

**STRUCTURAL STUDIES OF SUPRAMOLECULAR
HOST-GUEST SYSTEMS**

A Thesis Submitted to the College of
Graduate Studies and Research
In Partial Fulfillment of the Requirements
For the Degree of Doctor of Philosophy
In the Department of Chemistry
University of Saskatchewan
Saskatoon

By

ABDALLA H. KAROYO

Permission To Use

In presenting this thesis in partial fulfillment of the requirements for a Postgraduate degree from the University of Saskatchewan, I agree that the Libraries of this University may make it freely available for inspection. I further agree that permission for copying of this thesis in any manner, in whole or in part, for scholarly purposes may be granted by Professors L. D. Wilson and P. Hazendonk who supervised my thesis work or, in their absence, by the Head of the Department or the Dean of the College in which my thesis work was done. It is understood that any copying or publication or use of this thesis or part thereof for financial gain shall not be allowed without my written permission. It is also understood that due recognition shall be given to me and to the University of Saskatchewan in any scholarly use which may be made of any material in my thesis.

Requests for permission to copy or to make other use of material in this thesis in whole or part should be addressed to:

Head of the Department of Chemistry

University Of Saskatchewan

110 Science Place

Saskatoon, Saskatchewan

S7N 5C9 Canada

Acknowledgements

✧ *In The Name of Allah The Most Beneficent The Most Merciful* ✧

I would like to express my sincere thanks to my supervisors Drs. Lee D. Wilson and Paul Hazendonk, to whom am deeply indebted by the support and guidance they accorded me throughout the course of my PhD program.

My heartfelt thanks to the Department of Chemistry for the opportunity to do research and further my scientific career. I wish to thank the University of Lethbridge (U of L) for the opportunity to train and work on the solid-state NMR spectrometer; the University of Saskatchewan for the Graduate Teaching Fellowship; and the Natural Sciences and Engineering Research Council (NSERC) for the financial support.

I am grateful to members of my PhD advisory committee, Drs. Richard Bowles, Steve Reid, and Oleg Dmitriev for their expert guidance.

I wish to thank Drs. Sammynaiken and K. Brown, J. Maley, and K. Thoms (Saskatchewan Structural Sciences Center (SSSC)) for their technical support; Dr. P. Sidhu, Alex Borisov, and T. Montana (U of L) for their support in Solids NMR; Drs. Wajdi Zoghaib (Sultan Qaboos, Oman) and Hashim Ali (Arkansas State, USA) for their words of encouragement.

To my colleagues in the Lab; Drs. Mohamed, Rui Guo and Jae Kwon, Dawn Pratt, Louis Poon, Chen Xue, Shagufta Younis, Leila Dehabadi, and Inimfon for their help in the Lab.

I wish to thank Mohamed and Regeye, Denis and Catherine for making me feel at home away from home, especially during the early days of my stay in Canada.

Lastly, my special thanks go to the most important person in this journey; my wife, Mwanajuma. I never realized how strong a woman she was until I embarked on this journey; her patience, love and encouragement allowed me to finish this journey.

Dedications

This thesis is dedicated to my wife and my sons Hamisi, Faisal, and Fadhil.

To my parents; my mam Mwanasha Mwacharo, and my dad Hamisi Karoyo.

To my sisters Mwanamisi, Bibi (twin), Mwanaulu, and Mwanasiti;

and brothers Baya, Kassim, Dinar, and Juma.

Thank you for your love and support.

Abstract

This research work details a systematic study of the structure and function of supramolecular host-guest systems. Host-guest inclusion complexes were formed between β -Cyclodextrin (β -CD) and its copolymers (as hosts), with several types of guest molecules both in aqueous solution and the solid state. The research is divided into two themes; (1) structural characterization and dynamic properties of the inclusion compounds of β -CD with various guest systems in aqueous solution and the solid phase, and (2) heterogeneous adsorption and structural studies of β -CD based copolymers with various guest systems in aqueous solutions. The guest systems include alkyl and perfluoroalkyl carboxylates, perfluoroalkyl sulfonate, and *p*-nitrophenol (PNP) at variable experimental conditions.

In the first theme (chapters 2–5), perfluorinated compounds (PFCs), namely; perfluorooctanoic acid (PFOA), perfluorobutyric acid (PFBA), and sodium perfluorooctanoate (SPFO) represent the guest molecules. The host-guest complexes in the solid state were prepared using dissolution and slow cool methods at variable host/guest mole ratios (i.e., 1:1 and 2:1). The complexes were further characterized using $^{19}\text{F}/^{13}\text{C}$ DP/MAS and CP/MAS solid-state NMR spectroscopy. The solution state complexes were prepared in D_2O for structural characterization using $^1\text{H}/^{19}\text{F}$ NMR spectroscopy. The NMR studies were complemented using FT-IR, thermal analyses (DSC, and TGA), and powder X-ray diffraction (PXRD). Evidence for the formation of host-guest inclusion compounds (ICs) was provided using CP/MAS solids NMR spectroscopy and complexation-induced chemical shift (CIS) values of $^1\text{H}/^{19}\text{F}$ nuclei in aqueous solution. The β -CD/PFC ICs displayed variable guest geometry and hydration states as determined by the host-guest stoichiometry and the conformation of the guest. PFOA and SPFO form 1:1 and 2:1 ICs with β -CD, wherein the guest adopts a range of *gauche* and *trans* conformations, respectively.

1:1 host-guest complexes were concluded for short perfluorocarbon chains (i.e., PFBA) where the *gauche* conformation of the PFC guest in the bound state was favoured.

The phase purity of the β -CD/PFC ICs was assessed using DSC and ^{19}F DP/MAS NMR spectroscopy at ambient and variable temperature (VT) conditions. The complexes prepared by the slow cool method were found to be of relatively high phase purity when compared to complexes prepared by the dissolution method. However, a simple modified dissolution method was developed to afford complexes with greater phase purity. The phase purity of the complexes was further assessed using deconvolution analyses of the ^{19}F DP/MAS NMR resonance line shapes. $^1\text{H}/^{13}\text{C}/^{19}\text{F}$ NMR relaxation ($T_1/T_2/T_{1\rho}$) data of the phase pure β -CD/PFC ICs in the solid state revealed variable host and guest dynamics that were governed by dipolar coupling, H-bonding, and combinations of host-guest motional dynamics that involve peripheral and hydrate water within the cavity of β -CD. Coupling constants of the simulated ^{19}F spectra and deconvolution analyses of selected ^{19}F nuclei were used to supplement the ^{19}F NMR relaxation results. In general, two types of motional dynamics of the guest were concluded; (i) 120° rotational jumps of the fluoromethyl (CF_3) group at the termini of the PFC chain, and (ii) axial (libration) motion of the entire PFC chain. The rotational and axial dynamics of the guest in the complexes differ in their distribution and magnitude, in accordance with the host-guest stoichiometry and the geometry of the guest within the host.

In the second theme (chapters 6–8), β -CD based copolymers were used as host materials. The structural characterization of a soluble poly-CD material (known as HDI-1) revealed that the solution behaviour of such polymeric hosts are sensitive to the presence of guest compounds such as *p*-nitrophenol (PNP) (i.e. *chemo*-responsive), as well as temperature variations (i.e. *thermo*-responsive). The host-guest chemistry of the soluble poly-CD material, as studied by 2-D

solution NMR and induced circular dichroism (ICD) spectroscopy, indicates that PNP was bound within the cavity sites of β -CD and the interstitial domains of the copolymer (*cf.* Scheme 1.6 and chapter 6). The observed responsive nature of such polymeric host materials to temperature variation and chemical potential resembles behaviour characteristic of ‘*smart materials*’. Herein, ‘*smart materials*’ refer to systems which are responsive to external stimuli (e.g. temperature and chemical).

The adsorption properties of the soluble (HDI-1) and insoluble (HDI-3 and -6) poly-CD adsorbents with octyl and perfluorooctyl carboxylate and sulfonate anions were estimated using the Sips and BET models. The hydrocarbon (HC) and fluorocarbon (FC) anions form monolayer and multilayer structures at the surface of the polymeric adsorbents, respectively. The formation of layered structures was controlled by the relative hydrophobicity of the alkyl/perfluoroalkyl chains and their mutual miscibility with the adsorbent surface. Other factors include the inductive effects of the alkyl/perfluoroalkyl head groups and their interactions with aqueous solvent or dipolar domains of the adsorbent surface. The adsorbed species at the liquid-solid interface were characterized using FT-IR spectroscopy, thermal analyses, and contact angle.

TABLE OF CONTENTS

Permission To Usei
Acknowledgementsii
Dedicationsiii
Abstractiv-vi
Table of Contentsvii
Table of Contentsviii-xvi
Appendicesxvii-xviii
List of Tablesxix-xx
List of Schemesxxi-xxiv
List of Figuresxxv-xxxiii
List of Abbreviationsxxxiv-xxxv

Chapter 1.....	1
1. Introduction.....	1
1.1. Introduction to Supramolecular Chemistry.....	1
1.1.1. Supramolecular Chemistry: A Brief History.....	1
1.1.2. Supramolecular Host-Guest Chemistry.....	2
1.1.3. Classification of Supramolecular Host-Guest Systems.....	3
1.1.4. Nature of Supramolecular Interactions.....	4
1.2. Cyclodextrin Based Inclusion Compounds: Structural Aspects.....	6
1.2.1. Native Cyclodextrins.....	6
1.2.2. Modified Cyclodextrins.....	8
1.2.3. Interaction of Cyclodextrins with Organic Guests.....	9
1.2.4. Interaction of CD Based Polymers with Organic Guests.....	12
1.2.5. The Structure of Host-Guest Inclusion Complexes.....	13
1.2.5.1. Packing Arrangements of Cyclodextrin in Host-Guest Systems.....	16
1.2.5.2. Conformation of the Guest Molecule.....	17
1.3. Perfluorinated Compounds (PFCs).....	19
1.3.1. Perfluorinated Compounds: An Overview.....	19
1.3.2. Physicochemical Properties and Uses of PFCs.....	20
1.3.3. Sources and Environmental Concentration of PFCs.....	21
1.3.4. Toxicity of PFCs.....	23
1.3.5. Perfluorinated Compounds as Guest Molecules: Their Challenges.....	24
1.3.6. Other Organic Guest Compounds.....	26
1.4. Methods for Removing PFCs from the Environment.....	27
1.4.1. Adsorption Phenomena.....	28
1.4.2. Adsorption Isotherms.....	29
1.4.3. Equilibrium Isotherm Models.....	30
1.4.3.1.1. Langmuir Isotherm.....	30
1.4.3.1.2. Freundlich Isotherm Model.....	31
1.4.3.1.3. Sips Isotherm Model.....	31
1.4.3.1.4. BET Isotherm Model.....	32
1.5. NMR Spectroscopy of Host-Guest Systems.....	32

1.5.1.	NMR Spectroscopy: An Overview.....	32
1.5.2.	Matter, Spin and Magnetism.....	33
1.5.3.	Macroscopic Magnetization.....	36
1.5.4.	The Basic Pulsed NMR Experiment.....	37
1.5.4.1.	The Chemical Shift and Shielding.....	38
1.5.4.2.	Chemical Shift Anisotropy.....	40
1.5.5.	Overview of Solid-state NMR Spectroscopy.....	41
1.5.5.1.	Magic Angle Spinning (MAS).....	42
1.5.5.2.	Polarization Transfer Techniques.....	43
1.5.5.3.	High Power Decoupling Techniques.....	45
1.5.5.4.	Technical Aspects of High Resolution ¹⁹ F Solids NMR.....	46
1.5.6.	Relaxation.....	47
1.5.6.1.	Longitudinal and Transverse Relaxation Time constants.....	48
1.5.6.2.	Correlation Time.....	49
1.5.6.3.	Relaxation Mechanisms.....	52
1.5.6.3.1.	Dipole-Dipole Relaxation.....	52
1.5.6.3.2.	Chemical Shift Anisotropy.....	53
1.5.6.4.	Measurement of Relaxation Times.....	53
1.5.6.4.1.	Inversion Recovery (T ₁).....	53
1.5.6.4.2.	Spin Echoes (T ₂).....	54
1.5.6.4.3.	Spin Locking (T _{1ρ}).....	55
1.5.7.	The Nuclear Overhauser Effect (NOE).....	56
1.5.7.1.	Two-dimensional COSY.....	57
1.5.7.2.	Two-dimensional TOCSY.....	58
1.5.7.3.	Two-dimensional NOESY.....	58
1.5.7.4.	Two-dimensional ROESY.....	59
1.6.	Overall Research Objectives.....	60
1.7.	Specific Research Objectives (Hypotheses)	62
1.8.	Scope of Work	62
1.9.	References.....	65

Chapter 2.....	77
2. Formation of Host-Guest Complexes of β-cyclodextrin and Perfluorooctanoic Acid.....	79
2.1. Abstract.....	79
2.2. Introduction.....	80
2.3. Experimental Section.....	82
2.3.1. Materials.....	82
2.3.2. Preparation of Solid Inclusion Compounds.....	82
2.3.2.1. Method 1: <i>Dissolution</i>	82
2.3.2.2. Method 2: <i>Slow Cool</i>	82
2.3.3. Solution-state NMR Spectroscopy.....	82
2.3.4. Solid-state NMR Spectroscopy.....	83
2.3.5. Thermal Analyses (DSC and TGA).....	83
2.3.6. FT-IR Spectroscopy.....	84
2.3.7. Powder X-ray Diffraction (PXRD).....	84
2.4. Results and Discussion.....	84
2.4.1. Characterization of β -CD/PFOA Complexes.....	84
2.4.1.1. Stoichiometry of the Inclusion Complexes.....	84
2.4.1.2. DSC and TGA.....	85
2.4.1.3. FT-IR.....	88
2.4.1.4. PXRD	90
2.4.2. Solution-state NMR.....	91
2.4.2.1. $^1\text{H}/^{19}\text{F}$ Solution NMR Characterization.....	91
2.4.2.2. ^{19}F Solution NMR Dynamics.....	96
2.4.3. Solid-state NMR.....	100
2.4.3.1. $^{13}\text{C}/^{19}\text{F}$ Solid NMR Characterization.....	100
2.4.3.2. ^{19}F Solid NMR Dynamics.....	104
2.5. Conclusions.....	110
2.6. Acknowledgements.....	111
2.7. References.....	111

Chapter 3.....	115
3. Characterization and Dynamic Properties for the Solid Inclusion Complexes of β-Cyclodextrin and Perfluorooctanoic Acid.....	117
3.1. Abstract.....	117
3.2. Introduction.....	118
3.3. Experimental Section.....	119
3.3.1. Materials.....	119
3.3.2. Preparation and the Stoichiometry of the Solid β -CD/PFC Inclusion Compounds.....	119
3.3.3. Solid-state NMR Spectroscopy.....	120
3.3.3.1. $^{13}\text{C}/^{19}\text{F}$ NMR Spectroscopy.....	120
3.3.3.2. $^{13}\text{C}/^{19}\text{F}$ Relaxation Dynamics NMR.....	121
3.3.4. Thermal Analyses (DSC and TGA).....	121
3.3.5. FT-IR Spectroscopy	121
3.3.6. Powder X-ray Diffraction (PXRD)	122
3.4. Results and Discussion.....	122
3.4.1. DSC.....	122
3.4.2. FT-IR	124
3.4.3. PXRD.....	126
3.4.4. Solid-state NMR Characterization.....	127
3.4.4.1. ^{19}F DP/MAS NMR.....	127
3.4.4.2. ^{19}F DP/MAS NMR Dynamics at Variable Temperature.....	128
3.4.4.3. Chemical shift and Line Width Analyses.....	130
3.4.4.4. ^{13}C Solid-state CP/MAS NMR.....	131
3.4.5. Solid-state Dynamics and Relaxation Data.....	135
3.4.5.1. ^{19}F DP/MAS NMR Relaxation Dynamics at Ambient Temperature..	135
3.4.5.2. ^{19}F DP/MAS NMR Relaxation Dynamics at Variable Temperature..	141
3.5. Conclusions.....	145
3.6. Acknowledgements.....	146
3.7. References.....	146

Chapter 4.....	150
4. Characterization and Dynamic Properties for the Solid Inclusion Complexes of β-Cyclodextrin and Perfluorobutyric Acid.....	152
4.1. Abstract.....	152
4.2. Introduction.....	152
4.3. Experimental Section.....	155
4.3.1. Materials and Chemicals.....	155
4.3.2. Preparation of β -CD/SPFO Solid Inclusion Compounds.....	155
4.3.3. Solution-state NMR Spectroscopy	156
4.3.4. Solid-state NMR Spectroscopy.....	156
4.3.5. Differential Scanning Calorimetry (DSC).....	157
4.3.6. FT-IR Spectroscopy.....	157
4.3.7. Powder X-ray Diffraction (PXRD).....	157
4.4. Results and Discussion.....	157
4.4.1. DSC.....	157
4.4.2. FT-IR.....	159
4.4.3. PXRD.....	161
4.4.4. Solution-state NMR	162
4.4.4.1. $^1\text{H}/^{19}\text{F}$ Solution NMR Characterization.....	162
4.4.4.2. Coupling Constants of Simulated ^{19}F PFBA Spectrum.....	165
4.4.5. Solid-state MAS NMR.....	168
4.4.5.1. ^{19}F DP/MAS NMR Characterization.....	168
4.4.5.2. ^{19}F Deconvolution Analyses.....	169
4.4.5.3. $^1\text{H}\rightarrow^{13}\text{C}$ CP/MAS NMR.....	172
4.4.5.4. $^{19}\text{F}\rightarrow^{13}\text{C}$ CP/MAS NMR.....	174
4.4.6. ^{19}F Solids NMR Relaxation Dynamics.....	175
4.5. Conclusions.....	179
4.6. Acknowledgements.....	179
4.7. References.....	180

Chapter 5.....	183
5. Probing the Effect of Sodium Counterions on the Structure and Dynamics for the Solid Inclusion Complexes of β-Cyclodextrin and Sodium Perfluorooctanoate.....	185
5.1. Abstract.....	185
5.2. Introduction.....	186
5.3. Experimental Section.....	188
5.3.1. Materials.....	188
5.3.2. Preparation of β -CD/PFBA Solid Inclusion Compounds.....	188
5.3.3. Solution-state NMR Spectroscopy.....	189
5.3.4. Solid-state NMR Spectroscopy.....	189
5.3.5. Thermal Analyses (DSC/TGA).....	190
5.3.6. FT-IR Spectroscopy	190
5.3.7. Powder X-ray Diffraction (PXRD).....	190
5.4. Results and Discussion.....	190
5.4.1. DSC/TGA.....	190
5.4.2. FT-IR.....	193
5.4.3. PXRD.....	195
5.4.4. Solution-state NMR.....	197
5.4.4.1. ^1H NMR Characterization.....	197
5.4.4.2. ^{19}F NMR Characterization.....	199
5.4.5. Solid-state MAS NMR.....	204
5.4.5.1. $^1\text{H}\rightarrow^{13}\text{C}$ CP/ and DP/MAS NMR.....	204
5.4.5.2. $^{19}\text{F}\rightarrow^{13}\text{C}$ CP/MAS NMR.....	206
5.4.5.3. ^{19}F DP/MAS at Ambient Temperature.....	208
5.4.5.4. ^{19}F DP/MAS at Variable Temperature.....	212
5.4.6. ^{19}F Relaxation Dynamics NMR Data at Variable Temperature.....	215
5.5. Conclusions.....	219
5.6. Acknowledgements.....	220
5.7. References.....	221

Chapter 6.....	225
6. Structural Characterization of a Urethane-Based “Molecular Accordion” Copolymer in Aqueous Solution.....	227
6.1. Abstract.....	227
6.2. Introduction.....	227
6.3. Materials and Methods.....	229
6.3.1. Materials.....	229
6.3.2. Synthesis of β -CD Based Copolymer Materials.....	229
6.3.3. Structural Characterization of a Urethane Copolymer in Aqueous Solution.....	230
6.3.3.1. Raman Spectroscopy.....	230
6.3.3.2. ^1H Solution-state NMR Spectroscopy.....	230
6.3.3.3. Differential Scanning Calorimetry (DSC).....	231
6.3.3.4. Induced Circular Dichroism (ICD).....	231
6.3.3.5. Dynamic Light Scattering (DLS).....	232
6.4. Results and Discussion.....	232
6.4.1. Physicochemical Characterization of a Soluble β -CD-based Copolymer.....	232
6.4.2. Physicochemical Characterization of the HDI-1/PNP Complex in Aqueous Solution.....	236
6.4.2.1. 2-D ROESY NMR.....	236
6.4.2.2. 1-D Selective ROESY NMR.....	239
6.4.2.3. Raman Spectroscopy.....	241
6.4.2.4. Induced Circular Dichroism (ICD).....	246
6.4.2.5. DSC.....	248
6.4.2.6. Dynamic Light Scattering (DLS).....	250
6.5. Conclusions.....	252
6.6. Acknowledgements.....	253
6.7. References.....	253

Chapter 7.....	258
7. Tunable Macromolecular-Based Materials for the Adsorption of Perfluorooctanoic and Octanoic Acid.....	260
7.1. Abstract.....	260
7.2. Introduction.....	261
7.3. Materials and Methods.....	262
7.3.1. Chemicals.....	262
7.3.2. Adsorbents.....	263
7.3.3. Adsorbates.....	264
7.4. Batch Sorption Studies.....	265
7.4.1. Sorption of Perfluorooctanoate (PFOA)	265
7.4.2. Sorption of Octanoate (OA)	266
7.4.3. Sorption Isotherms.....	266
7.4.4. Models and Equations.....	266
7.5. Results and Discussion.....	268
7.5.1. PFOA Sorption.....	268
7.5.2. OA Sorption.....	272
7.6. Conclusions.....	276
7.7. Acknowledgements.....	277
7.8. References.....	277
 Chapter 8.....	 281
8. Investigation of the Adsorption Interactions of Alkyl and Perfluoroalkyl Carboxylates Anions onto Macromolecular Imprinted Materials.....	283
8.1. Abstract.....	283
8.2. Introduction.....	283
8.3. Chemicals.....	284
8.4. Methods.....	285
8.4.1. Synthesis of Macromolecular (β -CD)-Based Copolymers (MIMs).....	285
8.4.2. Preparation of MIMs/Carboxylate Anions Mixtures.....	286

8.4.3. FT-IR Spectroscopy.....	286
8.4.4. Differential Scanning Calorimetry (DSC).....	287
8.4.5. Contact Angle	287
8.4.6. Isothermal Titration Calorimetry (ITC).....	287
8.5. Adsorption Isotherms.....	288
8.6. Results and Discussion.....	290
8.6.1. Sorption Studies for PFOA, OA, and PFOS.....	290
8.6.1.1. Surface Coverage: Monolayer vs. Multilayer (PFOA, OA).....	290
8.6.1.2. Sorption and Equilibrium Binding Parameters for PFOA and OA...	292
8.6.2. Sorption and Binding Parameters for PFOS.....	294
8.6.3. Interaction of PFOA and OA with β -CD Based Copolymer Adsorbents (MIMs).....	299
8.6.3.1. DSC.....	299
8.6.3.2. FT-IR.....	303
8.6.3.3. Contact Angle.....	307
8.6.3.4. ITC.....	308
8.7. Conclusions.....	311
8.8. Acknowledgements.....	311
8.9. References.....	312
Chapter 9.....	315
9. Summary, Conclusion and Proposed Future Work.....	315
9.1. Summary.....	315
9.2. Concluding Remarks.....	317
9.3. On the Application of MIMs.....	321
9.4. Proposed Future Work.....	322
9.5. References.....	324

Appendices (Supplementary Information)	326
Fig. A2.1. DSC thermograms of Physical Mixtures of β -CD/PFOA at the 1:1 and 2:1 Mole Ratios.....	326
Fig. A2.2. FT-IR Spectra of Native β -CD, the 1:1, and 2:1 β -CD/PFOA Physical Mixtures, and PFOA.....	326
Fig. A2.3. PXRD Spectra of the 1:1, and 2:1 β -CD/PFOA Physical Mixtures.....	327
Fig. B3.1. TGA Thermograms of β -CD, PFOA, and the 1:1 and 2:1 β -CD/PFOA Complexes Prepared by the Modified Dissolution Method.....	327
Fig. B3.2. X-ray Powder Diffractograms of β -CD, PFOA, and the 1:1, and 2:1 β -CD/PFOA Physical Mixtures.....	328
Fig. B3.3. ^{19}F T_1 Relaxation times for the CF_3 group of SPFO, the 1:1 and 2:1 β -CD/PFOA inclusion complexes as a function of temperature.....	328
Table B3.1. ^{19}F NMR spectral parameters Generated by Fitting the CF_3 Signal of the 1:1 β -CD/PFOA Complex to Two Lorentzian Peaks (CF_3 -in Cavity, CF_3 -out of Cavity).....	329
Table B3.2. ^{19}F NMR spectral parameters Generated by Fitting the CF_3 Signal of the 2:1 β -CD/PFOA Complex to One Lorentzian Peak (CF_3 -in Cavity).....	329
Table C4.1a,b. Deconvolution Parameters for the CF_3 and the CF_2 high and low field resonance lines of ^{19}F spectrum of the (a) 1:1 and (b) 2:1 β -CD/PFBA Complex acquired at MAS 20 kHz and 295 K.....	330
Fig. D5.1. Weight Percentages for the dehydration processes for β -CD, and the 1:1 and 2:1 β -CD/SPFO complexes.....	331
Table D5.1. Deconvolution Parameters for the CF_3 Line Shape of pure SPFO, the 1:1, and 2:1 β -CD/SPFO Complexes.....	332
E6.1. 2-D ^1H COSY NMR Results of HDI-1 Copolymer Showing Connectivity of the Protons of the HDI Linker.....	332
E6.2. 1-D TOCSY NMR Results of HDI-1 Copolymer. The Proton Nuclei of β -CD (H1-	

H4) are Irradiated.....	333
E6.3. 1-D TOCSY NMR Results of HDI-1 Copolymer. The Proton Nuclei of HDI cross-linker are Irradiated.....	333
E6.4. 1-D TOCSY NMR Results of HDI-1 Copolymer. The Proton Nuclei of the Solvents (diethyl ether, Dimethyl Acetamide) are Irradiated.....	334
E6.5: 2-D ROESY NMR Results of HDI-1/PNP Complex. Cross peaks Showing directed Inclusion of PNP Within the Cavity of β -CD are Shown as Expanded Regions.....	334

List of Tables

Table 1.1. Non-covalent interactions and their strength for host-guest complexes.....	5
Table 1.2. Physicochemical properties of the native α -, β -, and γ -cyclodextrins.....	7
Table 1.3. Examples of the application of cyclodextrin-based cross-linked polymers for the adsorption of organic molecules.....	10
Table 1.4. Structural parameters of host-guest complexes and techniques of measurement.....	15
Table 1.5. Physicochemical properties of perfluorinated compounds and octanoic acid.....	21
Table 1.6. PFOA and PFOS levels ($\mu\text{g/L}$) in some aquatic samples.....	22
Table 1.7. PFOA and PFOS safe levels for various organizations and governments.....	24
Table 1.8. Properties of Some Common NMR Nuclides.....	34
Table 2.1. DSC and TGA Thermoanalytical Data.....	86
Table 2.2. Chemical Shift Data for Uncomplexed and Complexed PFOA Guest at Variable Spin Rates (Values in Bracket Indicate Chemical Shifts for Broad CF_3 Components).....	106
Table 3.1. ^{13}C -Detected $T_{1\rho}^{\text{H}}$ Relaxation Values for the ^{13}C Resonances of the Host and the 1:1 and 2:1 β -CD/PFOA Complexes at Ambient Temperature.....	135
Table 3.2. ^{13}C -detected T_1^{H} relaxation values for the ^{13}C resonances of the host and the 1:1 and 2:1 β -CD/PFOA complexes at ambient temperature.....	138
Table 3.3. ^{13}C T_2 relaxation values (T_2^{C}) for the ^{13}C resonances of the host and the 1:1 and 2:1 β -CD/PFOA complexes at ambient temperature.....	139
Table 3.4. ^{19}F Relaxation Values ($T_1^{\text{F}}/T_2^{\text{F}}/T_{1\rho}^{\text{F}}$) for the ^{19}F Resonances of Sodium Perfluorooctanoate (SPFO), and the 1:1 and 2:1 β -CD/PFOA Complexes at Ambient Temperature.....	140
Table 4.1. Physicochemical Properties of Various Perfluorocarbon Compounds.....	154
Table 4.2. The DSC Data for β -CD, and the 1:1 and 2:1 β -CD/PFBA Inclusion Complexes. Main Dehydration Transitions are indicated by Asterisks.....	158
Table 4.3. T_1 and T_2 Relaxation Values for the 1:1 β -CD/PFBA and 1:1 β -CD/PFOA Complexes.....	177
Table 4.4. Activation Energies (kJ/mol) of PFBA Guest as Estimated from T_1 and T_2 Data for β -CD/PFBA Complexes.....	178
Table 5.1. CIS Values (ppm) for the ^1H Nuclei of β -CD and Complexes with PFOA and SPFO in Solution at 295 K.....	199

Table 5.2. CIS Values (ppm) for the ¹⁹ F Nuclei of β-CD/SPFO and β-CD/PFOA Complexes in Solution at 295 K.....	200
Table 5.3 CIS Values (ppm) for the ¹³ C Nuclei of β-CD/SPFO and β-CD/PFOA Complexes in Solution at 295 K.....	208
Table 5.4 <i>T</i> ₁ Relaxation Values for the 19F Resonances of the SPFO and the 1:1 and 2:1 β-CD/SPFO Complexes at Variable Temperature.....	217
Table 5.5 <i>T</i> ₂ Relaxation Values for the 19F Resonances of the SPFO and the 1:1 and 2:1 β-CD/SPFO Complexes at Variable Temperature.....	217
Table 5.6 Summarized Structural Properties of PFOA, SPFO, and PFBA and their Complexes with β-CD.....	221
Table 6.1 Raman Shift Data for Host and Guest Raman Bands (1-9) for HDI-1/PNP Complexes at Various Mole Ratios (1:1 to 1:5) and Crystalline PNP at 295 K.....	244
Table 7.1 Physicochemical Properties of the Adsorbent Materials and the Dye-based Equilibrium Binding Constants.....	264
Table 7.2 Physicochemical Properties of Adsorbate Materials.....	264
Table 7.3 Isotherm Sorption Parameters for PFOA onto GAC and the Urethane-copolymers (MIMs) Obtained from the BET and Sips Models at 295 K and pH ~ 3.85.....	270
Table 7.4 Isotherm Sorption Parameters for Octanoate onto GAC and the Urethane-copolymers (MIMs) Obtained from the Sips Model at 295 K and pH ~ 8.50.....	276
Table 8.1. Physicochemical Properties of the Adsorbent and Adsorbate.....	291
Table 8.2. BET and Sips Isotherm Sorption Parameters for PFOA and OA with GAC and MIMs at 295 K and pH 4 and 8.5, respectively.....	293
Table 8.3. Molecular Structures and Physicochemical Properties of PFOA and PFOS.....	295
Table 8.4. BET Isotherm Sorption Parameters for PFOS with HDI-1 and -6 at 295 K and pH~ 3.....	299
Table 8.5. FT-IR Absorption Bands of HDI-6, PFOA and their Adsorbed Complexes.....	305
Table 8.6. FT-IR absorption bands for HDI-6, OA, and HDI-6/OA systems.....	306
Table 8.7. Static Contact Angles (θ) of PFOA and OA on an HDI-6 Copolymer Film at Variable Loading Levels at 295 K.....	307
Table 8.8. Binding constants (<i>K</i> _{<i>i</i>} ; <i>i</i> = 1:1 or 2:1) and Standard Enthalpy (Δ <i>H</i>) and Entropy Changes (TΔ <i>S</i>) for Inclusion Complexes of PFOA and OA with HDI-1 at pH ~4 (PFOA) and pH ~8.5 (OA, in phosphate buffer) at 298 K.....	310

List of Schemes

Scheme 1.1. The association of a host and a guest to form a host-guest complex, where K_i is the equilibrium binding constant corresponding to a 1:1 host-guest inclusion complex.....	2
Scheme 1.2. The hydrophobic effect is shown as the association of a host and a guest in the presence of an aqueous solvent.....	4
Scheme 1.3. Schematic representation of (a) a rotaxane showing a polymeric guest threading through a CD, and (b) a catenane showing two CDs interlocked in a chain.....	9
Scheme 1.4. A model describing the formation of a host-guest complex according to a 1:1, 1:2, and 2:1 binding stoichiometry.....	11
Scheme 1.5. Topology of cyclodextrin complexes; (a) complete, (b) axial, (c) partial, (d) sandwich-type inclusion; (e) 2:1 axial inclusion compound, and (f) non-inclusion compound (Adapted from ref. 33).....	11
Scheme 1.6. Association of a CD and a di-functional reagent to form a linear and a branched copolymer, where a guest can bind in the inclusion sites or within the interstitial regions.....	12
Scheme 2.1. The formation of a host-guest complex is shown for β -CD (toroid) and a perfluorinated guest molecule according to a 1:1 and 2:1 equilibrium binding process where K_i are the corresponding equilibrium binding constants for each host-guest stoichiometry. In the case of perfluorooctanoic acid (PFOA); R= -OH. The relative dimensions of the β -CD macrocycle and PFOA are not drawn to scale.....	92
Scheme 2.2. Representations of the supramolecular structure of β -CD structure. The left hand structure refers to the oligomer where $n = 7$ and the right hand structure represents the toroidal shape of the macrocycle.....	93
Scheme 3.1 Step-wise formation of the 1:1 and 2:1 host/guest complexes between β -CD (toroid) and PFOA, according to the 1:1 and 2:1 (host/guest) stoichiometric ratios. The corresponding equilibrium constants are presented as $K_{1:1}$ and $K_{2:1}$, respectively.....	120
Scheme 3.2. Schematic representation of the three types of complexes that can hypothetically be formed between PFOA and β -CD.....	128

Scheme 3.3. Representation of the molecular structure of β -CD; (a) the oligomer where $n = 7$, (b) the toroidal shape of the macrocycle showing the inclusion cavity protons, and (c) the toroidal shape of the macrocycle showing the rim and framework carbons.....	133
Scheme 4.1 The association of β -CD and PFBA to form a β -CD/PFBA inclusion complex forms according to a 1:1 host-guest stoichiometry.....	155
Scheme 4.2 Molecular Structure of (a) PFBA, and (b,c) β -CD. The structure of β -CD is shown as a truncated toroid where the primary and secondary hydroxyls, and glycosidic oxygen bridges are shown. The intracavity protons (H_3/H_5) are shown (b).....	164
Scheme 4.3 Schematic representation of the binding interaction postulated for PFBA guest and β -CD; (1) partial guest inclusion in a 1:2 host/guest ratio, (2) complete guest inclusion in a 1:1 host/guest ratio, and (3) complete inclusion with guest protruding to result in 2:1 host/guest ratio. Note: inclusion through the narrow rim of CD is possible.....	170
Scheme 5.1 Molecular Structures of (a) β -CD oligomer where $n = 7$, (b) β -CD represented as a toroidal macrocycle, and (c) SPFO.....	188
Scheme 5.2 Stepwise formation of the 1:1 and 2:1 complexes of β -CD (toroid) and SPFO according to the 1:1 and 2:1 host/guest mole ratios.....	189
Scheme 5.3 The proposed inclusion geometry of (a) PFOA, and (b) SPFO in the 2:1 β -CD/guest complex. (c) The proposed inclusion geometry of SPFO in the 1:1 β -CD/SPFO complex. Note the CD torus and SPFO structure are not drawn to scale.....	204
Scheme 6.1 Reaction between β -CD and 1,6-hexamethylene diisocyanate (HDI) to form the HDI-1 copolymer. Note that for 1:1 co-monomer mole ratios, the cross linker is hypothesized to attach covalently at the primary annular hydroxyl sites of β -CD.....	230
Scheme 6.2 Temperature induced switching between compact (i.e., coiled) and extended (i.e., uncoiled) forms of the HDI-1 copolymer in aqueous solution at ambient pH conditions; where n indicates the hypothetical repeat structure of the copolymer.....	234
Scheme 6.3 Numbering scheme for the 1H intracavity nuclei (H_3 , H_5) and external macrocycle (H_1 , H_2 , H_4 , H_6) nuclei of β -CD, and the nuclei of hexamethylene	

diisocyanate (HDI).....	236
Scheme 6.4 Inclusion binding mode between β -CD inclusion sites of HDI-1 with <i>p</i> -nitrophenol (PNP). The urethane bond linkage is denoted by the wavy line in the primary annular hydroxyl region. Note: The binding presentation is not drawn to scale.	238
Scheme 6.5 Guest-induced switching between compact (i.e., coiled) and extended (i.e., uncoiled) forms of the HDI-1 copolymer in aqueous solution at ambient pH conditions; where ovals represent the guest (PNP). The compact form may involve self-inclusion of the linker unit. The repeat structure of the copolymer is represented by n.....	245
Scheme 6.6 Equilibrium switching between <i>compact</i> and <i>extended</i> forms of HDI-1, according to temperature and the presence of guest (PNP).....	246
Scheme 7.1 Reaction between β -CD and 1,6-hexamethylene diisocyanate (HDI) to form the HDI-X copolymers; where X = 1, 3 and 6.....	263
Scheme 7.2 Sorption of PFOA and OA onto the hydrocarbon (HC) sorbents; Top: Binding of PFOA via the carboxylate head group and formation of tail-to-tail bilayer structures (with possible hemi-micelle and micelle formation), and Bottom: Monolayer binding of OA via the apolar alkyl chain.....	274
Scheme 7.3 Sorption modes of the PFOA/OA anion onto (a) activated carbon via electrostatic and hydrophobic interactions, (b) HDI-6 adsorption occurs via non-inclusion sites through ion-dipole interactions with hydroxyl groups and/or amide-NH groups as donor molecules and $-\text{COO}^-$ as the acceptor (the wavy line displays the perfluoroalkyl tail of PFOA), and (c) HDI-1 adsorption occur via inclusion and non-inclusion sites of the copolymer framework where the toroids represent β -CD, spheres with tails represents PFOA, and the zig-zag lines represent HDI linker sites. Note that the head group of PFOA and perfluoroalkyl chain is not drawn to scale.....	275
Scheme 8.1 Reaction between β -CD (toroid) and 1,6-hexamethylene diisocyanate (HDI) to form the HDI-X copolymers; where X = 1 or 6. Note that for the 1:1 mole ratio, the cross linker is hypothesized to attach at the primary annular hydroxyl sites ($-\text{C}_6\text{H}_2\text{-OH}$) of β -CD.....	285
Scheme 8.2 Schematic presentation of the sites of substitution of HDI cross linker to the primary (narrow rim) and secondary (wide rim) hydroxyl groups in the annular	

region of β -CD copolymer. The filled spheres represent covalently attached sites and illustrate low, medium, and high cross-linking; whereas, the open spheres represent unreacted sites. Adapted from ref. 15.....	286
Scheme 8.3 Proposed adsorption modes of the carboxylate anions within the inclusion sites of β -CD via tail groups and onto the linker domains of the copolymer for (a) PFOA via ion-dipole interactions of the head group and subsequent formation of multilayers, and (b) OA adsorption occurs via the alkyl tails to form a monolayer.....	294
Scheme 8.4 Proposed adsorption modes for (a) HDI-6/PFOA, and (b) HDI-6/PFOS systems. PFOA confers stronger ion-dipole interactions with the dipolar regions of the MIMs surface than PFOS. Adsorption via head group interactions prevail due to the low β -CD inclusion site accessibility and the greater number of urethane linkages of HDI-6 on the MIMs framework. Note: Inclusion sites accessibility for HDI-6 ~ 0 due to steric effects.....	300
Scheme 9.1 Organization of the PhD Thesis; The Boxes in Bold Represent the Two Main Themes of the Study, the Boxes under the Arrows Represent the Sub-topics, and the Box between the lines Represent the Intersection of the Structure and Function Themes.....	316

List of Figures

Figure 1.1. Schematic illustration of the association of a guest and (a) a cavitand to form a cavitate, and (b) a clathrand to form a clathrate. (c) Formation and self-assembly of a supramolecular complex.....	3
Figure 1.2. The molecular structure of Cyclodextrins showing (a) the macromolecule, (b) the toroid shape and, (c) a cross-section of the toroid showing the primary and secondary hydroxyl groups, intracavity protons, and the framework carbons.....	7
Figure 1.3. Schematic representation of the packing of cyclodextrin structure showing (a) head-to-head channel type, (b) head-to-tail channel type, (c) cage-type, and (d) layer-type packing structures.....	17
Figure 1.4. The Newman projection for the (a) <i>gauche</i> , and (b) <i>anti</i> conformers of a simple four-carbon system.....	18
Figure 1.5. The molecular structure of PFOA displaying; (b and d) the <i>gauche</i> and (a and c) <i>anti</i> -conformers of the perfluorocarbon chain. (c,d) Spartan generated ball and stick structures of PFOA.....	18
Figure 1.6. The molecular structure of (a) PFOA/SPFO, where $R' = H^+/Na^+$; (b) PFBA, and (c) PFOS.....	19
Figure 1.7(a) Molecular structure of <i>p</i> -nitrophenol, (b) three different inclusion modes of the phenolate guest within the cavity of a CD host as determined from intermolecular NOE spatial interactions	26
Figure 1.8. Types of Adsorption isotherms. Point A represents the regions where monolayer coverage is complete.....	29
Figure 1.9. The energy difference ΔE between two adjacent energy levels for spin-1/2 nuclei as a function of the magnetic flux density B_0	35
Figure 1.10. The orientations of the nuclear magnetic moments at equilibrium in the absence of external magnetic field are isotropically distributed.....	35
Figure 1.11. Precession of the spin magnetic moment in the presence of external Magnetic field.....	36
Figure 1.12. (a) A cluster of spins precessing at the Larmor frequency (ω_0) in the presence of external magnetic field (B_0) along the <i>z</i> -axis, and (b) the corresponding	

longitudinal magnetization vector.....	36
Figure 1.13. Net magnetization is shown (a) in longitudinal before the $\pi/2$ RF pulse, (b) rotated in the transverse plane by the $\pi/2$ RF pulse, and (c) Larmor precession of the transverse magnetization.....	37
Figure 1.14. One channel single-pulse NMR sequence.....	38
Figure 1.15. Distribution of spin orientation in (a) solution, and (b) solid samples. Rapid molecular tumbling in solution averages the orientation dependence to an isotropic value and sharp resonance line (a). Anisotropic effects in solid samples result in broad NMR spectral lines (b).....	42
Figure 1.16. Dipolar coupling of two spins presents a source of line broadening in solid NMR.....	42
Figure 1.17. Schematic interpretation of the magic angle ($\theta = 54.74^\circ$). Samples are spun at this angle with respect to the vertical axis.....	43
Figure 1.18. A typical cross polarization pulse sequence for observing dilute nucleus X where magnetization is transferred from an abundant nucleus e.g., ^1H to X during spin lock time t_{cp}	44
Figure 1.19. A cross polarization MAS NMR pulse sequence with TPPM heteronuclear decoupling of spin I.....	45
Figure 1.20. Relaxation drives the z -magnetization to its equilibrium value (dotted line) and the transverse to its value of zero.....	49
Figure 1.21. Typical NMR time-scales and related motional dynamics (Adapted from ref. 184).....	50
Figure 1.22. Relationship between longitudinal and transverse relaxation rate constants as a function of correlation time (Adapted from ref. 203).....	51
Figure 1.23. Inversion recovery pulse sequence for measuring the rate constant for longitudinal relaxation (T_1).....	54
Figure 1.24. The simple spin echo pulse sequence used to measure the rate constant for transverse relaxation (T_2).....	55
Figure 1.25. Pulse sequence for measuring ($T_{1\rho}$).....	55
Figure 1.26. Schematic two-dimensional COSY spectrum showing cross peaks (grey ovals) and diagonal peaks (black ovals) and scalar coupled peaks (dotted lines).....	57

Figure 1.27. Basic 2-D COSY pulse sequence.....	58
Figure 1.28. Basic 2-D TOCSY pulse sequence.....	58
Figure 1.29. Basic 2-D NOESY pulse sequence.....	59
Figure 1.30. Basic 2-D ROESY pulse sequence.....	59
Figure 2.1. DSC thermograms of native β -CD hydrate and PFOA (a), the 1:1 and 2:1 complexes prepared by slow cooling (b), and dissolution (c) methods.....	87
Figure 2.2. TGA plots for native β -CD hydrate, PFOA, and the 1:1 and 2:1 β -CD/PFOA complexes prepared by the slow cooling method.....	88
Figure 2.3. FT-IR spectra of native β -CD, 1:1 β -CD/PFOA complex, 2:1 β -CD/PFOA complex, and PFOA. The figure on the right is an expansion of the spectral region between 800 and 1400 cm^{-1}	89
Figure 2.4. Powder X-ray Diffraction (PXRD) spectra for native β -CD, unbound PFOA, 1:2 β -CD/PFOA dissolution (D) complexes, 1:1 and 2:1 β -CD/PFOA slow cooled (SC) complexes, and 1:1 and 2:1 β -CD/PFOA dissolution (D) complexes.....	91
Figure 2.5. ^1H NMR in D_2O solutions for β -CD, the 1:1, 2:1, and 3:1 β -CD/PFOA inclusion compounds acquired at pD~5 and 295K; where * indicates HOD signal.....	92
Figure 2.6. Expanded and assigned ^{19}F solution NMR spectra of PFOA, the 1:1 and 2:1 β -CD/PFOA inclusion compounds acquired at pD ~5 and 295 K.....	94
Figure 2.7. ^{19}F NMR spectra at variable temperature conditions for the 1:1 β -CD/PFOA complex in D_2O at pD~5 (heating cycle from 25 $^\circ\text{C}$ to 75 $^\circ\text{C}$).....	97
Figure 2.8. ^{19}F NMR spectra at variable temperature for the 1:1 β -CD/PFOA complex in D_2O at pD~5 (cooling cycle from 55 $^\circ\text{C}$ to 5 $^\circ\text{C}$).....	97
Figure 2.9. ^{19}F NMR spectra at variable temperature for the 2:1 β -CD/PFOA complex in D_2O at pD~5 (heating cycle from 25 $^\circ\text{C}$ to 75 $^\circ\text{C}$).....	99
Figure 2.10. ^{19}F NMR spectra at variable temperature for the 2:1 β -CD/PFOA complex in D_2O at pD~5 (cooling cycle from 55 $^\circ\text{C}$ to 5 $^\circ\text{C}$).....	100
Figure 2.11. Solid state ^{19}F DP/MAS spectrum of PFOA obtained at MAS 25 kHz and 295 K.....	100
Figure 2.12. Solid state ^{13}C H \rightarrow C CP/MAS spectrum for native β -CD hydrate at MAS 20 kHz and 295 K.....	101

Figure 2.13. ^{19}F DP MAS 25 kHz NMR spectra at 295 K for pure PFOA, and the 1:1 and 2:1 β -CD/PFOA complexes obtained by the slow cool method.....	102
Figure 2.14. ^{19}F DP/MAS 25 kHz NMR spectra at 295 K for pure PFOA, and the 1:1 β -CD/PFOA complexes obtained by dissolution and slow cool methods.....	103
Figure 2.15. ^{19}F DP NMR spectra for unbound (free) PFOA at variable spin rates (VSRs) at 295 K.....	105
Figure 2.16. ^{19}F DP NMR spectra of the 1:1 β -CD/PFOA complex prepared by the dissolution method and run at variable spin rates (VSR) at 295 K.....	106
Figure 2.17. ^{19}F DP NMR spectra of the 1:1 β -CD/PFOA complex prepared by the slow cool method and run at variable spin rates (VSR) at 295 K.....	107
Figure 2.18. ^{19}F DP/MAS NMR spectra at 14 kHz and variable temperature for the 1:1 β -CD/PFOA complex prepared by the dissolution method (warming from -90°C to 20°C).....	107
Figure 2.19. ^{19}F DP/MAS NMR spectra obtained at 14 kHz and variable temperature for the 1:1 β -CD/PFOA complex prepared by the dissolution method. The heating cycle was from 25°C to 90°C (A), and the cooling cycle was from 85°C to 25°C (B).....	109
Figure 2.20. ^{19}F DP/MAS NMR spectra obtained at 14 kHz and variable temperature for the 2:1 β -CD/PFOA complex prepared by the slow cool method. The heating cycle was from 25°C to 100°C (A), and the cooling cycle was from 90°C to 25°C (B).....	110
Figure 3.1. DSC thermograms of β -CD hydrate, unbound PFOA, and the 1:1 and 2:1 β -CD/PFOA inclusion compounds.....	123
Figure 3.2. FT-IR spectra of β -CD, unbound PFOA, and the 1:1 and 2:1 β -CD/PFOA inclusion compounds. The inset shows expanded region from $900 - 1500\text{ cm}^{-1}$	125
Figure 3.3. PXRD spectra of β -CD hydrate, PFOA, and the 1:1 and 2:1 β -CD/PFOA inclusion compounds. Differences in the PXRD patterns between the two complexes are shown by asterisks (*)......	126
Figure 3.4. ^{19}F DP/MAS (20 kHz) NMR spectra of PFOA, and the 1:1 and 2:1 β -CD/PFOA complexes at ambient temperature.....	127
Figure 3.5. ^{19}F DP/MAS (20 kHz) NMR spectra of (a) the 1:1, and (b) 2:1 β -CD/PFOA dissolution complexes at variable temperature.....	129

Figure 3.6. Deconvolution of the CF ₃ signal in the ¹⁹ F DP/MAS (20 kHz) NMR spectra of the 2:1 and 1:1 complexes at 25°C. The 2:1 complex is fit to one Lorentzian peak (CF ₃ -in cavity), while the 1:1 complex is fit to two Lorentzian peaks (CF ₃ -in cavity, CF ₃ -out of cavity).....	130
Figure 3.7. Plots of the (7a) chemical shift and (7b) linewidth estimates of the 2:1 (one component) and 1:1 (two components) NMR spectra from the deconvolution results illustrated in Figure 3.6.....	131
Figure 3.8. ¹³ C (¹ H→ ¹³ C) CP/MAS solid NMR spectra of β-CD, the 1:1 and 2:1 β-CD/PFOA complexes at ambient temperature.....	132
Figure 3.9. ¹³ C (¹⁹ F→ ¹³ C) CP/MAS 20 kHz NMR spectra of pure PFOA and the 1:1 β-CD/PFOA complex at variable contact times.....	134
Figure 3.10. ¹⁹ F T ₁ (open symbols) and T ₂ (filled symbols) values for the CF ₃ , main (C _m F ₂) and terminal C _e F ₂ groups for the (a) 1:1, and (b) 2:1 β-CD/PFOA complexes....	142
Figure 3.11. (a) ¹⁹ F T _{1ρ} 's for the CF ₂ and CF ₃ groups of the 1:1 and 2:1 βCD/PFOA complexes. (b) ¹⁹ F T _{1ρ} 's for the CF ₂ group of the 1:1 and 2:1 βCD/PFOA complexes on an expanded scale.....	144
Figure 4.1. The DSC thermograms of β-CD, and the 1:1 and 2:1 β-CD/PFBA inclusion complexes.....	158
Figure 4.2. The FT-IR for native β-CD, PFBA, and the 1:1 and 2:1 βCD/PFBA inclusion complexes. Inset: Expanded region from 1400 cm ⁻¹ –800 cm ⁻¹	160
Figure 4.3. The PXRD patterns for native β-CD, SPFB, and the 1:1 and 2:1 βCD/PFBA inclusion complexes.....	162
Figure 4.4. ¹ H solution NMR spectra for β-CD, and the 1:1 and 2:1 β-CD/PFBA inclusion complexes in D ₂ O at 295 K.....	163
Figure 4.5. ¹⁹ F solution NMR expanded spectra for PFBA, and the 1:2, 1:1, and 2:1 β-CD/PFBA inclusion complexes in D ₂ O at 295 K.....	164
Figure 4.6. ¹⁹ F simulated spectrum of PFBA (Hz) in D ₂ O at ambient temperature showing the splitting of the (a) –CF ₃ , (b) α-CF ₂ , and (c) β-CF ₂ signals. The satellite lines are shown by asterisks.....	165
Figure 4.7. The three possible rotamers of perfluorobutyric acid (PFBA),	

R = -COOH.....	166
Figure 4.8. ^{19}F DP NMR spectra for the 1:1, and 2:1 β -CD/PFBA inclusion complexes acquired at 20 kHz MAS and 295 K. Asterisks show spinning sidebands.....	168
Figure 4.9. (a) Deconvolution analyses of the CF_3 line shapes for the ^{19}F DP/MAS 20 kHz spectra of (i) the 1:1, and (ii) 2:1 β -CD/PFBA solid complexes at 295 K. (b) Deconvolution analyses of the CF_2 line shapes for the ^{19}F DP/MAS 20 kHz spectra of (i) the 1:1, and (ii) 2:1 β -CD/PFBA solid complexes at 295 K.....	171
Figure 4.10. ^{13}C $^1\text{H}\rightarrow^{13}\text{C}$ CP NMR results for β -CD, and the 1:1, and 2:1 β -CD/PFBA inclusion complexes at 20 kHz MAS and 295 K.....	173
Figure 4.11. ^{13}C $^{19}\text{F}\rightarrow^{13}\text{C}$ CP NMR results for the 1:1, and 2:1 β -CD/PFBA inclusion complexes at 20 kHz MAS and 295 K.....	175
Figure 4.12. ^{19}F T_1 (in seconds) and T_2 (in milliseconds) relaxation times for the 1:1, and 2:1 β -CD/PFBA complexes	176
Figure 5.1. The DSC traces for β -CD hydrate, SPFO, and the 1:1 and 2:1 β -CD/SPFO inclusion complexes.....	191
Figure 5.2. TGA traces for β -CD hydrate, SPFO and the 1:1 and 2:1 β -CD/SPFO inclusion compounds.....	192
Figure 5.3. FT-IR spectra of β -CD, SPFO, and the 1:1 and 2:1 β -CD/SPFO inclusion compounds.....	194
Figure 5.4. The PXRD patterns for β -CD hydrate, SPFO, and the 1:1, and 2:1 β -CD/SPFO inclusion compounds.....	196
Figure 5.5. ^1H NMR spectra for β -CD, and the 1:1 and 2:1 inclusion compounds with SPFO and PFOA in D_2O at 295 K, respectively.....	198
Figure 5.6. ^{19}F NMR expanded spectra for PFOA, and SPFO, and their 1:1, and 2:1 inclusion compounds with β -CD in D_2O at 295 K. The resonance lines are assigned according to the accompanying structure.....	200
Figure 5.7. The $^1\text{H}\rightarrow^{13}\text{C}$ CP and DP/MAS spectra for β -CD, and the 1:1 β -CD/SPFO, and β -CD/PFOA complexes. All spectra were acquired at MAS 20 kHz and 295 K....	205
Figure 5.8. The $^{19}\text{F}\rightarrow^{13}\text{C}$ CP results for SPFO, PFOA, and the respective 1:1 inclusion compounds with β -CD under MAS 20 kHz at 295K. The host and guest regions are labeled.....	207

Figure 5.9 ^{19}F DP NMR spectra for PFOA, SPFO, and the 1:1 and 2:1 β -CD/SPFO inclusion compounds under MAS 20 kHz at 295 K.....	209
Figure 5.10 The simulated CF_3 signal as a function of variable dipolar coupling strengths.....	210
Figure 5.11 Deconvolution of the CF_3 line shape for SPFO, and the 1:1 and 2:1 β -CD/SPFO complexes.....	211
Figure 5.12 (a-c) ^{19}F DP NMR spectra for SPFO, and the 1:1 and 2:1 β -CD/SPFO inclusion compounds under MAS 20 kHz at variable temperature. (d) ^{19}F DP/MAS-VT NMR spectra for 2:1 β -CD/PFOA inclusion compound.....	214
Figure 5.13 ^{19}F T_1 (open symbols) and T_2 (filled symbols) values for the CF_3 and main CF_2 groups for the 1:1, and 2:1 β -CD/SPFO complexes under MAS 20 kHz at variable temperature.....	218
Figure 6.1. 1-D ^1H NMR Spectra in D_2O at 500 MHz and 298 K; HDI-1 copolymer, HDI, and β -CD. * denotes residual solvent (i.e., DMA and ethyl ether).....	233
Figure 6.2. VT ^1H NMR spectra in D_2O at 500 MHz of HDI-1 without PNP in aqueous solution; (a) heating cycle, and (b) cooling cycle. The asterisk denotes residual solvent (i.e., DMA and ethyl ether).....	235
Figure 6.3. 2-D ^1H NMR ROESY spectra in D_2O at 500 MHz and 298 K; (a) 1:1 HDI-1/PNP, (b) 1:5 HDI-1/PNP.....	237
Figure 6.4. 1-D ^1H NMR ROESY spectra in D_2O at 500 MHz for HDI-1/PNP complexes at various host/guest ratios and a spin-lock time of 400 ms; (a) 1:3 HDI-1/PNP at 298 K; where the following nuclei were irradiated: <i>i</i>) $\text{H}_{3,7}$, <i>ii</i>) H_1 , <i>iii</i>) H_3 and H_6 , <i>iv</i>) $(\text{CH}_2)_{\beta,\gamma}$, <i>v</i>) $(\text{CH}_2)_{\beta,\gamma}$, and (b) 1:5 HDI-1/PNP at VT; where the following nuclei were irradiated: $\text{H}_{3,7}$ and $(\text{CH}_2)_{\beta,\gamma}$ (enlarged spectra are also shown), and (c) 1:5 HDI-1/PNP at VT; where the following nuclei were irradiated: $\text{H}_{3,7}$ and $(\text{CH}_2)_{\beta,\gamma}$	241
Figure 6.5 Raman spectra of solution evaporated films at 295 K for HDI-1 (Host), and PNP (Guest) and the 1:1, 1:2, 1:3, and 1:5 HDI-1/PNP (H/G) complexes. (A) Full spectral region ($600\text{--}3400\text{ cm}^{-1}$), (B) Expanded spectral region ($800\text{--}1640\text{ cm}^{-1}$), and (C) Expanded spectral region ($2300\text{--}3200\text{ cm}^{-1}$).....	243
Figure 6.6 ICD spectra of host-guest complexes in aqueous solution; (a) β -CD/PNP at various host-guest mole ratio, and (b) HDI-1/PNP at variable host-guest ratios and 295	

K.....	248
Figure 6.7. DSC results of β -CD, HDI-1, and HDI-1/PNP mixtures in aqueous solution from 20 to 70 °C. The dashed line is provided as a guide.....	249
Figure 6.8. DLS results recorded as change in hydrodynamic diameter of HDI-1 copolymer with (a) temperature (298 to 348 K), and (b) relative PNP mole ratio (the x-axis in Figure 8b represents moles PNP per 1 mole HDI-1 monomer, where zero means absence of PNP).....	251
Figure 7.1. Calibration results and “best-fit” linear regression for the (a) ESI-MS results for PFOA and (b) titration of OA.....	265
Figure 7.2. Sorption isotherms of PFOA onto GAC, HDI-1, HDI-3, and HDI-6 at pH 3.85 and 295 K. The “best-fit” lines correspond to the BET (copolymers) and Sips (GAC and copolymers; see inset) models.....	269
Figure 7.3. ^{19}F NMR chemical shifts (CF_2) and “best-fit” 1:1 equilibrium binding model for the titration of PFOA in the presence of HDI-1 (1 g/L) in aqueous solution at 298 K and pH ~ 5.....	272
Figure 7.4. Sorption isotherms of octanoate onto GAC, HDI-3, and HDI-6 at pH 8.50 and 298 K. The “best-fit” lines correspond to the Sips model.....	273
Figure 8.1. Typical ESI-MS spectra of the solutions of PFOA (pH 3.8) and PFOS (pH ~3) at low and high loading concentrations in the presence of HDI-6 copolymer.....	289
Figure 8.2. Sorption isotherms for MIMs/PFOA (Left) and MIMs/OA (Right) systems expressed as surface coverage (Θ) against equilibrium concentration (C_e).....	290
Figure 8.3. Sorption isotherms of PFOS onto HDI-1, and (b) HDI-6 MIMs at pH ~3 and 295 K. The “best-fit lines” correspond to the BET model. Insets: The corresponding sorption isotherms of PFOA onto HDI-1, and HDI-3 MIMs surfaces are compared where the circled regions at low C_e show favourable adsorbate-adsorbent interactions.....	297
Figure 8.4. DSC thermograms of the hydrated samples of PFOA and mixtures containing HDI-6 at different PFOA loadings.....	300
Figure 8.5. DSC thermograms of the hydrated samples of OA and its mixtures with HDI-6 at different loading levels of OA.....	302
Figure 8.6. FT-IR spectra of hydrated solids HDI-6, PFOA, and HDI-6/PFOA-1, HDI-	

6/PFOA-4, and HDI-6/PFOA-7 systems at 295 K. The numbered bands (1–3) show the CF ₂ /CF ₃ stretching bands of PFOA.....	303
Figure 8.7. FT-IR spectra of hydrated solids HDI-6, OA, and HDI-6/OA-1, HDI-6/PFOA-4, and HDI-6/PFOA-18 systems at 295 K.....	306
Figure 8.8a,b. Calorimetric titration of (a) β-CD/PFOA, and (b) HDI-1/ PFOA at pH ~ 4 and 298 K, respectively. The ITC isotherms reveal 1:1 and 2:1 β-CD/PFOA (a-II), and 1:1 HDI-1/PFOA (b-II).....	308
Figure 8.9. Calorimetric titration of (a) β-CD/OA, and (b) HDI-1/OA systems at pH ~8 and 298 K.....	309
Figure 9.1 Pulse Sequence for 2D J-Resolved NMR Technique.....	322

List of Abbreviations

BET	Brunauer-Emmett-Teller
CD	Cyclodextrin
CIS	Complexation Induced Chemical Shift
COSY	Correlation Spectroscopy
CP	Cross Polarization
DLS	Dynamic Light Scattering
DP	Direct Polarization
DSC	Differential Scanning Calorimetry
ESI	Electro Spray Ionization
FC	Fluorocarbon
FT-IR	Fourier Transform Infrared
HC	Hydrocarbon
HDI	Hexamethylene Diisocyanate
ICs	Inclusion Compounds
ICD	Induced Circular Dichroism
ITC	Isothermal Titration Calorimetry
MAS	Magic Angle Spinning
MIMs	Macromolecular Imprinted Materials
MS	Mass Spectrometry
NMR	Nuclear Magnetic Resonance

NOESY	Nuclear Overhauser Effect Spectroscopy
OA	Octanoic Acid
PFBA	Perfluorobutyric Acid
PFCs	Perfluorinated Compounds
PFOA	Perfluorooctanoic Acid
PFOS	Perfluorooctane Sulfonate
PNP	<i>p</i> -Nitrophenol
PU	Polyurethane
PXRD	Powder X-ray Diffraction
RF	Radio Frequency
ROESY	Rotating Frame Overhauser Enhancement Spectroscopy
SPE	Solid Phase Extraction
SPFO	Sodium Perfluorooctanoate
TDI	Toluene Diisocyanate
TGA	Thermogravimetric Analysis
TOCSY	Total Correlation Spectroscopy
TPPM	Two Phase Pulse Modulation
US-EPA	United States Environmental Protection Agency
UV-Vis	Ultra-violet Visible
VT	Variable Temperature
WWTP	Waste Water Treatment Plant

CHAPTER 1

1. Introduction

1.1 Introduction to Supramolecular Host-Guest Chemistry

1.1.1 Supramolecular Chemistry: A Brief History

Supramolecular chemistry refers to the area of chemistry beyond that of molecules and focuses on the collective chemical system made up of a discrete number of assembled molecular subunits or components.^{1,2} The concept of supramolecular chemistry can be traced back to the beginning of modern chemistry in the early 19th century. However, the field has seen significant development and major breakthroughs since the 1960's. Important concepts that have been demonstrated by supramolecular chemistry include molecular self-assembly, molecular folding, molecular recognition, host-guest chemistry, mechanically-interlocked molecular architectures, and dynamic covalent chemistry. While traditional chemistry focuses on the covalent bond, supramolecular chemistry deals with the weak non-covalent intermolecular interactions (e.g., hydrogen bonding, metal coordination, hydrophobic forces, van der Waals interactions, π - π interactions and electrostatic effects).

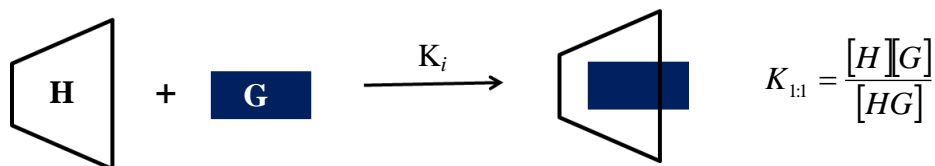
The existence of intermolecular forces was first postulated by Johannes Diderik van der Waals in 1873, but it was not until 1894 that Hermann Emil Fischer first introduced the concept of supramolecular chemistry.³ Fischer suggested that enzyme-substrate systems display the "lock and key" interaction which represents a key concept among the fundamental principles of molecular recognition and host-guest chemistry.

The breakthrough in synthetic supramolecular chemistry came with the synthesis of the crown ethers by Charles J. Pederson in the 1960s.⁴ This was followed by the works of Donald J. Cram, Jean-Marie Lehn, and Fritz Vogtle in the synthesis of *shape*- and *ion-selective* receptors, and the subsequent emergence of the concepts of mechanically interlocked molecular architectures in the 1980's.^{5,6} The rapid expansion of the field over the past few decades has seen a significant increase in the diversity of chemical systems. In the 1990's, supramolecular chemistry became even more sophisticated, with researchers such as James Fraser Stoddart developing molecular machinery and highly complex self-assembled structures, and Itamar Willner developing sensors and methods of electronic and biological interfacing. During this period, electrochemical and photochemical motifs became integrated into supramolecular systems in order to increase their functionality. Other related research

areas such as synthetic self-replicating systems, and studies on molecular information processing devices followed. The emergence of the field of nanotechnology has strongly influenced supramolecular chemistry where diverse building blocks such as fullerenes, nanoparticles, and dendrimers represent examples of some complex synthetic systems. Today, modern supramolecular chemistry is not just limited to elementary host-guest systems but includes other systems such as molecular devices and machines, mechanically-interlocked molecular architectures, which involve processes such as molecular recognition, self-assembly, self-organization and molecular folding.

1.1.2 Supramolecular Host-Guest Chemistry

The simplest definition of supramolecular host-guest chemistry involves non-covalent binding or complexation between a host and a guest as depicted in Scheme 1.1. The non-covalent interactions involved include hydrogen bonding, ion-pairing, π - π interactions, metal-to-ligand binding, van der Waals forces, solvent reorganization, and partial made and broken covalent bonds (transition states). Some of the most common and natural host-guest systems include antigen-antibody, DNA-ligand, enzyme-substrate, and protein-carbohydrate complexes.



Scheme 1.1 The association of a host (truncated cone) and a guest (rectangle) to form a host-guest complex, where K_i is the equilibrium binding constant corresponding to a 1:1 host-guest inclusion complex. Note that the contribution of solvent is omitted for the sake of clarity.

Donald Cram⁵ defined a host-guest relationship as the involvement of complementary stereoelectronic arrangement of binding sites between a host and guest. That is, the host must possess binding sites that are of the correct electronic character to complement those of the guest. The host is commonly defined as a large molecule or aggregate such as an enzyme or synthetic cyclic compound that possess a sizeable, pre-organized central hole or cavity (e.g., CDs, calixarenes, crown ethers, etc.). The guest may be an organic or inorganic cation, a

simple inorganic anion, an ion pair, or a more complicated organic molecule such as a hormone. The host and the guest, as described by Cram, are molecular entities that possess *convergent* (e.g., Lewis acid donor sites, hydrogen bond donors, etc.) and *divergent* (e.g., hydrogen bond acceptor, Lewis acidic acceptor sites or metal cation, etc.) binding sites, respectively.

1.1.3 Classification of Supramolecular Host-Guest Systems

Supramolecular host-guest systems can generally be divided into three classes; (1) cavitates, (2) clathrates, and (3) self-assemblies. The term ‘clathrate’ was coined by H. M. Powell in 1948 who gave one of the first formal definitions of a supramolecular *cage-like* host-guest structure. Generally speaking, the classification of host-guest systems is based on topological relationship of the host and the guest. Cavitands (host molecules that form cavitates, e.g., CDs, calixarenes, and cucurbiturils) possess permanent intramolecular cavities; whereas, clathrands possess extramolecular cavities that are created by gaps between two or more host molecules in a lattice (*cf.* Figure 1.1).

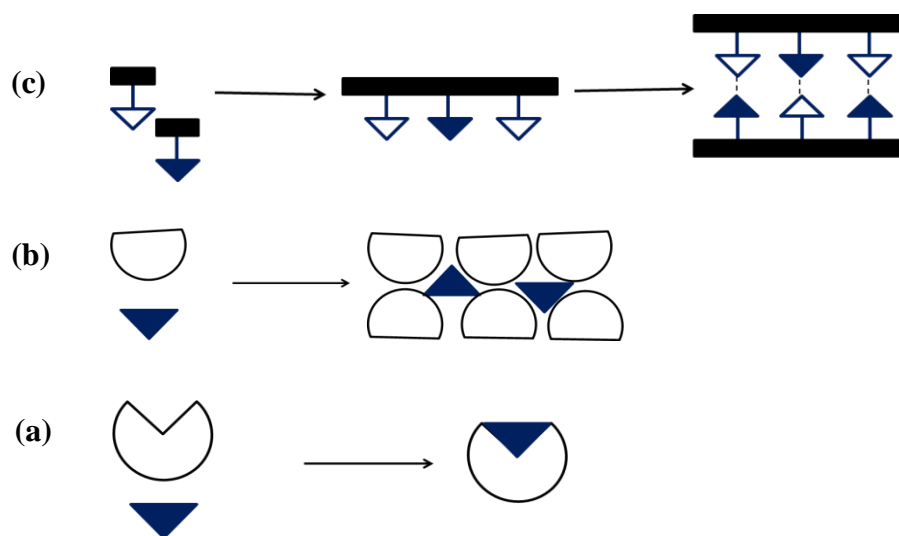
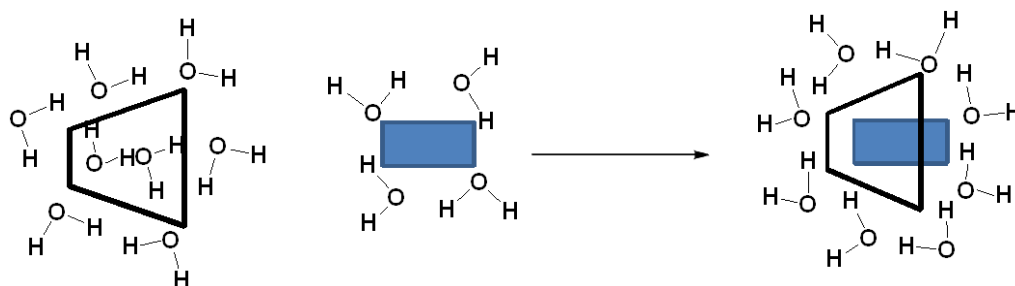


Figure 1.1 Schematic illustration of the association of a guest (triangle) and (a) a cavitand to form a cavitate, and (b) a clathrand to form a clathrate. (c) Formation and self-assembly of a supramolecular complex. Adapted from ref. 2

Traditionally, clathrates refer to polymeric hosts-molecular guests systems; however, the term has recently been used for self-associating molecules such as calixarenes and CDs, as well as inorganic lattices such as zeolites.⁷ IUPAC⁸ defines clathrates as inclusion compounds in which the guest molecules lie in a cage formed by the host molecule or by a lattice of host molecules. Therefore, the cavity in cavitands is an intrinsic property of the host, existing both in solution and the solid state. Contrary to the cavitands, clathrands are only relevant in the crystalline or solid state. Common examples of clathrates are methane hydrates and channels in urea crystals.^{9,10} Self-assembly includes a third category where two molecules, which do not fit the typical descriptions of host and guest, associate by non-covalent forces. The distinction between the two host classes, and self-assembly is illustrated schematically in Figure 1.1.

1.1.4 Nature of Supramolecular Interactions

Supramolecular host-guest chemistry concerns non-covalent bonding interactions between two or more molecules. These interactions often encompass an enormous range of attractive and repulsive effects. In fact, much of the emphases in the construction of supramolecular host molecules concerns bringing about summative or even multiplicative interactions. For example, most of host-guest systems involve a combination of more than two non-covalent interactions occurring simultaneously. Thus, the stability of a host-guest complex is fundamental and represents a key division within supramolecular host-guest chemistry. The most important non-covalent interactions in supramolecular host-guest chemistry are listed in Table 1.1, along with their approximate interaction energies.²



Scheme 1.2 The hydrophobic effect is shown as the association of a host (toroid) and a guest (rectangle) in the presence of an aqueous solvent.² Note that the molecular dimensions of the host, guest and solvent are not drawn to scale.

Among the various interactions listed above (*cf.* Table 1.1), hydrophobic effects and hydrogen-bonding are of crucial importance in the binding of organic guests by CDs and similar hosts in aqueous solution. Hydrophobic effects generally relate to the exclusion from polar solvents, particularly water, of large particles (solute species) or those that are weakly solvated by hydrogen bonding or dipolar interactions.¹⁷ Since host cavities such as CDs are hydrophobic in nature, intracavity water does not interact favourably with the cavity and is preferentially released into the bulk solvent where it can interact with other water molecules. The interaction of a host and a guest in the presence of an aqueous solvent is depicted in Scheme 1.2.

Table 1.1 Non-covalent Interactions and Their Strengths for Host-guest Complexes.^{2,11}

Type of interaction	Typical	
	Energy (kJ mol ⁻¹)	Examples
Ion-ion	200–300	Tetrabutylammonium chloride
Ion-dipole	50–200	cation-crown ether complex ⁴
Dipole-dipole	5–50	Dihydroxybenzoic acid-CD complex ¹²
Hydrogen bonding	4–120	R-CO ₂ H dimers, ¹³ enzyme-substrates
π-π	0–50	Protein-ligand complex ¹⁴
Cation-π	5–80	Fe ²⁺ -ferrocene complex ¹⁵
Van der Waals	<5	Toluene- calixarene complex ¹⁶
Hydrophobic	Variable	CD inclusion complexes

Generally, the importance of solvent in supramolecular chemistry cannot be overstressed, particularly for complexes formed between an apolar host and a guest. Even though the host-guest binding process can be simplistically regarded as an interaction between a pre-organized host with unsolvated guest (*cf.* Scheme 1.1); however, solvation processes of the host and guest are important considerations in solution (*cf.* Scheme 1.2). The difference in

Gibbs energy of solvation for an unbound host may be significantly different from those of the complexed state, particularly if there is significant conformation changes (induced fit) upon binding.¹⁸ In the solid state, the solvent is often included as a co-guest in the crystalline lattice and usually mediates the nucleation and deposition of a crystalline compound from solution. In solution, all complexation phenomena are in competition with solvation interactions and the solvent is often present in excess levels. Polar solvents such as water compete efficiently for binding sites through hydrogen bonding which reveals why hydrophobic (or solvophobic) effects are of paramount importance. In nonpolar solvents and in the gas phase, specific host-guest dipolar and hydrogen bonding interactions may be more significant due to the nature and importance of solvation.

1.2 Cyclodextrin Based Inclusion Compounds: Structural Aspects

1.2.1 Native Cyclodextrins

Recent research efforts have been directed towards the study of host-guest inclusion systems in supramolecular chemistry. Cyclodextrins (CDs) are among the most widely studied host molecules and the continued interest in the study of the inclusion complexes involving CDs and its copolymers stems from both fundamental science and practical application point of view. CDs are enormously important host compounds with a variety of applications in food, cosmetics, pharmaceuticals and the environment.¹⁹⁻²¹ CDs are a group of structurally related natural products formed during bacterial digestion of starch. These cyclic oligosaccharides consist of (α -1,4)-linked α -D-glucopyranose units and contain a lipophilic central cavity and a hydrophilic outer surface.²² Due to the chair conformation of the glucopyranose units, the CDs are toroidal-shaped like a truncated cone rather than cylindrically shaped. The hydroxyl groups are located at the periphery of the tori exterior with the primary groups at the narrow side of the torus and the secondary hydroxyl groups at the wider annulus region. The central cavity is lined with skeletal C-C, C-H, and ether groups from the glycosidic linkages, which impart lipophilic character to the CD interior. The native α -, β - and γ -CDs consist of six, seven, and eight glucopyranose units, respectively. An illustration of the molecular structure of the common types of CDs, along with the cavity sizes are shown in Figure 1.2, including their physicochemical properties in Table 1.2.

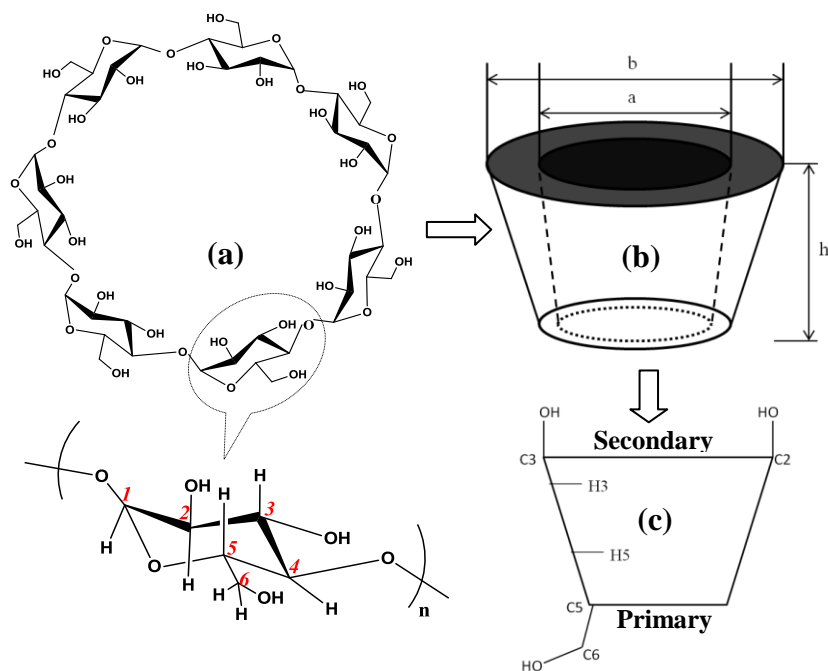


Figure 1.2 The molecular structure of cyclodextrins showing (a) the macromolecule with enlarged glucopyranose unit where $n = 6, 7$ or 8 , (b) the toroid shape, and (c) a systematic cross-section of the toroid showing the primary and secondary hydroxyl groups, intracavity protons, and the framework carbons

Table 1.2 Physicochemical Properties of Native α -, β -, and γ -Cyclodextrins.²

Type of Cyclodextrin	α -CD	β -CD	γ -CD
Number of glucose units	6	7	8
Height (h) of CD (Å)	7.80	7.80	7.80
Internal (a) cavity outer diameter (Å)	5.7	7.8	9.5
Internal cavity center diameter (Å)	5.0	6.2	8.0
Outer (b) diameter (Å)	13.7	15.3	16.9
Solubility in water (g/L, 25°C)	145	18.5	232
Cavity volume in 1g CD (cm ³)	0.10	0.14	0.20
Crystalline water (wt. %)	10.2	13.2–14.5	8.13–17.7
pKa (25°C, by potentiometry)	12.33	12.20	12.08

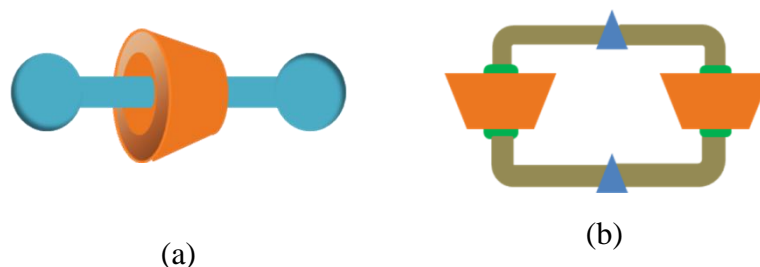
The native CDs, especially β -CD, have limited aqueous solubility (*cf.* Table 1.2) meaning that complexes resulting from interaction of lipophiles with CDs may have limited solubility resulting in precipitation of the complex from aqueous solutions. This characteristic of β -CD is important in the preparation of the inclusion compounds between β -CD and perfluorinated compounds (PFCs) using dissolution and evaporation methods reported herein (§Chapter 2). The low solubility of CDs is thought to be due to relatively strong intramolecular hydrogen bonding in the crystal state.²³

1.2.2 Modified Cyclodextrins

The use of modified CDs as host molecules is well established^{24,25} and provides a way to enhance various physical properties e.g. solubility of CDs for tailored application in areas such as pharmaceuticals and medicine, catalysis, and separation phenomena. A variety of CD derivatives containing one or more substituents at the primary or secondary positions were synthesized, many of which have shown improved molecular recognition.²⁵ Some of the most common CD derivatives that have been used as host materials include; methylated-,^{26,27} heptakis-methylated-,^{28,29} and hydroxyl-based^{30,31} CDs. Other types of derivatives have been reviewed elsewhere.^{22,25}

Recently, supramolecular chemistry has been expanding to supramolecular polymer chemistry as a way to enhance functionality and tune the physicochemical properties of supramolecular materials. CD-based host-guest complexes are presented by three types; (i) complex formation between a simple organic/inorganic guest molecule and a native CD host, (ii) complex formation between a simple guest and CD-based polymeric host, and (iii) complex formation between a native CD host and a polymeric guest. Host-guest supramolecular systems of the second type are common in the sorption of organic pollutants. The most common supramolecular architectures formed by association of the third type, where a CD (or a derivatized CD) with a polymeric guest are involved, include (poly)-rotaxanes and catenanes.³²⁻³⁴ These architectures represent a class of mechanically interlocked molecular structures which have potential application in the construction of molecular devices. (Poly)-rotaxanes are prepared from axial (*cf.* Scheme 1.5b) polymeric inclusion compounds with bulky terminal capping groups (stoppers) on the guest. Ogino³⁵ reported one of the first examples of rotaxanes utilizing host-guest inclusion phenomena, where an alkyl

chain with metallo-organic stoppers threaded through the α -CD cavity. Common polyrotaxanes containing polyethylene glycol threads and α -CD beads have been reported by Harada et al.^{36,37} Catenanes consist of two or more macrocyclic units that are interlocked in a ring or chain. The schematic representations of a rotaxane and a catenane are depicted in Scheme 1.3.



Scheme 1.3 Schematic representation of (a) a rotaxane showing a polymeric guest threading through a CD (truncated cone), and (b) catenane showing two CDs interlocked in a chain. The triangles represent functional groups that are of different complementarity to CD

The supramolecular association of CD-based polymeric materials with simple organic/inorganic guest molecules is important in this dissertation because of its sorption based applications.^{38,39} The design of CD-based polymers as sorbent materials is an extension of host-guest chemistry that offers unique opportunities to engineer new materials with tunable properties: (1) surface area, (2) pore structure, (3) solubility, (4) life-time (regeneration), and (5) the functionality (surface chemistry) of the sorbent to aid in the design of optimal sorption properties. Studies of the application of CD-based copolymers for the adsorption of organic pollutants have been reported⁴⁰⁻⁴⁷ and some examples are listed in Table 1.3.

1.2.3 Interaction of Cyclodextrins with Organic Guests

In general, apolar guest molecules (e.g., organic and inorganic molecules) may be favourably bound in the CD cavity (*cf.* Scheme 1.1). The interaction of a CD with an apolar guest molecule in aqueous solution results in the formation of 1:1 inclusion compounds, where the guest may be included within the host cavity. Higher order equilibria involving the formation of 1:2 and 2:1 complexes are known and may exist simultaneously. Therefore, a

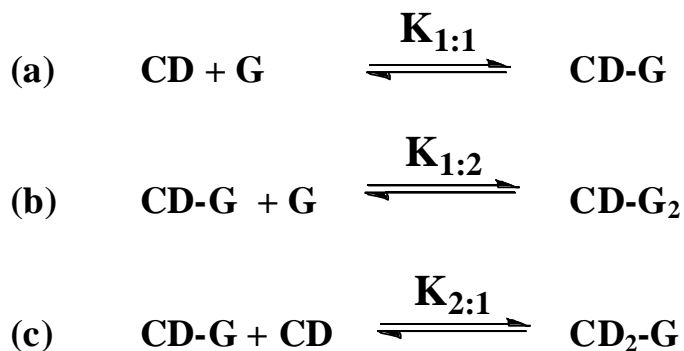
model that describes the formation of a host-guest complex must adequately account for the various types of host-guest stoichiometry.^{48,49}

Table 1.3 Examples of the Application of Cyclodextrin-based Cross-Linked Polymers for the Adsorption of Organic Molecules

Linker Agents	Guest molecules (Adsorbates)	Proposed Mode of Sorption	Ref.
Epichlorohydrin	Aromatic guests (e.g. Phenol, benzoic acid, β -naphthol, and dyes).	Cavity inclusion, adsorption onto polymer network, guest-guest interaction	40,41
Diisocyanate	Humic acid, geosmine.	Cavity inclusion	44
Diisocyanates	Cholesterol (as template).	Cavity inclusion	45
Epichlorohydrin	Dodecylbenzenesulfonic acid and benzalkonium chloride.	Cavity inclusion	46
2-Hydroxyethyl methacrylate and Di-isocyanate	Steroids (cholesterol, progesterone, testosterone).	Cavity inclusion	47

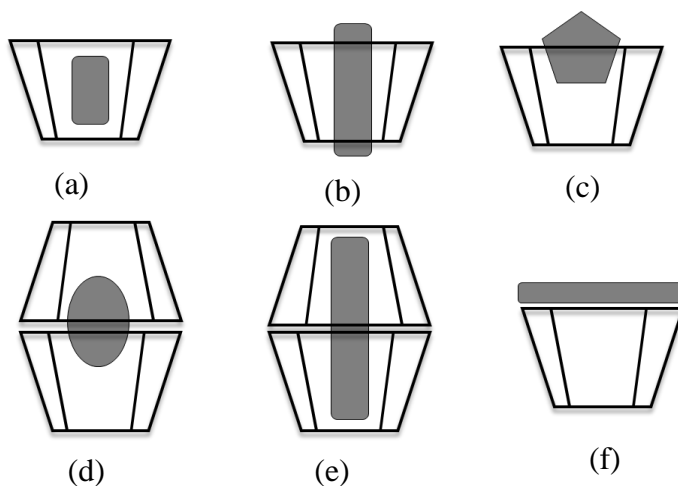
Scheme 1.4 describes various complexes that were considered in this work. It should be noted that multiple equilibria are possible in the case of aliphatic guests with longer alkyl chains due to the occurrence of channel structures (*cf.* Scheme 1.4c and §1.2.5.1). In order to form a stable inclusion complex, the guest molecules should fit, at least partly, into the CD cavity.^{19,20} Based on Scheme 1.4, the association of a CD with apolar guests can give rise to a variety of complexes with variable topologies. The topology of these complexes is determined predominantly by *size-fit* considerations according to the dimensions of the guest with respect to the host. Possible topologies of the guest include; (i) complete inclusion within the host cavity, (ii) partial inclusion with one end (short guest) or two ends (long guest) protruding from the rim(s) of the macrocycle, (iii) sandwich-like inclusion for short and thick guests, and

(iv) binding of the guest at the periphery or exterior of the cavity (non-inclusion binding). Several types of host-guest topologies of CD complexes are depicted in Scheme 1.5.



Scheme 1.4 A model describing the formation of a host-guest complex according to a 1:1, 1:2, and 2:1 binding stoichiometry.

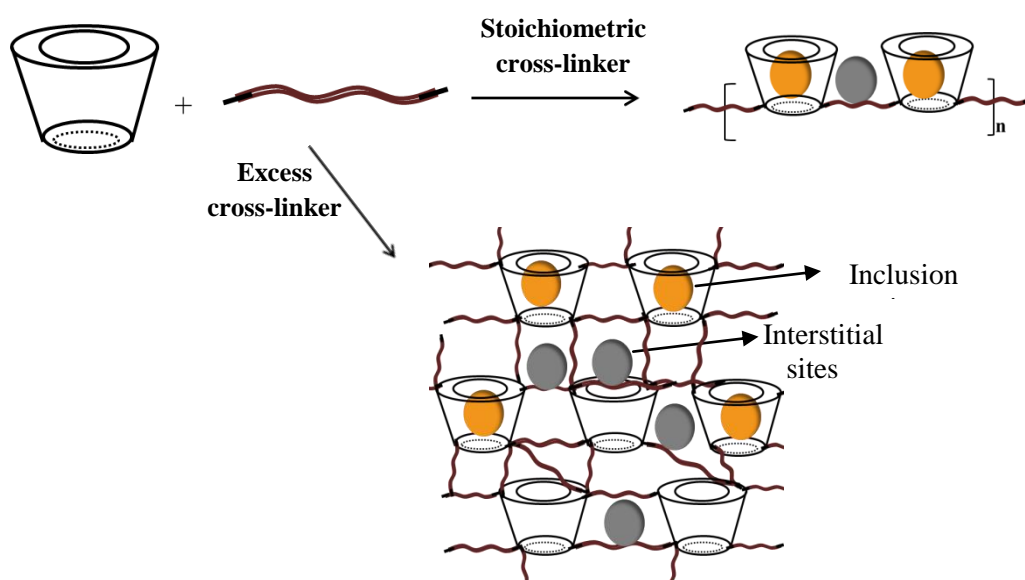
It is apparent that steric considerations contribute to the association of guest molecules to CDs in solution. Other factors such as the release of high energy water, hydrophobic effects, van der Waals interactions, dispersive forces, dipole-dipole interactions, charge-transfer interactions, electrostatic interactions, and hydrogen bonding are important as previously described (*cf.* §1.1.4). The relative cavity size (*cf.* Table 1.2) and chemical modification of the host (e.g., derivatization; *cf.* §1.2.2) determine the binding affinity of a CD host to its guest molecules. In general, the stability of CD inclusion compounds depends on the extent to which the cavity is filled by the hydrophobic part of the guest.



Scheme 1.5 Topology of cyclodextrin complexes; (a) complete, (b) axial, (c) partial, and (d) sandwich-type inclusion; (e) 2:1 (axial) inclusion compound, and (f) non-inclusion compound. Adapted from ref. 33

1.2.4 Interaction of CD-based Polymers with Organic Guests

The cross-linking reaction of bi-functional reagents such as epichlorohydrin,^{41,42,50} diisocyanates^{39,44,45,51,52} and di-acid chlorides^{53,54} with CD affords either soluble or insoluble linear or branched polymers, depending on the reaction conditions. The reaction of such cross-linker reagents with CDs to form a CD-based polymer is schematically represented in Scheme 1.6. Materials of the type shown in Scheme 1.6 are amorphous in nature and their properties vary according to the nature of the cross-linker molecule (i.e., epichlorohydrin, diisocyanates, di-acid chlorides, etc.). Such polymeric materials are useful as adsorbents for the removal of organic pollutants, such as PFCs and PNP, especially when the inclusion properties of the CD cavity are retained. Adsorption onto the linker domains (non-inclusion or interstitial sites; *cf.* Scheme 1.6) is possible. Therefore, these materials can be classified as both cavitands and clathrands (*cf.* Fig. 1.1a,b).



Scheme 1.6 Association of a CD (cone) and a bi-functional reagent (e.g., a diisocyanate urethane linker; wavy lines) to form linear (top) or branched (bottom) urethane based copolymer materials, where guest (spheres) can bind in the inclusion sites or within the interstitial regions.

A major strategy in the design of CD-based copolymer materials shown in Scheme 1.6 involves controlling the surface area and pore structure properties of the copolymer frameworks by controlling the composition and size of the cross-linker, in agreement with

studies of solid phase extraction (SPE) materials.⁵⁵ The positive correlation between sorption capacity and increasing surface area and pore structure properties have been concluded from a previous research reported elsewhere.⁵⁶ However, the precise molecular details of the sorption process in polymeric CD materials is poorly understood. In the case of PFCs, there is a need to address knowledge gaps with regard to their structure with both native and polymeric CDs in order to develop improved sorbent materials with tunable sorption properties.

In a study by Ma and Li,⁵² the synthesis of urethane-based β -CD materials was reported using hexamethylene diisocyanate (HDI) and toluene diisocyanate (TDI) linkers, respectively. These urethane-based CD polymers were reported to display very high binding affinity with PNP ($K = 10^8$ – 10^9), as compared with native β -CD ($K=10$ – 10^3). The determination of the binding constant (K) was obtained using UV-vis spectroscopy where the concentration of the residual (i.e. unbound) PNP was used to evaluate K. The underlying assumption in their model was that PNP was solely bound in the cavity of β -CD. In the case of polymeric β -CD, the binding constant relation simplifies because the activity of the poly-CD is unity and the value of K approximately equals to $[\text{PNP}]^{-1}$. The assumption that PNP is strictly bound within the cavity of CD is problematic since potential sorption occurs at interstitial sites within the polymeric framework (*cf.* Scheme 1.6) as shown by Mohamed et al.⁵⁶ Furthermore, the method used to evaluate K by Ma and Li was oversimplified since the total number of sorption sites for PNP were underestimated. Therefore, accurate measurement of K values requires a better understanding of the nature of the binding sites involved in the adsorption process.

1.2.5 The structure of Host-Guest inclusion complexes

The structure of host-guest inclusion compounds can be probed using several techniques. Job's method, also known as continuous variation method, was one of the first methods used for the determination of the stoichiometry of inclusion complexes.⁵⁷ The continuous variation method was used in conjunction with NMR^{58,59} and UV-vis⁶⁰ spectroscopy. Other techniques such as elemental analyses⁶¹⁻⁶³ and calorimetric⁶⁴ methods in solution have been used to provide information regarding the stoichiometry of host-guest systems. Acid-base titration methods can be used to evaluate the stoichiometry of host-guest systems involving acidic guests (e.g., PFOA).⁶⁵

Spectroscopic methods (NMR, FT-IR, and Raman) are important in probing the structure and motional dynamics of the host/guest, solvation properties and the presence of specific interactions e.g., hydrogen bonding interactions. In particular, multinuclear NMR spectroscopy with magic angle spinning (MAS) and cross polarization (CP) techniques have recently been used to provide unequivocal evidence for the inclusion of a guest within the host for a variety of systems.⁶⁶⁻⁶⁸ Other techniques have been used to probe through-space intermolecular interactions for host-guest systems such as 2D NMR techniques (e.g., ROESY and NOESY; §1.5.7).

NMR relaxation techniques can be used to measure the dynamic properties of the host and guest as influenced by the internal rotations, dipolar interactions, and dynamics of the host/guest complex, as well as hydrogen bonding and solvation effects. Thermal analyses (DSC and TGA) can reveal the formation of stable inclusion complexes and their hydration properties, while X-ray diffraction techniques can provide information about the periodic structure and packing arrangement of the complexes in the solid state.

In the case of Poly-CD adsorbent materials, equilibrium sorption parameters extracted from isotherm studies can provide important information regarding the possible intermolecular interactions. However, detailed structural information of the complexes requires additional techniques such as NMR,⁶⁸⁻⁷¹ FT-IR and Raman spectroscopy,^{72,73} ITC,⁷⁴ PXRD, thermal analyses⁷⁵ and measurement of contact angles.⁷⁶

The importance of solvent in supramolecular chemistry has been mentioned (§1.1.4). In the solid state the solvent is often co-included as a guest within the crystalline lattice. Therefore hydrophobic repulsion effects between the guest and solvent are hindered. However, the dynamics and interaction of water with the host or guest are anticipated to affect the structure and stability of the host-guest system. The structure of an inclusion complex in solution can be challenging to establish since inclusion may occur in several ways (*cf.* Scheme 1.5); through the wide or the narrow rim, in an axial or equatorial position with respect to the cavity long axis.⁷⁷ Several techniques have been used to study the structure of host-guest complexes, where NMR spectroscopic techniques are possible in the solid and solution phases, as described above. For example, the presence of the asymmetric environment of the cavity can induce a dichroic signal even for the achiral guests (e.g., PNP). According to the Harata-Kodaka rules,⁷⁸ the positive and negative sign of the ICD band indicates the axial and

equatorial inclusion of the guest, respectively. Table 1.4 summarizes some of the structural parameters and the experimental techniques that can be used for these types of measurements. Some of the structural parameters and experimental techniques are discussed in greater detail in the following sections.

Table 1.4 Some Structural Parameters of Host-guest Complexes and the Techniques of Measurement.

Parameter	Techniques of measurement	Description
Stoichiometry	Elemental analysis	C-H, C-F analyses
	NMR, UV-vis titration	Continuous variation
	Acid-base titration	Acidic guest (e.g. PFOA)
	ITC	Host-guest titration
Specific interactions	FT-IR and Raman spectroscopy	e.g. H-bonding or dimers
Thermal stability, hydration properties, purity	DSC and TGA	Melting, boiling, physical/phase transition.
Conformation, dynamics, solvation properties	$^1\text{H}/^{19}\text{F}$ NMR spectroscopy and Relaxation ($T_1/T_2/T_{1\rho}$) NMR	CIS effects, chain conformation, rotational/motional dynamics
Through-space interactions	2-D (ROESY, NOESY), CP/MAS NMR techniques	Spatial/dipolar interaction (Guest inclusion)
Packing arrangement, hydration properties	Powder X-ray diffraction	Channel, cage, and layer-type structures, crystalline structure.
Equilibrium binding constants	ITC	(Host-guest titrations):
	NMR spectroscopy	Thermodynamic parameters
Host-guest interaction	NMR, DSC/TGA, FT-IR, PXRD	

1.2.5.1 Packing Arrangements of Cyclodextrins in Host-Guest Systems

Single crystal X-ray diffraction is an unequivocal method for determining the structures of single crystals CD inclusion complexes and provides an understanding of the mode of inclusion, the nature of the host-guest interactions, and the role of solvent. In cases where good quality single crystal cannot be obtained (e.g., CD/PFCs complexes), powder X-ray diffraction (PXRD) is an alternative method for the identification and characterization of host-guest complexes.^{61,79} This is because it is not always possible to produce single crystals of adequate quality for X-ray analysis and PXRD is amenable to such amorphous materials with limited crystalline behavior. Qualitative analysis of PXRD results involves a comparison of the diffraction patterns of the host, guest, and the complex, relative to its physical mixtures. Other than providing evidence for the formation of unique host-guest complexes, PXRD can be used to characterize the packing arrangements of the CD inclusion complexes.

In a review of CD inclusion complexes,^{79,80} the solid state packing arrangement was generally classified into three broad categories; channel, cage and layered structures. Further divisions are observed for CDs depending on the relative orientation of the primary and secondary faces (*cf.* Figure 1.2) but are not of immediate interest to the present work. The three types of packing arrangements described above are determined by the orientation of the CD and the connectivity between one cavity and the next. *Cage-type* structures are observed when the guest molecule is small enough to be enclosed fully within the cavity (e.g., Scheme 1.5a). In fact, the CD macromolecule attains such a packing arrangement in its native form due to the random arrangement of the molecules.⁶¹ The *cage-type* structure results in a “herring-bone” arrangement of CD molecules and are common for α -CD. Such structures have been reported for complexes with short chain fatty acids such as acetic, propionic and butyric acids.⁸¹ There is no evidence that γ -CD forms *cage-type* compounds due to its large cavity size (*cf.* Table 1.2).

Channel-type structures can be formed by all three types of CDs with large guest molecules. A rearrangement from the *cage-type* to the *channel-type* structures occurs when the guest molecule is so large that it protrudes on both sides of the cavity (e.g., Scheme 1.5b). In the *channel-type* arrangement, the CD cavities are lined up in order to produce an extended hydrophobic channel into which guests can thread through in a similar fashion as beads through a string, as illustrated by rotaxane systems (*cf.* Scheme 1.3). Such structures are

observed for the α -CD complex of the pH indicator dye, methyl orange, where the guest spans three CD cavities.² *Channel-type* compounds are also known for β -CD complexes with long and medium chain PFCs⁶¹ and other systems.^{32,37,49,71,82,83} The formation of *channel-type* structures is further classified as either “head-to-head” or “head-to-tail” depending on the orientations of the neighboring CD molecules. β -CD is reported to have a strong tendency to form “head-to-head” dimers that are held together by multiple hydrogen bonds at the secondary rims, where at least one guest molecule can be accommodated.⁸⁰

The *layer-type* packing structure is generally associated with large guest molecules and has been reported for α -CD/*p*-bromophenol⁸⁴ and β -CD/cinnamoyl⁸⁵ complexes. In this type of structure the CD molecules pack in layers with their macrocyclic ring planes in parallel orientation, with alternate layers shifted to produce a ‘*brick-in-a-wall*’ pattern. The three possible packing modes are illustrated in Figure 1.3.

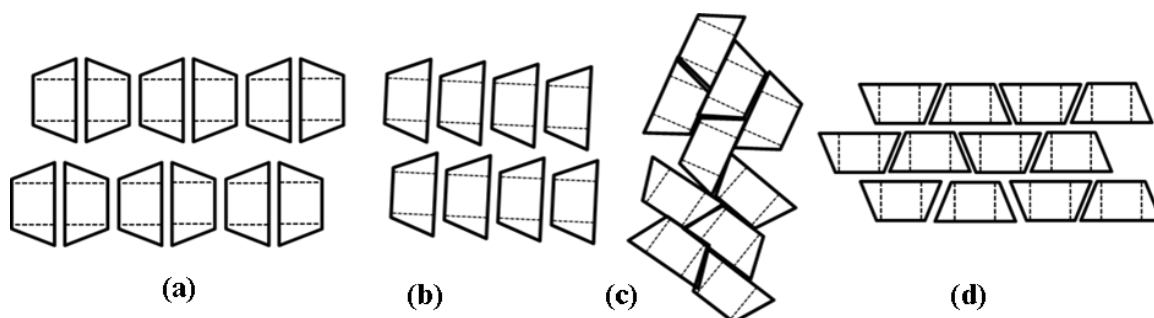


Figure 1.3 Schematic representation of the packing of cyclodextrin structure showing (a) head-to-head channel type, (b) head-to-tail channel type, (c) cage-type, and (d) layer-type structures. Adapted from ref. 80.

1.2.5.2 Conformation of the Guest Molecule

As mentioned earlier, conformation change of a guest may occur upon induced fit binding with a host. There are several classifications of isomeric conformers but only three; *ortho*-, *gauche*-, and *anti*-conformers, are discussed here with special reference to PFCs. The complexity of the subject of torsional energetics of perfluoroalkanes has been noted by many researchers and that particular topic is beyond the scope of this work. However, a brief and general description of the conformations of PFCs is presented here. The presence of three conformational energy minima for the C-C-C-C torsional profile of perfluoroalkanes is well established using n -C₄F₁₀ as the model compound.⁸⁶ The determination of the three conformers for fluorobutane were based on *ab initio* calculations⁸⁷⁻⁹² and N₂ matrix-isolation

Raman spectroscopy.⁸⁷⁻⁸⁹ Among the three conformers, the *gauche* and *anti* are most common for PFCs and are widely reported in the literature.^{61,93} For a simple four-carbon organic molecule of the type $AX_3AX_2AX_2AX_3$, the *gauche*- and *anti*-conformers can be viewed using the Newman projection as shown in Figure 1.4.

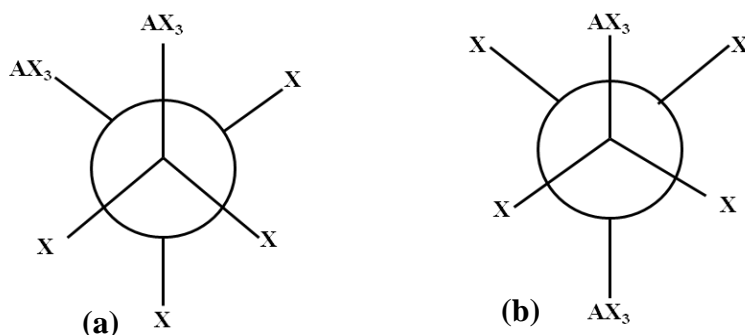


Figure 1.4 The Newman projection for the (a) *gauche*-, and (b) *anti*-conformers of a simple four carbon system.

In general, the *gauche*-conformers ($g+$, $g-$) have CCCC dihedral angles ca. $\pm 60^\circ$, the *ortho*- ($o+$, $o-$) ca. ± 90 and -90 , and the *anti*-conformers ($+a$, $-a$) have dihedral angles ca. 180° . Figure 1.5 below shows the *gauche*- and *anti*-conformers of PFOA.

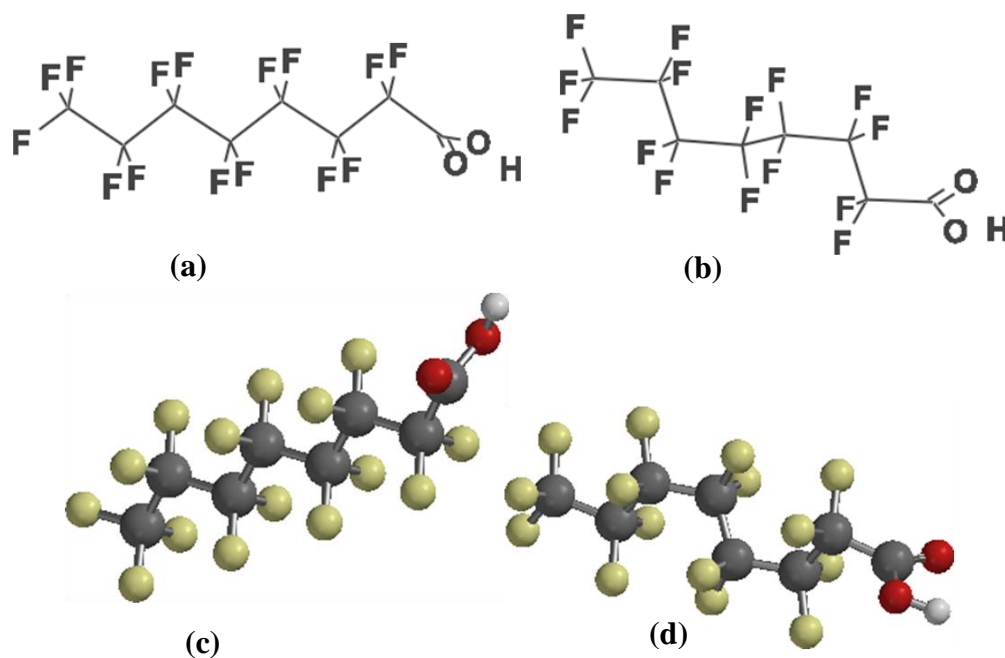


Figure 1.5 The molecular structure of PFOA displaying the *gauche*- (b and d) and *anti*-conformations (a and c) of the perfluorocarbon chain. Figures c and d represent the ball and stick structures of PFOA generated using Spartan '08 V1.2.0.

1.3 Perfluorinated compounds (PFCs)

1.3.1 Perfluorinated Compounds (PFCs): An Overview.

Perfluorinated compounds (PFCs) are a series of fluorine-containing chemicals that represent a growing list of persistent organic pollutants (POPs) accumulating in Canadian and global environments.^{94,95} PFCs have the general formula $\text{CF}_3\text{-(CF}_2\text{)}_n\text{-R}'$ and can be divided into the groups of sulfonic ($\text{R}' = \text{CF}_2\text{-SO}_3\text{H}$) and carboxylic ($\text{R}' = \text{COOH}$) acids, fluorotelomer alcohols ($\text{R} = \text{CF}_2\text{-OH}$), and perfluoroalkanamides ($\text{R} = \text{CONH}_2$). PFC chemicals that are of interest in this research work are PFOA ($\text{CF}_3\text{-(CF}_2\text{)}_6\text{-COOH}$), PFOS ($\text{CF}_3\text{(CF}_2\text{)}_7\text{-SO}_3\text{H}$), PFBA ($\text{CF}_3\text{(CF}_2\text{)}_2\text{-COOH}$) and SPFO ($\text{CF}_3\text{(CF}_2\text{)}_6\text{COO}^-\text{Na}^+$). These PFCs were selected to represent a carboxylic acid (PFOA) and its conjugate base (SPFO); long/medium (C8) and short chain (C4) PFCs; including PFCs with variable head groups (i.e., a carboxylate vs sulfonate head group). Within the class of PFC chemicals, PFOA and PFOS have received considerable attention because of their persistence in the environment, and their bioaccumulative and toxic properties.⁹⁶ These compounds are considered as useful reference materials, particularly from a toxicological standpoint. Perfluoroalkyl carboxylates and sulfonates are amphiphilic because they consist of a PFC alkyl chain that is both hydrophobic and oleophobic, while the anion group is hydrophilic in nature.^{96,97} The combination of hydrophobic and oleophobic character makes these substances useful as surfactants. The molecular structures of some representative PFCs are presented in Figure 1.6.

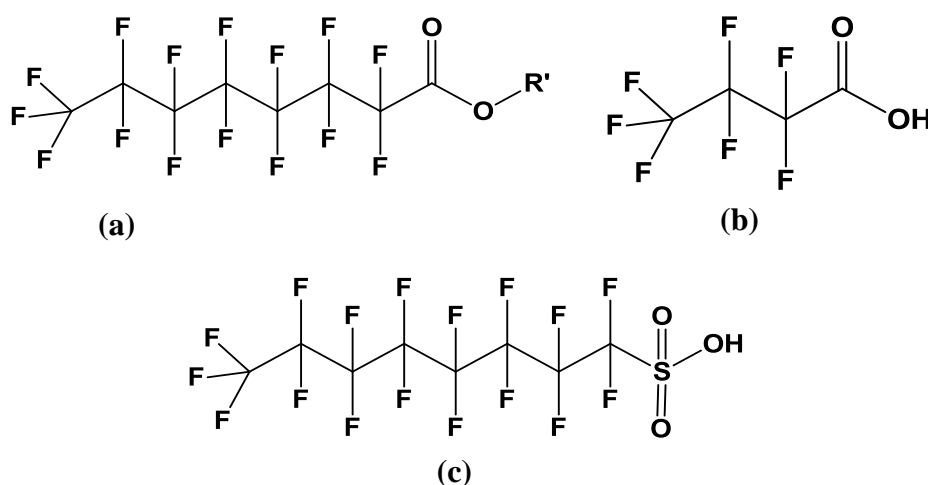


Figure 1.6 The molecular structures of (a) PFOA/SPFO, where $\text{R}' = \text{H}^+/\text{Na}^+$, (b) PFBA, and (c) PFOS

Perfluorinated surfactants have been synthesized by electrochemical fluorination (ECF) or telomerisation. Detailed procedures for the production of PFCs are reported elsewhere.⁹⁶⁻⁹⁸ Commercial production of PFOA and PFOS in the Americas is mostly based on ECF; whereas, telomerization process is used for the production of perfluoroalkyl carboxylates and fluorotelomer alcohols (FTOHs). Perfluorooctanesulfonyl fluoride (POSF)-based polymers and the volatile FTOHs can degrade to PFOS and PFOA, respectively.

1.3.2 Physicochemical Properties and Uses of PFCs

In general, PFCs of the type described above possess unique physicochemical properties, as compared with their hydrocarbon analogues. They are generally apolar, have relatively good solubility, low volatility and are very stable under extreme conditions. The presence of C-F bonds makes these compounds resistant to hydrolysis, photolysis, microbial degradation and metabolism.^{97,99} They generally have low vapor pressures (e.g., ~10 mmHg for PFOA at 25 °C)¹⁰⁰ and exhibit long residence times in the environment. They are very surface active and can therefore effectively lower the surface tension of aqueous and other solvent systems, even at low concentrations, by selective adsorption at the air/solvent interface. The relatively high surface activity of PFCs confers their application as high performance surfactants, emulsifiers, formulations for firefighting foams and cosmetics, and surface coatings for metals and paper.

The distribution of PFCs in water, air, and sediment depends on their physicochemical properties.¹⁰¹ Therefore, the propensity of these compounds to adsorb onto solid surfaces varies according to differences in various properties such as pK_a , solubility, and vapour pressure (*cf.* Table 1.5). In general, PFOA and PFOS have relatively high water solubility and therefore tend to stay in the aqueous phase but are also known to strongly bind to particles present in the atmosphere. The higher concentrations of PFBA in landfill leachates reported by Foen et al.¹⁰² are attributed to its greater water solubility and reduced propensity to adsorb onto solid materials. The short-chain PFCs (C₄) are often exclusively detected in dissolved solution phase; whereas, long-chain PFCs (C_{≥8}) are strongly adsorbed onto particulates. Some of the physicochemical properties for PFOA, SPFO, and PFBA are listed in Table 1.5 and are compared to those of octanoic acid (OA).

Table 1.5 Physicochemical properties of some perfluorinated compounds and octanoic acid.¹⁰³⁻¹⁰⁷

Physicochemical Properties	Alkyl/Perfluoroalkyl compounds			
	PFOA	PFOS	PFBA	OA
Molecular formula	C ₈ HF ₁₅ O ₂	C ₈ HF ₁₇ O ₃ S	C ₄ HF ₇ O ₂	C ₈ H ₁₆ O ₂
Molecular weight (g/mol)	414	500	235	144
Chain length (Å)(*Spartan)	~12	~13	~7	~11
Physical state (25°C)	Solid	Solid	Liquid	Liquid
Solubility (g/L, 25°C)	340	520	High	0.16
Melting point (°C)	45-55	>400	-17.5	16.7
Boiling point (°C)	189-192	133	120	240
Vapor pressure (mmHg)	4.1-10	~0	10	0.25
pK_a	2.5	<0	0.08–0.4	4.8
cmc (mM)	8.7-10.5	8.0	No data	No data

1.3.3 Sources and Environmental Concentrations of PFCs

In general, PFCs with 4–10 carbons were reported to be the dominant species detected in landfill leachates in the Americas and globally.¹⁰² PFOA, PFOS, and other PFCs are commonly found in soil, sediments, and aquatic environments because of their ability to infiltrate groundwater to varying extents. In particular, PFOA and PFOS do not occur naturally, but are mostly available in the environment as synthetic chemicals or as degradation products of volatile precursors.^{108,109} These chemicals have been reported to enter the environment directly during their production.^{110,111} Due to their low pK_a values (*cf.* Table 1.5), PFOA and PFOS are often present in solution in their anionic form at ambient environmental conditions. Environmental contamination by PFCs was reported due to the direct discharge of industrial waste, such as aqueous firefighting foams¹¹⁰⁻¹¹³ and wastewater effluents from water

treatment plants.¹¹⁴⁻¹¹⁷ Consumption of contaminated foods and inhalation of air laden with volatile PFCs (e.g., perfluorinated alcohols and esters) that may be further degraded to PFOA or PFOS are other potential ingestion pathways.¹¹⁷⁻¹²⁰

Based on the above mentioned activities, human beings are exposed to PFCs on a daily basis via a number of different pathways; e.g. pre- and post-natal exposures, drinking water, contaminated food, inhalation of contaminated dust, and occupational exposure.¹²¹ Detectable PFC levels vary from a few ng/L to several µg/L, depending on the matrix and the related activities (*cf.* Table 1.6). For example, studies from Canada, the USA, Germany, Denmark, and Japan reported elevated levels of PFOS and PFOA (3–17 µg/L) in the cord blood of humans.¹²¹⁻¹²⁴ Similar studies reported average PFOS and PFOA concentrations of ~0.04–0.40µg/L in human breast milk samples.^{125,126}

**Table 1.6 PFOA and PFOS Levels (µg/L) in Some Aquatic samples:
*-After Fire-fighting Activity, na - Not Analyzed.⁹⁸**

Matrix	Location	PFOA	PFOS
Tap water	Osaka and Tohoku area, Japan	0.040	0.012
	Ruhr, Germany	0.519	0.022
Ground water*	Air Force Base, Michigan, USA	105	110
River water	Kyoto area, Japan	0.110	0.010
	Pearl and Yangtze River, China	0.260	0.099
	Oder, Vistula, Poland	0.0038	Na
Lake water	Canadian Arctic	0.016	0.090
Waste water	WWTP, Kentucky, USA	0.334	0.993
	WWTPs, New York, USA	1.050	0.068

The environmental concentrations of PFOA and PFOS for several matrices (e.g., atmosphere, land, water, and living organisms) are well documented by Becker in her thesis

report.⁹⁸ Table 1.6 lists some of the PFOA and PFOS levels in aquatic samples, including waste water treatment plants (WWTPs).

1.3.4 Toxicity of PFCs

As we have seen previously, human beings are exposed to PFCs on a daily basis via a number of different pathways. However, most of the toxicological studies have been carried out in rats and other small animals, and it is uncertain whether the effects observed in animals may occur in humans. A wide range of toxicological studies have been carried out for PFOA and PFOS over the past decade. While PFOS and PFOA have been extensively studied, other PFCs including replacement chemicals such as perfluorobutanesulfonate (PFBS) and PFBA, have not been well characterized. Despite the relative lack of data available on these other PFCs, it has been assumed that they will display similar toxicology to PFOS or PFOA.

PFOA and PFOS are essentially nonvolatile and exposure is most likely via the oral route in contaminated food or water. They are well absorbed orally and are very slowly eliminated from the body in humans with a half-life of approximately nine and four years,¹⁰³ respectively. Animal data suggest that they have moderate acute oral toxicity with major effects on the gastrointestinal tract and the liver. Other risks associated with exposure to PFOA and PFOS include suppression of immunity and effects on developmental and reproductive organs.¹²⁷⁻¹³⁴ Reports have associated PFOA and PFOS with increased incidents of aborted pregnancies in animals.¹³⁵⁻¹³⁷ Several studies have shown both PFOA and PFOS to induce tumors in animals at relatively high doses.^{132,137-139} In other reports, high levels of serum POPs, mainly made up of PFCs, were suggested to be the cause of breast cancer risks among the Inuit population of Greenland and Canada.¹⁴⁰

Following reports of the global distribution and toxicity of PFOA and PFOS, several organizations and city councils have acted towards addressing the associated health and environmental concerns. For example, in 2000, 3M which is the largest producer of PFOS-related substances announced its intention to phase out production of such compounds by reformulating its entire range of “Scotch” brand products with chemistry based on the short chain PFBS, that is reported to be less bioaccumulative than PFOS. In addition to US-EPA and other health organization (e.g., UK-HPA) issuing ‘provisional health advisories’ for the acceptable levels of PFOS and PFOA for short term exposure, several city councils have

recently established drinking water guidelines for these chemicals. Table 1.7 presents some of the guidelines showing acceptable levels of PFOS and PFOA in drinking water.¹⁴¹

Table 1.7 PFOA and PFOS Safe Levels for Various Organizations and Governments.¹⁴¹ N/A; Not Applicable.

State/organization	PFOA (µg/L)	PFOS (µg/L)
US-EPA	0.2	0.4
UK-HPA	0.3	10
Canada	0.3	0.7
Minnesota	0.3	0.2
North Carolina	2	N/A
New Jersey	0.04	N/A
Germany	0.1 (sum of PFOA and PFOS)	

1.3.5 Perfluorinated Compounds as Guest Molecules: Their Challenges

The challenges associated with obtaining good quality crystals of inclusion complexes with β -CD have generally precluded detailed X-ray studies of PFCs in the solid state. The structure and distribution pathways of these surface active compounds are poorly understood because of their amphiphilic behaviour and non-ideal mixing behaviour with hydrocarbon materials. The solution and colloidal behavior of surface-active agents may be attenuated by their complexation with host compounds such as CDs, where NMR techniques both in the solution and solid phases offer possibilities to the study of the short-range order of such complexes.

A limitation to the study of low melting compounds such as PFOA (*cf.* Table 1.5) presents another challenge for solids NMR studies under MAS NMR conditions. This is because compounds with low melting points can cause rotor instability and damage to the NMR probe when spun at frequencies as low as 8 kHz or for longer periods due to the heat generated through fast spinning. The study of SPFO reported herein (chapter 5) enables its structural investigation as a model PFC in its unbound state. The structural and dynamic

information obtained from SPFO is expected to shed light into the structure of PFCs in their native states of such perfluorocarbon chains.

Numerous studies have reported the inclusion complexes involving CDs and PFCs in the solution phase. Reinsborough et al.¹⁴² and Guo et al.⁹³ were among the first groups to study CD/PFCs inclusion complexes using such techniques as conductometry and NMR spectroscopy, respectively. In particular, Guo et al. studied the association of α -, β -, and γ -CDs with C4-C9 sodium perfluoroalkyl salts using ¹⁹F NMR spectroscopy in solution. As well, Druliner and Wasserman¹⁴³ examined the interaction of α - and β -CD with unsubstituted acyclic and cyclic perfluoroalkanes in solution. The association of the various fluorocarbon surfactants with α -CD inclusion was found to be fairly weak because the size of the cavity is too small (*cf.* Table 1.2) to accommodate the guests. In contrast, the cavity size of β -CD is large enough to accommodate PFCs up to 8 carbons long in a 1:1 or 2:1 host/guest stoichiometry. In the case of γ -CD, favourable binding at the 1:1 and 1:2 (host/guest) mole ratios is anticipated for longer chain PFCs. Favourable association of PFC guests with β -CD in solution is controlled by the *size-fit* complementarity of the host and guest,¹⁴² as well as an induced fit via a conformation change of the guest. For instance, in the 1:1 and 2:1 β -CD/PFOA complexes, the perfluorocarbon guest may adopt the coiled (*gauche* or helical) and extended (*trans* or zigzag) conformations, respectively, in order to adopt the cavity dimensions of the host (*cf.* Table 1.2 and 1.5 and Fig. 1.5).

Among the three types of CDs, β -CD was chosen for this study due to its *size-fit* complementarity with the PFC guests (i.e., PFOA, SPFO, PFBA, and PFOS). In fact, complexes of β -CD/perfluoroalkyl carboxylates with variable chain length were concluded to form stable inclusion complexes in aqueous solution, according to ¹⁹F/¹H NMR spectroscopy,^{26,94,144} viscometry,¹⁴⁴ conductometry,^{142,145,146} and sound velocity¹⁴⁷ in aqueous solutions. In particular, β -CD and SPFO form more stable 1:1 and 2:1 host/guest complexes in solution.

There are relatively few examples of the formation of solid-state inclusion complexes between β -CD and PFC guests (e.g., PFOA) in the literature, relative to studies in aqueous solution. In fact, no studies have reported the inclusion complexes of β -CD and SPFO in the solid state. Tatsuno and Ando⁶¹ have examined the solid inclusion complexes of β -CD with C₉F₂₀ and C₂₀F₄₂ using solid state NMR, where 2:1 and 4:1 host-guest complexes were

reported, respectively. However, several other studies have examined modified PFCs¹⁴³ and semi-fluorinated polymers^{148,149} in the solid state. Recently, Koito et al.⁶⁶ studied inclusion complexes of β -CD and hydrofluoroether using solid state NMR spectroscopy and wide-angle X-ray diffraction. Thus, solid-state structural studies of CD/PFC inclusion compounds remain largely unexplored. This knowledge gap contributes to a limited understanding of the structure and dynamics properties of PFCs and their complexes. In contrast, single-crystal XRD studies of β -CD/hydrocarbon carboxylic acids have been reported.¹⁵⁰⁻¹⁵² Single-crystal XRD studies of CD complexes can provide rich structural information regarding the spatial orientation of the guest within the host, including the role of solvation properties in governing the structure and stability of the complex.^{151,152} In the absence of single crystal X-ray data, solid-state NMR spectroscopy provides the opportunity to obtain detailed structural information of such amorphous and crystalline host/guest materials.¹⁵³

1.3.6 Other Organic Guest Compounds

Phenolate guests, particularly PNP (*cf.* Figure 1.7a), represent commonly used model compounds of aromatic environmental pollutants owing to their structural relevance to pharmaceuticals, explosives, dyes and agrochemicals.¹⁵⁴

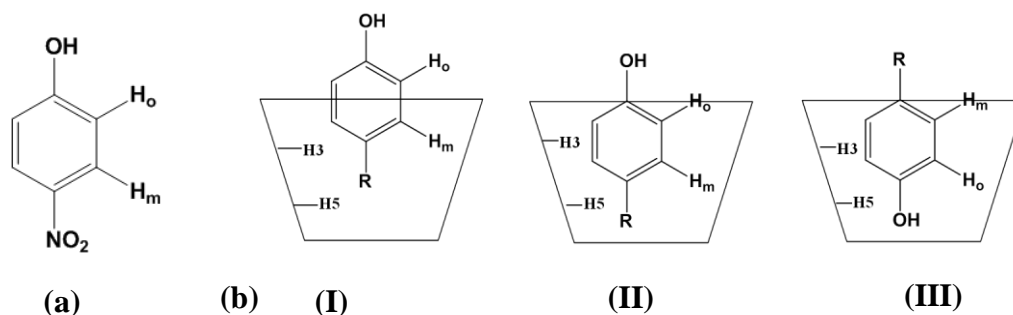


Figure 1.7 (a) Molecular structure of *p*-nitrophenol, and (b) three different inclusion modes of the phenolate guests within the cavity of a CD host as determined from intermolecular NOE spatial interactions.¹⁵⁵

PNP is a simple model guest for studying β -CD and its related copolymers because its complexes are amenable for study by using NMR¹⁵⁵ and UV-vis¹⁵⁶ spectroscopy, calorimetry,¹⁵⁷ electrospray ionization mass spectrometry¹⁵⁸ and X-ray crystallography.¹⁵⁹ Of

paramount importance to the study of CD/PNP complexes is the use of Nuclear Overhauser Effect (NOE) (*cf.* §1.5.7) NMR techniques in solution. Two-dimensional NMR methods such as NOESY and ROESY are useful in structural studies of through-space interactions between the guest and the host. More importantly, intermolecular NOEs provide information about the spatial interactions and inclusion modes of host/guest complexes. For example, Figure 1.7b illustrates a typical NOE application for phenolates with α -CD complexes, which may occur in three possible inclusion modes (I-III).¹⁵⁷ The 2D-ROESY spectrum of *p*-iodophenolate with α -CD showed the inclusion mode I.¹⁶⁰ The 2-D ROESY spectrum of β -CD/PNP is reported in greater detail in this study (§Chapter 6). The use of PNP in this work as a model guest for β -CD and its copolymers was based on the utility of various methods wherein studied in solution. Moreover, Ma and Li⁵² used PNP and their results provide a comparison for the binding affinity studies of urethane-based copolymers. The binding properties of the copolymers toward PNP constitute one of the research hypotheses for this work (*cf.* §1.7).

1.4 Methods for Removing PFCs from the Environment

Since most PFCs are resistant to hydrolysis, photolysis, microbial degradation and metabolism, these compounds are not amenable to conventional chemical or biological degradation methods. Alternative approaches for the removal of PFCs such as ultrasonic¹⁶¹ and UV irradiation¹⁶² are limited due to their demanding capital cost and time requirements. Adsorption with activated carbon¹⁶³⁻¹⁶⁷ offers a general utility, technical simplicity, and relatively low cost for the removal of such pollutants. Other carbonaceous materials (e.g., carbon nanotubes; CNTs)^{168,169} were recently evaluated as potential adsorbent materials for the removal of PFCs and HC surfactants from aqueous environment. However, carbonaceous materials were generally found to have limited uptake of PFCs due to their inert character and relative immiscibility of PFCs with HC adsorbent materials.^{170,171}

We hypothesized in this work that *improved molecular recognition of target substrates (e.g., PFOA) is possible using synthetically engineered adsorbent materials possessing macromolecular units (e.g., β -CD) within a copolymer framework (cf. Scheme 1.6)*. The incorporation of macromolecular porogens within copolymer frameworks is a *bottom-up* strategy which offers the possibility of tuning the physicochemical properties of the adsorbent by controlling the reagent ratios and reaction conditions. There are comparatively few studies

reported for the sorptive removal of PFCs using copolymer adsorbent materials. Most of these studies have reported the selective removal of PFOS from aqueous solution using molecularly imprinted polymers (MIPs) where PFOA and PFOS were used as molecular templates.^{172,173} In contrast, a number of reports have described the sorption of PFCs onto commercially available resins.^{174,175} The use of polymeric adsorbent materials (*cf.* Scheme 1.6) offers a potential strategy for the sorptive removal of PFCs with tunable properties such as ease of regeneration, high sorption capacity, and shorter equilibration times. We describe in this section some aspects of sorption phenomena that are necessary for understanding the thermodynamics of heterogeneous adsorption of organic molecules onto the surface of solid materials.

1.4.1 Adsorption Phenomena

Adsorption is the accumulation of molecules (the *adsorbate*) on a surface of the *adsorbent* in contact with air or a water phase. It is important to distinguish between the terms “adsorption” and “absorption”. While adsorption is the accumulation of molecules onto the surface of a solid adsorbent material, absorption is the partitioning of molecules within the inner structure (across the interface) of the adsorbent. Since both adsorption and absorption may occur simultaneously, the term *sorption* is often used to describe a combination of both processes. Therefore, the terms sorption and adsorption will be used interchangeably in the course of this thesis. Similarly, the terms sorbate/adsorbate and sorbent/adsorbent will be used interchangeably.

Adsorption processes can be categorized into two types; (1) Physisorption and (2) Chemisorption. *Physisorption* describes the non-covalent interaction between the adsorbate and the adsorbent through such forces as van der Waals interactions, surface charge interaction (i.e., electrostatic forces), dipolar (e.g., hydrogen bonding), and CH- π or π - π interactions. *Chemisorption* involves covalent bonding interactions between the adsorbate and adsorbent.

The interaction of the adsorbate with CD-based copolymer adsorbent involves one of the binding topologies described in Scheme 1.6, where multiple binding sites may be available as long as there are no steric effects. Non-covalent interactions are crucial in the binding process and for adsorptive applications. *The hypothesis considered here was related to understanding*

the structure and function of adsorbent-adsorbate systems, including nature and mode of interactions involved, and the role of the solvent (water) (cf. §1.6 - 1.7).

1.4.2 Adsorption Isotherms

Sorption phenomena are usually described using isotherms to provide a detailed understanding of the thermodynamic properties of the adsorbate/adsorbent system. Gas porosimetry measurements have been used to characterize the adsorption of gaseous species onto adsorbent materials.¹⁷⁶ Solid-gas isotherms have been used to classify adsorption profiles into six types. The adsorption profile of the gas at constant temperature is related to the adsorbent pore size and surface characteristics. Four common isotherms (types I–IV) are shown in Figure 1.8 and are discussed briefly herein. The other types of isotherms (not shown) have been described in detail elsewhere.¹⁷⁷

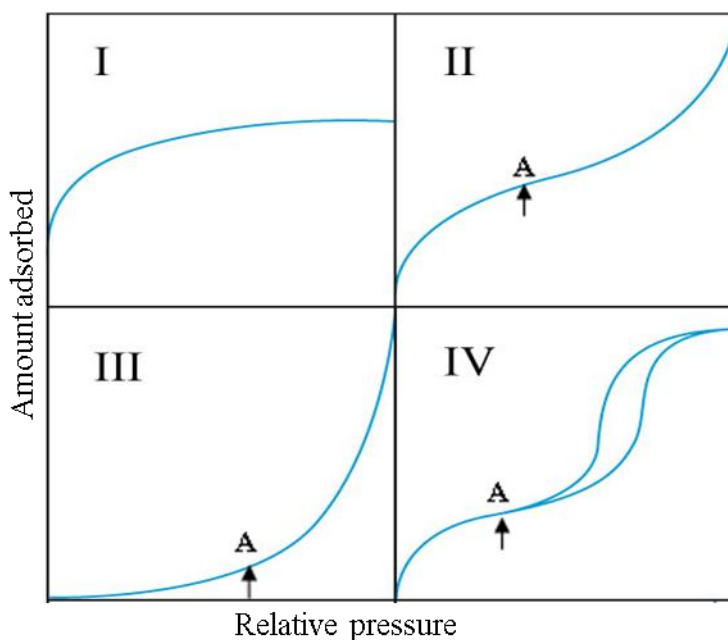


Figure 1.8 Types of adsorption isotherms. Point A represents the regions where monolayer coverage is complete.

The type I isotherm represents sorption behavior of micro-porous solids whose pore size does not exceed a few molecular diameters (typical pore width ≤ 2 nm) of the adsorbate. This type of isotherm depicts monolayer sorption that is well described by the Langmuir isotherm (§1.4.3). Physical adsorption for this type of isotherm involves adsorption within the micro-

pores. Upon saturation of these sites, no further adsorption occurs. Materials which exhibit type I isotherms include GAC and zeolites.

The type II isotherms are encountered when adsorption occurs on non-porous or macroporous materials (pore widths >50 nm). Type II behaviour involves multilayer adsorption which occurs after subsequent adsorption onto the first adsorbed monolayer after point A (*cf.* Figure 1.8).

Type III isotherm describes multilayer sorption which occurs in non-porous adsorbents with characteristic weak adsorbent-adsorbate interaction. As adsorption proceeds, further cooperative adsorption is facilitated because the adsorbate interaction with an adsorbed layer is greater than the interaction with the adsorbent surface.

Type IV isotherm is typical for meso-porous adsorbents (pore widths ~2–50 nm). It is a variation of type II, with a characteristic hysteresis loop. The hysteresis loop is associated with the secondary pore filling process of capillary condensation.

1.4.3 Equilibrium Isotherm Models

Many of the adsorption processes are described by one of the four adsorption isotherms above. The results of an adsorption process are usually expressed as a plot of equilibrium uptake of adsorbate species from aqueous solution by the adsorbent phase (Q_e ; mmol/g or mg/g) against the residual equilibrium concentration of unbound adsorbate species (C_e ; mmol/L or mg/L) as described by eqn 1.1. C_o refers to the initial adsorbate concentration prior to sorption, m is the mass (g) of adsorbent, and V is the volume (L) of the solution.

$$Q_e = \frac{C_o - C_e \times V}{m} \quad \text{Equation 1.1}$$

Sorption isotherms are analyzed using appropriate isotherm models to simulate the observed sorption behavior. The physical parameters obtained from fitting sorption isotherm data to an appropriate model provides insight about the thermodynamics of the adsorption process, including the sorption capacity and the affinity of the adsorbent.¹⁷⁸ Two sorption models (Sips and Brunauer-Emmett-Teller (B.E.T)) were considered in this work and are described along with the Langmuir and Freundlich models.

1.4.3.1 Langmuir Isotherm

In its formulation, the Langmuir isotherm¹⁷⁹ involves three assumptions; (1) monolayer adsorption occurs onto the adsorbent surface, (2) adsorption can only occur at equivalent adsorption sites, and (3) there is no lateral interaction or steric hindrance between adsorbed molecules, even at adjacent sites. Therefore, the model assumes homogeneous adsorption where all sites have equal affinity for the adsorbate with no lateral migration of the adsorbate in the plane of the surface. Since CD-based copolymers potentially contain two binding sites (*cf.* Scheme 1.6) with variable adsorption enthalpies, this model is not valid for such multi-site adsorption. The Langmuir isotherm model (eqn 1.2) is graphically represented and similar to the type I isotherm in Figure 1.8. Q_m is the monolayer surface coverage of the adsorbate on the surface and K_L is the equilibrium adsorption constant for the adsorbent/adsorbate system.

$$Q_e = \frac{K_L Q_m C_e}{1 + K_L C_e} \quad \text{Equation 1.2}$$

1.4.3.2 Freundlich Isotherm model

The Freundlich isotherm¹⁸⁰ (eqn 1.3) is the earliest known model which describes the non-ideal and reversible adsorption, not restricted to the formation of monolayer. This empirical model assumes heterogeneous adsorption that also applies to multilayer adsorption, with non-uniform distribution of adsorption activation energies and affinities over the heterogeneous surface. Such a model would be appropriate for the CD copolymer/PFCs systems. However, the model is limited in its ability to accurately determine Q_m since the ratio of the adsorbate onto a given mass of adsorbent varies at different solution concentrations.

$$Q_e = K_F C_e^{1/n_f} \quad \text{Equation 1.3}$$

1.4.3.3 Sips Isotherm Model

The Sips isotherm model¹⁸¹ (eqn 1.4) combines features of the Langmuir and Freundlich models. K_s is the Sips equilibrium constant and n_s is a heterogeneity parameter. Values of n_s that deviate from unity infer that the adsorbent is heterogeneous; while values of $n_s = 1$ indicate a homogenous surface that resembles the Langmuir isotherm. In the limit where $(K_s C_e)^{n_s} \ll 1$, the model converges with the Freundlich model. The versatility and general applicability of this model lies in the ability to describe Langmuir and Freundlich behavior. In

general, the model reduces to Freundlich isotherm at low adsorbate concentrations, whereas, it predicts a monolayer adsorption profile characteristic of the Langmuir model at higher concentration. Therefore, the Sips model is useful for GAC/PFC systems and for β -CD based polymeric adsorbents/PFC systems for monolayer adsorption.

$$Q_e = \frac{Q_m (K_s C_e)^{n_s}}{1 + (K_s C_e)^{n_s}} \quad \text{Equation 1.4}$$

1.4.3.4 BET Isotherm Model

Brunauer–Emmett–Teller (BET) isotherm¹⁷⁶ (eqn 1.5) is widely used to describe multilayer adsorption systems as first derived by Stephen Brunauer, Paul Emmett and Edward Teller. It is the model of choice for most adsorption systems that involve PFC adsorbates due to their tendency to aggregate and form multilayers. The BET model involves an initial adsorbed layer which acts as a substrate for subsequent adsorption. The BET model describes adsorbate-adsorbent systems that involve cooperative adsorption as anticipated for most systems that involve PFCs as adsorbates. The parameters K_{BET} and C_s are the equilibrium adsorption constant and saturated concentration of the adsorbate, respectively. For surface active compounds such as PFOA and PFOS, C_s values are interpreted as or close to the cmc values.

$$Q_e = \frac{Q_m K_{BET} C_e}{(C_s - C_e) [1 + (K_{BET} - 1)(C_e / C_s)]} \quad \text{Equation 1.5}$$

1.5. NMR Spectroscopy of Host-Guest systems

1.5.1. NMR spectroscopy: An Overview

Nuclear Magnetic Resonance, commonly known as NMR, is a spectroscopic technique that measures the intrinsic magnetic properties of atomic nuclei in the presence of an external magnetic field. The concept of NMR was first demonstrated in 1946 in condensed matter simultaneously by two research groups; that of Felix Bloch and that of Edward Mills Purcell. Bloch and Purcell were jointly awarded the Nobel Prize for Physics in 1952 for their discovery. Since then the field of NMR has seen tremendous developments in both the instrumental and experimental aspects. Recent experimental advances have made the NMR

technique a method of choice for many solution and solid sample analyses. The development of two-dimensional NMR experiments during the 1970s signaled the start of a new era in NMR spectroscopy.

This overview begins by describing aspects of magnetic properties of nuclei as a prerequisite for understanding the basic theory of NMR spectroscopy. From there, more advanced NMR techniques will be explained. Attention will be confined mostly to ^1H , ^{19}F , and ^{13}C nuclei in our discussion. A detailed theory of NMR spectroscopy with reviews on quantum mechanics, which is beyond the scope of this work, is provided elsewhere.¹⁸²⁻¹⁸⁴

1.5.2 Matter, Spin and Magnetism

Matter is made up of atoms, which are made up of electrons and nuclei. The four important physical properties that define a nucleus include mass, electric charge, magnetism and spin. Nuclear magnetism and spin have almost no effect on the normal chemical and physical behavior of substances, but provide a wonderful tool for NMR.

NMR involves detailed manipulations of nuclear spins. A spinning object possesses a quantity called *angular momentum*, \mathbf{P} , which is quantized:

$$P = \sqrt{I(I+1)\hbar} \quad \text{Equation 1.6}$$

In eqn 1.6, $\hbar = h/2\pi$ (where h is Planck's constant = 6.6256×10^{-34} J.s) and I is the angular momentum quantum number or simply, the nuclear spin. Spin is a form of angular momentum; however, unlike angular momentum, spin is not produced by the rotation of a particle but rather it is an intrinsic property of nuclei, as described above. The overall spin quantum number I of the magnetic particle is determined by the number of neutrons and protons in the nucleus and is given by either a half-integer or a whole number as shown in Table 1.8.

The angular momentum \mathbf{P} has associated with it a *magnetic moment* $\boldsymbol{\mu}$, both of which are vector quantities and are proportional to each other:

$$\boldsymbol{\mu} = \gamma\mathbf{P} \quad \text{Equation 1.7}$$

The proportionality factor γ is the *gyromagnetic ratio* and is a property of each nuclide (i.e., each isotope of each element; cf. Table 1.8). The detection sensitivity of a nuclide in the NMR experiment depends on γ ; nuclides with a large value of γ (e.g., ^1H and ^{19}F) are said to

be sensitivity, while those with small γ (e.g., ^{13}C) are said to be insensitive. Also, nuclides with spin $I = 0$ (e.g., ^{12}C) have no nuclear magnetic moment (ref. to eqns 1.6 and 1.7, cf. Table 1.) and are NMR inactive or silent.

Table 1.8 Properties of Some Common NMR Spectroscopy Nuclides.¹⁸⁴

Nuclide	Spin I	Natural abundance (%)	Magnetic Moment μ_z/μ_M	Electric quadrupole moment (10^{-30}m^2)	Magnetogyric ratio γ ($10^7\text{ rad T}^{-1}\text{ s}^{-1}$)	NMR frequency (MHz; B_0 ; 2.3488 T)	Relative receptivity
^1H	$1/2$	99.9885	2.7928	-	26.7522	100	1.00
^2H	1	0.0115	0.8574	0.2860	4.1066	15.3506	9.65×10^{-3}
^{12}C	0	98.9	-	-	-	-	-
^{13}C	$1/2$	1.07	0.7024	-	6.7283	25.1450	1.59×10^{-2}
^{14}N	1	99.63	0.4038	2.044	1.9338	7.2263	1.01×10^{-3}
^{15}N	1/2	0.368	-0.2832	-	-2.7126	10.1348	1.04×10^{-3}
^{16}O	0	99.96	-	-	-	-	-
^{17}O	5/2	0.038	-1.8938	-2.558	-3.6281	13.5565	2.91×10^{-2}
^{19}F	$1/2$	100	2.6269	-	25.1815	94.0940	8.32×10^{-1}
^{23}Na	3/2	100	2.2177	10.4	7.0809	26.4519	9.27×10^{-2}
^{31}P	$1/2$	100	1.1316	-	10.8394	40.4807	6.65×10^{-2}

If a nucleus with angular momentum P and magnetic moment μ is placed in a static magnetic field B_0 , the angular momentum takes $2I+1$ possible orientations defined by $m = I, I-1, \dots, -I$. For a nucleus with $2I+1$ possible orientations, there are also $2I+1$ energy states known as the nuclear *Zeeman levels*. For ^1H and ^{13}C nuclei, both of which have $I = 1/2$, there are two energy levels in the magnetic field corresponding to the two m values $+1/2$ (spin up) and $-1/2$ (spin down) as shown in Figure 1.9. These energy states are not degenerate, i.e. the nuclear magnetic moments of the nuclei (e.g. ^1H) can align with B_0 in a manner that it either reinforces it (spin up) or opposes it (spin down). The energetically preferred orientation has the magnetic moment aligned parallel with the applied field. Thus, the lower energy orientations (spins) of spins- $1/2$ (e.g., ^1H and ^{19}F) and spins-1 (e.g., ^2H and ^{14}N) nuclei are $1/2$ and 1, respectively.

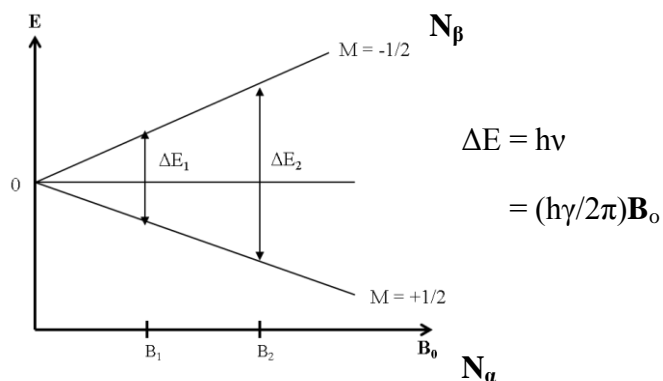


Figure 1.9 The energy difference ΔE between two adjacent energy levels for spin-1/2 nuclei as a function of the magnetic flux density B_0 .

In the absence of external fields at equilibrium, the energy states are degenerate and the spin angular momenta are isotropically (uniformly) distributed in all possible directions as depicted in Figure 1.10.

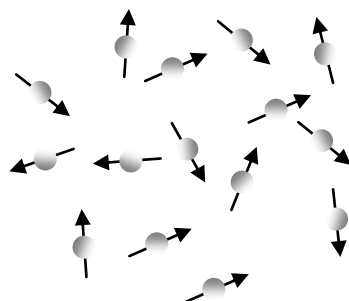


Figure 1.10 The orientations of the nuclear magnetic moments at equilibrium in the absence of external magnetic field are isotropically distributed.^{182,183}

Note that the rotational axis of the spinning nucleus cannot be oriented exactly parallel (or anti-parallel) with the direction of the applied field \mathbf{B}_0 , which is arbitrarily chosen to be the z -axis, but must precess about this field at an angle Θ as depicted in Figure 1.11. Thus, the magnetic moment μ experiences a torque perpendicular to its direction causing it to precess in a cone along the magnetic field direction with a frequency termed as the nuclear *Larmor frequency* (ω_o) described by eqn 1.8, where B^o is the magnetic field at the site of the particle.

$$\omega_o = -\gamma B^o \quad \text{Equation 1.8}$$

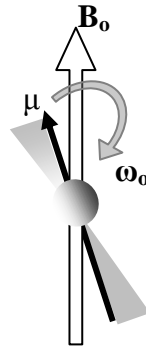


Figure 1.11 Precession of the spin magnetic moment in the presence of external field \mathbf{B}_0

1.5.3 Macroscopic Magnetization

As described above, the spin polarizations are isotropically distributed in the absence of an external magnetic field (\mathbf{B}_0). However, if a magnetic field is suddenly turned on, all nuclear spins begin to experience a Larmor precession around the field. On a macroscopic level, the sample in the presence of a magnetic field consists of an ensemble of magnetic moments with slightly different magnitude and direction. This is because small fluctuations in the fields due to the thermal motion of the environment cause a gradual breakdown of the constant angle cone precession (*cf.* Figure 1.11) of the nuclear spins. Over time, the magnetic moment of each nuclear spin moves between different ‘precession cones’ and eventually sampling the entire range of possible orientations.

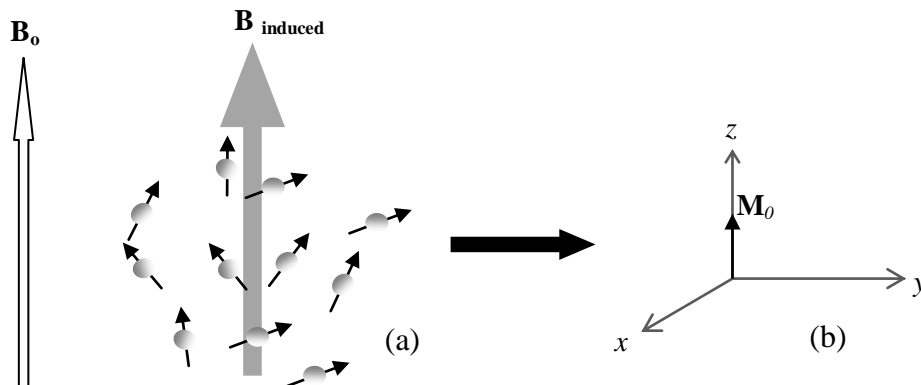


Figure 1.12 (a) A cluster of spins precessing at the Larmor frequency (ω_0) in the presence of external magnetic field \mathbf{B}_0 along the z -axis, and (b) the corresponding longitudinal magnetization vector.

The net distribution of spin orientations with magnetic moments along the field (z -axis) are more probable than orientations with magnetic moments opposed to the field as shown in Figure 1.12. This gives rise to a longitudinal *net* magnetization M_0 due to *thermal equilibrium*. The vector M_0 plays an important role in the description of all types of pulsed NMR experiments.

1.5.4. The Basic Pulsed NMR Experiment

The longitudinal nuclear spin magnetization described above is very small and not detectable. NMR measures nuclear spin magnetization perpendicular to the field (i.e., in the x - y plane). Transverse magnetization is achieved by rotating the polarization of every single spin at thermal equilibrium by $\pi/2$ radians (90°) around the z -axis (cf. Figure 1.13). This is equal to applying a radio frequency (RF) pulse to bring the polarization to the x - y plane in order to generate a transverse magnetization, which is the basis of a simple NMR pulse sequence. Once the RF pulse is turned off, a fraction of the nuclear spins are bunched together in phase as they begin to precess about the field direction. This condition is called *phase coherence*. The precessing nuclear spins eventually lose their coherence due to slight fluctuations of local fields. The transverse magnetization decays slowly as it is impossible to maintain exact synchrony between the precessing nuclear magnets. The precessing transverse magnetization after an RF pulse is very small. Nevertheless, it is detectable because it oscillates at a very well-defined frequency.

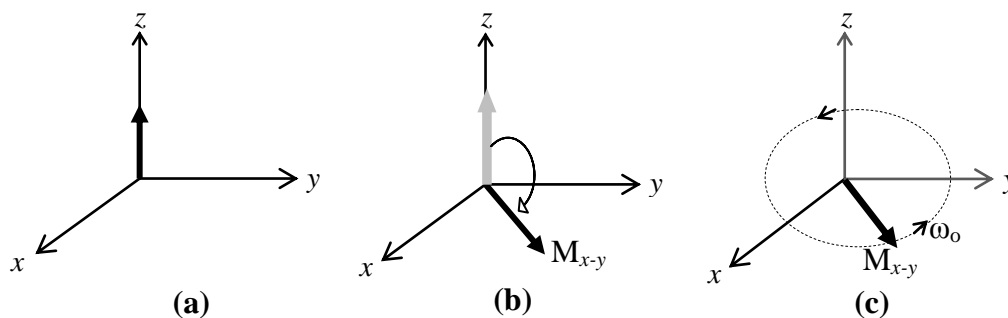


Figure 1.13 Net magnetization is shown (a) in longitudinal (z -axis) before the $\pi/2$ RF pulse, (b) rotated in the transverse plane by the $\pi/2$ RF pulse, and (c) Larmor precession of the transverse magnetization.

For a one channel single-pulse sequence, an NMR spectrum is recorded using a pulsed experiment as the one shown in Figure 1.14. First a delay of the order of a few seconds, known as the *relaxation* or *recycle delay* (t_d), is left in order to allow the spins to come to equilibrium. Then the sample is irradiated with a pulse from a dedicated transmitter that produces an RF signal at a frequency (ν_1) close to the Larmor frequency of the selected nuclear isotope defined by eqn 1.9.

$$\nu_1 = \left(\frac{\gamma}{2\pi} \right) B_0 \quad \text{Equation 1.9}$$

This RF pulse disturbs the equilibrium of the nuclear spin system and creates transverse nuclear magnetization. The pulse sequence is switched off during detection. The precession of the nuclear spin magnetization sets up oscillations in the tuned circuit, which gives rise to a transient signal known as *free induction decay* (FID), which is a function of time. The FID is recorded for a time called the *acquisition time* (t_{acq}) which usually lasts between 50 ms to a few seconds. Finally, the FID signal is subjected to mathematical operations called *Fourier transformation* which converts the NMR signal into an NMR spectrum, which is a plot of the intensity of absorption (or emission) on the vertical axis against frequency (ppm) on the horizontal axis.

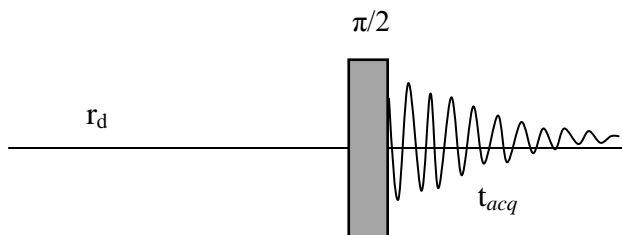


Figure 1.14 One channel single-pulse NMR sequence.

1.5.4.1 The Chemical Shift and Shielding

Only a single peak would be expected from the interaction of RF energy and a strong magnetic field in accordance with eqn 1.9. Luckily that is not the case, because if it were, NMR technique would be of no use. The nucleus in a molecule is shielded to some extent by its electron cloud, the density of which varies with the chemical environment, giving rise to

differences in chemical shift positions. The ability to efficiently discriminate among the individual absorptions (resonance lines) describes high-resolution NMR spectroscopy.

The basic NMR equation (i.e., eqn 1.9) for all spins in a nucleus can be modified to give the effective frequency that accounts for the shielding factor as shown in eqn 1.10, where the symbol σ is the shielding constant. Note that at any given B_0 , $\nu_1 < \nu_{eff}$.

$$\nu_{eff} = \left(\frac{\gamma}{2\pi} \right) B_0 (1 - \sigma) \quad \text{Equation 1.10}$$

The degree of shielding depends on the density of the circulating electrons, as well as on the inductive effect of neighboring atoms, among other factors. The difference in the absorption position of a particular nucleus in a molecule from the absorption position of a reference peak is called the *chemical shift* of that nucleus. Further detailed information on chemical shift is given elsewhere.¹⁸⁴⁻¹⁸⁶ The focus here is on the factors that influence the chemical shift. The main factors relevant to this work that influence chemical shift include; electron density and inductive effects. Other influences such as ring current effect and hybridization also exist¹⁸⁶ but are not discussed here.

Electrons under the influence of a magnetic field circulate generating their own magnetic field known as the *local field*, either increasing or decreasing the influence of the applied external magnetic field. The shielding of nuclei can generally be expressed as the sum of four terms;

$$\sigma = \sigma_{dia} + \sigma_{para} + \sigma_{neig} + \sigma_{solv} \quad \text{Equation 1.11}$$

Where σ_{dia} is the diamagnetic shielding, σ_{para} is the paramagnetic shielding, σ_{neig} is the neighbouring group shielding, and σ_{solv} is the solvent shielding. For ^1H and other nuclei with spherically symmetric charge distribution, the diamagnetic shielding term reduces the strength of the external magnetic field resulting in chemical shifts moving to a higher field (also upfield or low frequency). Paramagnetic shielding effects arise only for nuclei in non-spherical molecules (e.g., electrons in p-orbitals). Paramagnetic shielding terms tend to increase the strength of the external magnetic field, consequently, resulting in chemical shift moving to lower field (also downfield or high frequency).

Shielding arising from the neighboring groups also plays an important role in determining the chemical shifts. This term may be expressed in terms of the contributions from one of the electronic effects i.e. inductive and γ -*gauche* effects. The inductive effect of, for instance, an electron-withdrawing group (e.g., fluorine) connected to a proton on the same carbon atom in a molecule, will decrease the electron density around the proton resulting in higher chemical shifts (deshielding). Since the inductive effect propagates through the σ -bonds of the molecule and decrease with the inverse cube of the distance ($1/r^3$), much smaller shielding effects are observed for protons on the β -carbon. On the contrary, the protons on the γ -carbon will experience a significant shielding effect due to what is termed as the γ -*gauche* effect.

Concentration and solvent molecules also have very significant contribution to the shielding constant, particularly in solution NMR. The most important contributions occur in terms of diamagnetic and neighboring group shielding. For example, the inclusion of a guest within the cavity of host (e.g., β -CD) in aqueous solution presents a typical example where the influence of electron density and neighboring group shielding are at play. The effect of solvent on NMR chemical shifts comes from several contributions such as bulk magnetic susceptibility, magnetic anisotropy, and contributions from van der Waals and hydrogen-bonding interactions.^{187,188} van der Waals interactions make a relatively large contribution to ^{19}F chemical shifts and such interactions depend upon solute size as well as on the polarizability and ionization potential of the solvent.¹⁸⁸ For instance, the ^{19}F nuclei are highly polarizable in polar aqueous solvent resulting in increased van der Waals interactions and upfield shifts in their environment.

1.5.4.2 Chemical Shift Anisotropy

For most molecules, the secondary (or local) field induced by the electrons, and hence the size of the chemical shift, depends on the orientation of the molecule with respect to the applied magnetic field (*cf.* Figures 1.10 and 1.12). This is generally described by saying that the chemical shift is *anisotropic*. In liquid samples, the molecules are tumbling so rapidly that they experience an average local field, and hence have an average chemical shift, called the *isotropic shift*. Nevertheless, at any instant, the local field is different for molecules at different orientations. The local field due to the chemical shift is not necessarily parallel to the

applied field, it can point in any direction and therefore this local field can be a source of relaxation mechanism (§1.5.6).

The extent to which the local field varies as the molecule tumbles depends on the anisotropy of the chemical shift. With the exception of nuclei at sites of high symmetry, such as isolated atoms or nuclei in octahedral or tetrahedral sites, all chemical shifts are anisotropic. As a rough guide, the shift anisotropy is of the order of the chemical shift range for that nucleus. Thus, for protons the shift anisotropy is a few (~5) ppm; whereas, for ^{13}C and ^{19}F , the anisotropy can easily be in the order of 100 ppm or more.

1.5.5 Overview of Solid-state NMR Spectroscopy

Solid-state NMR is perhaps the most important technique for determining the structure and dynamics of a variety of systems e.g. polymers, host-guest systems, and proteins. An informative introduction to the basics of solid-state NMR with an emphasis on applications in supramolecular chemistry has been described by Ripmeester and Ratcliffe.¹⁸⁹ The fundamental difference in spectrometer design for solid samples is based on the anisotropic effects of powder samples. Thus, the spectra of solid samples are characterized by broader peaks compared to narrow lines for similar samples in the solution phase. For isolated spins-1/2 nuclei (e.g., ^{19}F and ^{13}C) in the solid state, CSA is the major source of line broadening. As previously described, NMR spectra of samples in solution experience rapid random molecular tumbling that averages the orientation dependence of the shielding to an isotropic value. However, appreciable CSA may still be observed in solution and only affects relaxation processes where it is the dominant mechanism for rare spins such as ^{13}C (§1.5.6).

In contrast to NMR spectra in solution, the full effects of anisotropic interactions are observed in the spectra of solid samples. The NMR line shapes of powder samples are a summation of the statistical distribution of multiple crystallite orientations, as shown in Figure 1.15. Consequently, broader lines are generated for solid samples compared to solution samples. Furthermore, the presence of direct nuclear dipole-dipole (D-D) interactions in solids, which are averaged to zero in solution, leads to an additional source of broadening in solid samples^{190,191} as shown in Figure 1.16. For nuclei with spins $>1/2$ (e.g., ^{23}Na), the quadrupolar interaction is often the dominant source of line broadening.

High resolution solid-state NMR can provide similar information that is available from corresponding solution NMR spectra if specialized techniques are incorporated such as magic angle spinning (MAS), cross polarization (CP), and 2D NMR methods. Furthermore, NMR relaxation offers an option for the study of the motional dynamics of host/guest complexes, including the role of solvent in the complex.

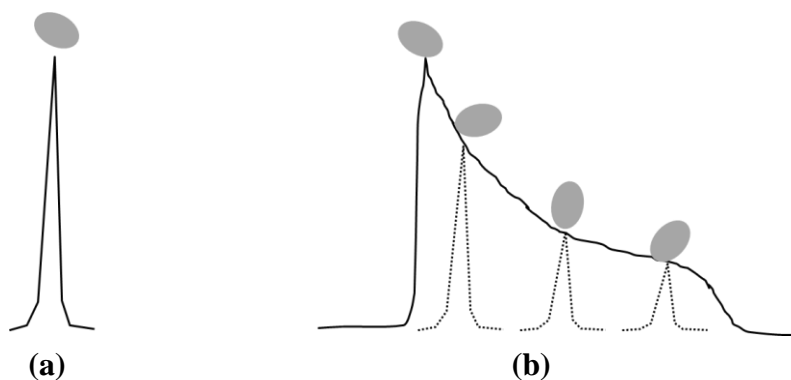


Figure 1.15 Distribution of spin orientation (ovals) in (a) solution, and (b) solid samples. Rapid molecular tumbling in solution averages the orientation dependence to an isotropic value and sharp resonance line (a). Anisotropic effects in solid samples result in broad NMR spectral lines (b).

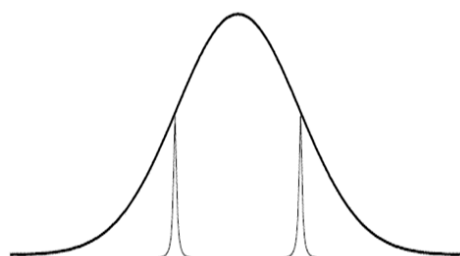


Figure 1.16 Dipolar coupling of two spins presents a source of line broadening in solid NMR.

1.5.5.1 Magic Angle Spinning (MAS)

The dipolar and chemical shielding interactions contain $(3\cos^2\Theta - 1)$ terms. In Magic-angle spinning (MAS), the axis of the sample rotor is placed at the magic angle (54.74°) with respect to \mathbf{B}_0 , where the term $3\cos^2\Theta - 1 = 0$, when $\Theta = 54.74^\circ$. The rate of spinning must be greater than or equal to the magnitude of the anisotropic interaction to average it to zero. Solid samples are normally packed tightly into rotors and spun at rates of up to 60 kHz at the magic

angle (*cf.* Figure 1.17), depending on the rotor size and type of the spectrometer. If the sample is spun at a rate that is less than the magnitude of the anisotropic interaction, a series of *spinning sidebands* which are separated by the rate of spinning (in Hz) are observed.

It is important to note that the presence of broad line shapes can be used to provide important information about the structure and dynamics in the solid state. For example, relaxation and cross polarization (CP) techniques are dependent on dipole-dipole interactions.

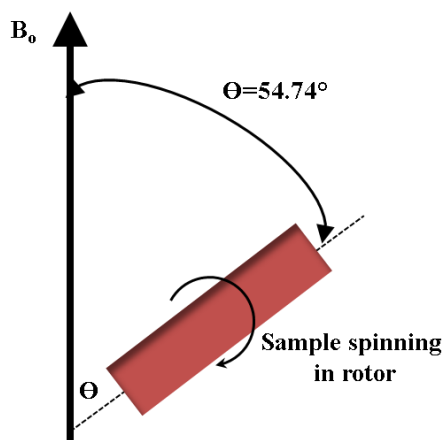


Figure 1.17 Schematic interpretation of the magic angle ($\Theta = 54.74^\circ$). Samples are spun at this angle with respect to the vertical axis.

1.5.5.2 Polarization Transfer Techniques

Cross polarization (CP) is one of the most important techniques in solid-state NMR spectroscopy which is mediated by dipolar interactions. In this technique, polarization from abundant spins such as ^1H or ^{19}F is transferred to dilute spins (e.g. ^{13}C) to aid in their spin states. CP techniques can also be used to perform some spectral editing and to obtain information about the proximity of spins in space.¹⁹² Observing dilute spins such as ^{13}C presents a number of problems; 1) the low abundance of the nuclei means that the signal-to-noise (S/N) ratio is generally poor, and 2) the relaxation times of low abundant nuclei tend to be long because of the absence of strong homonuclear dipolar interactions which can drive such relaxation transitions. Long relaxation times often require longer recycle delays (§1.5.4), sometimes on the order of several minutes between successive scans. Such problems can be eliminated by using CP techniques which can enhance the signal from dilute spins potentially by a factor of $\gamma(^1\text{H})/\gamma(\text{X})$, where $\gamma(^1\text{H})$ and $\gamma(\text{X})$ are the gyromagnetic ratios of the protons (or

any other abundant spin) and dilute spins, respectively. Secondly, there is a potential reduction in the acquisition time through elimination of the wait time for slowly relaxing dilute nuclei since the recycle delay is dependent upon the $T_{1\rho}$ of the abundant nuclei (e.g., ^1H and ^{19}F).

The pulse sequence of a typical CP experiment is shown in Figure 1.18.¹⁹³ Polarization is transferred during the spin locking period or the contact time, t_{cp} . Spin locking involves applying a resonant RF field to suppress the free evolution of transverse magnetization, locking it to a particular direction in the x - y plane (rotating frame). The $\pi/2$ pulse is only made on the abundant nucleus, followed by decoupling of the abundant nucleus to eliminate splitting patterns and inhomogeneous line broadening. A direct polarization (DP) pulse sequence would be similar to the simple $\pi/2$ pulse (*cf.* Figure 1.14) except for an additional decoupling channel, as required.

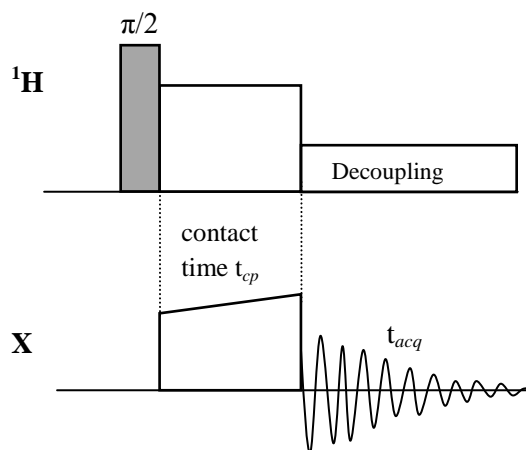


Figure 1.18 A typical cross polarization pulse sequence for observing dilute nucleus X where magnetization is transferred from an abundant nucleus e.g., ^1H to X during spin lock time (t_{cp}).

Cross polarization requires that nuclei are dipolar coupled to one another and the method works even when samples are spun rapidly at the magic angle, as long as the spinning rate does not exceed the anisotropic interaction. The key to obtaining efficient cross polarization is setting the Hartmann-Hahn¹⁹⁴ match (eqn 1.12) properly. In this case, the RF fields of the dilute spin (e.g., $\omega_{\text{C-13}}$) are set equal to that of the abundant spin (e.g., $\omega_{\text{H-1}}$). This is usually achieved experimentally by keeping the power on the ^1H channel constant while

adjusting the power level on the X channel so that the most intense ^1H spin spectrum is observed.

$$\gamma_X B_X = \gamma_{1H} B_{1H} \quad \text{Equation 1.12}$$

1.5.5.3 High Power Decoupling Techniques

The use of heteronuclear dipolar decoupling in the presence of MAS techniques is one of the key factors to obtaining high resolution spectra in solid-state NMR spectroscopy. The use of multiple decoupling techniques over the conventional continuous wave (CW) decoupling becomes more important in MAS NMR because the residual line width under CW conditions increase with higher spinning frequency.¹⁹⁵⁻¹⁹⁷ The CW decoupling sequence was originally used in liquid-state NMR and later applied in SS-NMR under MAS,¹⁹⁸⁻²⁰¹ but it was soon realized that resonance offsets could result in inefficient decoupling and residual line splitting.^{202,203} It is essential to apply efficient decoupling at higher MAS conditions. In high power CW decoupling, the abundant spins (e.g., ^1H , *cf.* Figure 1.18) are irradiated with a strong RF field of typically 20–250 kHz, where the decoupling quality improves with increasing field strength.

The two-pulse phase modulated (TPPM) decoupling sequence was the first multi-pulse heteronuclear decoupling method that was applicable for solid samples with dense homonuclear coupling network. There are a number of variations and modifications of the TPPM decoupling sequence, but a typical TPPM decoupling sequence consists of a train of RF pulses separated by a duration of one rotation, τ_r , and alternating phases ($-\phi/2$, $+\phi/2$, $-\phi/2$...etc.), as illustrated in Figure 1.19.

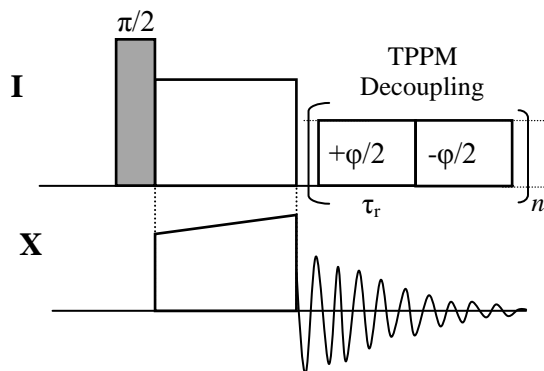


Figure 1.19 A cross polarization MAS NMR pulse sequence with TPPM heteronuclear decoupling of spin **I**.

1.5.5.4 Technical Aspects of High Resolution ^{19}F Solids NMR

Now that we have an understanding of the basic NMR concepts, we provide an overview of the properties of the ^{19}F nuclide and its NMR features since ^{19}F NMR spectroscopy represents a common technique used in this thesis.

^{19}F has a spin of $\frac{1}{2}$ and natural abundance of 100 %, and along with ^1H is considered as one of the easiest nuclides to observe. It has a relatively high resonance frequency, close to that of the proton, which along with the other properties makes this nucleus possess very favourable sensitivity (*cf.* Table 1.8). The chemical shift range of ^{19}F is comparable to that of ^{13}C and considerably wider (several orders of magnitude) than that for ^1H . Thus, the spectra of ^{19}F are simpler than those of the analogous hydrogen compounds since there is less overlapping between the groups of the peaks. Since fluorine forms compounds with nearly all other elements, such nucleus presents a wealth of structural information. It follows that, when it comes to choosing a nucleus to study the structure of fluorinated materials containing ^{19}F , ^{13}C and ^1H , fluorine will often be preferred.

The total amount of high-resolution ^{19}F solids NMR work on host-guest supramolecular systems containing ^{19}F and ^1H is relatively limited, and may be due to technical problems associated with ^{19}F solids NMR measurements. Ando et al.²⁰⁴ cited the two advantages of the nucleus, namely the 100% natural abundance and its high magnetic moment, as the reason for some of the technicalities of high-resolution ^{19}F NMR spectroscopy in the solid state. This is because homo- and heteronuclear dipolar interactions are likely to be extremely strong making discrimination of individual ^{19}F lines a challenge. Some technical problems associated with high resolution ^{19}F NMR of fluorinated systems containing ^1H can be summarized as:

- 1) The presence of extremely strong ^1H - ^{19}F heteronuclear dipolar interactions means that very high decoupling powers and very fast MAS (>20 kHz) are required.
- 2) Fast MAS conditions present the same degree of line narrowing throughout the experiment which defeats the purpose of NMR, i.e. the possibility to manipulate and separate interactions. Therefore, even under high-speed MAS, proton-fluorine double/multiple resonance experiments, e.g., CP experiments with simultaneous decoupling are desirable.

- 3) Achieving high resolution ^{19}F spectra of perfluorinated systems may still present a challenge even with efficient ^1H decoupling because of the strong ^{19}F - ^{19}F dipolar interactions. Such homonuclear dipolar interactions often require either multi-pulse decoupling techniques (e.g. TPPM) or very fast MAS (≥ 20 kHz) conditions.
- 4) Finally, the low melting point of some perfluorinated compounds e.g. PFOA (~ 45 - 55 °C) implies that NMR measurements of such samples under conditions of fast MAS are only possible at extremely low temperature (< 0 °C).

1.5.6 Relaxation

We have already seen that at equilibrium we have magnetization along z -axis, and none in the transverse x - y plane. The thermal equilibrium of the spin system is disturbed by irradiating at the resonance frequency. This alters the population ratios and creates transverse magnetic field components M_x and M_y . When the perturbation ceases the system relaxes until it reaches equilibrium again. Relaxation is how the bulk magnetization from the spins reaches its equilibrium value. We distinguish between two types of relaxation processes; the relaxation in the z direction, which is characterized by the spin-lattice or longitudinal relaxation time T_1 , and relaxation in the x - y plane, which is characterized by the spin-spin or transverse relaxation time T_2 .

Relaxation in NMR is generally on the order of between milliseconds and a few seconds or even hours in extreme cases. Comparing that to the lifetime of an excited electronic state which is a few microseconds, or the lifetimes of vibrational and rotational energies of molecules which are a few nanoseconds, we see that relaxation processes in NMR are unusually slow. The advantage of slow relaxation is that it gives ample time for the transverse magnetization to be manipulated and observed. Slow relaxation also means that the FID persists for long enough for us to obtain high-resolution spectra. The disadvantage of slow relaxation is that it limits the rate at which an experiment can be repeated since sufficient relaxation delay is required to allow the equilibrium magnetization to be re-established (relax) before the experiment can be repeated. Referring to the pulse sequence in Figure 1.14, after the 90° pulse the transverse magnetization relaxes with a rate that is a function of the longitudinal relaxation time, T_1 , of the nucleus. Thus, a recycle delay of 5 - $7T_1$ must be

allowed to ensure that the magnetization has recovered to approximately 99-100% of its original value.

We will see in the forthcoming sections that in NMR the rate of relaxation is sensitive to the physical environment and the nature of motion of the nuclei. Thus, relaxation can be conveniently used to probe both the environment and dynamics of the nuclei. Furthermore, relaxation processes can manifest in the Nuclear Overhauser Effect (NOE; *cf.* §1.5.7), which is a very important phenomenon in characterizing the spatial orientations of host-guest systems.

1.5.6.1. Longitudinal and Transverse Relaxation Time Constants

Relaxation in the direction of applied field (z -axis) is characterized by the spin-lattice or longitudinal time T_1 . Such relaxation is brought about by the transverse components of local magnetic fields which are oscillating at the Larmor frequency. These oscillating local fields are generated by the spins and act like a pulse but are highly localized. Recall that at equilibrium there is magnetization along the z -axis ($M_z = M_z(t)$) and none in the transverse plane ($M_{xy} = 0$). A 90° RF pulse equalizes the populations of the two energy levels; whereas, a 180° pulse inverts the population ratio. Spin-lattice relaxation is always associated with a change in the energy between two reservoirs; the magnetic energy of the spins and the energy of thermal motion. After the perturbation, the equilibrium condition $M_z = M_z(t)$ reasserts itself (*cf.* Figure 1.20).

Typical T_1 values range from a few seconds for ^{19}F and ^1H nuclei, to hundreds of seconds for ^{13}C nuclei in small molecules. T_1 largely depends on the time scale of the local fluctuating fields and is often dependent on the temperature and viscosity of the material.

The transverse relaxation (T_2) is the decay of the transverse magnetization to its equilibrium value of zero (*cf.* Figure 1.20). The significance of T_2 values lie in their relationship to the line width of the observed NMR signals (half-height width = $1/\pi T_2$). There are two contributions to transverse relaxation; the transverse components of local fields which are oscillating at the Larmor frequency, and the distribution of the z -components of the local fields. Recall that an RF pulse creates phase coherence between spins (§1.5.4). Fluctuations caused by the local time-dependent magnetic fields cause the loss of this synchronization over time. This loss of coherence can be observed as a decaying transverse magnetization. The

transverse relaxation is characterized by the time constant, T_2 , which is different from T_1 . Note that the energy of the spin system is not altered by spin-spin relaxation, only the phase coherence of the nuclear spins is lost. Decays of longitudinal and transverse magnetizations at rates defined by T_1 and T_2 , respectively, are graphically shown in Figure 1.20. In order to be able to compare T_1 and T_2 , we need to define correlation time, τ_c , which is used to determine and quantify random thermal motion.

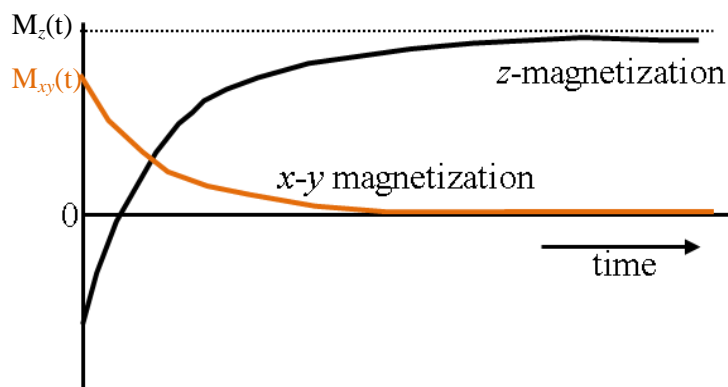


Figure 1.20 Relaxation drives the z -magnetization to its equilibrium value (dotted line) and the transverse magnetization to its equilibrium value of zero.¹⁸³

1.5.6.2 Correlation Time

As described above, to cause longitudinal relaxation the transverse component of the local field must be oscillating at or near the Larmor frequency (ω_0). A molecule is likely to be executing two distinct types of motion: vibrations/librations (which modulate the dipolar interaction), and overall rotation (which modulates the local fields due to both the dipolar interaction and CSA). Molecular vibrations typically take place at frequencies of 10^{11} to 10^{13} Hz, which represent a time-scale of ~ 10 ps ($\nu = 1/2\pi\tau_c$). On the other hand, molecular rotations are in the order of 10^9 Hz (~ 10 ns) (*cf.* Figure 1.21).^{182,183} The highest attainable Larmor frequency is in the order of $\sim 10^9$ Hz.

Vibrational and rotational motions are generally characterized by their correlation times (τ_c), which is the average time needed by a molecule to achieve an orientation one radian away from its starting position. τ_c depends on the temperature, and size and viscosity of the molecule. Only those molecular motions whose frequencies match the Larmor frequencies lead to rapid/efficient relaxation of the molecule. Note that molecular libration and rotation

can be reduced significantly particularly in host-guest systems where the dynamics of the guest are relatively hindered by the host.

The relationship between the Larmor frequency and correlation time is important in understanding relaxation processes as it helps define the motional regimes of a molecule. For a random fluctuating field (B_x) along the x -axis, the amount of motion present at the required frequency can be represented by the spectral density function, $J(\nu)$, which is related to the correlation time and given as shown in eqn 1.13.

$$J(\nu) = \frac{2\tau_c}{1 + (2\pi\nu\tau_c)^2} \quad \text{Equation 1.13}$$

The higher the value of $J(\nu)$, the more efficient the relaxation. Efficient spin-lattice relaxation (T_1) requires fluctuations in the local field at frequencies of hundreds of megahertz (Larmor time-scale) and this roughly equates to correlation times of nanoseconds. On the other hand, spin-lattice relaxation in the rotating frame ($T_{1\rho}$) requires fluctuations of tens of kilohertz (spectral time-scale), equating to correlation times on the order of microseconds. Typical NMR time-scales are depicted in Figure 1.21.

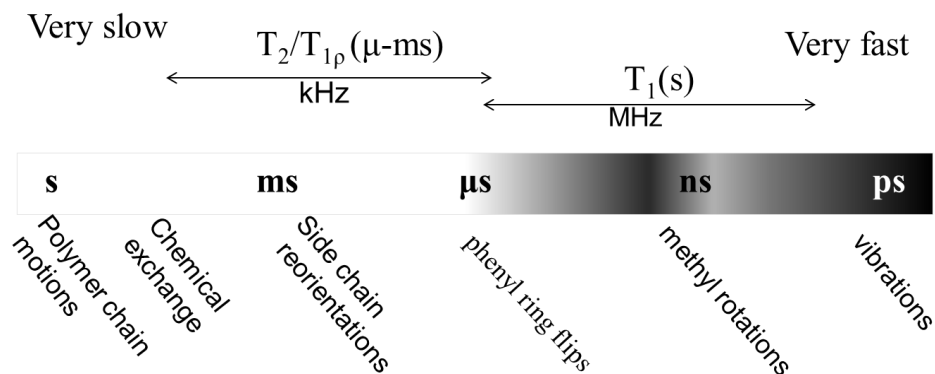


Figure 1.21 Typical NMR time-scales and related motional dynamics. Adapted from ref. 184.

Thus, if the transverse field fluctuates rapidly, the correlation time (τ_c) is short and the spectral density is broad such that the value of J at any particular frequency is small. Similarly, if the transverse field fluctuates slowly, the correlation time is long and the spectral density is sharply peaked around $\nu = 0$, so that the value of J at any frequency is zero. Relaxation at frequency (ν), which might be the resonance frequency (ω_0) of the spins in the

sample, is most efficient when the molecular motion results in a fluctuating magnetic field of the same frequency. Relaxation is therefore most effective at an intermediate value of τ_c where the spectral density is neither too broad nor too narrow. There is a value of correlation time when the spectral density is maximum, defined as $2\pi\nu\tau_c = 1$ or $\tau_c = 1/2\pi\nu$. It follows that T_1 will also be most efficient when $\tau_c = 1/2\pi\nu$, as this is the correlation time that gives the maximum spectral density at the Larmor frequency. Therefore, for the most efficient T_1 relaxation the correlation time must neither be too long nor too short, but must be within a reasonable range ($1/2\pi\nu$).

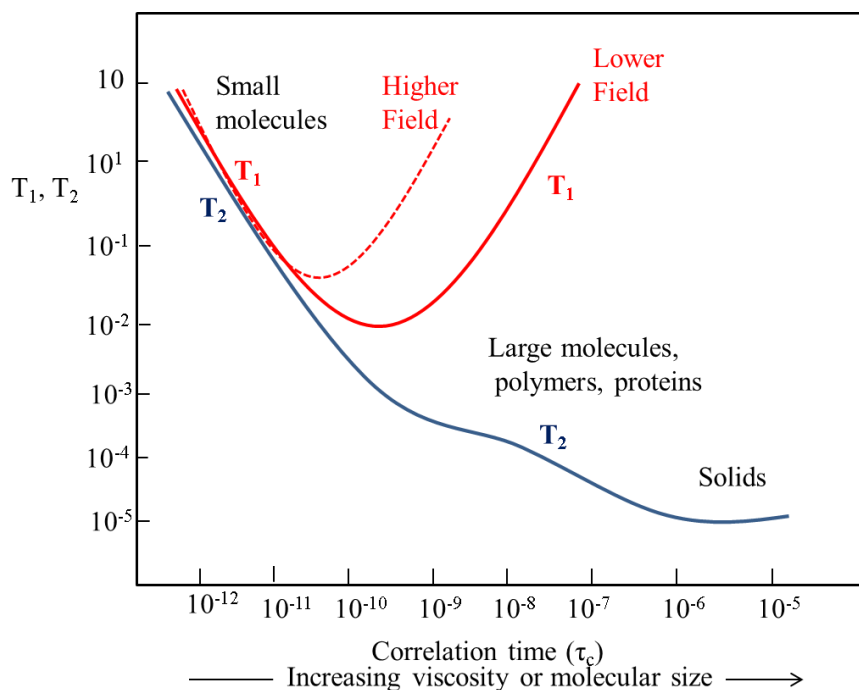


Figure 1.22 Relationship between longitudinal and transverse relaxation rate constants as a function of correlation time. Adapted from ref. 205.

From here, we distinguish two motional regimes; the fast motion or extreme narrowing ($2\pi\nu\tau_c \ll 1$) and slow motion or spin diffusion limit ($2\pi\nu\tau_c \gg 1$) regimes. In the extreme narrowing, the motion of the molecule is very fast (i.e. the correlation time is very short) and the spectral density is independent of the Larmor frequency (i.e. $J(\nu) \sim \tau_c$). At very short rotational correlation times (at the extreme narrowing limit), the values of T_1 and T_2 are nearly equal. That is the case for small molecules or mobile fluids where static dipolar fields are averaged out. As the correlation time is increased (slow motion), T_1 passes through a

minimum and then increases. The transverse relaxation time constant T_2 , continues to decrease which means that the NMR peaks get progressively broader as the molecular mass is increased. In the solid state, T_2 is generally shorter than T_1 (i.e. $T_2 < T_1$), because return of magnetization to the z -axis inherently causes loss of magnetization in the x - y plane. The relationship between T_1 and T_2 as a function of correlation time is depicted in Figure 1.22.

In practice, T_1 depends on temperature because the random field fluctuations originate in the molecular environment, and τ_c is temperature dependence. The effect of temperature on T_1 depends on the location of τ_c with respect to the minimum. For example, for systems with long τ_c (right side of the T_1 minimum on Fig. 1.22), warming the sample reduces T_1 . Conversely, for systems with short τ_c , warming the sample increases T_1 (Refer to the T_1 curve in Figure 1.22).

1.5.6.3 Relaxation Mechanisms

A particular source of a local magnetic field is called a *relaxation mechanism*. Generally, for spins-1/2 nuclei, relaxation is caused by fluctuating magnetic fields at the sites of the nuclear spins, caused by thermal motion of the molecules. Various relaxation mechanisms are recognized as contributing to the spin-lattice and spin-spin relaxation processes. Of the various mechanisms, two are common and more relevant to this work; dipole-dipole (D-D or dipolar) interactions and chemical shift anisotropy (CSA).

1.5.6.3.1 Dipole-dipole (DD) relaxation

The dipolar mechanism is due to the magnetic moment (or magnetic dipole) experienced by a spin from a neighboring spin. D-D relaxation shows very strong distance dependence, and operates most effectively between directly bonded nuclei or those that are in close proximity. Generally, the precise role of D-D and CSA relaxation effects depends on details of the system. For example, for host-guest systems involving β -CD and organic guest molecules (e.g., PFCs), contributions to T_1/T_2 generally come from heteronuclear ($^1\text{H}/^{19}\text{F}$, $^{13}\text{C}/^{19}\text{F}$) dipolar interactions modulated by the dynamics of the guest. $^{19}\text{F}/^{19}\text{F}$, $^1\text{H}/^1\text{H}$ homonuclear dipolar interactions are also known to drive such relaxations. In general, the main contribution to T_1 relaxation comes from D-D interactions. Structural peculiarities of a molecule determine how D-D interactions affect T_1 relaxation.¹⁸⁴ For example, the T_1 of a

terminal methyl (CH₃ or CF₃) group can be appreciably longer due to its internal rotation that tends to reduce dipolar coupling. As well, hydroxyl (e.g., in the case of β-CD) and carboxyl groups (e.g., in carboxylic acids) can form H-bonds limiting the mobility of part or the entire molecular segments. Also, individual parts of a molecule can move at different rates, where the rigid parts can act as anchors for the side chains decreasing T_1 values for the groups adjacent to the anchor point.

1.5.6.3.2 Chemical shift anisotropy (CSA)

The CSA mechanism results from the presence of a strong applied field which is thought to induce local fields from the electrons. The magnitude of the induced local field depends on the orientation (anisotropy) of the molecule with respect to the applied magnetic field. Molecules in liquids rapidly experience all the possible orientations relative to the direction of applied magnetic field so that the observed σ is an averaged value. However, the tumbling motions that produce this value cause oscillations of the local magnetic field and these time-varying fields lead to relaxation. CSA gives rise to T_1/T_2 of elements such as ¹⁹F and ¹³C nuclei, but not the ¹H nucleus since it has a relatively small CSA (5 ppm). CSA has generally been shown to make a minor contribution to ¹⁹F T_1 relaxation, but adds significantly to the ¹⁹F signal line width (T_2 relaxation).²⁰⁶

1.5.6.4 Measurement of Relaxation Times ($T_1/T_2/T_{1\rho}$)

This part describes the measurement of spin-lattice relaxation time constants in the laboratory (T_1), and rotating ($T_{1\rho}$) frames, as well as spin-spin relaxation constant (T_2).

1.5.6.4.1 Inversion Recovery: Measurement of T_1

As noted above, T_1 characterizes the return of the bulk magnetization of a sample to its equilibrium state, after it has been isolated from its equilibrium state by some form of perturbation (such as an applied RF pulse). The usual technique for measuring T_1 is called *inversion recovery*, as illustrated in Fig. 1.23.¹⁸²

The first 180° pulse inverts the magnetization in the negative z -axis (“inversion”), and then the magnetization is allowed to recover (by a spin lattice relaxation process) for a specified period of time τ (“recovery”). The final 90° “read” pulse places the partially relaxed

magnetization into the x - y plane where the amount of recovery (i.e. signal intensity) is measured.

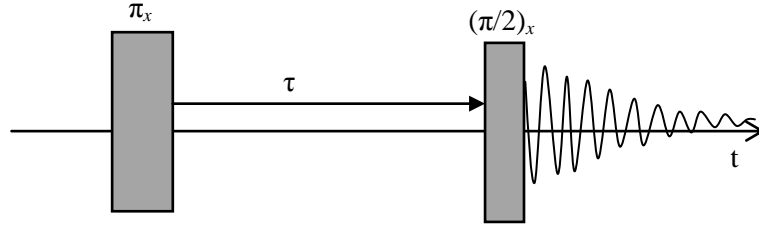


Figure 1.23 Inversion recovery pulse sequence for measuring the rate constant for longitudinal relaxation (T_1).

Typically, 15-20 recovery times (τ) are chosen for a single T_1 measurement, where the inversion recovery process is characterized by equation 1.14.

$$M_\tau = M_o \left[1 - 2e^{(-\tau/T_1)} \right] \quad \text{Equation 1.14}$$

Equation 1.14 can be rearranged to:

$$\ln \frac{M_o - M_\tau}{M_o} = \ln 2 - \frac{\tau}{T_1} \quad \text{Equation 1.15}$$

The initial condition ($\tau = 0$) immediately after the 180° pulse is given by $M_\tau = -M_o$ (i.e. the initial magnetization is along the $-z$ -axis). The equilibrium condition at $\tau = \infty$ is given as $M_\tau = +M_o$ (i.e., the magnetization is in its equilibrium position along $+z$ -axis).

From Equation 1.15, a plot of $\ln[(M_o - M_\tau)/M_o]$ vs. τ will yield a slope of $-1/T_1$. For solids, T_1 values are usually on the order of a few milliseconds to seconds in magnitude.

1.5.6.4.2 Spin Echoes: Measurement of T_2

Recall that T_2 represents the time constant for the decay of magnetization from some non-zero value to zero. T_2 can be measured using a Hahn echo²⁰⁷ pulse sequence, as shown in Figure 1.24, by variation of the τ spacing between the 90° and the 180° pulses.

The 90° pulse places the magnetization in the x - y plane, where it begins to dephase under relaxation for a period of τ_1 . The 180° pulse is a refocusing pulse, where after τ_2 delay the spectral intensity reflects solely T_2 relaxation, with magnetic field inhomogeneities being refocused.

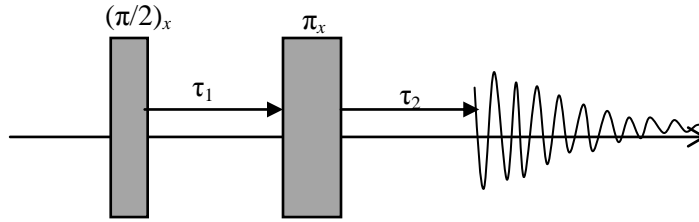


Figure 1.24 The simple spin echo pulse sequence used to measure the rate constant for transverse relaxation.

T_2 measurements are characterized by eqn 1.16 or its rearranged form (Eqn 1.17).

$$M_{\tau} = M_o e^{-\tau/T_2} \quad \text{Equation 1.16}$$

$$\text{Ln} \frac{M_{\tau}}{M_o} = \frac{-\tau}{T_2} \quad \text{Equation 1.17}$$

A plot of $\ln(M_{\tau}/M_o)$ vs. τ yields a slope of $-1/T_2$. For solids, the T_2 values are on the order of a few milliseconds to tens or hundreds of microseconds.

1.5.6.4.3 Spin Locking: Measurement of $T_{1\rho}$

Another property that is routinely measured in the study of relaxation and dynamics is the spin-lattice relaxation in the rotating frame, or $T_{1\rho}$. Experimentally $T_{1\rho}$ is measured by rotating the longitudinal magnetization to the transverse plane using a 90° pulse. This is followed by subsequent application of a lower amplitude pulse (also known as spin-locking pulse or field) with the same phase as the resulting transverse magnetization, for a period τ . The applied spin-locking pulse is typically on the order of milliseconds, as opposed to microseconds for ordinary $\pi/2$ pulses. The pulse sequence for measuring $T_{1\rho}$ is shown below;²⁰⁸

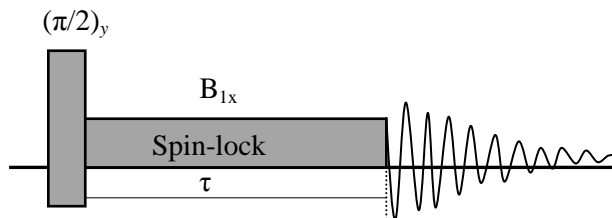


Figure 1.25 Pulse sequence for measuring $T_{1\rho}$

If the spin-lock field strength is large enough (50-100 kHz), the spin magnetization is locked into position along the axis corresponding to the phase of the locking pulse and precession occurs about this axis. After period τ , B_1 is turned off allowing the magnetization to decay in a “ T_1 -like” process which is governed by the time scale of the locking power rather than the Larmor frequency. The equation describing $T_{1\rho}$ decay is the same as that for T_2 decay, and the same graphical treatment can be applied for $T_{1\rho}$ if the T_2 is replaced with $T_{1\rho}$ in Equation 1.17.

1.5.7 The Nuclear Overhauser Effect (NOE)

The Nuclear Overhauser Effect (NOE) is an important consequence of D-D relaxation. It is the transfer of nuclear spin polarization from one nuclear spin population to another via cross-relaxation. The NOE is an extension of the seminal work of American physicist Albert Overhauser who in 1953 proposed that nuclear spin polarization could be enhanced by the microwave irradiation of the conduction electrons in certain metals.²⁰⁹ The general Overhauser effect was demonstrated experimentally by other scientists and in 1963 it was experimentally observed and explained by Kaiser in an NMR experiment where the spin polarization was transferred from one population of nuclear spins to another.²¹⁰

Subsequent to its discovery, the NOE process was shown to be highly useful in NMR spectroscopy for characterizing and refining organic chemical structures. A distinction is made between 2D NMR methods that exploit the NOE effect (e.g., ROESY and NOESY) and those that use spin-spin or J-coupling (e.g., COSY and TOCSY). While NOE occurs through space, the latter occurs through chemical bonds. Thus, atoms that are in close proximity to each other can yield a measurable NOE, whereas scalar or J-coupling is observed only when the atoms are connected by 2–3 chemical bonds. The inter-atomic distances derived from the observed NOE can often help to confirm a precise molecular conformation, i.e. the three-dimensional structure of a molecule. In 2002, Kurt Wüthrich was awarded the Nobel Prize in Chemistry for demonstrating that the NOE could be exploited using two-dimensional NMR spectroscopy to determine the three-dimensional structures of biological macromolecules in solution. Some two-dimensional NMR experimental techniques exploiting spin coupling and the NOE effect are described below.

1.5.7.1 2-D COSY

The COSY (Correlation Spectroscopy) experiment is one of the most popular and useful of all 2-D experiments. It is a homonuclear 2-D technique that is used to correlate the chemical shifts of mostly ^1H (also ^{19}F) nuclei which are J-coupled.²¹¹ From a COSY NMR spectrum it is possible to identify the chemical shifts of spins which are scalar coupled, enabling interpretation of the J-coupling network in the molecule. Figure 1.26 shows a schematic COSY NMR spectrum which consists of two types of peaks; cross peaks and diagonal peaks. Cross peaks (grey ovals) have different frequency coordinates in F1 and F2. Diagonal peaks (black ovals) have the same frequency coordinates in F1 and F2, and are centered at the chemical shift of each spin and serve to locate the chemical shift values in the spectrum. The spectrum in Figure 1.26 shows that a resonance line at δ_A is coupled to a peak at δ_B , or more generally the following couplings are present: A-B, B-C, and F-D.

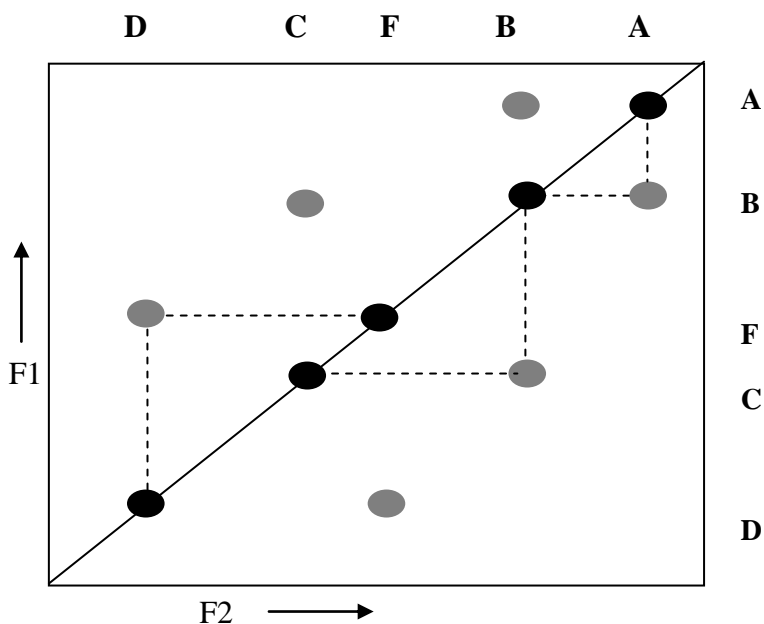


Figure 1.26 A Schematic 2-D COSY spectrum showing cross peaks (grey ovals) and diagonal peaks (black ovals) and scalar coupled peaks (shown by dotted

The pulse sequence for COSY in Figure 1.27 can be explained as follows; the first $\pi/2$ pulse creates transverse magnetization components which evolve under the chemical shift and homonuclear J-coupling during the evolution period t_1 . The second pulse ($\pi/2$ or $\pi/4$) mixes the magnetization components among all the transitions that belong to the same coupled spin

systems. The final distribution of labeled magnetization components is detected by measuring their precession frequencies during the detection period t_2 .

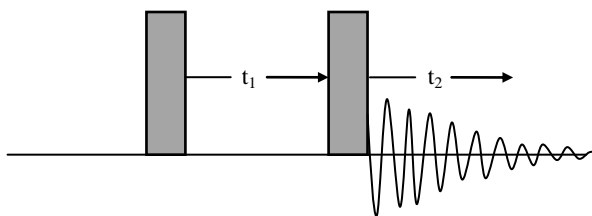


Figure 1.27 Basic 2-D COSY pulse sequence.

1.5.7.2 TOCSY

Total correlation spectroscopy (TOCSY) is similar to COSY in that cross peaks of coupled spins are observed. However, unlike in COSY where coherence transfer is restricted to directly spin coupled nuclei, in TOCSY oscillatory exchange is established which proceeds through the entire coupling network so that there is net magnetization transfer from one spin to another even in the absence of direct coupling. For example, if spin A is coupled to spin B and B is coupled to C, then in a TOCSY experiment cross peaks between A and C will be observed even though they are not directly coupled. The isotropic mixing which occurs during the spin-lock period of the TOCSY sequence (Fig. 1.28)^{183,212} exchanges all of the *in-phase* as well as *anti-phase* coherences.

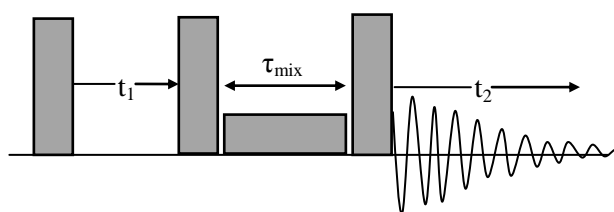


Figure 1.28 Basic 2-D TOCSY pulse sequence.

1.5.7.3 NOESY

A 2-D NOESY (Nuclear Overhauser Effect Spectroscopy) spectrum looks similar to a COSY, except that the cross peaks are generated not by coherence transfer through couplings, but by cross relaxation through direct dipolar coupling.²¹³ Thus, the cross peaks of a NOESY spectrum indicates which protons are close to each other in space.

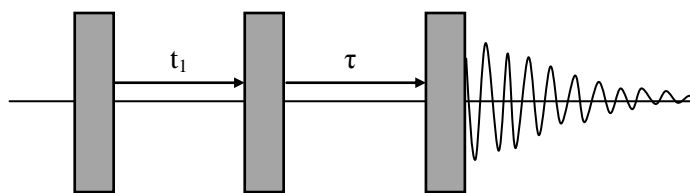


Figure 1.29 Basic 2-D NOESY pulse sequence.

The basic NOESY sequence consists of three $\pi/2$ pulses (*cf.* Figure 1.29). The sequence will be analyzed for two spins that are undergoing dipolar relaxation and assuming there is no scalar coupling between the two spins. The first part of the sequence $\pi/2$ - t_1 - $\pi/2$ has already been analyzed in the COSY experiment (*cf.* §1.5.7.1). During t_1 , transverse magnetization acquires a phase label according to the offset (δ); this transverse magnetization is rotated onto the z -axis by the second pulse. During the mixing time τ cross polarization may transfer this labeled z -magnetization to other spins. The final pulse rotates the z -magnetization into the transverse plane, allowing a signal to be detected.

1.5.7.4 ROESY

ROESY (Rotating-frame Overhauser Effect Spectroscopy) is analogous to NOESY experiment, except that instead of generating cross peaks by cross relaxation between the z -magnetization of different spins, the cross peaks in ROESY arise from cross relaxation between spin-locked transverse magnetization. The experiment is a useful alternative for NOESY as the cross peaks in a ROESY NMR spectrum always have the same sign, regardless of the value of the correlation time (τ_c). ROESY is therefore used to look for NOE enhancements in molecules with intermediate (~ 1000 – 5000 Da) molecular weights or in molecules whose τ_c make the conventional NOEs zero or close to zero.^{214,215} The pulse sequence for a 2-D ROESY is shown in Fig. 1.30.

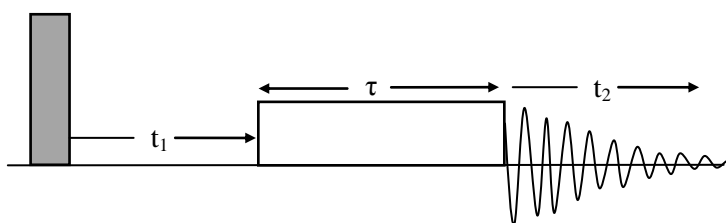


Figure 1.30 Basic 2-D ROESY pulse sequence

The pulse sequence for 2-D ROESY is very similar to that for NOESY in that frequency labeled magnetization is prepared during t_1 . The difference arises from the mixing time. In NOESY, the frequency magnetization is rotated to the z -axis, where cross relaxation takes place. In ROESY, it is the x -magnetization present at the end of t_1 which is spin-locked so that transverse cross relaxation can take place.

1.6. Overall Research Objectives

The overall objectives of this research work can be classified into two main themes: (1) To study the structure of β -CD based supramolecular host-guest inclusion compounds (ICs) using perfluorinated compounds (PFCs) as guest molecules, and (2) To examine the host-guest properties of β -CD based copolymers as potential adsorbent materials for hydrocarbon (HC) and fluorocarbon (FC) compounds. Based on the overall objectives, the thesis is sub-divided into five main projects;

- 1) Preparation and characterization of β -CD/PFCs host-guest inclusion compounds (ICs) in aqueous solution and the solid state,
- 2) Investigation of the structural and dynamic properties of the β -CD/PFCs host-guest ICs,
- 3) Structural characterization of β -CD-based copolymers (Poly-CDs) and their inclusion properties with a model phenolic guest molecule (i.e. PNP) in aqueous solution,
- 4) Application of synthetically engineered CD-based copolymers (or MIMs) for the adsorption of alkyl and perfluoroalkyl carboxylates, and
- 5) Structural investigation of the adsorptive interactions of the alkyl and perfluoroalkyl carboxylates/sulfonates onto the (MIMs).

The motivation to carry out a detailed and systematic study of the complexes formed between β -CD and PFCs was based on the fact that there are no detailed X-ray and spectroscopic studies documenting the structure of β -CD/PFCs complexes in the solid state. Moreover, reports on the adsorption of perfluorinated contaminants using synthetic polymeric adsorbents containing cyclodextrins are relatively limited.

The main objectives of the first theme of this thesis which comprises projects 1 and 2 (chapters 2 – 5) were to develop better methods for preparing host-guest inclusion complexes containing β -CD and PFCs at various host/guest mole ratios (i.e. 1:1 and 2:1), and to further characterize the structural and dynamic properties of the guest in the complexes. Two

methods (dissolution and slow cool) were developed by comparison to prepare β -CD/PFC complexes using PFOA as the model guest. A modified dissolution method was later adopted to afford host-guest complexes with greater phase purity where various PFCs guests were used. The guests were chosen to represent long chain (PFOA; C8) and short chain (PFBA; C4) acids, and the conjugate base of PFOA (SPFO; C8). The complexes formed between β -CD and PFCs were characterized using $^1\text{H}/^{19}\text{F}/^{13}\text{C}$ solution/solid-state NMR and FT-IR spectroscopy, thermal analyses (DSC and TGA), and PXRD. Complexes of β -CD/PFCs in solution were studied using NMR with D_2O as the solvent system.

The second theme of the thesis comprises projects 3 – 5 (chapters 6 – 8). The main objectives of this part of the thesis were to characterize the structure of CD-based polymeric host materials and to evaluate their adsorption properties towards fluorocarbon and hydrocarbon guests. The polymeric host materials were synthetically engineered from hexamethylene diisocyanate (HDI) linker at different loading ratios (i.e., 1, 3, and 6 with respect to β -CD) to form HDI-1, -3, and -6 copolymers, respectively. The copolymer materials were referred to as macromolecular imprinted materials (MIMs), because they contain β -CD which serves as a macromolecular imprint site where guests can be preferentially bound. This part of the thesis starts with the structural characterization of the soluble copolymer (HDI-1) where its complexes with PNP as a model guest in aqueous solution were characterized using NMR, FT-IR and Raman spectroscopy, thermal analyses (DSC, TGA), induced circular dichroism (ICD), and dynamic light scattering (DLS) (chapter 6). The structure of HDI-1 copolymer was characterized in aqueous solution as a function of guest concentration and temperature.

The adsorption properties of a series of polymeric adsorbent materials (i.e., HDI-1, -3, and -6 or MIMs) were evaluated towards perfluorooctyl (PFOA) and octyl (OA) carboxylate anions, as well as perfluorooctyl sulfonate (SPFO) anions. The main objectives were to compare the adsorption properties of the different MIMs towards a variety of guest molecules in order to be able to propose possible interaction modes between the host/guest systems. The adsorption results for MIMs were compared to similar results using conventional activated carbon adsorbent materials. Spectroscopic methods were later employed to provide unequivocal evidence for the types and nature of interactions involved in the binding of the guests onto the surface of MIMs.

The adoption of the urethane-based host copolymers grew out of the PhD research work of M. H. Mohamed.⁵⁴ The research presented in this thesis report was aimed at extending the study of simple host-guest systems to polymeric hosts whilst preserving the unique host-guest chemistry of β -CD.

1.7. Specific Research Objectives

This PhD thesis research was aimed at addressing various knowledge gaps and hypotheses:

- 1) To develop improved preparative methods for producing phase pure β -CD/PFCs ICs in the solid state.
- 2) To understand the structure and conformational preferences of PFC chains in their unbound and bound states in aqueous solution and the solid state.
- 3) To characterize and understand the motional dynamic properties of PFC guests in host-guest complexes in the solid state.
- 4) To study the effect of guest concentration and temperature variations on the structure of urethane-based copolymer materials in aqueous solution.
- 5) To characterize the types and nature of the active binding sites present in polymeric hosts, such as inclusion and interstitial (polymeric framework) regions. In a controversial study by Ma and Li,⁵¹ an anomalously high binding affinity was reported between urethane-based copolymers and PNP (10^8 – 10^9), as compared to native β -CD (10 – 10^3). The assumption by Ma and Li⁵¹ indicates that PNP is bound solely in the cavity sites of β -CD and not within the interstitial regions.
- 6) To understand the sorption behaviour of alkyl and fluoroalkyl carboxylate anions using CD-based urethane copolymer adsorbents in aqueous solution.

The end goal of this work is to gain further insights about the structure/dynamics relationship of host-guest systems in order to be able to rationalize the design of polymeric adsorbent materials for improved function.

1.8. Scope of Work

As described above, this PhD thesis mainly deals with the structural studies of supramolecular host-guest systems. β -cyclodextrin (β -CD) and β -CD-based copolymers were

used as host materials where several fluorocarbon and hydrocarbon guest molecules were studied (PFOA, PFOS, SPFO, PFBA, and OA).

The thesis work is divided into 9 chapters; where chapters 1 and 9 are the introductory and concluding chapters, respectively. Chapters 2–7 are published articles and submitted manuscripts as outlined below;

1. **Karoyo, A. H.**; Borisov, A.; Hazendonk, P.; Wilson, L. D. Formation of Host-Guest Complexes of β -Cyclodextrin and Perfluorooctanoic Acid. *J. Phys. Chem. B* **2011**, *115*, 9511–9527. (Chapter 2)
2. **Karoyo, A. H.**; Sidhu, P.; Hazendonk, P.; Wilson, L. D. Characterization and Dynamic Properties for the Solid Inclusion Complexes of β -Cyclodextrin and Perfluorooctanoic Acid. *J. Phys. Chem. B* **2013**, *117*, 8269–8282. (Chapter 3)
3. **Karoyo, A. H.**; Sidhu, P.; Hazendonk, P.; Wilson, L. D. Characterization and Dynamic Properties for the Solid Inclusion Complexes of β -Cyclodextrin and Perfluorobutyric Acid. *J. Phys. Chem. C* **2014**, *118*, 15460–15473 (Chapter 4).
4. **Karoyo, A. H.**; Sidhu, P.; Borisov, A.; Wilson, L. D.; Hazendonk, P. Probing the Effect of Sodium Counterions on the Structure and Dynamics of the Solid inclusion complexes of β -Cyclodextrin and Sodium Perfluorooctanoate. *Manuscript in Preparation* (Chapter 5)
5. Wilson, L. D.; **Karoyo, A. H.** Structural Characterization of a Urethane-based “Molecular Accordion” in Aqueous Solution. Submitted to *Langmuir* August **2014** (Chapter 6)
6. **Karoyo, A. H.**; Wilson, L. D. Tunable Macromolecular-based Materials for the Adsorption of Perfluorooctanoic and Octanoic Acid Anions. *J. Colloid. Interf. Sci.* **2013**, *402*, 196–203. (Chapter 7)
7. **Karoyo, A. H.**; Wilson, L. D. Investigation of the Adsorption Processes of Alkyl and Perfluoroalkyl Carboxylates onto Macromolecular Imprinted Materials. Submitted to *J. Am. Chem. Soc.* August **2014** (Chapter 8).

In Chapter 2, the thesis firstly introduces the formation of the inclusion complexes between β -CD and PFCs, where two preparative methods were developed. PFOA is used as the model compound to prepare solid ICs with β -CD at the 1:1 and 2:1 host/guest mole ratios

using dissolution and slow cool methods. The β -CD/PFOA ICs were characterized using NMR and FT-IR spectroscopy, thermal analyses (DSC and TGA), and PXRD methods. The results were further complemented using solution NMR spectroscopy of the complexes in D_2O .

In chapter 3, the preparative conditions for the dissolution method developed in chapter 2 were optimized to obtain β -CD/PFOA ICs with greater phase purity, where the solid complexes were characterized as above. The phase purity of the complexes prepared by the modified dissolution method was assessed using thermal analyses and ^{19}F DP/MAS NMR spectroscopy at ambient and variable temperature conditions. Multinuclear and relaxation NMR techniques were used to provide unequivocal evidence for the inclusion of the PFOA guest within the CD cavity and to study the dynamics of the guest in the complexes, respectively.

In chapter 4, the modified dissolution method was used to prepare β -CD/PFBA complexes. These complexes were characterized using the techniques described above in the solid state and complemented by NMR spectroscopy in D_2O . The dynamics of the guest were further characterized through interpretation of the coupling constants from simulated ^{19}F PFBA spectrum to supplement the NMR relaxation data.

In chapter 5, the structure and dynamic properties of the inclusion complexes formed between β -CD and SPFO were studied. This work was aimed at probing the effect of counterions (i.e., Na^+ vs. H^+) on the structure of the complexes formed between SPFO and PFOA with β -CD, respectively. CIS values of $^1H/^{19}F/^{13}C$ nuclei in aqueous solution and the solid state were quantitatively used to elucidate the geometry of the guest in the 1:1 and 2:1 β -CD/SPFO complexes. Simulated ^{19}F CF_3 lines at MAS 25 kHz and variable dipolar coupling strengths were used in conjunction with deconvolution analyses of the CF_3 line shapes to probe the dynamics of the sodium-rich guest and its complexes with β -CD and to supplement NMR relaxation data. The physical, structural and dynamic properties for the PFOA, PFBA, and SPFO guests and their complexes with β -CD, respectively, were compared and tabulated (*cf.* Table 5.6).

In chapter 6, a soluble CD-based copolymer material was used as the host system, where the physicochemical properties of the copolymer in aqueous solution were characterized using various methods. The structure of the inclusion complexes formed between the soluble

copolymer with a model guest molecule (i.e. PNP) in aqueous solution was characterized using such techniques as 1-D/2-D NMR spectroscopy, ICD, and DLS.

In chapter 7, the adsorption properties of PFCs onto CD-based copolymer adsorbent materials were studied. PFOA was used as the model PFC guest due to its abundance as an environmental marker and the fact that this PFC has widely been studied from a toxicological viewpoint. In this study, both the soluble and insoluble copolymer materials (referred to as MIMs) were used as adsorbents, and the sorption results were compared to similar results for activated carbon adsorbents. As well, the adsorption properties of PFOA onto MIMs/GAC adsorbent systems were compared to the adsorption results of the hydrocarbon analogue (octanoic acid; OA).

Chapter 8 focused on characterizing the molecular details of the sorption interactions for the fluorocarbon/hydrocarbon carboxylate anions (PFOA/OA) with the MIMs, respectively. This study involved analyses of the host-guest interactions at the liquid-solid interface and the molecular structures related to the sorption of PFOA/OA onto the surface of the MIMs. The sorptive mechanism of PFOA onto MIMs was further probed by comparing its sorption behavior to that of PFOS, according to the nature of the head group.

1.9 References

1. Lehn, J. –M. *Science* **2002**, 295(5564), 2400–2403.
2. (a) Steed, J. W.; Atwood, J. L. *Supramolecular Chemistry: A Concise Introduction*. 2000. Chichester; New York; John Wiley and Reference therein; (b) Steed, J.W.; Atwood, J.L. In *Supramolecular Chemistry*, 2nd ed.; John Wiley & Sons, Ltd.: West Sussex, UK, 2009.
3. Fischer, E. Einfluss der Configuration auf die Wirkung der Enzyme, *Chem. Ber.* **1894**, 27(3), 2985–2993.
4. Pedersen C. J. Cyclic polyethers and their complexes with metal salts. *J. Am. Chem. Soc.* **1967**, 89(26), 7017–7036; Pedersen, C. J. *J. Am. Chem. Soc.* **1967**, 89, 2495–2496
5. Cram, D. J. Preorganization – from solvents to spherands. *Angew. Chem., Int. Ed. Engl.* **1986**, 25, 1039-1134; Cram, D. J. *Angew. Chem.* **1988**, 27(8), 1009–1020.
6. Vögtle, F. *Supramolecular Chemistry*, John Willey & Sons, Ltd: Chichester, 1991.

7. Atwood, J. L.; Steed, J. W. *Encyclopedia of Supramolecular Chemistry*. Vol 1, 2004, MerceL Dekker Inc. 270 Madison Avenue, New York.
8. <http://goldbook.iupac.org/C01097.html>
9. Taouss, C.; Thomas, L.; Jones, P. G. *Cryst. Eng. Comm.* **2013**, *15*(34), 6829–6836.
10. Knott, B. C.; Molinero, V.; Doherty, M. F.; Peters, B. *J. Am. Chem. Soc.* **2012**, *134*, 19544–19547.
11. Steed, J. W.; Turner, D. R.; Wallace, K. J. *Core Concepts in Supramolecular Chemistry and Nanochemistry*. John Wiley & Sons, Ltd. The Atrium, Southern Gate, Chichester, West Sussex, 2007, Ch. 1, Pg. 17–18.
12. Mele, A.; Malpezzi, L. *J. Am. Soc. Mass Spectrom.* **2000**, *11*, 228–236.
13. Chen, J.; Brooks III, C. L.; Scheraga, H. A. *J. Phys. Chem. B* **2008**, *112*(2), 242–249.
14. Meyer, E. A.; Castellano, R. K.; Diederich, F. *Angew. Chem. Int. Ed.* **2003**, *42*, 1210–1250
15. Ma, J. C.; Dougherty, D. A. *Chem. Rev.* **1997**, *97*, 1303–1324.
16. Motta, L.; De Vains, J-B. R.; Bavoux, C.; Perrin, M. *J. Chem. Crystallogr.* **1995**, *25*(7), 401–406.
17. Blokzijl, W.; Engberts, J. B. F. N. *Angew. Chem. Int. Ed. Engl.* **1993**, *32*, 1545–1579.
18. Rekharsky, M.; Inoue, Y. *Solvation Effects in Supramolecular Recognition*. John Wiley & Sons (Online).
19. Del Valle, E. M. M. *Process Biochem.* **2004**, *39*, 1033–1046
20. Szejtli, J. *J. Mater. Chem.* **1997**, *7*(4), 575–587
21. Singh, M.; Sharma, R.; Banerjee, U. C. *Biotechnol. Adv.* **2002**, *20*, 341–359
22. Szejtli, J. *Chem. Rev.* **1998**, *98*, 1743–1753
23. Loftsson, T.; Jarho, P.; Masson, M.; Jarvonen, T. *Expert Opin. Drug Deliv.* **2005**, *2*, 335–351.
24. Easton, C. J.; Lincoln, S. F. *Modified Cyclodextrins: Scaffolds and Templates for Supramolecular Chemistry*, World Scientific Publishing Company, London, 1999.
25. Wenz, G.; Strassnig, C.; Thiele, C.; Engelke, A.; Morgenstern, B.; Hegetschweiler, K. *Chem. Eur. J.* **2008**, *14*, 7202–7211; and references cited therein.
26. Wilson, L. D.; Verrall, R. E. *Langmuir* **1998**, *14*, 4710–4717.
27. Hirlekar, R.; Kadam, V. *J. Incl. Phenom Macrocycl Chem.* **2009**, *63*, 219–224.

28. Yu, Z.; Cui, M.; Yan, C.; Song, F.; Liu, Z.; Liu, S. *Rapid Commun. Mass Spectrom.* **2007**, *21*, 683–690.
29. Pereira, C. C. L.; Diogo, C. V.; Burgeiro, A.; J. Oliveira, P. J.; Marques, M. P. M.; Braga, S. S.; Paz, F. A. A.; Pillinger, M.; Goncalves, I. S. *Organometallics* **2008**, *27*, 4948–4956.
30. Baboota, S.; Agarwal, S. P. *J. Incl. Phenom Macrocycl Chem.* **2005**, *51*, 219–224.
31. Melani, F.; Bettinetti, G. P.; Mura, P.; Manderioli, A. *J. Inclusion Phenom. Mol. Recognit. Chem.* **1995**, *22*, 131–143.
32. Miyawaki, A.; Miyauchi, M.; Takashima, Y.; Yamaguchi, H.; Harada, A. *Chem. Commun.* **2008**, 456–458
33. Wenz, G. *Angew. Chem. Int. Ed. Engl.* **1994**, *33*, 803–822; and Refs cited therein.
34. Herrmann, W.; Schneider, M.; Wenz, G. *Angew. Chem. Int. Ed. Engl.* **1997**, *36*, 2511–2514.
35. Ogino, H. *J. Am. Chem. Soc.* **1981**, *103*, 1303–1304.
36. Harada, A.; Li, J.; Kamachi, M. *J. Am. Chem. Soc.* **1994**, *116*, 3192–3196
37. Harada, A.; Takashima, Y.; Yamaguchi, H. *Chem. Soc. Rev.*, 2009, *38*, 875–882.
38. Crini, G.; Morcellet, M. *J. Sep. Sci.* **2002**, *25*, 789–813; Crini, G. *Prog. Polym. Sci.* **2005**, *30*, 38–70.
39. Malefetse, T. J.; Mamba, B. B.; Krause, R. W.; Mahlambi, M. M. *Water SA.* **2009**, *35*(5), 729–734.
40. Crini, G. *Bioresource Technol.* **2003**, *90*, 193–198.
41. Crini, G.; Bertini, S.; Torri, G.; Naggi, A.; Sforzini, D.; Vecchi, C.; Janus, L.; Lekchiri, Y.; Morcellet, M. *J. Appl. Polym. Sci.* **1998**, *68*, 1973–1978.
42. Morin-Crini, N.; Crini, G. *Prog. Polym. Sci.* 2013, *38*, 344–368.
43. Mamba, G.; Mbianda, X. Y.; Govender, P. P. *Carbohydr. Polym.* **2013**, *98*, 470–476.
44. Mamba, B. B.; Krause, R. W.; Malefetse, T. J.; Sithole, S. P.; Nkambule, T. I. *Water SA.* **2009**, *35*(1), 117–119.
45. Asanuma, H.; Kakazu, M.; Shibata, M.; Hishiya, T.; Komiyama, M. *Supramol. Sci.* **1998**, *5*, 417–421.
46. Murai, S; Imajo, S; Inumaru, H; Takahashi, K; Hattori, K. *J. Colloid Interf. Sci.* **1997**, *190*, 488–490.

47. Sreenivasan, K. *Polym. Int.* **1997**, *42*, 22–24.
48. Connors, K. A. *In Binding Constants: The Measurement of Molecular Complex Stability*. Wiley: New York, 1987, Ch. 5.
49. Wilson, L. D.; Verrall, R. E. *Can. J. Chem.* **1998**, *76*, 25–34.
50. a) Szejtli, J.; Fenyvesi, E.; Zsardon, B. *Sturch/Sturke* **1978**, *30*, 127–131; b) Cserhati, T.; Oros, G.; Fenyvesi, E.; Szejtli, J. *J. Inclusion Phenom.* **1984**, *1*, 395–402.
51. Hirai, H.; Komiyama, M.; Yamamoto, H. *J. Inclusion Phenom.* **1984**, *2*, 655 Hirai, H.; Komiyama, M.; Yamamoto, H. *J. Inclusion Phenom.* **1984**, *2*, 655–660.
52. Ma, M.; Li, D. *Chem. Mater.* **1999**, *11*, 872–874.
53. Stoddart, J. F. et al. *Chem. Eur. J.* **1995**, *1*, 33–55.
54. Krause, R. W. M.; Mamba, B. B.; Bambo, F. M.; Malefetse, T. J. *Cyclodextrins: Chemistry and Physics*, 2010, Ed. Jie Hu.
55. Pesek, J. J.; Matyska, M. T. *SPE Sorbents and Formats: 2000*; Taylor & Francis Group LLC.
56. Wilson, L. D.; Mohamed, M. H.; Headley, J. V. *J. Colloid Interf. Sci.* **2011**, *357*, 215–222.
57. Job, P. *Ann. Chim.* **1928**, *9*, 113–120
58. Hammer, B. C.; Russell, R. A.; Warrenner, R. N.; Collins, J. G. *Eur. J. Biochem.* **1989**, *178*, 683–688.
59. Sohajda, T.; Hu, W. H.; Zeng, L. L.; Li, H.; Szente, L.; Noszal, B.; Beni, S. *Electrophoresis* **2011**, *32*, 2648–2654
60. Iacovino, R. Rapuano, F.; Caso, J. V.; Russo, A.; Lavorgna, M.; Russo, C.; Isidori, M.; Russo, L.; Malgieri, G.; Isernia, C. *Int. J. Mol. Sci.* **2013**, *14*, 13022–13041
61. Tatsuno, H.; Ando, S. *J. Phys. Chem. B* **2006**, *110*, 25751–25760.
62. Larionov, S. V. et al. *Chemistry for Sustainable Development* **2006**, *14*, 147–155
63. Bonefeld-Jorgensen, E. C. et al. *Environ. Health* **2011**, *10(88)*, 1–16.
64. Eftink, M.R.; Harrison, J.C. *Bioorg. Chem.* **1981**, *10*, 388–398.
65. Hattori, T.; Katai, K.; Kato, M.; Izume, M.; Mizuta, Y. *Bull. Chem. Soc. Jpn.* **1999**, *72*, 37–41.
66. Koito, Y.; Yamada, K.; Ando, S. *J. Incl. Phenom. Macrocycl. Chem.* **2013**, *76*, 143–150.
67. Fyfe, C. A.; Brouwe, D. H. *Can. J. Chem.* **2006**, *84*, 345–355.

68. Levebvre, F.; Mentzen, B. F. *Mater. Res. Bull.* **1994**, *29*, 1049–1056.
69. Rüdiger, V.; Schneider, H. -J. *Chem. Eur. J.* **2000**, *6*, 3771–1776.
70. Saalwächter, K. *Macromol. Rapid Commun.* **2002**, *23*, 286-291; Lu, J.; Mirau, P. A.; Tonelli, E. *Prog. Polym. Sci.* **2002**, *27*, 357–401.
71. Braga, S. S.; Gonçalves, I. S.; Herdtweck, E.; Teixeira-Dias, J. J. C. *New J. Chem.* **2003**, *27*, 597–601.
72. Lamcharfi, E.; Kunesch, G.; Meyer, C.; Robert, B. *Spectrochim. Acta A*, **1995**, *51*, 1861–1870.
73. Wang, X. M.; Schneider, H. -J. Vibrational Spectroscopy Studies on the Inclusional Complexation by β -Cyclodextrin. Coleman, AW. P543–546, 1998.
74. Sun, D. -Z.; Li, L.; Qiu, X. -M.; Liu, F.; Yin, B. -L. *Int. J. Pharm.* **2006**, *31*, 7–13.
75. Caira, M. R.; Griffith, V. J.; Brown, G. R.; Nassimbeni, L. R. *J. Incl. Phenom. Mol. Recogn. Chem.* 1996, *25*, 141–144.
76. Godínez, L. A.; Lin, J.; Muñoz, M.; Coleman, A. W.; Rubin, S.; Parikh, A.; Zawodzinski, Jr., T. A.; Loveday, D.; Ferraris, J. P.; Kaifer, A. E. *Langmuir*, **1998**, *14*, 137–144.
77. Tablet, C.; Dumitrache, L.; Minea, L.; Hillebrand, M. *Rev. Roum. Chim.* **2012**, *57*, 665–673
78. Harata, K.; Uedaira, H. *Bull. Chem. Soc. Japan*, **1975**, *48*, 375–378
79. Caira, M. N. *Rev. Roum. Chim.* **2001**, *46(4)*, 371–386; and references cited therein.
80. Saenger W. *J. incl. Phenom.* **1984**, *2*, 445–454; and references cited therein.
81. Saenger, W.; Beyer, K.; Manor, P. C. *Acta Cryst.* **1976**, *B32*, 120–128.
82. Huang, L.; Allen, E.; Tonelli, A. E. *Polym.* **1998**, *39*, 4857–4865.
83. Lo Nostro, P.; Santoni, I.; Bonini, M.; Baglioni, P. *Langmuir*, **2003**, *19*, 2313–2317.
84. Kamitori, S.; Toyama, Y.; Matsuzaka, O. *Carbohydr. Res.* **2001**, *332*, 235–240.
85. Harada, A.; Takashima, Y.; Yamaguchi, H. *Chem. Soc. Rev.* **2009**, *38*, 875–882.
86. Albinsson, B.; Michl, J. *J. Am. Chem. Soc.* **1995**, *117*, 6378–6379.
87. Watkins, E. K.; Jorgensen, W. L. *J. Phys. Chem. A* **2001**, *102*, 4118–4125; and references cited therein.
88. Albinsson, B.; Michl, J. *J. Phys. Chem.* **1996**, *100*, 3418–3429.

89. Neumann, F.; Teramae, H.; Downing, J. W.; Michl, J. *J. Am. Chem. Soc.* **1998**, *120*, 573–582.
90. Smith, G. D.; Jaffe, R. L.; Yoon, D. Y. *Macromolecules* **1994**, *27*, 3166–3173.
91. Okada, O.; Oka, K.; Kuwajima, S.; Tanabe, K. *Mol. Simul.* **1999**, *21*, 325–342.
92. Chen, K.-H.; Walker, G. A.; Allinger, N. L. *J. Mol. Struct. (THEOCHEM)* **1999**, *490*, 87–107.
93. Guo, W.; Fung, B. M.; Christian, S. D. *Langmuir* **1992**, *8*, 446–451.
94. S. Fujii, C. Polprasert, S. Tanaka, N.P.H. Lien, Y. Qiu, *J. Water Supply: Res. Technol. AQUA* **2007**, *56* (5), 313–326.
95. Shoeib, M.; Harner, T.; Webster, G. M.; Lee, S. C. *Environ. Sci. Technol. Lett.* **2011**, *45*(19), 7999-8005.
96. Schultz, M.M., Barofsky, D.F., Field, J.A. *Environ. Eng. Sci.* **2003**, *20*, 487–501.
97. Kissa, E. *Fluorinated Surfactants and Repellents*, Second Ed. Marcel Dekker, New York. 2001
98. Becker, A. M. Faculty of Biology, chemistry and Geosciences; University of Bayruth, 2008 Thesis.
99. Richardson, S. D. *Anal. Chem.* **2009**, *81*, 4645–4677.
100. Fujii, S.; Polprasert, C.; Tanaka, S.; Nguyen, P. H. L.; Yong, Q. J. *J. Water Supply Res. T.* **2007**, *56*, 313–326.
101. Ahrens, L.; Taniyasu, S.; Yeung, L. W. Y.; Yamashita, N.; Lam, O. K. S.; Ebinghaus, R. *Chemosphere* **2010**, *79*(3), 266–293.
102. Substance Flow Analysis for Switzerland; Perfluorinated surfactants perfluorooctanesulfonate (PFOS) and perfluorooctanoic acid (PFOA): Foen, Bern, **2009**.
103. US-EPA. Emerging Contaminants; Perfluorooctane sulfonate (PFOS) and Perfluorooctanoic acid (PFOA). May 2012.
104. Margot, R.; Berger, U.; Broman, D.; Cousins, I. T.; Nilsson, E. D.; McLachlana, M. *S. Environ. Chem.* **2011**, *8*, 381–388
105. Yoo, H.; Guruge, K. S.; Yamanaka, N.; Sato, C.; Mikami, O.; Miyazaki, S.; Yamashita, N.; Giesy, J. P. *Ecotox. Environ. Safe* **2007**, *72*(1), 26–36.
106. Beare-rogers, J.; Dieffenbacher, A.; Holm, J. V. *Pure Appl. Chem.* **2001**, *73*(4), 685–744.

107. Hoffmann, H.; Würtz, J. *J. Mol. Liq.* **1997**, *72*, 191–230.
108. Ellis, D.A.; Martin, J. W.; De Silva, A. O.; Mabury, S. A.; Hurley, M. D.; Andersen, M. P. S.; Wallington, T. J. *Environ. Sci. Technol.* **2004**, *38*, 3316–3321.
109. Lange, C.C., 2002. 3M Environmental Laboratory. Biodegradation Screen Study for Telomer Type Alcohols. Docket AR226–1149; U.S. Environmental Protection Agency: Washington, DC, November 6.
110. Hansen, K. J.; Johnson, H. O.; Eldridge, J. S.; Buttenhoff, J. L.; Dick, L. A. *Environ. Sci. Technol.* **2002**, *36*, 3316–3321.
111. Prevendouros, K.; Cousins, J. T.; Buck, R. C.; Korzeniowski, S. H. *Environ. Sci. Technol.* **2006**, *40*, 32–44.
112. Moody, C.A., Field, J.A. *Environ. Sci. Technol.* **1999**, *33*, 2800–2806.
113. Moody, C.A., Martin, J.W., Kwan, W.C., Muir, D.C.G., Mabury, S.A. *Environ. Sci. Technol.* **2002**, *36*, 545–551.
114. Boulanger, B.; Vargo, J. D.; Schnoor, J. I.; Hornbuckle, K. C. *Environ. Sci. Technol.* **2005**, *39*, 5524–5530.
115. Schultz, M. M.; Barofsky, D. F.; Field, J. A. *Environ. Sci. Technol.* **2006**, *40*, 289–295; Schultz, M. M.; Higgins, C. P.; Huset, C. A.; Luthy, R. G.; Barofsky, D. F.; Field, J. A. *Environ. Sci. Technol.* **2006**, *40*, 7350–7357.
116. Sinclair, E.; Mayack, D. T.; Roblee, K.; Yamashita, N.; Kannan, K. *Archiv. Environ. Contam. Toxicol.* **2006**, *50*, 398–410.
117. Loganathan, B. G.; Sajwan, K. S.; Sinclair, E.; Kumar, K. S.; Kannan, K. *Water Res.* **2007**, *41*, 4611–4620.
118. Martin, J. W.; Muir, D. C. G.; Moody, C. A.; Ellis, D. A.; Kwan, W.; Solomon, K. R.; Mabury, S. A. *Anal. Chem.* **2002**, *74*, 584–590.
119. Stock, N. L.; Lau, F. K.; Ellis, D. A.; Martin, J. W.; Muir, D. C. G.; Mabury, S. A. *Environ. Sci. Technol.* **2004**, *38*, 991–996.
120. Shoeib, M., Harner, T., Wilford, B.H., Jones, K.C., Zhu, J. *Environ. Sci. Technol.* **2005**, *39*, 6599–6606.
121. Stahl, T.; Mattern, D.; Brunn, H. *Environ. Sci. Eur.* **2011**, *23(38)*, 1–52; and references cited therein.
122. Tittlemier, S. A.; Pepper, K.; Edwards, L. *J. Agric. Food Chem.* **2006**, *54*, 1180–1185

123. Inoue, K. et al. *Environ. Health Perspect.* **2004**, *112*, 1204–1207.
124. Fei, C.; McLaughlin, J. K.; Tarone, R. E.; Olsen, J. *Environ Health Perspect.* **2007**, *115*, 1677–1682.
125. Karrman, A.; Ericson, I.; van Bavel, B.; Darnerud, P. O.; Aune, M.; Glynn, A.; Lignell, S.; Lindstrom, G. *Environ. Health Perspect.* **2007**, *115*, 226–230
126. So, M. K.; Yamashita, N.; Taniyasu, S.; Jiang, Q.; Giesy, J. P.; Chen, K.; Lam, P. K. S. *Environ. Sci. Technol.* **2006**, *40*, 2924–2929.
127. Guruge, K. S.; Yeung, L. W. Y.; Yamanaka, N.; Miyazaki, S.; Lam, P. K. S.; Giesy, J. P.; Jones, P. D.; Yamashita, N. *Toxicol. Sci.* **2006**, *89*, 93–107.
128. Fei, C.; McLaughlin, J. K.; Lipworth, L.; Olsen, J. *Hum. Reprod.* **2009**, *1*, 1–6.
129. Yang, Q; Abedi-Valugerdi, M.; Xie, Y.; Zhao, X. Y.; Muller, G.; Nelson, B. D.; DePierre, J. W. *Int. Immunopharmacol.* **2002**, *2*, 389–397.
130. Peden-Adams, M. M.; Keller, J. M.; EuDaly, J. G.; Berger, J.; Gilkeson, G. S.; Keil, D. E. *Toxicol. Sci.* **2008**, *104*, 144–154.
131. Dewitt, J. C.; Copeland, C. B.; Strynar, M. J.; Luebke, R. W. *Reprod. Toxicol.* **2009**, *27*, 409–416.
132. Kennedy, G. L. Jr.; Butenhoff J. L; Olsen G. W.; O'Connor J. C.; Seacat, A. M.; Perkins, R. G.; Biegel, L. B.; Murphy, S. R.; Farrar, D. G. *Crit. Rev. Toxicol.* **2004**, *34*, 351–384.
133. Lau, C.; Butenhoff, J. L.; Rogers, J. M. *Toxicol. Appl. Pharmacol.* **2004**, *198*, 231–241.
134. Lau, C., Thibodeaux, J. R.; Hanson, R. G.; Narotsky, M. G.; Rogers, J. M.; Lindstrom, A. B.; Strynar, M. J. *Toxicol. Sci.* **2006**, *90*, 510–518.
135. Butenhoff, J. L.; Kennedy, G. L. Jr.; Frame, S. R.; O'Connor, J. C.; York, R. G. *Toxicology* **2004**, *196*, 95–116.
136. Case, M. T.; York, R. G.; Christian, M. S. *Int. J. Toxicol.* **2001**, *20*, 101–109.
137. Kawashima, Y.; Kobayashi, H.; Miura, H.; Kozuka, H. *Toxicol.* **1995**, *99*, 169–178.
138. Kudo, N.; Iwase, Y.; Okayachi, H.; Yamakawa, Y.; Kawashima, Y. *Toxicol. Sci.* **2005**, *86*, 231–238
139. Gilliland, F. D.; Mandel, J. S. *J. Occup. Environ. Med.* **1993**, *35*, 950–954.
140. Bonefeld-Jorgensen, E. C. et al. *Environ. Health* **2011**, 10:88

141. Perfluorinated Compounds (PFC's), Maxxam Analytics International Corporation Technical Bulletin 2007, Missassauga Canada.
142. Palepu, R.; Reinsborough, V. C. *Can. J. Chem.* **1989**, *67*, 1550–1553.
143. Druliner, J. D.; Wasserman, E. *J. Fluorine Chem.* **1995**, *72*, 75–78.
144. Zhang, H. H.; Hogen-Esch, T. E.; Boschet, F.; Margailan, A. *Langmuir* **1998**, *14*, 4972–4977.
145. Palepu, R.; Richardson, J. M.; Reinsborough, V. C. *Langmuir* **1989**, *5*, 218–221.
146. Saint-Aman, E.; Serve, D. *J. Colloid Interface Sci.* **1990**, *138*, 365–375.
147. Junquera, E.; Aicart, E.; Tardajos, G. *Langmuir* **1993**, *9*, 1213–1219.
148. Nostro, P. L.; Santoni, I.; Bonini, M.; Baglioni, P. *Langmuir* **2003**, *19*, 2313–2317.
149. Geppi, M.; Pizzanelli, S.; Veracini, C. A.; Cardelli, C.; Tombari, E.; Lo Nostro, P. *J. Phys. Chem. B* **2002**, *106*, 1598–1605.
150. Yannakopoulou, K.; Mavridis, I. M. *Curr. Org. Chem.* **2004**, *8*, 25–34.
151. Bojinova, T.; Heinz, G.; Viguerie, N. L.; Rico-Lattes, I. *Carbohydrate Research* **2003**, *338*, 781–785.
152. Wang, E.; Chen, G.; Han, C. *Chin. J. Chem.* **2011**, *29*, 617–622.
153. Borisov, A. S.; Hazendonk, P.; Hayes, P. G. *J. Inorg. Organomet. Polym.* **2010**, *20*, 183–212.
154. Kozarac, Z.; Ćosović, B.; Gašparović, B. *Langmuir* **1991**, *7*, 1076–1081.
155. Schneider, H-J.; Hacket, F.; Rüdiger, V. *Chemical Reviews* **1998**, *98*, 1755–1786.
156. Wilson, L. D.; Mohamed, M. H.; Guo, R.; Pratt, D. Y.; Kwon, J. H.; Mahmud, S. T. *J. Agromedicine* **2010**, *15*(2), 105–116.
157. Watanabe, D.; Ohta, M.; Jang, Z. J.; Yonemochi, E.; Oguchi, T.; Yamamoto, K. *Chem. Pharm. Bull.* **1996**, *44*(4), 833–836.
158. Shahgholi, M.; Copper, C. L.; Callahan, J. *Supramol. Chem.* **1998**, *9*, 263–276
159. Harata, K. *Chem. Rev.* **1998**, *98*, 1803–1827
160. Rudinger, V.; Eliseev, A.; Svetlana, S.; Schneider, H, -J.; Blandamer, M. J.; Cullis, P. M.; Meyer, A. *J. Chem. Soc., Perkin Trans. 2*, **1996**, *10*, 2119–2123.
161. Moriwaki, H.; Takagi, Y.; Tanaka, M.; Tsuruho, K.; Okitsu, K.; Maeda, Y. *Environ. Sci. Technol.* **2005**, *39*, 3388–3392.

162. Yamamoto, T.; Noma, Y.; Sakai, S. I.; Shibata, Y. *Environ. Sci. Technol.* **2007**, *41*, 5660–5665.
163. Hansen, M. C.; Børresen, M. H.; Schlabach, M.; Cornelissen, G. *J. Soil Sediment* **2010**, *10*, 179–185.
164. Ochoa-Herrera, V.; Sierra-Alvarez, R. *Chemosphere* **2008**, *72*, 1588–1593.
165. Zhao, D.; Cheng, J.; Vecitis, C. D.; Hoffmann, M. R. *J. Phys. Chem. A* **2011**, *115*, 2250–2257.
166. Yu, Q.; Zhang, R.; Deng, S.; Huang, J.; Yu, G. *Water Res.* **2009**, *43*, 1150–1158.
167. Qu, Y.; Zhang, C.; Li, F.; Bob, X.; Liu, G.; Zhou, Q. *J. Hazard. Mater.* **2009**, *169*, 146–153.
168. Li, X.; Chen, S.; Quan, X.; Zhang, Y. *Environ. Sci. Technol.* **2011**, *45*, 8498–8505.
169. Deng, S.; Zhang, Q.; Nie, Y.; Wang, H. W. B.; Huang, J.; Yu, G. *Environ. Pollut.* **2012**, *168*, 138–144.
170. Qaqish, S. E.; Urquhart, S. G.; Lanke, U.; Brunet, S. M. K.; Paige, M. F. *Langmuir* **2009**, *25*, 7401–7409.
171. Asakawa, T.; Amada, K.; Miyagishi, S. *Langmuir* **1997**, *13*, 4569–4573.
172. Deng, S.; Shuai, D.; Yu, Q.; Huang, Y.; Yu, G. *Front. Environ. Sci. Eng. China* **2009**, *3*, 171–177.
173. Yu, Q.; Deng, S.; Yu, G. *Water Res.* **2008**, *42*, 3089–3097.
174. Senevirathna, S. T. M. L. D.; Tanaka, S.; Fujii, S.; Kunacheva, C.; Harada, H.; Shivakoti, B. R.; Okamoto, R. *Chemosphere* **2010**, *80*, 647–651.
175. Xiao, F.; Davidsavor, K. J.; Park, S.; Nakayama, M.; Phillips, B. R. *J. Colloid Interface Sci.* **2012**, *36*, 505–511.
176. Bruanuer, S.; Emmett, P. H.; Teller, E. *J. Am. Chem. Soc.* **1938**, *60*, 309–316.
177. Lowell, S.; Shields, J. E. *Characterization of Porous Solids and powders: Surface Area, Pore Size and Density.* Kluwer Academic Publishers,
178. Foo, K. Y.; Hameed, B. H. *Chem. Eng. J.* **2010**, *156*, 2–10.
179. Langmuir, I. *J. Am. Chem. Soc.* **1916**, *38(11)*, 2221–2295.
180. Freundlich, H.M.F. *J. Phys. Chem.* **1906**, *57*, 385–471.
181. Sips, R. *J. Chem. Phys.* **1948**, *16*, 490–495.

182. Levitt, M. L. *Spin Dynamics: Basics of Nuclear Magnetic Resonance*. 2nd ed. John Wiley & Sons Ltd. The Atrium, Southern Gate, Chichester, West Sussex, England, **2005**.
183. Keeler, J. *Understanding NMR Spectroscopy*. 1st Ed. John Wiley & Sons Ltd. The Atrium, Southern Gate, Chichester, West Sussex, England, 2005; Keeler, J. *Understanding NMR Spectroscopy*. 2nd ed. John Wiley & Sons Ltd. The Atrium, Southern Gate, Chichester, West Sussex, England, **2010**.
184. Friebolin, H. *Basic One- and Two-Dimensional NMR Spectroscopy*. 4th ed. WILEY-VCH Verlag GmbH & Co. KGaA, Weinheim, **2005**; and references cited therein.
185. Silverstein, R. M.; Webster, F. X.; Kiemle, D. J. *Spectrometric Identification of Organic Compounds*. 7th ed. John Wiley & Sons, Inc. USA; **2005**.
186. Balci, M. *Basic ¹H-¹³C-NMR Spectroscopy*. Elsevier B. V.; Amsterdam, The Netherlands, **2005**.
187. Emsley, J. W.; Feeney, J.; Sutcliffe, L. H. *Progress in NMR Spectroscopy*. Pergamon Press: New York, 1971; Vol. 7, p11.
188. Nanny, M. A.; Minear, R. A.; Leenheer, J. A. *Nuclear Magnetic Resonance Spectroscopy in Environmental Chemistry*. Oxford University Press, 1997, ch. 3.
189. J. A. Ripmeester and C. I. Ratcliffe, In “*Comprehensive Supramolecular Chemistry*”, Vol. 8, J. L. Atwood, J. E. D. Davies, D. D. MacNicol and F. Vogtle, Eds., Pergamon Press, Amsterdam, 1996, ch. 8.
190. R. E. Wasylishen, In “*Encyclopedia of Nuclear Magnetic Resonance*”, D. M. Grant and R. K. Harris, Eds., John Wiley & Sons, New York, 1996, p.1685.
191. David L. Bryce, Guy M. Bernard, Myrlene Gee, Michael D. Lumsden, Klaus Eichele, and Roderick E. Wasylishen *Can. J. Anal. Sci.Spectrosc.* **2001**, *46*, 46–82 and references cited therein.
192. Duer, M. *Solid State NMR Spectroscopy*. Blackwell Science Ltd. 23 John St London Ch1, pg61
193. Kolodziejewski, W.; Klinowski, J. *Chem. Rev.* **2002**, *102*, 613–628
194. Hartmann, S. R.; Hahn, E. L. *Phys. Rev.* **1962**, *128*, 2042–2053.
195. Scholz, I.; Hodgkinson, P.; Meier, B. H.; Ernst, M. *J. Chem. Phys.* **2009**, *130*, 114510–114517.

196. Shannon, I. J.; Harris, K. D. M.; Arumugan, S. *Chem. Phys. Lett.* **1992**, *196*, 588–594.
197. Ernst, M.; Zimmermann, H.; Meier, B. H. *Chem. Phys. Lett.* **2000**, *317*, 581–588.
198. Ernst, R. R.; Bodenhausen, G.; Wokaun, A. *Principles of Nuclear Magnetic Resonance in One and Two Dimensions*, Clarendon, Oxford, **1987**.
199. Haeberlen, U. *High Resolution NMR in Solids: Selective Averaging*. Academic Press New York, **1976**.
200. Mehring, M. *Principles of High Resolution NMR in Solids*, 2nd ed. Springer-Verlag, Berlin, **1983**.
201. Schmidt-Rohr, K.; Spiess, H. W. *Multidimensional Solid-State NMR and Polymers*. Academic Press, London, **1994**.
202. Reich, H. J.; Jautelat, M.; Messe, M. T.; Weigert, F. J.; Roberts, J. D. *J. Am. Chem. Soc.* **1969**, *91*, 7445–7454.
203. Birdsall, B.; Birdsall, N. J. M.; Feeney, J. *J. Chem. Soc. Chem. Commun.* **1972**, *6*, 316–317.
204. Ando, S.; Harris, R. K.; Scheler, U. *Fluorine-19 NMR of Solids Containing Both Fluorine and Hydrogen*. John Wiley & Sons, Ltd, Chichester, 2002.
205. <http://www.chem.wisc.edu/areas/reich/nmr/08-tech-01-relax.htm>
206. Gerig, J. T. *Fluorine NMR*. University of California, USA. Online 2001.
207. Hu, J. Z.; Zhou, J.; Deng, F.; Feng, H.; Yang, N.; Li, L.; Ye, C. *Solid State Nucl. Magn. Reson.* **1996**, *6*, 85–94.
208. Samson, A. O.; Chill, J. H.; Anglister, J. *Biochem.* **2005**, *44*, 10926–10934
209. Overhauser, A. W. *Physical Review* **1953**, *92*(2): 411–415.
210. Kaiser, R. *J. Chem. Phys.* **1962**, *39*(1), 2435–2442.
211. Nagayama, K.; Kumar, A.; Wuthrich, K.; Ernst, R. R. *J. Magn. Reson.* **1980**, *40*, 321–334.
212. Braunschweiler, L.; Ernst, R. R. *J. Magn. Reson.* **1983**, *53*, 521–528.
213. Jeener, J.; Meier, B. H.; Bachmann, P.; Ernst, R. R. *J. Chem. Phys.* **1979**, *71*, 4546–4553
214. Bax, A.; Davis, D. G. *J. Magn. Reson.* **1985**, *63*, 207–213.
215. Jeener, J.; Meier, B. H.; Bachmann, P.; Ernst, R. R. *J. Phys. Chem.* **1979**, *69*, 4546–4553.

CHAPTER 2

Manuscript no. 1

Description

In this work, the inclusion complexes of β -CD and PFOA were prepared using two methods, namely; dissolution and slow cool (*cf.* §2.3.2). The two protocol methods were developed by comparison for the preparation of β -CD/PFCs complexes. The β -CD/PFOA complexes were prepared at the 1:1 and 2:1 host/guest mole ratios and were characterized using NMR and FT-IR spectroscopic methods, thermal analyses (DSC and TGA), and PXRD.

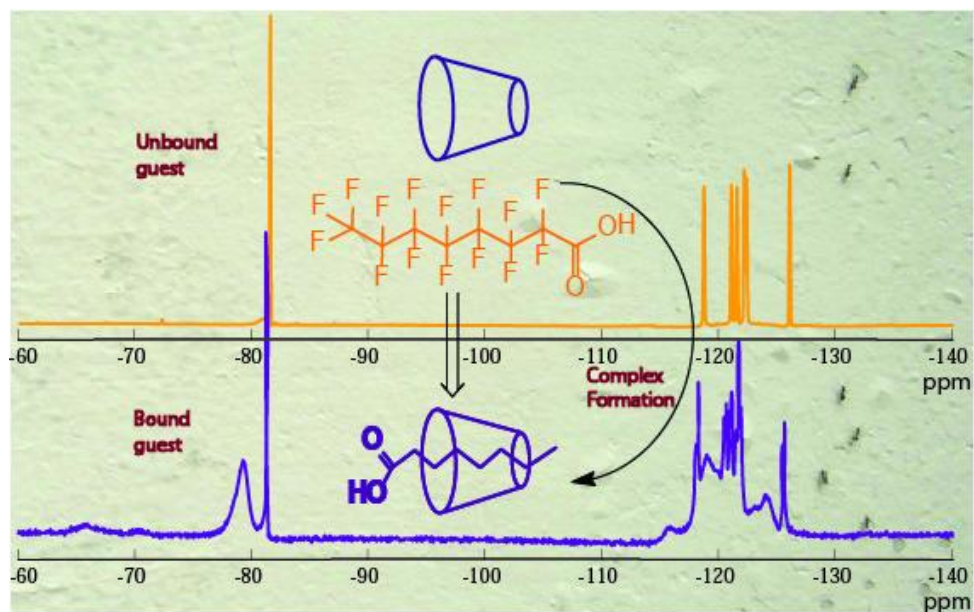
Author's Contribution

The idea to prepare and characterize the structure of the inclusion compounds formed between β -CD and PFCs was proposed by Drs. Lee Wilson and Paul Hazendonk (University of Lethbridge; UofL). The preparation and characterization of the β -CD/PFOA complexes were done entirely by myself. Most of the initial solid state NMR measurements for this work were done by Alex Borisov at the UofL NMR facility; while the solution NMR, FT-IR, PXRD, and thermal analyses were done by myself. I prepared the first draft of the manuscript and subsequent drafts were edited by Drs. Wilson and Hazendonk.

Relation of Manuscript 1 to Overall Objective of this Project

The work of this manuscript was very important to the overall objective of the research project because it served as a preliminary study to the preparation and characterization of the inclusion complexes of β -CD and PFCs. The β -CD/PFOA complexes were used as a model system for the preparation and characterization of β -CD/PFCs complexes; where two preparative methods, namely dissolution and slow cool, were developed.

Graphical Abstract



Research Highlights

- Two preparative methods (dissolution and slow cool) for the inclusion complexes between β -CD and PFOA were developed. The complexes were prepared at the 1:1 and 2:1 β -CD/PFOA mole ratios.
- The host-guest stoichiometry was estimated by acid/base titration in conjunction with gravimetry and revealed host/guest stoichiometric ratios (r) slightly exceeding 1:1 or less than 2:1. The host-guest ratios, $2:1 > r > 1:1$, arose from excess host, reduced guest, or formation of small amounts of both the 1:1 and 2:1 complexes.
- The β -CD/PFOA complexes formed in this work were generally found to be phase impure, i.e. there was a possible formation of inclusion and non-inclusion compounds, in addition to small amounts of unbound guest.

2. Formation of Host-Guest Complexes of β -Cyclodextrin and Perfluorooctanoic Acid

Abdalla H. Karoyo,[†] Alex S. Borisov,[‡] Lee D. Wilson,^{,†} and Paul Hazendonk^{*,‡}*

[†]University of Saskatchewan, Department of Chemistry, Saskatoon, SK, S7N 5C9, Canada.

[‡]University of Lethbridge, Department of Chemistry and Biochemistry, Lethbridge, AB, Canada.

*Corresponding Authors.

§Supplementary Information (Appendix A)

2.1 Abstract

Solid inclusion complexes of β -cyclodextrin (β -CD; host) and perfluorooctanoic acid (PFOA; guest) were prepared by comparison using two methods; dissolution and slow cool. The structure and dynamic properties of the β -CD/PFOA complexes were further characterized using $^1\text{H}/^{19}\text{F}/^{13}\text{C}$ NMR spectroscopy in aqueous solution and the solid state. Thermal analyses (DSC and TGA), PXRD, and FT-IR results provided complementary support that inclusion complexes were formed between β -CD and PFOA with variable stoichiometry and guest inclusion geometry. The dynamics of the guest molecules in the complexes prepared by the two methods were studied using ^{19}F DP/MAS solids NMR at variable temperature (VT). The guest molecules were observed to be in several different molecular environments, providing evidence of variable host/guest stoichiometry and inclusion geometry, in accordance with the preparation method of the complex and the conformational preference of PFOA. It was concluded from PXRD that β -CD and PFOA form inclusion complexes with “channel-type” structures. ^{19}F DP/MAS solids NMR at variable spin rate (VSR) was used to assess the phase purity of the two types of complexes (i.e., dissolution and slow cool) and it was revealed that slow cooling resulted in relatively pure phases. $^1\text{H}/^{19}\text{F}$ spectra for β -CD/PFOA complexes in solution were acquired using D_2O as the solvent system, where complexation-induced chemical shifts (CIS) of the ^1H and ^{19}F nuclei provided additional support for the formation of 1:1 and 2:1 β -CD/PFOA inclusion complexes. The dynamics of the guest molecule in the β -CD/PFOA complexes in D_2O solutions were probed using ^{19}F NMR at variable temperature and revealed variable guest conformations and exchange dynamics as a function of temperature, and the relative host/guest mole ratios.

2.2 Introduction

Many fluorine-containing compounds such as pharmaceuticals, pesticides, coatings, adhesives, and surface active agents represent a growing list of persistent organic pollutants (POPs) accumulating in Canadian and global environments. This is particularly true for recalcitrant perfluorinated compounds (PFCs) of the type; $\text{CF}_3\text{-(CF}_2)_n\text{-R}'$, where $\text{R}' = \text{CF}_2\text{-OH}$, COOH , CONH_2 , or $\text{CF}_2\text{-SO}_3\text{H}$. There is a considerable interest in developing innovative green strategies that involve the sequestration of such PFCs with suitable sorbent materials that exhibit good sorption capacity and molecular selectivity. For example, Deng et al. developed a molecular imprinted polymer with good sorption toward perfluorooctane sulfonic acid (PFOS; $\text{R}' = \text{CF}_2\text{-SO}_3\text{H}$) in aqueous solution.¹

PFCs of the type described above possess unique physicochemical properties, as compared with their hydrocarbon analogues since they are generally apolar and relatively inert owing to the stability of the C-F bond.² They generally have low vapor pressures (~ 10 mmHg for PFOA; $\text{R}' = \text{CF}_2\text{-CO}_2\text{H}$, at 25°C)³ and exhibit long residence times in the environment. The relatively high surface activity of PFCs confers their application as high performance surfactants, emulsifiers, and surface coatings for metals and paper.³ PFOA and PFOS are commonly found in soil, sediments, and aquatic environments because of their ability to infiltrate ground water to varying extents. Environmental contamination by PFCs was reported from direct discharge of industrial activities, for example, aqueous fire-fighting foams⁴ and wastewater effluents from water treatment plants.⁵ Consumption of contaminated foods and inhalation of air laden with volatile PFCs (e.g., perfluorinated alcohols and esters) that may be degraded to PFOA are regarded as other possible ingestion pathways.^{3,4}

Despite the human health and environmental concerns of PFOA, the distribution pathways are not fully understood; however, researchers have linked its exposure to cancer,⁶ birth defects, infertility,⁷ liver damage,⁸ and suppression of immunity.⁹⁻¹¹ Thus, there is a need to further study PFOA due to its widespread use and the associated health and environmental risks. Perfluorinated surfactants are generally more surface active than their hydrogenated analogues, as evidenced by their lower critical micelle concentrations (cmc). A comparison of the cmc values for PFOA (~ 0.0105 M),¹² SPFO (sodium perfluorooctanoate, 0.032 M),¹³ and sodium octanoate (~ 0.4 M),¹⁴⁻¹⁸ illustrates the differences in surface activity between PFCs and

hydrocarbon surfactants. The solution and colloidal behaviour of surface active agents may be attenuated by their complexation with host compounds such as cyclodextrins.¹⁹⁻²¹

Cyclodextrins (CDs) are macrocyclic (1→4)-linked oligomers of α -D-glucopyranose and the most commonly studied CDs are α -, β -, and γ -CD, consisting of 6-, 7-, and 8-glucopyranose units, respectively.²² β -CD displays the remarkable ability of forming stable inclusion complexes with perfluorinated alkanes, in part, because of the good “size-fit” complementarity²³ of the guest and the host. Complexes of β -CD/perfluoroalkyl carboxylates of variable chain length were concluded to form stable inclusion complexes in aqueous solution, according to $^{19}\text{F}/^1\text{H}$ NMR spectroscopy,^{13,24,25} viscometry,²⁵ conductometry,^{23,26,27} and sound velocity.²⁸ In particular, SPFO forms very stable 1:1 and 2:1 CD/SPFO inclusion complexes. In contrast to solution studies, there are relatively few detailed examples documenting the formation of solid state inclusion complexes between β -CD and perfluorinated guests (e.g., PFOA), and this may be attributed to challenges associated with obtaining good quality single crystals. Tatsuno et al.²⁹ have reported a solid state NMR study of CD inclusion compounds consisting of medium (C-9) chain and long (C-20) chain perfluorocarbon compounds; however, several other studies have examined modified perfluorocarbons^{25,30} and semi-fluorinated polymers^{31,32} in the solid state. Thus, solid state structural studies of inclusion compounds of CDs and PFCs remains largely unexplored. In contrast, a single crystal XRD (X-ray diffraction) study of β -CD/hydrocarbon carboxylic acids has been reported.³³ Recent advances in solid state NMR spectroscopy have provided the opportunity to obtain detailed structural information of such amorphous and crystalline host-guest materials.^{34,35}

In this article, we report a detailed study of the formation of inclusion complexes between β -CD and PFOA using two different preparation methods (dissolution and slow cool) using solid/solution state NMR, FT-IR, PXRD, and thermoanalytical (DSC and TGA) methods. The β -CD/PFOA complex is a very interesting system because it can adopt variable host-guest stoichiometry and inclusion geometry in condensed phases that depend on thermodynamic parameters such as relative host-guest concentrations and temperature. β -CD/PFOA complexes are amenable to the use of HFX solid state and multi-nuclear NMR techniques;³⁶ therefore, the dynamics of the free and complexed PFOA were investigated using ^{19}F NMR techniques in the solid and solution states at ambient and variable temperature conditions. ^{19}F DP/MAS solids

NMR at variable spinning rates (VSR) was used to study the phase purity and stability of the complexes prepared by the dissolution and slow cool methods, respectively.

2.3 Experimental Section

2.3.1 Materials

β -CD hydrate (~10 % w/w) and PFOA (96 %) were purchased from Sigma Aldrich Chemical Co., and were used as received without any further purification. The water contents of the materials were accounted for when preparing samples for each method. Potassium hydrogen phthalate (KHP) and sodium hydroxide were purchased from Merck and EMD chemicals, respectively.

2.3.2 Preparation of solid inclusion compounds

2.3.2.1 Method 1: *Evaporation/Dissolution*. In the dissolution method, β -CD and PFOA at the 1:1 and 2:1 (β -CD:PFOA) mole ratios were mixed in glass vials containing deionized water with continuous stirring and mild heating (~40 °C) to dissolve the solid mixtures. The solution mixtures were allowed to cool to room temperature and the solvent was gradually evaporated over several days (~4–5) to obtain the solid products. The solid products were ground into fine powders and characterized using NMR, DSC, TGA, PXRD and FT-IR.

2.3.2.2 Method 2: *Slow cool*. In slow cool method, saturated solutions of β -CD and PFOA (1:1 and 2:1 mole ratios) were prepared in glass vials using deionized water to form thick slurry. More deionized water was added drop-wise to the mixtures with continuous stirring under heating at ~80°C until clear solutions were formed. The resulting solution mixtures were slow-cooled over several hours (~2h) by placing the vials containing the mixtures in hot water bath housed within an insulated box to ensure gradual cooling of the solutions. The solvent of the slow-cooled solutions was air-evaporated to obtain the solid products.

2.3.3 Solution-state NMR Spectroscopy

Solution NMR experiments were performed on a 3-channel Bruker Avance (DRX) spectrometer operating at 500.13 MHz for ^1H and 470.30 MHz for ^{19}F . All ^1H NMR spectra were referenced externally to tetramethylsilane (TMS, $\delta = 0.0$ ppm) and ^{19}F spectra were referenced externally to

2,2,2-trifluoroethanol (TFE, $\delta = -79.21$ ppm). Samples for ^1H NMR were prepared in D_2O at pD ~ 5 in mole ratios of 1:1, 2:1 and 3:1 β -CD/PFOA. Samples for ^{19}F NMR were similarly prepared in D_2O at pD ~ 5 and at variable β -CD/PFOA mole ratios (1:1 and 2:1). The external reference TFE solutions for the ^{19}F NMR samples were prepared in D_2O at pD ~ 5 in sealed capillary tubes at a concentration of ~ 0.5 mM. All the NMR spectra obtained in the solution state were acquired at 295 K. Dry nitrogen gas was used to control the temperature for the VT ^{19}F NMR dynamic studies.

2.3.4 Solid-State NMR Spectroscopy

All solid state NMR spectra were obtained using a Varian INOVA spectrometer operating at 470.33 MHz (^{19}F) and 125.55 MHz (^{13}C). ^{19}F and ^{13}C solids NMR spectra were referenced externally to liquid hexafluorobenzene (not spun) (HFB, $\delta = -164.9$ ppm) and adamantane ($\delta = 38.5$ ppm), respectively. All samples were spun at the magic angle with a spinning rate between 10 kHz to 25 kHz using 2.5 mm and 3.2 mm Vespel rotors equipped with Kel-F turbine caps, inserts and seal screws. All NMR spectra were obtained using a 100 kHz sweep width with 8192 points in the FID, and were zero-filled to 64 k data points, unless stated otherwise. For all DP experiments, a one-pulse sequence was used where the 90° excitation pulse lengths for the ^{19}F channel were set to 2.5, 3.25, 4.25 and 4 μs , and relaxation delays were set to 4, 4, 4, and 8 s, respectively. $^{19}\text{F}\{^1\text{H}\}$ and $^{13}\text{C}\{^1\text{H}\}$ spectra of all solid samples were acquired using a two pulse phase modulation (TPPM) decoupling mode,^{34,37} where the powers of the ^1H and ^{19}F decoupled channels were set to 35.7 and 38.5 kHz, respectively, as determined by peak-to-peak voltage. Curve and width for the $^1\text{H} \rightarrow ^{13}\text{C}$ ramped CP experiments were set to 50 and 10000 Hz, respectively, and optimal Hartmann-Hahn matching conditions were achieved by setting contact times to 1 ms and CP powers to 54.2 kHz and 59.5 kHz for the proton and carbon channels, respectively.

2.3.5 DSC and TGA

Differential scanning calorimetry (DSC) of the native β -CD, PFOA and the inclusion complexes were acquired using a TA Q20 thermal analyzer, while the thermogravimetric analysis (TGA) was performed on a TA Q50 over a temperature range of 30 to 350 $^\circ\text{C}$. The scan rate for DSC was set to 10 $^\circ\text{C}/\text{min}$ while that for TGA was 5 $^\circ\text{C}/\text{min}$, and dry nitrogen gas was used in both

cases to regulate the sample temperature and sample compartment purging. DSC samples were run in hermetically sealed aluminum pans; whereas, an open pan geometry was used for the TGA measurements.

2.3.6 FT-IR Spectroscopy

Fourier Transform-IR spectra were obtained using a Bio-Rad FTS-40 spectrometer with a resolution of 4 cm^{-1} . All spectra were obtained with spectroscopic grade KBr which constituted ~80% (w/w) of the total sample. Samples were run as finely ground powders in reflectance mode.

2.3.7 PXRD

Powder XRD spectra were collected with a Rigaku Rotaflex RU-200 rotating anode X-ray diffractometer using Cu K α radiation ($\lambda = 0.154\text{ nm}$). The applied voltage and current were set to 40 kV and 80 mA, respectively. The samples were prepared by adding drops of hexane to the fine powder on the quartz sample holder to form a suspension resulting in a homogeneous film. The samples were mounted in a vertical pan configuration in the diffractometer, and XRD patterns were measured in the continuous mode for a 2θ angle range of $5\text{--}20^\circ$ with a scan rate of 0.5 degree/min . Finely powdered silica was used to calibrate the positions of the diffraction lines.

2.4 Results and Discussion

2.4.1 Characterization (DSC, TGA, FT-IR and PXRD)

2.4.1.1 Stoichiometry of the Inclusion Complexes

The stoichiometry of the β -CD/PFOA ICs was determined by acid/base titration in conjunction with gravimetry. The amounts of PFOA in the washed and unwashed complexes were evaluated by titration with 0.01 M NaOH (standardized with KHP) and the amounts of β -CD were estimated by difference. The preparations of 1:1 β -CD/PFOA complexes (i.e. dissolution vs slow cool) yielded the following host:guest ratios; unwashed ($0.95:1.0$ vs $1.1:1.0$) and washed ($1.2:1.0$ vs $1.3:1.0$), respectively. The 2:1 β -CD/PFOA complexes yielded the following host:guest ratios: $1.6:1.0$ vs $1.7:1.0$ (unwashed) and $1.6:1.0$ vs $1.7:1.0$ (washed) for the dissolution vs slow cool methods, respectively. In general, the products prepared by the slow cool method showed relatively greater β -CD:PFOA mole ratios compared to complexes prepared

by the dissolution method. The results are not straight forward to interpret unequivocally since the host:guest mole ratios >1:1 may arise from the occurrence of excess β -CD, reduced guest, or a possible contribution of 2:1 complexes.²⁸ In the case of 2:1, host/guest ratios <2:1 may arise due to the formation of small amounts of 1:1 complexes. Nonetheless, the experimental values for the 1:1 and 2:1 β -CD/PFC complexes are consistent with the relative magnitude of the binding constants (e.g., $\sim 7 \times 10^4 \text{ M}^{-1}$ (1:1) and $\sim 9 \times 10^2 \text{ M}^{-2}$ (2:1))^{24,38} in aqueous solution. The preparative methods for the 2:1 complex yield a mixture of 1:1 and 2:1 complexes; whereas, the preparative methods for the 1:1 product yield chiefly 1:1 complexes. Washing of the solid state products did not appear to affect the host/guest stoichiometry to any significant extent.

2.4.1.2 DSC and TGA

The DSC thermograms for native β -CD, PFOA, and the 1:1 and 2:1 β -CD/PFOA complexes prepared by the slow cool and dissolution methods are shown in Figure 2.1. In Figure 2.1a, the thermogram for β -CD hydrate shows two endothermic transitions centered at 110 and 320 °C, and are attributed to its dehydration and decomposition processes, respectively. PFOA shows three endothermic transitions at ~ 60 , 100, and 170 °C; these are attributed to the melting, dehydration and vaporization transitions, respectively. The DSC curves for the inclusion complexes of β -CD/PFOA prepared at the 1:1 and 2:1 mole ratios, using the slow cool (SC) and dissolution (D) methods are shown in Figure 2.1b and c, respectively. The thermograms in Figure 2.1b-c indicate the presence of several unique endothermic events between $\sim 120 - 250$ °C, as compared with native β -CD and PFOA. The thermal events are attributed to the variable phase transitions of the complex and the loss of hydrate water from β -CD occurring between $\sim 120 - 150$ °C. In the context of the above-noted phase transitions, this may refer to the relative spatial orientation of the guest within the host-guest complex.

The 1:1 complexes are consistently characterized by two features at ~ 180 and 210 °C, while the 2:1 complexes have only one feature at 210 °C. The presence of two thermal transitions supports the existence of additional topologies for the 1:1 complex. The slow-cooled complexes are characterized by sharp and pronounced features at 250 °C, which may reveal the greater phase purity for the complexes prepared by slow cool method compared to complexes prepared by dissolution (*cf.* Figure 2.1b).³⁹ According to the DSC results and table 2.1, the increased thermal stability of PFOA observed for the 1:1 and 2:1 complexes with β -CD provides

support that β -CD/PFOA inclusion complexes are formed, and this is consistent with the favourable complex formation stability.⁴⁰ The DSC thermograms of the β -CD/PFOA physical mixtures are presented in the supporting information in appendix A (Fig. A2.1), and are distinct since they reveal endotherms at ~ 60 °C corresponding to the melting of PFOA. The thermophysical properties of bound PFOA within the cavity of β -CD are anticipated to exceed those for pure PFOA due to the occurrence of favourable van der Waals interactions within the complex, as summarized in Table 2.1.

Table 2.1 DSC and TGA Thermoanalytical Data*

Systems	DSC Results (°C)				TGA Results (°C)	
	M.P./ Phase transitions*	Hydrate Water loss	Vaporization	Decompose	Melt (guest)	Melt (Host)
Native β-CD	-	110	-	~ 320	-	310
Unbound PFOA	60	100	~ 175	-	100	-
β-CD:PFOA (1:1)	Range*	$\sim 120 - 150$	~ 250	> 300	~ 220	320
β-CD:PFOA (2:1)	Range*	$\sim 120 - 150$	~ 250	> 300	~ 220	320

* indicates range between ~ 150 and 250 °C.

In Figure 2.2, the TGA results for PFOA and β -CD show mass losses ~ 100 and 320 °C, respectively. The differences in the two temperatures observed between DSC and TGA transitions are attributed to the sample pan configuration and the nature of the physical measurement. DSC is generally sensitive to thermal phase transitions whereas TGA reveals weight loss events due to chemical changes.

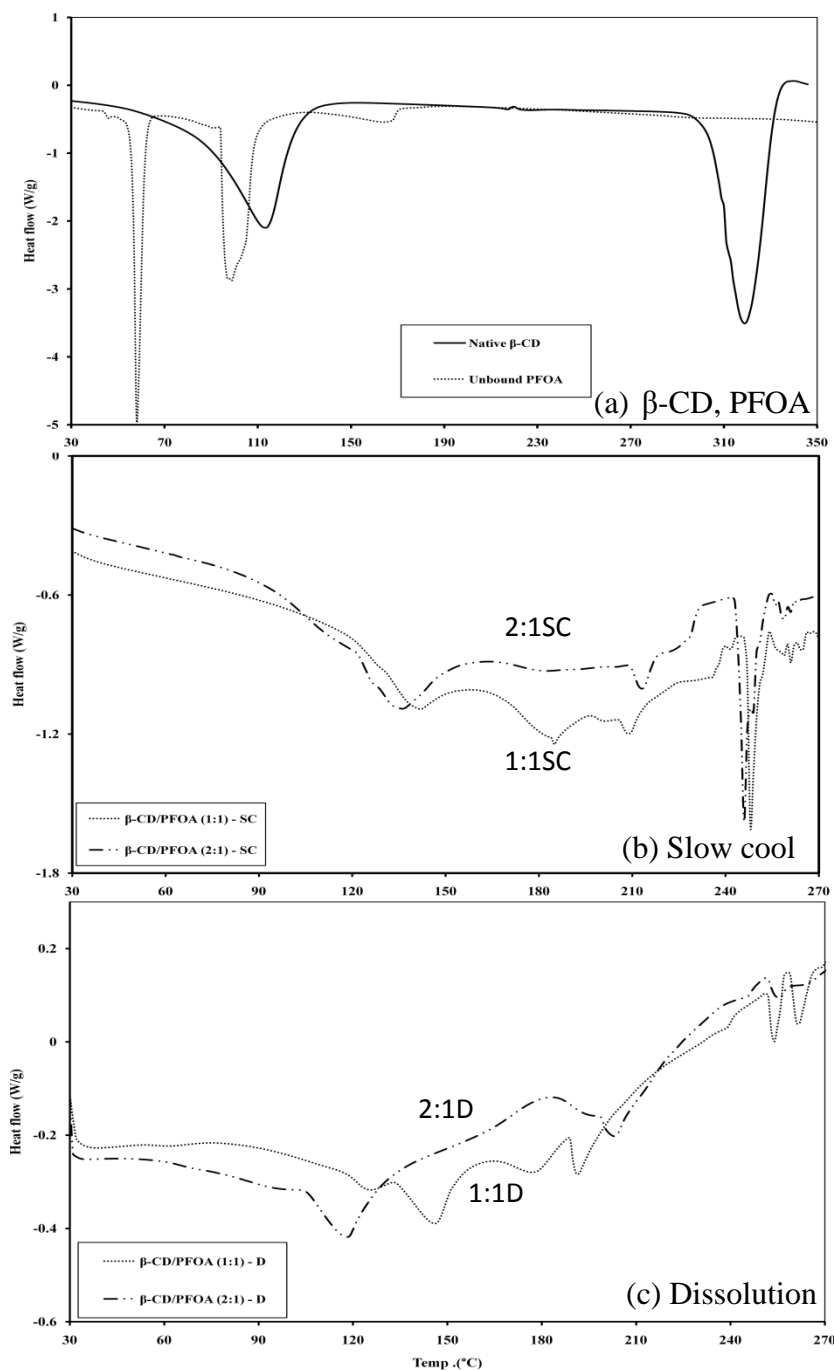


Figure 2.1 DSC thermograms of (a) native β -CD hydrate and PFOA, and the 1:1 and 2:1 complexes prepared by (b) slow cool, and (c) dissolution methods.

The thermal events at 220 °C in Figure 2.2 for PFOA for the 1:1 and 2:1 slow cooled complexes provide evidence for the volatilization of the guest; whereas, the event at 310°C is attributed to the decomposition of β -CD. The pure PFOA vaporizes immediately after dehydration at the conditions employed in the TGA experiments since the sample is heated in an

open system. However, the TGA results support the formation of inclusion complexes between β -CD and PFOA since the physicochemical properties of guests are altered in the bound state⁴¹ (*cf.* Table 2.1).

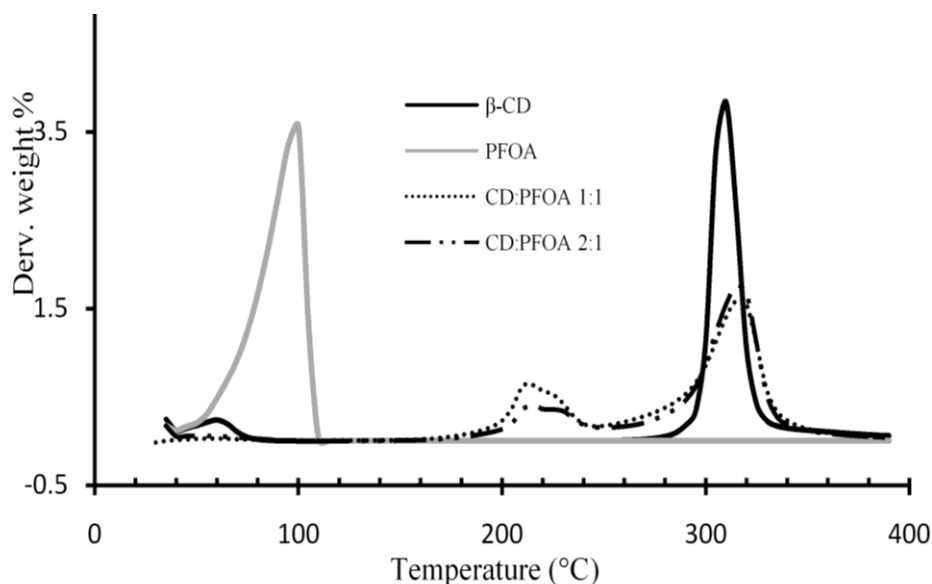


Figure 2.2 TGA plots for native β -CD hydrate, PFOA, and the 1:1 and 2:1 β -CD/PFOA complexes prepared by the slow cool method.

2.4.1.3 FT-IR

FT-IR spectroscopy can provide useful information on guest conformational preferences (*i.e. gauche vs trans* (also *anti*)) of the alkyl chain of the guest in the β -CD/PFOA inclusion complexes.²⁹ Figure 2.3 shows the FT-IR spectra for the native β -CD, pure PFOA, and both 1:1 and 2:1 β -CD/PFOA complexes in the region between 500–4000 cm^{-1} (left) and its enlargement of the area between 800–1400 cm^{-1} (right). The IR spectra of the physical mixtures are compared and are presented in the supplementary information (*cf.* Fig. A2.2). Figure 2.3 (L) shows the vibrational bands for the carbonyl group of pure PFOA at $\sim 1750 \text{ cm}^{-1}$, and its bound form in the 1:1 and 2:1 β -CD/PFOA complexes. The hydroxyl and C-H vibrational bands (~ 3300 and 2900 cm^{-1} , respectively) exhibit stronger intensity for the 2:1 β -CD/PFOA complex and the spectrum is consistent with the greater mole fraction of β -CD hydrate.

The expanded spectra reveal three bands for PFOA and its complexes with β -CD appearing at ~ 1230 (**1**), 1210 (**2**), and 1150 (**3**) cm^{-1} ; which have been previously reported.^{29,42,43} Vibrational bands **1** and **3** are attributed to CF_2 asymmetric and symmetric stretching; whereas, band **2** is assigned to the C-C and C-C-C stretching and bending modes, respectively. The most notable feature for the spectra in Figure 2.3 are the relative changes in intensity of the bands (**1–3**) for the 1:1 and 2:1 complexes. These bands are attributed to different conformational isomers (i.e. *anti*, *gauche* and *ortho*), as concluded for solid and liquid forms of C_4F_{10} ⁴⁴ where the *anti*- and *gauche*-conformers are favoured. The attenuation of band **2** at ~ 1210 cm^{-1} for the 2:1 complex indicates an alteration of the relative population of PFOA for the *trans*- and *gauche*-conformers in this complex. Tatsuno et al.²⁹ indicated that band **2** (1230 cm^{-1}) for the β -CD/ C_9F_{20} complex was attributed mainly to the *anti*-conformer. In the absence of quantum mechanical calculations and detailed spectroscopic evidence, the unequivocal assignment of the FT-IR bands of PFOA is beyond the scope of the present work, as compared to the published results for C_9F_{20} . In addition, the foregoing IR results for various vibrational bands are susceptible to potential changes in dipole moment when accompanied by a conformational change of PFOA as a consequence of changes in electron density.²⁴ The relative intensities of the β -CD and/or PFOA lines in the 1:1 and 2:1 complexes in Fig. 2.3 provide further evidence for variable conformations and dynamic properties of the guest.⁴⁵

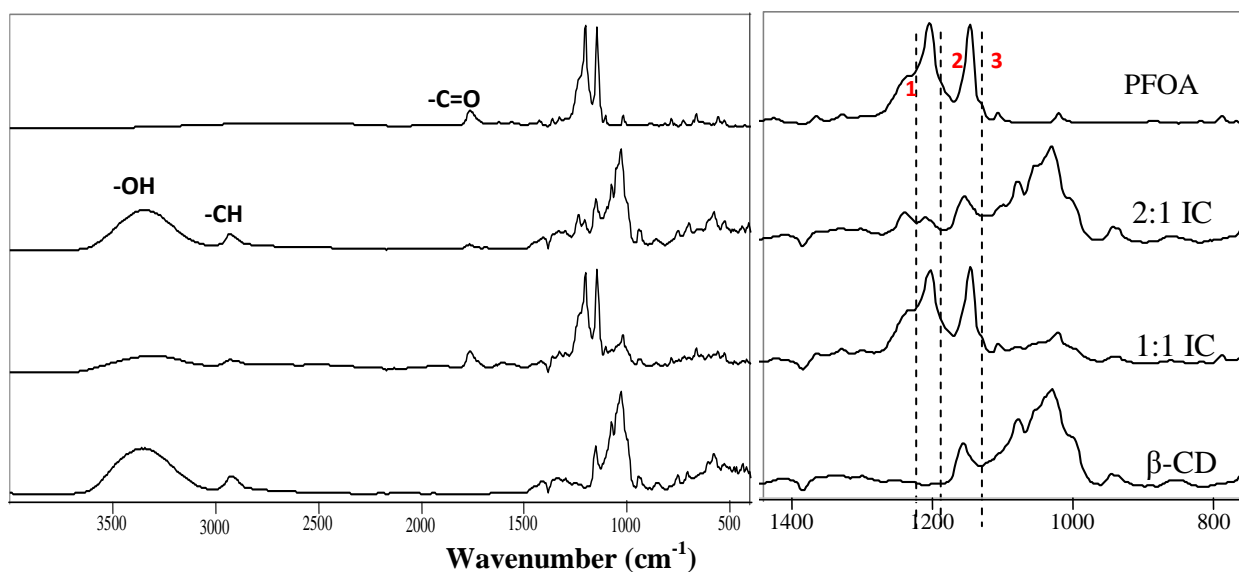


Figure 2.3 FT-IR spectra of native β -CD, 1:1 β -CD/PFOA complex, 2:1 β -CD/PFOA complex, and PFOA. The figure on the right is an expansion of the spectral region between 800 and 1400 cm^{-1} .

The FT-IR results in Figure 2.3 provide evidence that conformational changes of the perfluorocarbon chain in the 1:1 and 2:1 complexes are variable and may be attributed to *trans* and *gauche*-conformers of PFOA. There is a significant decrease in the contribution of the *gauche*- and/or *trans*-conformer of the PFOA chain in the 2:1 complex. The included PFOA chain in the 1:1 complex may adopt a similar configuration to that of the free PFOA (*cf.* Fig. 2.3) since a portion of the chain may extend outside of the β -CD macrocycle. In this regard, the PFOA chain in the 1:1 complex may adopt variable inclusion topologies with multiple configurations of the guest perfluoroalkyl chain, as previously concluded from the DSC results. Further elaboration on the conformational effects of the PFOA chain is made in the discussion of the NMR results (*vide infra*). The FT-IR results may provide a semi-quantitative estimate of the relative host-guest composition from the relative intensity of respective vibrational bands of certain functional groups. A more detailed understanding of the host-guest complex can be obtained from NMR studies of these systems.

2.4.1.4 PXRD

Figure 2.4 shows the PXRD patterns for β -CD, PFOA, and the 1:2, 1:1 and 2:1 β -CD/PFOA inclusion complexes that were prepared by slow cool and dissolution methods. The XRD patterns of the physical mixtures (*cf.* Fig. A2.3) are simple superpositions of the patterns of unbound host and guest, respectively. On the other hand, the XRD patterns for the 1:1 and 2:1 β -CD/PFOA complexes presented in Figure 2.4 represent unique solid phase materials, as evidenced by the appearance of unique diffraction lines. The XRD results for the complexes cannot be simulated from the additive patterns of the β -CD and PFOA components, and provides further evidence that the complexes are unique phases. The XRD pattern for β -CD exhibits major signatures at various 2θ values; 10.8° , 12.6° , 17.8° , and other minor signatures at higher 2θ values. Such patterns are characteristic of a “cage-type” lattice structure arising from the random packing arrangement of β -CD.⁴⁶⁻⁴⁸ The 1:1 and 2:1 complexes derived from slow cool and dissolution methods show slightly different XRD patterns, as indicated in Figure 2.4.

Two prominent peaks at $2\theta \sim 11.8$ and 17.8° observed for the 1:1 and 2:1 complexes indicate that “channel-type” crystalline structures⁴⁶⁻⁴⁹ may be formed, and are distinctly different from the PXRD pattern for β -CD hydrate. Such low angle scattering lines outlined above are consistent with spacings in the crystal framework ~ 5.0 and 7.60 \AA ($d = n\lambda/2\sin\theta$; where $\lambda =$

1.54Å), and these have been attributed to the inter- and intra-spacings of β -CD.²⁹ Furthermore, the XRD patterns for the 1:1 β -CD/PFOA complexes are characterized by a small shoulder above the main signature at $\sim 11.8^\circ$ (indicated by asterisk). The additional XRD lines for the 1:1 complexes provide further support for the existence of additional configurations due to the conformational preference of PFOA, in agreement with the DSC and FT-IR results. In the case of the 1:2 β -CD/PFOA complex, a low angle 2θ ($\sim 7.8^\circ$) signature is attributable to contributions arising from unbound PFOA and to those of the pure 1:1 complex. The general features of the PXRD spectra for the 1:1, 1:2, and 2:1 complexes resemble the results for native β -CD since the former are anticipated to have similar unit cell dimensions relative to that of the macrocyclic host, as observed in Figure 2.4.

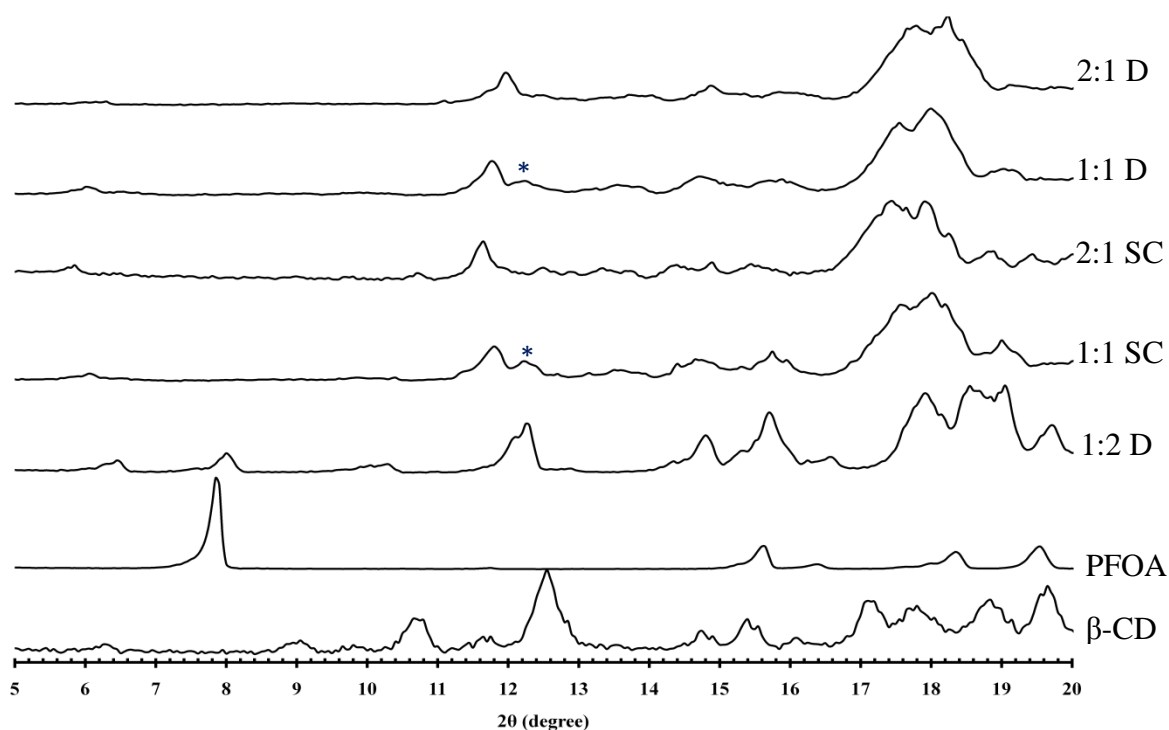


Figure 2.4 Powder X-ray Diffraction (PXRD) spectra for native β -CD, unbound PFOA, 1:2 β -CD/PFOA dissolution (D) complexes, 1:1 and 2:1 β -CD/PFOA slow cooled (SC) complexes, and 1:1 and 2:1 β -CD/PFOA dissolution (D) complexes.

2.4.2 Solution-state NMR

2.4.2.1 $^1\text{H}/^{19}\text{F}$ Solution NMR Characterization

Complexation-induced ^1H and ^{19}F NMR chemical shifts (CIS) in aqueous solution were used to provide evidence for the formation of inclusion complexes between β -CD and PFOA.

Figures 2.5 and 2.6 illustrate the respective ^1H and ^{19}F NMR spectra for PFOA and its inclusion complexes with $\beta\text{-CD}$. The assignment of the ^1H NMR signals agree with previous assignments.^{50,51} The ^1H NMR chemical shifts of the interior cavity protons (H_3 and H_5) of $\beta\text{-CD}$ in Figure 2.5 provide estimates of the extent of PFOA inclusion within the $\beta\text{-CD}$ cavity.^{50,51}

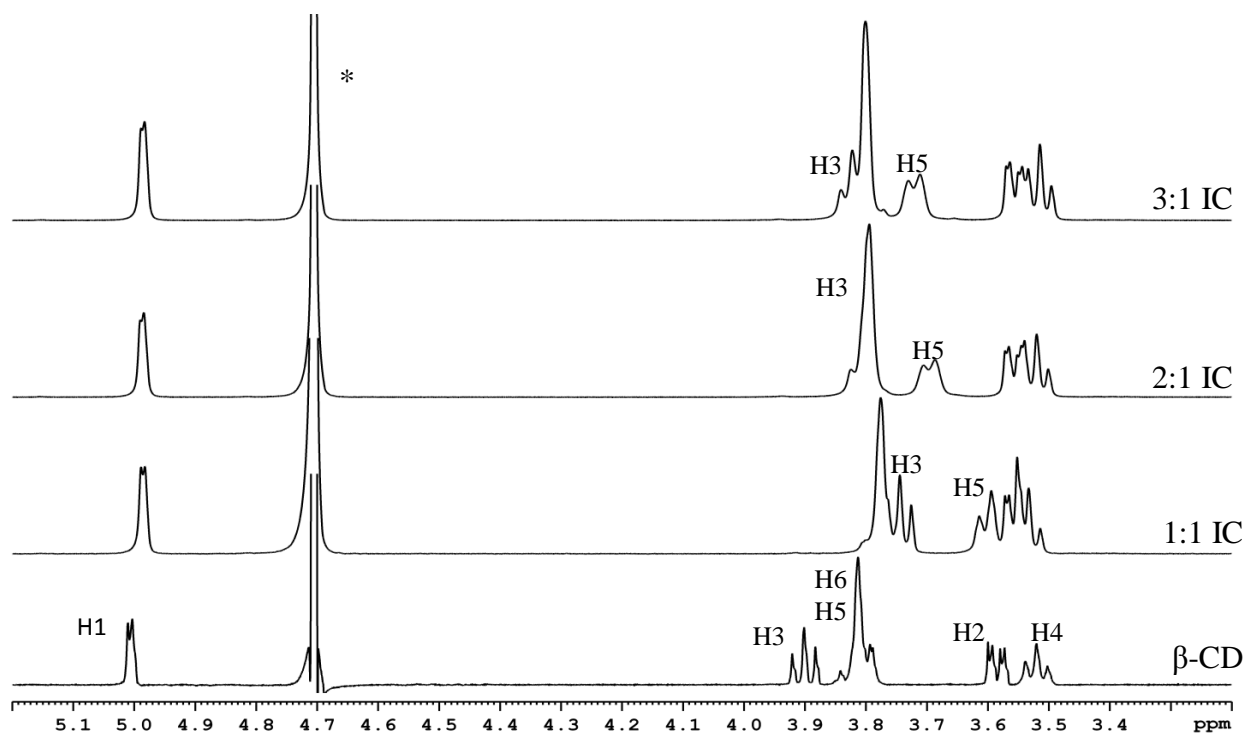
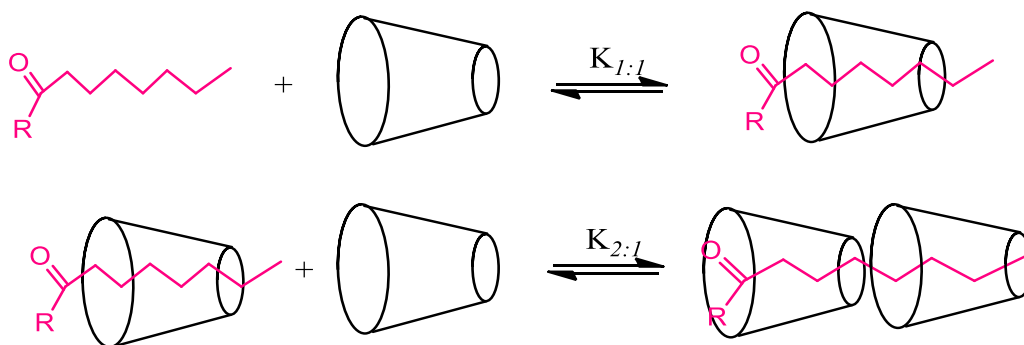
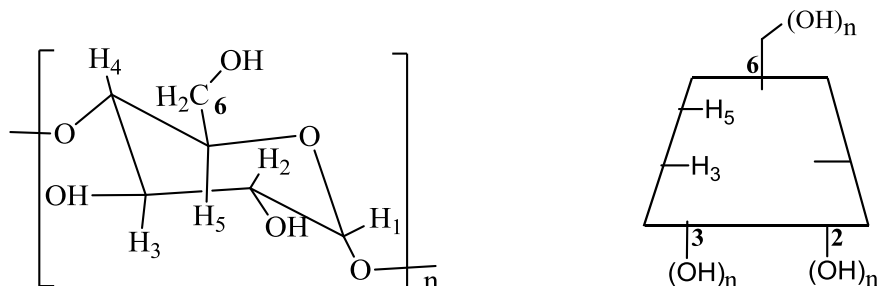


Figure 2.5 ^1H NMR in D_2O solutions for $\beta\text{-CD}$, the 1:1, 2:1, and 3:1 $\beta\text{-CD}$ /PFOA inclusion compounds acquired at $\text{pD}\sim 5$ and 295K; where * indicates HOD signal.



Scheme 2.1 The formation of a host-guest complex is shown for $\beta\text{-CD}$ (toroid) and a perfluorinated guest molecule according to a 1:1 and 2:1 equilibrium binding process where K_i are the corresponding equilibrium binding constants for each host-guest stoichiometry. In the case of perfluorooctanoic acid (PFOA); $\text{R} = \text{-OH}$. The relative dimensions of the $\beta\text{-CD}$ macrocycle and PFOA are not drawn to scale.

Scheme 2.1 illustrates the formation of a β -CD/PFC inclusion complex, where K_i is the equilibrium binding constant. Scheme 2.2 outlines the molecular structure of β -CD structure with a schematic side view showing the interior cavity host protons.



Scheme 2.2 Representations of the supramolecular structure of β -CD structure. The left hand structure refers to the oligomer where $n = 7$ and the right hand structure represents the toroidal shape of the macrocycle.

The results illustrated in Figure 2.5 are consistent with the fact that the guest molecule displaces the polar solvent from the host cavity according to the upfield chemical shifts of the complex for the H_3 and H_5 protons (*cf.* Scheme 2.2). The shift of these protons to higher field is a consequence of their increased chemical shielding effects resulting from the guest complexation process.⁴² The inclusion of an apolar PFOA guest molecule within the apolar cavity of β -CD is thermodynamically favoured according to the hydrophobic effect.²⁹ However, as the mole ratio of the host increases beyond the 1:1 ratio (i.e. for 2:1 and 3:1 complexes), the intra-cavity protons (H_3 , H_5) become less shielded and move to higher frequency (downfield) with respect to the 1:1 complex because of the greater mole fraction contribution of the unbound host. Note that the observed chemical shift is a weighted average of the bound and unbound species.^{24,42} In contrast, the 1:1 complex shows the most attenuated CIS effects for the H_3 and H_5 nuclei, and this is due to the increased steric and shielding effects and the variable conformation of the PFOA chain²⁴ (*cf.* Scheme 2.1).

The ^{19}F NMR results in Figure 2.6 reveal somewhat different shielding/deshielding patterns for the 1:1 and 2:1 complexes, and further support the occurrence of variable stoichiometry and conformational effects of the PFOA chain. Perfluorinated alkyl chains in the solid state have been reported to assume helical (*gauche*) and zigzag (*trans*) conformations for long chains ($C > 12$) and short chains ($C \leq 8$), respectively.⁴² A mixture of conformations (*gauche* and *trans*) may be present in intermediate chain lengths of 8–12 carbon atoms.⁵² The

helical structure was shown to be the stable form for PFOA⁵³ and PFOS⁵⁴ according to density functional theory (DFT) and semi-empirical molecular calculations, respectively. The assignment of ¹⁹F signals for long chain PFCs may be difficult due to the long range couplings (over at least four bonds),⁵⁵ and possible spectral overlap of resonance lines. However, the assignment of the ¹⁹F spectrum of PFOA in Figure 2.6a is in good agreement with previous results by Goecke et al.⁵⁶ and Buchanan et al.⁵⁷

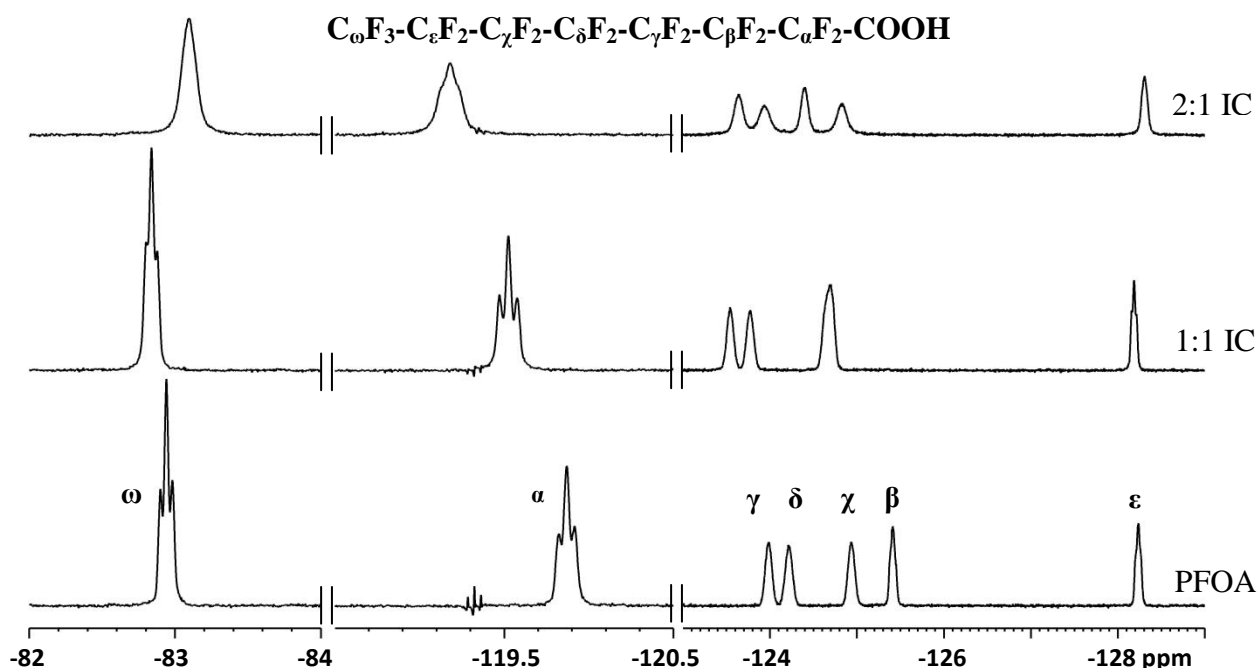


Figure 2.6 Expanded and assigned ¹⁹F solution NMR spectra of PFOA, the 1:1 and 2:1 β -CD/PFOA inclusion compounds acquired at pD ~5 and 295 K.

In general, complex formation between PFOA and β -CD results in downfield shifts of most of the ¹⁹F resonances with respect to unbound guest. The contribution of van der Waals interactions presents the largest effects on ¹⁹F chemical shifts and depends on the polarizability of the solvent. Fluorine is highly polarizable in bulk aqueous solvent compared to the CD environment, particularly near the rim which is composed of hydrocarbon (C-H) and hydroxyl groups. Therefore, the guest molecule experiences reduced van der Waals interactions near the CD rim resulting in increased chemical shifts. Furthermore, van der Waals interactions between

the guest and ether-like oxygens in the apolar interior of CD will result in shielding of the ^{19}F nuclei in its environment.

The chemical shift changes for the $\text{C}_\alpha\text{F}_2$ group are affected by the inductive effects of the carboxylate ion due to H-bonding interactions with the -OH groups of CD and/or bulk aqueous solvent. The result is a downfield shift of the $\text{C}_\alpha\text{F}_2$ resonance. The chemical shifts of the ^{19}F nuclei are also affected by the conformation of the guest. The end-to-end stacking of β -CD in the 2:1 complex (*cf.* Scheme 2.1) will force PFOA to adopt an extended *all-trans* conformation in order to occupy the inclusion sites of two host macrocycle moieties. This conformational change from *gauche* to *trans* results in the maximization of the through-space F-F distance between neighboring CF_2 groups and subsequent optimization of favourable van der Waals interactions within the β -CD interior.¹³ A combined *all-trans* conformation (deshielding) of the perfluorocarbon chain and the occurrence of favourable van der Waals interactions within the CD interior (shielding) for the 2:1 complex may result in a composite deshielding/shielding effect.

In the case of the 1:1 complex, the deshielding effect observed for the C_βF_2 group may be associated with the loss of the γ -*gauche* shielding effect that is commonly observed for alkyl carboxylate groups in the *gauche* configuration,⁵⁸⁻⁶⁰ as the PFC chain untwists itself. Knochenhauer et al. have shown that perfluorocarbon chains unwind from a helical to an extended chain configuration when packed in a periodic lattice.⁶¹ The *gauche/trans* conformational inter-conversion of the perfluorocarbon chain of the complexes is consistent with the IR results shown in Figure 2.3. In the 1:1 β -CD/PFOA complex, unequal populations of the helical and zigzag conformers of PFOA may exist.⁵²

The chemical shift of the terminal CF_3 group in the complexed state may reveal the proximity of the perfluorocarbon chain relative to the interior or the periphery of the host.¹³ The observed chemical shifts in Figure 2.6 indicate that the CF_3 group in the 2:1 inclusion complex is in closer contact with the interior of the apolar CD cavity than within the bulk solvent environment. The interior of CD is composed of ether-like oxygens which can take part in van der Waals interactions with the fluorines of the guest, as previously described. Note that the influence of conformational change is minimal in the case of the CF_3 group. In contrast to the 2:1 complex, the CF_3 group in the 1:1 inclusion complex can reside near the rim of the CD macrocycle (*cf.* Scheme 2.1) or in the extra-cavity environment in the bulk solvent. The

environment near the CD rim has a small polarizability compared to that of the bulk aqueous phase. Such an environment will result in reduced van der Waals interactions between the fluorocarbon guest and the CD causing deshielding of the CF₃ group. The chemical shift pattern of the guest for the 1:1 and 2:1 complexes is consistent with the length of β-CD cavity (~7.9 Å)²⁹ which is about one half of the extended chain length of PFOA.

The overlapping signals of the C_γF₂ and C_βF₂ groups in the 1:1 complex in Figure 2.6 and the variable line shapes of the ¹⁹F signals for PFOA in the 1:1 and 2:1 complexes may be attributed to the differences in the conformation and geometry of the PFOA guest in the complexes geometries. These dynamics are further explained in the VT NMR studies. However, the CIS values provide strong evidence that complexes are formed between β-CD and PFOA in aqueous solution. The results in Figure 2.6 are consistent with reported CIS values for β-CD/SPFO system.²⁴

2.4.2.2 Solution NMR Dynamics

The motional dynamics of PFOA in the complexed state were probed by ¹⁹F NMR at variable temperature (VT) in aqueous solution. Figure 2.7 shows ¹⁹F (VT) NMR stack plot results for complexes of β-CD and PFOA at the 1:1 mole ratio. There is an overall increase of the ¹⁹F chemical shifts as the temperature is increased. The downfield trend in the NMR chemical shifts may be attributed to the conformational changes of the perfluorocarbon chain. According to ¹⁹F (VT) NMR and spin relaxation studies in solution, Ellis et al. suggested that PFC chains may adopt a helical twist (*gauche*) conformation;⁵² however, slow untwisting of the helix may occur, and the perfluorocarbon chain may adopt an *all-trans* conformation at elevated temperatures.^{61,62} Bunn and Howell concluded from their XRD studies that PFC chains undergo variable rotation about the chain axes (helical conformation) and longitudinal zigzag displacement at temperatures above ambient conditions.⁶² Thus, temperature effects may induce CF₂ groups with variable conformations. The helical nature of perfluorocarbon chains is generally explained by the greater van der Waals radius of fluorine relative to that of hydrogen, as well as the correspondingly greater repulsive interactions between alternating CF₂ groups.^{61,62} The helical structure can be viewed as the rotation about the perfluorocarbon chain in an attempt of the chain to increase the distance between alternate CF₂ groups and minimize the repulsive interactions.

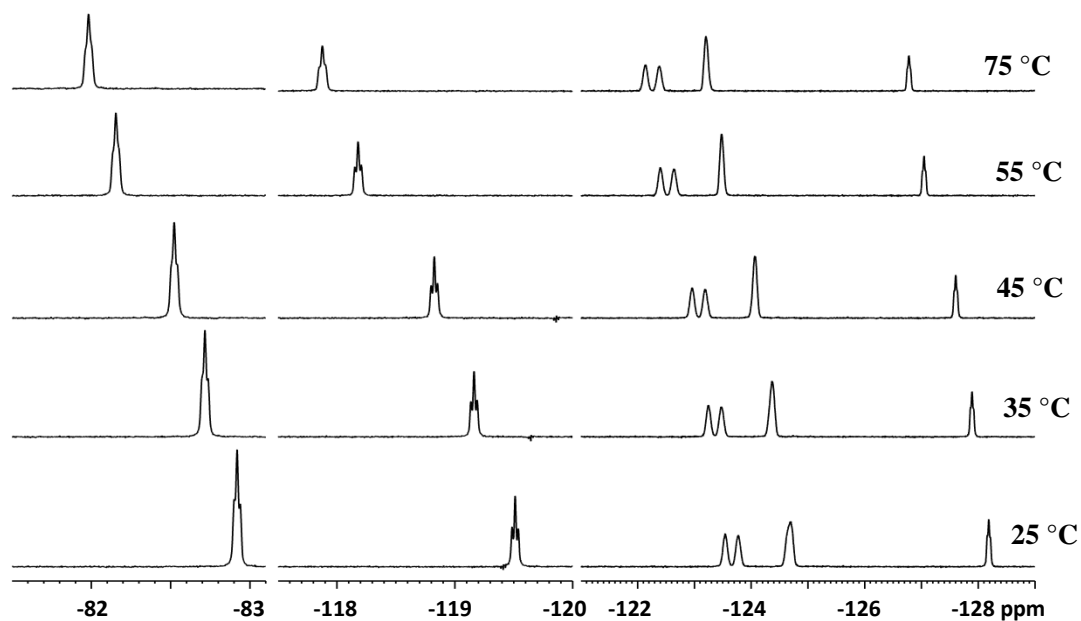


Figure 2.7 ^{19}F NMR spectra at variable temperature conditions for the 1:1 β -CD/PFOA complex in D_2O at pD \sim 5 (heating cycle from 25 $^\circ\text{C}$ to 75 $^\circ\text{C}$).

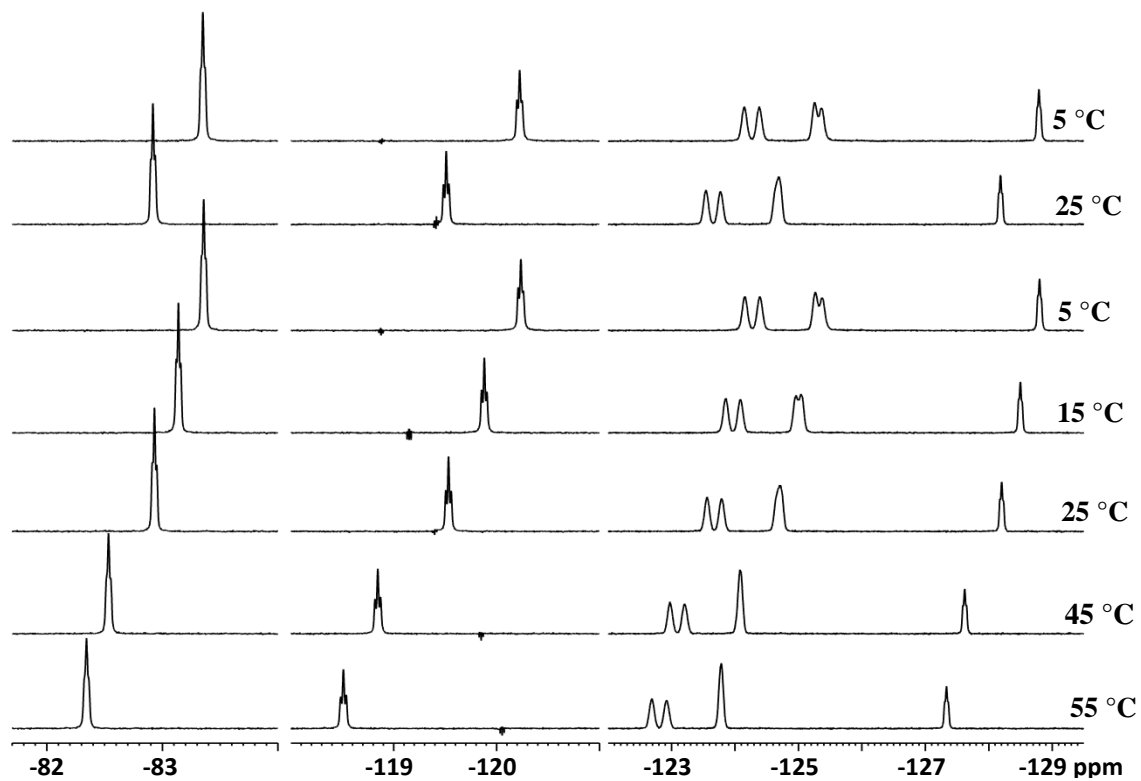


Figure 2.8 ^{19}F NMR spectra at variable temperature for the 1:1 β -CD/PFOA complex in D_2O at pD \sim 5 (cooling cycle from 55 $^\circ\text{C}$ to 5 $^\circ\text{C}$).

In Figure 2.7, the CD-bound PFOA chain can be interpreted as undergoing a conformational change from *gauche* to an extended *all-trans* configuration at elevated temperatures. This is consistent with the downfield shifts of the ^{19}F signals as the temperature is increased. Apart from the chemical shift changes, another unique feature is the overlap and separation of the C_χF_2 and C_βF_2 (*cf.* Figure 2.6) signals at ca. -125 ppm as a function of temperature and this is similarly observed in the stack plots of Figures 2.8–2.10. As the temperature increases, averaging and sharpening of the ^{19}F signals for the C_χF_2 and C_βF_2 is observed. The results are attributed to the increased motional dynamics (i.e. shorter correlation time) for the 1:1 complex in relation to that of the 2:1 complex because of the difference in relative molecular weights. Furthermore, the guest molecule in the 1:1 complex may experience less restricted dynamics because it can exist in the extra-cavity environment. The 1:1 and 2:1 complexes are expected to be stable at and above the temperature conditions employed for the VT NMR studies according to the DSC results. The positions of C_χF_2 and C_βF_2 may be regarded as pseudo-symmetric points along the perfluorocarbon chain, and for temperatures below 15 °C (Figure 2.8) these signals start to separate. This is attributed to changes in the conformational preference of the perfluorocarbon chain about the C_χ and C_β positions. The presence of a conformational dependence (i.e., coiled and uncoiled forms) of the γ -*gauche* shielding effect at the C_βF_2 group may contribute to the overlap and separation of the $\text{C}_\chi\text{F}_2/\text{C}_\beta\text{F}_2$ resonance lines for these temperature conditions. The reversibility of the exchange dynamics is shown by the heating and cooling cycle between 5 and 25 °C in Figure 2.8.

In contrast to the 1:1 complex, a different spectral pattern is observed for the 2:1 complex where the C_χF_2 and C_βF_2 signals overlap at higher temperatures (*cf.* Figure 2.9). At low temperatures, the motional dynamics of the PFOA molecule may have greater variability given the longer “channel-like” host space of two β -CD molecules. Additionally, the greater molecular weight of the 2:1 complex results in a decreased tumbling rate, which in turn results in broader resonance lines accompanied by the divergence of the C_χF_2 and C_βF_2 signatures at ambient temperature. As the temperature is increased, the C_χ and C_β methylene groups undergo further conformational changes due to the increased motional dynamics and the formation of a 1:1 complex where a portion of the PFOA chain extends outside of the β -CD cavity. These factors result in the overlapping of the C_χF_2 - C_βF_2 signals observed at higher temperatures. However, a more quantitative study of the relaxation times (T_1 , T_2 , $T_{1\rho}$) and the coupling constant

measurements of the ^{19}F groups of interest (*cf.* chapter 3 - 5), along with 2-D NMR experiments may be required to further characterize the conformational features adopted by these host-guest systems.

A distinct feature shown for the 2:1 complex is the broadening of the ^{19}F signals at temperatures below 15 °C (Figure 2.10) and this is due to the attenuation of the exchange kinetics observed for the 2:1 complexes (*cf.* Figure 2.6). The decreased tumbling rate for the 2:1 complex discussed earlier results in an increased correlation time (τ_c) that yields broader resonance lines at reduced temperatures, and may be attributed to reduced exchange kinetics of the guest between the bulk and inclusion sites of β -CD. Previous studies have shown that the T_1 values of bound guest for 1:1 and 2:1 complexes are markedly different relative to the unbound guest.⁵⁹ In general, the variable temperature studies provide support that the PFC chains of PFOA may interconvert between *all-trans* and *gauche* conformations during the heating and cooling cycles.

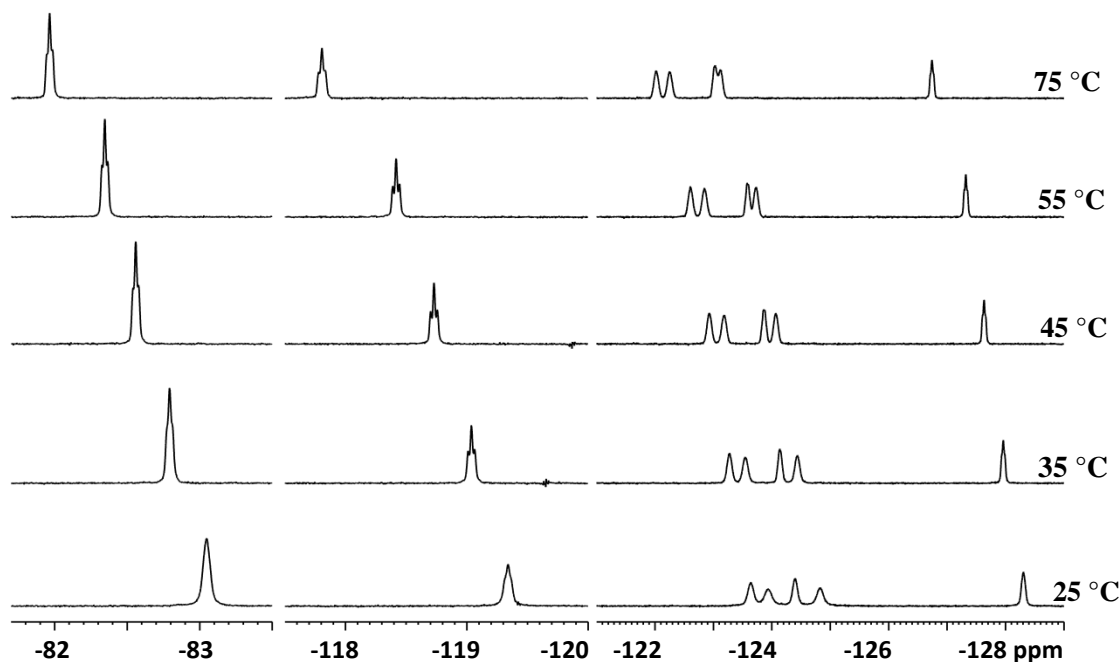


Figure 2.9 ^{19}F NMR spectra at variable temperature for the 2:1 β -CD/PFOA complex in D_2O at pD \sim 5 (heating cycle from 25 °C to 75 °C).

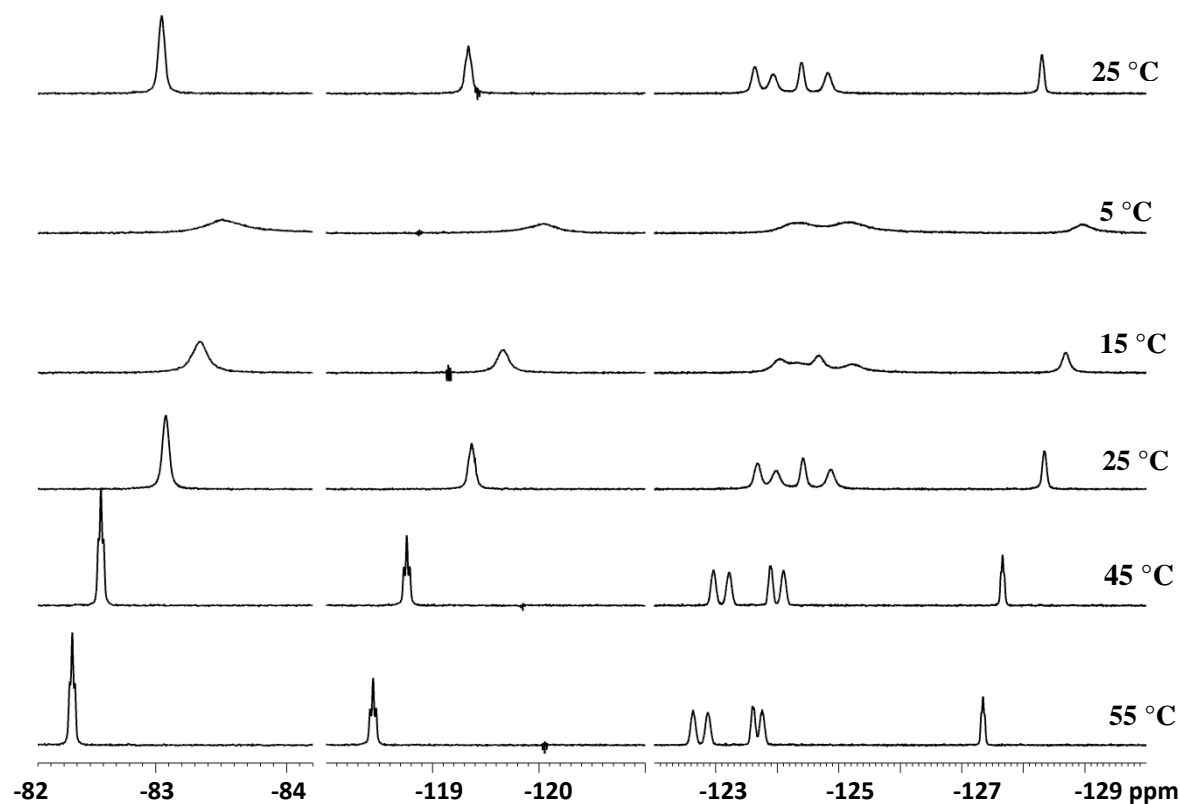


Figure 2.10 ^{19}F NMR spectra at variable temperature for the 2:1 β -CD/PFOA complex in D_2O at pD \sim 5 (cooling cycle from 55 $^\circ\text{C}$ to 5 $^\circ\text{C}$).

2.4.3. Solid-state NMR

2.4.3.1 Solid NMR Characterization

^{19}F NMR was used to characterize the structure of unbound PFOA and its inclusion complexes with β -CD. ^{19}F NMR spectroscopy in the solid state is unique because of the high natural abundance and the wide chemical shift dispersion of the ^{19}F nuclei. The opportunity to simultaneously observe several independent nuclei provides useful structural and quantitative information for host-guest complexes.

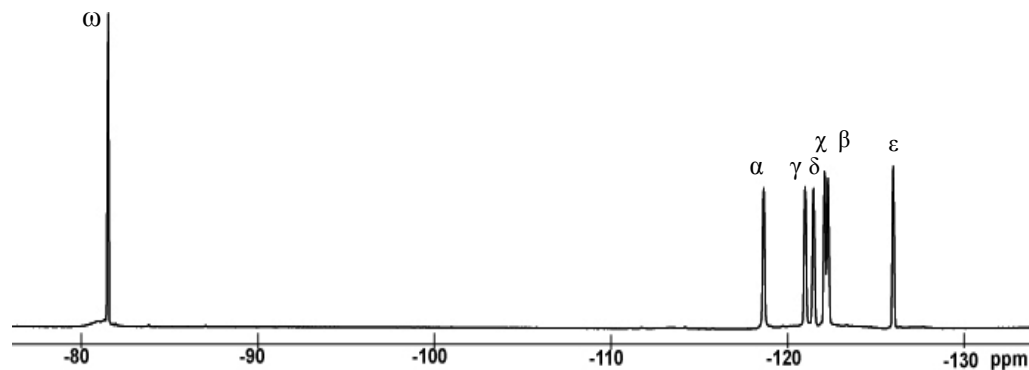


Figure 2.11 Solid state ^{19}F DP/MAS spectrum of PFOA obtained at MAS 25 kHz and 295 K.

The results in Figure 2.11 show a ^{19}F NMR spectrum acquired under DP conditions with MAS at 25 kHz. The spectrum of the unbound PFOA shows well resolved ^{19}F signals and the assignment is in good agreement with the high resolution solution NMR spectrum (*cf.* Figure 2.6). On the other hand, Figure 2.12 shows a well resolved ^{13}C NMR spectrum for β -CD hydrate obtained using $^1\text{H}\rightarrow^{13}\text{C}$ CP/MAS at 20 kHz conditions. Although β -CD is comprised of seven glucose monomers, the individual ^{13}C nuclei are not completely resolved in the CP/MAS spectrum, and this is attributed to the crystallographic inequivalence of the pyranose units and coincidental overlap of certain resonance lines because of the variable hydration states and amorphous characteristics of powdered samples with mixtures of non-stoichiometric β -CD hydrate.

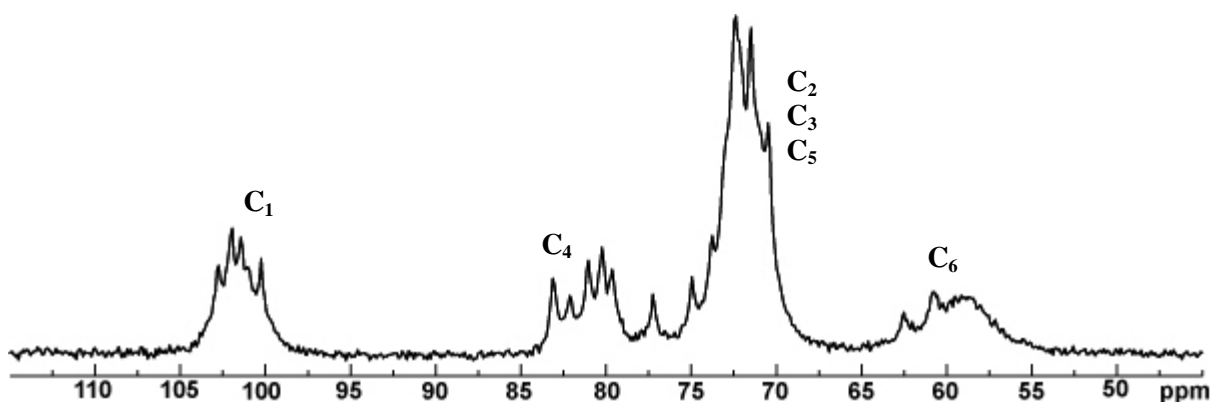


Figure 2.12 Solid state ^{13}C H \rightarrow C CP/MAS spectrum of native β -CD hydrate at MAS 20 kHz and 295 K.

The ^{19}F DP/MAS spectra for pure PFOA and its 1:1 and 2:1 slow cool complexes with β -CD are shown in Figure 2.13. The ^{19}F NMR results provide evidence for the formation of 1:1 and 2:1 β -CD/PFOA inclusion complexes prepared using the slow cool method. Complex formation between β -CD and PFOA results in reduced motional averaging of the ^{19}F homonuclear dipolar couplings which result in broadening of the ^{19}F signals and the appearance of spinning side bands²⁹ (*cf.* asterisks in Figures 2.13 and 2.14). As the PFOA becomes increasingly bound (i.e. conversion of 1:1 to 2:1), the stoichiometry of the complex coincides with the attenuation of the sharp component at ca. -82 ppm for the 2:1 complex and the presence of increasingly broadened ^{19}F signatures, compared to the 1:1 complex. The presence of the

sharp CF_3 component at -82 ppm in the 1:1 complex indicates that there may be greater motional dynamics of coiling and uncoiling of segments of the PFC chain.

The structure of 1:1 complex can be described as a dynamic pseudo-rotaxane complex; wherein the β -CD macrocycle can encapsulate $\sim 4 - 5$ CF_2 groups with an ensemble of potential configurations, depending on the conformation of the guest.⁶⁴ In contrast to the 1:1 complex, the 2:1 complex represents a more static pseudo-rotaxane type complex in which a greater proportion of the PFC chain is included within two host cavities (*cf.* Scheme 2.1). As a consequence of this inclusion geometry, a potentially lower energy state configuration confines the motional chain dynamics of the guest. These results are consistent with the solution NMR results (*cf.* Figure 2.6). Furthermore, the presence of sharp and broad signatures for the CF_3 group (ca. -79 and -82 ppm) in the 1:1 slow cool complex provides support that it may reside in two or more microenvironments (i.e. inside vs outside the β -CD macrocycle), and this conclusion is consistent with results for DSC, FT-IR and PXRD presented above. For example, the DSC of the 1:1 complex was consistently characterized by two transitions at 180 and 210 °C (*cf.* Fig. 2.1). It should be noted that contributions from free unbound guest cannot be ignored, particularly in the 1:1 complex and may also account for the broad and narrow feature at high frequency.

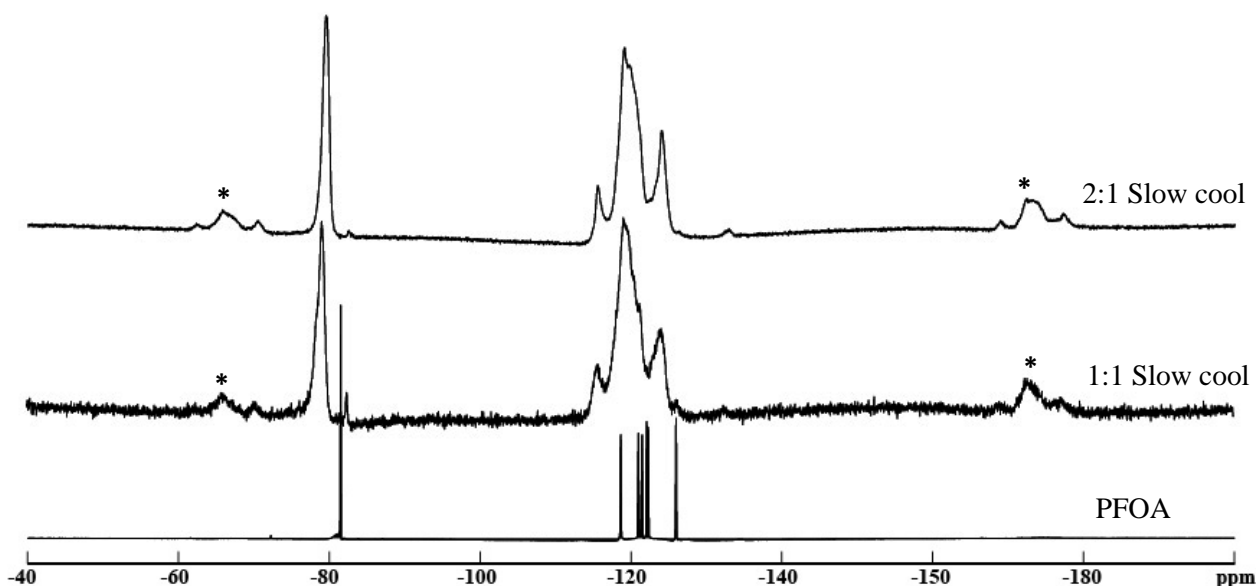


Figure 2.13 ^{19}F DP MAS 25 kHz NMR spectra at 295 K for pure PFOA, and the 1:1 and 2:1 β -CD/PFOA complexes obtained by the slow cool method.

Figure 2.14 depicts the ^{19}F DP/MAS NMR spectra of the 1:1 β -CD/PFOA inclusion complexes prepared by the slow cool and dissolution methods, respectively. The product obtained by slow cool is characterized by relatively broad ^{19}F signatures due to a microenvironment in which the motional dynamics of PFOA are attenuated, as compared with the complex prepared by dissolution (*cf.* Fig. 2.14). The DSC results (*cf.* Figure 2.1) have shown greater phase purity for the complexes prepared by slow cool relative to the products obtained by dissolution. In the latter case, the appearance of numerous sharp resonance lines is consistent with increased motional dynamics of PFOA.

The sharp resonance lines observed for PFOA are attributed to the unrestricted motional dynamics of unbound guest, as compared with the bound forms of the 1:1 and 2:1 β -CD/PFOA complexes. In Figure 2.14, the chemical shift trends for the sharp CF_3 line for the dissolution complex follows a similar trend as that observed in the solution NMR spectra in Figure 2.6. In contrast to the dissolution complex, the slow cooled product does not follow the same trend. This observation provides support for the presence of variable conformations of the PFOA chain in solid complexes, in accordance with the type of preparative method (*i.e.* dissolution vs slow cool). In general, the PFOA chain in the 1:1 complex has a distribution of the *gauche*- and *trans*-conformers. However, the results provide strong evidence for the formation of β -CD/PFOA inclusion complexes with variable stoichiometry and inclusion geometry in the solid state.

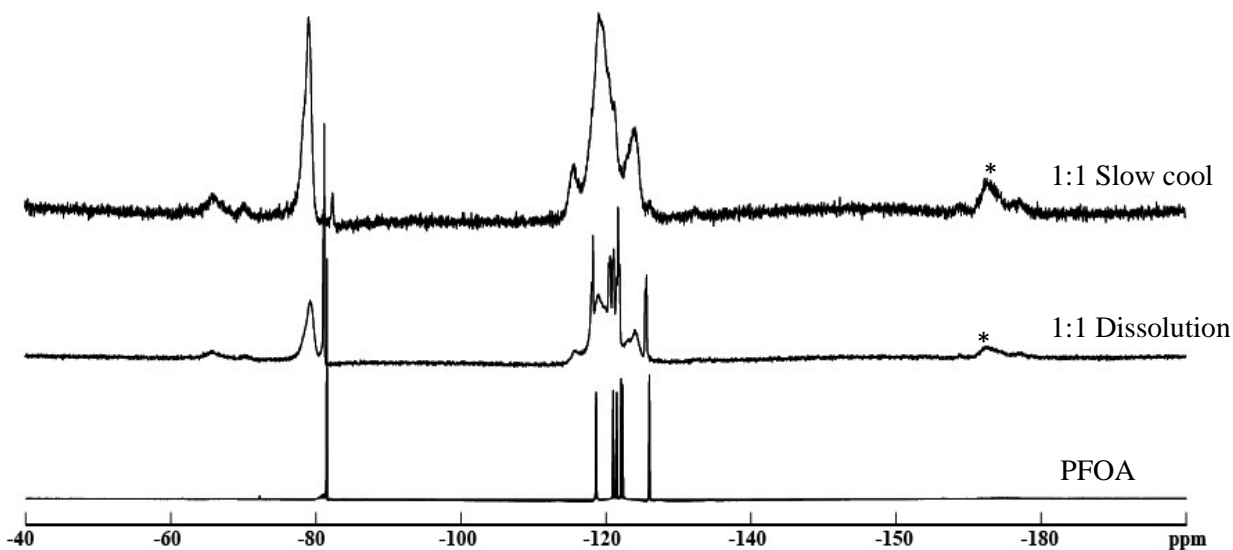


Figure 2.14 ^{19}F DP/MAS 25 kHz NMR spectra at 295 K for pure PFOA, and the 1:1 β -CD/PFOA complexes obtained by dissolution and slow cool methods.

2.4.3.2 ¹⁹F Solid NMR Dynamics

The foregoing results have illustrated that β -CD forms stable inclusion complexes with PFOA in the solution and solid states, respectively, with variable host-guest stoichiometry and inclusion geometry. It is well known that the physicochemical properties (stability, solubility, surface tension etc.) of the guest molecules in the bound state are dramatically altered for inclusion complexes with β -CD.¹⁹⁻²¹ However, the relationship between the mode of preparation of these complexes and their structure in the solid state are poorly understood and requires further study.

An understanding of the structure, dynamics, and molecular recognition properties of such solid state complexes is afforded by multi-nuclear NMR studies described herein. As previously observed, the complexes prepared by the slow cool and dissolution methods yield distinct differences in their NMR line shape patterns (*cf.* Figure 2.14) and this was concluded as being due to the inclusion geometry and guest conformation. The dynamic properties of the complexes prepared by the different preparative methods were studied using ¹⁹F DP/MAS conditions with variable spin rate (VSR; 10 to 25 kHz) at 295 K. The unbound PFOA (Figure 2.15) and the 1:1 dissolution complex (Figure 2.16) display well-resolved ¹⁹F resonances with broad and sharp components for the specified VSR conditions, as anticipated. As the spinning rate increases, dipolar couplings are scaled down and the different phases possessing variable configurations of the guest are revealed.

In Figure 2.17, the 1:1 complex prepared by slow cool appears more static for these VSR conditions, as supported by the absence of sharp ¹⁹F guest signatures. In contrast, variable microenvironments and configurations are revealed for the 1:1 complex prepared by dissolution (*cf.* Figure 2.16). Following the interpretation of the results in Figure 2.15, the 1:1 complex (Figure 2.16) is made up of two types of bound guest; a mobile and static phase. The results are consistent with the variable binding conformation of the PFOA chain in the 1:1 complex, as previously described. Note that the effects of free unbound guest cannot be ignored as previously described and may contribute to the overall dynamics. The frequencies of the narrow components due to the complexed and pure PFOA are provided in Table 2.2.

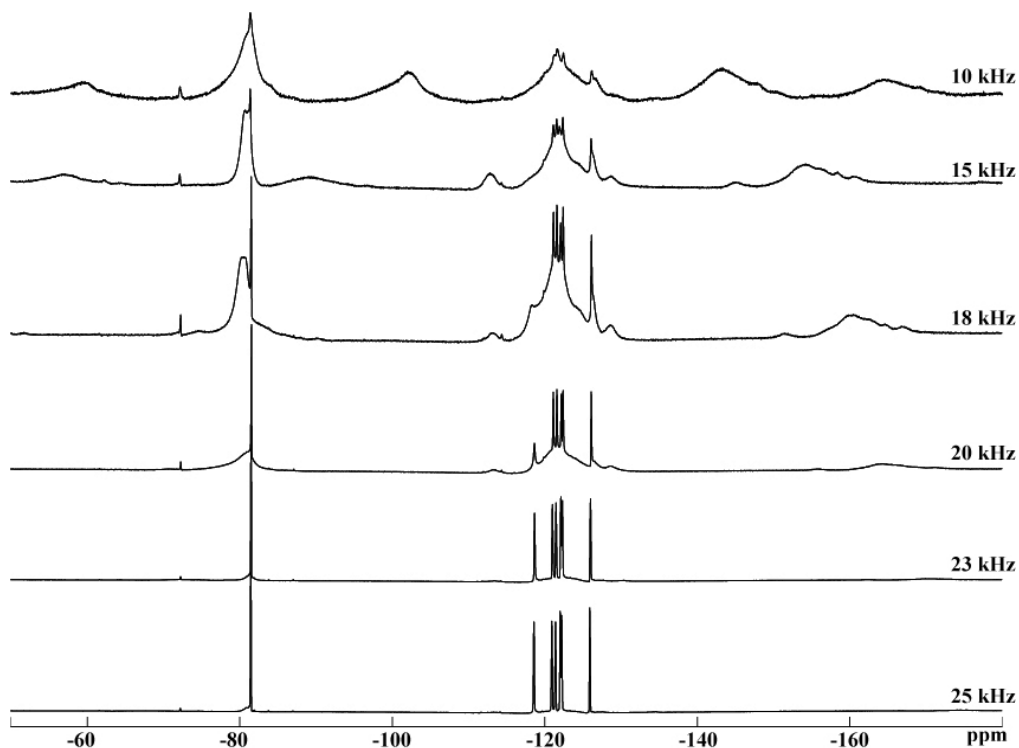


Figure 2.15 ^{19}F DP NMR spectra for unbound (free) PFOA at variable spin rates (VSRs) at 295 K.

The dynamics of PFOA in the complexed state were studied using VT ^{19}F DP/MAS NMR. The ^{19}F NMR experiments were obtained at moderate MAS rate (14 kHz) while varying the temperature from -90 to 100 °C. Figure 2.18 illustrates the ^{19}F DP MAS spectra where the system is heated from -90 to 22 °C. The guest dynamics of the 1:1 complex prepared by the dissolution method are observed to increase as the temperature increases. A sharply resolved ^{19}F signature for the CF_3 group appears upfield at ca. -82 ppm and temperatures $\geq 0^\circ\text{C}$. This peak is attributed to the occurrence of greater rotational dynamics for these conditions. However, the signatures for the CF_2 groups are relatively invariant over the temperature range investigated, and this is attributed to insufficient motional averaging of the ^{19}F homonuclear dipolar couplings because of the static nature of the PFOA chain. It is clear that the guest dynamics are expected to be more pronounced as the temperature is increased above the phase transition of the guest molecule according to observed thermo-physical transitions observed for the guest at temperatures $\geq 60^\circ\text{C}$ (*cf.* Figure 2.1).

As shown in Figure 2.19, a further increase in the temperature for the 1:1 complex prepared by dissolution reveals significant dynamic effects with increasing temperature. Figures

2.19A and B show the ^{19}F (VT) DP/MAS NMR results for the heating (25 to 90 °C) and cooling (90 to 25 °C) cycles, respectively.

Table 2.2 Chemical Shift Data for Uncomplexed PFOA and Complexed PFOA Guest at Variable Spin Rates (Chemical Shifts for Broad CF_3 Components are shown in brackets)

Signal	Uncomplexed PFOA		β -CD/PFOA 1:1 Dissolution	
	δ (25 kHz)	δ (23 kHz)	δ (25 kHz)	δ (23 kHz)
1 (ω)	-81.53	-81.56	-81.24 (-79.38)	-81.24 (-79.34)
2 (α)	-118.6	-118.7	-118.3	-118.3
3 (γ)	-121.0	-121.1	-120.6	-120.6
4 (δ)	-121.5	-121.5	-121.1	-121.0
5 (χ)	-122.1	-122.2	-121.7	-121.8
6 (β)	-122.3	-122.4	-122.0	-122.0
7 (ϵ)	-126.0	-126.1	-125.6	-125.6

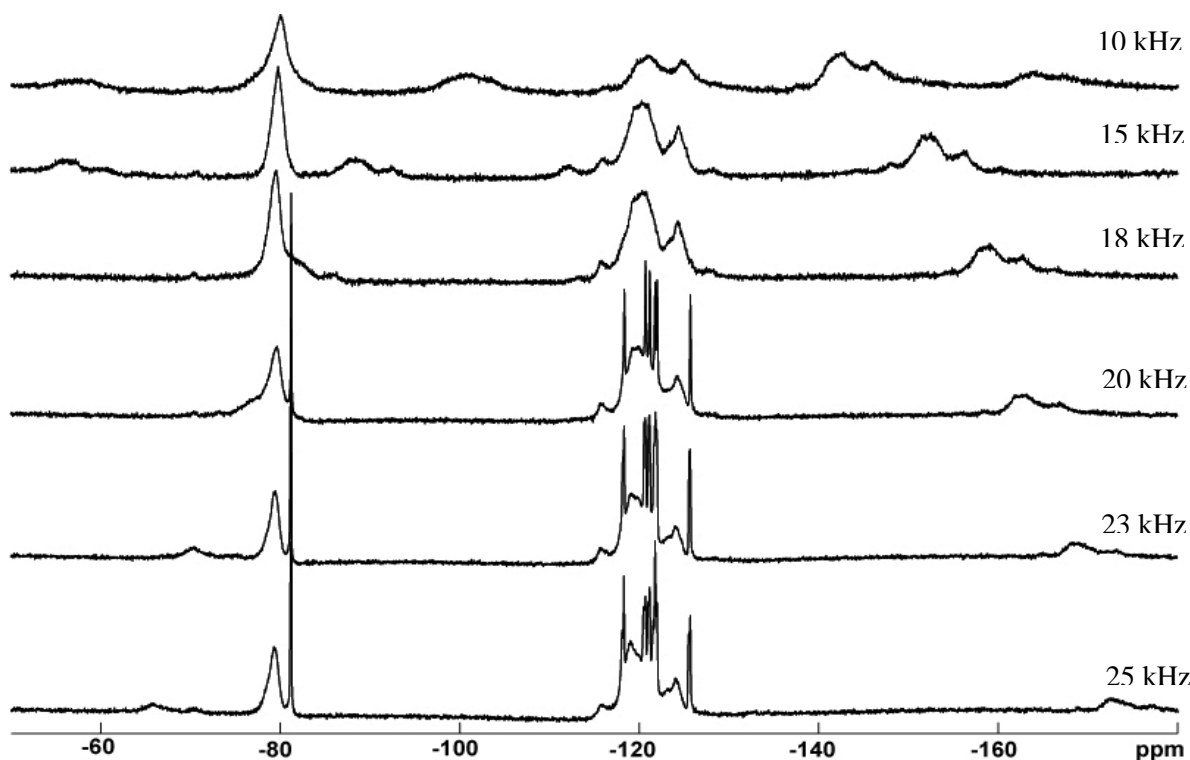


Figure 2.16 ^{19}F DP NMR spectra of the 1:1 β -CD/PFOA complex prepared by the dissolution method and run at variable spin rates (VSR) at 295 K.

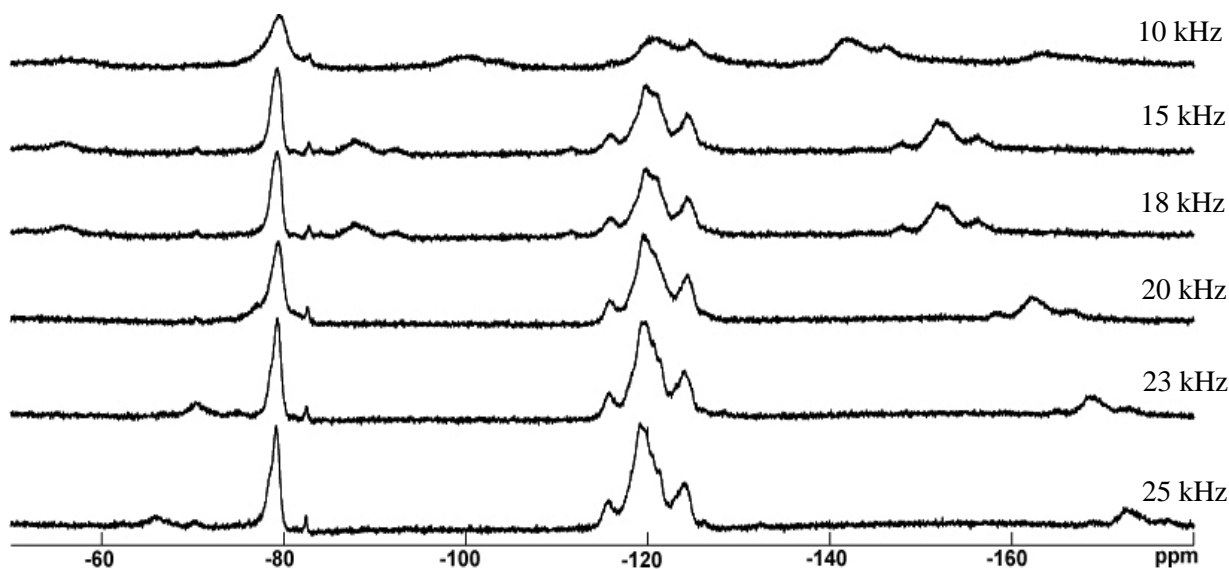


Figure 2.17 ^{19}F DP NMR spectra of the 1:1 β -CD/PFOA complex prepared by the slow cool method and run at variable spin rates (VSR) at 295 K.

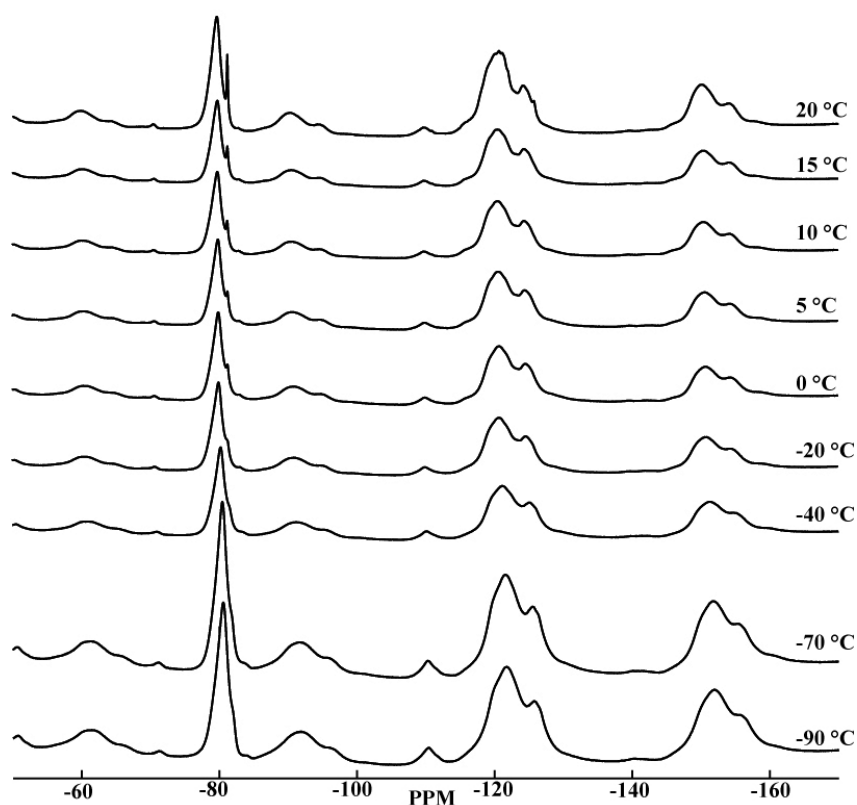


Figure 2.18 ^{19}F DP/MAS NMR spectra at 14 kHz and variable temperature for the 1:1 β -CD/PFOA complex prepared by the dissolution method (warming from -90°C to 20°C).

During the heating cycle, the ^{19}F signals for the guest become more resolved as the temperature is increased. The relative intensity of the sharp CF_3 group signature at ca. -82 ppm increases at the expense of the broad CF_3 component at ca. -79 ppm up to $\sim 80^\circ\text{C}$, revealing variable distribution of conformational effects as a function of temperature. The other ^{19}F signals for the CF_2 groups (ca. -120 ppm) become more resolved as the temperature is increased to $\sim 80^\circ\text{C}$. This observation is consistent with the inter-conversion between conformational states of PFOA, as previously discussed. We conclude that the broad and narrow CF_3 components correspond to the *gauche*- and *trans*-conformers, respectively. The broadening of the CF_3 signal is suspected to arise from the strong coupling between the inequivalent fluorines in the *gauche*-conformer; whereas, the equivalent fluorines in the *trans*-conformer are expected to exhibit narrowing of the CF_3 signal. Above 80°C , unique line shape changes are observed for the CF_2 region (~ 120 ppm) and this supports that changes in the microenvironment and dynamics of the PFOA chain occur. The guest environment undergoes a change because the host may undergo desolvation at these temperature conditions, as evidenced by the DSC results in Figure 2.1. The process of dehydration may occur at temperatures $< 120^\circ\text{C}$ (*cf.* DSC results, Fig. 2.1) since the sample rotor is an open system. In addition, the apparent temperature recorded during the experiment is expected to be less than the in situ temperature within the sample rotor since the mechanical effects of spinning are expected to generate heat. The role of hydrate water and guest molecular dynamics are supported from independent ultrasonic relaxation studies by Aicart et al.⁶³ Tatsuno and Ando²⁹ reported similar conclusions, according to their VT NMR studies of β -CD and long chain *n*-alkyl PFCs.

Upon cooling (90 to 25°C) in Figure 2.19B, the trends in line shapes of the guest are observed not to be reversible, as compared with the heating cycle (*cf.* Fig. 2.19A). The observed irreversibility is attributed to changes resulting from the loss of hydrate water during the heating cycle because the purge gas stream irreversibly removes hydrate water from the system. The void volume arising from dehydration causes a microenvironment change which subsequently affects the motional dynamics of the PFC chain in the host framework.²⁹ In addition, slight but observable shift changes for the ^{19}F signals are observed for the guest in the complexed state during the heating and cooling processes, respectively. The heating and cooling processes may be accompanied by different populations of *trans*- and *gauche*-conformers of PFOA. The

chemical shift changes are as high as ~ 1.3 ppm in the solution state and ~ 0.8 ppm for the solid state spectra over the specified temperature ranges.

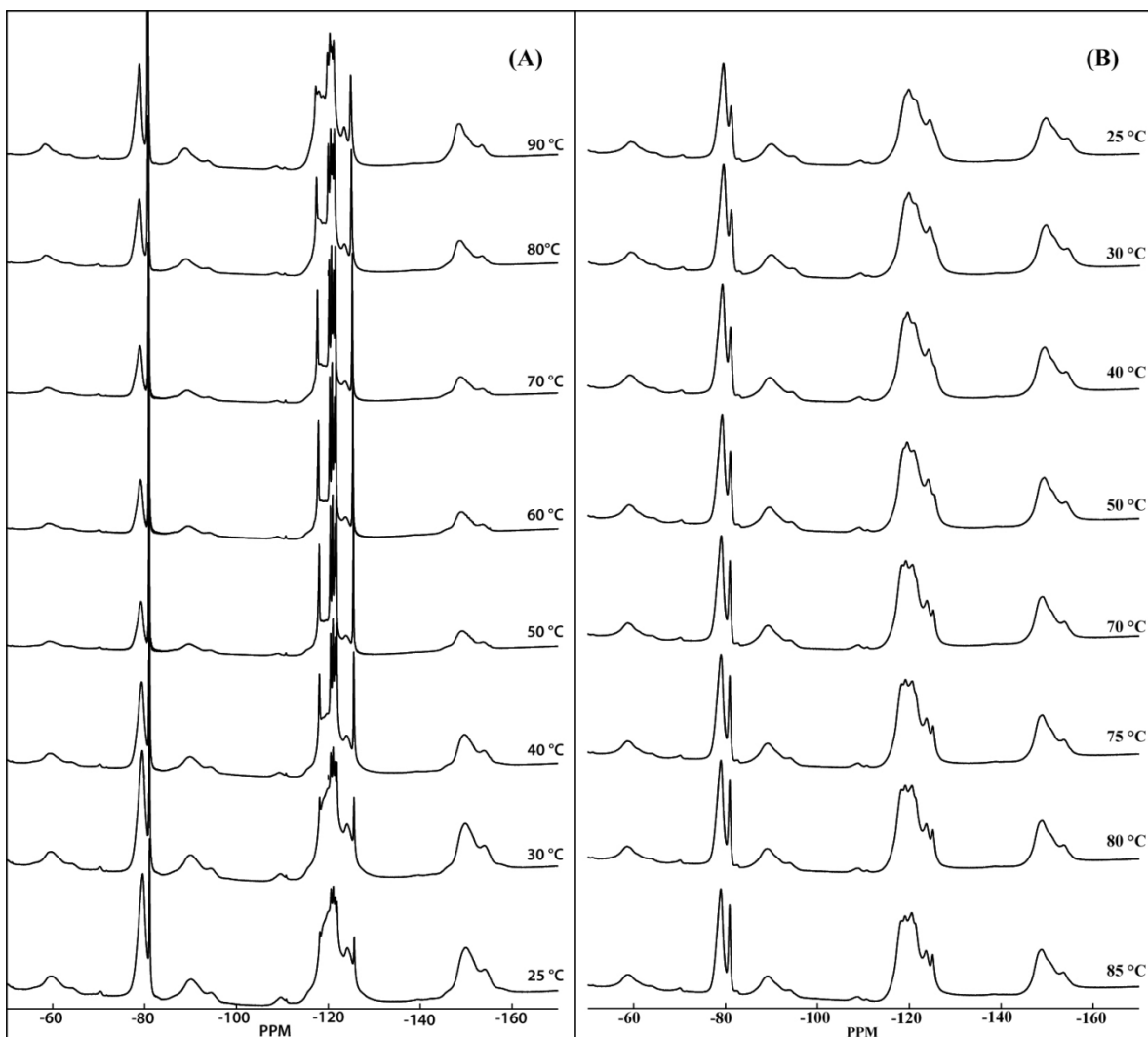


Figure 2.19 ^{19}F DP/MAS NMR spectra obtained at 14 kHz and variable temperature for the 1:1 β -CD/PFOA complex prepared by the dissolution method. The heating cycle was from 25 °C to 90 °C (A), and the cooling cycle was from 85 °C to 25 °C (B).

Variable dynamic effects were observed for the 2:1 complexes prepared by the slow cool method (*cf.* Figure 2.20). The absence of a sharp component for the terminal CF_3 group at ca. -82 ppm in Figure 20A suggests that the complex formed by the slow cool method is different in nature than the corresponding 1:1 complex (*cf.* Figure 2.14c). The broad resonance lines for the 2:1 complex are consistent with attenuated motional dynamics with a different inclusion

geometry compared to the 1:1 complex. Minor dynamic effects are observed above 80 °C for the ^{19}F guest signals at ca. -120 ppm and this is related to the loss of hydrate water, as described above. The reduced temperature dependence of the ^{19}F line shapes for the 2:1 complexes prepared by slow cooling is observed due to the greater stability of this complex, in agreement with the DSC results. However, there are minor upfield and downfield chemical shifts for the ^{19}F guest signals during the heating and cooling cycles, and these are related to the inter-conversion between *trans*- and *gauche*-conformers of the PFC chain of PFOA, as described above.

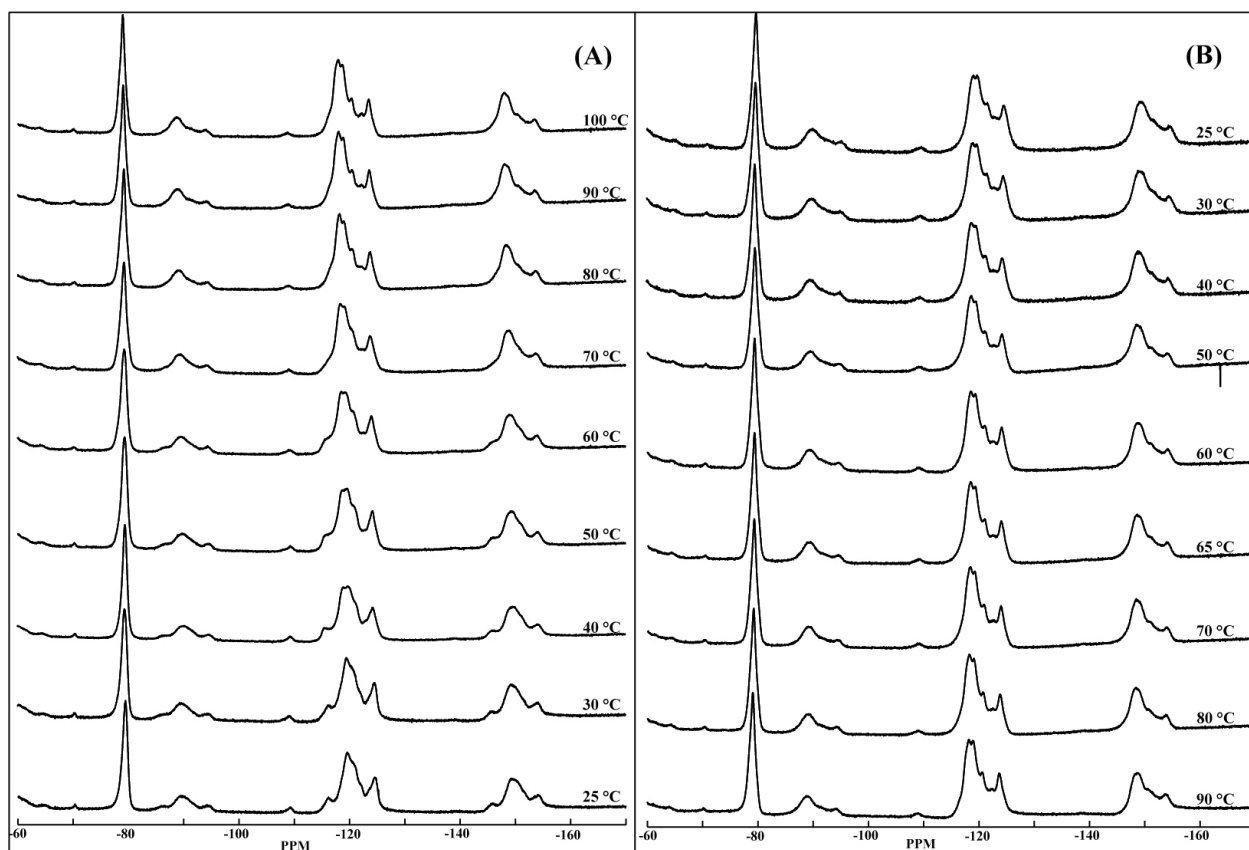


Figure 2.20 ^{19}F DP/MAS NMR spectra obtained at 14 kHz and variable temperature for the 2:1 β -CD/PFOA complex prepared by the slow cool method. The heating cycle was from 25 °C to 100 °C (A), and the cooling cycle was from 90 °C to 25 °C (B).

2.5. Conclusions

Two preparative methods, slow cool and dissolution, were developed and used to prepare 1:1 and 2:1 β -CD/PFOA solid state complexes. $^1\text{H}/^{19}\text{F}$ NMR spectroscopy and CIS effects

provide support for the formation of 1:1/2:1 β -CD/PFOA complexes with variable guest geometry and conformation. The NMR results were complemented using results from FT-IR, thermal analyses (DSC and TGA), and PXRD. IR results revealed that PFOA adopts the *gauche*- and *trans*-conformations in the 1:1 and 2:1 host-guest complexes, respectively. “Channel-type” structures were reported for the 1:1/2:1 complexes which are distinctly different from the cage structures formed by native β -CD according to PXRD results.

According to variable spinning rates (VSR) and temperature (VT) NMR studies, the complexes prepared by slow cool method were characterized to possess less mobile components, as compared with complexes prepared by dissolution. ^{19}F (VT) NMR results in solution and the solid state indicate that PFOA undergoes variable temperature-induced intramolecular conformations as a function of host/guest mole ratio and the preparative method. $^1\text{H}/^{19}\text{F}$ NMR, IR and DSC support the presence of variable conformations and the greater phase purity of the complexes prepared by slow cool method.

The structure and conformational dynamics for the solid complexes formed between β -CD and PFOA are generally affected by host-guest mole ratios, temperature changes, and hydrate content of β -CD. Complexes prepared by slow cool method display reduced dynamics than complexes prepared by dissolution, and this may be related to the greater stability and phase purity of the complexes prepared by the slow cool method.

2.6. Acknowledgements

We wish to acknowledge the University of Saskatchewan, the University of Lethbridge and the National Sciences and Engineering Research Council (NSERC) for support of this research.

2.7. References

1. Deng, S.; Shuai, D.; Yu, Q.; Huang, J.; Yu, G. *Environ. Sci. Eng. China* **2009**, *3*, 171–177
2. Richardson, S. D. *Anal. Chem.* **2009**, *81*, 4645–4677.
3. Fujii, S.; Polprasert, C.; Tanaka, S.; Nguyen, O. H. L.; Yong, Q. J. *J. Water Supply Res. Technol. AQUA*, **2007**, *56*, 313–326.
4. Saito, N.; Harada, K.; Inoue, K.; Sasaki, K.; Yoshinaga, T.; Koizumi, A. *J. Occup. Health* **2004**, *46*, 49–59.

5. Boulanger, B. ; Vargo, J. D. ; Schnoor, J. L.; Hornbuckle, K. C. *Environ. Sci. Technol.*, **2005**, 39, 5524–5530.
6. Gilliland, F. D.; Mandel, J. S. *J. Occup. Environ. Med.* **1993**, 35, 950–954.
7. Guruge, K. S.; Yeung, L. W. Y.; Yamanaka, N.; Miyazaki, S.; Lam, P. K. S.; Giesy, J. P.; Jones, P. D.; Yamashita, N. *Toxicol. Sci.* **2006**, 89, 93–107.
8. Fei, C.; McLaughlin, J. K.; Lipworth, L.; Olsen, J. *Human Reprod.* **2009**, 1, 1–6.
9. Yang, Q.; Abedi-Valugerdi, M.; Xie, Y.; Zhao, X. Y.; Müller, G.; Nelson, B. D.; DePierre, J. W. *Int. Immunopharmacol.* **2002**, 2, 389–397.
10. Peden-Adams, M. M.; Keller, J. M.; EuDaly, J. G.; Berger, J.; Gilkeson, G. S.; Keil, D. E. *Toxicol. Sci.* **2008**, 104, 144–154.
11. Dewitt, J. C.; Copeland, C. B.; Strynar, M. J.; Luebke, R. W. *Reprod. Toxicol.* **2009**, 27, 409–416.
12. Hoffmann, J.; Würtz, J. *J. Mol. Liq.* **1997**, 72, 191–230.
13. Guo, W.; Fung, B. M.; Christian, S. D. *Langmuir* **1992**, 8, 446–451.
14. Wilson, L. D.; Siddall, S. R.; Verrall, R. E. *Can. J. Chem.* **1997**, 75, 927–933; and references cited therein.
15. Zemb, T.; Drifford, M.; Hayoun, M.; Jehanno, A. *J. Phys. Chem.* **1983**, 87, 4524–4528; and references cited therein.
16. Picquart, M.; Lacrampe, G. *J. Phys. Chem.* **1992**, 96, 9114–9120.
17. D'Angelo, M.; Onori, G.; Santucci, A. *Prog. Colloid Polym. Sci.* **1994**, 97, 154–157.
18. Gonzalez-Perez, A.; Ruso, J. M.; Prieto, G.; Sarmiento, F. *Colloid Polym. Sci.* **2004**, 282, 1133–1139.
19. Kitamura, S.; Fujimura, T.; Kohda, S. *J. Pharm. Sci.* **1999**, 88, 327–330.
20. Nicolle, G. M.; Merbach, A. E. *Chem. Commun.* **2004**, 854–855
21. Dias, A. M. A.; Andre-Dias, C.; Lima, S.; Countinho, J. A. P.; Teixeira-Dias, J. J. C.; Marrucho, I. M. *J. Coll. Int. Sci.* **2006**, 303, 552–556.
22. Szejtli, J.; Osa, T. *In Comprehensive Supramolecular Chemistry*. Eds.; Pergamon Press: New York, 1996; and references cited therein.
23. Palepu, P.; Reinsborough, V. C. *Can. J. Chem.* **1989**, 67, 1550–1553.
24. Wilson, L. D.; Verrall, R. E. *Langmuir* **1998**, 14, 4710–4717.

25. Zhang, H. H.; Hogen-Esch, T. E.; Boschet, F.; Margaillan, A. *Langmuir* **1998**, *14*, 4972–4977.
26. Palepu, R.; Richardson, J. M.; Reinsborough, V. C. *Langmuir* **1989**, *5*, 218–221.
27. Saint Aman, E.; Serve, D. *J. Coll. Int. Sci.* **1990**, *138*, 365–375.
28. Junquera, E.; Aicart, E.; Tardajos, G. *Langmuir* **1993**, *9*, 1213–1219.
29. Tatsuno, H.; Ando, A. *J. Phys. Chem. B* **2006**, *110*, 25751–25760.
30. Druliner, J. D.; Wasserman, E. *J. Fluorine Chem.* **1995**, *72*, 75–78
31. Nostro, P. L.; Santoni, I.; Bonini, M.; Baglioni, P. *Langmuir* **2003**, *19*, 2313–2317
32. Geppi, M.; Pizzanelli, S.; Veracini, C. A.; Cardelli, C.; Tombari, E.; Lo Nostro, P. *J. Phys. Chem. B* **2002**, *106*, 1598–1605
33. Yannakopoulou, K.; Mavridis, I. M. *Curr. Org. Chem.* **2004**, *8*, 25–34.
34. Borisov, A. S.; Hazendonk, P.; Hayes, P. G. *J. Inorg. Organomet. Polym.* **2010**, *20*, 183–212.
35. Ripmeester, J. A.; Ratcliffe, C. I. *Compr. Supramol. Chem.* **1996**, *8*, 323–380.
36. Battiste, J.; Newmark, R. A. *Prog. Nucl. Magn. Reson. Spectrosc.* **2006**, *48*, 1–23.
37. Bennett, A. E.; Rienstra, C. M.; Auger, M.; Lakshmi, K. V.; Griffin, R. G. *J. Chem. Phys.* **1995**, *103*, 6951–6958.
38. Xing, H.; Lin, S.; Yan, P.; Xiao, J.; Chen, Y. *J. Phys. Chem. B* **2007**, *111*, 8089–8095
39. Zainal Abidin, S.; Ling, G. K. F.; Abdullah, L. C.; Ahmad, S.; Yunus, R.; Choong, T. S. Y. *Euro. J. Sci. Res.* **2009**, *33*, 3, 471–479
40. Bruylants, G. Wouters, J.; Michaux, C. *Curr. Med. Chem.* **2005**, *12*, 2011–2020
41. J. Szejtli. *J. Inclus. Phenom. Mol.* **1992**, *14*, 25–36.
42. Moynihan, R. E. *J. Am. Soc.* **1959**, *81*, 1045–1050.
43. Pawsey, S.; Reven, L. *Langmuir* **2006**, *22*, 1055–1062.
44. Albinsson, B.; Michl, J. *J. Phys. Chem.* **1996**, *100*, 3418–3429.
45. Drużbicki, K.; Mikuli, E.; Ossowska-Chruściel, M. D. *Vib. Spectrosc.* **2010**, *52*, 54–62
46. Okumura, H.; Kawaguchi, Y.; Harada, A. *Macromolecules* **2001**, *34*, 6338–6343.
47. Jiao, H.; Goh, S. H.; Valiyaveetil, S. *Macromolecules* **2002**, *35*, 3997–4002.
48. Li, N.; Liu, J.; Zhao, X.; Gao, Y.; Zheng, L.; Zhan, J.; Yu, L. *Colloids Surf. A*, **2007**, *292*, 196–201.
49. Caira, M. R. *Rev. Roum. Chim.* **2001**, *46*, 371–386.

50. Schneider, H. J.; Hacket, F.; Rüdiger, V. *Chem. Rev.* **1998**, *98*, 1755–1786.
51. Webb, G. A. *Annual Reports on NMR spectroscopy*. London, New York, Academic Press Inc.; **1993** (Vol. 7) and references cited therein.
52. Ellis, D. A.; Denkenberger, K. A.; Burrow, T. E.; Mabury, S. A. *J. Phys. Chem. A*, **2004**, *108*, 10099–10106.
53. Raynea, S.; Forest, K. *J. Mol. Struct. THEOCHEM* **2010**, *949*, 60–69.
54. Erkoç, S.; Erkoç, F. *J. Mol. Struct. THEOCHEM* **2001**, *549*, 289–293.
55. Battais, A.; Boutevin, B.; Moreau, P. *J. Fluorine Chem.* **1978**, *12*, 481–496.
56. Goecke, C. M.; Jarrot, B. M.; Reo, N. V. *Chem. Res. Toxicol.* **1992**, *5*, 512–519.
57. Buchanan, G. W.; Munteanu, E.; Dawson, B. A.; Hodgson, D. *Magn. Reson. Chem.* **2005**, *43*, 528–553.
58. Dalling, D. K.; Grant, D. M. *J. Am. Chem. Soc.* **1967**, *89*, 6612–6620.
59. Perlin, A. S.; Koch, H. J. *Can. J. Chem.* **1970**, *48*, 2639–2643.
60. Roberts, J. D.; Weigert, F. J.; Kroschwitz, J. I.; Reich, H. J. *J. Am. Chem. Soc.* **1970**, *92*, 1338–1347.
61. Knochenhauer, G.; Reiche, J.; Brehmer, L.; Barbeka, T.; Woolley, M.; Tredgold, R.; Hodge, P. *J. Chem. Soc., Chem. Commun.* **1995**, 1619–1620.
62. Bunn, C. W.; Howells, E. R. *Nature* **1954**, *174*, 549–551.
63. Jobe, D. J.; Verrall, R. E.; Janquera, E.; Aicart, E. *J. Phys. Chem.* **1993**, *97*, 1243–12483.
64. Wilson, L. D.; Verrall, R. E. *J. Phys. Chem. B* **2000**, *104*, 1880–1886.

CHAPTER 3

Manuscript no. 2

Description

In this work, the dissolution preparative method described in chapter 2 was modified to afford β -CD/PFOA inclusion complexes with greater phase purity. The phase purity was assessed using ^{19}F DP/MAS NMR spectroscopy and DSC. Multinuclear $^{13}\text{C}/^{19}\text{F}$ MAS NMR spectroscopy and relaxation NMR techniques were used to further characterize the structure of the complexes and dynamic properties of the host/guest system, respectively.

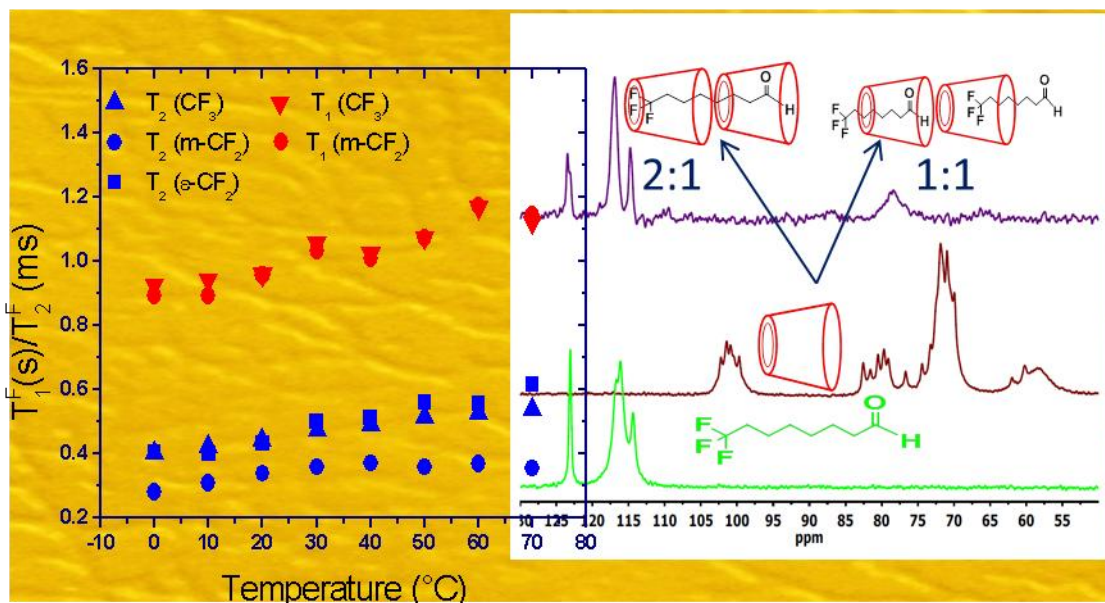
Author's Contribution

I proposed the idea to modify the dissolution preparative method developed in chapter 2 in order to obtain phase pure β -CD/PFOA ICs. The idea of using multinuclear and relaxation NMR techniques was proposed by Dr. Paul Hazendonk (UofL) and seconded by Dr. Lee Wilson. The preparation and characterization (FT-IR, DSC, and PXRD) of the β -CD/PFOA complexes were done by myself. The solid state NMR characterization was done by myself, while the NMR relaxation measurements and data analyses were done in collaboration with Dr. Paul Sidhu (UofL). I prepared the first draft of the manuscript and all the subsequent revisions/edits were done by Drs. Wilson, Hazendonk and Sidhu.

Relation of Manuscript 1 to Overall Objective of this Project

The work of this manuscript was important to the overall objective of the research project because it ensured that we obtain phase pure inclusion complexes which would be used to afford more reliable spectroscopic measurements. The developed modified method could also be used to prepare the complexes of PFBA and SPFO with β -CD, respectively.

Graphical Abstract



Research Highlights

- The modified dissolution method gave rise to inclusion complexes with improved phase purity.
- ^{13}C ($^{19}F \rightarrow ^{13}C$ CP) MAS NMR techniques provided unequivocal evidence for the inclusion of the guest within the host.
- Two types of motional dynamics were characterized for the guest; rotational motion of the terminal fluoromethyl (CF_3) group, and axial (librational) motion of the entire perfluorocarbon chain.

3. Characterization and Dynamic Properties for the Solid Inclusion Complexes of β -Cyclodextrin and Perfluorooctanoic Acid

Abdalla H. Karoyo,[†] Paul Sidhu,[‡] Lee D. Wilson,^{†,} Paul Hazendonk^{‡,*}*

[†]University of Saskatchewan, Department of Chemistry, Saskatoon, SK, S7N 5C9, Canada.

[‡]University of Lethbridge, Department of Chemistry and Biochemistry, Lethbridge, AB, Canada.

*Corresponding Authors.

§Supplementary Information (Appendix B)

3.1 Abstract

The structural characterization and dynamic properties for the solid inclusion complexes (ICs) formed between β -cyclodextrin (β -CD; host) and perfluorooctanoic acid (PFOA; guest) were investigated using ^{13}C NMR spectroscopy. The 1:1 and 2:1 host/guest solid state complexes were prepared using a modified dissolution method to obtain complexes with greater phase purity. These complexes were further characterized using differential scanning calorimetry (DSC), FT-IR spectroscopy, powder X-ray diffraction (PXRD), ^{19}F direct polarization (DP) and ^{13}C cross polarization (CP) with magic-angle spinning (MAS) NMR spectroscopy. The $^{19}\text{F} \rightarrow ^{13}\text{C}$ CP results provided unequivocal support for the formation of well-defined inclusion compounds. The phase purity of the complexes formed between β -CD and PFOA were assessed using ^{19}F DP/MAS NMR technique at 20 kHz and variable temperature (VT). The complexes were found to be of high phase purity when prepared in accordance with the modified dissolution method. The motional dynamics of the guest in the solid complexes were studied using $T_1/T_2/T_{1\rho}$ relaxation NMR methods at ambient and variable temperatures. The relaxation data revealed reliable and variable guest dynamics for the 1:1 vs 2:1 complexes at the variable temperatures investigated. The motional dynamics of the guest molecules involve an ensemble of axial motions of the whole chain and 120° rotational jumps of the methyl (CF_3) group at the termini of the perfluorocarbon chain. The axial and rotational dynamics of the guest in the 1:1 and 2:1 complexes differ in distribution and magnitude in accordance with the binding geometry of the guest within the host.

3.2 Introduction

Perfluorinated compounds (PFCs) are of continued interest due to their widespread applications (e.g., firefighting foams, cosmetics, pesticides, emulsifiers, etc.) and their related environmental and health concerns.¹ Their recalcitrant nature make these compounds environmentally persistent leading to potential bio-accumulation, bio-magnification, and global distribution.² PFOS (perfluorooctane sulfonate; C₈F₁₇SO₃H) and PFOA (C₈F₁₇O₂H) have been reported as the most abundant types of PFCs in the environment, especially in aquatic biota.^{2,3}

The occurrence of PFCs in other matrices include ground water, fish and animals, soil, and sediments.⁴ PFCs have also been discharged in the environment directly through firefighting foams, industrial waste effluents, and pesticide application.^{5,6} Indirectly, PFCs are formed through degradation pathways of precursor compounds such as fluorotelomer alcohols and perfluoroalkyl sulfonamides.³ These compounds have been widely used in applications ranging from pharmaceuticals to surface active agents⁷⁻⁹ despite their potential adverse health risks as endocrine disruptors,¹⁰ infertility¹¹ and immunotoxin agents.¹²⁻¹⁴

The fate and transport pathways of PFCs in various environments and ecosystems are poorly understood in spite of the numerous studies over the past decade. In part, this may be due to the variation in the physicochemical properties of PFCs, such as surface activity, chemical mobility, and their chemical stability, as compared with their hydrocarbon analogues.^{15,16} In previous studies,¹⁷⁻²⁰ cyclodextrins (CDs)²¹ were reported to attenuate the surface activity of PFCs due to the formation of stable noncovalent host/guest complexes between the apolar PFC guest and the apolar CD interior. An improved understanding of the structure of β -CD/PFC ICs will contribute to the knowledge related to the physical and biophysical processes involving the fate and transport of PFCs in the environment. Considerable effort has been invested in studying the molecular structure of such ICs in solution and the solid state. Tatsuno²² and Druliner²³ reported ¹⁹F solids NMR studies of the complexes formed between aliphatic- and aromatic-based PFCs with CDs. By contrast, there are numerous reports of high resolution NMR studies of CD/PFC complexes in aqueous solution.²⁴⁻²⁶ In the case of solid state NMR, there is a paucity of structural studies, particularly those employing HFX and multi-nuclear NMR techniques²² of such β -CD/PFC host-guest systems. Recently, Koita et. al.²⁷ reported a detailed ¹⁹F→¹³C CP/MAS NMR study of the host-guest complex formed between β -CD and a semi-fluorinated hydrofluorether.

The aim of this study was to prepare well-defined highly phase pure β -CD/PFOA inclusion compounds at various host-guest ratios (e.g., 1:1 and 2:1) using a preparative method adapted from a previous study.¹⁷ The method was modified to obtain phase pure inclusion compounds to allow for more reliable dynamic relaxation studies of the guest in the complexed state. The inclusion compounds were characterized by DSC, FT-IR, PXRD and solid-state ^{19}F DP/MAS and $^1\text{H}/^{19}\text{F}\rightarrow^{13}\text{C}$ CP/MAS NMR. ^{19}F NMR under DP conditions at MAS 20 kHz and variable temperature was used to assess the phase purity of the complexes. Spin-lattice (T_1) and spin-spin (T_2) relaxation times in the laboratory frame, and spin-lattice relaxation times in the rotating frame ($T_{1\rho}$), were used to study the motional dynamics of the guest molecule in the 1:1 and 2:1 host/guest complexes at ambient and variable temperature conditions.

3.3 Experimental Section

3.3.1 Materials

β -CD hydrate (~10 % w/w) and PFOA (96 %) were purchased from Sigma-Aldrich Canada Ltd. (Oakville, ON), and were used as received without any further purification. The water content of the materials was determined using thermogravimetric analysis during preparation of the sample mixtures.

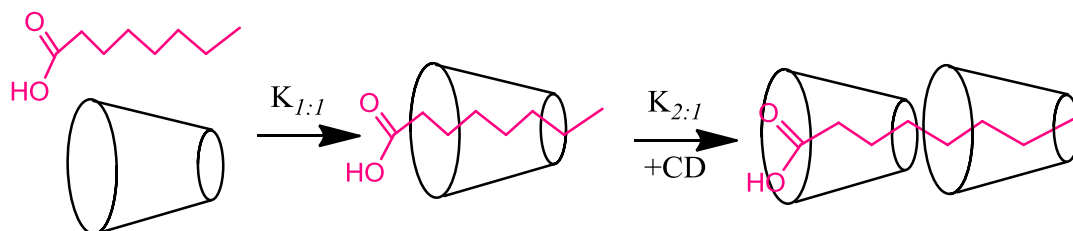
3.3.2 Preparation and the stoichiometry of the solid β -CD/PFOA ICs.

The solid β -CD/PFC complexes were prepared using a dissolution (evaporation) method modified from a previously reported method.¹⁷ Appropriate masses of the host and guest were weighed and dissolved in ~10 mL of high purity MilliQ water in 50 mL beakers to prepare the 1:1 and 2:1 host:guest complexes (*cf.* Scheme 3.1). The solutions were continuously stirred under mild heating of ~40 °C. Upon dissolution, the solution was allowed to cool to room temperature, and the solvent was evaporated over ~ 2 days in an open system to obtain the solid products.

The stoichiometric ratios of the solid complexes were independently analyzed by acid-base titration. The relative amounts of the guest in the washed and unwashed complexes were determined by titration with 0.01 M NaOH (standardized with potassium hydrogen phthalate) and the amounts of the host were estimated by gravimetric difference. The experimental host/guest values were shown to be comparable with previously reported¹⁷ values (1:1 unwashed = 1.0:1.1 and washed = 1.0:0.95; 2:1 unwashed = 1.7:1.0 and washed = 1.7:1.0). The results

suggest that the 2:1 complexes yield a mixture of 1:1 and 2:1 complexes, while the 1:1 products yield 1:1 complexes predominantly.^{28,29}

The modified preparation method allows for the isolation of complexes with greater phase purity because compounds (e.g., PFOA) that melt incongruently are susceptible to phase separation upon cooling or solvent evaporation at slower rates.³⁰ Inclusion compounds with greater phase purity allow for more reliable dynamic relaxation studies of the guest molecule within the host.³¹



Scheme 3.1 Step-wise formation of the 1:1 and 2:1 host/guest complexes between β -CD (toroid) and PFOA, according to the 1:1 and 2:1 (host/guest) stoichiometric ratios. The corresponding equilibrium constants are presented as $K_{1:1}$ and $K_{2:1}$, respectively.

3.3.3 Solid-State NMR Spectroscopy

3.3.3.1 $^{13}\text{C}/^{19}\text{F}$ NMR for characterization

All solid state NMR spectra were obtained using a Varian INOVA spectrometer operating in a triple channel HFC mode using a 3.2 or 2.5 mm T3 HFX probe operating at 125.55 MHz for ^{13}C , 499.99 MHz for ^1H , 469.89 for ^{19}F . Solid state ^{13}C NMR MAS spectra were referenced externally to adamantane ($\delta = 38.5$ ppm) as a secondary standard with respect to TMS, while ^{19}F MAS spectra were referenced to hexafluorobenzene. Samples were spun at the magic angle with variable spinning rates (14, 20 and 25 kHz) using 3.2 and 2.5 mm Vespel rotors equipped with Kel-F turbine caps, inserts, and end caps. All NMR spectra were obtained using a 100 kHz sweep width in 8192 points in the FID and were zero-filled to 64 k data points, unless stated otherwise. The curve and width parameters for the adiabatic $^1\text{H} \rightarrow ^{13}\text{C}$ CP experiments were set between 50 and 10,000 Hz, while those for $^{19}\text{F} \rightarrow ^{13}\text{C}$ were set between 50 and 50,000 Hz, respectively. Optimal Hartmann-Hahn matching conditions were achieved at a contact time of ≥ 2 ms and powers ranging from 68 kHz and 59.5 kHz for the ^{19}F and ^{13}C channels, respectively. ^{13}C $\{^1\text{H}, ^{19}\text{F}\}$ spectra of all solid samples were acquired using a two-pulse phase modulation

(TPPM) decoupling mode,^{32,33} using a pulse phase of 13.5 degrees and pulse powers of 35.7 and 38.5 kHz in the ¹H and ¹⁹F decoupled channels, respectively, as determined by the peak-to-peak voltage.

3.3.3.2 ¹³C/¹⁹F NMR for Relaxation Dynamics

The ¹⁹F T_1 values (T_1^F) were measured by inversion recovery (180°- τ -90°-acquire), whereas the T_2^F values were obtained with a Hahn echo³⁴ (90°- τ -180°- τ -acquire). The $T_{1\rho}^F$ relaxation times were measured with a pulse sequence that contains a spin-lock (SL) pulse in phase by 90° with respect to an initial 90° pulse (e.g., 90°_x-SL_y-acquire).³⁵ The ¹³C T_2 relaxation times were obtained by using a post-CP Hahn echo in the ¹³C channel. The ¹³C-detected T_1^H and $T_{1\rho}^H$ were measured with a pre-CP 180° pulse followed by a variable delay τ , and a pre-CP spin locking pulse in the ¹H channel, respectively. All relaxation measurements were obtained at ambient and variable temperature (0–70 °C). The error estimates (brackets) correspond to the standard deviation of the linear least-squares fitting parameters.

3.3.4 DSC and TGA

Differential scanning calorimetry (DSC) of the native β -CD, PFOA and the ICs were acquired using a TA Q20 thermal analyzer over a temperature range of 30–380 °C. The scan rate was set at 10 °C/min and dry nitrogen gas was used to regulate the sample temperature and sample compartment gas purging. Solid samples were analyzed in hermetically sealed aluminum pans where the sample mass ranged from 3.50 to 3.80 mg. TGA was carried out using a TGA Q50 over a temperature range of 30–400 °C. The scan rate was set to 10 °C/min with dry nitrogen gas to regulate the sample temperature and the compartment purging. TGA samples were measured using an open pan configuration.

3.3.5 FT-IR Spectroscopy

Fourier Transform-IR spectra were obtained using a Bio-Rad FTS-40 spectrometer with a resolution of 4 cm⁻¹. All spectra were obtained with spectroscopic grade KBr which constituted ~80% (w/w) of the total sample. Samples were run as finely ground powders in reflectance mode.

3.3.6 Powder X-ray Diffraction (PXRD)

PXRD spectra were collected using a PANalytical Empyrean powder x-ray diffractometer using monochromatic Cu-K α 1 ($\lambda = 0.154$ nm) radiation. The applied voltage and current were set to 45 kV and 40 mA, respectively. The samples were mounted in a vertical configuration as evaporated hexane films and PXRD patterns were measured in a continuous mode over a 2θ angle range of 5–20° with a scan rate of 25 degree/min.

3.4 Results and Discussion

3.4.1 DSC

DSC is used to provide evidence for the purity and the formation of host-guest ICs. It can also be used to provide experimental support for the occurrence of variable guest conformations in host-guest systems.^{36,37} In particular, the disappearance of the melting endotherms of the free guest in the DSC thermograms can be used to indicate the formation of host-guest inclusion compounds.^{38,39} As well, changes in the enthalpy of dehydration³⁶ of the host is an indicator of the formation of host-guest complexes.

Figure 3.1 illustrates the DSC results for the host (hydrate), guest, and the 1:1 and 2:1 β -CD/PFOA complexes. Two endotherm peaks are shown in Figure 3.1 for the host at ~115 and 320 °C which are attributed to dehydration and decomposition processes, respectively. The DSC results for the guest reveal endothermic peaks at ~60, 100, and 170 °C; attributed to the melting, dehydration and vaporization transitions, respectively. The observed thermograms of the complexes are distinct relative to the unbound host and guest, and illustrate the disappearance of the guest melting endotherm at ~60 °C. The unique endotherms of the 1:1 and 2:1 complexes provide support that a unique solid phase is formed corresponding to the host-guest (i.e., β -CD/PFC) IC.

It is worthwhile to mention that some minor differences are observed between the thermograms of the dissolution complexes reported in this study with those of a previous study (*cf.* Chapter 2, Figure 2.1). The appearance of additional endothermic transitions ~180–270 °C in Figure 2.1 for the host-guest complexes prepared by slower rates of evaporation (~4–5d) were attributed to variable phase transitions of the bound guest in the complexes. These phase transitions were described in terms of the variable inclusion modes of the guest within the host. This is because the PFC guest may undergo phase separation in solution when cooled at a slower

rate or at non-uniform temperatures resulting in variable phases of the β -CD/PFOA complexes or even a slightly greater fraction of unbound guest. The variable phases are expected to have different thermal stabilities which manifest as unique endothermic transitions in the DSC. For example, the slow cool inclusion complexes reported previously were characterized to have greater phase purity relative to the dissolution complexes. This is because the slow cool complexes were cooled gradually under controlled temperature conditions in an insulated box before evaporating the solvent. The relative amounts of the host and guest in the complexes reported in this study (*cf.* §3.3.2) relative to those reported previously (as determined by titration with NaOH) are consistent with a lesser fraction of unbound guest. The preparation method in this study was modified such that the amount of solvent and duration (~2 days) of evaporation were controlled in order to afford phase pure β -CD/PFOA ICs.³⁰

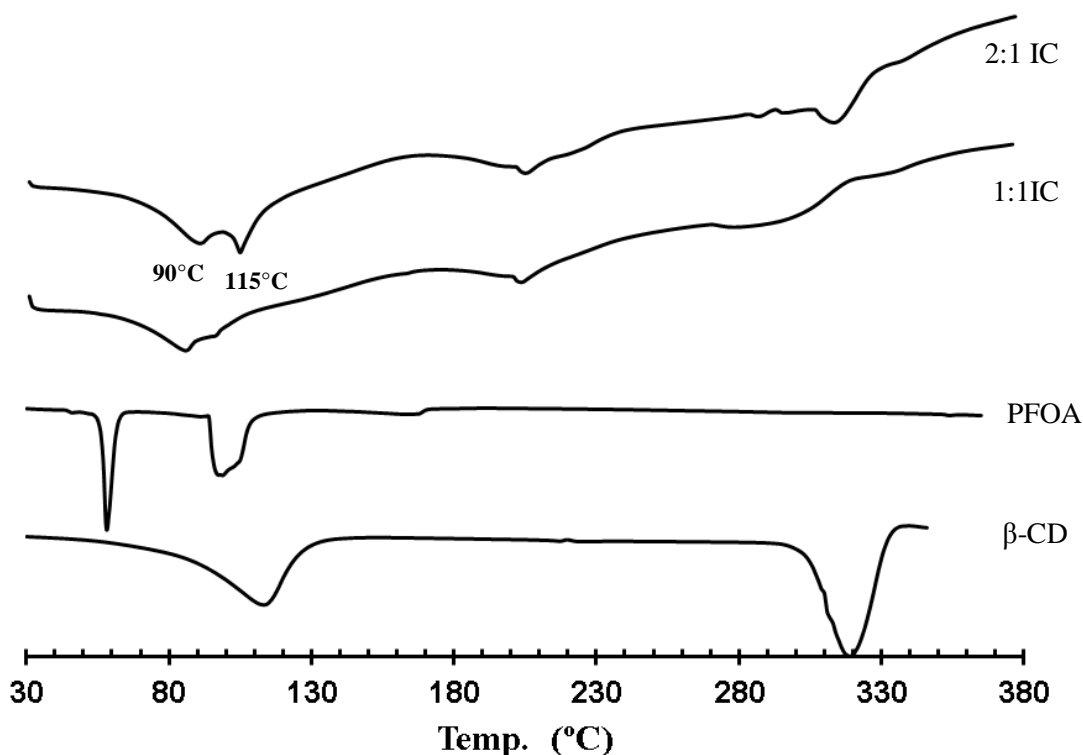


Figure 3.1 DSC thermograms of β -CD hydrate, unbound PFOA, and the 1:1 and 2:1 β -CD/PFOA inclusion compounds.

Two endothermic features are revealed for the inclusion compounds in Figure 3.1 at ~90 and 115 °C due to transitions involving dehydration. In general, the onset of dehydration for the 1:1 complexes occurs at a lower temperature than for the 2:1 complexes, and this is attributed to

the differences in the amount of inclusion bound water and the overall hydration state of these β -CD complexes.⁴⁰ For example, the relative intensities of the two peaks at 90 and 115 °C reveal that the 2:1 complexes possess a greater proportion of the cavity bound water than the 1:1 complexes. The occurrence of cavity bound and interstitial bound water is anticipated to have variable enthalpic characteristics, as evidenced by the desolvation temperature observed herein. Moreover, the displacement of the dehydration endotherm to lower temperatures for the 1:1 IC indicates reduced interactions and entropic characteristics of the hydrate water with the CD interior,⁴¹ consistent with the favourable binding affinity of the guest in this complex.^{28,29}

The decomposition endotherms of the two solid complexes ~320 °C in Figure 3.1 reveal distinct features. The 1:1 complex is made up of a single broad endotherm (at lower temperature ~270–320 °C); whereas, the 2:1 complex is composed of a prominent sharp feature (~320 °C) and other minor contributions over the temperature range observed for the 1:1 complex. This may be due to the variable binding configurations of the guest for the 1:1 and 2:1 complexes. Furthermore, the results reveal that the 2:1 complex may be a mixture of 1:1 and 2:1 ICs, in agreement with previous findings.^{17,25} In general, the differences in the DSC patterns of the host-guest complexes reported in this study when compared to a previous study reveal that complexes prepared by slower cooling rates or uncontrolled temperatures may result in phase separation of the host and guest. The tendency of the perfluorocarbon guest to undergo phase separation is more pronounced for the 1:1 relative to the 2:1 complexes due to the greater mole fraction of the free guest in the case of 1:1 complex formation. Thermogravimetric results for β -CD/PFOA complexes prepared by the modified dissolution method are presented as supplementary information in appendix B and reveal increased stability for the complexes (*cf.* Fig. B3.1).

3.4.2 FT-IR

Figure 3.2 shows the FT-IR spectra as stack plots for the host, guest, and the 1:1 and 2:1 host/guest inclusion complexes in the 500–4000 cm^{-1} spectral region. It is worthwhile to note that the FT-IR results reveal some minor spectral differences as compared with previous results.¹⁷ This was attributed to the different preparative methods employed in this study which result in more phase pure inclusion compounds as previously reported. However, changes in the relative intensity of bands **1–3** are consistently observed in the FT-IR results. Furthermore, the -

OH band of the guest is broad and shifted in comparison to the inclusion compounds and may indicate the formation of well-defined β -CD/PFOA ICs with variable hydration characteristics.⁴²

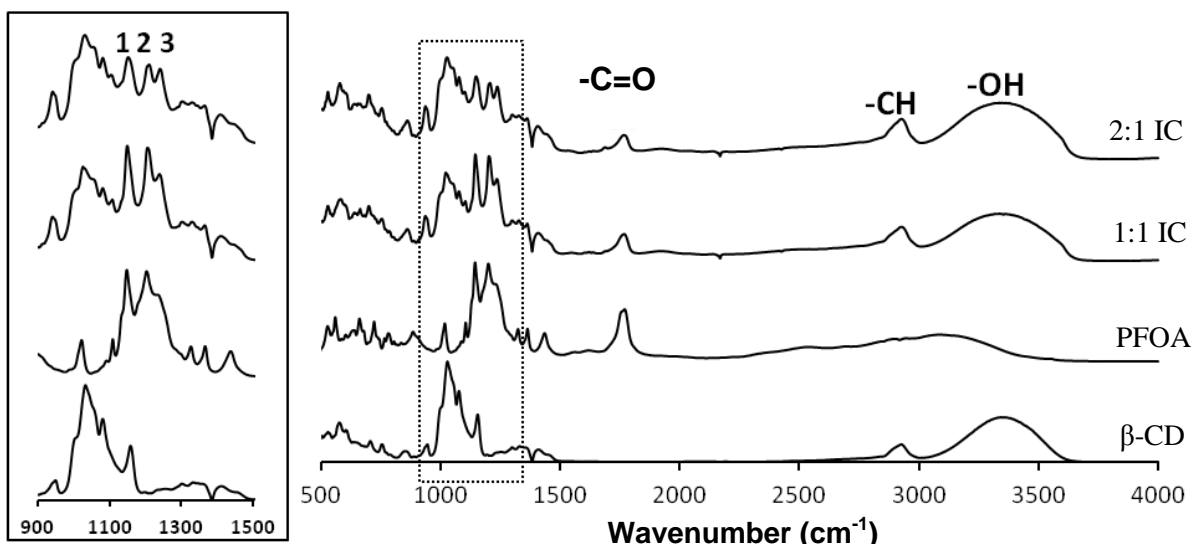


Figure 3.2 FT-IR spectra of β -CD, unbound PFOA, and the 1:1 and 2:1 β -CD/PFOA inclusion compounds. The inset shows expanded region from 900 – 1500 cm^{-1} .

The relative intensity and shift of the carbonyl vibrational bands ($-\text{C}=\text{O} \approx 1750 \text{ cm}^{-1}$) for the ICs relative to the pure guest reveal some information regarding the variable stoichiometry and/or inclusion mode of the guest within the host. The relative changes in the intensity of the IR bands: **1** ($\sim 1150 \text{ cm}^{-1}$; $\nu_{\text{asym}}-\text{CF}_2$), **2** ($\sim 1215 \text{ cm}^{-1}$; δ -CCC and β -CC), and **3** ($\sim 1250 \text{ cm}^{-1}$; $\nu_{\text{sym}}-\text{CF}_2$) (refer to the inset of Figure 3.2), for the 1:1 and 2:1 ICs were previously reported and assigned to the *gauche* and *trans* conformations of the guest in the complexed state.^{43,a,b} The attenuation of these bands, especially band 2 for the 2:1 complex (*cf.* Figure 3.2) is related to conformational changes of the guest in the 2:1 complex and are distinct to those of the conformation of PFOA in the 1:1 complex. The FT-IR results reveal that the bound guest in the 2:1 complex exists in an ensemble of *gauche*- and *trans*-conformers, with the latter being the preferred conformation (*cf.* Scheme 3.1) as described previously.¹⁷ In contrast to the 2:1 host/guest complex, the guest molecule in the 1:1 complex adopts a conformation similar to that of the unbound guest, as supported by the solid state NMR results described herein.

3.4.3 PXRD

Figure 3.3 shows the PXRD results for the host, guest, along with the 1:1 and 2:1 β -CD/PFOA ICs. The PXRD patterns of the physical mixtures (*cf.* Fig. B3.2) are well described as a direct superposition of weighted fractions of the individual spectra of the free host and guest. However, the PXRD results for the ICs in Figure 3.3 show unique diffraction lines and provide further support that unique phases are formed in accordance with the formation of host-guest inclusion compounds.

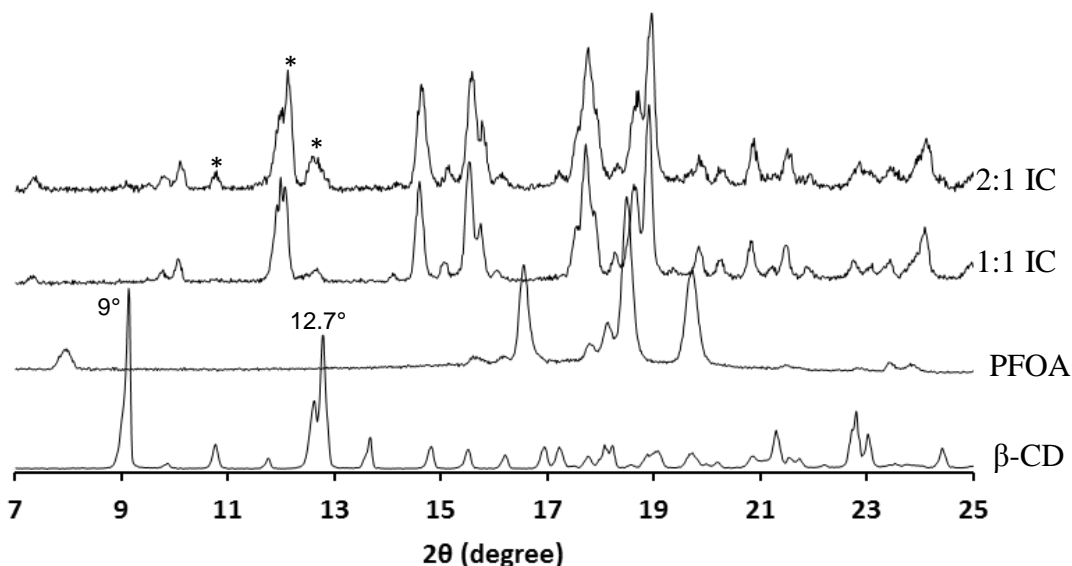


Figure 3.3 PXRD spectra of β -CD hydrate, PFOA, and the 1:1 and 2:1 β -CD/PFOA inclusion compounds. Differences in the PXRD patterns between the two complexes are shown by asterisks (*).

The PXRD patterns of the host (*cf.* Fig. 3.3) exhibit prominent lines at $\sim 9^\circ$, 12.7° , with minor signatures at higher 2θ values that are characteristic of a “cage-type” lattice arrangement due to the random packing arrangement of β -CD.⁴⁴ In contrast to the PXRD results of β -CD hydrate, the 1:1 and 2:1 complexes show intense diffraction lines at $2\theta \sim 7, 9.8, 12.0, 14.6, 17.8,$ and 18.9° , indicating the formation of “channel-type” structures.⁴⁵ In particular, the appearance of a strong peak at $2\theta \approx 18^\circ$ in the PXRD patterns of the ICs was previously reported and suggests that the complexes adopt *head-to-head* channel structures.⁴⁶ The PXRD spectra of the complexes reveal distinct XRD features that are unique relative to the host lattice structure, with minor perturbations to the unit cell. It is noteworthy that there are no observable features

corresponding to unbound PFOA, in agreement with IR and DSC results presented above. The quantitative indexing of PXRD lines to obtain unit cell dimensions of β -CD and various types of inclusion complexes is outside the scope of this study and are not reported herein. We speculate that the slight differences in the PXRD patterns of the 1:1 vs 2:1 complexes as shown with asterisks (*) are associated with the variable conformation or binding topologies of the guest and variable hydration states of the compounds,⁴⁷ as described in the DSC, FT-IR, and NMR results reported herein.

3.4.4. Solid-state NMR Characterization

3.4.4.1 ¹⁹F DP/MAS NMR

Figure 3.4 shows the ¹⁹F NMR results under DP conditions and MAS at 20 kHz and ambient temperature. The spectrum of the pure guest is comprised of well-resolved ¹⁹F resonances, and the assignments are supported by a previous report⁴⁸ according to the labeled structure in Figure 3.4. The spectra of the 1:1 and 2:1 complexes in Figure 3.4 consist of four contributions at ca. -82 ppm due to the methyl (CF₃) group, -117 ppm (C _{α} F₂), -120 ppm (main C _{m} F₂ groups), and -128 ppm (terminal C _{ϵ} F₂). For the sake of discussion, the respective ¹⁹F resonances at ca. -82, -117, -120, and -128 ppm will hereafter be referred to as CF₃, α -CF₂, main (C _{m} F₂) and the terminal (ϵ -CF₂) signals as denoted in Figure 3.4.

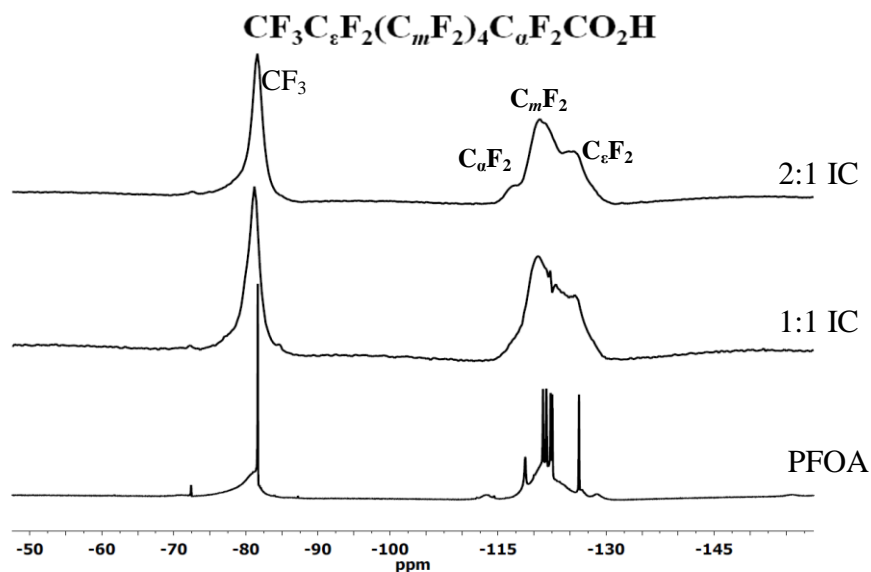


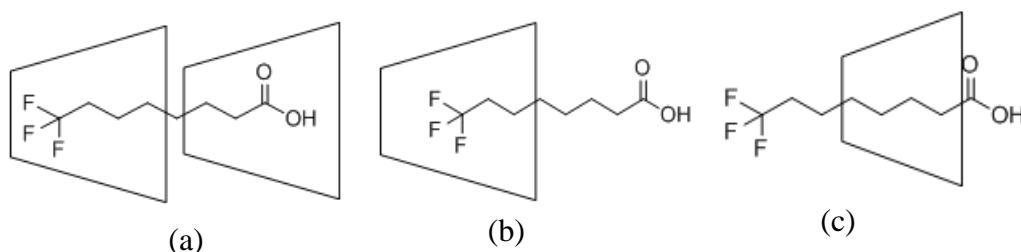
Figure 3.4 ¹⁹F DP/MAS (20 kHz) NMR spectra of PFOA, and the 1:1 and 2:1 β -CD/PFOA complexes at ambient temperature.

Note that the ^{19}F resonances of the guest in the bound state are broader relative to the pure guest and this is due to reduced motional averaging of the weak ^{19}F dipolar couplings along the PFOA chain, along with increased heterogeneity in the ^{19}F environments.²² In fact, the ^{19}F resonances of the 2:1 IC are relatively broad when compared to the 1:1 IC and this is related to the faster dynamics of localized domains or the entire guest within the 1:1 complex. A sharp spectral component at ca. -83 ppm was reported in a previous study¹⁷ and was attributed to the rotational dynamics of the CF_3 group of the guest and/or the presence of free domain of the guest in the complex.

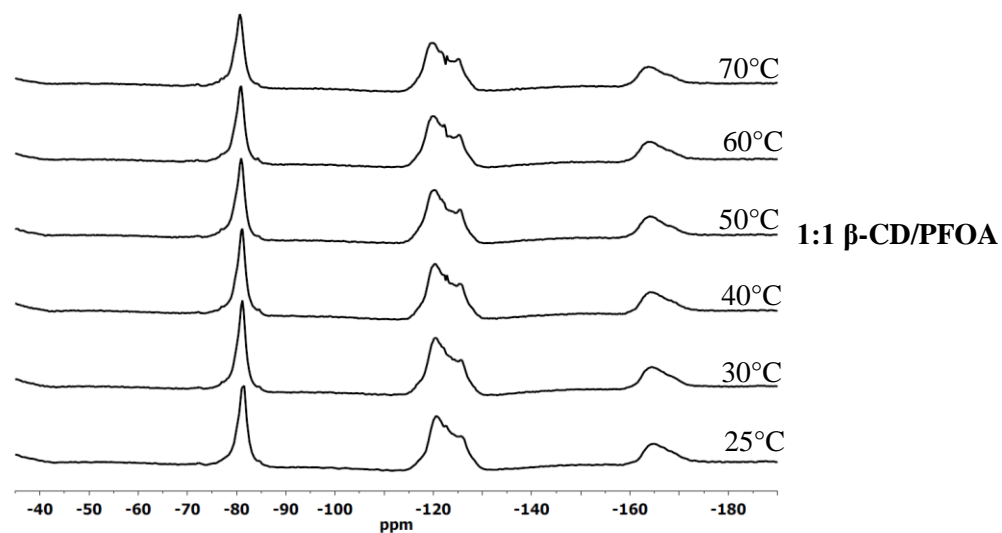
3.4.4.2 ^{19}F DP/MAS NMR Dynamics at Variable Temperature (VT)

The phase purity of the 1:1 and 2:1 host/guest inclusion compounds was further assessed in a VT (25–70 °C) ^{19}F DP/MAS NMR dynamic study at 20 kHz as shown in Figure 3.5a and b, respectively. The CF_2 regions at ca. -130 to -115 ppm in the 1:1 and 2:1 complexes did not show any noticeable line shape changes. However, the deconvolved CF_3 line shapes displayed variable guest dynamics in the 1:1 vs the 2:1 complexes.

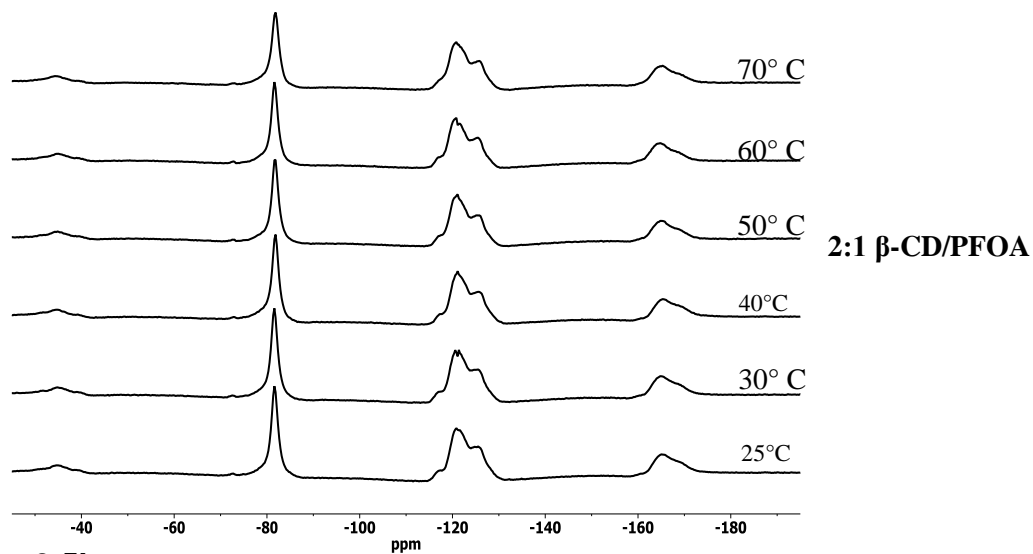
The expanded regions showing deconvolutions of the CF_3 resonances in the 1:1 and 2:1 complexes are shown in Figure 3.6, where CF_3 -*in* and -*out* represent the intra- and extra-cavity environments of the CF_3 group, respectively. The CF_3 resonance of the 2:1 complex can be fit to a single Lorentzian lineshape (2:1 CF_3 -*in*; cf. Scheme 3.2a). On the other hand, there is a shoulder on the high frequency side of the CF_3 resonance of the 1:1 complex, and the line shape is fit as a combination of two Lorentzian line shapes (1:1 CF_3 -*in* and 1:1 CF_3 -*out*; cf. Scheme 3.2b,c). The assignment of the three components to their respective complexes appears in Figure 3.6. Line shape fitting for both the 1:1 and 2:1 host/guest complexes were performed for all the temperatures measured, where the deconvolution parameters are presented in the supplementary data (Tables B3.1-3.2).



Scheme 3.2 Schematic representation of the three types of complexes that can hypothetically be formed between PFOA and β -CD.



3.5 a



3.5b

Figure 3.5 ^{19}F DP/MAS (20 kHz) NMR spectra of (a) the 1:1, and (b) 2:1 β -CD/PFOA dissolution complexes at variable temperature.

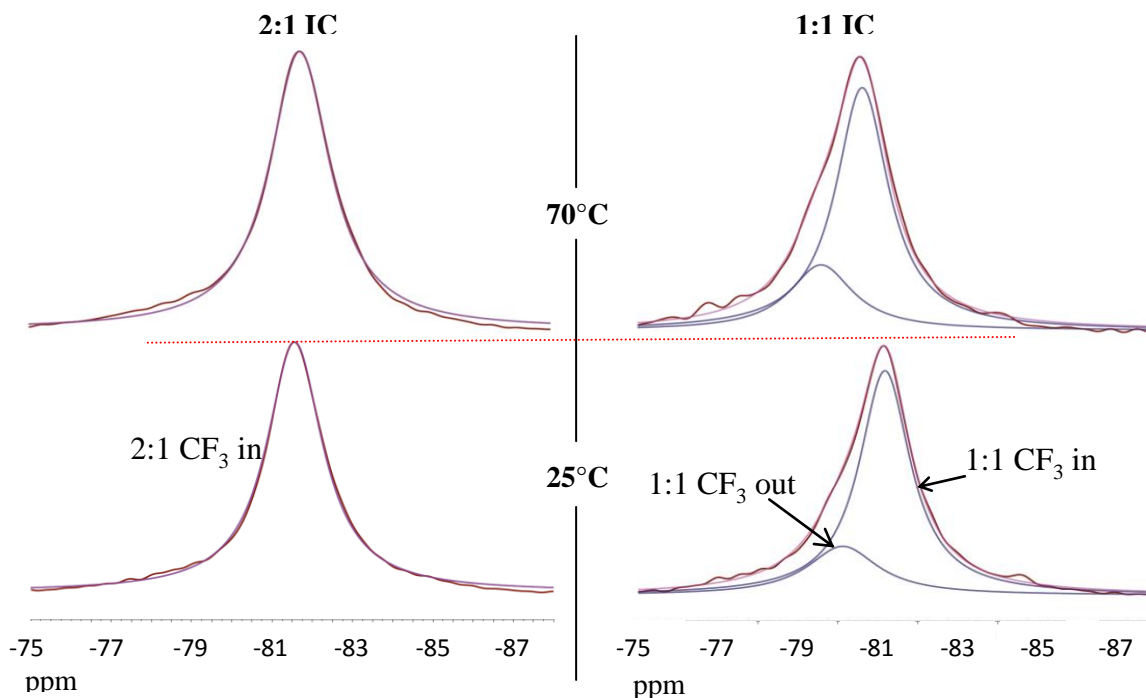
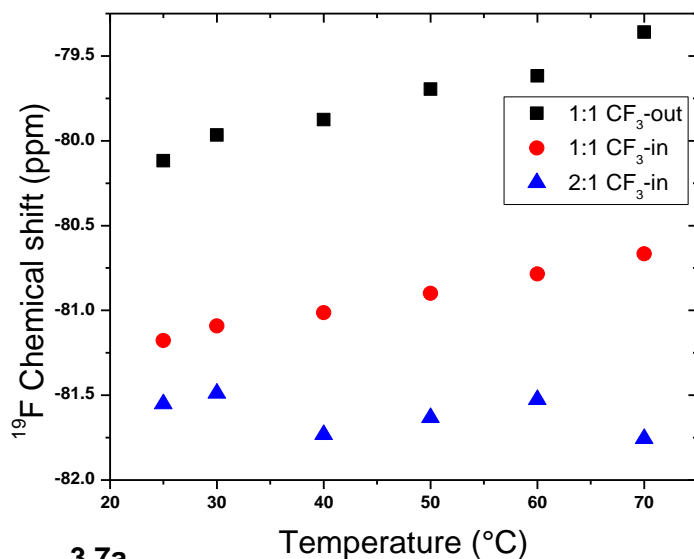


Figure 3.6 Deconvolution of the CF_3 signal in the ^{19}F DP/MAS (20 kHz) NMR spectra of the 2:1 (L) and 1:1 (R) complexes at 25 °C (bottom) and 70 °C (top). The 2:1 complex is fit to one Lorentzian peak (CF_3 -in cavity), while the 1:1 complex is fit to two Lorentzian peaks (CF_3 -in cavity, CF_3 -out of cavity).

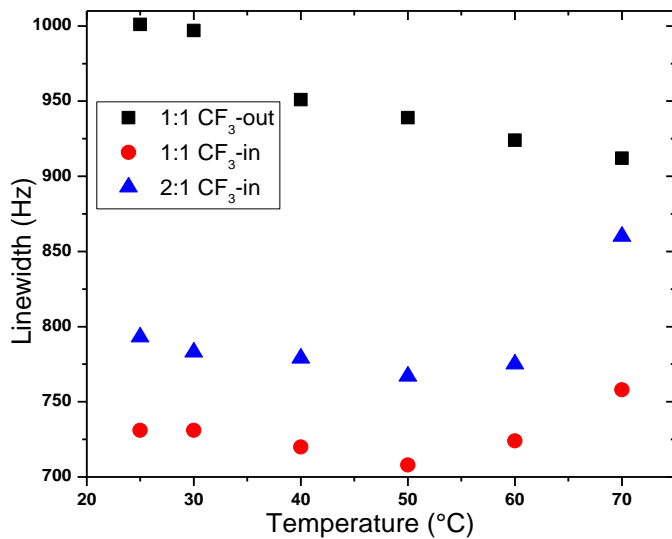
3.4.4.3 Chemical Shift and Line Width Analyses

A plot of the ^{19}F chemical shift and line width of the three components are shown in Figure 3.7a and b, respectively. The chemical shifts of both components in the 1:1 complex (i.e., 1:1 CF_3 -out and 1:1 CF_3 -in) shift to higher frequency (less negative ^{19}F shift) with increasing temperature; while the chemical shift of the 2:1 complex (2:1 CF_3 -in) appears to have no simple dependence on temperature. The chemical shift of the two CF_3 contributions (i.e. 2:1 CF_3 -in and 1:1 CF_3 -in) occur at similar shifts (between ca. -80.5 and -82.0 ppm), while that of the minor 1:1 CF_3 -out contribution appears at much higher frequency (-79.0 to -80.5 ppm). The line width of the 1:1 CF_3 -out component becomes narrower with increasing temperature, while that for the CF_3 -in component in both the 1:1 and the 2:1 ICs decrease to a minimum at 50°C and then increase again at higher temperatures. The apparent increase in the mobility of the CF_3 inside of the cavity suggests the possibility of exchange with the CF_3 outside of the cavity. Further details

of the dynamics of the guest in the 1:1 and 2:1 complexes will be discussed in the relaxation experiments (cf. §3.4.5).



3.7a



3.7b

Figure 3.7 Plots of the (a) chemical shift and (b) linewidth estimates of the 2:1 (one component) and 1:1 (two components) NMR spectra from the deconvolution results illustrated in Figure 3.6

3.4.4.4 ^{13}C Solid-state CP/MAS NMR

^{13}C solid-state NMR techniques which employ CP/MAS and high power decoupling afford well-resolved ^{13}C NMR spectra and provide useful structural information, as evidenced by the characterization of polymers and related host-guest systems.⁴⁹ The ^{13}C NMR CIS values and

line shape changes in the solid state can be used to probe conformational effects and molecular dynamics of the guest in a host-guest system.⁵⁰ Figure 3.8 shows the $^1\text{H}\rightarrow^{13}\text{C}$ CP/MAS spectra of the native host and the inclusion compounds at variable host/guest stoichiometry (i.e. 1:1 and 2:1).

The assignment of the ^{13}C resonance lines agrees with previous reports^{46,51} (*cf.* Scheme 3.3). A broad range of carbon resonance frequencies results from a range of host/host interactions and various hydrated forms.⁴⁶ The presence of sharp features for the line shapes of the ^{13}C nuclei in the 1:1 complex relative to the 2:1 complex (e.g., the rim carbons C_2 , C_3 , and C_5 ; *cf.* Scheme 3.3c) of the host in Figure 3.8 is associated with the greater motional dynamics of the guest molecule in the 1:1 complex. For example, the 1:1 complex was previously reported to show the most attenuated CIS for the intracavity ^1H nuclei (H_3 , H_5 ; *cf.* Scheme 3.3b) in solution (*cf.* Fig. 2.5).¹⁷

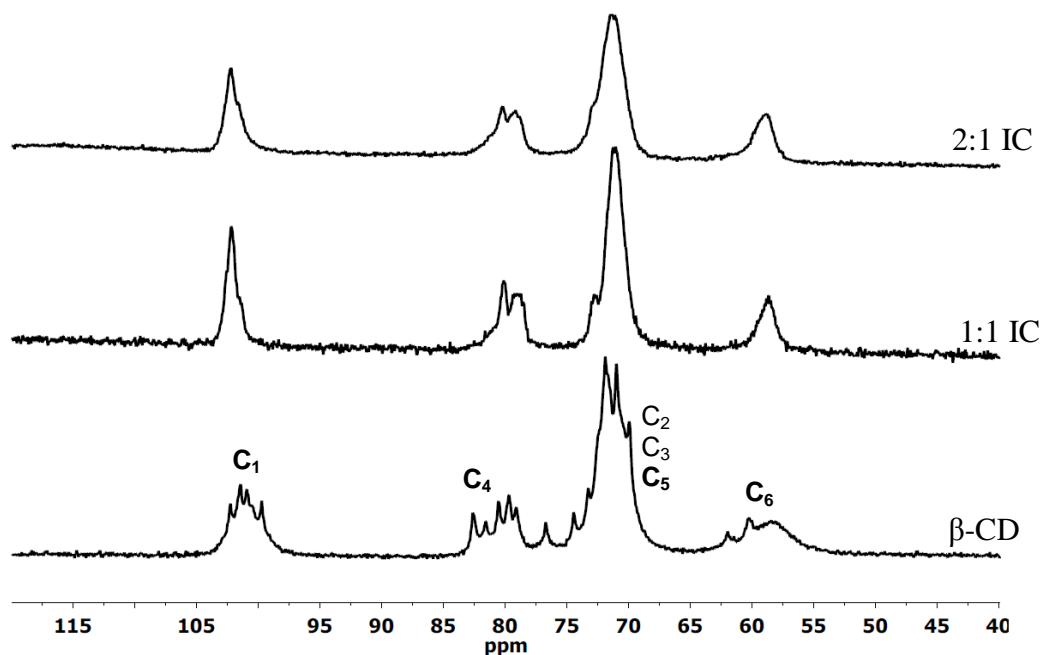


Figure 3.8 ^{13}C ($^1\text{H}\rightarrow^{13}\text{C}$) CP/MAS solid NMR spectra of β -CD, the 1:1 and 2:1 β -CD/PFOA complexes at ambient temperature.

The differences in ^{13}C line shapes of the host nuclei are attributed to the variety of hydration configurations of the 1:1 and 2:1 complexes, as described in Section 3.4.1. Furthermore, the ^{13}C CIS values are difficult to assess, in part, due to the resolution and line

In fact, C₁ and C₄ signals in Figure 3.9 are beginning to emerge at t_{CP} >7.5 ms (denoted by asterisks).

Similar CP transfer was not observed in the case of the 2:1 complex (data not shown) and this may be attributed to the less efficient ¹⁹F→¹³C CP transfer due to the variable dynamics and conformation of the guest in this complex. For example, an extended *all-trans* conformation of the guest molecule in the 2:1 complex in solution was reported in a previous study.¹⁷ The lack of CP transfer in the 2:1 complex implies that the intermolecular heteronuclear couplings inside the host cavity are weak which can result from large C-F distances. That, in combination with moderate internal motion (millisecond time scale) of the guest and fast MAS dynamics will destroy any prospects of CP transfer in the 2:1 complex. In contrast to the 2:1 complex, strong binding in the form of possible H-bonding can be thought to occur in one of the binding geometries in the 1:1 complex. This would exhibit favourable rotational dynamics and heteronuclear distances for improved CP conditions in the 1:1 complex. Despite the increased CP efficiency in the 1:1 complex, the carbon signal intensity is smaller than expected, which is readily explained by the major binding geometry being more dynamic and thereby lacking efficient CP transfer like in the 2:1 complex.

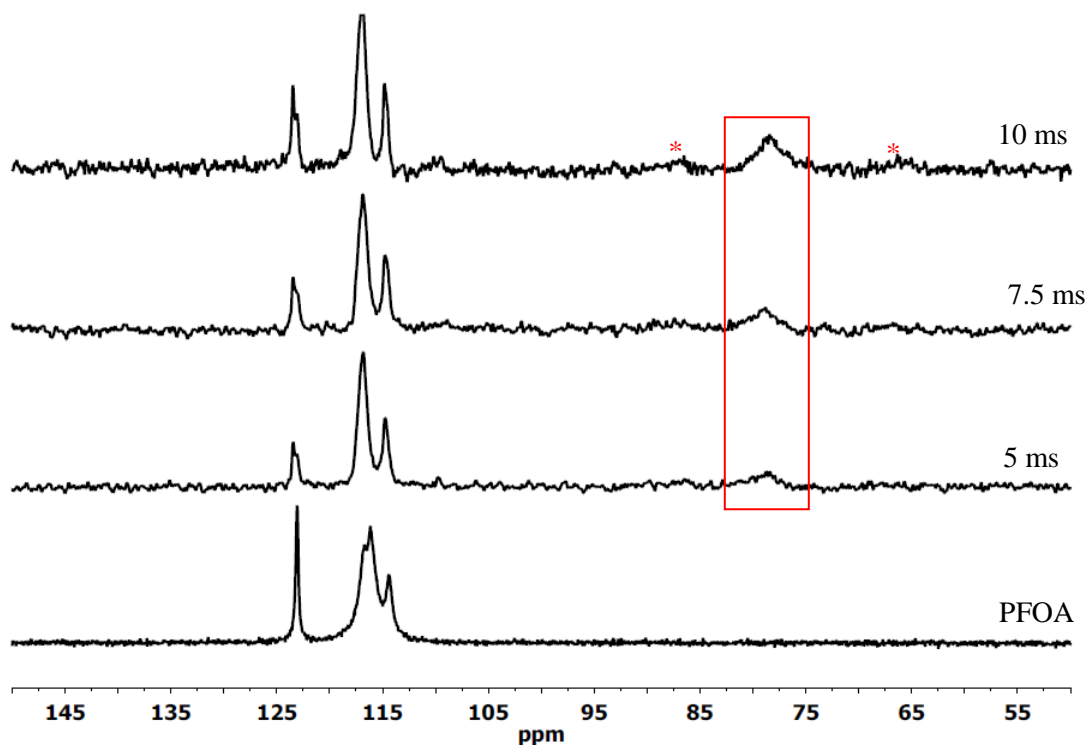


Figure 3.9 ¹³C (¹⁹F→¹³C) CP/MAS 20 kHz NMR spectra of pure PFOA and the 1:1 β-CD/PFOA complex at variable contact times.

3.4.5 Solid-state Dynamics and Relaxation Data

3.4.5.1 ^{19}F DP/MAS Dynamics at Ambient Temperature

Table 3.1 lists the ^{13}C -detected $T_{1\rho}^{\text{H}}$ relaxation times (under CP conditions) for the host, and the 1:1 and 2:1 host-guest complexes. In general, increased rates of $T_{1\rho}$ relaxation are observed for protons on all of the carbons upon formation of the complexes. The relaxation times in Table 3.1 are all between 2 and 3 ms for β -CD hydrate, while the complexes display significantly shorter values between 1 and 2 ms. The shorter $T_{1\rho}^{\text{H}}$ for the complexes explains their much reduced $^1\text{H}\rightarrow^{13}\text{C}$ CP efficiency in comparison to β -CD hydrate⁵⁴ (*cf.* Figure 3.8).

Table 3.1 ^{13}C -Detected $T_{1\rho}^{\text{H}}$ Relaxation Values for the ^{13}C Resonances of the Host and the 1:1 and 2:1 β -CD/PFOA Complexes at Ambient Temperature.

^{13}C shift (ppm)	Host (ms)	1:1 IC (ms)	2:1 IC (ms)
100 (C_1)	2.67 (± 0.07)	1.70 (± 0.02)	1.56 (± 0.04)
78 (C_4)	2.40 (± 0.06)	1.38 (± 0.05)	1.89 (± 0.10)
70 ($\text{C}_2, \text{C}_3, \text{C}_5$)	2.20 (± 0.03)	1.61 (± 0.02)	1.66 (± 0.01)
56 (C_6)	2.21 (± 0.09)	1.74 (± 0.06)	1.48 (± 0.09)

Note that $T_{1\rho}^{\text{H}}$ relaxation is governed primarily by the strength of the ^1H - ^1H dipolar interactions and the time scale of their fluctuations.⁵⁵ These interactions are influenced by local motion and packing arrangement in the lattice, which in turn are both strongly dependent on the degree of hydration. Furthermore, because there are few modes of motion available to the host overall, one must consider the motion of water and its influence on librational motion of the hydroxyl and methylene moieties of β -CD.

The dynamics of complex formation in solution between β -CD and alkanoate anions are near the diffusion-controlled limit but vary as the lipophilicity of the guest increases where the forward rate constant is in the order of $\sim 10^8 \text{ M}^{-1}\text{s}^{-1}$.^{56a} Ultrasonic relaxation measurements of cyclodextrin complexes further indicate that several relaxation processes occur; (i) a relaxation in

the 1 MHz range ($\sim\mu\text{s}$ /spectral time-scale) is attributed to “wig-wagging” of the host glycosidic bonds, (ii) a relaxation process in the 3–30 MHz range is attributed to hydration of the host cavity, and (iii) a relaxation in the 100 MHz range ($\sim\text{ns}$ /Larmor time-scale) is attributed to rotation of the $\text{C}_5\text{-C}_6$ bonds of the host.^{56b} In the case of complexes in the solid state, the guest, host, and solvent motional dynamics are considered to be strongly coupled. In these $T_{1\rho}^{\text{H}}$ relaxation experiments, a locking field of 66 kHz was used; this form of relaxation is sensitive to motion on the time-scale of ca. 15 μs . In this case we will assume that the slow motion (millisecond time scale) regime applies, where a decrease in the relaxation time indicates reduced correlation time and increased motion (*cf.* Fig. 1.21 and 1.22). Thus, faster motion on the ns scale will have less prominent effect on this relaxation process, but will feature more prominently in T_1 and T_2 processes.

In Table 3.1, one realizes that the $T_{1\rho}^{\text{H}}$ relaxation times for protons on the rim carbons $\text{C}_2/\text{C}_3/\text{C}_5$ (2.20 ms) and C_6 (2.21 ms) are the shortest for $\beta\text{-CD}$ hydrate (*cf.* Scheme 3.3c). In contrast, the relaxation times for protons on the anomeric carbons C_1 (2.67 ms) and C_4 (2.40 ms) are relatively longer. This reflects the influence of the extra-cavity environment of the host in driving $T_{1\rho}^{\text{H}}$; whereas protons on the rim carbons would be affected the most by hydration dynamics in the interstitial region, protons on the anomeric carbons would likely be more shielded from this influence as there is scant and less mobile water in the cavity.

The increased rates of relaxation observed for the complexes may come from two sources, namely (1) dipolar interactions between ^{19}F and ^1H coupled to the motion of the guest, and (2) $^1\text{H}\text{-}^1\text{H}$ homonuclear dipolar interactions. The former is predicated on the various inclusion geometries, and modulated by a range of dynamic processes of the guest; hence the relaxation of the protons on the anomeric carbons (C_1 and C_4) would be most affected. The latter is sensitive to changes in lattice structure, namely the breakup of the tight packing arrangements observed in $\beta\text{-CD}$ hydrate resulting in much less long range order and increased dynamics in the extra-cavity environment; hence relaxation of the protons on the rim carbons ($\text{C}_2/\text{C}_3/\text{C}_5$, and C_6) would be most influenced.

On going from the pure host to the 1:1 complex in Table 3.1, the anomeric carbons C_1 and C_4 on the interior surface of the macrocycle show the greatest decrease in $T_{1\rho}^{\text{H}}$ (ca. -1.0 ms), while the rim carbons $\text{C}_2/\text{C}_3/\text{C}_5$ and C_6 exhibit a smaller decrease (ca. -0.5 ms). This highlights the point that for the 1:1 complex, dipolar interactions between ^{19}F and ^1H coupled to the motion

of the guest are prominent drivers of $T_{1\rho}^H$ relaxation, in contrast to changes in homonuclear proton dipolar interactions associated with changes in host geometry and packing. The protons on C₄ have the shortest $T_{1\rho}^H$ in the 1:1 complex (1.38 ms), which suggests that the inclusion geometry of the guest places the CF₃ group closest to C₄, resulting in its enhanced relaxation driven by rotation of the CF₃ group. Conversely, the protons on C₆ in the 2:1 complex exhibit the shortest $T_{1\rho}^H$ (1.48 ms) while those of the C₄ protons are much longer (1.89 ms). This suggests an altered binding geometry of the guest in the 2:1 complex where the CF₃ group is nearer to the protons on the narrow rim of the host macrocycle as depicted in Scheme 3.2. However, one still has to allow for concomitant contributions from changes in host geometry and packing. Note that the protons on C₁ are more isolated from the extra-cavity environment (*cf.* Scheme 3.3); hence a reduced $T_{1\rho}^H$ on C₁ in the 1:1 complex is much less pronounced than that recorded for C₄, suggesting that the CF₃ group is more remote from C₁ (or the intra-cavity environment). Interestingly, $T_{1\rho}^H$ of the C₁ protons in the 2:1 complex is much smaller suggesting a binding geometry where the CF₃ geometry is much closer to the intra-cavity environment and this is consistent with the stoichiometry of the complexes and the deconvolution and chemical shift analyses in Figures 3.6 and 3.7, respectively. The end-to-end stacking of β -CD in the 2:1 complex (*cf.* Scheme 3.1) will ensure that the dynamics of the guest are limited to the intra-cavity environment of the host.

Recall that the T_1^H process is sensitive to the time scale predicated on the proton Larmor frequency.⁵⁷ More specifically, assuming that the dipolar mechanism dominates and the slow motion limit applies, the contribution from the zero-quantum transitions is most prominent; hence T_1 will be sensitive to differences in the proton frequencies implying a timescale of milliseconds. Table 3.2 shows the ¹³C-detected ¹H spin-lattice (T_1^H) relaxation times for the host, and those for the 1:1 and 2:1 ICs. In the case of β -CD hydrate, the T_1^H of the proton on the wide annular rim (C₂ and C₃) is significantly longer than the other protons, indicating possible increased dynamics in its environment.

The T_1^H s of the protons on C₁ show almost no change on going from β -CD to the complexes, while C₄ shows only a slight decrease (ca. 0.2 s) for 1:1 and no change for 2:1. In contrast, C₂ and C₃ (ca. 70 ppm, on the wide rim) show significant decrease in T_1^H (up to 0.4 s) upon going from β -CD hydrate to the complexes. As well, C₆ (56 ppm, on the narrow rim) shows a large decrease in T_1^H for the 1:1 complex (ca. 0.4 s) with minimal change for the 2:1 complex

(ca. 0.1 s). In the case of the complexes, the T_1^H of the anomeric carbons, namely C_1 (100 ppm) and C_4 (78 ppm), are least affected by the presence of the guest; whereas, the host nuclei near the rim, $C_2/C_3/C_5$ (70 ppm), and C_6 (56 ppm), are attenuated to a greater extent. These results are consistent with decreased order and enhanced dynamics of the host upon complexation. These observations are consistent with the ^{13}C CP/MAS NMR spectra in Figure 3.8 and PXRD patterns in Figure 3.3. Dynamic disorder results in narrowed distribution and larger line widths of the ^{13}C signals when compared to the spectrum of β -CD hydrate. Furthermore the characteristic and intense low angle reflection at 9° is greatly reduced indicating the loss of long range order.⁵⁸

Table 3.2 ^{13}C -detected T_1^H Relaxation Values for the ^{13}C Resonances of the host and the 1:1 and 2:1 β -CD/PFOA Complexes at Ambient Temperature.

^{13}C shift (ppm)	pure β -CD (s)	β -CD/PFOA 1:1 (s)	β -CD/PFOA 2:1 (s)
100 (C_1)	1.160 (± 0.009)	1.065 (± 0.035)	1.097 (± 0.018)
78 (C_4)	1.066 (± 0.018)	0.861 (± 0.017)	1.080 (± 0.011)
70 (C_2, C_3, C_5)	1.312 (± 0.025)	0.948 (± 0.023)	0.974 (± 0.013)
56 (C_6)	1.126 (± 0.011)	0.735 (± 0.005)	1.023 (± 0.005)

Table 3.3 shows the ^{13}C T_2 values of β -CD hydrate and the 1:1 and 2:1 complexes. Carbon relaxation times are governed by the chemical shielding anisotropy (CSA) contribution in the absence of homonuclear dipolar contributions, and where heteronuclear dipolar contributions are removed by proton decoupling. This relaxation process is driven by the carbon single quantum transitions; hence, the time scale is determined by the carbon Larmor frequency.

Assuming the slow motion regime applies, the relaxation time will increase slowly with decreasing dynamics frequency. For β -CD hydrate (and also the complexes to some extent), the much shorter T_2^C values for C_6 (1.84 ms for β -CD, 2.01 ms for the 1:1 complex and 2.06 ms for the 2:1 complex) are likely due to the increased dynamic disorder of this CH_2OH primary hydroxyl at the narrow rim, as it is tethered to the macrocycle framework by only one bond (*cf.* Scheme 3.3). All of the other carbons (C_1 , C_4 and $C_2/C_3/C_5$) are tethered to the framework by two

bonds, and as a result are much less dynamic, resulting in longer T_2 values. Again the anomeric carbon (C_4) indicates much greater rigidity than C_1 as its relaxation time is 1.2 ms longer.

Table 3.3 ^{13}C T_2 relaxation values (T_2^C) for the ^{13}C resonances of the host and the 1:1 and 2:1 β -CD/PFOA complexes at ambient temperature.

^{13}C shift (ppm)	β -CD (ms)	β -CD/PFOA 1:1 (ms)	β -CD/PFOA 2:1 (ms)
100 (C_1)	7.89 (± 0.25)	8.66 (± 0.13)	8.06 (± 0.20)
78 (C_4)	9.14 (± 0.37)	5.82 (± 0.09)	6.17 (± 0.21)
70 (C_2, C_3, C_5)	7.93 (± 0.21)	4.19 (± 0.13)	4.49 (± 0.11)
56 (C_6)	1.84 (± 0.08)	2.01 (± 0.03)	2.06 (± 0.06)

In the case of the complexes, heteronuclear ^{13}C - ^{19}F dipolar couplings contribute to T_2 relaxation as ^{19}F decoupling was not employed in these experiments. Upon formation of the 1:1 complex the carbons on the wide rim (C_2 and C_3 ; *cf.* Scheme 3.3c) experience enhanced relaxation, while those on the narrower rim (C_6) remain unchanged (within error limits). The anomeric carbon (C_1) is relatively unaffected; however, the T_2^C of C_4 is reduced significantly by 3.3 ms. As the C_6 carbon already exhibits significant motional freedom, further increases would have little incremental effect on its relaxation rate. The wide-rim carbons are sensing changes in H-bonding which modulates the carbon CSA, enhancing its relaxation. Again C_1 is isolated from the extra-cavity environment, and remote from the CF_3 ; hence, the relaxation rate does not change significantly. In contrast, C_4 is closer to the CF_3 group, whose motion and heteronuclear dipolar interactions drive the relaxation and reduce the relaxation time. The same observation is made in the 2:1 complex; however the relaxation times of the anomeric carbons are altered slightly where C_1 is reduced and C_4 increased. This is consistent with an inclusion binding geometry in the 2:1 complex where the CF_3 group is closer to C_1 (intracavity environment) than in the 1:1 complex.

Table 3.4 ^{19}F Relaxation Values ($T_1^{\text{F}}/T_2^{\text{F}}/T_{1\rho}^{\text{F}}$) for the ^{19}F Resonances of Sodium Perfluorooctanoate (SPFO), and the 1:1 and 2:1 β -CD/PFOA Complexes at Ambient Temperature.

^{19}F shift	$^{19}\text{F } T_1$		
	SPFO (s)	1:1 IC (s)	2:1 IC (s)
-80 ppm (CF_3)	2.655 (± 0.003)	0.917 (± 0.003)	1.199 (± 0.004)
-125 ppm (main CF_2)	3.104 (± 0.005)	0.978 (± 0.005)	1.138 (± 0.003)
^{19}F shift	$^{19}\text{F } T_2$		
	SPFO (ms)	1:1 IC (ms)	2:1 IC (ms)
-80 ppm (CF_3)	0.158 (± 0.003)	0.488 (± 0.005)	0.490 (± 0.005)
-125 ppm (main CF_2)	0.114 (± 0.002)	0.329 (± 0.008)	0.358 (± 0.006)
^{19}F shift	$^{19}\text{F } T_{1\rho}$		
	SPFO (ms)	1:1 IC (ms)	2:1 IC (ms)
-80 ppm (CF_3)	0.232 (± 0.004)	0.329 (± 0.003)	0.350 (± 0.009)
-125 ppm (main CF_2)	0.088 (± 0.003)	0.173 (± 0.005)	0.186 (± 0.004)

In Table 3.4, the ^{19}F relaxation times (T_1^{F} , T_2^{F} and $T_{1\rho}^{\text{F}}$) for the β -CD/PFOA complexes at ambient temperature are listed. Free PFOA was not studied in the solid state due its low melting point (*cf.* Table 1.5). Alternatively, the relaxation parameters of the sodium salt (SPFO; sodium perfluorooctanoate) were measured. The longer T_1^{F} s for the pure SPFO in Table 3.4 relative to the complexes is related, in part, to the less efficient spin diffusion of the perfluorocarbon chain due to rapid dynamics.^{56,22} Note that, the T_1^{F} and T_2^{F} values in Table 3.4 differ in excess of 3 orders of magnitude at ambient temperature, which suggests that the PFOA guest is in the slow motion regime at room temperature, where motion of the guest occurs at rates significantly smaller than the differences in ^{19}F chemical shifts (<20 kHz) under these conditions. The very short $T_{1\rho}^{\text{F}}$ for the CF_3 group in the complexes (~ 0.33 ms) are as much as 8 times shorter than the

$T_{1\rho}^H$ values of the host (*cf.* Tables 3.1 and 3.4). This explains why $^{19}\text{F} \rightarrow ^{13}\text{C}$ CP transfer was much less efficient than $^1\text{H} \rightarrow ^{13}\text{C}$ CP (*cf.* Figures 3.8 and 3.9), as seen in the dramatic disparity in the number of transients required in their respective experiments. In general, the relaxation data provide strong support for the formation of well-defined β -CD/PFOA ICs. Furthermore, it also provides support that the binding geometries of PFOA in the 1:1 and 2:1 complexes are distinct, and that the guest is more dynamic in former. Further details regarding the dynamics are explored in the temperature-dependent ^{19}F relaxation parameters.

3.4.5.1 ^{19}F DP/MAS Dynamics at Variable Temperature

Figure 3.10 (a,b) shows the variation of spin-lattice (T_1^F) and spin-spin (T_2^F) relaxation times as a function of temperature. The T_1^F values for the $-\text{CF}_3$ group of SPFO are presented in the supplementary data (Fig. B3.3) and are much longer than the corresponding values for the 1:1 and 2:1 ICs at various temperatures.⁵⁹ As previously described, longer T_1 values for a perfluoroalkyl guest relative to its complexed form with β -CD can be attributed to motional quenching via spin diffusion. In the solid state, long alkyl chains undergo axial rotation as a consequence of successive rotational events in fragments of the chain. In these complexes, axial rotation occurs at a rate similar or greater than the differences in the ^{19}F resonance frequencies (<20 kHz), while C-C bond rotation of the CF_3 moiety occurs at rates far exceeding the ^{19}F Larmor frequency. Thus, two different motional time scales potentially apply, where an axial motion is most likely in the slow motion regime, and the CF_3 bond rotation would be in the fast motion regime.

Relaxation of ^{19}F nuclei results from fluctuations in local fields arising from both the CSA and dipole-dipole coupling interactions modulated by localized reorientational motion. Molecular motions at frequencies that greatly exceed the CSA and dipolar interactions attenuate them significantly, and may eliminate them completely with rapid isotropic reorientational dynamics.^{22,57} Hence, the faster the rate the less efficient the dipole-dipole (DD) and the CSA relaxation mechanisms become, and results in longer T_1 relaxation times.

SPFO is expected to have a completely different lattice environment than the inclusion complexes; therefore, the axial motion and CF_3 bond rotation will occur at very different rates. Furthermore, the conformational properties of the SPFO chain are unlikely to correspond to the nuclei of PFOA in the complexed state; hence, the homonuclear dipolar couplings are expected

to be very different. The longer relaxation times are consistent between the ^{19}F environments and indicate that the fast motion regime applies, where the CF_3 motion drives ^{19}F relaxation throughout the chain via efficient spin diffusion.

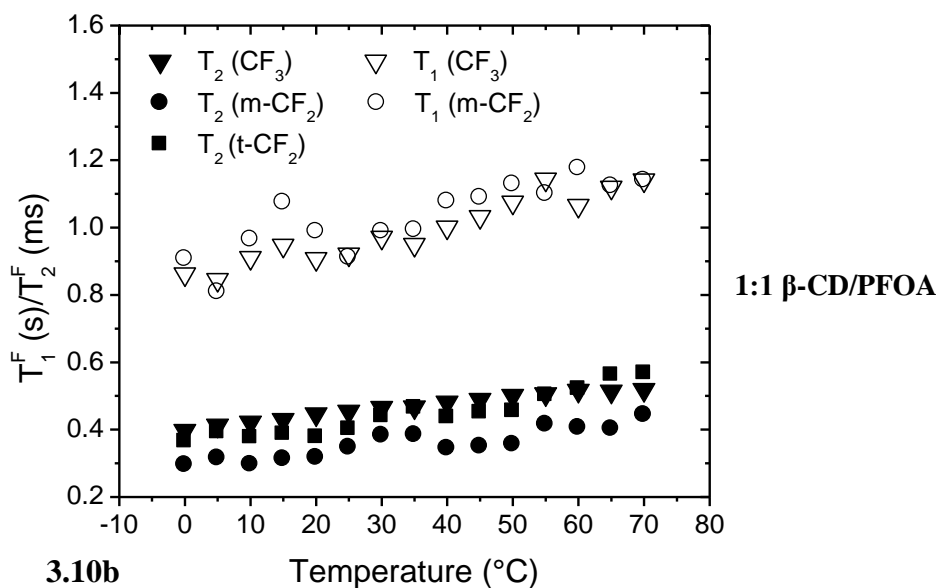
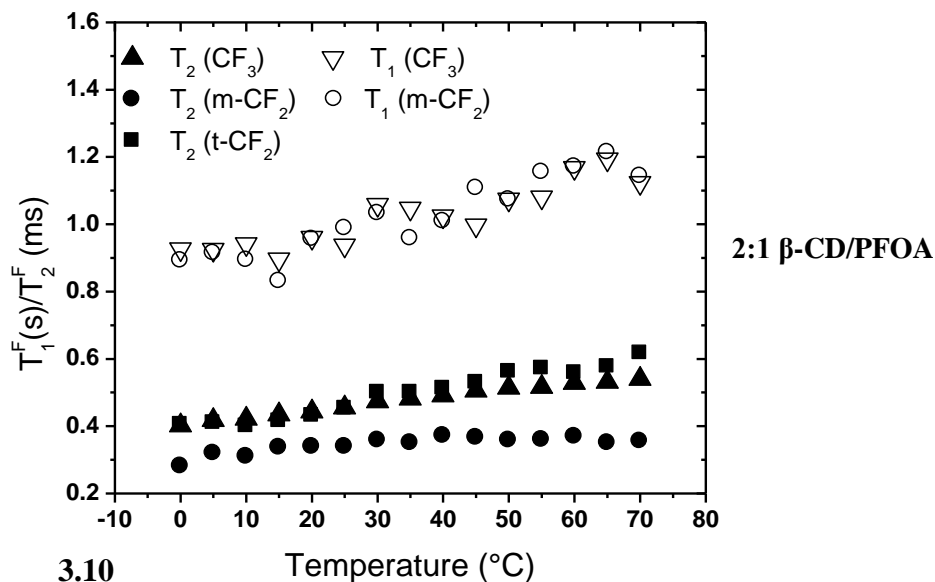


Figure 3.10 ^{19}F T_1 (open symbols) and T_2 (filled symbols) values for the CF_3 , main (C_mF_2) and terminal C_tF_2 groups for the (a) 1:1, and (b) 2:1 $\beta\text{-CD/PFOA}$ complexes.

The inclusion compounds exhibit more comparable dynamics and local environments than SPFO, hence their relaxation times would be expected to be similar. The 1:1 complex has two different inclusion geometries, while the 2:1 complex appears to have one geometry, as

described previously. One form of the 1:1 complex involves binding near the wide-rim carbons (Scheme 3.2c), while the other appears to be intracavity, as is the case with the 2:1 complex (Scheme 3.2a,b). The former is expected to be more constrained near the carbonyl end as suggested in the ^{19}F to ^{13}C CP dynamics, while the latter does not appear to be constrained to the same extent. Hence, one would expect very different rates of axial motion along the chain for the constrained form of the 1:1 complex. Axial rotation on both forms would be expected to be well within the slow motion regime. Consequently, the efficiency in spin diffusion is expected to vary along the chain in the constrained form and thereby directly influencing the degree to which CF_3 rotation is able to drive relaxation along the chain. This would cause the relaxation times to vary along the chain in the constrained form and to much lesser extent in the more mobile form. However, the manner in which they change with increasing temperature is determined by the activation of CF_3 bond rotation which will be the same for each. As a result, the T_1 and T_2 values are expected to increase gradually with temperature, consistent with the behaviour in the fast motion regime.

Figures 3.10a and b show the variation of ^{19}F T_1 and T_2 values as a function of temperature for the 1:1 and 2:1 complexes, respectively. Note that the T_2 values are generally several orders of magnitude shorter than the T_1 values at the same temperature. Generally, both T_1 and T_2 increase monotonically with temperature, where the values for the ^{19}F T_1 (open symbols in Figure 3.10a,b) of the $-\text{CF}_3$ and the main $-\text{CF}_2$ groups (ca. -120 ppm) are similar in both the 1:1 and 2:1 complexes. Thus, the motion of the guest that drives T_1 affects all perfluoroalkyl groups in a comparable way for both complexes.

In contrast to the T_1 's, the ^{19}F T_2 values (filled symbols in Figure 3.10a,b) for the CF_3 , $\text{C}_\epsilon\text{F}_2$ and C_mF_2 groups of the 1:1 complex are different. Although T_2 is driven by rapid CF_3 rotation, spin diffusion propagates it along the chain less efficiently. This will result in a reduced relaxation time for the CF_2 groups further removed from the CF_3 group (i.e., the main C_mF_2 groups). As the T_2 data contain less scatter than the T_1 data, it was possible to distinguish between T_2 's of the main (C_mF_2) and terminal ($\text{C}_\epsilon\text{F}_2$) signals and determine that they are statistically distinct. In the case of the 2:1 complex (Figure 3.10b), the difference in T_2 between the terminal and main CF_2 moieties is less pronounced, and follows a similar trend at higher temperatures. In contrast to the 2:1 complex, the difference in T_2 's in the 1:1 complex is quite

prominent. Thus, the axial dynamics of PFOA differ sufficiently and lead to unique T_2 relaxation behavior along the chain for each of the complexes.

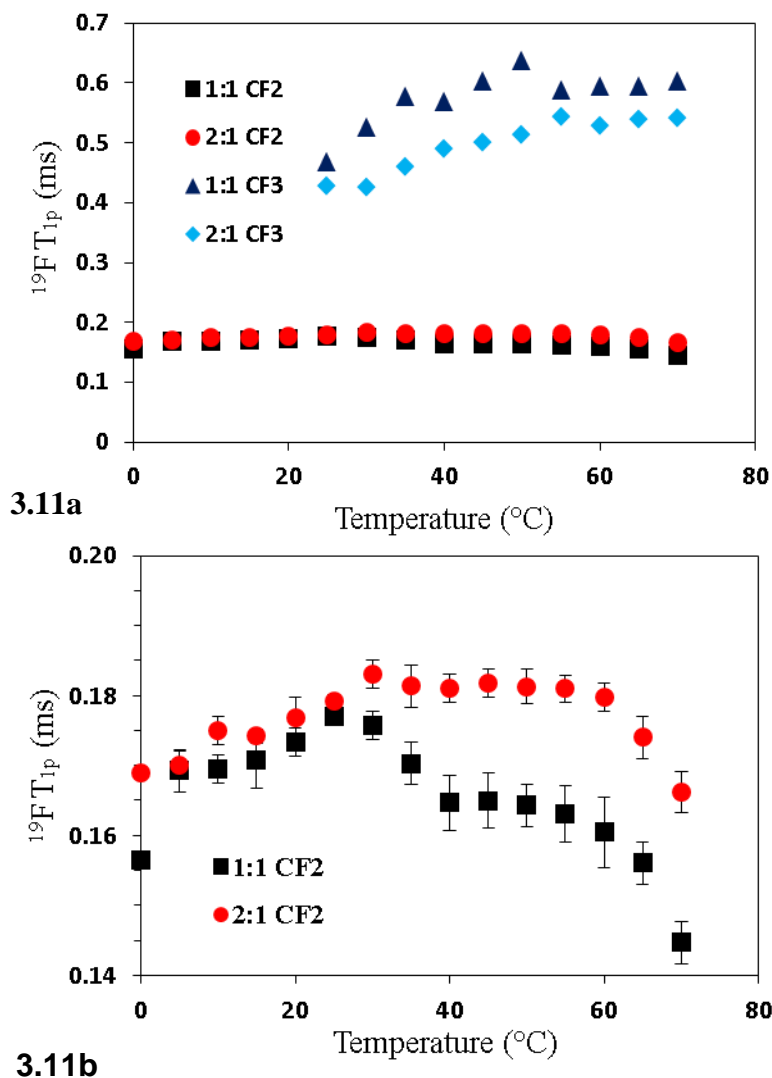


Figure 3.11 (a) ^{19}F $T_{1\rho}$'s for the CF₂ and CF₃ groups of the 1:1 and 2:1 $\beta\text{CD}/\text{PFOA}$ complexes. (b) ^{19}F $T_{1\rho}$'s for the CF₂ groups of the 1:1 and 2:1 $\beta\text{CD}/\text{PFOA}$ complexes on an expanded scale.

The ^{19}F $T_{1\rho}$ data at variable temperature for the 1:1 and 2:1 complexes appear in Figure 3.11a for the CF₃ (25 to 70 $^{\circ}\text{C}$) and main CF₂ (0 to 70 $^{\circ}\text{C}$) signals. The $T_{1\rho}$ of the CF₃ is governed by rotation about the C-C bond. The $T_{1\rho}$'s increase with increasing temperature, indicating that the CF₃ rotation rate is greater than the spin-lock frequency (ca. 100 kHz). The 1:1 complex appears to have a faster rate of CF₃ rotation which could be a consequence of one of the favoured

binding geometries. The geometry where the CF₃ points out of the β-CD cavity would make rotation less restricted than the geometry where the CF₃ is confined to the cavity as in the 2:1 complex (*cf.* Scheme 3.2).

The ¹⁹F T_{1ρ}'s of the CF₂ groups are much shorter than that for CF₃, and show little difference between the 1:1 and 2:1 complexes. The ¹⁹F T_{1ρ} of the CF₂ groups may be influenced by the librational motion of the chain of the PFOA guest, and the lack of clear temperature dependence indicates that the rate of the librational motion is reduced in comparison to the rate of CF₃ rotation.

When comparing T_{1ρ} of the CF₃ and the CF₂ groups, it can be seen that the T_{1ρ} (CF₃) shows a much greater difference between 1:1 and 2:1 complexes, while T_{1ρ} (CF₂) of the 1:1 and 2:1 complexes are almost the same. This indicates that the dynamics of the CF₃ group is quite different between the 1:1 and 2:1 complexes. In contrast, the librational motion of the whole PFOA chain that drives ¹⁹F T_{1ρ} of the CF₂ groups is occurring at practically the same rate in the 1:1 and 2:1 complexes. In the case of the complexed CF₂ groups, the ¹⁹F T_{1ρ} relaxation times are much less scattered than their CF₃ counter parts, as observed on the expanded scale in Figure 3.11b where significant differences are seen. The 1:1 complex shows a more complex dependence of T_{1ρ} with temperature than that observed for the 2:1 complex. In both cases the T_{1ρ} are near their minima, where each seem to have several local minima at different temperatures indicating several dynamic modes differing significantly in timescale. This is especially evident from T ≥ 40 °C (40 - 70 °C in this case) and coincides with the DSC results where significant differences are observed.

3.5 Conclusions

Solid-state ¹H/¹⁹F→¹³C CP/MAS NMR spectroscopy, DSC, FT-IR, and PXRD were used to study the structure and dynamic properties of β-CD/PFOA host-guest complexes. β-CD/PFOA inclusion complexes were prepared using a modified dissolution method with improved phase purity and were further characterized by the various complementary methods described herein. β-CD forms complexes with a unique channel-type structure with PFOA and differs when compared to the cage-type structure of β-CD hydrate. PFOA adopts variable alkyl chain conformation for the 1:1 and 2:1 complexes, where the 1:1 complex prefers a *gauche* conformation, similar in nature to the helical structural form of unbound PFOA. PFOA adopts a

mixture of *gauche*- and *trans*-conformers for the 2:1 complex, as evidenced from the FT-IR results. Two modes of rotational dynamics were concluded in the complexes; the axial rotation of the entire chain, and the C-C/C-F bond rotation of the CF₃ group at the termini of the perfluorocarbon chain. The guest molecules in the 1:1 and 2:1 complexes were described to undergo both the axial and CF₃ bond rotations in varying magnitudes; whereas the latter dynamics can be concluded to occur at practically the same rate in the 1:1 and 2:1 complexes. Overall, the relaxation data reveal greater motional dynamics of PFOA in the 1:1 complex providing further support that the 1:1 and 2:1 complexes exhibit different dynamic properties. Furthermore, the relaxation data provide an insight into the binding geometry of the guest in the complexes; whereas the location of the guest in the 1:1 is both extra- and intra-cavity, while that of the 2:1 complex is mainly intra-cavity. For example, the wide rim carbons of the host underwent significant changes in H-bonding as revealed by the relaxation data and the ¹H→¹³C CP/MAS results. ¹⁹F→¹⁹C CP/MAS results in the solid state provided unique and unequivocal proof that the guest is included within the host cavity as a well-defined inclusion complex according to the nature of the host-guest stoichiometry.

3.6 Acknowledgements

The authors gratefully acknowledge the Natural Sciences and Engineering Research Council (NSERC), the University of Saskatchewan, and the University of Lethbridge for support of this research.

3.7 References

- (1) Li, B.; Danon-Schaffer, M. N.; Li, L. Y.; Ikonomou, M. G.; Grace, J. R. *Water Air Soil Pollut.* **2012**, *223*, 3365–3372
- (2) Houde, M. ; De Silva, O. A. ; Muir, D. C. G. ; Letcher, J. R. *J. Environ. Sci. Technol.*, **2011**, *45*, 7962–7973.
- (3) Houde, M.; Martin, J. W.; Letcher, R. J.; Solomon, K. R.; Muir, D. C. G. *Environ. Sci. Technol.* **2006**, *40*, 3463–3473.
- (4) Wang, T.; Chen, C.; Naile, J. E.; Khim, J. S.; Giesy, J. P.; Lu, Y. *Bull Environ Contam. Toxicol.* **2011**, *87*, 74–79

- (5) Fujii, S.; Polprasert, C.; Tanaka, S.; Nguyen, P. H. L.; Yong, Q. J. *J. Water Supply Res. Technol. AQUA* **2007**, *56*, 313-326.
- (6) Saito, N.; Harada, K.; Inoue, K.; Sasaki, K.; Yoshinaga, T.; Koizumi, A. *J. Occup. Health* **2004**, *46*, 49-59.
- (7) Key, B. D.; Howell, R. D.; Criddle, C. S. *Environ. Sci. Technol.* **1997**, *31*, 2445-2454.
- (8) Rao, N. S.; Baker, B. E.; Tatlow, J. C. *Organofluorine Chemistry Principles and Commercial Applications*; Plenum Press: New York, **1994**.
- (9) Kissa, E. *Fluorinated Surfactants and Repellants*, 2nd ed., Marcel Dekker; New York, **1994**.
- (10) Guruge, K. S.; Yeung, L. W. Y.; Yamanaka, N.; Miyazaki, S.; Lam, P. K. S.; Giesy, J. P.; Jones, P. D.; Yamashita, N. *Toxicol. Sci.* **2006**, *89*, 93-107.
- (11) Fei, C.; McLaughlin, J. K.; Lipworth, L.; Olsen, J. *Human Reprod.* **2009**, *24*(5), 1200-1205.
- (12) Peden-Adams, M. M.; Keller, J. M.; EuDaly, J. G.; Berger, J.; Gilkeson, G. S.; Keil, D. E. *Toxicol. Sci.* **2008**, *104*, 144-154.
- (13) Dewitt, J. C.; Copeland, C. B.; Strynar, M. J.; Luebke, R. W. *Environ. Health Perspect.* **2008**, *166*(5), 644-650.
- (14) Hoffmann, H. *J. Mol. Liq.*, **1997**, *72*, 191-230.
- (15) Lemal, D. M. *J. Org. Chem.* **2004**, *69*, 1-11.
- (16) US EPA. World Wide Web site: <http://www.epa.gov/opptintr/pfoa/index.htm>.
- (17) Karoyo, A. H.; Borisov, A.; Hazendonk, H.; Wilson, L. D. *J. Phys. Chem. B* **2011**, *115*, 9511-9527
- (18) Kitamura, S.; Fujimura, T.; Kohda, S. *J. Pharm. Sci.* **1999**, *88*, 327-330.
- (19) Nicolle, G. M.; Merbach, A. E. *Chem. Commun.* **2004**, 854-855
- (20) Dias, A. M. A.; Andre-Dias, C.; Lima, S.; Countinho, J. A. P.; Teixeira-Dias, J. J. C.; Marrucho, M. *J. Coll. Int. Sci.* **2006**, *303*, 552-556.
- (21) Szejtli, J.; Osa, T. *In Comprehensive Supramolecular Chemistry*, Eds.; Pergamon Press: New York, **1996**.
- (22) Tatsuno, H.; Ando, S. *J. Phys. Chem. B* **2006**, *110*, 25751-25760.
- (23) Druliner, J. D.; Wasserman, E. *J. Fluor. Chem.* **1995**, *72*, 75-78.
- (24) Guo, W.; Fung, B. M.; Christian, S. D. *Langmuir* **1992**, *8*, 446-451.
- (25) Wilson, L. D.; Siddall, S. R.; Verrall, R. E. *Can. J. Chem.* **1997**, *75*, 927-933.

- (26) Zhang, H. H.; Hogen-Esch, T. E.; Boschet, F.; Margaillan, A. *Langmuir* **1998**, *14*, 4972–4977.
- (27) Koito, Y.; Yamada, K.; Ando, S. *J. Incl. Phenom. Macrocycl. Chem.* **2013**, *76*, 143-154.
- (28) Junquera, E. ; Aicart, E. ; Tardajos, G. *Langmuir* **1993**, *9*, 1213–1219.
- (29) Wilson, L. D.; Verrall, R. E. *Langmuir* **1998**, *14*, 4710–4717.
- (30) Liu, Y.; Pellerin, C. *Polymer* **2009**, *50*, 2601–2607
- (31) Power, G.; Vij, J. K.; Johari, G. P. *J. Chem. Phys.* **2007**, *126*, 0345121-0345129.
- (32) Borisov, A. S.; Hazendonk, P.; Hayes, P. G. *J. Inorg. Organomet. Polym.* **2010**, *20*, 183–212.
- (33) Bennett, A. E.; Rienstra, C. M.; Auger, M.; Lakshmi, K. V.; Griffin, R. G. *J. Chem. Phys.* **1995**, *103*, 6951–6958.
- (34) Hu, J. Z.; Zhou, J.; Deng, F.; Feng, H.; Yang, N.; Li, L.; Ye, C. *Solid State Nucl. Mag.* **1996**, *6*, 85–94
- (35) Samson, A. O.; Chill, J. H.; Anglister, J. *Biochemistry* **2005**, *44*, 10926–10934
- (36) Cairo, P.; Artuso, F.; Alcaro, S.; Fontananova, E.; Tocci, E.; Drioli, E. *Chem. Phys. Lett.* **2008**, *454*, 374–381.
- (37) Marques, H. M. C.; Hadgraft, J.; Kellaway, I. W. *Int. J. Pharm.* **1990**, *63*, 259-266
- (38) Rotich, M. K.; Brown, M. E.; Glass, B. D. *J. Therm. Anal. Cal.* **2003**, *73*, 671-705.
- (39) Mura, P.; Maestrelli, F.; Cirri, M.; Furlanetto, S.; Pinzauti, S. *J. Therm. Anal. Cal.* **2003**, *73*, 635–646.
- (40) Reddy, M. N.; Rehana, T.; Ramakrishna, S.; Chowdary, K. P. R.; Diwan, P. V. *AAPS Pharm. Sci.* **2004**, *6*, 1–9.
- (41) Villaverde, J. ; Morillo, E. ; Pérez-Martínez, J. I. ; Ginés, J. M. ; Maqueda, C. *J. Agric. Food Chem.* **2004**, *52*, 864–869.
- (42) Subramaniam, P.; Mohamad, S.; Alias, Y. *Int. J. Mol. Sci.* **2011**, *11*, 3675–3685.
- (43) Albinsson, B. ; Michl, J. *J. Phys. Chem.* **1996**, *100*, 3418–3429.
- (44) (a) Okumura, H.; Kawaguchi, Y.; Harada, A. *Macromolecules*, **2001**, *34*, 6338–6343; (b) Jiao, H.; Goh, S. H.; Valiyaveetil, S. *Macromolecules* **2002**, *35*, 3997–4002.
- (45) (a) Caira, M. R. *Rev. Roum. Chim.* **2001**, *46*, 371–386; (b) Fernandes, J. A.; Lima, S.; Braga, S. S.; Ribeiro-Claro, P.; Rodriguez-Borges, J. E.; Teixeira, C.; Pillinger, M.; Teixeira-Dias, J. J. C.; Goncalves, I. S. *J. Organomet. Chem.* **2005**, *690*, 4801–4808.

- (46) Abbate, V.; Bassindale, A. R.; Brandstadt, K. F.; Taylor, P. G. *J. Incl. Phenom. Macrocycl. Chem.* **2012**, *74*, 223–230.
- (47) Sidhu, P. S.; Enright, G. D.; Ripmeester, J. A.; Penner, G. H. *J. Phys. Chem. B* **2002**, *106*, 8569–8581.
- (48) Pawsey, S.; Reven, L. *Langmuir* **2006**, *22*, 1055–1062.
- (49) Lu, J.; Mirau, P.; Tonelli, A. E. *Prog. Polym. Sci.* **2002**, *27*, 357–401.
- (50) Derome, A. E. In *Modern NMR Techniques for Chemistry*; Pergamon: New York, 1987.
- (51) Cunha-Silva, L.; Teixeira-Dias, J. J. C. *J. Phys. Chem. B* **2002**, *106*, 3323–3328.
- (52) Gidley, M. J.; Bociek, S. M. *J. Am. Chem. Soc.* **1988**, *110*, 3820–3829
- (53) Lichtenthaler, F. W.; Immel, S. *Starch* **1996**, *48*, 145–154; and references cited therein.
- (54) Thurber, K. R.; Tycko, T. *J. Chem. Phys.* **2012**, *137*, 084508–084514
- (55) Steiner, E.; Yemloul, M.; Guendouz, L.; Leclerc, S.; Robert, A.; Canet, D. *Chem. Phys. Lett.* **2010**, *495*, 287–291
- (56) a) Nishikawa, S.; Kondo, M. *J. Phys. Chem. B* **2006**, *110*, 26143–26147, and b) Jobe, D. J.; Verrall, R. E.; Reinsborough, V. C. *Can. J. Chem.* **1990**, *68*, 2131–2136.
- (57) Levitt, M. H. *In Spin Dynamics*; John Wiley & Sons Ltd.: Chichester, **2001**.
- (58) Bagshaw, S. A.; Prouzet, E.; Pinnavaia, T. J. *Science* **1995**, *269* (5228), 1242–1244.
- (59) Tycho, R. *Nuclear Magnetic Resonance Probes of Molecular Dynamics*; Kluwer Academic Publishing: The Netherlands, **1994**.

CHAPTER 4

Manuscript no. 3

Description

In this work, solid state and solution phase inclusion complexes of β -CD and a short perfluorocarbon compound (C4; PFBA) were prepared at various host/guest mole ratios (i.e. 1:1 and 2:1) using the modified dissolution method. The complexes were characterized using solid/solution NMR spectroscopy, FT-IR, thermal analyses (DSC), and PXRD. Interpretation of the splitting patterns of the simulated NMR spectra for PFBA in solution was used to understand the dynamics of PFBA.

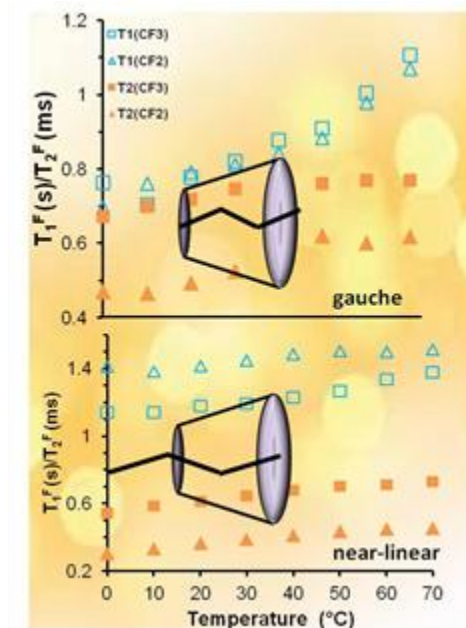
Author's Contribution

The idea of preparing inclusion complexes of β -CD and PFBA was based on the original plan of the overall research project laid out by Drs. Wilson and Hazendonk. The preparation and characterization (FT-IR, DSC, and PXRD) of the β -CD/PFOA complexes were done by myself. The solid state NMR characterization was done by myself, while the NMR relaxation measurements and data analyses were done in collaboration with Dr. Paul Sidhu. All simulations were done by Dr. Hazendonk. The first draft of the manuscript was prepared by me with subsequent editing by Drs. Wilson, Hazendonk, and Sidhu.

Relation of Manuscript 4 to Overall Objective of this Project

The work of this manuscript was important to the overall objective of the research project because the use of a short (C4) chain PFC (i.e., PFBA) provided the opportunity to compare and better understand the structures of PFCs. Also, PFBA forms exclusively 1:1 complexes with β -CD.

Graphical Abstract



Research Highlights

- ^{13}C ($^{19}\text{F} \rightarrow ^{13}\text{C}$ CP) MAS NMR technique provided unequivocal evidence for the inclusion of the guest within the host.
- PFBA forms “cage-type” structures with β -CD in the solid state, where the guest adopts *gauche* conformation in the 1:1 complex.
- PFBA exists in at least two distinct geometries that resemble 1:1 and 2:1 host/guest configurations.
- Dynamic relaxation and coupling constants simulation data reveal that the CF_3 group has free internal rotation, whereas the rest of the chain is not locked in a particular rotamer configuration but experiences significant C-C bonds rotation.

4. Characterization and Dynamic Properties for the Solid Inclusion Complexes of β -Cyclodextrin and Perfluorobutyric Acid

Abdalla H. Karoyo,[†] Paul Sidhu,[‡] Lee D. Wilson,^{†,*} Paul Hazendonk^{‡,*}

[†]University of Saskatchewan, Department of Chemistry, Saskatoon, SK, S7N 5C9, Canada.

[‡]University of Lethbridge, Department of Chemistry and Biochemistry, Lethbridge, AB, Canada.

*Corresponding Authors.

§Supplementary data (Appendix C)

4.1. Abstract

The structural characterization of the solution and solid state inclusion complexes (ICs) of β -cyclodextrin (β -CD; host) with perfluorobutyric acid (PFBA; guest) is presented in this study. Complexes in the solid state were prepared at various host/guest mole ratios (i.e., 1:1 and 2:1) using a modified dissolution method. Thermal analyses and multinuclear ^{13}C NMR methods employing direct polarization (DP) and cross polarization (CP) techniques with magic angle spinning (MAS) and high power $^1\text{H}/^{19}\text{F}$ decoupling were used to characterize the solid state host-guest complexes. Unequivocal evidence for the formation of β -CD/PFBA inclusion compounds was provided using $^{19}\text{F} \rightarrow ^{13}\text{C}$ CP/MAS NMR results. PXRD reveals that PFBA forms a “cage-type” structure with β -CD, in which the guest adopts *gauche* and near-linear conformations in the 1:1 and 2:1 complexes, respectively, according to FT-IR results. Interpretation of the NMR splitting patterns of PFBA spectrum in solution reveals that PFBA undergoes fast rotation of the CF_3 group on a three-fold axis, while the remainder of the chain experiences a significant C-C bond rotation, hence not locked in a particular rotamer configuration. The distribution of the rotational and axial motions in the β -CD/PFBA complexes in the solid state as revealed by NMR relaxation dynamic studies is a function of the host/guest mole ratios and is determined by the binding geometry of the guest.

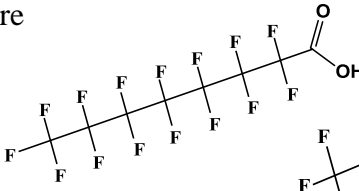
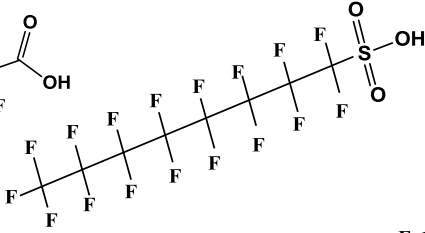
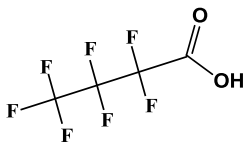
4.2. Introduction

There is vast research interest in perfluorinated compounds (PFCs) because they represent a new class of persistent organic pollutants (POPs) found in Canada and globally. PFCs are a class of fluorine containing compounds that are surface active and generally resistant to

chemical and thermal degradation.¹ Their use is found in many applications such as surfactants, adhesives, cosmetics, pesticides, and firefighting foams and powders.¹⁻² Several studies have documented the occurrence of several main classes of PFCs in the environment; namely, perfluoroalkyl carboxylic acids (PFCAs e.g., PFOA) and perfluoroalkyl sulfonates (PFSs e.g., PFOS).³⁻⁸ PFCAs ($\text{CF}_3(\text{CF})_n\text{CO}_2\text{H}$) and PFSs ($\text{CF}_3(\text{CF})_n\text{SO}_3\text{H}$) have been detected in soil and sediments, ground water, fish and animal tissues, sewage effluent, and other matrices.⁷⁻⁸ In general, PFCAs with alkyl chains that are 4–10 carbons long were reported to be the most dominant species detected in landfill leachates in the Americas.^{9,10} The distribution of PFCs in water, air, and sediment was found to depend on their physicochemical properties.⁶ Therefore, the distribution of such compounds onto solid surfaces varies according to differences in properties such as pK_a , solubility, and vapor pressure. These properties are directly related to the alkyl chain length and the structure of the head group.¹¹ On the basis of known physical properties (*cf.* Table 4.1), PFOS is essentially non-volatile and more soluble than PFOA and displays a strong tendency to exist in aqueous solution. PFBA is much more mobile than PFOA and PFOS due to its greater water solubility and shorter alkyl chain length. Therefore, PFBA can favourably reside in ground and surface water environments. The short-chain PFCAs are primarily detected as dissolved species; whereas, long-chain PFCAs are mostly adsorbed onto solid interfaces such as suspended solids and sediments. The structures and physicochemical properties of several PFCs are given in Table 4.1.

We previously reported¹² the formation of solid inclusion complexes between β -CD and PFOA (chapters 2-3). As well, similar complexes were formed using the conjugate base of PFOA (i.e., sodium perfluorooctanoate; SPFO; chapter 5).¹³ Such complexes were generally characterized using a variety of techniques including NMR and FT-IR spectroscopy, thermal analyses and PXRD. Understanding the structure of PFCs and their complexes with CDs¹⁴ is crucial because it helps develop better host systems for immobilizing these compounds in the environment. PFOA (and SPFO) were previously shown to form both 1:1 and 2:1 ICs with β -CD with variable binding configurations. Ellis et al.⁵ and other researchers^{15,16} have demonstrated that changes in the chain length of a perfluorocarbon compound correlates with changes in its conformation and physicochemical properties (e.g., cmc, pK_a , melting and boiling points, solubility, and viscosity). Many of the aforementioned physical properties play a vital role in the environmental fate and distribution of PFCs in the environment.

Table 4.1 Physicochemical Properties of Selected Perfluorocarbon Compounds*^{16,20-24}

	PFOA	PFOS	PFBA
Molecular Formula and Structure	$C_8HF_{15}O_2$ 	$C_8HF_{17}O_3S$ 	$C_4HF_7O_2$ 
Molecular weight (g/mol)	414	500	214
Solubility (g/L, 25°C)	3.4 ^a	0.57	High
Melting Point (°C)	45–55	>400	-17.5
Boiling Point (°C)	188	133	120
pK _a	2.5	0.14	0.08–0.4
cmc (mmol/L)	8.5–10	2.0	No data
Vapor pressure (mmHg, 25°C)	0.017	2.48x10 ⁻⁶	10

*Note that the conformation and stereochemistry of the PFCs are not accurately depicted.^aA value of 9.5 g/L (25 °C) has also been reported. It is unclear which value represents true solubility and which value represents microdispersity of micelles.

The conformational preference of a perfluorocarbon chain in its native state influences the way PFCs interact with CDs to form host-guest complexes. Bunn et al.¹⁷ explained that the helical conformation adopted by medium and long perfluoroalkyl chains results in a significant increase (~3 units) in pK_a from PFBA (0.40) and trifluoroacetic acid (TFA; 0.23)¹⁸ to PFOA (2.5–3.8).¹⁶ In general, the chain conformation of perfluorocarbon compounds is best described as being fully zigzag (or *trans*) for alkyl chain lengths ≤8 carbons, a mixture of zigzag and helical for alkyl chain lengths 8–12 carbons, and fully helical (*gauche*) for alkyl chain lengths >12 carbon atoms. Thus, the general trend in the geometry of perfluoroalkyl chains is the progression of a planar zigzag to helical geometry with increasing chain length. Thus, the physicochemical properties in Table 4.1 vary with the perfluoroalkyl chain length.

In this paper, we report the structural characterization of the complexes formed between PFBA and β -CD. We also report on the dynamic properties of PFBA in its pure form in solution and its complexed form with β -CD in the solid state. PFBA represents a model guest compound possessing a relatively short PFC chain (C4). The study of the formation of complexes of PFBA with β -CD will provide an improved understanding of the structure of hydrophilic PFCs with relatively short carbon chains. The complexes were prepared at the 1:1 and 2:1 host/guest mole ratios using a modified dissolution method¹⁹ and they were further characterized using $^1\text{H}/^{19}\text{F}/^{13}\text{C}$ solids/solution NMR spectroscopy, FT-IR, DSC and PXRD.

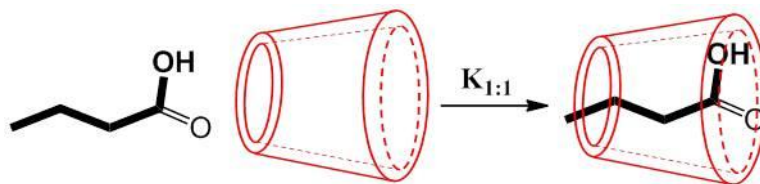
4.3. Experimental Section

4.3.1 Materials and Chemicals

β -CD hydrate (~10 % w/w) and PFBA (98 %) were purchased from Sigma-Aldrich Canada Ltd. (Oakville, ON) and were used as received without any further purification. The water content of the materials was determined from thermogravimetric analysis when preparing the sample mixtures.

4.3.2 Preparation of the solid β -CD/PFBA ICs.

The solid complexes of β -CD/PFC were prepared at the 1:1 and 2:1 host/guest mole ratios using a modified dissolution method adapted from a previous report,¹⁹ as depicted in Scheme 4.1. Upon evaporation of the solvent, the solid products were ground into fine powders and were further analyzed.



Scheme 4.1 The association of β -CD and PFBA in a 1:1 host-guest stoichiometry yields a β -CD/PFBA inclusion complex

4.3.3 Solution-state NMR Spectroscopy

^1H solution NMR experiments were carried out on a three-channel Bruker Avance (5mm DRX probe) spectrometer operating at 500.13 MHz, while the ^{19}F solution NMR spectra were acquired at 282.4 MHz using a 300 MHz Bruker Avance 2 spectrometer outfitted with a 2 channel (H/FX) 5mm BBO probe. All NMR spectra of samples in solution were prepared in D_2O at host-guest mole ratios of 1:1 and 2:1 at 295 K, where the chemical shifts (δ) of ^1H and ^{19}F were measured with respect to tetramethylsilane (TMS; ^1H 0.0 ppm) and trifluoroborane (BF_3 ; ^{19}F -131 ppm) as internal standards, respectively. Typical acquisition parameters were as follows: a spectral window of 6250 Hz, and a $\pi/2$ pulse width of 8.5 μs for the ^1H spectra; a file size of 64 k data points, a spectral window of 56818 Hz and a 10.3 μs ($\pi/2$) pulse width for the ^{19}F spectra, where 100 transients were acquired in all cases, with an acquisition time of 1.15 s, with a file size of 32 k data points and 1 s relaxation delay.

4.3.4 Solid-State NMR Spectroscopy

All solids NMR spectra were obtained using a Varian INOVA spectrometer operating in triple channel HFC mode using a 2.5 mm T3 HFX probe operating at 125.55 MHz for ^{13}C , 499.99 MHz for ^1H , 469.89 for ^{19}F . Solid state ^{13}C CP/MAS spectra were referenced externally to adamantane (δ 38.5 ppm) as a secondary standard with respect to TMS. ^{19}F NMR spectra were referenced with respect to hexafluorobenzene (δ -164.9 ppm) as a secondary standard with respect to CFCl_3 (0 ppm). All samples were spun at the magic angle with a spinning rate of 20 kHz (or as stated) using 2.5 mm zirconium oxide rotors equipped with Vespel (low fluorine background) turbine caps, inserts, and end caps. All NMR spectra were obtained using a 100 kHz spectral window in transients of 8 k points, which were zero-filled to 64 k, unless stated otherwise. The curve and width parameters for the adiabatic $^1\text{H} \rightarrow ^{13}\text{C}$ CP experiments were set at 50 and 10,000 Hz respectively, while those for $^{19}\text{F} \rightarrow ^{13}\text{C}$ were set at 50 and 50,000 Hz, respectively. Optimal Hartmann-Hahn matching conditions were achieved at a 1 ms contact time and spin locking powers of 68 kHz and 59.5 kHz for the ^{19}F and ^{13}C channels, respectively. ^{13}C spectra of all solid samples were acquired using a two-pulse phase modulation (TPPM) decoupling mode,²⁵ using a pulse phase of 13.5 degrees and decoupling frequencies of 125 and 100 kHz in the ^1H and ^{19}F decoupled channels, respectively, as determined by 360° pulse width measurement in each channel.

4.3.5 Differential Scanning Calorimetry (DSC)

DSC experiments were acquired using a TA Q20 thermal analyzer over a temperature range of 30 °C to 380 °C. The scan rate was set at 10 °C/min and dry nitrogen gas was used to regulate the sample temperature and sample compartment purging. Solid samples were analyzed in hermetically sealed aluminum pans where the sample masses ranged from 3.50 to 3.80 mg.

4.3.6 FT-IR Spectroscopy

Fourier Transform-IR spectra were obtained using a Bio-Rad FTS-40 spectrometer with a resolution of 4 cm⁻¹. All spectra were obtained with spectroscopic grade KBr which constituted ~80% (w/w) of the total sample. Samples were run as finely ground powders in reflectance mode.

4.3.7 Powder X-ray Diffraction (PXRD)

PXRD spectra were collected using a PANalytical Empyrean powder X-ray diffractometer using monochromatic Cu-K α 1 radiation. The applied voltage and current were set to 45 kV and 40 mA, respectively. The samples were mounted in a vertical configuration as evaporated hexane films and PXRD patterns were measured in the continuous mode over a 2 θ angle range of 5–20° with a scan rate of 0.5 degree/min.

4.4. Results and Discussion

4.4.1 DSC

DSC and TGA are complementary techniques that have been used to characterize thermal properties of polymeric²⁶ and other host-guest systems.^{27,28} Changes in the enthalpy of dehydration of the host due to displacement of cavity water have been used to indicate formation of host/guest complexes.²⁹ The DSC thermograms of the native β -CD hydrate, the 1:1 complex and 2:1 β -CD/PFBA ICs are depicted in Figure 4.1. The corresponding transition temperatures are listed in Table 4.2. Generally, the DSC spectra show three major endothermic transitions which are related to dehydration, vaporization and decomposition processes. The peaks at ~115° and 320 °C (*cf.* Figure 4.1) are related to dehydration and decomposition transitions of the pure host, respectively. The guest molecule in the bound state vaporizes and decomposes at ~200° and 310 °C (*cf.* Fig. 4.1), respectively. The dehydration transitions for the complexes display three

endothermic contributions at ~80°, 100°, and 120 °C (*cf.* Figure 4.1 and Table 4.2) and exhibit variable hydration levels and nature of the stoichiometry (i.e., 1:1 and 2:1) for the host-guest complexes. It should be noted here that PFBA was reported to form mainly 1:1 host/guest complexes with β -CD in aqueous solution due to *size-fit* complementarity of the host and the guest.³⁰ However, host-guest complexes with other host/guest ratios (e.g., 2:1 and 1:2) may arise in the solid phase.^{31,32} β -CD/PFBA complexes with variable stoichiometric ratios (e.g., 2:1 and 1:2) may result from different binding configurations, e.g., a 2:1 association where the guest is strongly bound by one CD and weakly bound to a second CD macrocycle.

Table 4.2 The DSC Data for β -CD, and the 1:1 and 2:1 β -CD/PFBA Inclusion Complexes. Main Dehydration Transitions are Indicated by Asterisks.

	Dehydration (°C)			Vaporization (°C)	Decomposition (°C)
β -CD	-	-	113	-	319
1:1 IC	~80*,90	~102	117	195	310
2:1 IC	~80	~100*	114	198	310

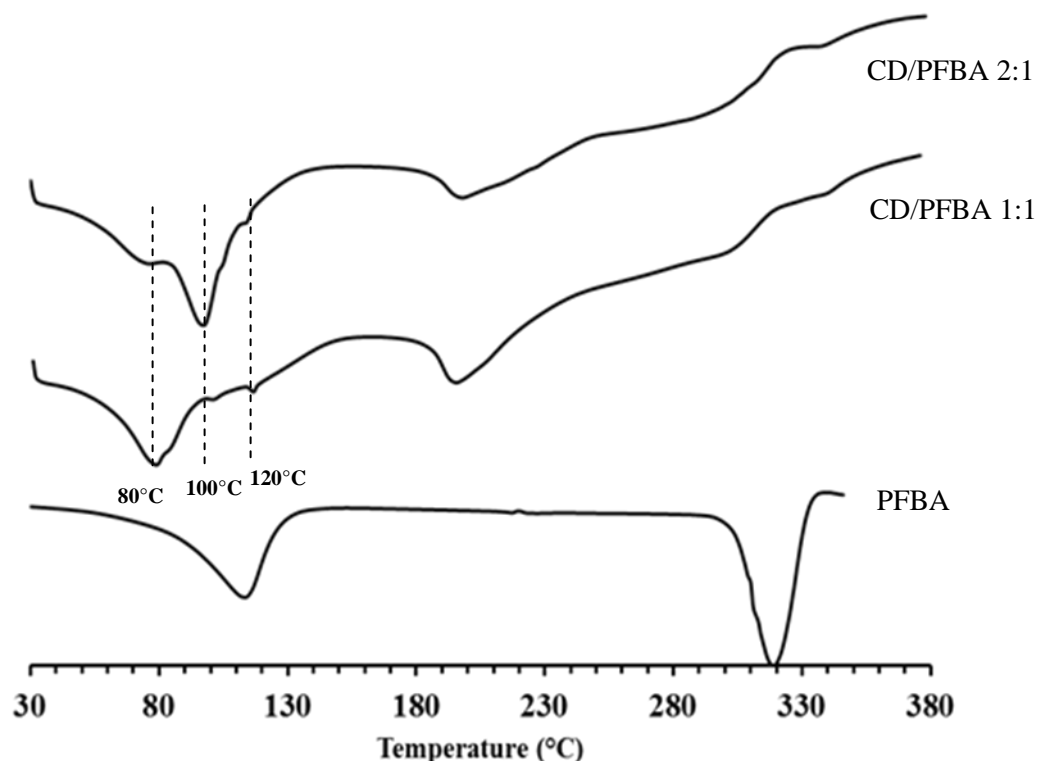


Figure 4.1 The DSC thermograms for β -CD, and the 1:1 and 2:1 β -CD/PFBA complexes

According to Figure 4.1, the variable enthalpies of dehydration evidenced by the desorption temperatures correlate with different hydration states that exist due to the different guest binding configurations. For example, the displacement of the main dehydration process to lower temperature (80 °C) for the 1:1 complex relative to the 2:1 complex (~100 °C) may be associated with a reduced contribution of cavity bound water due to its removal upon guest binding. The host cavity for the 1:1 complex is fully occupied by the guest molecule. Moreover, the deconvolution of the broad DSC peak for the 1:1 complex at ~80 °C displays a shoulder at higher temperature (~90 °C) and this may suggest an additional guest environment in this complex. In contrast, the 2:1 host-guest association reveals a greater level of H-bound water due to the greater mole fraction of the host. Hence, the dehydration process shifts to higher temperature (100 °C). A minor enthalpic contribution at a temperature corresponding to the main dehydration process for the 1:1 complex (~80 °C) is displayed for the 2:1 complex, suggesting minor contributions of the 1:1 guest configuration for this complex. When comparing the vaporization temperature of pure PFBA (b.p. 120°C, *cf.* Table 4.1), the vaporization temperature of the guest in the bound state is increased (195°-198°C) providing thermodynamic evidence of the formation of stable inclusion compounds. The minor transitions at 120 °C for the complexes may be related to the melting of small amounts of non-inclusion bound, unbound (free) PFBA guest, or hydrate water.

4.4.2 FT-IR

FT-IR has been widely used to study the structure of CD-based ICs in which the guest molecule bears a carbonyl group because the CO-stretching band is sensitive to changes in guest conformation as well as possible H-bonding with the CD.^{33,34} The FT-IR spectra of the host, guest, and the 1:1 and 2:1 β -CD/PFBA ICs are shown in Figure 4.2. The relative intensities of the -OH (~3400 cm⁻¹), -CH (~2900 cm⁻¹) and -C=O (~1700 cm⁻¹) vibrational bands for the 1:1 (weaker) and 2:1 (stronger) inclusion complexes (*cf.* Figure 4.2) correlate with the relative mole ratios of the host/guest relative to the unbound species. The unbound PFBA is characterized by a broad, low intensity -OH band ~3600–2500 cm⁻¹ that is typical of fatty acids.³⁵ The attenuation of the carbonyl band in the 1:1 and 2:1 complexes is related to H-bond formation and supports the formation of β -CD/PFBA inclusion complexes. The visibly attenuated carbonyl band in the 1:1 complex in Figure 4.2 indicates formation of multiple of H-bonds,³⁶ as this band displays two

distinct contributions. The IR results further support that the guest exists in the 1:1 complex in two distinct microenvironments, in agreement with the DSC results in Figure 4.1.

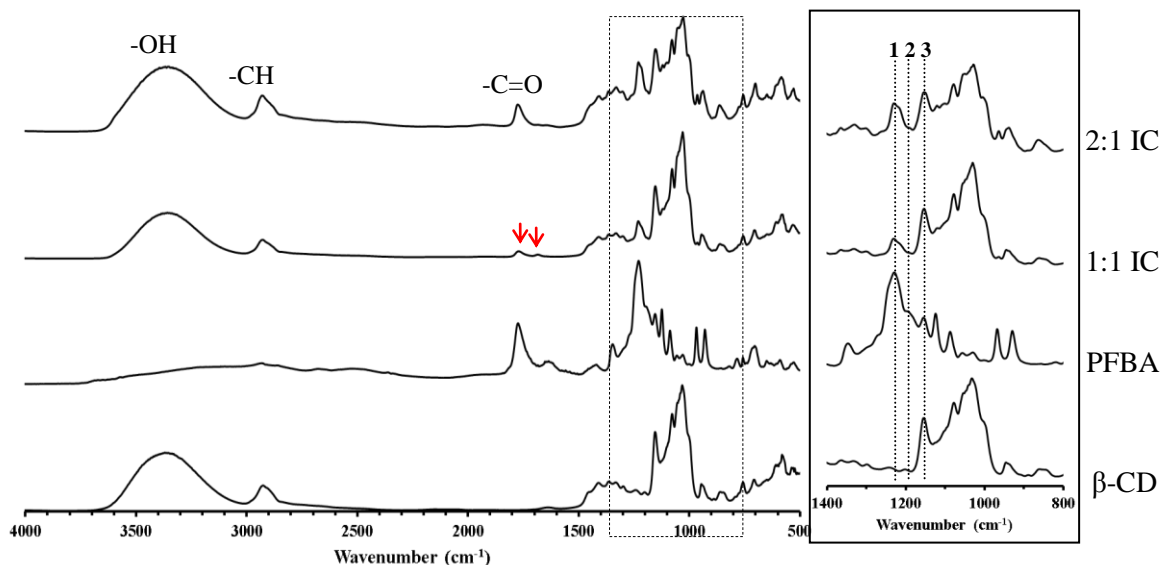


Figure 4.2 The FT-IR traces for native β -CD, PFBA, and the 1:1 and 2:1 β CD/PFBA inclusion complexes. **Inset:** Expanded region from 1400 cm^{-1} – 800 cm^{-1} .

The FT-IR spectral region from ~ 1400 – 800 cm^{-1} is of interest in terms of the conformational preference of the guest molecule. This expanded FT-IR region is shown as an inset in Figure 4.2. Bands **1** ($\sim 1230\text{ cm}^{-1}$), **2** (1200 – 1210 cm^{-1}), and **3** (1150 cm^{-1}) in the expanded region of Figure 2 were reported previously^{17,37} and assigned to the CF_2 asymmetric stretching mode, CC bending and CCC stretching modes, and CF_2 symmetric stretching modes. Note that the wavenumber position of band **2** is not straight forward to assign as this band may be partly overlapped with band **1**. However such band position is assigned to be within 1200 – 1210 cm^{-1} range. Changes in the relative intensities of these bands, particularly band **2**, were related to the *trans* and *gauche* conformations of the PFC chain. As described previously, perfluorocarbon chains ≤ 8 carbons (e.g., PFBA) generally adopt a fully zigzag (*trans*) conformation in the solid phase;³⁸ whereas, composite zigzag/helical conformations were reported for C8–C12 chains.³⁹ Ellis et al.⁵ reported using NMR simulation of coupling constants that the PFBA chain in solution does not adopt a fully *trans* conformation. However, such conformation is the generally accepted form of C4 perfluorocarbons in the solid phase.⁴⁰

Bands **1–3** in Figure 4.2 were observed for gaseous $n\text{-C}_4\text{F}_{10}$ where band **2** $\sim 1200\text{--}1210\text{ cm}^{-1}$ was attributed to the *trans*-conformer,⁴⁰ as described in previous chapters. A decrease in intensity of this band was previously attributed to a *trans-to-gauche* conformational change of the perfluorocarbon chain. Recall that PFBA adopts a full *trans* conformation in its unbound form in the solid state. However, a variable conformation may result if the environment of the guest is varied.

Erkoc and Erkoc³ reported that the conformation of PFOS changed from helical to near-linear (zigzag) when H was replaced with F due to changes in the dipole moment of the various molecular fragments. Similarly, the conformation of PFOA changed from a helical to zigzag when packed into a periodic lattice.³⁹ We believe that the significant decrease in the intensity of band 2 for the $\beta\text{-CD}$ /PFBA complexes is related to the *trans-to-gauche* conformational change of the perfluorocarbon chain. The guest molecule in the 1:1 and 2:1 complexes is expected to adopt variable conformation with variations in the CF_2 asymmetric stretching modes (band 1) and CC bending/CCC stretching modes (band 2), according to the FT-IR results.

4.4.3 PXRD

The PXRD patterns for the host, and the 1:1 and 2:1 host/guest inclusion (ICs) complexes prepared by the modified dissolution method are shown in Figure 4.3. The PXRD of sodium perfluorobutyrate (SPFB) is shown for comparison since it is the salt form of the conjugate base of PFBA. The hydrate form of the host ($\beta\text{-CD}$) exhibits intense diffraction lines at lower 2θ values $\sim 9^\circ$, 12° and minor signatures at higher 2θ that are characteristic of a “cage-type”⁴¹ crystalline structure. SPFB exhibits intense diffraction lines at $\sim 7^\circ$ and $\sim 17\text{--}22^\circ$ with minor reflections at higher 2θ values.

The diffraction patterns for the 1:1 and 2:1 ICs in Figure 4.3 consist of 2θ values $\sim 6^\circ$, and $9\text{--}17^\circ$, where the higher 2θ region is comprised of minor reflections that are characteristic of “cage-type” structures. We conclude that $\beta\text{-CD}$ forms “cage-type” structures with PFBA, similar to its structure in the native unbound form. The relative shift and intensity of 2θ reflection at $\sim 6^\circ$ in the 1:1 and 2:1 complexes with respect to pure SPFB (at 7°) reveal the variable conformations/configurations of the guest in these complexes.

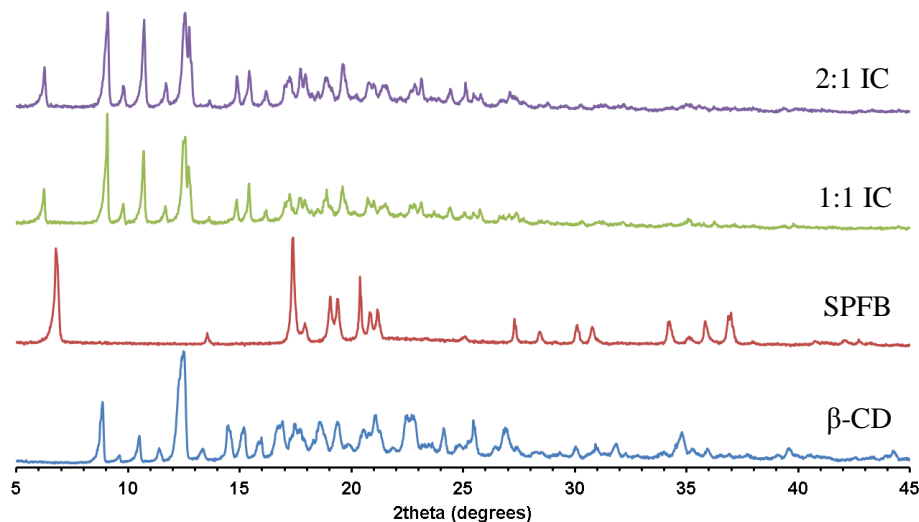


Figure 4.3 The PXRD patterns for native β -CD, SPFB, and the 1:1 and 2:1 β CD/PFBA inclusion compounds.

4.4.4 Solution-state NMR Spectroscopy

4.4.4.1 $^1\text{H}/^{19}\text{F}$ NMR Characterization

$^1\text{H}/^{19}\text{F}$ solution NMR spectroscopy was used to characterize the inclusion compounds of β -CD and PFBA through complexation induced shifts (CIS), as shown in Figures 4.4 and 4.5, respectively. In Figure 4.4, the ^1H solution NMR spectra for β -CD and the 1:1 and 2:1 β -CD/PFBA ICs are shown. The ^1H solution NMR spectra were assigned according to literature reports.⁴² The intracavity protons (i.e., H_3 and H_5 , *cf.* Scheme 4.2b) are the most affected nuclei providing evidence for the formation of inclusion compounds between β -CD and PFBA. The H_3/H_5 CIS values are greater in the 1:1 complex and this is related to the greater steric effect on the intracavity nuclei upon complexation. It should be noted here that the complexation induced shifts are a weighted average due to the bound and unbound species.⁴³ The observed chemical shift changes for the extracavity ^1H nuclei (i.e., H_1 , H_2 , H_4) in the 1:1 and 2:1 complexes may be associated with the extracavity environment of the PFBA guest in these complexes or possibly the complexation-induced conformational change of the host. The extracavity environment (e.g., H_1) experiences variable steric effects from the guest in the 1:1 complex (shielding) vs. the 2:1 complex (deshielding). The shielding/deshielding effects of the 1:1/2:1 complexes may be related to the variable conformations of the guest as described in the FT-IR results. The increase in line broadening upon complexation can be readily ascribed to the increase in correlation times

expected upon complexation, which decreases T_2 , leading to a wider natural line width. The greater line width further supports the formation of the complexes.

We believe that the guest molecule preferentially adopts the *gauche* conformation in the 1:1 complex in solution phase; whereas a fully *trans* conformation is favoured in the 2:1 complexes. A *gauche* conformation is anticipated to impart a greater steric strain (shielding) on the host compared to a fully *trans* conformation, in agreement with the ^1H solution NMR results.

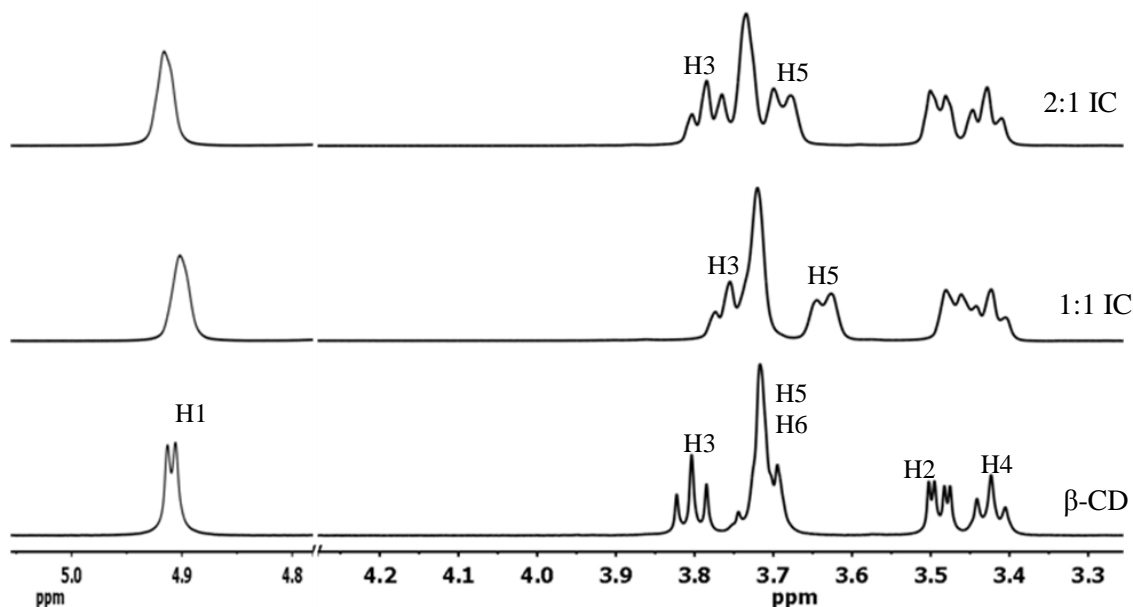
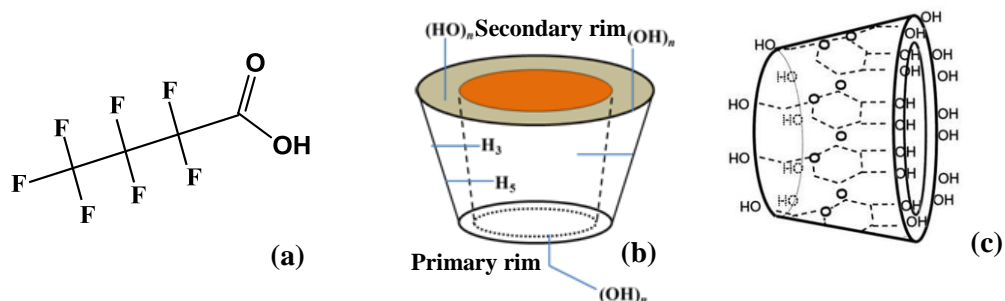


Figure 4.4 ^1H solution NMR spectra for β -CD, and the 1:1 and 2:1 β -CD/PFBA inclusion compounds in D_2O at 295 K.

Figure 4.5 shows the expanded ^{19}F solution NMR spectra for PFBA and the β -CD/PFBA inclusion compounds prepared at the 1:1 and 2:1 mole ratios. Similar results for the 1:2 host/guest preparation were included for comparison. The assignment of the ^{19}F solution NMR agrees well with previous literature reports.⁵ The formation of host-guest ICs results in an overall downfield shift of the ^{19}F resonances due to reduced polarizability of the host interior relative to the environment of bulk aqueous solution.⁴⁴ This provides evidence for the formation of β -CD/PFBA inclusion compounds in solution. Note that the CIS values did not increase further beyond the 1:1 mole ratio supporting the fact that PFBA forms mainly 1:1 complexes with β -CD in solution phase. The ^{19}F CIS values for the 1:2 host/guest complexes are the least affected

relative to unbound PFBA and may be due to the lower mole ratio of the host and increased fraction of unbound guest.



Scheme 4.2 Molecular Structure of (a) PFBA, and (b,c) β -CD. The structure of β -CD is shown as a truncated toroid where the primary and secondary hydroxyls, and glycosidic oxygen bridges are shown. The intracavity protons (H_3/H_5) are shown in (b).

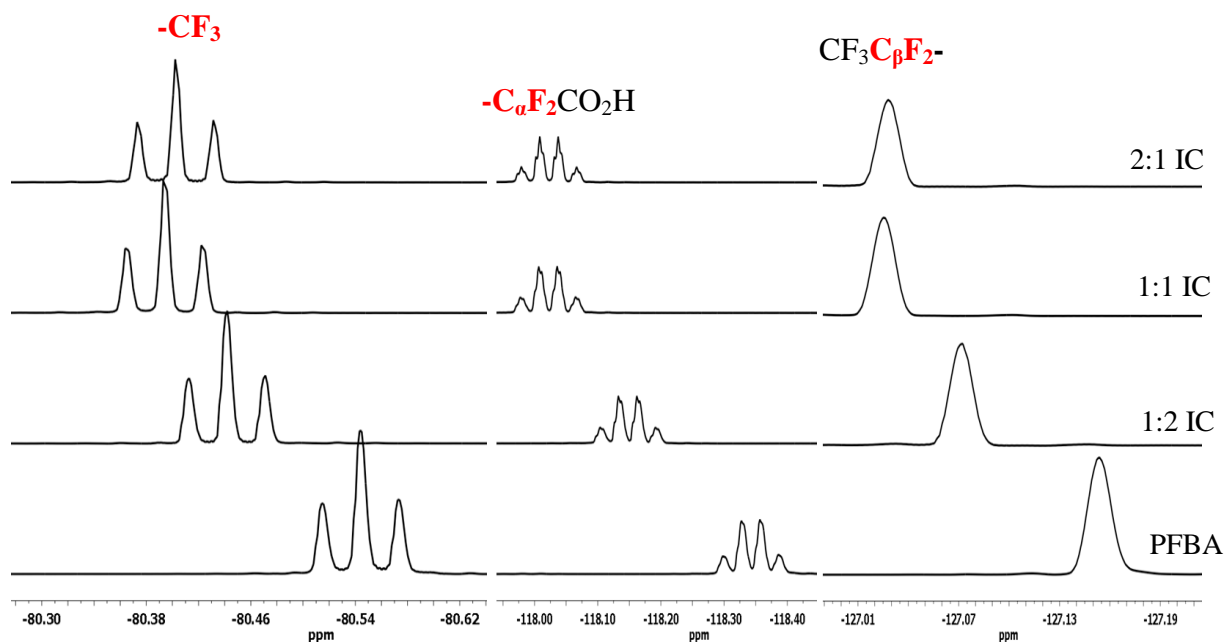


Figure 4.5 ^{19}F solution NMR spectra for PFBA, and the 1:2, 1:1, and 2:1 β -CD/PFBA inclusion compounds in D_2O at 295 K.

The inherent line widths in the spectra of Figure 4.5 are about 1 Hz, where slight distortions due to differences in shimming cause slight lineshape changes between samples which could easily be confused for subtle changes in the splitting patterns between the

complexes and pure PFBA. As one follows the ^{19}F shifts of all the signals, one realizes that the trend is the increase in δ of the ^{19}F resonance lines with the degree of complexation. This cannot only be ascribed to the effect of the host entirely, but is evidence of the guest conformational changes occurring. According to the IR results, the guest molecule adopts the *gauche* conformation in the complexed state. However, since such results clearly suggest that the *trans* contribution in the complexed form increases with the degree of complexation (i.e., 2:1>1:1), we should expect to see a reduction in the *gamma-gauche* shielding effect. As a result, the chemical shift should increase from the 1:2 through the 1:1 to 2:1 host/guest complexes (*cf.* Fig. 4.6).

4.4.4.2 Coupling Constants of Simulated ^{19}F NMR Lines

^{19}F NMR in solution can be a very important tool in understanding the structure of perfluorocarbon materials. For example, the ability to discern the coupling constants of all the ^{19}F nuclei in highly fluorinated materials in liquid form is an important technique in determining and understanding molecular dynamics and conformation of such materials. Coupling constants in perfluorinated carboxylic acids have largely been indiscernible due to long range coupling (over 4 bonds) and coincidental spectral overlap.^{45,46} The ^{19}F solution spectrum of PFBA in D_2O was simulated using MestreNova to determine the individual coupling constants. The simulated spectrum of pure PFBA in D_2O along with its labeled structure are shown in Figure 4.6.

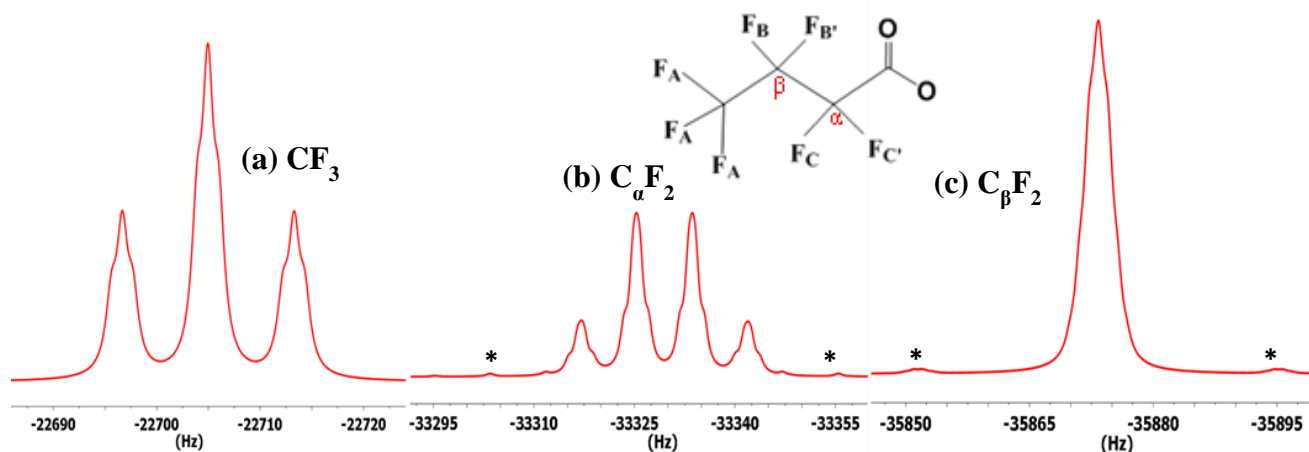


Figure 4.6 ^{19}F simulated spectrum of PFBA (Hz) in D_2O at ambient temperature showing the splitting of the (a) $-\text{CF}_3$, (b) $\alpha\text{-CF}_2$, and (c) $\beta\text{-CF}_2$ signals. The satellite lines are shown by asterisks.

The spectrum of PFBA can be determined by seven coupling constants; ${}^4J_{AC} = {}^4J_{AC'} = 8.3$ Hz, ${}^3J_{AB} = 1.4$ Hz, ${}^3J_{AB'} = 0.7$ Hz, ${}^3J_{BC} = {}^3J_{B'C'} = 6.9$ Hz, ${}^3J_{B'C} = {}^3J_{BC'} = -5.8$ Hz, ${}^2J_{BB'} = -263.1$ Hz, and ${}^2J_{CC'} = -283.1$ Hz. The values of coupling constants reported herein agree well with reported values in the literature,⁴⁷ however at this resolution they cannot represent a unique solution. According to the splitting pattern, the ${}^{19}\text{F}$ spectra of pure PFBA and the complexes in D_2O are $\text{A}_3\text{BB}'\text{CC}'$ spin systems where the CF_2 groups are magnetically inequivalent. Figure 4.7 represents the three possible rotamers of PFBA; one *trans* (*t*) and two equivalent *gauche* (*g*, *g'*) conformers. Note that fast rotational averaging on the NMR time scale in solution at ambient temperature is such that the spectrum of PFBA is represented by spectral parameters which are averages of the chemical shifts and coupling constants in the three rotational isomers, weighted according to their populations. Therefore, the couplings do not reflect a single configuration, but an average over all three rotamers,⁴⁸ which in this case constitute one *trans* and two symmetrically equivalent *gauche* configurations.

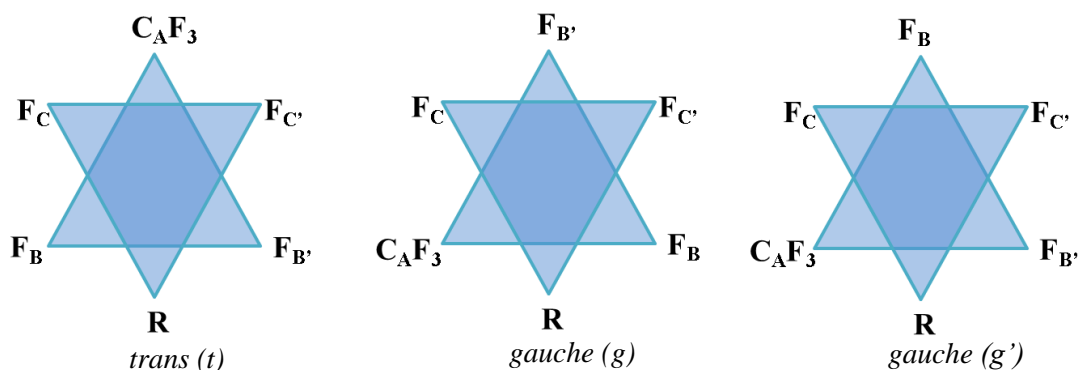


Figure 4.7 The three possible rotamers of perfluorobutyric acid (PFBA),

The $\text{F}_\text{B}/\text{F}_\text{B}'$ and $\text{F}_\text{C}/\text{F}_\text{C}'$ spins are strongly coupled by two geminal couplings whose difference (${}^2J_{\text{BB}'} - {}^2J_{\text{CC}'}$) is 20 Hz. This resonance spacing (i.e. ~ 20 Hz) can be seen occurring between the satellite lines and the main signals in both sub-spectra (*cf.* Figure 4.6b,c). These are second order satellites, which can only result from very strong coupling. A second set of such satellites (at very low intensity) should appear in the spectrum of Figure 4.6b (not shown in the scale) for the $\text{C}_\alpha\text{F}_2$ group at ~ 546.2 Hz. Hence the 2J couplings are -283.1 and -263.1 Hz. Reported geminal couplings in acyclic $-\text{CF}_2-\text{CF}_2-$ groups range between 260 and 290 Hz.⁴⁹

The coupling constants cannot be determined from the splittings observed in the BB' and CC' as the individual spectral lines are not resolved; however, some observed splittings can be attributed to the sum of the various geminal and vicinal coupling constants. Hence the inability to obtain a unique solution for the spectral parameters since a spectral resolution of less than 0.3 Hz would be required in this case. For example, the ${}^3J_{AB}$ and ${}^3J_{AB'}$ couplings add up to 2.1 Hz. The two couplings do not have to be equal, so any combination that adds up to 2.1 Hz is valid up to a limit determined by the two geminal couplings. Similarly, the sum of the two vicinal couplings ${}^3J_{BC}/{}^3J_{B'C'}$ and ${}^3J_{B'C'}/{}^3J_{BC}$ is 1.1 Hz. Again, these couplings cannot be determined separately at this resolution. Resolution enhancement allowing the identification of some characteristic spacings in the F_{CC'} regions places ${}^3J_{BC}$ and ${}^3J_{B'C'}$ at the 6.9 and -5.8 Hz. The ${}^4J_{AC}$ and ${}^4J_{AC'}$ couplings add up to 16.6 Hz. Again these couplings cannot be determined separately at this resolution. They do not have to be equal; however, in the simulation they were assumed to be equal at 8.3 Hz. Changing the magnitudes of 4J couplings, but preserving their sum does not change the appearance of the A3 and CC' regions in the spectrum up to a limit determined by the two geminal couplings.

The nearly constant splitting patterns between all the ${}^{19}\text{F}$ spectra of neat PFBA and its complexes cannot be used as evidence for the lack of conformational changes occurring upon complex formation, as any change that preserves the sums of the 3J couplings will have the same pattern. As the 3J couplings are an average of their counterparts in the individual rotamers (i.e. *t*, *g*, and *g'*, cf. Figure 4.7), they will change only subtly upon stabilization of the *trans* conformation. Thus, the sum of these couplings cannot be expected to increase significantly. The interpretation of the splitting pattern of PFBA reveals that the F atoms on the CF₂ groups are non-equivalent as indicated in a previous report.⁵ Thus, the results suggest that there must be fast rotation about the CF₂-CF₂ bonds of PFBA chain in aqueous solution, but each configuration (i.e. *t*, *g*, and *g'*) does not contribute equally. Therefore, the main chain cannot be rigid, because if it were, one would expect to observe the sub-spectra corresponding to all three rotamers. Note also that the *trans* configuration is likely to be the least stable, compared to the two *cis* (*gauche*) configurations, which have equal populations as they have the same energy. Thus, as the *trans* configuration is stabilized, the average 3J and 4J reflect this by an increased contribution from the coupling constants in the *trans* rotamer to the average. This leads to the conclusion that the PFBA chain undergoes free rotation of the -CF₃ group about the three-fold axis and appreciable

rotation about the $\text{CF}_2\text{-CF}_2$ bonds of the main chain. The structure of PFBA in the complexed form in the solid state is expected to vary, especially with respect to its bond rotation dynamics, which may be influenced by steric interactions with the host. ^{19}F DP/MAS NMR and dynamic relaxation results are presented to further understand the structure and dynamic properties of PFBA and its complexes with $\beta\text{-CD}$, respectively.

4.4.5 Solid-state NMR

4.4.5.1 ^{19}F DP/MAS NMR Characterization

NMR methods where the nucleus of interest is observed provide an opportunity to study the structure of host-guest systems. Figure 4.8 shows assigned ^{19}F DP/MAS solid NMR spectra of the 1:1 and 2:1 solid complexes prepared by the modified dissolution method. The ^{19}F DP/MAS spectrum of the guest was not acquired because PFBA is a liquid at room temperature. Minor changes in the CIS values for the methyl (CF_3) and methylene (CF_2) groups in the 1:1 and 2:1 $\beta\text{-CD}$ /PFBA complexes reveal variable environments and dynamics of the guest as previously described.

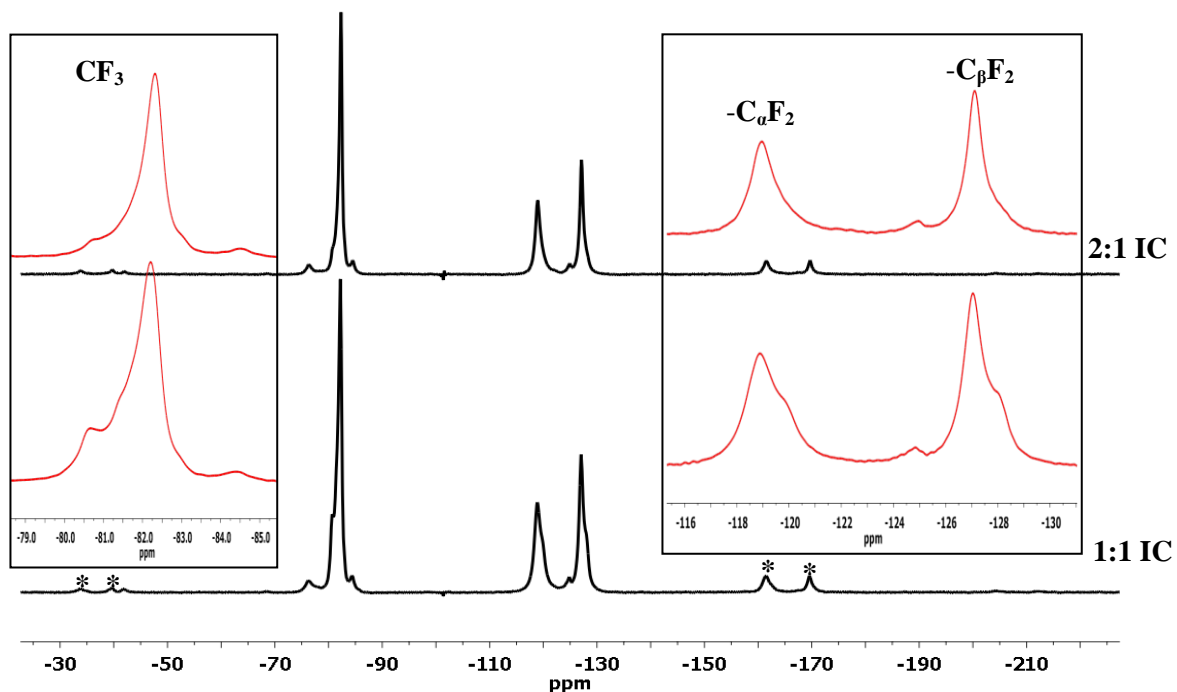


Figure 4.8 ^{19}F DP NMR spectra for the 1:1, and 2:1 $\beta\text{-CD}$ /PFBA complexes acquired at 20 kHz MAS and 295 K.

The ^{19}F resonance lines of the 1:1 and 2:1 complexes are characterized by various contributions which may be due to the presence of various microenvironments of the guest and/or the presence of unbound guest. Note that the fast rotation of the short chain PFBA guest, particularly the CF_3 group as described in the simulation studies, affects the line width/shape of the adjacent ^{19}F lines. The motional dynamics of the PFBA chain are generally expected to be much faster compared to that of C8 (e.g., PFOA and SPFO) perfluorocarbon chains. In Figure 4.8, the CF_3 group displays the sharpest resonance line followed by the methylene group connected directly next to it (C_βF_2) and then the CF_2 group connected next to the carbonyl group ($\text{C}_\alpha\text{F}_2$). The ^{19}F resonance lines of the 1:1 complex reveal prominent line shape features compared to the 2:1 complex and may suggest variable guest binding configurations consistent with the results from DSC and FT-IR. Deconvolution analyses of the ^{19}F resonance lines were carried out to further understand the structure of the complexes and the dynamics of the guest.

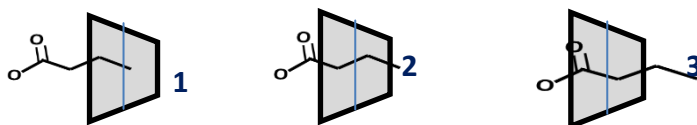
4.4.5.2 Deconvolution Analyses of ^{19}F NMR Line Shapes

Deconvolution analyses of NMR line shapes were previously used to assign the various phases (e.g., crystalline and amorphous) of a compound.⁵⁰ The deconvolution results for the CF_3 and CF_2 lines at 295 K appear in Figure 4.9a,b for the 1:1 and 2:1 complexes, respectively. The CF_3 and CF_2 resonances of the 1:1 and 2:1 complexes are generally characterized by two or three components (1–3, *cf.* Figure 4.9a,b). In a previous report,¹⁹ three topologies of β -CD/PFOA complexes were concluded from the deconvolution analyses of the CF_3 line shapes (chapter 3). These topologies corresponded to a 1:1 β -CD/PFOA complex where two configurations (CF_3 -out of and CF_3 -in cavity) were possible, and a 2:1 complex with a CF_3 -in cavity configuration (*cf.* Scheme 2, ref. 19/Scheme 3.2). The three topologies (two for 1:1 complex and one for 2:1 complex) reported for β -CD/PFOA complexes were determined by the length of the perfluorocarbon chain (~ 15 Å) with respect to that of the CD cavity (~ 7.9 Å). In the case of β -CD/PFBA complexes, higher order stoichiometries (e.g., 2:1, and 1:2) may arise in the solid phase, in addition to the 1:1 stoichiometry; indicating that a number of binding configurations are possible as suggested by DSC, FT-IR and ^{19}F DP/MAS NMR results. As was the case with the β -CD/PFOA complexes, the different binding configurations formed by PFBA with β -CD are determined by the *size-fit* complementarity (length of PFBA is about half that of PFOA) and interactions between the different components of the host and guest. For example, the edges of β -

CD are lined with hydroxyl groups, whereas the internal cavity is lined with H atoms and glycosidic O bridges (*cf.* Scheme 4.2c). Therefore, the internal cavity is hydrophobic, whereas the annular hydroxyl groups are hydrophilic in nature. Several binding interactions are therefore possible between the perfluorinated carboxylate anion and the various segments of the macrocycle.

The relative distribution of components 1–3 for the CF₃ and CF₂ groups in the 1:1 and 2:1 complexes in Fig. 4.9 were estimated from the deconvolution parameters, and reveal variable binding geometries and stoichiometries in these complexes. Deconvolution parameters showing chemical shifts, areas under curves, and relative Lorentzian/Gaussian ratios are presented as supplementary data (Table C4.1a,b). Whereas component 2 is more prominent in the 1:1 complex, the 2:1 complex is mainly defined by component 3. On the other hand, component 1 is the least prominent in both the 1:1 and 2:1 complexes, and may be missing entirely in the latter. Thus, we conclude that components 1–3 may correspond to guest binding configurations that resemble 1:2 (1), 1:1 (2), and 2:1 (3) host/guest stoichiometries, respectively. Scheme 4.3 represents the various possible binding configurations of PFBA within the CD cavity. Note that guest penetration through the narrow rim is possible. As well, formation of channel or cage structures, as described in the PXRD results, are known to occur in CD complexes but are omitted for clarity.

Configuration 1 in Scheme 4.3 is the least stable from a thermodynamic point of view and may represent a 1:2, or more accurately a 0.5:1 host/guest stoichiometry, but may also represent a free guest. According to the deconvolution analyses in Figure 4.9a,b-i), the 1:1 preparation gives rise to approximately equimolar amounts (refer to Table C4.1a) of 1:1 (configuration 2) and 2:1 (configuration 3) host/guest stoichiometries, and small amounts of the 1:2 stoichiometry (configuration 1). The presence of the 1:1 and 2:1 complexes in the 1:1 preparation may coincide with the two DSC dehydration transitions at ~80° and 90 °C, respectively.



Scheme 4.3 Schematic representation of the binding interaction postulated for PFBA guest and β -CD host; (1) partial guest inclusion in a 1:2 H/G ratio, (2) complete guest inclusion in a 1:1 H/G ratio, and (3) complete inclusion with guest protruding to result in 2:1 H/G ratio. Note: inclusion through the narrow rim of CD is possible.

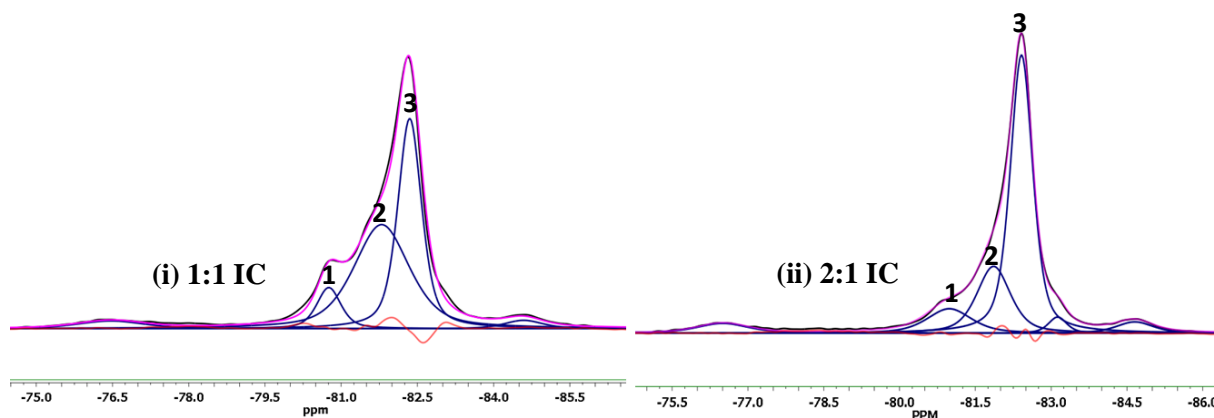


Figure 4.9a Deconvolution analyses of the CF_3 line shapes for the ^{19}F DP/MAS 20 kHz spectra of (i) the 1:1, and (ii) 2:1 β -CD/PFBA solid complexes at 295 K.

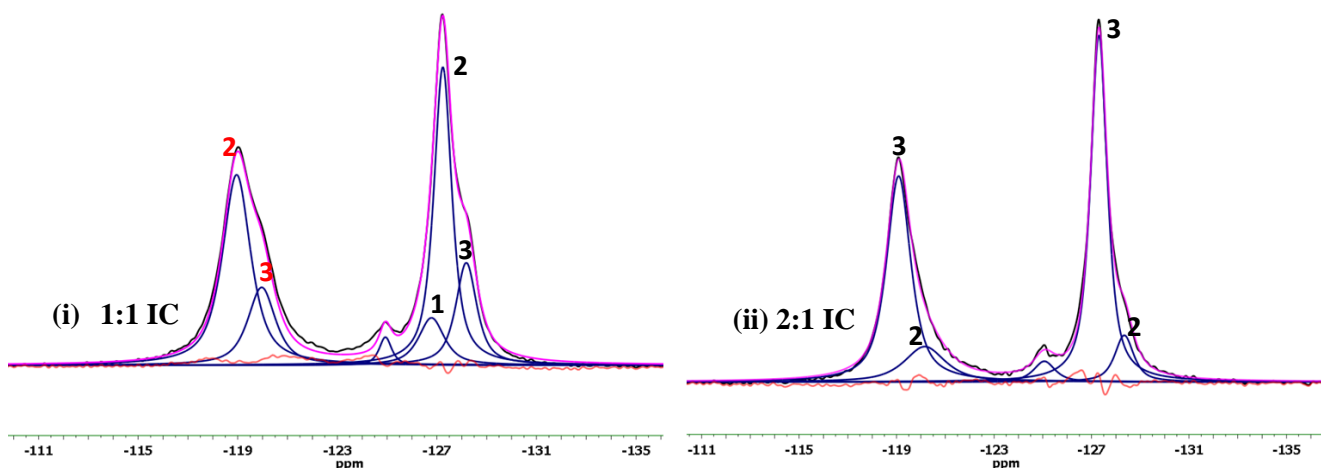


Figure 4.9b Deconvolution analyses of the CF_2 line shapes for the ^{19}F DP/MAS 20 kHz spectra of (i) the 1:1, and (ii) 2:1 β -CD/PFBA solid complexes at 295 K.

In contrast, the 2:1 preparation is composed primarily of the 2:1 complex, with a small contribution of the 1:1 host/guest complex (*cf.* Fig. 4.9a,b-ii and Table C4.1b) consistent with the minor DSC dehydration transition at ~ 80 °C. The 1:2 host/guest contributions are either attenuated or are missing entirely in the 2:1 preparation due to the greater mole fraction of the host. The presence of appreciable amounts of the 1:2 contributions in the 1:1 preparation is consistent with the greater mole ratio of the guest and may suggest the presence of a free guest in this preparation. The hydration and H-bonding behaviour described in the DSC and FT-IR, respectively, agree well with the findings of the deconvolution analyses. Complexes with variable host/guest configurations where different stoichiometric distributions (i.e., 2:1, 1:1, and 1:2) may be present are expected to experience different hydration and H-bonding effects.

4.4.5.3 $^1\text{H}\rightarrow^{13}\text{C}$ CP/MAS NMR

Multinuclear NMR techniques employing polarization transfer have been used to provide unequivocal evidence for the formation of inclusion complexes.⁵¹⁻⁵³ Additionally, solid state ^{13}C NMR CIS values and line shape variations can be used to probe conformational effects and molecular dynamics of host-guest systems.⁵⁴ The NMR spectra of the native β -CD, the 1:1 and 2:1 host-guest inclusion compounds obtained using $^1\text{H}\rightarrow^{13}\text{C}$ CP under conditions of 20 kHz MAS at ambient temperature are depicted in Figure 4.10. The ^{13}C resonance lines were assigned in agreement with previous reports.^{53,55} The individual ^{13}C nuclei for β -CD hydrate in Fig. 4.10 are not completely resolved due to the amorphous nature and variable hydration state of the material, in addition to the spectral overlap of certain ^{13}C resonance lines. Note that the $^1\text{H}\rightarrow^{13}\text{C}$ CP/MAS NMR spectra in Figure 4.10 show ^{13}C host nuclei and since the guest has no protons, any changes in line shape/width are attributed to hydration properties of the 1:1 and 2:1 complexes. Therefore, the extent and nature of hydration is influenced by the guest binding configuration in these complexes. CIS patterns similar to those observed in solution ^1H NMR are observed in the ^{13}C solid NMR results, further supporting the presence of variable hydration states and guest motional dynamics.

The most attenuated CIS values are observed in the spectrum of the 1:1 complex for the intracavity carbon nuclei (i.e., C_3 and C_5). This further supports the inclusion of the guest within the cavity. The deshielding pattern in the 2:1 complex reveals less steric hindrance of the guest for the intracavity nuclei compared to the 1:1 complex (shielding). As well, there are prominent chemical shift changes to lower field in the 2:1 complex for the framework carbon nuclei (C_1 and C_4); whereas, the chemical shift (δ) of C_6 is unaffected in both complexes. In general, the 1:1 complex experiences reduced δ for almost all of its ^{13}C nuclei. We infer from the ongoing discussion that the host cavity in the 1:1 complex experiences greater steric effects from the included guest compared to the 2:1 complex. We conclude that the guest molecule may adopt a *trans* conformation in the 2:1 complex as compared to a *gauche* conformation in the 1:1 complex, in accordance with the configurations in Scheme 4.3, the IR and solution NMR results. Variations in the relative intensities of IR bands 1 ($\nu_{\text{asym}}/\text{CF}_2$) and 2 (β/CC and ν/CCC) were observed for the 1:1 and 2:1 complexes and may be related to differences in the conformation of the guest in these compounds. A near-linear conformation of the guest in the 2:1 complex is

generally expected to cause minimal constraints on the host framework thereby resulting in a downfield shift for such ^{13}C nuclei.

The spectrum of the 1:1 complex in Figure 4.10 is characterized by narrow resonance lines; whereas, the resonance lines for the 2:1 complex are relatively broad. The observed differences in line width may be due to differences in guest dynamics. The guest molecule in the 1:1 complex is expected to be more dynamic than in the 2:1 complex where the guest may be completely encapsulated by two host macromolecules. In the case of the 1:1 complex, part of the guest may extend outside of the CD cavity as shown in Scheme 4.3. The deshielding effect observed for the extra- and intra-cavity carbon nuclei of the host in the 2:1 complex may be related to a variable guest conformation, as described above, and in agreement with FT-IR and solution/solid NMR results. For PFBA to form a 2:1 host/guest complex with CD, the guest must adopt a near-linear conformation. We conclude that while PFBA guest adopts a *gauche* conformation in the 1:1 (and 1:2) host/guest complexes, the conformation in the 2:1 complex is not *gauche* but a linear one.

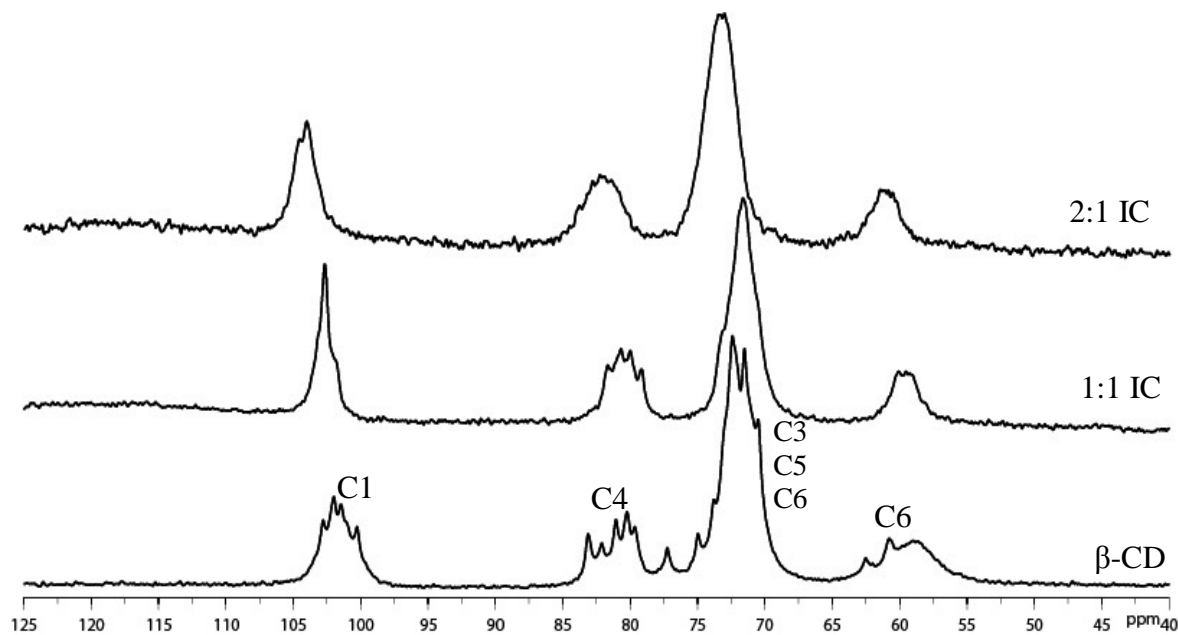


Figure 4.10 ^{13}C $^1\text{H} \rightarrow ^{13}\text{C}$ CP NMR results for β -CD, and the 1:1, and 2:1 β -CD/PFBA complexes at 20 kHz MAS and 295 K.

4.4.5.4 $^{19}\text{F}\rightarrow^{13}\text{C}$ CP/MAS NMR

$^{19}\text{F}\rightarrow^{13}\text{C}$ CP/MAS NMR techniques allow for dipolar interactions between the host and guest to be detected. Figure 4.11 shows the $^{19}\text{F}\rightarrow^{13}\text{C}$ CP/MAS NMR spectra of the host/guest complexes prepared at variable mole ratios (i.e., 1:1 and 2:1) assigned according to spectra of Figures 4.5 and 4.10. The ^{13}C resonance of the carbonyl group for the β -CD/PFBA inclusion compounds is observed at a much higher field ($\delta \sim 160$ ppm) compared to $\delta \sim 170$ ppm for the carbonyl carbon of the PFOA complexes in a previous study (chapter 3).¹⁹ Carbonyl carbon nuclei in general resonate in the characteristic region between 150–220 ppm, whereas carbonyl groups of carboxylic acids appear in the range of 160–180 ppm.⁵⁶ The observed δ value for the carbonyl carbon of PFBA reported herein is in good agreement with a reported value in solution by ^{13}C NMR.⁵⁷ The most remarkable observation in the $^{19}\text{F}\rightarrow^{13}\text{C}$ CP/MAS results is the appearance of a host signal centered ~ 78 ppm. This signal indicates that ^{19}F polarization from the guest has been transferred to the ^{13}C nuclei of the host cavity (i.e., C₃ and C₅) and provides unequivocal evidence for the inclusion of the PFBA guest within the host cavity. The relative intensities of this signal for the 1:1 (low) and 2:1 (high) complexes reveals a more efficient polarization transfer for the latter and this is related to the differences in guest conformation and dynamics in the two complexes. The appearance of a similar resonance ~ 85 ppm (i.e., C₄) for only the 2:1 complex further supports an altered binding configuration and conformation of the guest in this product. Note that C₄ is closer to the center of the CD macrocycle, and supports complete encapsulation in the 2:1 complex.

The dynamics and conformation of the guest in the 2:1 complex contribute to more efficient polarization transfer as evidenced from the greater intensity of the resonance at ~ 78 ppm. The guest molecule in the 2:1 complex is believed to adopt a near-linear conformation, in which the guest is entirely encapsulated within the host cavity space as described above. In the case of the 1:1 complex, the *gauche* conformation coupled with faster dynamics of the guest are expected to reduce efficient dipolar coupling between the host and guest, thus reducing CP transfer. The ^{13}C peaks of the PFBA guest in Fig. 4.11 are broader for 2:1 and narrower for 1:1 and this suggests that guest dynamics are faster in the 1:1 complex. In general, differences in line shapes and δ values observed in the $^{19}\text{F}\rightarrow^{13}\text{C}$ CP/MAS NMR results reveal the differences in the guest geometry, mobility and solvent effect in these complexes and are in agreement with the DSC, FT-IR, and ^{19}F NMR results.

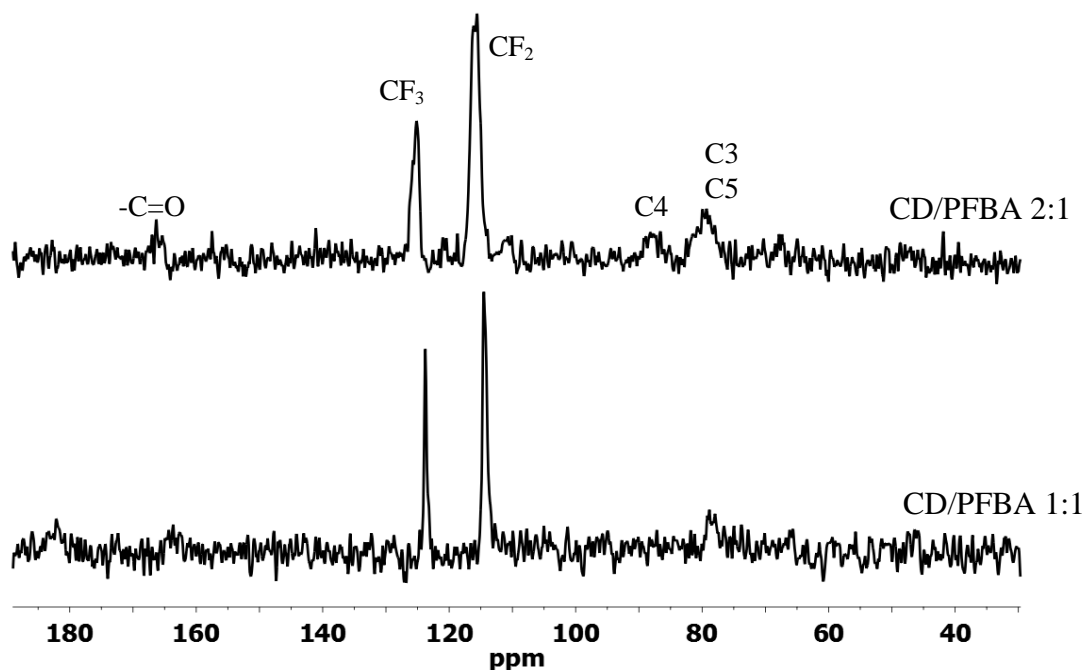


Figure 4.11 $^{13}\text{C } ^{19}\text{F} \rightarrow ^{13}\text{C}$ CP NMR results for the 1:1, and 2:1 β -CD/PFBA complexes at 20 kHz MAS and 295 K.

4.4.6 ^{19}F Solids NMR Relaxation Dynamics

The dynamics of the guest in the complexes were studied using ^{19}F relaxation (T_1/T_2) NMR methods at variable temperature (VT; 20–70 °C). The T_1/T_2 data as a function of temperature are shown in Figure 4.12 for the 1:1 and 2:1 complexes. The T_1 process of the 1:1 complex shows a bi-exponential behaviour as a function of temperature; whereas, the 2:1 (T_1) preparation shows relatively linear behavior (*cf.* Fig. 4.12). The bi-exponential behaviour of the 1:1 preparation suggests that this material consists of two contributions and may be consistent with the presence of equimolar amounts of 1:1 and 2:1 host/guest complexes as illustrated by the ^{19}F NMR deconvolutions of the CF_3 peaks in Figure 4.9a-i. In contrast, the linear behaviour of the 2:1 preparation is consistent with the presence of the 2:1 complex as the predominant product in this material. It should be noted here that the bi-exponential behaviour of the 1:1 (T_1) complex could be the result of multiple dynamic processes at work.

The relaxation of spin-1/2 (e.g., ^{19}F) nuclei results from fluctuations in local fields arising from chemical shift anisotropy (CSA) and dipole-dipole (DD) coupling interactions modulated by localized motions.⁵⁸ The faster the rate of motion, the less efficient the CSA and DD relaxation mechanisms and the longer the T_1/T_2 relaxation times. Notice from Figure 4.12 that

the T_1 relaxation times increase monotonically with temperature, and this suggests that the motions that give rise to T_1 are faster than the Larmor frequency (469 MHz) at the measured conditions. However, the T_2 values (~ 0.2 – 1.3 milliseconds) are about three orders of magnitude smaller than the corresponding T_1 values (~ 0.4 – 1.0 seconds, *cf.* Table 4.3). This implies that the types of motion causing T_1 and T_2 relaxation are different. Starting with T_1 plots from Figure 4.12, we observe that the T_1 relaxation values for the different segments of the chain at each temperature are indistinguishable in both the 1:1 and 2:1 complexes. This suggests that the type of motion that drives T_1 relaxation affects different segments of the chain similarly. That motion must be a librational (axial) motion of the guest as a whole. In contrast to the T_1 values, the T_2 values are different for the different segments of the chain in the 1:1/2:1 ICs at each temperature. We therefore conclude that the internal rotation of the CF_3 is causing T_2 relaxation, where the group furthest removed from the CF_3 group (i.e., $\text{C}_\alpha\text{F}_2$) experiences the most attenuated relaxation time due to less efficient spin diffusion.⁵⁴

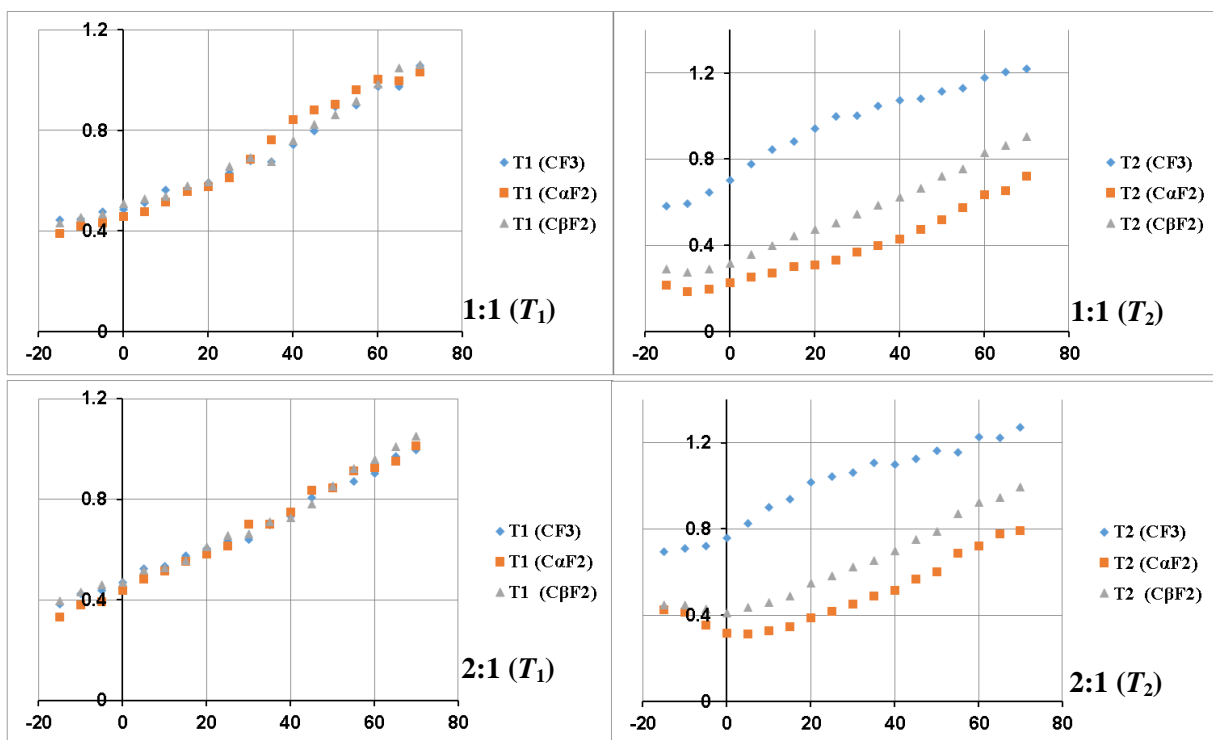


Figure 4.12 ^{19}F T_1 (in seconds) and T_2 (in milliseconds) relaxation times for the 1:1, and 2:1 β -CD/PFBA complexes

Table 4.3 T_1/T_2 Relaxation Values for the 1:1 β -CD/PFBA and 1:1 β -CD/PFOA Complexes.*

T (°C)	1:1 β -CD/PFBA				1:1 β -CD/PFOA			
	T ₁ (s)	T ₂ (ms)			T ₁ (s)	T ₂ (ms)		
	CF ₃	CF ₃	CF ₂ α	CF ₂ β	CF ₃	CF ₃	CF ₂ <i>m</i>	CF ₂ <i>t</i>
0	0.487	0.704	0.226	0.318	0.926	0.402	0.281	0.405
10	0.563	0.844	0.272	0.400	0.941	0.422	0.31	0.400
20	0.593	0.943	0.311	0.474	0.960	0.443	0.339	0.431
30	0.679	1.002	0.368	0.543	1.058	0.473	0.358	0.499
40	0.742	1.072	0.430	0.624	1.024	0.491	0.372	0.512
50	0.895	1.116	0.517	0.723	1.074	0.514	0.358	0.562
55	0.901	1.126	0.574	0.754	1.080	0.516	0.360	0.572
60	0.976	1.179	0.636	0.828	1.168	0.528	0.369	0.558
65	0.975	1.203	0.652	0.862	1.193	0.531	0.350	0.577
70	1.059	1.218	0.720	0.903	1.123	0.540	0.355	0.617

*Error estimates are within 0.003 s and 0.05 ms for T_1 and T_2 values, respectively.

In general, the T_2 values of the CF₃ group for the complexes reported herein are about twice as long compared to similar values reported previously for β -CD/PFOA complexes (*cf.* Table 4.3). This is because the motional dynamics of the short PFBA chain are expected to be significantly faster compared to the dynamics of PFOA. Furthermore, it is evident from Figure 4.12 that the T_2 relaxation values of the methylene groups of PFBA are significantly reduced relative to those of the CF₃ group. In a previous study of β -CD/PFOA complexes,¹⁹ the T_2 values of the methylene groups were close to the corresponding T_2 values of the CF₃ group (*cf.* chapter 3, Fig. 3.10). Since T_2 relaxation is driven by CF₃ rotation, the reduced relaxation times for the methylene groups of the complexes reported herein further support the relative dynamics of the main PFBA chain, as described in the ¹⁹F NMR simulation results in solution. The PFBA chain

was described to experience extensive rotation of the CF₃ group at the termini and appreciable rotation of the CF₂ bonds in the main chain. Thus, spin diffusion propagates the CF₃ rotational motion along the chain less efficiently resulting in reduced T_2 relaxation values for the CF₂ groups of PFBA. The increased disparity between the T_2 values of the methyl and methylene groups in the 1:1 complex compared to the 2:1 complex in Figure 4.12 may be related to the increased rotation of the CF₃ group in the former complex in accordance with the configurations in Scheme 4.3.

The activation energies for the methyl and methylene groups were estimated from the slope of the Arrhenius plots to further evaluate the structure of the β -CD/PFBA complexes. The results are presented in Table 4.4. Note that the energies of activation (E_a) for the T_1 processes are similar for all the segments (CF₃, C _{α} F₂, and C _{β} F₂) of the chain in both the 1:1 and 2:1 complexes. This supports the fact that the type of motion that drives T_1 relaxation is libration of the whole body and affects all the fluorines in the same way. Recall that T_2 is caused by the free rotation of the CF₃ group which affects segments of the guest in different ways. This is manifested by the disparity in E_a values for the T_2 relaxation between the methyl and methylene groups (*cf.* Table 4.4).

Table 4.4 **Activation Energies (kJ/mol) of PFBA Guest as Estimated from T_1/T_2 Data of β -CD/PFBA Complexes.**

	Parameter	CF ₃	C _{α} F ₂	C _{β} F ₂
β-CD/PFBA 1:1	T_1	7.83	9.33	8.06
	T_2	4.12	14.4	11.1
β-CD/PFBA 2:1	T_1	8.26	9.21	8.45
	T_2	3.56	12.6	10.3

The CF_3 groups displayed low $E_a(T_2)$ values (~ 4.0 kJ/mol), while much greater values ($\sim 10\text{--}14$ kJ/mol) were recorded for the CF_2 groups. The lower $E_a(T_2)$ values for the CF_3 groups are understood in terms of the relative ease with which this group can freely rotate around its three-fold axis. In contrast, the rotation of the $\text{CF}_2\text{--CF}_2$ bonds is relatively constrained in the complexes compared to the pure PFBA. The greater $E_a(T_1)$ for the 2:1 complex relative to the 1:1 complex suggests that the libration of the PFBA guest is more hindered in the 2:1 complex.

4.5. Conclusions

β -CD/PFBA host/guest inclusion compounds were prepared and characterized using multinuclear solid/solution NMR techniques, FT-IR, DSC and PXRD. The solid phase compounds were prepared using a modified dissolution methods at various host/guest mole ratios (1:1 and 2:1). The $^{19}\text{F}\rightarrow^{13}\text{C}$ CP results provided unequivocal evidence for the formation of β -CD/PFBA inclusion compounds. PXRD results have shown the host to form “cage-type” structures with the guest. The enthalpy of dehydration revealed various binding configurations of the guest in the 1:1 and 2:1 complexes. According to the deconvolution analyses of the ^{19}F resonance line shapes, the guest molecule in the 1:1 preparation exists in at least two distinct configurations that resemble an equimolar mixture of 1:1 and 2:1 complexes and supported by DSC results. In the 2:1 preparation, the contribution of the guest configuration corresponding to the 2:1 complex is predominant. The guest molecule in the 1:1 complex adopts a *gauche* conformation and is different from the fully linear conformation of the guest in the 2:1 complex. Simulation of the ^{19}F spectrum of pure PFBA and its complexes with β -CD in solution reveal that the CF_3 group experiences an extensive rotation about its three-fold axis, whereas a significant rotation of the CF_2 is present in the main chain. NMR relaxation dynamic parameters reveal that these dynamics depend on the host/guest mole ratios and are determined by the geometry of the guest within the host. The CF_2 bond rotations are more hindered in the 2:1 complex due to full encapsulation of the guest in this product.

4.6. Acknowledgements

We wish to acknowledge the University of Saskatchewan, the University of Lethbridge, and the National Sciences and Engineering Council (NSERC) for supporting this research.

4.7. References

1. Kissa, E., Fluorinated Surfactants and Repellents. 2 ed.; Marcel Dekker, Inc.: New York, 2001; Vol. 97, pp 228-231.
2. Rao, N. S.; Baker, B. E. Organofluorine Chemistry Principles and Commercial Applications. Ed. Banks, R. E.; Smart, B. E.; Tatlow, J. C. Plenum Press: New York: 1994; pp 61.
3. Erkoc, S.; Erkoc, F. *J. Mol. Struct-Theochem* **2001**, *549*, 289-293.
4. Schultz, M. M.; Barofsky, D. F.; Field, J. A. *Environ. Eng. Sci.* **2003**, *20*, 487-501.
5. Ellis, D. A.; Denkenberger, K. A.; Burrow, T. E.; Mabury, S. A. *J. Phys. Chem.A* **2004**, *108*, 10099-10106.
6. Ahrens, L.; Taniyasu, S.; Yeung, L. W. Y.; Yamashita, N.; Lam, P. K. S.; Ebinghaus, R. *Chemosphere* **2010**, *79*, 266-272.
7. Giesy, J. P.; Kannan, K. *Environ. Sci. Technol.* **2001**, *35*, 1339-1342.
8. Prevedouros, K.; Cousins, I. T.; Buck, R. C.; Korzeniowski, S. H. *Environ. Sci. Technol.* **2006**, *40*, 32-44.
9. Huset, C. A. Determination of Fluorochemicals in Waste-Dominated Aqueous Systems. Oregon State University, 2007.
10. Huset, C. A.; Barlaz, M. A.; Barofsky, D. F.; Field, J. A. *Chemosphere* **2011**, *82*, 1380-1386.
11. Higgins, C. P.; Luthy, R. G. *Environ. Sci. Technol.* **2006**, *40*, 7251-7256.
12. Karoyo, A. H.; Borisov, A. S.; Wilson, L. D.; Hazendonk, P. *J. Phys. Chem. B* **2011**, *115*, 9511-9527.
13. Karoyo, A. H.; Borisov, A. S.; Wilson, L. D.; Hazendonk, P. Probing the Effect of Sodium Counterions on the Structure and Dynamics for the Solid inclusion complexes of β -Cyclodextrin and Sodium Perfluorooctanoate. *Manuscript in Preparation*.
14. Szejtli, J. *J. Mater. Chem.* **1997**, *7*, 575-587.
15. Moroi, Y.; Yano, H.; Shibata, O.; Yonemitsu, T. *Bull. Chem. Soc. Jpn* **2001**, *74*, 667-672.
16. Rayne, S.; Forest, K. *J. Mol. Struct-Theochem* **2010**, *949*, 60-69.
17. Bunn, C. W.; Holmes, D. R. *Discuss. Faraday Soc.* **1958**, *25*, 95-103.
18. Milne, J. B.; Parker, T. J. *J. Solution Chem.* **1981**, *10*, 479-487.
19. Karoyo, A. H.; Sidhu, P.; Wilson, L. D.; Hazendonk, P. *J. Phys. Chem. B* **2013**, *117*, 8269-8282.

20. US-EPA. Emerging Contaminants; Perfluorooctane sulfonate (PFOS) and Perfluorooctanoic acid (PFOA). May 2012.
21. Margot, R.; Berger, U.; Broman, D.; Cousins, I. R.; Nilsson, E. D.; McLachlana, M. S. *Environ. Chem.* **2001**, *8*, 381-388.
22. Yoo, H.; Guruge, K. S.; Yamanaka, N.; Sato, C.; Mikami, O.; Miyazaki, S.; Yamashita, N.; Giesy, J. P. *Ecotox. Environ. Safe* **2007**, *72*, 26–36.
23. Beare-Rogers, J.; Dieffenbacher, A.; Holm, J. V. *Pure Appl. Chem.* **2001**, *73*, 685–744.
24. Hoffmann, H.; Würtz, J. *J. Mol. Liq.* **1997**, *72*, 191–230.
25. Bennett, A. E.; Rienstra, C. M.; Auger, M.; Lakshmi, K. V.; Griffin, R. G. *J. Chem. Phys.* **1995**, *103*, 6951-6958.
26. Riga, A.; Collins, R.; Mlachak, G. *Thermochim. Acta* **1998**, *324*, 135-149
27. Yang, X.; Zhao, Y.; Chen, Y.; Liao, X.; Gao, C.; Xiao, D.; Qin, Q.; Yi, D.; Yang, B. *Mater. Sci. Eng. C Mater. Biol. Appl.* **2013**, *33*, 2386-2391.
28. Cwiertnia, B.; Hladon, T.; Stobiecki, M. *J. Pharm. Pharmacol.* **1999**, *51*, 1213-1218.
29. Venkatesh, G.; Sivasankar, T.; Karthick, M.; Rajendiraan, N. *J. Incl. Phenom. Macrocycl. Chem.* **2013**, *77*, 309-318.
30. Palepu, R.; Reinsborough, V. C. *Can. J. Chem.-Revue Canadienne De Chimie* **1988**, *66* (2), 325-328.
31. Wenz, G. *Angew. Chem. Int. Ed. Engl.* **1994**, *33*, 803-822.
32. Wilson, L. D.; Verrall, R. E. *Langmuir* **1998**, *14*, 4710–4717.
33. Dong, T.; He, Y.; Shin, K.; Inoue, Y. *Macromolecular Bioscience* **2004**, *4* (12), 1084-1091.
34. Lamcharfi, E.; Kunesch, G.; Meyer, C.; Robert, B. *Spectrochim. Acta A* **1995**, *51*, 1861–1870.
35. Harry-O’kuru, R. E.; Isbell, T. A.; Weisleder, D. *J. Am. Oil Chem. Soc.* **2001**, *71*, 219-222.
36. Labuschagne, P. W.; Kazarian, S. G.; Sadiku, R. E. *Spectrochim. Acta A* **2011**, *78*, 1500-1506.
37. Moynihan, R. E. *J. Am. Chem. Soc.* **1959**, *81*, 1045-1050.
38. Wang, J.; Ober, C. K. *Liq. Cryst.* **1999**, *26*, 637-648.
39. Knonchehuer, G.; Reiche, J.; Brehmwer, L.; Berberka, T.; Woolley, M.; Tredgold, R.; Hodge, P. J. *Chem. Soc., Chem. Commun.* **1995**, 1619-1620.
40. Albinsson, B.; Michl, J. *J. Phys. Chem.* **1996**, *100*, 3418–3429.

41. Okumura, H.; Kawaguchi, Y.; Harada, A. *Macromolecules* **2001**, *34*, 6338–6343.
42. Schneider, H-J.; Hacket, F.; Rüdiger, V. *Chem. Rev.* **1998**, *98*, 1755–1785.
43. Steed, J.W.; Atwood, J.L. In *Supramolecular Chemistry*, 2nd ed.; John Wiley & Sons, Ltd.: West Sussex, UK, **2009**.
44. Guo, W.; Fung, B. M.; Christian, S. D. *Langmuir* **1992**, *8*, 446–451.
45. Yonemori, S.; Sasakura, H. *J. Fluorine Chem.* **1995**, *75*, 151–156.
46. Emsley, J. W.; Feeney, J.; Sutcliffe, L. J. *High-Resolution Magnetic Resonance Spectroscopy*. Pergamon: New York, 1966; Vol. 2, p 877.
47. Newmark, R. A. *J. Flu. Chem.* **2009**, *130*, 383-393.
48. Foris, A. *Magn. Reson. Chem.* **2001**, *39*, 386–398.
49. Gutowsky, H. S.; Belford, G. G.; McMahon, P. E. *J. Chem. Phys.* **1962**, *36*, 3353–3368.
50. Borisov, A. S.; Hazendonk, P.; Hayes, P. G. *J. Inorg. Organomet. Polym.* **2008**, *18*, 163–174.
51. Koito, Y.; Yamada, K.; Ando, S. *J. Incl. Phenom. Macrocycl. Chem.* **2013**, *76*, 143–150.
52. Fyfe, C. A.; Brouwer, D. H. *Can. J. Chem.* **2006**, *84*, 345–355.
53. Lefebvre, F.; Mentzen, B. F. *Mater. Res. Bull.* **1994**, *29*, 1049–1056.
54. Derome, A. E. In *Modern NMR Techniques for Chemistry*; Pergamon: New York, 1987.
55. Jiao, H.; Goh, S. H.; Valiyaveetil, S. *Macromolecules* **2002**, *35*, 3997–4002.
56. Balci, M. *Basic 1H-13C-NMR Spectroscopy*. 1st ed. Elsevier B. V.; Amsterdam, The Netherlands, 2005; chp 13, pp 315-319.
57. Lim, K.T.; Ganapathy, H. S.; Lee, M. Y.; Yuvaraj, H.; L. W.-K.; Heo, H. *J. Fluorine Chem.* **2006**, *127*, 730-735.
58. Levitt, M. L. *Spin Dynamics: Basics of Nuclear Magnetic Resonance*. 2 Ed. John Wiley & Sons Ltd. The Atrium, Southern Gate, Chichester, West Sussex, England, 2005.

CHAPTER 5

Manuscript no. 4

Description

The modified dissolution preparative method developed in chapter 3 was used to prepare β -CD/SPFO inclusion complexes at the 1:1 and 2:1 host-guest mole ratios. Complexation-induced shifts of the $^1\text{H}/^{19}\text{F}/^{13}\text{C}$ nuclei in solution and the solid state for β -CD/SPFO complexes were compared with similar values for β -CD/PFOA complexes in order to probe the effect of the counterion species (i.e. sodium and hydronium) in the binding of the guests. Simulated CF_3 signals at MAS 25 kHz and variable dipolar coupling strengths were used in conjunction with deconvolution analyses of the CF_3 line shapes to probe the dynamics of SPFO and its complexes with β -CD. Structural properties for PFOA, SPFO and PFBA and their complexes with β -CD were compared and summarized.

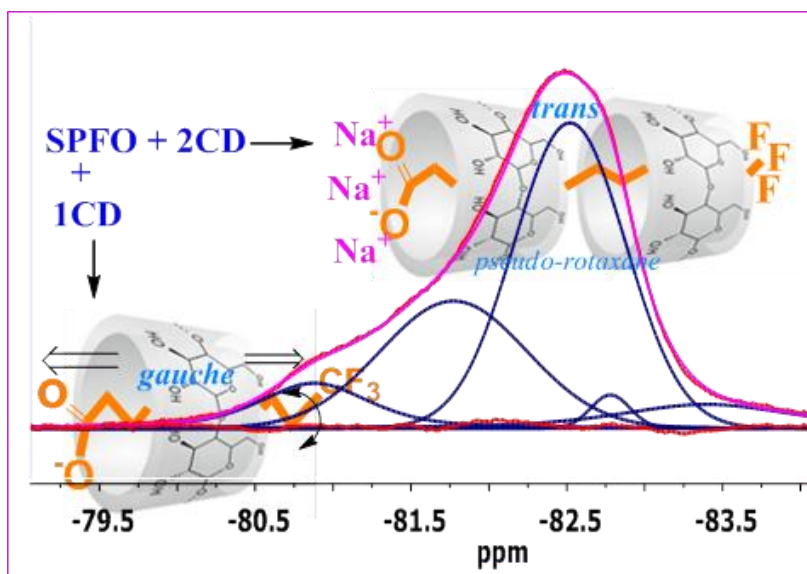
Author's Contribution

The idea of preparing β -CD/SPFO ICs was proposed by Drs. Wilson and Hazendonk as part of the original research plan. The idea of using simulations to probe dynamics was proposed by Dr. Hazendonk. I carried out the preparation and characterization (solution NMR, FT-IR, DSC, and PXRD) of the β -CD/SPFO complexes. The solid state NMR characterization, relaxation measurements and data analyses were done in collaboration with Alex Borisov and Dr. Paul Sidhu. All simulations were done by Dr. Hazendonk. The first draft of the manuscript was prepared by me and subsequently edited by Drs. Wilson, Hazendonk, and Sidhu.

Relation of Manuscript 4 to Overall Objective of this Project

The main objective of this work was to provide a structural comparison between the CD complexes of SPFO and PFOA, respectively, in terms of the dynamics and geometry of the guest as determined by the presence of different counterion species (i.e. H^+/Na^+).

Graphical Abstract



Research Highlights

- ^{13}C ($^{19}\text{F} \rightarrow ^{13}\text{C}$ CP) MAS NMR technique provided unequivocal evidence for the inclusion of the SPFO guest within the host cavity.
- The binding geometry and dynamics of the guests in the β -CD/SPFO vs. β -CD/PFOA complexes were compared and found to be variable as determined by the presence of sodium vs. hydronium counterion species.
- The dynamics of β -CD/SPFO involve extensive motions of the CF_3 rotations in the 1:1 β -CD/SPFO; whereas, the axial motions of the central body dominate the dynamics of the guest in the 2:1 complex in accordance with the role of the sodium counterion in the binding of the guest.

5 Probing the Effect of Sodium Counterions in the Structure and Dynamics of Solid Host-Guest Complexes of β -Cyclodextrin and Sodium Perfluorooctanoate

Abdalla H. Karoyo,[†] Paul S. Sidhu,[‡] Alex Borisov,[‡] Lee D. Wilson,^{†,} Paul Hazendonk.^{‡,*}*

[†]University of Saskatchewan, Department of Chemistry, Saskatoon, SK, S7N 5C9, Canada.

[‡]University of Lethbridge, Department of Chemistry and Biochemistry, Lethbridge, AB, Canada.

Supplementary Information (Appendix D)

5.1. Abstract

Structural characterization of the inclusion complexes (ICs) of β -Cyclodextrin (β -CD; host) and sodium perfluorooctanoate (SPFO; guest) was carried out using $^1\text{H}/^{19}\text{F}/^{13}\text{C}$ NMR spectroscopy. The 1:1 and 2:1 β CD/SPFO solid complexes were prepared using a modified dissolution method. Evidence for the formation of β -CD/SPFO ICs was provided using ^{13}C DP (direct polarization) and CP (cross polarization) solid-state NMR spectroscopy with magic angle spinning (MAS) at 20 kHz. Complexation-induced shifts (CIS) for $^1\text{H}/^{19}\text{F}/^{13}\text{C}$ nuclei in solution and the solid state for β -CD/SPFO complexes were compared with similar values for the complexes of perfluorooctanoic acid (PFOA) with β -CD in order to probe the effect counterion species in the binding of the guests. Analyses of the CIS values provided evidence for the formation of inclusion compounds and variable guest geometry for SPFO and PFOA as determined by the presence of sodium and hydronium counterions, respectively. DSC, TGA, FT-IR, and powder X-ray diffraction (PXRD) were used to complement the NMR results. Simulated CF_3 lines at MAS 25 kHz and variable dipolar coupling strengths were used in conjunction with deconvolution analyses of the CF_3 line shapes to probe the dynamic properties of SPFO and its complexes with β -CD. The dynamics of the guest are modulated by the nature of the guest and the stoichiometry of the complex, and involve three-fold rotation of the CF_3 group as well as rotations of the C-F bonds. ^{19}F DP/MAS NMR results, spin-lattice (T_1) and spin-spin (T_2) relaxation times in the laboratory frame at variable temperatures in the solid phase support that the dynamics of SPFO in β -CD/SPFO complexes are unique due to the role of sodium counterion in the binding of the guest with β -CD.

5.2. Introduction

Perfluorinated compounds (PFCs) of the type $\text{CF}_3\text{-(CF}_2)_n\text{-R}'$ have diverse functional groups ($\text{R}' = \text{CF}_2\text{-OH, COOH, CO-NH}_2, \text{ or CF}_2\text{-SO}_3\text{H}$) and chain lengths and have received vast research attention due to environmental and health related concerns. Such materials have been used in applications ranging from fire-fighting foams to pesticides and surface active agents.¹⁻³ They have unique physicochemical properties in comparison to their hydrocarbon analogues. For example, a comparison of the critical micelle concentrations (cmc) of perfluorooctanoic acid (PFOA; $\text{CF}_3\text{-(CF}_2)_6\text{-CF}_2\text{-OH}$, $\sim 0.0087\text{--}0.010\text{ M}$), perfluorooctane sulfonate (PFOS; $0.0060\text{--}0.0080\text{M}$), and sodium perfluorooctanoate (SPFO: $\text{CF}_3\text{-(CF}_2)_6\text{-CF}_2\text{-O}^-\text{Na}^+$, $\sim 0.032\text{M}$),³⁻⁷ and sodium octanoate ($\sim 0.40\text{ M}$),⁸ illustrates the differences in surface activity that occur between PFCs and hydrocarbon surfactants. PFOA and PFOS are the most common PFCs and exist predominantly as anions in aqueous environments due to their low pKa values (PFOA; 2.5, PFOS; <0).^{9,10} SPFO and APFO (ammonium perfluorooctanoate) are salts of PFOA commonly used as surfactants and as essential processing agents in fluorotelomer-based formulations for making consumer products (e.g., films and membranes for non-stick cookware and outerwear, and cleaning agents for carpets).¹¹ Most of the toxicological effects of PFCs are related to the anionic forms in aquatic environments and biological samples. For example, evidence of liver damage was noted in primates that were treated with APFO.¹²

Cyclodextrins (CDs) have been widely used to lower the surface activity of perfluorocarbon compounds through formation of host-guest complexes.^{13,14} CDs are a family of macrocyclic oligomers consisting of 6 (α -CD), 7 (β -CD) or 8 (γ -CD) glucopyranose units that are linked by α -(1 \rightarrow 4) glycosidic linkages (cf. Scheme 5.1a,b).¹⁵ We reported in previous work^{16,17} the structural and dynamic properties for the complexes formed between β -CD and PFOA (C8) in the solution and solid states (chapters 2,3). We also recently reported similar studies for short chain perfluorobutyric acid (C4) (chapter 4).¹⁸ It was concluded from these studies that PFOA forms 1:1 and 2:1 inclusion compounds with β -CD with variable conformation and dynamics of the guest. In contrast to PFOA, PFBA was reported to form mainly 1:1 host-guest complexes.

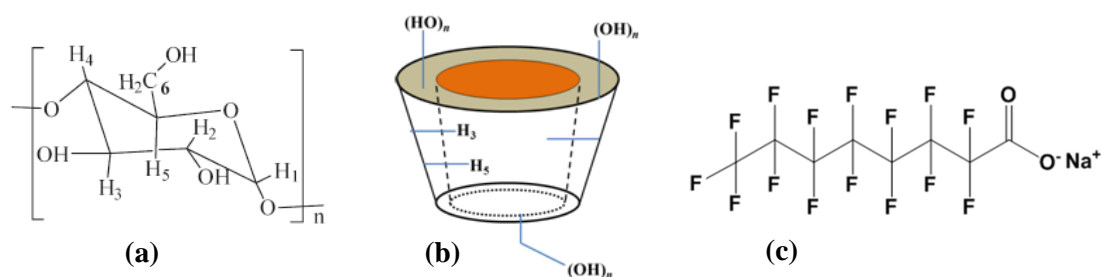
SPFO (C8) is the most widely studied^{7,19-25} perfluorocarbon salt because it shows strong affinity for CDs due to its unique amphiphilic nature. The research groups of Reinsborough¹⁹⁻²¹ and Guo⁷ were among the first to study CD/SPFO complexes using conductometry and solution NMR spectroscopy, respectively. Guo et al.⁷ reported a detailed study of the complex formation

in solution between CDs and a series of sodium perfluoroalkanoates comprising 4–9 carbon atoms. In that study, it was reported that the association of CDs to shorter sodium perfluorocarbon chains favors 1:1 host-guest formation; whereas longer chains favor 2:1 or a combination of 1:1 and 2:1 formation. A preferred extended (*all-trans*) conformation of the perfluorocarbon guest was reported in the 2:1 complexes in solution. Similar conclusions were drawn from our studies on the β -CD/PFOA system in aqueous solution and the solid state.^{16,17} For structural considerations, Wenz²⁶ described the association of the host and guest to form complexes as consisting of one or more CDs or guest molecules; in this case these complexes can form *inclusion* as well as *non-inclusion* associations with a variety of topologies. Wilson and Verrall^{27,28} showed that higher order (e.g. 2:1 and 1:2) host-guest complexes were formed in aqueous solution between modified β -CD and long chain PFCs.

Other reports of CD/SPFO complexes in solution have focused on analyzing the effects of SPFO monomer-micelle exchange rates on CD addition,²² measurements of binding constants using native and substituted-CDs,^{23,24} and selective association of CD to SPFO in the presence of other hydrocarbon surfactants.²⁵ Recently, it was demonstrated that complexation of SPFO to CDs is important to the biomedical field since these perfluorocarbon surfactants are used as oxygen-carrying, pulmonary drug and gene delivery agents.^{29,30} The widespread use of these recalcitrant perfluorocarbon compounds, along with their extreme inertness, are responsible for their environmental persistence. The fate and transport pathways of such materials are poorly understood, in part due to their unique physicochemical properties including surface activity, chemical mobility and stability, in comparison to their hydrocarbon counterparts. Despite their widespread use and related potential health and environmental concerns, detailed studies of the structural characterization of the solid complexes of β -CD and SPFO have not yet been reported. This may be due to the challenges associated with obtaining good quality single crystals. High resolution multinuclear solid state NMR techniques may offer a versatile option to the study of such complexes.

In this study we report the complex formation of SPFO with β -CD in the solution and solid states using $^1\text{H}/^{19}\text{F}/^{13}\text{C}$ NMR and FT-IR spectroscopy, thermal analyses (DSC/TGA), and powder X-ray diffraction (PXRD). The complexes in the solid state were prepared at the 1:1 and 2:1 β -CD/SPFO mole ratios using a modified dissolution method described previously.¹⁷ The CIS values for solution/solid phase β -CD/SPFO complexes were compared to similar values for

β -CD/PFOA complexes to aid in probing the geometry of the guests within the host and to determine the role of sodium ion in the binding of the guest. The dynamic properties of the SPFO guest in the free and bound states were examined using a combination of simulation and deconvolution analyses of the CF_3 resonance and NMR relaxation studies in the solid state. The results of this study are anticipated to contribute to a better understanding of the detailed structures of both native SPFO and its complexes with β -CD both in the solution and solid phases. Previous results of the structures of the complexes of β -CD with PFOA and PFBA, respectively, are highlighted to provide comparison and further understanding of the structure of SPFO and its complexes with β -CD.



Scheme 5.1 Molecular Structures of (a) β -CD oligomer where $n = 7$, (b) β -CD represented as a toroidal macrocycle, and (c) SPFO.

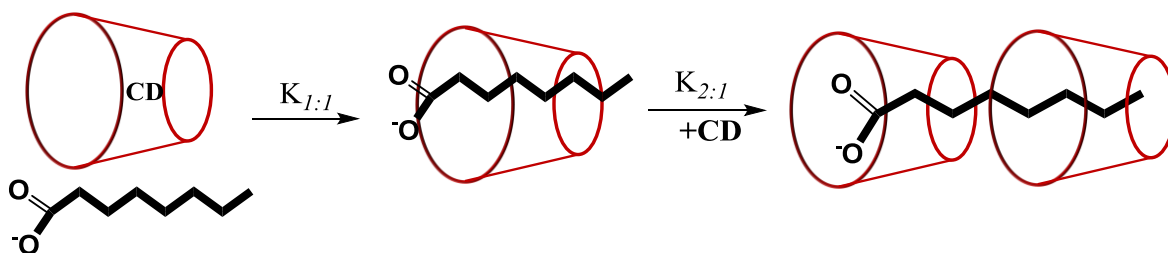
5.3. Experimental Section

5.3.1 Materials and Chemicals

β -CD hydrate (~10 % w/w H_2O) was purchased from Sigma-Aldrich Canada Ltd. (Oakville, ON), while SPFO (98 %) was purchased from SynQuest Labs Inc. (USA). All chemicals were used as received without any further purification. The water contents of the materials were determined using thermogravimetric analysis during preparation of the sample mixtures.

5.3.2 Preparation of β -CD/SPFO Solid Inclusion Compounds

The solid β -CD/SPFO complexes were prepared at the 1:1 and 2:1 mole ratios (*cf.* Scheme 5.2) using a modified dissolution (evaporation) method adapted from a previous report.¹⁷ The solid products were ground into fine powder for characterization with solid-state NMR, DSC/TGA, FT-IR and PXRD.



Scheme 5.2 Stepwise formation of the 1:1 and 2:1 complexes of β -CD (toroid) and SPFO according to the 1:1 and 2:1 host/guest mole ratios.

5.3.3 Solution-state NMR Spectroscopy

Solution NMR experiments were performed on a three-channel Bruker Avance DRX 500 NMR spectrometer operating at ca. 500 MHz for ^1H and ca. 470 MHz for ^{19}F . ^1H NMR spectra were referenced externally to tetramethylsilane (TMS; δ 0 ppm) while ^{19}F spectra were referenced externally to 2,2,2-trifluoroethanol (TFE; δ -79.21 ppm). Samples for ^1H and ^{19}F NMR were prepared in D_2O at pH \sim 5 in mole ratios of 1:1 and 2:1 β -CD/SPFO. All NMR spectra obtained in the solution state were acquired at 295 K.

5.3.4 Solid-state NMR Spectroscopy

All solid state NMR spectra were obtained using a Varian INOVA NMR spectrometer operating in triple channel HFC mode using a 2.5 mm T3 HFX probe operating at 125.55 MHz for ^{13}C , 499.99 MHz for ^1H , 469.89 for ^{19}F . Solid state ^{13}C MAS spectra were referenced externally to adamantane ($\delta = 38.5$ ppm) as a secondary standard with respect to TMS, while ^{19}F MAS spectra were referenced to hexafluorobenzene ($\delta = -164.9$ ppm). All samples were spun at the magic angle with a spinning rate of 20 kHz using 2.5 mm Vespel rotors equipped with Kel-F turbine caps, inserts, and end caps, unless stated otherwise. All ^{13}C NMR spectra were obtained using a 100 kHz sweep width with 8192 points in the FID and were zero-filled to 64 k data points, unless stated otherwise. The curve and width parameters for the adiabatic $^1\text{H} \rightarrow ^{13}\text{C}$ CP experiments were set at 50 and 10,000 Hz respectively, while those for $^{19}\text{F} \rightarrow ^{13}\text{C}$ were set at 50 and 50,000 Hz respectively. Optimal Hartmann-Hahn matching conditions were achieved with a contact time of 5 ms and approximate powers of 68 kHz and 59.5 kHz for the ^{19}F and ^{13}C channels, respectively. The ^{19}F T_1 values (T_1^{F}) were measured by inversion recovery (180° - τ - 90° -acquire), while the T_2^{F} values were obtained with a rotor synchronous Hahn echo (90° - τ - 180° - τ -acquire).³¹ The $T_{1\rho}^{\text{F}}$ relaxation times were measured with a pulse sequence that contains a spin-lock (SL) pulse out of

phase by 90° with respect to the initial 90° pulse (e.g., 90°_x-SL_y-acquire).³² Relaxation time measurements were obtained at ambient and variable temperatures (0–70 °C). Simulation analyses of CF₃ resonance as a function of dipolar coupling strength (Hz) were done using MestreNova.

5.3.5 Thermal Analyses (DSC and TGA)

Differential scanning calorimetry (DSC) of the native β-CD, unbound SPFO, and the inclusion compounds was performed using a TA Q20 thermal analyzer over a temperature range of 30 to 370 °C. The scan rate was set at 10 °C/min and dry nitrogen gas was used to regulate the sample temperature and purge the sample compartment. Solid samples were analyzed in hermetically sealed aluminum pans where the sample mass ranged from 3.80 to 4.00 mg. Thermogravimetric analysis (TGA) was performed on a TA Q50 over a temperature of 30–400 °C. Solid samples for TGA were heated in open pans where sample masses ~7.0–8.0 mg were analyzed.

5.3.6 FT-IR Spectroscopy

Fourier Transform (FT) IR spectra were obtained using a Bio-Rad FTS-40 spectrometer with a resolution of 4 cm⁻¹. All samples were prepared with spectroscopic grade KBr which constituted ~80% (w/w) of the total sample. Samples were run as finely ground powders in reflectance mode.

5.3.7 Powder X-ray Diffraction (PXRD)

PXRD spectra were collected using a PANalytical Empyrean Powder X-ray diffractometer using monochromatic Cu-Kα1 radiation. The applied voltage and current were set at 45 kV and 40 mA, respectively. The samples were mounted in a vertical configuration as evaporated hexane films and PXRD patterns were measured in a continuous mode over a 2θ angle range of 5–45° with a scan rate of 0.5 degree/min.

5.4. Results and Discussion

5.4.1 DSC/TGA

DSC and TGA are complimentary techniques that have been used to characterize thermal properties of polymeric³³ and host-guest systems.^{34,35} In general, DSC provides a

measure of physical phase transition temperatures and phase purities as a function of heat rate; whereas, TGA reveals thermal events accompanied by weight losses. The DSC and TGA traces of β -CD, SPFO, and the 1:1 and 2:1 solid inclusion compounds prepared by the modified dissolution method are shown in Figures 5.1 and 5.2, respectively. In Figure 5.1, the DSC thermogram of native β -CD exhibits two endothermic peaks at ca. 115 and 320 °C that are attributed to dehydration and decomposition transitions, respectively. The main endotherm of the unbound SPFO consists of a sharp peak at ca. 275 °C that is related to melting of the compound. The thermograms of the 1:1 and 2:1 β -CD/SPFO ICs display endothermic transitions at ca. 130 °C due to dehydration processes. The exothermic transitions lying in the temperature ranges between ca. 250–285 °C and 300–350 °C for the β -CD/SPFO ICs may be related to the decomposition of the guest and host, respectively. The appearance of the exothermic peaks for the inclusion compounds is telling and provides evidence for the formation of β -CD/SPFO inclusion complexes.³⁵ In a previous study of β -CD/PFOA complexes, the decomposition of the guest/host were shown as endothermic processes,¹⁷ and highlights some structural differences with the complexes reported herein.

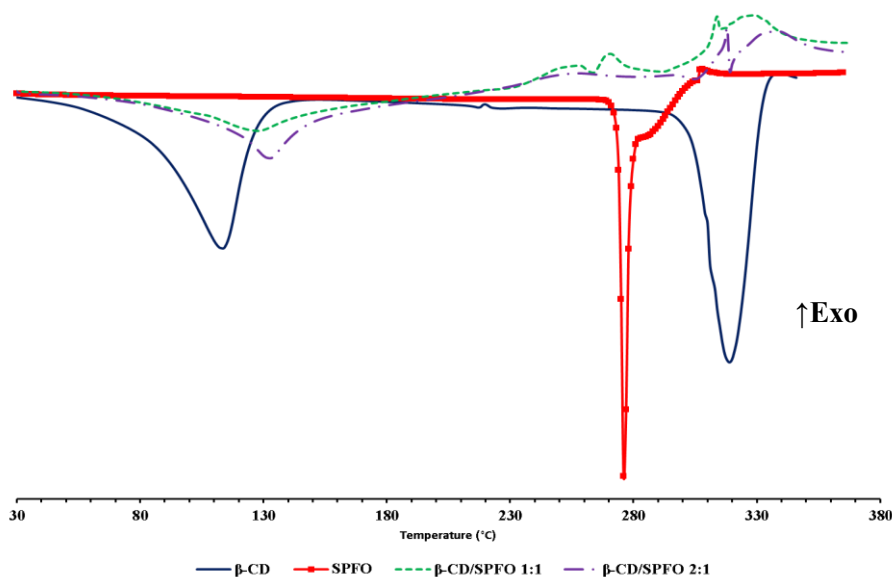


Figure 5.1 The DSC traces for β -CD hydrate, SPFO, and the 1:1 and 2:1 β -CD/SPFO inclusion complexes

The dehydration endotherms for the inclusion compounds are distinct and reveal variable hydration environments. The 2:1 complex revealed a relatively sharp and more intense dehydration endotherm with offset to higher temperature (ca. 135 °C); whereas, a broader signal was observed for the 1:1 complex at ca. 130 °C. The dehydration endotherms for the complexes may reveal variable microenvironments for the 1:1 complex with a greater amount of extra-cavity water. In contrast, the 2:1 complex may contain a greater amount of highly ordered cavity bound water.³⁶ The decomposition of the guest in the 1:1 complex (between 250–285 °C) revealed two distinct thermal events which support the presence of more than one environment of the guest in this complex.

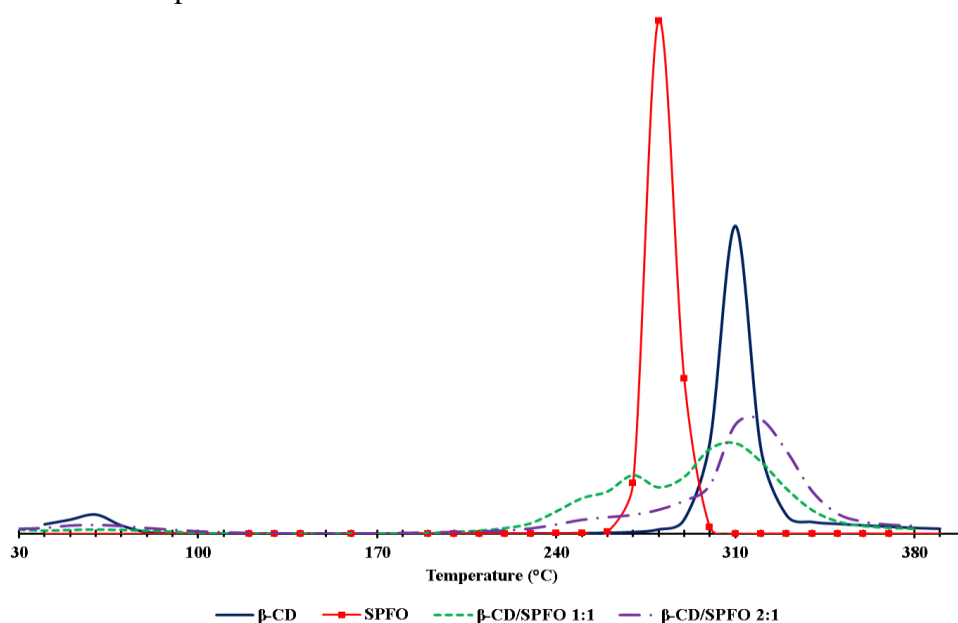


Figure 5.2 TGA traces for β -CD hydrate, SPFO and the 1:1 and 2:1 β -CD/SPFO inclusion compounds.

The DSC results suggest that the guest molecule of the 2:1 complex may be fully encapsulated within the cavity of β -CD; whereas, the guest in the 1:1 complex is partially included with variable microenvironments.²⁶ The inclusion compounds decomposed at higher temperatures relative to native β -CD and pure SPFO and this supports the formation of stable β -CD/SPFO inclusion compounds. The DSC results of the β -CD/SPFO complexes were complemented by the TGA results in Fig. 5.2.

The TGA results in Fig. 5.2 are presented as weight derivatives in the y-axis versus temperature in the x-axis. It is worthwhile to note that the differences in the temperatures for the DSC and TGA results may be related to differences in the sample configuration, as described in Section 5.3.5. The thermal events in Fig. 5.2 at ca. 280 °C for SPFO and 310 °C for β -CD are associated with melting and decomposition processes, respectively. The inclusion compounds revealed several thermal events at ca. 60, 260 and 310 °C due to dehydration, guest volatilization, and host decomposition processes, respectively. The TGA of the 1:1 complex revealed two distinct peaks at ca. 250 and 270 °C which support the presence of multiple microenvironments of the guest for this complex, in agreement with the DSC results. The 2:1 complex is characterized by a broad range of thermal events between 240–290 °C which suggest a unique guest conformation that is different from that of the 1:1 complex. As illustrated by the DSC and TGA results, the thermal stability of the 2:1 complex is similar or slightly greater than that of the 1:1 complex. Greater magnitudes of the binding constants were reported for the 1:1 β -CD/SPFO complex ($K_{1:1}$) compared to $K_{2:1}$ values according to solution studies.^{7,27} The slight differences in the thermal stabilities of the 1:1 and 2:1 complexes reported herein may be a result of artefacts arising from possible formation of mixtures of 1:1, 2:1 and 1:2 β -CD/SPFO complexes.

The TGA % weight losses for the different thermal events are presented in the Supporting Information (Fig. D5.1). The weight loss (%) due to the dehydration processes at ca. 60 °C were evaluated as ca. 9 % (β -CD), 3 % (1:1 complex) and 6 % (2:1 complex), and are in agreement with results from DSC. In general, the formation of the inclusion compounds tends to increase the thermal stability of β -CD host and suggests the formation of stable β -CD/SPFO ICs.³⁷ Differences in thermal stabilities, enthalpies of dehydration, and the number of thermal transitions suggest that there are structural differences between the 1:1 and 2:1 β -CD/SPFO complexes. Further details on the molecular structures of the complexes are presented in the FT-IR and NMR results in the forthcoming sections.

5.4.2 FT-IR

FT-IR spectroscopy is a useful technique for systems that contain functional groups such as the carbonyl and hydroxyl groups. For example, this technique has been used to characterize guest conformational changes (i.e., *gauche* vs *trans*) of perfluoroalkyl chains^{38,39} and other

systems.^{40,41} The FT-IR spectra of β -CD, SPFO, and the 1:1 and 2:1 host-guest complexes prepared by the modified dissolution method are displayed in Fig. 5.3. The relative intensities of the -OH ($\sim 3400\text{ cm}^{-1}$), -CH ($\sim 2900\text{ cm}^{-1}$), and -C=O ($\sim 1700\text{ cm}^{-1}$) vibrational bands in Fig. 5.3 for the 1:1 and 2:1 host-guest complexes correlate with the relative mole ratios of the host/guest relative to the unbound species. Red-shifts of ca. 8 cm^{-1} and 6 cm^{-1} for the frequencies of the -C=O bands for the 1:1 and 2:1 β -CD/SPFO ICs respectively, relative to the IR frequency of the unbound SPFO (1694 cm^{-1}) are noted. These shifts reveal differences in dipolar interactions between the host and guest and variable binding geometry and conformation of the guest for the 1:1 vs 2:1 host-guest complexes.

The IR spectral region between $1100\text{--}1250\text{ cm}^{-1}$ was previously used to characterize the conformational preferences of perfluorocarbon chains in the solid phase. Vibrational bands (**1–3**) are labeled in Fig. 5.3 and are assigned to CF_2 asymmetric stretching mode (**1** $\nu_{\text{asym}}/\text{CF}_2$; 1250 cm^{-1}), CC bending and CCC stretching modes (**2** $\beta/\text{C-C}$, $\nu/\text{C-C}$; 1215 cm^{-1}), and CF_2 symmetric stretching (**3** $\nu_{\text{sym}}/\text{CF}_2$; 1150 cm^{-1}).⁴² In particular, band **2** was previously used to provide useful structural information regarding the conformational change of a PFC guest in a host-guest system.³⁸

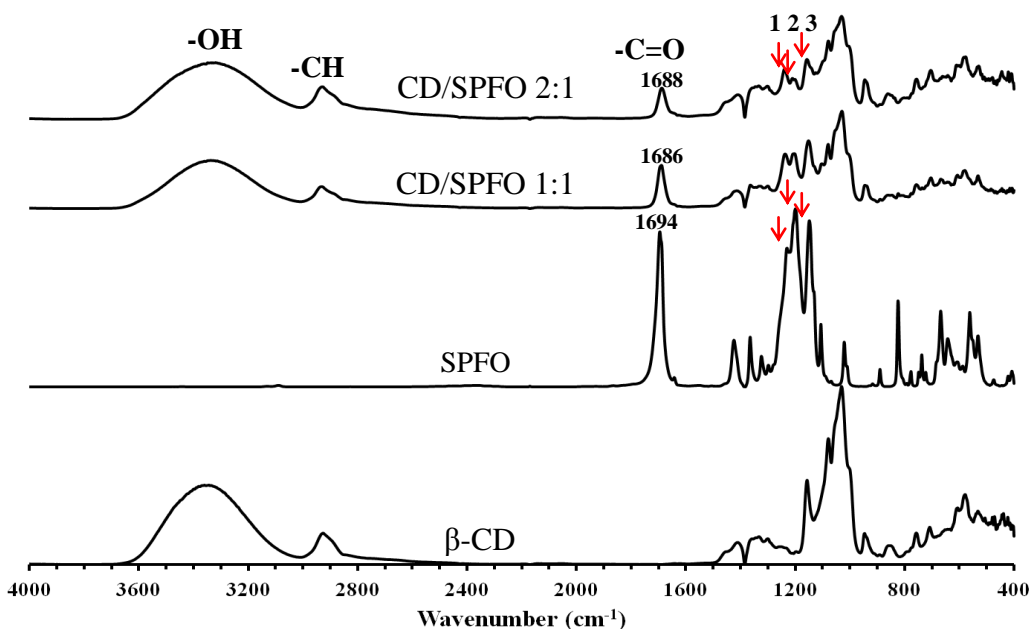


Figure 5.3 FT-IR spectra of β -CD, SPFO, and the 1:1 and 2:1 β -CD/SPFO inclusion compounds.

In a previous report on β -CD/SPFO complexes in solution,⁷ a preferred *all-trans* conformation of the perfluorocarbon chain was reported for the 2:1 complex. PFOA and other C8 perfluorocarbon chains have generally been reported to adopt helical (*gauche*) conformations in the pure solid compared to the zigzag (*trans*) conformation adopted by PFCs with chain lengths less than 8 carbons (e.g. PFBA).^{43,44} A conformational change of the perfluorocarbon chain may occur if its environment is changed.^{45,46} The attenuation of band **2** in Fig. 5.3 for the 2:1 complex may be attributed to a conformational change of the SPFO chain in this complex. According to the IR results, the native conformation of the guest is not completely retained even in the 1:1 complex where observable attenuation of band **2** is noted. In previous reports^{16,17} of β -CD/PFOA complexes (Chapters 2 and 3), the guest molecule was concluded to adopt a *gauche* conformation in the 1:1 host-guest complex, similar to the unbound guest in the solid phase. In contrast to the *gauche* conformation adopted by the guest in the 1:1 complex, a preferred *all-trans* conformation of the guest was reported for the 2:1 complex. This is in contrast to the *gauche* conformation formed by the C4 PFBA guest (chapter 4) in the 1:1 complex with β -CD.¹⁸

5.4.3 PXRD

Powder X-ray diffraction is sensitive to long-range order or to the periodic structure of the framework. PXRD has been used to study the structure of host-guest complexes and to confirm the formation of a new compound from parent molecules.⁴⁷ The PXRD patterns for the native β -CD, free SPFO and the 1:1 and 2:1 β -CD/SPFO ICs are shown in Fig. 5.4. The PXRD patterns due to the host molecule in Fig. 5.4 consist of prominent lines near 2θ values 9 and 12° , and other minor signatures at higher 2θ values that are characteristic of “cage-type” crystalline structure.⁴⁸⁻⁵⁰ Native SPFO reveals its signature 2θ values at 7.5 and 11.3° , and several minor peaks at higher 2θ . The PXRD patterns of the inclusion compounds are uniquely characterized by some sharp reflections and provide evidence for the formation of β -CD/SPFO inclusion compounds. The patterns of the 1:1 and 2:1 complexes show major peaks at 2θ values 11.5 and 17.5° and represent *head-to-head* “channel-type” structure,^{51,52} similar to those reported for β -CD/PFOA complexes in chapters 2-3.¹⁷ However, such structures are different from those of β -CD and the native SPFO guest reported herein, as well as from those of β -CD/PFBA complexes reported previously,¹⁸ which form “cage-type” structures (chapter 4). β -CD is known to have a strong tendency to form *head-to-head* dimeric units with long chain PFCs ($C \geq 8$) that are held

together by multiple H-bonds at the secondary rim of CD (*cf.* Scheme 5.1), in which one or more guests can be accommodated.⁵³

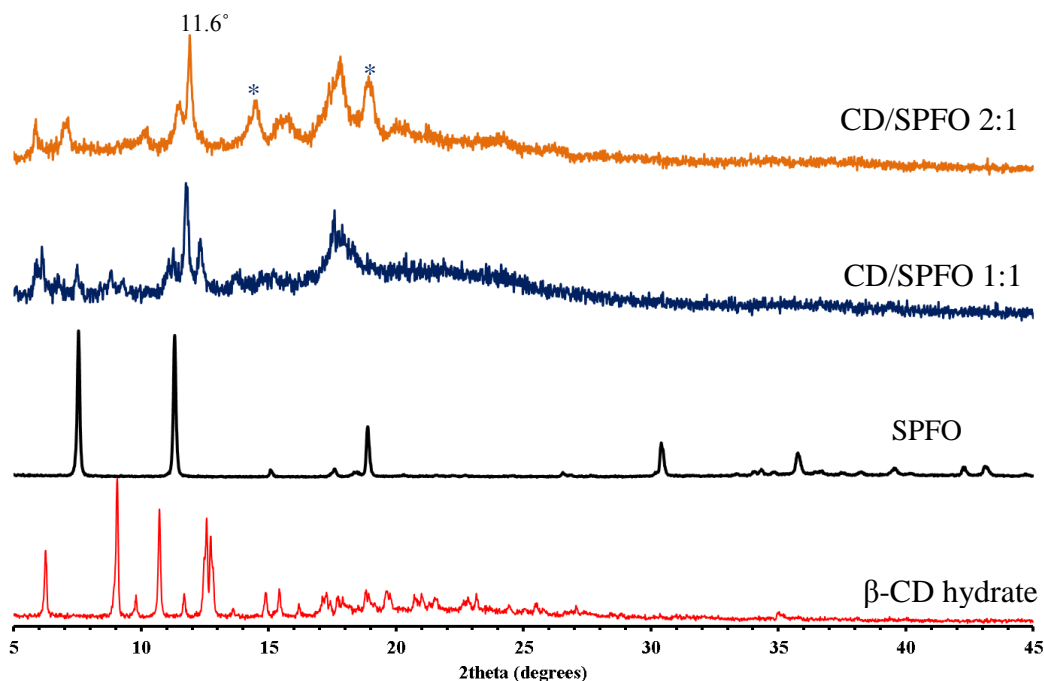


Figure 5.4 The XRD patterns for β -CD hydrate, SPFO, and the 1:1, and 2:1 β -CD/SPFO inclusion compounds.

The broad patterns at values of $2\theta > 20^\circ$ for the inclusion compounds in Fig. 5.4 may reveal that the inclusion of the sodium-rich perfluorocarbon guest within the host results in significant loss of long-range order. The XRD results of the 2:1 complex in Fig. 5.4 are characterized by peaks at 2θ angles 14.5° , 15.7° , and 18.9° (noted by asterisks in Fig. 5.4) that are not present or are significantly attenuated in the patterns of the 1:1 complex. The additional reflections may indicate that the structure of the 2:1 complex is distinct from that of the 1:1 complex. Wenz²⁶ described the packing of the cyclodextrin host-guest compounds to depend on the dimensions of the guest relative to those of the host, as previously described. The guest can either be partially or completely encapsulated by the host, with variable conformations as described in the IR results. Aside from the variable guest topologies and conformations, differences in the amount of encapsulated water in the 1:1 vs 2:1 complexes is revealed by the DSC results, and contributes to differences in structural order.³⁸

5.4.4 Solution-state NMR Spectroscopy

5.4.4.1. ¹H Solution NMR Characterization

Numerous studies have been reported on the structure of host-guest inclusion systems using complexation-induced ¹H/¹⁹F NMR shifts (CIS) in solution.^{7,25,27,28} Comparative results for PFOA and its complexes with β-CD will be presented in this and the following sections, to aid in understanding the structure of SPFO and its complexes with β-CD. Fig. 5.5 shows stack plots of the ¹H solution NMR spectra for β-CD and the 1:1 and 2:1 β-CD/SPFO host-guest inclusion compounds. Similar results for β-CD/PFOA complexes are shown in Fig. 5.5 for comparison. The assignment of the resonance lines for the ¹H spectra in Fig. 5.5 agrees well with previous literature reports^{54,55} and with the structures illustrated in Scheme 5.1a,b. The δ values for the ¹H/¹⁹F nuclei were measured to within ±0.001 ppm and the CIS values are listed as the difference, Δδ, given by eqn 5.1 where the results are presented in Table 5.1. The determination of the δ values for the partly overlapped signals in Fig. 5.5 was confirmed from the known signal splitting patterns and the corresponding integrated coupling constants.

$$\Delta\delta = \delta_{complex} - \delta_{free} \quad \text{Equation 5.1}$$

The CIS values for the intra-cavity protons (i.e. H₃, H₅) in Fig. 5.5 are the most affected due to steric effects of the included guest, providing evidence for the formation of host-guest inclusion compounds (*cf.* Scheme 5.2). In particular, the Δδ values for the intra-cavity protons are more attenuated in the 1:1 compared to the 2:1 complexes due to increased steric effects of the guest in the *gauche* conformation for the 1:1 complex, as described in the IR results.

Comparison of the CIS values for the SPFO and PFOA inclusion complexes with β-CD, respectively, allows for estimation of the relative positions of the guest within the host. The CIS values of the intra-cavity nuclei for the 1:1 complexes (*cf.* Fig. 5.5) are relatively constant compared to similar values for the 2:1 complexes as shown in the expanded spectra in Fig. 5.5-2 and Table 5.1. Therefore, the latter can be used to probe the relative positions of the guests in the complexes. Notice that the CIS values changed by -0.006 ppm (upfield) for H₃ and +0.010 ppm (downfield) for H₅, going from the 2:1 β-CD/PFOA to the 2:1 β-CD/SPFO complex. That is, H₅ is less shielded and H₃ is more shielded in the 2:1 β-CD/SPFO complex relative to the shifts of the PFOA counterpart. Similarly, H₃ is less shielded and H₅ is more shielded in the 2:1 β-CD/PFOA complex.

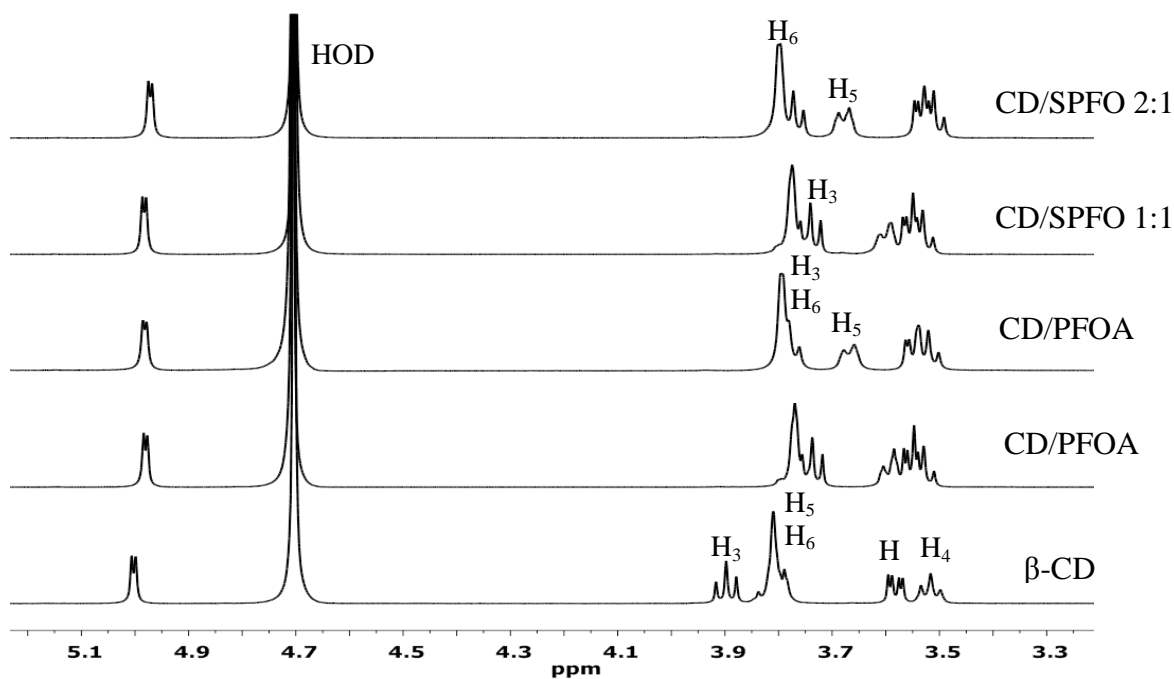


Figure 5.5-1 ^1H NMR spectra for β -CD, and the 1:1/2:1 β -CD/PFOA and β -CD/SPFO inclusion compounds in D_2O at 295 K.

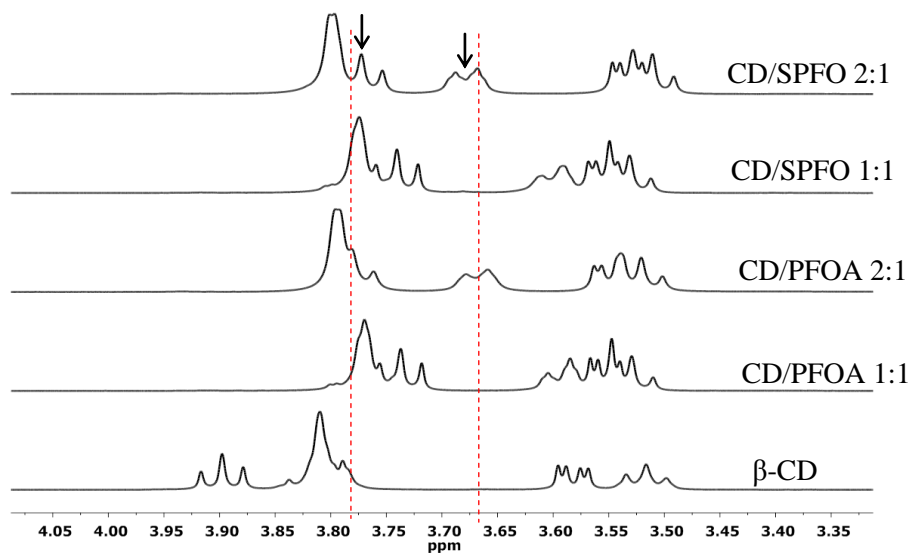


Figure 5.5-2 ^1H NMR expanded spectra for β -CD, and the 1:1/2:1 β -CD/PFOA, and β -CD/SPFO inclusion compounds showing CIS patterns for H_3 and H_5 signals for the 2:1 β -CD/PFOA (dotted lines) and 2:1 β -CD/SPFO (arrows) complexes.

The trends in the CIS values for the intra-cavity protons of the two complexes (i.e. β -CD/PFOA and β -CD/SPFO) suggest the presence of variable guest geometry/conformations in

the two samples. Part of the SPFO guest chain must be in close proximity to H₃ group of CD causing increased shielding effects due to steric hindrance. Furthermore, increased δ of the host in the 2:1 β -CD/SPFO complex for H₅ means reduced steric effects at its environment. Note that contributions of $\Delta\delta$ from other sources such as solvation effects are possible. ¹⁹F solution NMR results are presented to further understand the geometry of the guests in the complexes.

Table 5.1 CIS Values (ppm) for the ¹H Nuclei of β -CD and its Complexes with PFOA and SPFO in Solution at 295 K

Nuclei	δ_{free}	$\Delta\delta$			
	β -CD	β -CD/PFOA	β -CD/PFOA	β -CD/SPFO	β -CD/SPFO
		1:1	2:1	1:1	2:1
H ₁	5.002	-0.022	-0.020	-0.019	-0.030
H ₃	3.897	-0.160	-0.117	-0.157	-0.123
H ₆ H _{6'}	3.810	-0.040	-0.017	-0.036	-0.013
H ₅	3.798	-0.203	-0.129	-0.196	-0.119
H ₂	3.582	-0.029	-0.032	-0.028	-0.039
H ₄	3.516	+0.013	+0.005	+0.015	-0.005

5.4.4.2. ¹⁹F Solution NMR Characterization

The ¹⁹F NMR results of the solution complexes formed between PFOA and SPFO with β -CD respectively are shown in Fig. 5.6. The assignments of the ¹⁹F resonance lines for PFOA/SPFO in Fig. 5.6 were made in agreement with COSY results of Guzman⁵⁶ reported by Guo⁷ and according to the accompanying structure (*cf.* Fig. 5.6). The well resolved ¹⁹F resonance lines in Fig. 5.6 allow for more accurate quantitative analysis of the CIS values. Note that the chemical shift changes of the individual ¹⁹F resonance lines of the guests in the complexed state are assumed to be subtle relative to the unbound guest, such that any coalesced peaks are assumed to be from two neighboring signals.

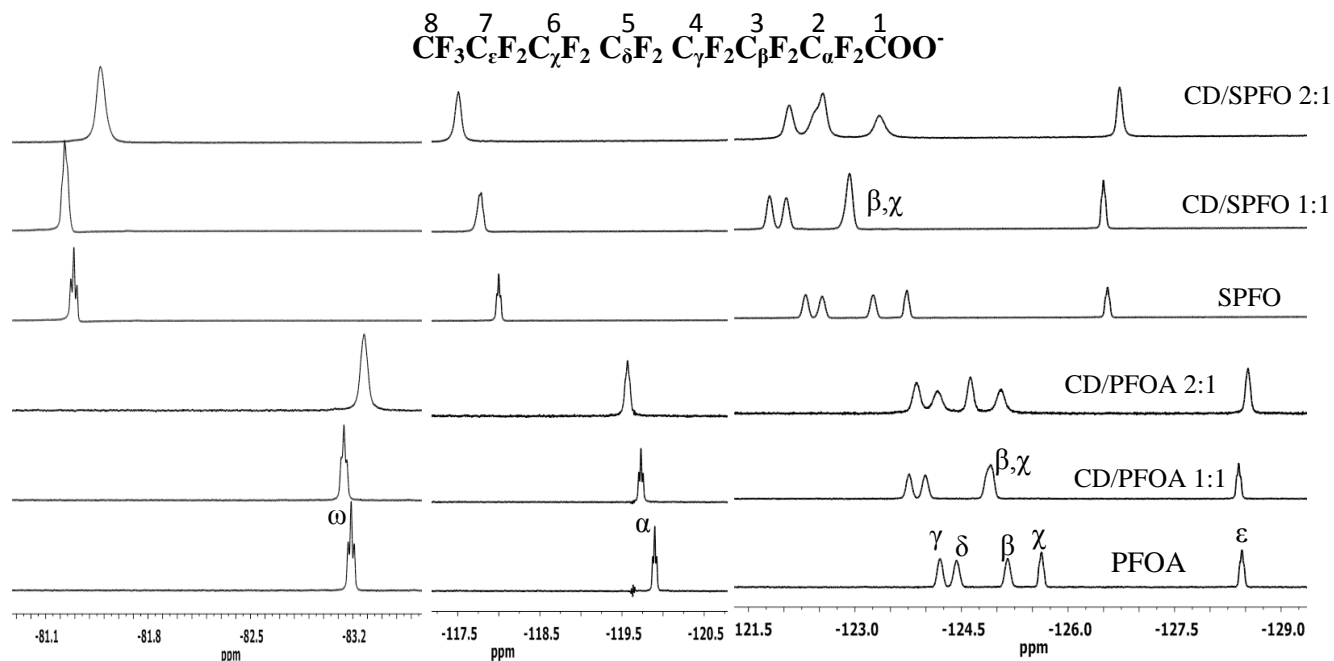


Figure 5.6 ^{19}F NMR expanded spectra for PFOA, SPFO, and the 1:1/2:1 inclusion compounds with β -CD in D_2O at 295 K. The resonance lines are assigned according to the accompanying structure.

Table 5.2 CIS Values (ppm) for the ^{19}F Nuclei of β -CD/SPFO and β -CD/PFOA Complexes in Solution at 295 K.

Nuclei	δ_{free}	$\Delta\delta$		δ_{free}	$\Delta\delta$	
	PFOA	β -CD/PFOA 1:1	β -CD/PFOA 2:1		SPFO	β -CD/SPFO 1:1
$\text{C}_\alpha\text{F}_2$	-119.899	0.168	0.331	-118.000	0.226	0.492
C_βF_2	-125.152	0.248	0.527	-123.256	0.333	0.710
$\text{C}_\gamma\text{F}_2$	-124.197	0.436	0.328	-122.307	0.511	0.233
$\text{C}_\delta\text{F}_2$	-124.429	0.437	0.262	-122.541	0.508	0.121
C_χF_2	-125.624	-	-	-123.730	-	-
$\text{C}_\varepsilon\text{F}_2$	-128.450	0.045	-0.086	-126.558	0.059	-0.169
$\text{C}_\omega\text{F}_2$	-83.189	0.049	-0.088	-81.294	0.063	-0.181

Wilson and Verrall^{27,28} have used ^{19}F CIS values to elucidate the binding geometry of a series of fluorocarbon alkyl carboxylate guests in CD-based complexes since such guests can

undergo significant environment changes between the free and bound states.^{27,54} Therefore, changes in δ values of the host/guest nuclei can provide a measure of the degree of complex formation in host-guest systems. The CIS values for PFOA and SPFO in their bound state with β -CD are listed in Table 5.2.

In general, the spectra of the 1:1 and 2:1 host-guest complexes (Fig. 5.6) are characterized by shifts of most of its ^{19}F resonance lines to higher frequency (lower field or downfield) with respect to unbound perfluorocarbon guest. More positive CIS values in Table 5.2 mean that the shifts are towards lower field (deshielding) with respect to unbound guests and vice versa. Palepu et al.^{19,20} observed downfield shifts for most of the ^{19}F resonances in β -CD/SPFO equimolar mixtures relative to pure SPFO guest in solution. As the guest is included within the cavity of the host it displaces water from the cavity. The fluorine atoms are strongly polarizing in the bulk aqueous phase compared to the CD environment. Thus, the perfluorocarbon chain interacts differently in these two environments.

The CIS values for the terminal ($\text{C}_\alpha\text{F}_3$ and $\text{C}_\epsilon\text{F}_2$) groups of the perfluorocarbon guests in the 2:1 complexes reveal negative $\Delta\delta$ numbers. This suggests variable binding geometry/conformation of the guests in the 2:1 relative to the 1:1 complexes as described in the DSC/TGA, IR, and ^1H solution NMR results. The contributions of conformation, van der Waals interactions and inductive effects to ^{19}F chemical shift changes were discussed in chapter 2 (§2.4.2) but will be reiterated here. Guo et al.⁷ and Wilson and Verrall²⁷ described the interaction of SPFO with β -CD in solution as composed of several contributions. (i) The negatively charged carboxylate head group may be located near the annulus of the host forming H-bonds with the CD-hydroxyl groups, as well as with bulk water. This would cause deshielding of the $\text{C}_\alpha\text{F}_2$ resonance due to the inductive effects of the carboxylate head group; (ii) the guest molecule may be forced to adopt an extended *all-trans* conformation as in the case of the 2:1 complex and as concluded from the IR results, in order to accommodate the cavity space of two β -CD hosts. Such a conformation will result in an increase of the F-F distances between adjacent CF_2 groups of the guest resulting in intramolecular deshielding effects on the ^{19}F nuclei; (iii) optimized van der Waals interactions between fluorine groups of the guest and ether-like oxygens within the apolar interior of the host cavity will result in an overall shielding effect; (iv) weakly polarizing fluorine atoms within the CD environment (especially near the rims) relative to the bulk polar aqueous phase will result in the deshielding of the guest nuclei in its environment; and (v)

combined shielding/deshielding effects may arise depending on the geometry and conformation of the guest according to contributions *i-iv*.

Considering the CIS data presented in Table 5.2, similar trends in $\Delta\delta$ values for the individual ^{19}F nuclei are generally observed between the 1:1 and 2:1 β -CD/guest complexes with some notable differences in their relative magnitudes. The chemical shift values for unbound PFOA (δ_{free}) are generally upfield by ca. 2.0 ppm compared to similar values for SPFO. Differences in cmc values between PFOA (ca. 10 mM) and SPFO (ca. 30 mM) suggest that PFOA more readily forms micelles in solution. The association of perfluorocarbon chain to form micelles in solution was reported to result in upfield shifts of ^{19}F resonances.²⁰

Attention will be focused on the groups at the head ($\text{C}_\alpha\text{F}_2$ and C_βF_2) and tail ($\text{C}_\omega\text{F}_3$ and $\text{C}_\varepsilon\text{F}_2$) ends of the two guests (i.e. SPFO and PFOA) in order to evaluate their geometry within the CD cavity. The occurrence of negative $\Delta\delta$ values (upfield shifts) for the terminal ^{19}F nuclei in the 2:1 complexes indicates the presence of contribution (*iii*) due to interactions between the fluorine atoms and the apolar interior of CD. Notice that the $\Delta\delta$ values for 2:1 β -CD/SPFO complex are twice as greater compared to similar values for the 2:1 β CD/PFOA complex. We conclude from the above results that the SPFO guest experiences greater interaction with the apolar interior of the host and may suggest a deeper inclusion of the guest.

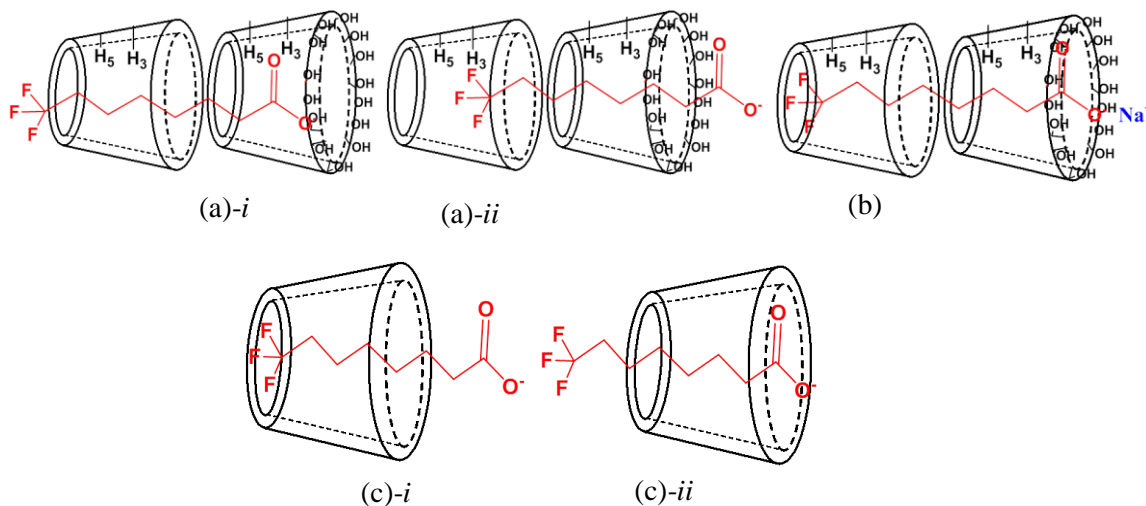
In contrast to the 2:1 complexes, the 1:1 complexes show small positive ^{19}F CIS values ($\Delta\delta \sim 0.05$ ppm) for the terminal nuclei relative to the CIS values of the other ^{19}F nuclei. As described previously, two geometries are possible for the 1:1 complexes; one where the CF_3 is in the extra-cavity environment in the bulk polar aqueous solvent and another where it is intra-cavity near the rim of the host molecule. Contributions due to interaction (*iv*) will affect the chemical shifts of the terminal groups in the 1:1 complexes differently with respect to their proximity with the CD and the bulk water, respectively. It should be noted here that the fluorocarbon guests in the 1:1 CD-complex experience both the extra- and intra-cavity environments such that a composite shielding/deshielding effects may occur. This result in $\Delta\delta \sim 0$ for the $\text{C}_\omega\text{F}_3$ and $\text{C}_\varepsilon\text{F}_2$ resonances (*cf.* Table 5.2). Note also that the fluorine atoms near the rim of the CD host are weakly polarizing since such an environment is composed mainly of C-H and O-H groups.^{7,57} Therefore, reduced van der Waals interactions in such an environment will result in increased δ values relative to the bulk aqueous environment where the δ values are reduced.

The CIS values for the $C_{\alpha}F_2$ resonance in both the 1:1 and 2:1 host-guest complexes are affected by contributions from interaction (i). In general, the 2:1 host-guest complexes display greater CIS values for $C_{\alpha}F_2$ nuclei compared to the corresponding 1:1 complexes. The guest molecules in the 2:1 complexes experience strong dipolar interactions from CD-hydroxyl groups and aqueous solvent which result in increased deshielding of the $C_{\alpha}F_2$ group due to inductive effects. The increased deshielding effects of $C_{\alpha}F_2$ observed for the SPFO complexes relative to the PFOA complexes (*cf.* Table 5.2) highlight the different roles played by the respective counterions in the interactions of the guests with the host. The carboxylate head group of SPFO contains sodium (Na^+) counterion as an alternative to the hydronium (H^+) counterion, for PFOA above its pKa. Therefore, some structural differences are expected for the CD complexes formed between each of these two guests. Sodium ion electrode studies indicate that the Na^+ ion of SPFO is closely associated with the carboxylate anion of the β -CD/SPFO complex in solution. Palepu et al.^{19,20} have provided evidence that the encapsulated surfactant not only retains its counterions but immobilizes them at the hydrophilic exterior of the β -CD torus, thus promoting cooperative binding of the perfluorooctanoate guest with β -CD. A sodium counterion is expected to impart a more favourable binding environment for the perfluorooctanoate guest with β -CD than a hydronium counterion.

We conclude from the $^1H/^{19}F$ CIS data in solution and the above discussion that SPFO experiences deeper inclusion within the apolar CD cavity compared to PFOA. Furthermore, the sodium counterion in SPFO is closely associated with the guest promoting its binding with β -CD. Based on the 1H and ^{19}F solution NMR results, we propose the binding geometries of the guests for the 2:1 β -CD/SPFO and β -CD/PFOA complexes as depicted in Schemes 5.3a and b, respectively. Scheme 5.3c depicts the proposed binding geometry of the CD-bound fluorocarbon guests in the 1:1 host-guest mole ratio.

The reduced $\Delta\delta$ values for the central ^{19}F resonances (i.e. $C_{\gamma}F_2$ - $C_{\chi}F_2$; *cf.* Table 5.2) in the 2:1 complex relative to the 1:1 complex may be a result of contributions (ii) and (iii) where the effects of contribution (iii) are more pronounced. Note that the $\Delta\delta$ values of the central ^{19}F nuclei are further reduced in the 2:1 β -CD/SPFO complex suggesting optimized van der Waals in this complex. The overlapping of $C_{\gamma}F_2$ and $C_{\beta}F_2$ resonance lines in the 1:1 host-guest complex is a result of increased deshielding of the $C_{\beta}F_2$ group associated with the loss of γ -*gauche* shielding effect that is commonly observed for alkyl carboxylate groups in the *gauche* conformation. The δ

values for the $C_{\delta}F_2/C_{\beta}F_2$ resonance lines for the 2:1 complexes were estimated from the deconvolved peaks (*cf.* Table 5.2 and Fig. 5.6). As well, the δ values for $C_{\chi,\beta}F_2$ could not be accurately determined due to signal overlap.



Scheme 5.3 Proposed inclusion geometry of (a) *i-ii* PFOA, and (b) SPFO in the 2:1 β -CD/guest complex. c (*i-ii*) proposed inclusion geometry of the 1:1 β -CD/guest complex. Note the CD torus and SPFO/PFOA structures are not drawn to scale.

5.4.5 Solid-State MAS NMR Spectroscopy

Solid-state NMR spectroscopy is a versatile technique that can be used to study the structure and dynamic properties of host-guest systems.^{38,39,58-60} In particular, multi-nuclear NMR methods can provide unequivocal evidence for the inclusion of a guest within the host.⁶⁰ Additionally, relaxation techniques in the solid state can provide detailed information on the motional dynamics of the guest within the host.⁶¹

5.4.5.1 $^1H \rightarrow ^{13}C$ CP/MAS and DP/MAS NMR

^{13}C MAS NMR spectroscopy with DP and CP techniques were employed to provide evidence for the formation of β -CD/SPFO inclusion compounds. The $^1H \rightarrow ^{13}C$ CP and DP results for β -CD, the 1:1 β -CD/SPFO and 1:1 β -CD/PFOA complexes at MAS conditions of 20 kHz are shown in Fig. 5.7. The ^{13}C resonances in Fig. 5.7 were assigned according to previous reports⁵⁰ and the structures in Scheme 5.1a,b. The spectra of the inclusion complexes in Fig. 5.7 are generally characterized by broad ^{13}C signals relative to the resonance lines of the host molecule and this suggests increased symmetry of the host macromolecule upon inclusion of the guest.

The DP/MAS spectra of the 1:1 complexes reveal resonance lines for both the host (ca. 60- 105 ppm) and guest (ca. 110 – 125 ppm) molecules and further support formation of host-guest complexes.

The CP/MAS NMR resonance lines for the host in Fig. 5.7 could not easily be resolved into its individual glucopyranose units due to the amorphous nature of the host and spectral overlap of various resonance lines. However, the ^{13}C CP and DP spectra of the complexes display variable line shapes/widths and signal intensities (*cf.* Fig. 5.7). For example, the line shapes of the PFOA complexes consist of sharp features, whereas the spectra of the SPFO complexes are comprised of relatively broad lines. Furthermore, the relative intensity of C_6 resonance for the 1:1 β -CD/SPFO complex is greater compared to similar line for the 1:1 β -CD/PFOA complex, particularly for the DP spectra. The differences in line shapes/widths and signal intensities highlights the differences in the structure and dynamic properties of the complexes formed between SPFO and PFOA with β -CD, respectively.

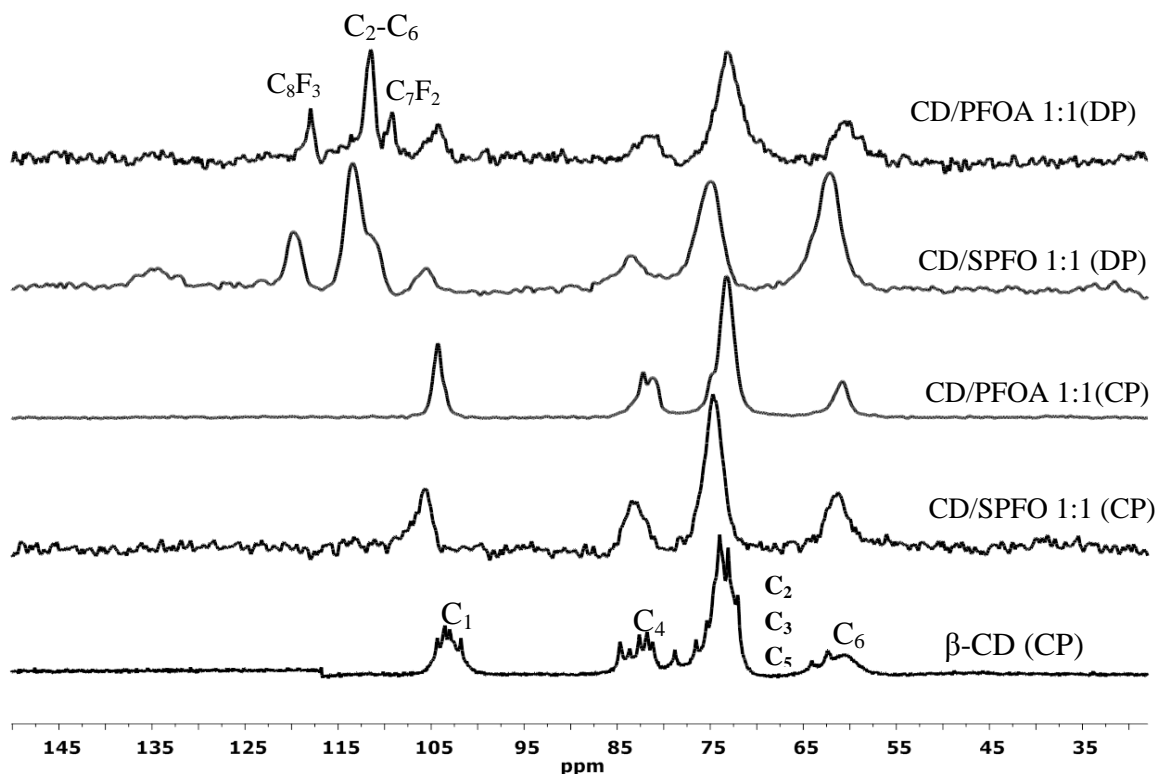


Figure 5.7 The $^1\text{H}\rightarrow^{13}\text{C}$ CP and DP/MAS spectra for β -CD, and the 1:1 β -CD/SPFO and β -CD/PFOA complexes. All spectra were acquired at MAS 20 kHz and 295 K.

The C₆ group in the respective complexes experiences variable dynamics as a function of the structure and geometry of the guests in the bound states. The relative intensities of individual resonance lines in NMR spectroscopy depend upon the rate at which equilibrium magnetization recovers after a radio frequency pulse. Optimum signal intensity requires that the recycle delay (d1) be greater than about 5T₁ to ensure complete recovery of equilibrium longitudinal relaxation (T₁) between transients. ¹³C-detected ¹H T₁ values for C₆ in β-CD/PFOA complexes were determined to be ~1.0 s.¹⁷ Similar T₁ values for β-CD/SPFO complexes were not measured. Since d1 values ~6.0 – 8.0 s were applied in the ¹H→¹³C CP and DP experiments for the β-CD/SPFO and β-CD/PFOA complexes, differences in relaxation properties for the pendant C₆ group may be responsible for the different relative intensities. Based on the ongoing discussion and the geometries depicted in Scheme 5.3, the β-CD/SPFO complex can be thought as a pseudo-rotaxane where the host-guest system is relatively rigid and the pendant C₆ group experiences efficient orientational motion. Further discussions on the dynamics of the guests in the complexes are provided in the ¹⁹F DP/MAS characterization results and relaxation studies.

5.4.5.2 ¹⁹F→¹³C CP/MAS NMR

The ¹⁹F→¹³C CP NMR results in Fig. 5.8 were used to provide unequivocal evidence for the inclusion of the guest within the host by probing through space dipolar interactions. Moreover, ¹³C CIS values from the ¹⁹F→¹³C CP results were evaluated to supplement the solution NMR CIS results. The ¹⁹F→¹³C CP results for the 1:1 complexes revealed host resonance lines at ca. 60 ppm (C₆), 75 ppm (C₂C₃C₅), and 85 ppm (C₄) (*cf.* Fig. 5.8 and Scheme 5.1a,b). The resonance line at ca. 75 ppm is due to the intra-cavity carbon nuclei and is the most intense. This signal indicates that magnetic polarization has been transferred from the ¹⁹F nuclei of the guest to the ¹³C nuclei of the host. Such CP transfer suggests that the perfluorocarbon guest is in spatial proximity to the β-CD cavity and provides unequivocal evidence for the inclusion of the guest within the host cavity.

The emergence of two carbonyl signals at ca. 165 and 170 ppm for the β-CD/SPFO complex further supports the presence of two configurations of the guest in the 1:1 complexes as previously described. The absence of similar signal in the 1:1 β-CD/PFOA complex is related to the differences in guest geometry and dynamics. Faster dynamics of the PFOA guests coupled

with fast MAS conditions may reduce prospects for efficient CP transfer to some of its ^{13}C nuclei.

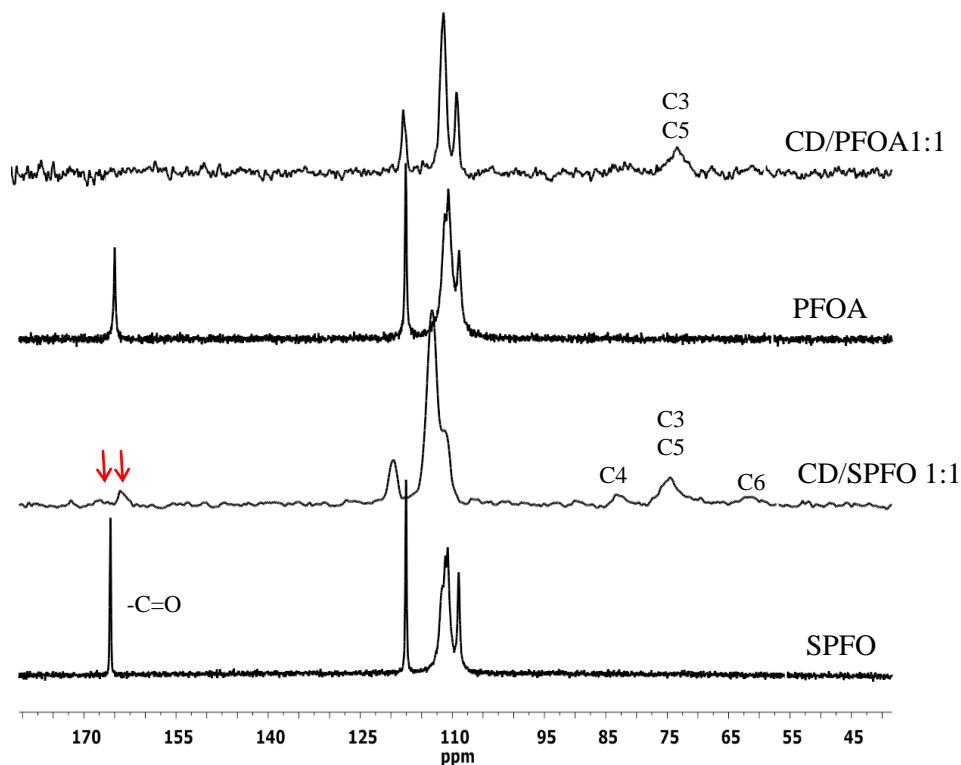


Figure 5.8 The $^{19}\text{F} \rightarrow ^{13}\text{C}$ CP results for SPFO, PFOA, and the 1:1 β -CD/SPFO and β -CD/PFOA inclusion compounds under MAS 20 kHz at 295K. The host and guest regions are labeled.

The ^{13}C δ values for the respective 1:1 complexes of SPFO and PFOA with β -CD were extracted from the deconvolved ^{19}F resonance lines and the $\Delta\delta$ values (in brackets) are presented in Table 5.3. The increased $\Delta\delta$ values for the $\text{C}_\alpha\text{F}_2$ group in the β -CD/SPFO complex (~ 1.62 ppm) is related to inductive effects due to increased dipolar interactions as described in the solution NMR results. There are no significant $\Delta\delta$ values observed for the $\text{C}_\alpha\text{F}_2$ of the β -CD/PFOA complex. The differences in the extent of dipolar interactions for PFOA and SPFO with CD further highlight the different structural roles played by the H^+ and Na^+ counterions, respectively. Greater $\Delta\delta$ values (>2.00 ppm) for the terminal groups of the 1:1 β -CD/SPFO complex compared to values for the 1:1 β -CD/PFOA ($\Delta\delta < 0.50$ ppm) are related to differences in guest geometry and conformation, and the extent to which the guests interact with the host. Note that the guest molecules in the 1:1 complexes can bind to the CD cavity in one of the two configurations depicted in Scheme 5.3(c). Note also that the effect of solvent is limited in the solid state.

Table 5.3 CIS Values (ppm) for the ^{13}C Nuclei of $\beta\text{-CD/SPFO}$ and $\beta\text{-CD/PFOA}$ Complexes in Solution at 295 K.

Nuclei	^{13}C ($^{19}\text{F} \rightarrow ^{13}\text{C}$ CP)			
	PFOA	$\beta\text{CD/PFOA}$ 1:1	SPFO	$\beta\text{CD/SPFO}$ 1:1
1 ($\text{C}=\text{O}$)	165.00	-	165.69	163.73, 167.35
2 (C_aF_2)	111.31	111.78 (+0.47)	111.73	113.35 (+1.62)
3-6	110.56, 110.60	111.31 (+0.71)	110.73, 110.88, 111.17	
7 ($\text{C}_\epsilon\text{F}_2$)	108.87	109.27 (+0.40)	108.96	111.08 (+2.12)
8 ($\text{C}_\omega\text{F}_3$)	117.58	117.65 118.04 (+0.46)	117.55	119.65 (+2.10)
C4	-	81.89	-	82.78
C3C5	-	73.38	-	74.50
C6	-	61.12	-	61.62

5.4.5.3 ^{19}F DP/MAS NMR at Ambient Temperature

Solid-state NMR in which the nucleus of interest can be observed may provide detailed information regarding the microenvironment and dynamics of the guest in a host-guest system. The ^{19}F DP/MAS NMR spectra of the $\beta\text{-CD/SPFO}$ complexes prepared by the modified dissolution method are presented in Fig. 5.9. The ^{19}F NMR results of PFOA are compared at MAS 20 kHz. As compared with the spectrum of pure PFOA in Fig. 5.9, pure SPFO displays broad ^{19}F signals for both the methyl (CF_3) and methylene (CF_2) resonances. The broad signals for SPFO relative to PFOA may be related to the limited dynamics of coiling and uncoiling in the former. However, the ^{19}F NMR spectra of the $\beta\text{-CD/SPFO}$ complexes give rise to relatively well-resolved ^{19}F resonance lines compared to those of the PFOA complexes in a previous study (*cf.* Fig. 4 ref. 17 or Fig. 3.4). The different line shapes of the complexes formed by $\beta\text{-CD}$ with PFOA and SPFO, respectively, reveal that the structural and dynamic properties of the two compounds (i.e. $\beta\text{-CD/PFOA}$ and $\beta\text{-CD/SPFO}$) are distinct.

The methylene (CF_2) signals for the 2:1 $\beta\text{-CD/SPFO}$ complex in Fig. 5.9 revealed relatively sharp features for the terminal $\text{C}_\epsilon\text{F}_2$ (ca. -128 ppm) and to some extent the main C_mF_2 (ca. -120 ppm) resonances; while the C_aF_2 signal (ca. -115 ppm) appeared to be broader in shape relative to the 1:1 complex. The broad C_aF_2 signals in the 2:1 complex is related to increased H-

bonding effects as described in the solution NMR and the $^{19}\text{F} \rightarrow ^{13}\text{C}$ CP results. The relatively narrow lines for the 2:1 complex may be related to dynamics of the guest that are distinct compared to the 1:1 complex. The presence of spinning sidebands at slower MAS conditions (20 kHz in this case) are known to interfere with the direct comparison of the line shapes for the spectra of the 1:1 and 2:1 complexes relative to those of unbound guest. This is because possible overlap between the resonance lines and the signals due to sidebands may occur. Therefore, comparisons were made at MAS 25 kHz where the deconvolution of the CF_3 lines provided an insight into the dynamics of the three products (i.e. the 1:1, 2:1, and unbound SPFO). Prior analyses of the simulated CF_3 lines at MAS 25 kHz and variable dipolar coupling strengths (100 Hz to 10,000Hz) were carried out as a model to characterize the line shape behavior of the CF_3 groups as a function of dipolar couplings as modulated by molecular dynamics.

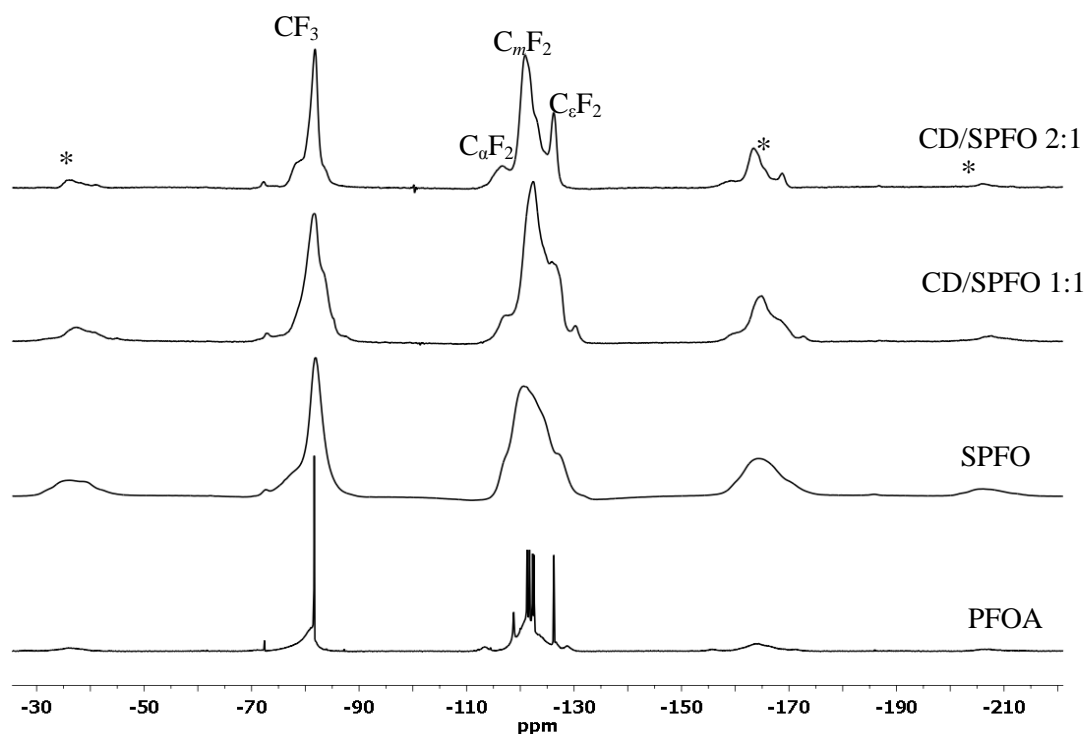


Figure 5.9 ^{19}F DP NMR spectra of PFOA, SPFO, and the 1:1 and 2:1 β -CD/SPFO inclusion compounds under MAS 20 kHz at 295 K.

The simulated CF_3 resonance lines at variable dipolar coupling strengths and MAS 25 kHz are presented in Fig. 5.10. Higher coupling strengths (e.g. 10 kHz) in Fig. 5.10 means slower dynamics, and lower strengths (e.g. 100 Hz) means faster dynamics. At slower dynamics

where the dipolar coupling is strong (e.g. 10,000 - 5,000 Hz), the CF₃ resonance is characterized by at least five different components. As the dynamics increase progressively and dipolar couplings are scaled down, the CF₃ signal is reduced to a single line.

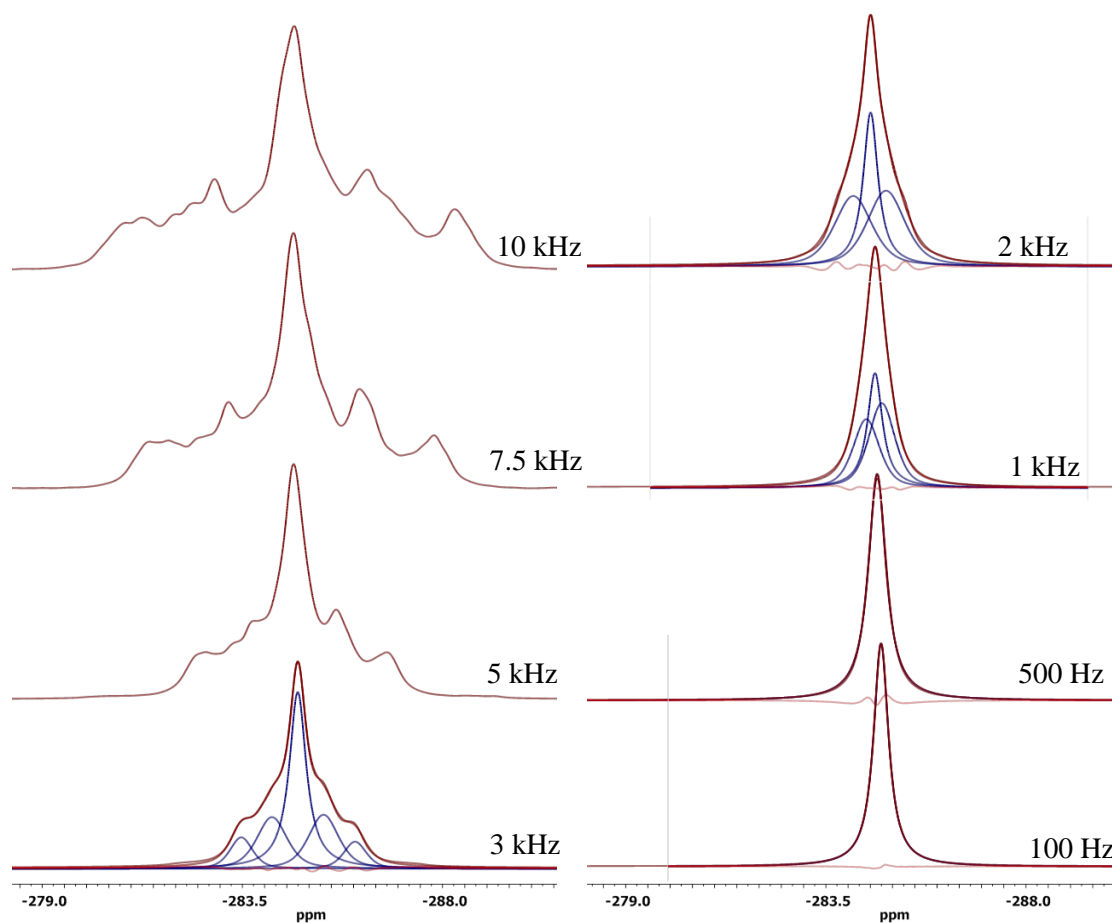


Figure 5.10 The simulated CF₃ signal as a function of variable dipolar coupling strengths

The deconvolved CF₃ signals for SPFO and the 1:1 and 2:1 β -CD/SPFO complexes at MAS 25 kHz are presented in Fig. 5.11. Based on the simulation results in Fig. 5.10, increased dynamics of the CF₃ group result in a single resonance line. Therefore, the dynamics of the CF₃ group for SPFO and its complexes generally appear to decrease in the order; SPFO>2:1>1:1. Since the component at higher field (ca. -84.0 ppm) may arise due to contribution from unbound

guest, it is not surprising that the various components in the deconvolved signals represent various guest environments, host-guest stoichiometries, or motional regimes of the guest. The structures of macromolecules have generally been described to involve an ensemble of distinct conformations that reflect distinct internal motions sampled over defined time-scales.⁶² Thus, individual lines in the deconvolved resonances may represent distinct structures, as well as variable dynamic regimes within a sample.

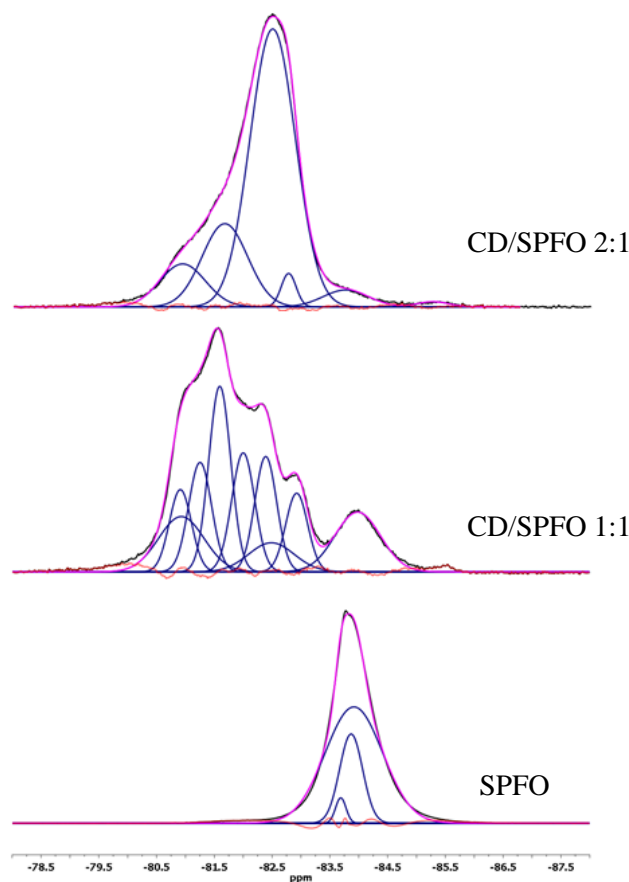


Figure 5.11 Deconvolution of the CF₃ line shape for SPFO, and the 1:1 and 2:1 β -CD/SPFO complexes acquired at 25 kHz.

The CF₃ line for SPFO in Fig. 5.11 is centered at around -84.0 ppm (similar shift as the upfield component in the complexes) and shows broad, narrow, and minor components. These components may be associated with the slow, intermediate, and fast dynamics, respectively. The deconvolution analysis of the CF₃ resonance line for the 2:1 complex is characterized by three

main broad components. In contrast to the 2:1 complex, the 1:1 complex reveals a mixture of broad and narrow components that closely resemble those in the simulations at ca. 3 – 2 kHz coupling strengths. It appears from the simulation data and the deconvolution analyses that the CF₃ group experiences faster dynamics in the 2:1 complex relative to the 1:1 complex. These results are consistent with the narrow CF₃ line in the ¹⁹F DP results for the 2:1 complex (*cf.* Fig. 5.8). However, contributions from other mixtures e.g. 1:2 and 1:1 complexes as mentioned in the DSC/TGA results (*cf.* §5.4.1) cannot be ignored and may account for the additional CF₃ components in the 1:1 and 2:1 host/guest complexes, respectively. Notice that the most intense component observed for the CF₃ resonance of the 1:1 at ca. -81.6 ppm is ca. 210 Hz wide compared to a similar line at ca.-82.5 ppm for the 2:1 complex that is twice as wide. The deconvolution parameters for SPFO and the complexes are presented in the supplementary information (Table D5.1).

5.4.5.4 ¹⁹F DP/MAS at Variable Temperature (VT)

¹⁹F DP NMR spectra under MAS 20 kHz at variable temperature (0–70 °C) were obtained for SPFO and the 1:1 and 2:1 host-guest inclusion compounds to gain further understanding into the dynamics of the bound guest in the complexes. Fig. 5.12 a–c show the stack plots of ¹⁹F DP NMR spectra at VT and MAS 20 kHz for SPFO (a), and the 1:1 (b) and 2:1 (c) β-CD/SPFO complexes. Similar results for the 2:1 β-CD/PFOA complexes (Fig. 5.12d) are presented for comparison. Note that the spectra of CD/PFC complexes are not readily amenable at variable temperature and/or faster (>20 kHz) MAS conditions because of instability of the spinning rotor. The spectra of unbound SPFO are characterized by relatively narrow lines for the CF₃ signal (ca. -83 ppm) and broad line for the methylene signals (ca. -120 ppm). Similarly, the CF₃ signal for the 2:1 complex (c) is relatively narrow compared to similar signal for the 1:1 complex (b). The CF₃ signal of the 1:1 complex reveals a shoulder at lower field which may be associated with externally bound or free guest. The methylene signals of the 2:1 complex (c) are relatively more resolved compared to similar lines for the unbound guest and the 1:1 complex, respectively.

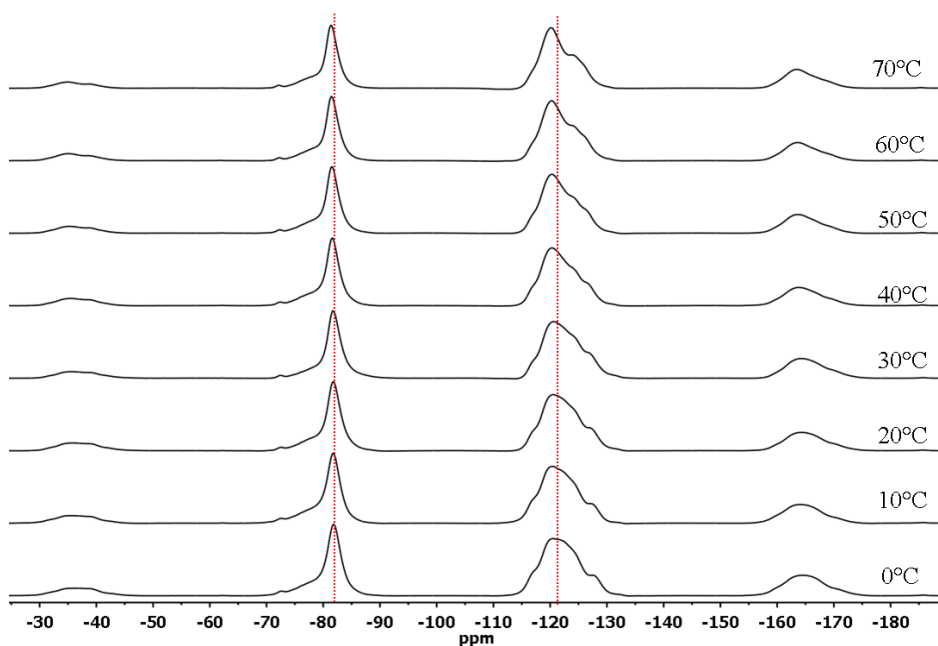


Figure 5.12a ^{19}F DP NMR spectra of SPFO under MAS 20 kHz at variable temperature

From the ongoing discussion, the dynamics of the CF_3 group as a function of temperature appear to decrease in the order; SPFO>2:1 \geq 1:1. The characterization of the CF_3 dynamics based on the comparison of the simulation and deconvolution results of the CF_3 group and the complexes, respectively, may not be entirely conclusive. This is because broad lines, for example in the spectra of the 1:1 complex, may arise from a number of factors; e.g. variable guest geometries, artifacts from higher order host/guest mixtures (e.g. 2:1 and 1:2), as well as the presence of free guest, as previously described. In the case of the dynamics of the main chain, the 2:1 complex is expected to experience increased dynamics of the C-F bonds. The relatively well-resolved methylene lines at ca. -130 – 120 ppm region for the 2:1 host-guest complex are consistent with increased C-F dynamics in their environment. The geometry of the guest in this complex as depicted in Scheme 3b is such that the sodium counterion and the fluoromethyl group can act as anchors where the rotation of the C-F bonds can be facilitated. In contrast to the 2:1 complex, the rotations of the C-F bonds are significantly reduced in the 1:1 complex because of the competing rotational motions of the CF_3 group around its three-fold axis and in accordance with the binding geometry of the guest (*cf.* Scheme 5.3c). In the case of the unbound

guest, the reduced motions of the C-F bonds can be explained in terms of the restricted dynamics of coiling and uncoiling for the sodium-rich SPFO guest, as previously described.

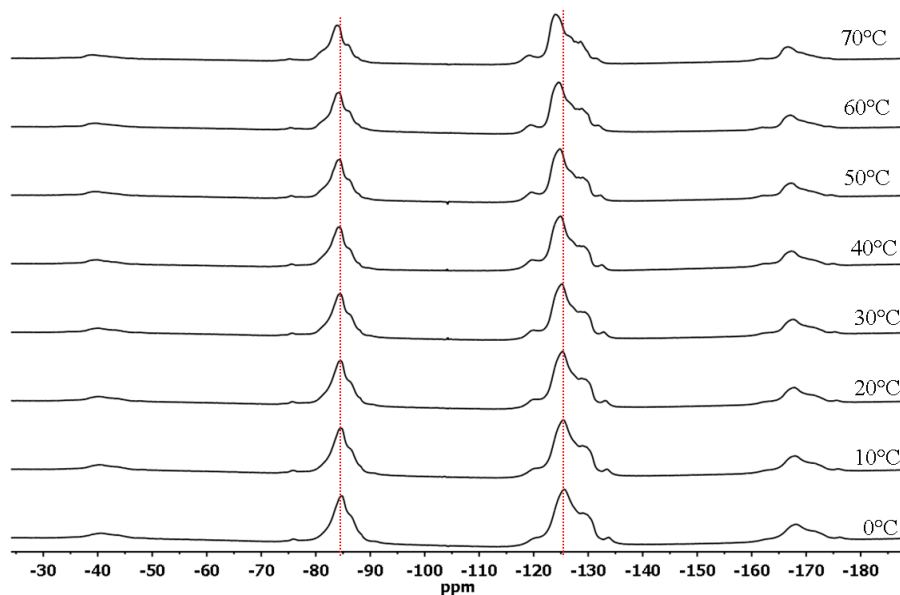


Figure 5.12b ^{19}F DP NMR spectra of the 1:1 β -CD/SPFO inclusion compound under MAS 20 kHz at variable temperature.

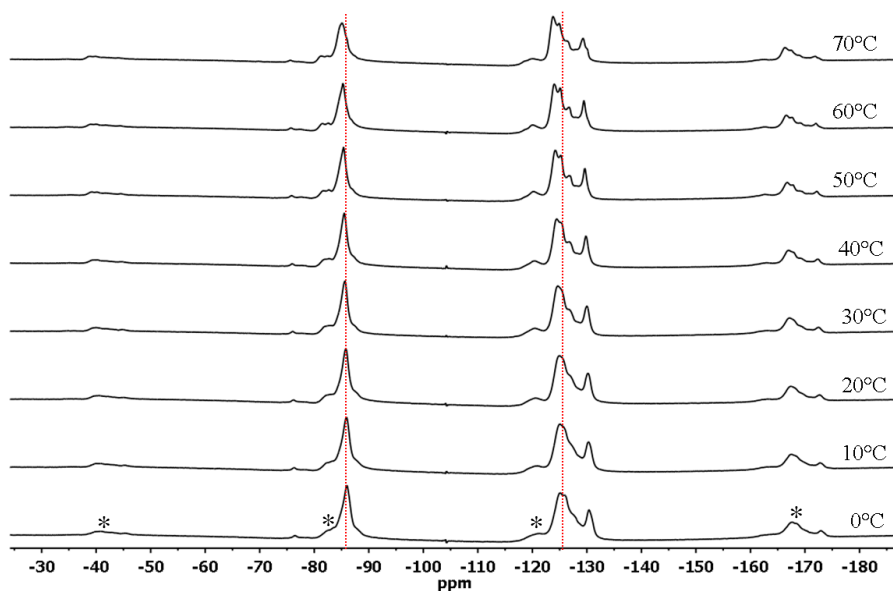


Figure 5.12c ^{19}F DP NMR spectra of the 2:1 β -CD/SPFO inclusion compound under MAS 20 kHz at variable temperature.

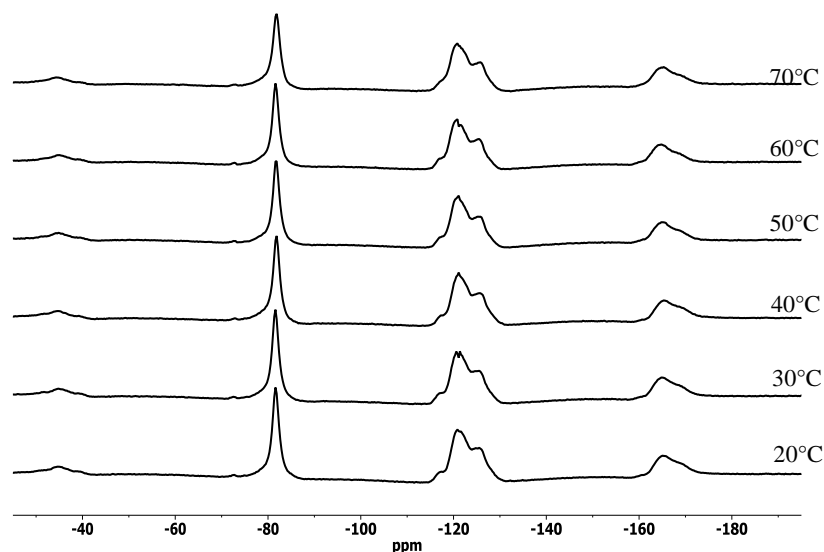


Figure 5.12d ^{19}F DP/MAS (20 kHz) NMR spectra of the 2:1 β -CD/PFOA dissolution complex at variable temperature.

On considerations of the structural differences between β -CD/SPFO and β -CD/PFOA complexes, further comparisons show well-resolved CF_2 resonance lines for the spectra of the 2:1 β -CD/SPFO complexes relative to the spectra of 2:1 β -CD/PFOA complexes (*cf.* Fig. 5.12c and d). The presence of sodium vs. hydronium counterions for SPFO and PFOA, respectively, accounts for the differences in the structures of the two complexes. We conclude that the rotaxane-like structure of the β -CD/SPFO complex facilitates rotation of the C-F bonds in this product, as well as reducing internal rotation of the CF_3 group relative to the dynamics of the guest in the β -CD/PFOA complex. The CF_3 group experiences increased rotational motion in the 2:1 CD/PFOA complex relative to the SPFO counterpart (*cf.* Fig. 5.12c and d).

5.4.6 Solid-state ^{19}F Relaxation Studies at Variable Temperature

The ^{19}F T_1 and T_2 relaxation times as a function of temperature (0–70 °C) for the unbound SPFO and the inclusion compounds are listed in Tables 5.4 and 5.5, respectively. It should be noted here that the relaxation parameters were measured on the CF_3 (ca. -83 ppm) and the main methylene (C_mF_2) groups at ca. -125 ppm. In general, relaxation of spin-1/2 nuclei (e.g., ^{19}F) is

stimulated by fluctuation of local fields that results from chemical shift anisotropy (CSA) and dipole-dipole (DD) coupling interactions in combination with random molecular (rotational and translational) motions.^{63,64} The nature and rate of such motions affect T_1 and T_2 relaxation times differently.⁶⁴ Molecular motions that occur at a rate comparable to the Larmor frequency are most effective for T_1 relaxation, and result in the minimum values for T_1 . The values of T_2 will be decreased even further as the molecular motions become slower than the Larmor frequency, but T_1 will eventually increase again (cf. Fig. 1.22).

The T_2 values in Table 5.5 are generally shorter than the T_1 values (cf. Table 5.4) by over four orders of magnitude. The longer T_1 relaxation for SPFO (~2–6 s) relative to the inclusion compounds (~0.7–1.5 s) can be explained in terms of less efficient spin diffusion of the guest in the unbound state.⁶⁴ This is because motions that are faster than the Larmor frequency such as libration of C-F bonds or internal rotation of CF_3 can eliminate homonuclear dipolar couplings between ^{19}F nuclei resulting in longer relaxation times. The relaxation of the CF_3 group in SPFO is more efficient than that of the C_mF_2 group. The SPFO chain was previously described to experience significant CF_3 rotation and reduced axial motion of the C-F bonds. The rapid internal rotation of the methyl group results in reduced T_1 values in the absence of dipolar coupling with other fluorines.

From the ongoing discussion and based on ^{19}F VT studies, two types of motions can be defined for the SPFO guest molecule; namely, the internal rotation of the fluoromethyl group on a three-fold axis and librational (axial) motions of the C-F bonds. Thus, two different motional time scales potentially apply, where axial motion is most likely in the slow motion regime and the rotation of the CF_3 group occurs at rates that exceed the ^{19}F Larmor frequency. Since relaxation processes are generally caused by fluctuations in local fields arising from CSA and DD coupling interactions, molecular motions that far exceed these two terms attenuate them significantly and can eliminate them completely with rapid isotropic reorientational dynamics. That is, the faster the rate, the less efficient the CSA and the DD relaxation mechanisms become, which results in longer T_1 relaxation. Note that pure SPFO is expected to display a completely different lattice environment than that of the guest in the inclusion compounds as described in the deconvolution analyses; therefore, the axial motion and the CF_3 bond rotation will occur at different rates.

Table 5.4 T_1 Relaxation Values for the ^{19}F Resonances of the SPFO and the 1:1 and 2:1 β -CD/SPFO Complexes at Variable Temperature.*

T (°C)	SPFO (s)		1:1 IC (s)		2:1 IC (s)	
	CF ₃	C _m F ₂	CF ₃	C _m F ₂	CF ₃	C _m F ₂
0	1.971	4.490	1.143	1.141	0.763	0.696
10	2.038	4.254	1.143	1.385	0.703	0.761
20	2.202	4.636	1.177	1.417	0.777	0.789
30	2.461	4.873	1.192	1.448	0.819	0.811
40	2.765	5.453	1.231	1.487	0.878	0.841
50	2.894	5.269	1.268	1.505	0.910	0.885
60	3.356	5.865	1.339	1.498	1.005	0.979
70	3.759	6.588	1.379	1.516	1.106	1.070

*Error estimates are within 0.001-0.005 s

Table 5.5 T_2 Relaxation Values for the ^{19}F Resonances of the SPFO and the 1:1 and 2:1 β -CD/SPFO Complexes at Variable Temperature.*

T (°C)	SPFO (ms)		1:1 IC (ms)		2:1 IC (ms)	
	CF ₃	C _m F ₂	CF ₃	C _m F ₂	CF ₃	C _m F ₂
0	0.158	0.116	0.543	0.308	0.672	0.472
10	0.166	0.101	0.587	0.336	0.699	0.468
20	0.164	0.101	0.617	0.366	0.719	0.494
30	0.167	0.101	0.647	0.391	0.745	0.527
40	0.169	0.101	0.682	0.414	0.749	0.583
50	0.178	0.112	0.704	0.439	0.760	0.620
60	0.177	0.111	0.712	0.450	0.770	0.601
70	0.181	0.112	0.731	0.455	0.770	0.620

*Error estimates are within 0.002-0.008 ms

The T_1^{F} (open symbols) and T_2^{F} (filled symbols) relaxation data for the 1:1 and 2:1 β -CD/SPFO complexes are summarized in the plots of Fig. 5.13a and b, respectively. The relaxation data for SPFO are omitted in the plots for clarity. The T_1/T_2 values increase monotonically as a function of temperature which suggests that the motion of the guest is faster than the Larmor frequency under the applied temperature conditions. In the case of the 1:1

complex (Fig. 5.13a), the T_1 and T_2 values are distinct for the CF_3 and C_mF_2 groups, respectively, which may suggest that different types of motions drive T_1 and T_2 processes. Since the rotational motion of the CF_3 group is in the fast motion regime, spin diffusion may propagate along the chain less efficiently resulting in distinct relaxation times for the CF_3 and C_mF_2 moieties at the different temperatures. In contrast to the 1:1 complex, the 2:1 complex (Fig. 5.13b) displays similar T_1 values for the different segments of the guest chain at different temperatures.

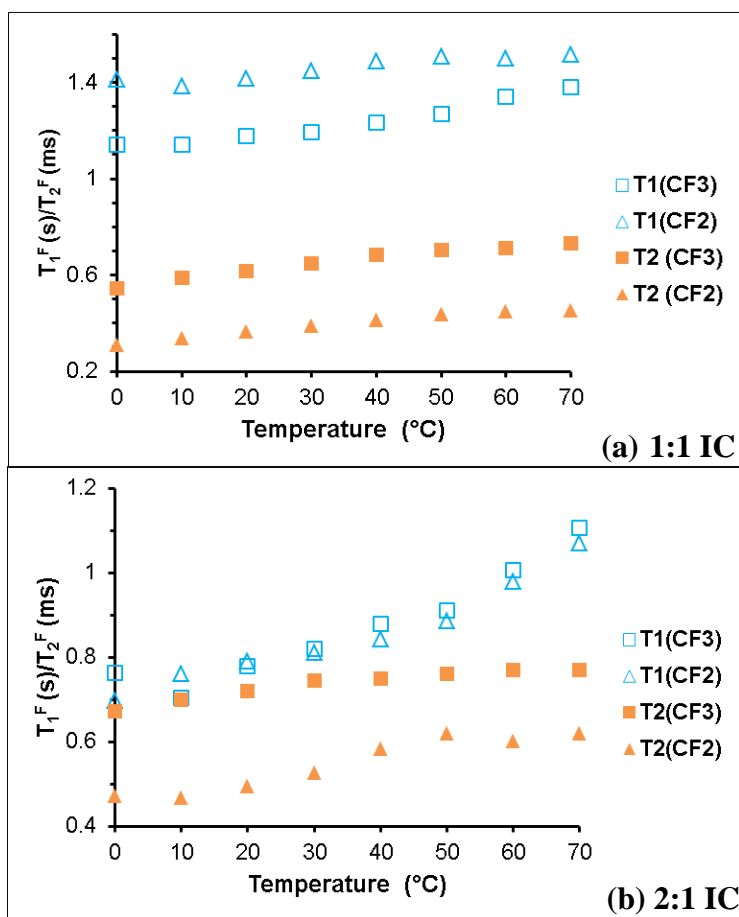


Figure 5.13 ^{19}F T_1 (open symbols) and T_2 (filled symbols) values for the CF_3 and main CF_2 groups for (a) the 1:1, and (b) 2:1 $\beta\text{-CD}/\text{SPFO}$ complexes under MAS 20 kHz at variable temperature.

It appears that librational motion of the C-F bonds drives T_1 relaxation, while T_2 is driven by rapid CF_3 rotation. The rotation of the CF_3 may be less restricted in the 1:1 complex considering the possible binding geometry of the guest in this product (*cf.* Scheme 5.3c). In contrast to the

1:1 complex, the guest molecule in the 2:1 complex may experience sufficient rotation of the CF₃ group as well as rotations of the C-F bonds, as described in the ¹⁹F DP-MAS/VT NMR results. The librational motion of the guest affects the CF₃ and C_mF₂ segments of the chain similarly which results in similar T₁ values for the 2:1 complex.

In a previous study,¹⁷ the librational motion of the C-F bonds in β-CD/PFOA complexes affected the entire guest chain (T₁) in a similar way for the 1:1 and 2:1 complexes (*cf.* Fig. 3.10). That is, these motions were synchronized along the perfluorocarbon chain in the two samples, respectively. While this may be true for the 2:1 β-CD/SPFO complex reported herein, in the case of the 1:1 complex such axial motions are affected by the extensive CF₃ rotation and therefore appear to be unevenly distributed along the chain. The 2:1 β-CD/SPFO complex has been described above as a pseudo-rotaxane where the ends are relatively capped and the central body experiences evenly distributed axial motions. In contrast to the 2:1 complex, the guest molecule in the 1:1 complex experiences rapid rotational motion of the CF₃ group due to its extra-cavity environment.

5.5. Conclusions

A detailed study of the solid inclusion complexes of β-CD and SPFO was reported to understand the structure of the guest and the role of sodium counterion in the binding of the guest with CD. The 1:1 and 2:1 β-CD/SPFO complexes were prepared using a modified dissolution method and were further characterized using NMR and FT-IR spectroscopy, thermal analysis (DSC/TGA), and powder X-ray diffraction. ¹⁹F/¹H/¹³C CIS values in solution and the solid state were used to provide evidence for the formation of β-CD/SPFO inclusion compounds and to understand the effect of sodium counterion on the structure of the complexes. The CIS effects for the C_αF₂ resonance of the β-CD/SPFO complexes experienced increased δ values compared to similar values for β-CD/PFOA complexes. The results reveal that the complexes in the former experience increased dipolar interactions in accordance with the geometry and conformation of the sodium-rich guest molecule.

¹⁹F→¹³C CP/MAS and ¹³C DP/MAS NMR results provided unequivocal evidence for the formation of β-CD/SPFO inclusion compounds in the solid state. The guest molecule of the 2:1 β-CD/SPFO complex adopts an extended *all-trans* conformation as it spans the cavity space of two CD macromolecules and as concluded from FT-IR results. The DSC/TGA results revealed

variable hydration states and thermal stabilities of the guest for the 1:1 and 2:1 β -CD/SPFO complexes. A greater fraction of cavity bound water was detected for the 2:1 complex as compared with the 1:1 complex, which is a direct consequence of the variations in the guest conformation and binding geometry for the two complexes. PXRD results indicate that SPFO forms *head-to-head* channel type structure with β -CD, and the XRD patterns reveal significant loss of long-range order which may arise from the structural disorder caused by a significant amount of bound water.

A combination of simulated spectra and deconvolution analyses of the CF_3 in conjunction with the ^{19}F DP/MAS NMR results at ambient and variable temperatures revealed variable guest dynamics for the pure SPFO guest and the 1:1 and 2:1 host-guest complexes. The structure of the 2:1 β -CD/SPFO complex represents a pseudo-rotaxane where the carbonyl and fluoromethyl ends are capped and rotations of the central C-F bonds are facilitated. The dynamics of the guest in the 1:1 complex are characterized by significant rotations of the CF_3 group in accordance with a binding geometry where the guest can either be extra- or intra-cavity bound. Comparisons for the dynamics of PFOA guest in its bound state with CD revealed that the C-F bond rotations were synchronized along the entire guest chain segment for the 1:1 and 2:1 complexes. In contrast, such motions were unevenly distributed in the 1:1 β -CD/SPFO complex due to more rapid rotational motion of the CF_3 group coupled with structural differences arising from electrostatic interactions between the carboxylate group and its sodium counterion. ^{19}F T_1 and T_2 relaxation results support the unique dynamics of SPFO in the complexes and provide further evidence for the rotaxane-like structure of the 2:1 β -CD/SPFO complex. Some of the structural properties of SPFO, PFOA, and PFBA and their complexes with β -CD are summarized in Table 5.6.

5.6. Acknowledgements

The authors gratefully acknowledge the Natural Sciences and Engineering Research Council (NSERC), the University of Saskatchewan, and the University of Lethbridge for support of this research. AHK wishes to acknowledge Esther Aluri for her assistance with PXRD measurements.

Table 5.6 Summarized Structural Properties of PFOA, SPFO, and PFBA and their Complexes with β -CD.

Guest Molecule	PFOA	SPFO	PFBA
Physical state	Solid	Solid	Liquid
Host:Guest Stoichiometry	1:1 and 2:1	1:1 and 2:1	Mainly 1:1
Native Conformation	<i>Gauche</i>	<i>Gauche</i>	<i>Trans</i>
Conformation in bound state	<i>Gauche</i> (1:1) and <i>trans</i> (2:1)	<i>Gauche</i> (1:1) and <i>trans</i> (2:1)	<i>Gauche</i>
Proposed guest geometry	Intra-/extra-cavity inclusion	Intra-/extra-cavity, deep guest inclusion.	Intra-/extra-cavity, variable topologies.
Packing structure	<i>Channel-type</i>	<i>Channel-type</i>	<i>Cage-type</i>
Dynamics of native guest	Free coiling and uncoiling	Restricted coiling and uncoiling	n/a
Dynamics of bound guest	Significant CF ₃ rotation and axial motions in both the 1:1 and 2:1 complexes	Reduced CF ₃ rotations and facilitated C-F bonds rotation in the 2:1 complex	Extensive CF ₃ rotation and appreciable axial motions of C-F bonds

5.7. References:

- (1) Key, B. D.; Howell, R. D.; Criddle, C. S. *Environ. Sci. Technol.* **1997**, *31*, 2445–2454.
- (2) Rao, N. S.; Baker, B. E.; Tatlow, J. C. *Organofluorine Chemistry Principles and Commercial Applications*; Plenum Press: New York, 1994, Ch. 3, pp.61–64.
- (3) Kissa, E. *Fluorinated Surfactants and Repellents*, Marcel Dekker, Inc., New York, 2nd ed., 2001, vol. 97, Ch. 6, pp. 228-231.
- (4) Hoffmann, H.; Würtz, J. *J. Mol. Liq.* **1997**, *72*, 191-230.
- (5) Giesy, J. P.; Kannan, K. *Environ. Sci. Technol.*, **2002**, *36*, 147A–152A.
- (6) Margot, R.; Berger, U.; Broman, D.; Cousins, I. T.; Nilsson, E. D.; McLachlana, M. S. *Environ. Chem.* **2011**, *8*, 381–388.
- (7) Guo, W.; Fung, B. M.; Christian, S. D. *Langmuir* **1992**, *8*, 446–451.
- (8) D'Angelo, M.; Onori, G.; Santucci, A. *Prog. Colloid. Polym. Sci.* **1994**, *97*, 154–157.
- (9) Rayne, S.; Forest, K. *J. Mol. Struct-Theochem* **2010**, *949*, 60-69.
- (10) Becker, A. M. Ph.D. Thesis, University of Bayreuth, Bayreuth, 2008.

- (11) Washburn, S. T.; Bingman, T. S.; Braithwaite, S. K.; Buck, R. C.; Buxton, W.; Clewell, H. J.; Haroun, L. A.; Kester, J. E.; Rickard, W. R.; Shipp, A. M. *Environ. Sci. Technol.* **2005**, *39*, 3904–3910.
- (12) Butenhoff, J.; Costa, G.; Elcombe, C.; Farrar, D.; Hansen, K.; Iwai, H.; Jung, R.; Kennedy, G. Jr.; Lieder, P.; Olsen, G.; Thomford, P. *Toxicol. Sci.* **2002**, *69*, 244–257.
- (13) Kitamura, S.; Fujimura, T.; Kohda, S. *J. Pharm. Sci.* **1999**, *88*, 327–330.
- (14) Nicolle, G. M.; Merbach, A. E. *Chem. Commun.* **2004**, 854–855.
- (15) Szejtli, J.; Osa, T. In *Comprehensive Supramolecular Chemistry*, Eds.; Pergamon Press: New York, 1996, vol. 3, Ch. 1, pp. 1–2.
- (16) Karoyo, A. H.; Borisov, A.; Wilson, L. D.; Hazendonk, P. *J. Phys. Chem. B*, **2011**, *115*, 9511–9527.
- (17) Karoyo, A. H.; Sidhu, P.; Wilson, L. D.; Hazendonk, P. *J. Phys. Chem. B* **2013**, *117*, 8269–8282.
- (18) Karoyo, A. H.; Sidhu, P.; Wilson, L. D.; Hazendonk, P. *J. Phys. Chem. C* **2014** (jp-2014-02325e).
- (19) Palepu, R.; Richardson, J. E.; Reinsborough, V. C. *Langmuir* **1989**, *5*, 218–221.
- (20) Palepu, R.; Reinsborough, V. C. *Can. J. Chem.* **1989**, *67*, 1550–1553.
- (21) Jobe, D. J.; Verrall, R. E.; Reinsborough, V. C. *Can. J. Chem.* **1990**, *68*, 2131–2136.
- (22) Jobe, D. J.; Verall, R. E.; Junquera, E.; Aicart, E. *J. Phys. Chem.* **1994**, *98*, 10814–10818
- (23) Wilson, L. D.; Siddall, S. R.; Verrall, R. E. *Can. J. Chem.* **1997**, *75*, 927–933.
- (24) Junquera, E.; Peña, L.; Aicart, E. *J. Inclusion Phenom. Mol. Recogn. Chem.* **1996**, *24*, 233–239.
- (25) Xing, H.; Lin, S. -S.; Yan, P.; Xiao, J. -X.; Chen, Y. -M. *J. Phys. Chem. B* **2007**, *111*, 8089–8095.
- (26) Wenz, G. *Angew. Chem. Int. Ed. Engl.* **1994**, *33*, 803–822.
- (27) Wilson, L. D.; Verrall, R. E. *Langmuir* **1998**, *14*, 4710–4717.
- (28) Wilson, L. D.; Verrall, R. E. *Can. J. Chem.* **1998**, *76*, 25–34.
- (29) Messina, P. V.; Prieto, G.; Salgado, F.; Varela, C.; Nogueira, M.; Dodero, V.; Ruso, J. M.; Sarmiento, F. *J. Phys. Chem. B* **2007**, *111*, 8045–8052.
- (30) Dias, A. M. A.; Andrade-Dias, C.; Lima, S.; Coutinho, J. A. P.; Teixeira-Dias, J. J. C.; Marrucho, I. M. *J. Colloid Interf. Sci.* **2006**, *303*, 552–556.

- (31) Hu, J. Z.; Zhou, J.; Deng, F.; Feng, H.; Yang, N.; Li, L.; Ye, C. *Solid State. Nucl. Magn. Reson.* **1996**, *6*, 86–94.
- (32) Samson, A. O.; Chill, J. H.; Anglister, J. *Biochemistry*, **2005**, *44*, 10929–10943.
- (33) Riga, A.; Collins, R.; Mlachak, G. *Thermochim. Acta* **1998**, *324*, 135–149.
- (34) Yang, X.; Zhao, Y.; Chen, Y.; Liao, X.; Gao, C.; Xiao, D.; Qin, Q.; Yi, D.; Yang, B. *Mater Sci. Eng. C Mater Biol. Appl.* **2013**, *33*, 2386–2391.
- (35) Cwiertnia, B.; Hladon, T.; Stobiecki, M. *J. Pharm. Pharmacol.* **1999**, *51*, 1213–1218.
- (36) Cursaru, B.; Stănescu, P. O.; Teodorescu, M. *U.P.B. Sci. Bull., Series B* **2010**, *72(4)*, 99–114.
- (37) Sambasevam, K. P.; Mohamad, S.; Sarih, N. M.; Ismail, N. A. *Int. J. Mol. Sci.* **2013**, *14*, 3671–3682.
- (38) Tatsuno, H.; Ando, S. *J. Phys. Chem. B* **2006**, *110*, 25751–25760.
- (39) Pawsey, S.; Reven, L. *Langmuir* **2006**, *22*, 1055–1062.
- (40) Lamcharfi, E.; Kunesch, G.; Meyer, C.; Robert, B. *Spectrochimica Acta Part A* **1995**, *51*, 1861–1870.
- (41) Crupi, V.; Majolino, D.; Rossi, B.; Verrochio, P.; Viliiani, G. *J. Phys. Chem. A* **2010**, *114*, 6811–6817.
- (42) Albinsson, B.; Michl, J. *J. Phys. Chem.* **1996**, *100*, 3418–3429.
- (43) Moynihan, R. E. *J. Am. Chem. Soc.* **1959**, *81* (5), 1045–1050.
- (44) Ellis, D. A.; Denkenberger, K. A.; Burrow, T. E.; Mabury, S. A. *J. Phys. Chem. A* **2004**, *108* (46), 10099–10106.
- (45) Knochehuer, G.; Reiche, J.; Brehmwer, L.; Berberka, T.; Woolley, M.; Tredgold, R.; Hodge, P. J. *Chem. Soc., Chem. Commun.* **1995**, 1619–1620.
- (46) Erkoc, S.; Erkoc, F. *J. Mol. Struct-Theochem* **2001**, *549* (3), 289–293.
- (47) Lo Nostro, P.; Santoni, I.; Bonini, M.; Baglioni, P. *Langmuir* **2003**, *19*, 2313–2317.
- (48) Okumura, H.; Kawaguchi, Y.; Harada, A. *Macromolecules* **2001**, *34*, 6338–6343.
- (49) Jiao, H.; Goh, S. H.; Valiyaveetil, S. *Macromolecules* **2002**, *35*, 3997–4002; Jiao, H.; Goh, S. H.; Valiyaveetil, S.; Zheng, J. *Macromolecules* **2003**, *36*, 6422–6429.
- (50) Gao, Y. –A.; Li, Z. –H.; Du, J. –M.; Han, B. –X.; Li, G. –Z.; Hou, W. –G.; Shen, D.; Zheng, L. –Q.; Zhang, G. –Y. *Chem. Eur. J.* **2005**, *11*, 5875–5880.
- (51) Liu, J.; Alvarez, J.; Ong, W.; Roman, E.; Kaifer, A. E. *Langmuir* **2001**, *17*, 6762–6764.

- (52) Abbate, V.; Bassindale, A. R.; Brandstadt, K. F.; Taylor, P. G. *J. Incl. Phenom. Macrocycl. Chem.* **2012**, *74*, 223–230.
- (53) Saenger, W. *J. Incl. Phenom.* **1984**, *2*, 445–454.
- (54) Schneider, H. J.; Hacket, F.; Rudinger, V. *Chem. Rev.* **1998**, *98*, 1755–1786.
- (55) Goecke, C. M.; Jarnot, B. M.; Reo, N. V. *Chem. Res. Toxicol.* **1992**, *5*, 512–519.
- (56) Guzman, E. K. M.S. Thesis, university of Oklahoma, Norman, OK, 1989.
- (57) Emsley, J. W.; Feeney, J.; Sutcliffe, L. H. *Progress in NMR Spectroscopy*. Pergamon Press: New York, 1971; Vol. 7, p11.
- (58) Rudinger, V.; Eliseev, A.; Svetlana, S.; Schneider, H, -J.; Blandamer, M. J.; Cullis, P. M.; Meyer, A. *J. Chem. Soc. Perkin Trans. 2*, **1996**, *10*, 2119–2123.
- (59) Lu, J.; Mirau, P. A.; Tonelli, A. E. *Prog. Polym. Sci.* **2002**, *27*, 357–401.
- (60) Koito, Y.; Yamada, K.; Ando, S. *J. Incl. Phenom. Macrocycl. Chem.* **2013**, *76*, 143-150.
- (61) Ceccato, M.; Lo Nostro, P.; Rossi, C.; Bonechi, C.; Donati, A.; Baglioni, P. *J. Phys. Chem. B* **1997**, *101*, 5094–5099.
- (62) Kleckner, I. R.; Foster, M. P. *Biochim. Biophys. Acta* **2011**, *1814*, 942-968.
- (63) Levitt, M. H. *In Spin Dynamics*, 2nd ed., John Wiley & Sons Ltd.: Chichester, **2001**.
- (64) James, T. L. *Fundamentals of NMR*, University of Carlifonia, **1998**.

CHAPTER 6

Manuscript 5

Description

A soluble CD-based copolymer, denoted HDI-1, was used to prepare host-guest inclusion compounds where PNP was used a model guest. The copolymer was synthesized using β -CD as the macrocyclic comonomer and hexamethylene diisocyanate (HDI) as the linker at the 1:1 (β -CD/HDI) mole ratio. The structure of the copolymer host material and its complexes with PNP in aqueous solution were investigated using various spectroscopic (e.g., 1-D/2-D NMR spectroscopy, FT-IR, etc.), and thermoanalytical (e.g., DSC) methods, induced circular dichroism (ICD), and dynamic light scattering (DLS) techniques.

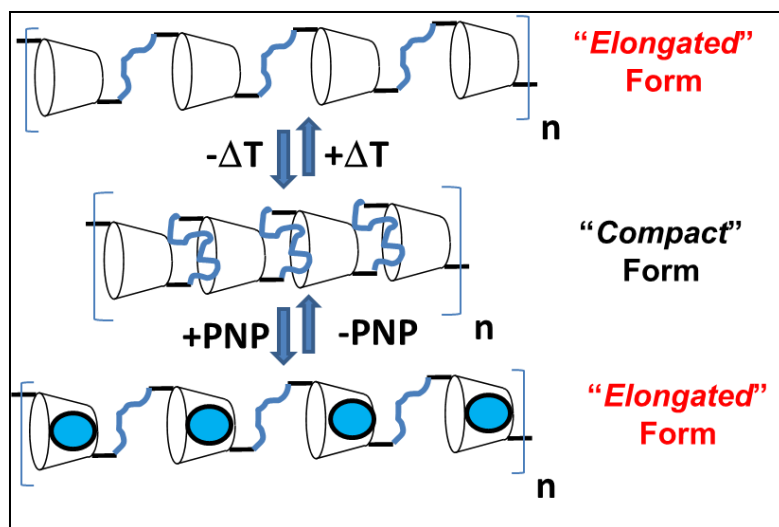
Author's Contribution

The idea of using polymeric host materials to study the structure of host-guest systems was proposed by myself. All the structural characterizations were done by myself. The HDI-1 copolymer material for the initial preliminary investigations was contributed by Dr. M. H. Mohamed. I prepared the experimental data/section and abstract, and the rest of the manuscript was prepared by Dr. Wilson.

Relation of Manuscript 5 to Overall Objective of this Project

The work of this manuscript provided a model system to the study of the structure of host-guest systems at a much more complex (3-dimensional) structural level by using linear polymeric hosts that have more than one binding site. The main objective of this study was to investigate the structure of the soluble copolymer material in aqueous solution in order to gain an understanding of how the material behaves in the absence/presence of a guest. The effect on the conformation of the copolymer as a function of temperature variation was also investigated.

Graphical Abstract



Research Highlights

- The conformation of HDI-1 copolymer material switched between "compact" (coiled) and "extended" (uncoiled) forms in the absence and presence of a guest/heat, respectively.
- 1-D ^1H ROESY NMR was used to provide unequivocal evidence for the formation of an inclusion compound between β -CD and PNP
- PNP was bound primarily within the cavity of β -CD; whereas, the HDI linker domains of the copolymer material acted as a secondary site where PNP could bind.

6. Structural Characterization of a Urethane-Based “*Molecular Accordion*” Copolymer in Aqueous Solution

Lee D. Wilson* and Abdalla H. Karoyo

Department of Chemistry, University of Saskatchewan, 110 Science Place, Saskatoon, Saskatchewan, S7N 5C9

*Corresponding Author.

§Supplementary Information is provided in Appendix E.

6.1 Abstract

A novel urethane-based copolymer material containing β -cyclodextrin (β -CD) was obtained from the reaction of 1,6-hexamethylene diisocyanate (HDI) with β -CD in a 1:1 mole ratio, denoted HDI-1. In aqueous solution at ambient conditions, HDI-1 adopts a *compact* (i.e., coiled) conformation in which the cross-linker units are coiled and partially self-included in the annular hydroxyl (i.e., interstitial) region of β -CD. As the temperature is raised or as *p*-nitrophenol (PNP) is included within the β -CD cavity sites of the copolymer, it adopts an *extended* (i.e., uncoiled) conformation. The equilibrium switching between the *extended* and the *compact* forms of HDI-1 is thermo- and chemo-reversible, in accordance with the hydrophobic effect and the formation of host-guest inclusion complexes. The molecular structure of this water-soluble urethane copolymer and its complex with PNP was investigated using spectroscopic (Raman, ^1H NMR, and induced circular dichroism (ICD)), dynamic light scattering (DLS), and calorimetric methods in aqueous solution at pH \sim 6. The results for HDI-1 were compared with native β -CD throughout this study.

6.2 Introduction

The use of polymers, colloids, and supramolecular tectons as porogens in nanocasting strategies yields a wide variety of novel imprinted porous materials.¹ By analogy, the development of macromolecular porous materials with tunable morphology, textural parameters, and physicochemical properties is possible through the incorporation of a macrocyclic porogen into a cross-linked copolymer framework. Cyclodextrins (CDs) such as α -, β -, and γ -CDs are among the most widely studied macrocyclic host compounds, in part, due to their remarkable ability to form inclusion complexes with a diverse range of organic guest molecules in

condensed phases and gaseous states.^{2,3} Incorporation of a β -CD co-monomer within a copolymer framework represents a novel modular design approach with significant potential for the controlled tuning of the molecular recognition properties of macromolecular sorbent materials.^{4,5} Carbohydrate-based copolymers represent an emerging class of “*smart*” or “*functional*” porous materials with improved solid phase extraction (SPE) and molecular recognition properties.^{2,5,6-10} The sorption and host/guest recognition properties of β -CD copolymers^{9,11,5} are influenced by the surface area, pore structure, and the relative accessibility of the binding sites of the copolymer framework. Inclusion site accessibility for copolymers containing β -CD is required for the formation of well-defined host/guest inclusion complexes.¹¹⁻¹³

CD-based copolymer materials are known to display tunable physicochemical properties that extend the range of conventional sorbent materials.^{10,14} The sorption properties of β -CD urethane copolymers indicate that the framework structure (e.g., inclusion and interstitial domains) may provide multiple binding sites for adsorbates with variable hydrophile-lipophile characteristics. Thus, rational sorbent design accounts for the inclusion site accessibility of β -CD, the interstitial framework domains, cross-link density of the copolymer, and the physicochemical properties of the cross linking agent.^{9,13,14}

Ma and Li¹⁵ reported that *p*-nitrophenol (PNP) forms remarkably stable ($K_{eq} \sim 10^9 \text{ M}^{-1}$) inclusion complexes with urethane copolymers when compared with native β -CD ($K_{eq} \sim 197 \text{ M}^{-1}$).¹⁶ We propose that the greater apparent binding constant for the copolymer is an artifact arising from the secondary adsorption sites (i.e., interstitial domains) that were previously unaccounted for in the study reported by Ma and Li.¹⁵ The measurement of the residual (i.e., unbound) equilibrium concentrations of PNP does not adequately account for the occurrence of multiple binding sites in such copolymer framework materials. Silva et al.¹⁷ reported an amphiphilic CD with two recognition sites; whereas, Mohamed et al.¹⁸ reported two types of binding sites (i.e., inclusion and interstitial domains) in a sorption isotherm study of PNP with urethane-based copolymers. Dual mode adsorption was independently reported for the sorption properties of several types of copolymer sorbents containing β -CD.¹⁹ Evidence of multiple types of sorption sites may be inferred from thermodynamic sorption parameters (*cf.* Scheme 2 in ref. 20) for such copolymers. However, there is a need to carry out further structural studies that define the nature of these sorption sites.

In this paper, we report a structural study of the equilibrium complexes formed between a urethane copolymer (HDI-1) and β -CD with PNP at various conditions using spectroscopic (Raman, ^1H NMR, and ICD), DLS, and differential scanning calorimetry (DSC) methods. The studies were carried out in aqueous solution at 295 K and variable temperature (VT), in the presence and absence of PNP at pH 6. HDI-1 is a urethane-based water-soluble copolymer containing β -CD and 1,6-hexamethylene diisocyanate (HDI) in an equimolar ratio. The results of this study are anticipated to provide a greater understanding of the sorption mechanism of urethane copolymers in aqueous solution and contribute to the further development of “*smart*” SPE sorbent materials with tunable molecular recognition properties.^{1,5,6,9}

6.3 Materials and Methods

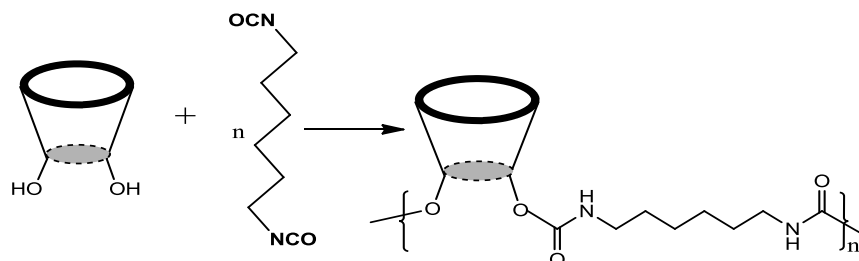
6.3.1. Materials

β -CD was purchased from VWR Canada Ltd. 1,6-hexamethylene diisocyanate (HDI), dimethyl acetamide (DMA), *p*-nitrophenol (PNP), methanol, anhydrous ethyl ether, potassium bromide, and 4Å (8–12 mesh) molecular sieves were purchased from Sigma-Aldrich Canada Ltd. Deuterium oxide (D_2O) was obtained from Cambridge Isotope Laboratories Inc. All materials were used as received unless specified otherwise. None of the materials in this study required any specialized safety precautions.

6.3.2. Synthesis of β -CD-Based Copolymer Materials

The synthesis of CD-based polyurethane materials was adapted from a previous report,²¹ as outlined in the following procedure. DMA was dried with 4Å (8–12 mesh) molecular sieves. The ^1H NMR spectrum of DMA was recorded before and after the addition of molecular sieves, and the water content was estimated to be ~0.5%. The 1:1 β -CD/diisocyanate HDI copolymer (*cf.* Scheme 6.1) was prepared by adding 1 mmol of dried β -CD to a round bottom flask with stirring until dissolved in 10 mL of DMA followed by the addition of 1 mmol HDI in 30 mL of DMA to the reaction mixture. The solution was stirred with heating at 68 °C for 24 h under argon and cooled to room temperature. The excess DMA was removed under vacuum (pressure ~1 mbar). The subsequent addition of cold methanol (~0°C) to the gelled product was followed by filtration through Whatman no. 2 filter paper. The crude product was washed with methanol in a Soxhlet extractor for 24 h to remove unreacted reagents and low molecular weight oligomers.

The copolymer product was dried in a pistol dryer for 24 h, ground into a powder, and passed through a size 40 mesh sieve to ensure a uniform particle size. A second cycle of washing in the Soxhlet extractor with anhydrous diethyl ether for 24 h was followed by drying, grinding, and sieving, as outlined above.



Scheme 6.1 Reaction between β -CD and 1,6-hexamethylene diisocyanate (HDI) to form the HDI-1 copolymer. Note that for 1:1 co-monomer mole ratios, the cross linker is hypothesized to attach covalently at the primary annular hydroxyl sites of β -CD.

The HDI-1-copolymer material was characterized using FT-IR and NMR spectroscopy, thermoanalytical methods, and elemental analyses, as outlined previously.²¹ The nomenclature of the HDI-1 copolymer is defined in accordance with the diisocyanate acronym and a numeric designation to indicate the co-monomer mole ratio, 1:1 (β -CD:hexamethylene diisocyanate), where the relative molar quantity of β -CD is taken to be unity.

6.3.3. Structural Characterization of a Urethane Copolymer in Aqueous Solution

6.3.3.1 Raman Spectroscopy

Raman spectra were obtained using a Renishaw system 2000 with an instrumental resolution ($\lambda/2$) of 0.257 μm (laser spot size). Raman shifts of the samples were obtained as evaporated liquid films on a glass microscope slide by evaporation of water at ambient temperature (295 K), followed by analysis of different regions to ensure sample homogeneity and reproducibility. The validity of this methodology has been documented in a recent report.²² The Argon ion laser excitation wavelength was 514 nm with the following operating conditions: scan range of 3500–500 cm^{-1} , 10 mW laser power with 100 % load, objective lens of 50 \times , cosmic ray removal, 30 s detection time, and 15 accumulative scans.

6.3.3.2 ¹H Solution NMR Spectroscopy

All ¹H NMR experiments (1-D ¹H NMR, COSY, TOCSY, ROESY)^{23,24} were performed on a 3-channel Bruker Avance (DRX) spectrometer operating at a proton resonance frequency of 500.13 MHz and equipped with a temperature control unit. NMR samples were prepared in D₂O at pD ~5–6 at HDI-1/PNP mole ratios of 1:1, 1:3 and 1:5 (i.e., with respect to β-CD mole content of HDI-1 to PNP). All ¹H NMR spectra were referenced externally to tetramethylsilane (TMS, δ = 0.0 ppm) with a recycle delay (2 s) and a 90° pulse length (10 μs). For all selective pulse 1-D total correlation spectroscopy (TOCSY)^{24c,d} experiments, the spin-lock power level (8.46 dB), spin-lock time (200 ms), number of acquisitions (8), spectral width (12 ppm), and spectral data were collected with 32k data points. For all 2-D rotating-frame Overhauser effect spectroscopy (ROESY)^{24b} and selective pulse (1-D gROESY)^{24c,d} experiments, the spin-lock times were varied from 100–500 ms. The spectra were acquired with a spectral width of 12 ppm in 2k data points (2-D ROESY) and 32 k data points (1-D ROESY) with 16 scans. The spin-lock power levels for the 2-D ROESY and 1-D ROESY experiments were set to 21.33 dB. All the NMR spectra were acquired at 298 K except for variable temperature (VT) studies, where the VT was varied from 295 to 348 K. Dry nitrogen gas was used to regulate the temperature of the heating and cooling cycles, respectively.

6.3.3.3 Differential Scanning Calorimetry

Differential scanning calorimetry (DSC) of the copolymer or β-CD in the presence and absence of PNP in aqueous solution were acquired using a TA Q20 thermal analyzer with hermetically sealed pans. The copolymer or β-CD were prepared as 1% (w/w) aqueous solution in deionized water and scanned over a temperature range of 25 to 70 °C with a scan rate of 10 °C/min. Dry nitrogen gas was used to regulate the sample temperature and to purge atmospheric gases from the sample compartment.

6.3.3.4 Induced Circular Dichroism

Induced Circular dichroism (ICD) spectra of β-CD and HDI-1 in the presence and absence of PNP were recorded on a PiStar 180 spectrophotometer (Applied Photophysics) at a scan rate of 50 nm/min and a resolution of 0.1 nm. The quartz sample cell had a 10.0 mm path length and the 250–400 nm spectral region was analyzed. The spectra were recorded as an average of 30 scans

and the wavelength calibration was performed with a camphor sulphonic acid solution (0.89 mg/mL) in water ($\Delta\epsilon = 2.40 \text{ dm}^3 \text{ mol}^{-1} \text{ cm}^{-1}$ at 290.5 nm).

6.3.3.5 Dynamic Light Scattering (DLS)

The average hydrodynamic diameters of HDI-1 solution and its complexes with PNP were measured using diffusion light scattering (DLS) on a Nano-ZS (Malvern Instrument Inc.) at a scattering angle of 90° . Aqueous solutions of HDI-1 ($\leq 1\%$ w/w) and their complexes with PNP (1:1, 1:2, 1:3, and 1:5 HDI-1:PNP with respect to the HDI-1 monomer concentration) were prepared and analyzed at pH ~ 7 and variable temperature (VT) from 298–348 K (HDI-1 solution). The solution samples were filtered using Acrodisc PTFE microfilters with a pore size of $0.2 \mu\text{m}$ to eliminate dust particles from the samples. Each experiment was performed at least 15 times in triplets to obtain statistical information with minimal error.

6.4 Results and Discussion

6.4.1 Physicochemical Characterization of the HDI-1 Copolymer

Figure 6.1 illustrates the ^1H NMR spectra for HDI-1 and the respective co-monomers (HDI and β -CD) at pD ~ 6 in D_2O at 295 K. The unequivocal ^1H NMR assignments of the hexamethylene groups of the HDI-1 copolymer was established using a combination of 1-D/2-D TOCSY and COSY ^1H NMR experiments and the results are presented as supplementary data (§Appendix E). A comparison of the HDI-1 copolymer material with β -CD indicates similar ^1H NMR signatures for the β -CD monomer. The resonance lines of the permethylene ($-\text{CH}_2$) groups of HDI-1 are broadened and shifted upfield relative to the HDI monomer species (*cf.* Figure 6.1). The observed chemical shift (δ) values are attributed, in part, to the formation of the urethane linkage for the α - and β - CH_2 groups (*cf.* Scheme 6.1), hydration characteristics of HDI-1, and/or conformational preference of the polymethylene linker of HDI-1. Published spectra of related HDI copolymers do not generally show such broadened NMR lines for the permethylene linker unit, in part, because the ^1H NMR spectra are often reported in organic solvents (e.g., $\text{DMSO-}d_6$).^{21,25,26} The observed line broadening in D_2O is attributed to hydrophobic hydration phenomena^{22,27} which are known to affect the conformational preference and phase behaviour of such substituents.²⁸

The conformation of the HDI cross-linker in the HDI-1 copolymer is expected to vary relative to the unbound species. For example, the coiling of the HDI permethylene chain within the annular hydroxyl region of CD (*cf.* Scheme 6.2) is anticipated to lower the surface area and the Gibbs free energy of hydration. The CD environment is more shielding relative to the bulk aqueous solvent and thus the upfield shift of the permethylene chain of HDI-1.

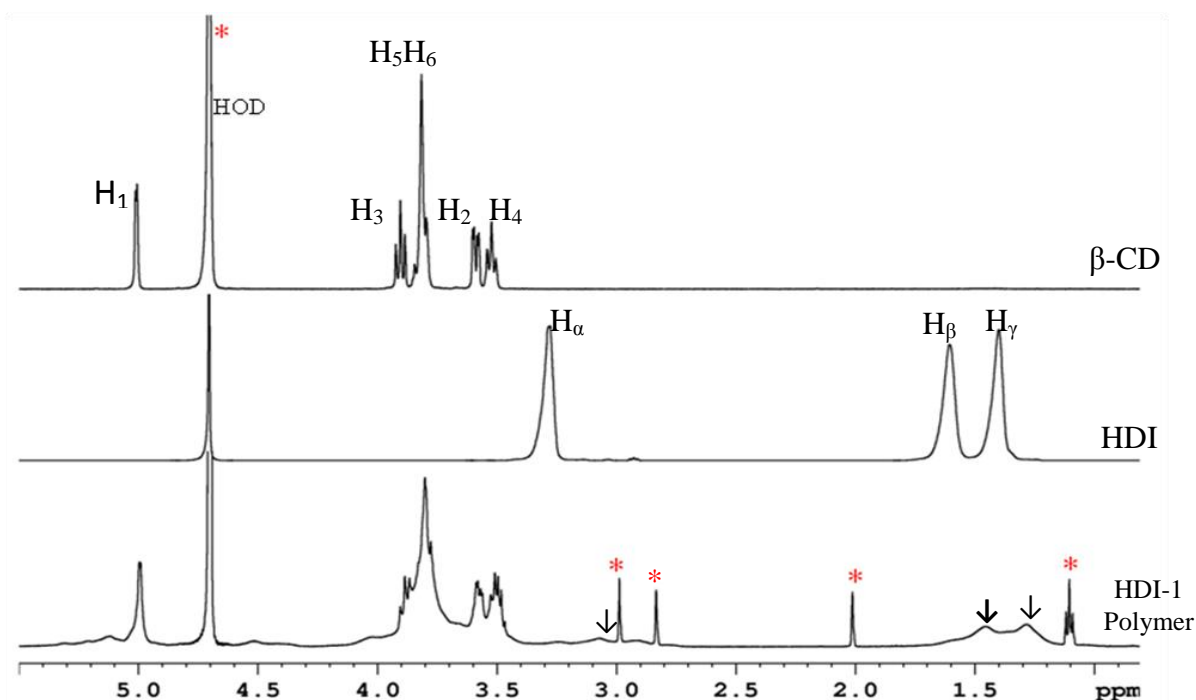
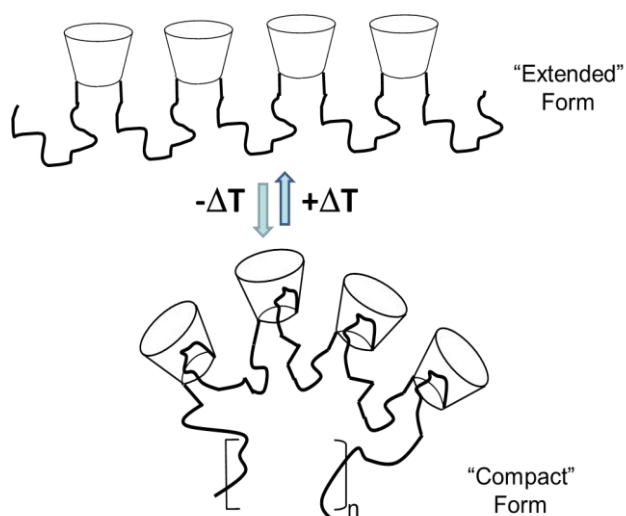


Figure 6.1 1-D ^1H NMR Spectra in D_2O at 500 MHz and 298 K; HDI-1 copolymer, HDI, and β -CD. * denotes residual solvent (i.e., DMA and ethyl ether).

To further understand the nature of the broadening of the hexamethylene resonance lines observed in Figure 6.1 for the polymer, a series of VT ^1H NMR experiments were performed at variable temperatures between 295 and 348 K, as shown in Figure 6.2a,b.

The effect of temperature on chemical shifts provides important information about the conformation of polymeric materials in solution. This is because temperature changes can affect the degree of H-bonding as well as how polymeric units aggregate in solution, and such effects can provide a source of chemical shift changes. The ^1H NMR signatures for β -CD and the hexamethylene cross-linker display continuous downfield shifts as the temperature increases (*cf.* Figure 6.2a). Upon cooling, the δ values observed in Figure 6.2a for the copolymer shift upfield and exhibit thermo-reversible changes as observed in Figure 6.2b. The copolymer solution was

further cooled to 278 K (Fig. 6.2b) and substantial broadening of the resonance lines for the permethylene unit of HDI-1 was observed. The observed line broadening and temperature effects indicate that the equilibrium process depicted in Scheme 6.2 is exothermic in nature and the hexamethylene linker undergoes substantial changes in solvation and conformation of the *n*-alkyl chain over the observed temperature conditions. The extended form of the copolymer is expected to result in deshielding effects; whereas, the compact form results in shielding effects.



Scheme 6.2 Temperature induced switching between compact (i.e., coiled) and extended (i.e., uncoiled) forms of the HDI-1 copolymer in aqueous solution at ambient pH conditions; where *n* indicates the hypothetical repeat structure of the copolymer.

Similar NMR line broadening effects were previously reported²⁷ for noncovalent complexes between β -CD and *n*-alkyl carboxylates in D₂O (*cf.* Fig. 8 in ref. 27). The NMR observations were attributed to coiling of the *n*-alkyl chain upon complex formation within the β -CD cavity. Alkylated β -CD derivatives were observed to undergo self-inclusion^{28,29} according to the nature of the alkyl substituent and its conformational motility. The structure of HDI-1 contains an average of two urethane bonds per macrocycle with the primary hydroxyl groups of β -CD, as previously reported (*cf.* Scheme 3 in ref. 12). The lipophilic contribution of two proximal hexamethylene chains in the case of HDI-1 may interact cooperatively, as compared with two isolated hexamethylene groups at opposite annular regions of β -CD. The observation that the resonance lines of the permethylene chain do not sharpen significantly over the temperature

range provides further support that hydrophobic hydration plays an important role for the processes shown in Scheme 6.2. Cooperative association (i.e., monomers→micelles→large aggregates) of oligoethylene grafted β -CD monomers was recently shown in a small-angle X-ray and light scattering study.³⁰

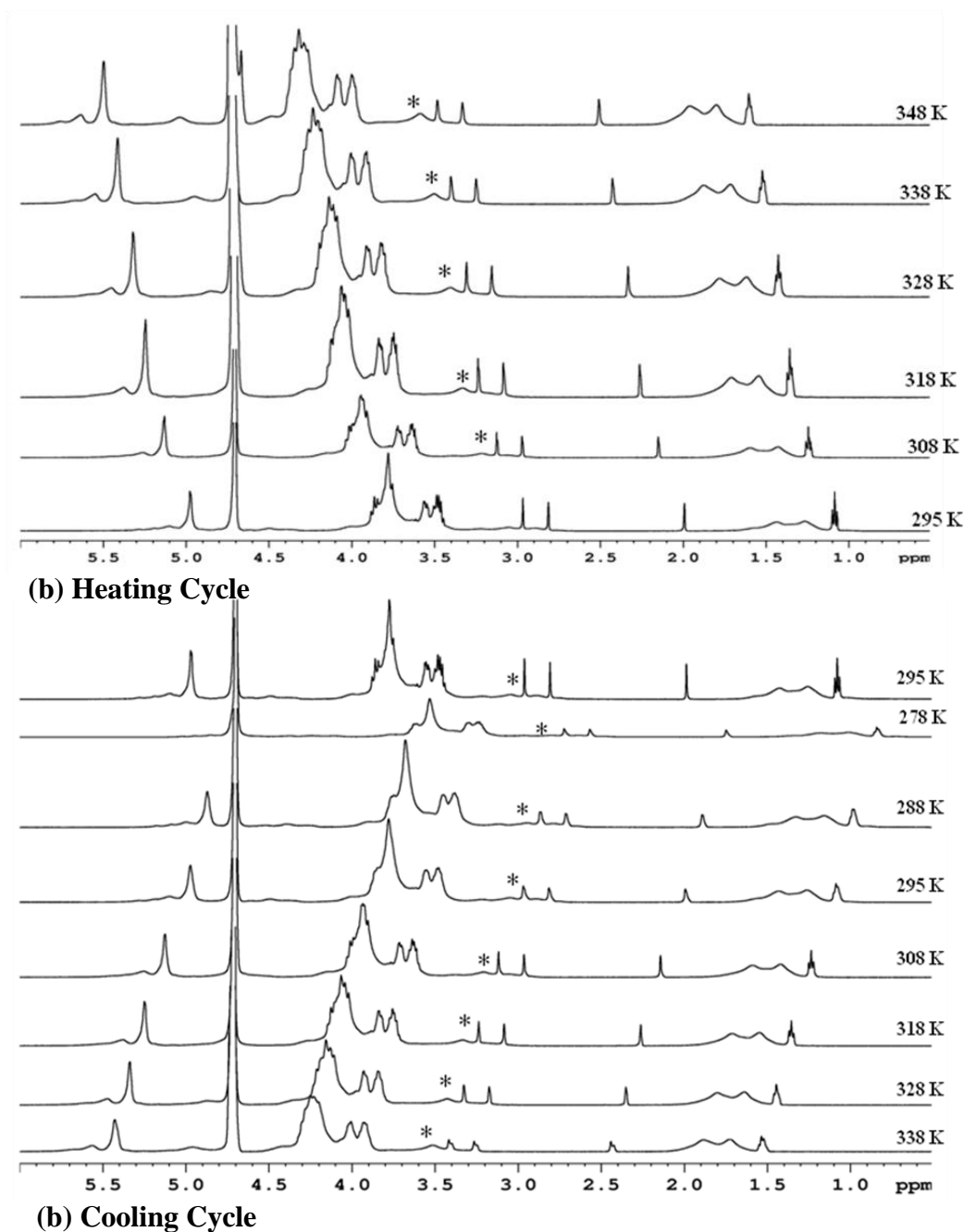


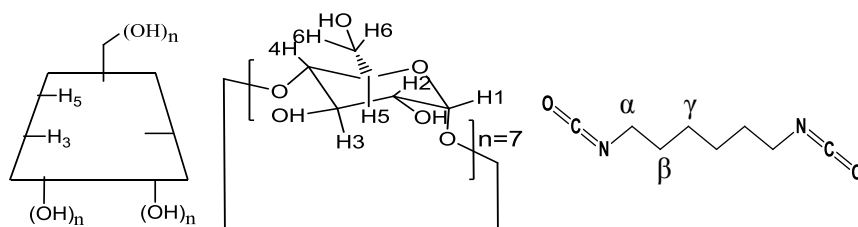
Figure 6.2 VT ^1H NMR spectra in D_2O at 500 MHz of HDI-1 without PNP in aqueous solution; (a) heating cycle, and (b) cooling cycle. The asterisk denotes residual solvent (i.e., DMA and ethyl ether).

The observed temperature effects and observed NMR chemical shift changes for HDI-1 are consistent with the partial inclusion/association of several methylene groups in the annular region of β -CD, in agreement with the results of Nozaki et al. for β -CDpNIPAAm gels.³¹ The volume of the host cavity of β -CD is sufficient to accommodate ~ 8 CH₂ groups.²⁷ The pronounced downfield/upfield δ values with increasing and decreasing temperatures are consistent with the uncoiling and coiling of the hexamethylene unit from its *compact* and *extended* states, respectively, described in Scheme 6.2. The VT induced equilibrium switching between the *compact* and *extended* forms of the HDI cross-linker units are consistent with such exothermic^{32,33} processes governed by the hydrophobic effects.³⁴

6.4.2 Physicochemical Characterization of the HDI-1/PNP Complex

6.4.2.1 2-D ROESY NMR

The inclusion properties of β -CD and the urethane copolymer (HDI-1) were studied with PNP using 2-D NMR methods to evaluate the occurrence of dipolar interactions for these host/guest systems in aqueous solution.^{35,36} Figure 6.3a,b illustrates the ¹H 2-D ROESY NMR spectra for HDI-1 and PNP at the 1:1 and 1:5 mole ratios, respectively, in aqueous solution at ambient pH (where pH < pK_a). The appearance of trace residual solvents (i.e., DMA ~ 2 – 3 ppm and diethyl ether ~ 1.1 ppm (not in scale); $\sim 2\%$ w/w) is noted in the 2-D spectra (*cf.* Figure 6.3b). The origin of these solvents has been described elsewhere²¹ and are not anticipated to interfere with the NMR measurements described herein.



Scheme 6.3 Numbering scheme for the ¹H intracavity nuclei (H₃, H₅) and external macrocycle (H₁, H₂, H₄, H₆) nuclei of β -CD, and the nuclei of hexamethylene diisocyanate (HDI).

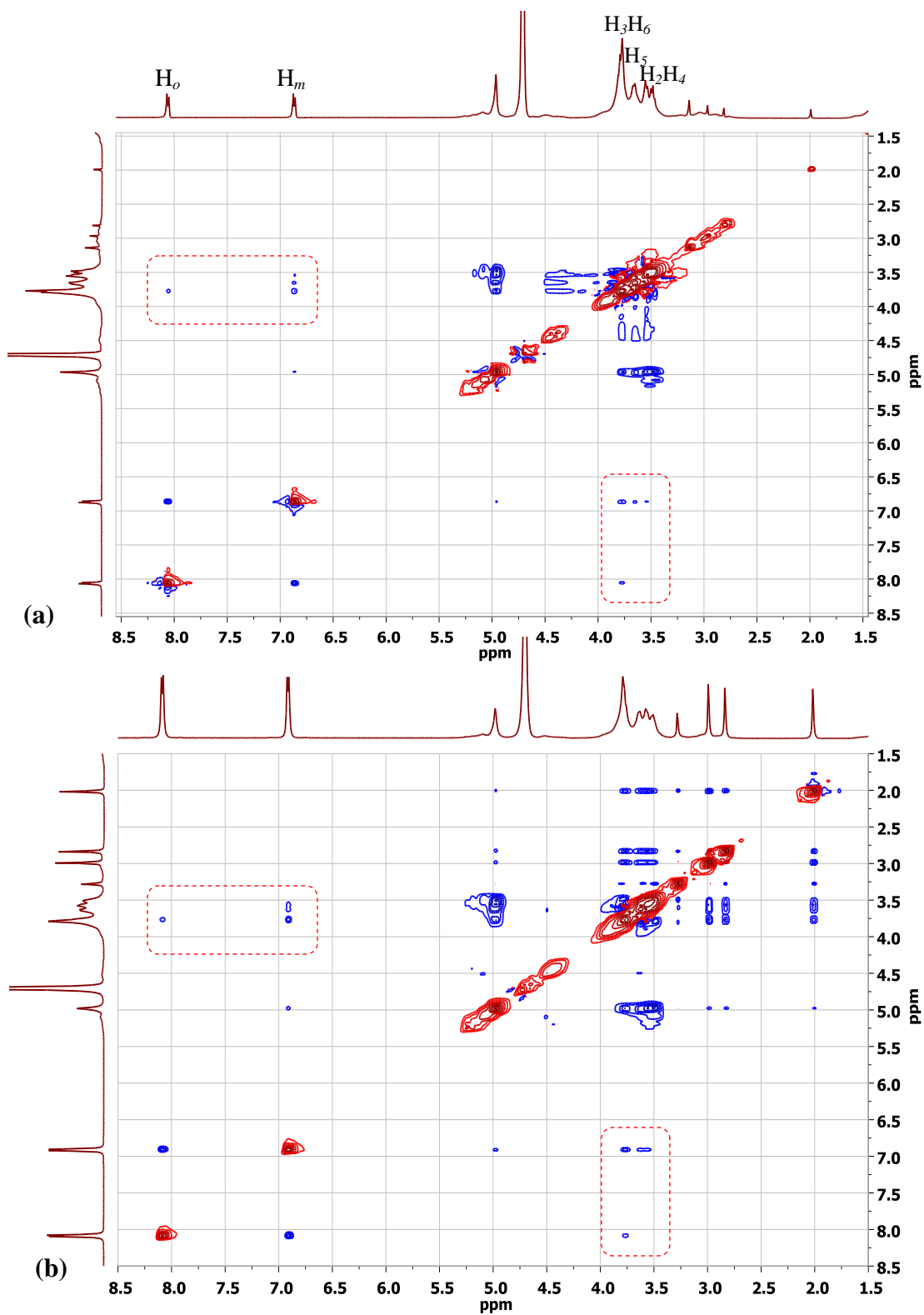
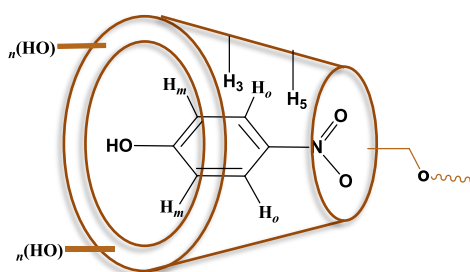


Figure 6.3 2-D ^1H NMR ROESY spectra in D_2O at 500 MHz and 298 K; (a) 1:1 HDI-1/PNP, (b) 1:5 HDI-1/PNP. β -CD/PNP correlations are shown by rectangles. The resonance region for HDI nuclei (1.5 – 1.0 ppm) is not shown in the scale.

Figure 6.3b depicts the 2-D ROESY NMR results of HDI-1 with PNP in the presence of excess guest (1:5) where the relative mole ratio is based on the β -CD content of HDI-1 relative to PNP, as described above. The results are comparable to those observed in Figure 6.3a; however, the dipolar correlations which correspond to the inclusion of PNP within the CD inclusion site (H_3 , H_5) are quite evident. The dipolar correlations are enhanced as the equilibrium fraction of bound guest species increases.



Scheme 6.4 Inclusion binding mode between β -CD inclusion site of HDI-1 with *p*-nitrophenol (PNP). The urethane bond linkage is denoted by the wavy line in the primary annular hydroxyl region. Note: The binding presentation is not drawn to scale.

In a published sorption study¹⁸ of CD-based urethane copolymers, the linker domains and β -CD inclusion sites were involved in the sorption of PNP. The linker domains were reported to play a greater role as the degree of cross linking increases for HDI-based copolymer materials (*cf.* Figure 2a in ref.18). An increase in the degree of cross linking for such materials correlates with decreased water solubility. The 2-D NMR results in solution (*cf.* Figure 6.3a,b) do not reveal any significant dipolar correlations between the ^1H nuclei of PNP ($\sim 6.8\text{-}8.0\text{ppm}$) and those of the permethylene units of HDI-1 ($\sim 1.2\text{-}1.5\text{ppm}$; not shown in scale) for these conditions. Copolymers with greater cross-link density (*i.e.*, HDI-2 and -3) are anticipated to exhibit stronger dipolar correlations with the interstitial sites (*i.e.*, linker domains); however, these materials were precluded from this study due to their low water solubility. According to Scheme 6.2, the compact form of HDI-1 may attenuate dipolar interactions between the permethylene units of HDI-1 and PNP at 295 K. The formation of a self-included complex between β -CD and the hexamethylene substituent is favored at these conditions, according to Scheme 6.2. The 2-D ROESY experiment may be subject to sensitivity limitations which results

from the observed line broadening of the ^1H NMR signatures of the permethylene unit of HDI-1.³⁶ The resulting effect is an attenuation of the measured dipolar correlations with PNP when weak NOEs occur or if the solubility of the host-guest system is limited.^{23,24,38}

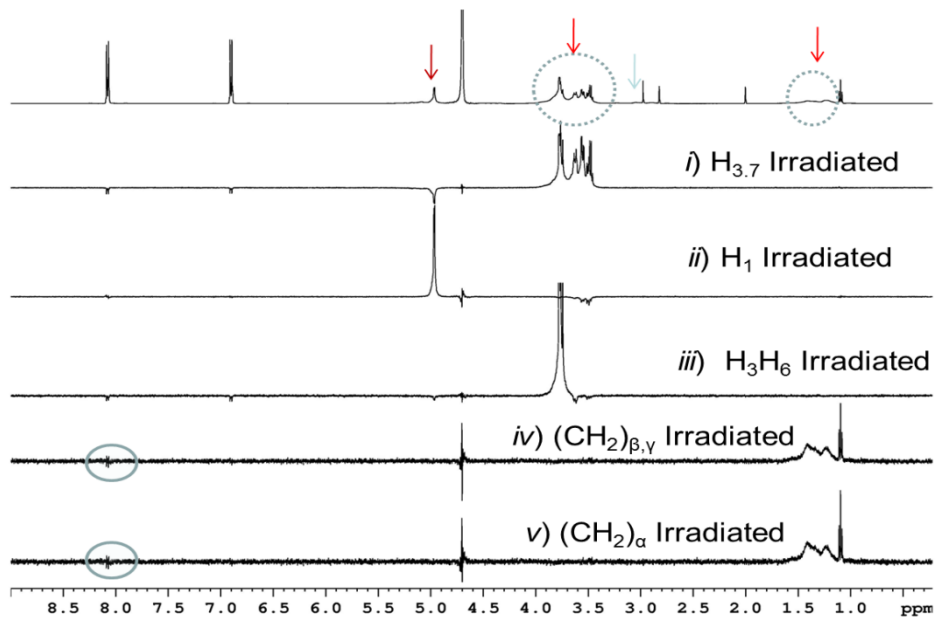
6.4.2.2 1-D Selective ROESY NMR

To enhance the sensitivity of the dipolar interactions, a series of 1-D selective ROESY NMR spectra were obtained for the HDI-1/PNP system at variable guest mole ratios (1:3 and 1:5) and VT, as illustrated in Figure 6.4a–c. The optimal spin-lock pulse was determined to be ~400 ms at 295 K for β -CD and HDI-1 copolymer, respectively. The use of 1-D ROESY was reported³⁸ to improve the reliability and sensitivity of NOEs for low abundance natural products. The ^1H nuclei of β -CD and the permethylene unit of the HDI-1 copolymer were selectively irradiated while the corresponding dipolar correlations with PNP were observed as inverted resonance signals. Noncovalent dipolar correlations were evident between the intracavity β -CD nuclei (i.e., H_3 and H_5) and PNP (*cf.* Figure 6.4a,b).

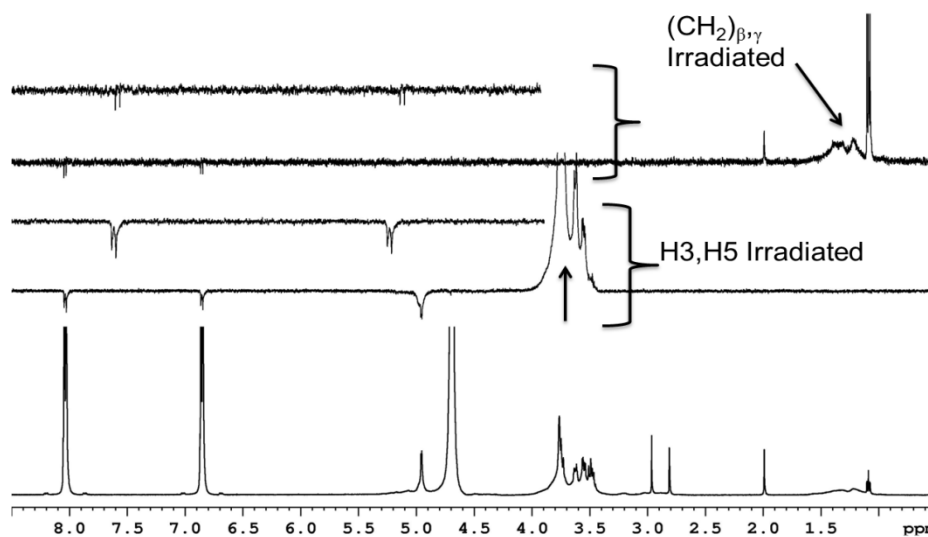
In the case of β -CD/PNP inclusion complexes, the resonance lines of PNP are influenced by irradiation of the collection of β -CD nuclei at 3.7 ppm (i.e., H_3 , H_5 , H_2 , H_4 , H_6 in Figure 6.4a-*i* and 6.4a-*iii*) denoted $\text{H}_{3,7}$; however, no such correlations were observed for the exterior (i.e., H_1) nuclei (*cf.* Figure 6.4a-*ii*). In contrast, irradiation of the nuclei of the permethylene unit of HDI-1 at 298 K (Figure 6.4a *iv,v*) revealed minor effects on the intensity of the guest (PNP) resonance lines. Similar conclusions were made from inspection of Figure 6.4b where greater (1:5) HDI-1/PNP mole ratio shows slightly enhanced correlations between the *ortho* and *meta* protons of PNP with the β -CD cavity nuclei and with the permethylene domains of the linker unit, respectively.

The interaction of the HDI-1 framework with PNP is affected by increased mole ratio of the guest and temperature-induced conformational changes of the HDI-1 copolymer. In Figure 6.4c, the effect of temperature on the conformational changes of the HDI-1 copolymer is shown. The COSY-type peaks in Figure 6.4a for the HDI-1/PNP interactions have been reduced in Figure 6.4b,c while the contrary is observed for the β -CD/PNP interactions when the $\text{H}_{3,7}$ is irradiated (*cf.* Figure 6.4c). Furrer et al³⁸ attributed these COSY-type peaks in 1-D selective ROESY spectra to non-dephased coherence from other unwanted nuclei. The enhanced correlations observed in Figure 6.4b are understood according to the greater equilibrium fraction

of bound guest at these conditions. In Figure 6.4c, it is interesting to note that the intensity of the dipolar correlations between PNP and the β -CD cavity interior are attenuated as temperature increases. In contrast, the dipolar correlations between PNP and the permethylene domains (i.e., $(\text{CH}_2)_{\beta,\gamma}$) of the linker unit are slightly increased from 298 to 323 K. The latter is understood in terms of the greater number of linker methylene sites as the chain uncoils with increasing temperature, as described by Scheme 6.2.



(a)



(b)

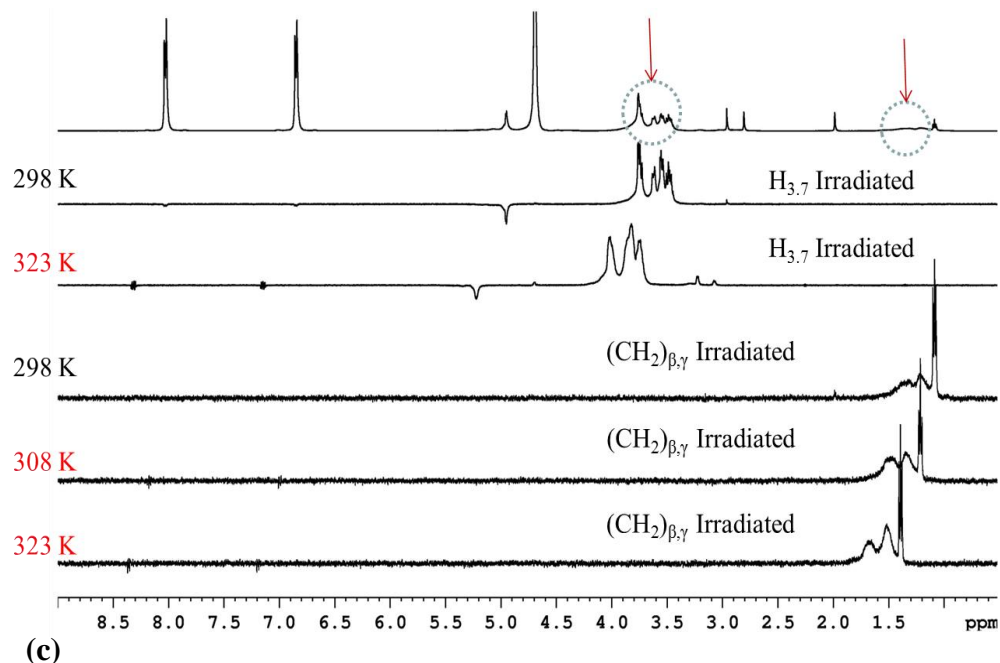
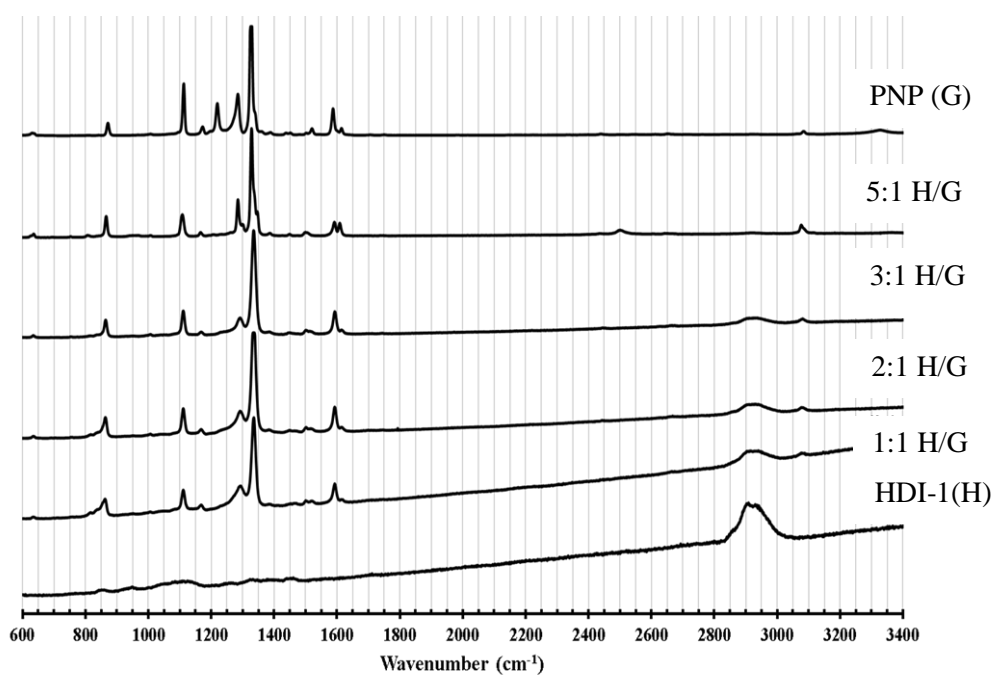


Figure 6.4 1-D ^1H NMR ROESY spectra in D_2O at 500 MHz for HDI-1/PNP complexes at various host/guest ratios and a spin-lock time of 400 ms; (a) 1:3 HDI-1/PNP at 298 K; where the following nuclei were irradiated: *i*) $\text{H}_{3,7}$, *ii*) H_1 , *iii*) H_3 and H_6 , *iv*) $(\text{CH}_2)_{\beta,\gamma}$, *v*) $(\text{CH}_2)_{\beta,\gamma}$, and (b) 1:5 HDI-1/PNP at 298 K; where the following nuclei were irradiated: $\text{H}_{3,7}$ and $(\text{CH}_2)_{\beta,\gamma}$ (enlarged spectra are also shown), and (c) 1:5 HDI-1/PNP at VT; where the following nuclei were irradiated: $\text{H}_{3,7}$ and $(\text{CH}_2)_{\beta,\gamma}$.

6.4.2.3 Raman Spectroscopy

The presence of various types of functional groups (e.g., $-\text{OH}$, $-\text{NO}_2$, C-H , C=C , C-O , etc.) offers an opportunity to investigate the spectroscopic signatures of the interactions between HDI-1 and PNP.³⁹⁻⁴¹ Figure 6.5a illustrates the Raman spectra for the host (i.e., HDI-1), guest (i.e., crystalline PNP), and the respective host/guest mole ratios (1:1 to 1:5) copolymer/PNP mixtures. The expanded Raman spectra are shown in Figures 6.5b and c. Table 6.1 lists the main Raman bands observed in Figure 6.5. The spectra for HDI-1 were recorded as air-dried films on glass slides; whereas, PNP was analyzed in its crystalline powder form. The Raman spectrum of pure PNP (*cf.* Fig. 6.5a) is comparable to that of PNP in aqueous solution reported by Ni et al.⁴¹ The spectral lines for pure PNP are relatively sharp in contrast to the Raman signatures for HDI-1 which display relatively broad bands (*cf.* Fig. 6.5a). In general, the Raman shifts for PNP in the presence of HDI-1 are relatively small ($\Delta\nu \leq 10 \text{ cm}^{-1}$; *cf.* Table 6.1); whereas the line

broadening for certain Raman signatures (i.e., bands 1,2,4-7; *cf.* Expanded spectra in Fig. 6.5b,c) of PNP in the complexes are more pronounced relative to pure PNP in its crystalline form. The Raman frequency shifts and the appearance of broader spectral lines are attributed to differences in the molecular environment of PNP in its bound state (i.e., inclusion sites and linker domains) within the HDI-1 copolymer.⁴²⁻⁴⁵ The polarizability characteristics of bulk solution and the copolymer are different which contribute to small Raman shifts and relatively large intensity variations in accordance with variable hydration and microenvironment.⁴⁶⁻⁴⁹



(a)

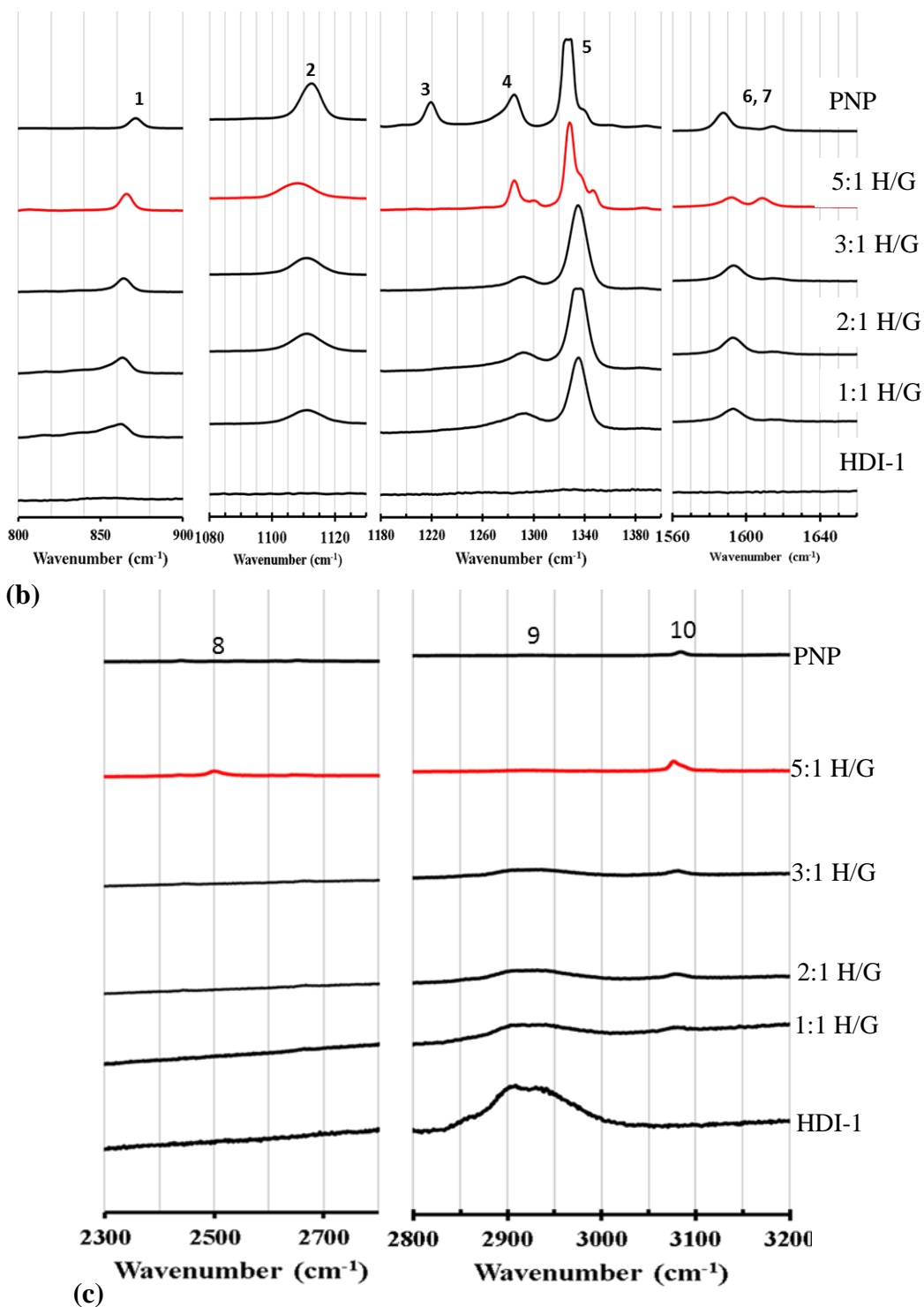


Figure 6.5 Raman spectra of solution evaporated films at 295 K for HDI-1 (Host), and PNP (Guest) and the 1:1, 1:2, 1:3, and 1:5 HDI-1/PNP (H/G) complexes. (a) Full spectral region (600–3400 cm⁻¹), (b) Expanded spectral region (800–1640 cm⁻¹), and (c) Expanded spectral region (2300–3200 cm⁻¹).

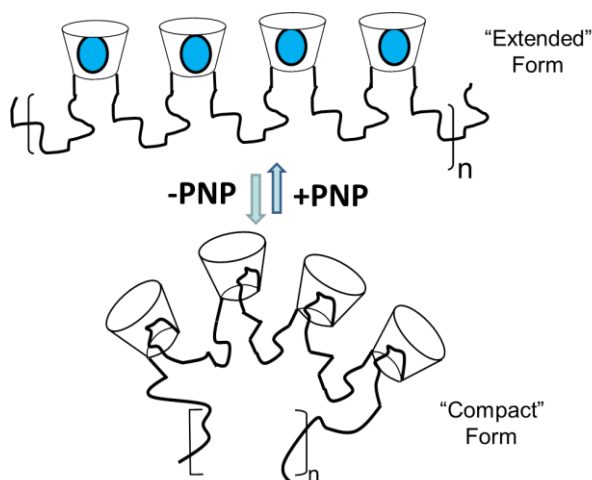
Table 6.1 Raman Shift Data for the Host and Guest Raman Bands (1-9) for HDI-1/PNP Complexes at Various Mole Ratios (1:1 to 1:5) and Crystalline PNP at 295 K.

Bands	1	2	3	4	5	6,7	8	9	10
HDI-1/PNP	$\nu_s(\text{C-C})$	$\nu_s(-\text{NO}_2)$	$\nu_s(-\text{NO}_2)$	$\nu_s(\text{C-O})$	ν_s	$\nu(-\text{C}=\text{C})$		$\nu(-\text{CH}_2)$	$\nu(=\text{C-H})$
Ratios		$\delta(\text{-CH})$			$-\text{C}(\text{NO}_2)$	$\delta(\text{C-N})$			
HDI	-	-	-		-	-	*	2896	-
1:1	862	1112	-	1288	1334	1592, 1612	*	2901	3074
1:2	863	1112	-	1288	1334	1592, 1612	*	2901	3075
1:3	865	1112	-	1288	1334	1592, 1612	*	2901	3074
				1282,			2485,		
1:5	867	1108	-	1297	1328**	1591, 1606	*	2901*	3072
		1113							
	871	(1167) ¹		1282		1585, 1612			3078
PNP	(850) ¹	(1117) ¹	1215	(1284) ¹	1326*	(1586) ²	-	-	(3084) ²

(-) No Signal, (*) Broad signal, ¹Ref 41, ²Ref 50

Raman spectroscopy has been successfully applied to the study of noncovalent host-guest complexes.⁵⁰⁻⁵⁸ Recently, Choi et al.⁵⁰ examined the Raman spectra of freeze dried complexes formed between α -CD, β -CD, and modified β -CD with *o*-, *m*-, and *p*-nitrophenol, respectively. Despite the limited quantitative analyses of the results, the authors concluded that small Raman shifts (i.e., $\leq 6 \text{ cm}^{-1}$) were observed for the phenyl C=C and C-H stretching bands of the nitrophenol guests. Sardo et al.⁵⁸ reported *ab initio* calculations in their Raman study of α -, β -, and γ -CD with methylated phenols. They concluded that the guest Raman bands could be attributed to bound and unbound species, respectively (*cf.* Table 3 in ref. 58). DFT calculations of the Raman intensity and normal mode analysis of the β -CD/permethrin system provided information on the structure of the host-guest complex, as reported by Li et al.⁵⁷ Witlicki et al.⁵⁶

demonstrated that a thorough quantitative analysis of the Raman intensity variations of the cyclobis(paraquat-*p*-phenylene)/tetrathiafulvalene system provided binding constants in good agreement with independent estimates obtained from UV-Vis-NIR titrations.

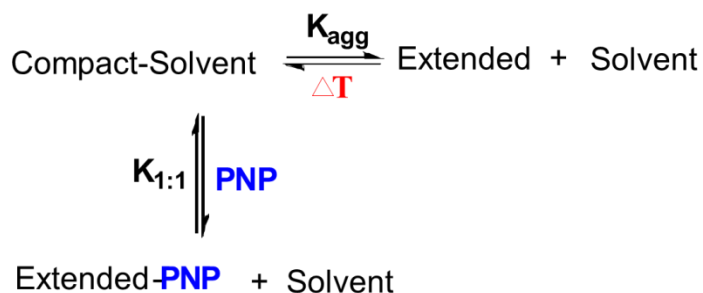


Scheme 6.5 Guest-induced switching between compact (i.e., coiled) and extended (i.e., uncoiled) forms of the HDI-1 copolymer in aqueous solution at ambient pH conditions; where ovals represent the guest (PNP). The compact form may involve self-inclusion of the linker unit. The repeat structure of the copolymer is represented by *n*.

The guest Raman signatures for the HDI-1/PNP systems reported herein reveal some interesting features that vary over the range of the host-guest mole ratios investigated (1:1 to 1:5). A notable feature in Figure 6.5a,b is the appearance of a new Raman signature $\sim 1610\text{ cm}^{-1}$ (bands 6, 7) where its intensity increases as the relative amount of PNP increases (*cf.* Expanded region; Figure 6.5b). This band corresponds to an enhancement of one of the skeletal bands of (C=C) of copolymer bound PNP.⁴⁶ At the lower 1:1 PNP mole ratios, the ring breathing (band 1), sym. NO₂ (band 2 and 5), C-O (band 4), C-C (band 6), and C-H stretching (band 9) for PNP are slightly shifted and broadened significantly (*cf.* Table 6.1). In particular, bands 2, 4, 7, and 10 appear significantly broader relative to pure crystalline PNP (*cf.* Figure 6.5a–c). The broader vibrational bands of complexed PNP in addition to the intensity variations indicate that the guest is in a distribution of bound and unbound environments. The results of Witlicki et al.⁵⁶ for the cyclobis(paraquat-*p*-phenylene)/tetrathiafulvalene similarly illustrate that substantial intensity changes of specific Raman bands occur upon complex formation.⁵⁶ Comparable results were

reported for PNP which further supports that noncovalent complexes are formed with β -CD and HDI-1, respectively.⁵⁰ As the copolymer/PNP mole ratio increases from 1:1 to 1:5, the resonance lines sharpen and resemble those of crystalline PNP arising from the greater contribution of unbound PNP at these conditions.

HDI-1 polymer adopts a linear morphology as described by the extended form illustrated in Schemes 6.2 and 6.5, with increasing temperature and relative guest concentration.^{59,60} The linear topology of the HDI-1 copolymer is a consequence of the cross linking at the primary hydroxyl groups at the narrow side of the β -CD annulus (*cf.* Scheme 6.3). The hexamethylene cross linker units are lipophilic in nature and the accessibility of the β -CD inclusion sites depend on the hydration state and the equilibrium state between the compact and extended forms (*cf.* Scheme 6.2) of the HDI-1 copolymer. We hypothesize that the preparation of air-dried films for Raman analysis (*cf.* §6.3.3.1) may bias the conformational preference of the linker unit for HDI-1 and its complexes to a pseudo-compact form. In contrast, the topology of HDI-1 and its complexes are anticipated to be more closely described by the coupled equilibria illustrated in Scheme 6.6 because of the presence of solvent, guest, and the accompanying effects of temperature on the position of equilibrium.



Scheme 6.6 Equilibrium switching between *compact* and *extended* forms of HDI-1, according to temperature and the presence of guest (PNP).

6.4.2.4 Induced Circular Dichroism (ICD)

Induced circular dichroism (ICD) has been widely used for the study of cyclodextrin inclusion complexes.^{61,62} The magnitude of the ICD effect is reflected by the amount of elliptical polarized light generated upon inclusion of an achiral guest within the cavity of β -CD. Figure 6.6a,b illustrates the ICD spectra in aqueous solution at pH ~6 for the titration of β -CD and

HDI-1 with PNP, respectively. The ICD spectra are plotted as ellipticity (θ ; degrees) against wavelength (nm). In the case of β -CD with no added guest, no apparent ICD is observed in the 250–400 nm region. The addition of incremental amounts of PNP gives rise to an ICD band centered \sim 320 nm and its intensity increases as the guest concentration increases up to the 1:5 β -CD/PNP mole ratio. The maximum ICD intensity corresponds to the greatest fraction of bound β -CD and provides unequivocal support of the formation of a host-guest inclusion complex. Mendicuti and González-Álvarez⁶² have quantitatively investigated the ICD spectra for complex formation between naphthyl guests and β -CD, and binding constants were estimated by analyzing the ellipticity values against increasing guest concentration.

The ICD spectra for the HDI-1 copolymer in aqueous solution with variable concentration of PNP are shown in Figure 6.6b for similar conditions described in Figure 6.6a. An ICD band centered \sim 320 nm is observed as the guest concentration increases in a similar fashion as that observed for the β -CD/PNP system. However, the highest mole ratio (\sim 1:5 HDI-1/PNP) examined yields a lower ellipticity relative to the β -CD/PNP system. The observed attenuation of the ICD band for the copolymer is attributed to competitive binding in the interstitial domains of the permethylene region of HDI-1. These secondary binding sites of HDI-1 result in a reduction of the inclusion bound PNP. The ICD results in Figure 6.6b provide strong support that inclusion complexes are formed between β -CD and its copolymer with PNP. However, it should be noted that secondary binding interactions between PNP and the linker sites of HDI-1 are supported from the ICD results, in addition to previously reported¹⁸ thermodynamic parameters for this system.

The ICD, NMR and Raman presented above for β -CD and HDI-1 provide unequivocal support for the formation of inclusion complexes for β -CD and HDI-1 with PNP, respectively. As well, NMR and Raman results indicate that PNP may be bound onto the linker domains and the β -CD inclusion sites of the HDI-1 copolymer framework. The binding affinity for HDI-1/PNP ($K_{eq} \sim 10^2 \text{ M}^{-1}$; pH =10.5) is similar to the 1:1 β -CD/PNP complex in aqueous solution at 295 K. In contrast, the attenuated binding affinity ($K_{eq} < 10^1 \text{ M}^{-1}$; pH 4.6) observed for HDI-1 is attributed to steric effects of the inclusion sites due to its *compact* form (*cf.* Schemes 6.2 and 6.5) and the competitive binding equilibria with the interstitial sites (i.e., permethylene linker domains) of HDI-1.

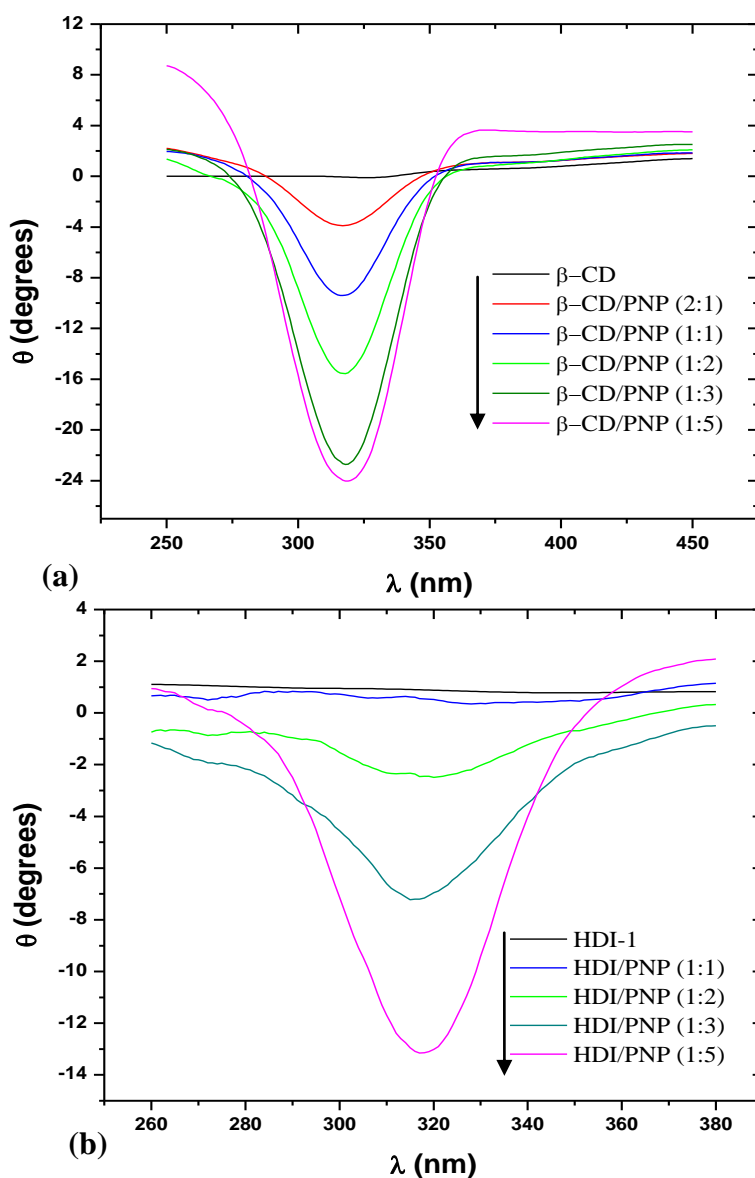


Figure 6.6 ICD spectra of host-guest complexes in aqueous solution; (a) β -CD/PNP at various host-guest mole ratio, and (b) HDI-1/PNP at variable host-guest ratios and 295 K.

6.4.2.5 DSC

Figure 6.7 illustrates DSC results for β -CD, HDI-1, and HDI-1/PNP complexes at variable mole ratios in aqueous solution at pH 6 over the temperature range 20 to 70°C. The occurrence of several weak endotherm peaks for β -CD provides evidence of hydration processes of the macrocycle over this temperature range.³⁴ The results in Figure 6.7 agree with the DSC transitions observed with α -CD for related hydration processes of the intracavity and external macrocycle sites.⁶² Similar DSC plots are observed for HDI-1 and HDI-1/PNP systems;

however, a unique endotherm is evident for the copolymer ~ 54 °C which is not observed for the HDI-1/PNP systems.

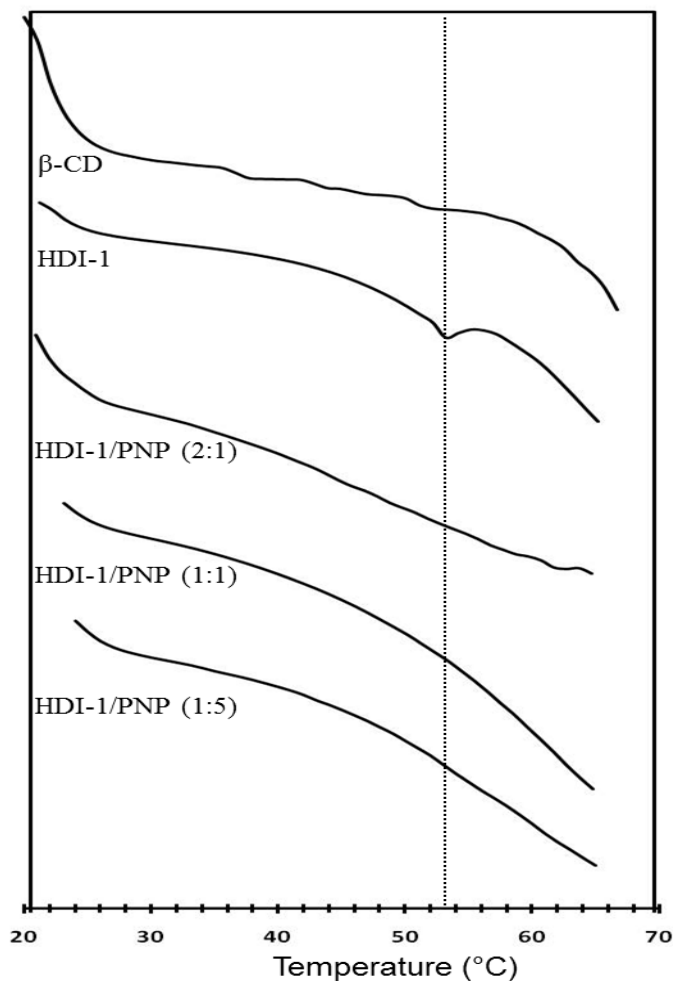


Figure 6.7 DSC results of β -CD, HDI-1, and HDI-1/PNP mixtures in aqueous solution from 20 to 70 °C. The dashed line is provided as a guide.

The results in Figure 6.7 agree with the DSC transitions observed with α -CD for related hydration processes of the intracavity and external macrocycle sites.⁶² Similar DSC plots are observed for HDI-1 and HDI-1/PNP systems; however, a unique endotherm is evident for the copolymer ~ 54 °C which is not observed for the HDI-1/PNP systems. A comparison of the HDI-1/PNP complexes (1:1 to 1:5) reveals the absence of the endotherm transition at ~ 54 °C. The endotherm for HDI-1 is attributed to the guest induced equilibrium switching between the compact and extended forms of the copolymer^{64,65} (*cf.* Scheme 6.5). Hu et al.⁶³ observed a similar reversible temperature-induced swelling for a urethane copolymer-based hydrogel using

DSC, as compared with results for HDI-1 in Figure 6.7. Similarly, hydrogel nanoparticles of hydrophobized pullulan have been observed to undergo thermal transition with refolding of carbonic anhydrase B in aqueous solution.⁶⁴ Comparable phase transitions were observed over a wide temperature range (28 to 40 °C) by Xie and Hsieh for poly(N-isopropylacrylamide) composite hydrogels containing cellulose.⁶⁵ The absence of the endothermic transition for the HDI-1/PNP complexes is related to the favoured *extended* form of the hexamethylene linkers when complexed with PNP (*cf.* Schemes 6.5 and 6.6). In the bound state, the changes in hydration in the annular hydroxyl region of β -CD favor the *extended* form of the copolymer and this may be related to intermolecular H-bonding interactions between PNP and the urethane linkage in the interstitial region. Thermo-gelling copolymers containing methylated β -CD grafted onto PPG and PEG reveal glass transition temperatures (~42–43 °C) where a reversible transition occurs from clear sol \rightarrow gel \rightarrow turbid sol over a similar temperature range (~22–55 °C).⁶⁶ A related thermo-reversible expansion/contraction was observed between 20–40 °C for gold nanoparticles with an elastin-like polymer coating.⁶⁷ The thermodynamics of solvation for HDI-1 and the formation of a supramolecular complex with PNP result in substantive hydration changes of the copolymer which affects the preferred conformation of the cross linker domains.

6.4.2.6 Dynamic Light Scattering (DLS)

The DLS technique has successfully been used to study protein folding conformation by monitoring changes in the hydrodynamic radius (R_H).^{68,69} The DLS of the HDI-1 copolymer in aqueous solution was acquired as a function of variable temperature (Figure 6.8a) and relative PNP mole fraction (Figure 6.8b), respectively, and both experiments indicated significant changes in hydrodynamic diameters (D_H). In Figure 6.8a, the VT-DLS experiment resulted in the change of D_H from ~105 nm at 298 K to ~170 nm at 348 K. Similarly, an increase in D_H (~100 to 200 nm) was recorded as HDI-1 copolymer was complexed with incremental amounts of PNP (Figure 6.8b). Galantini et al.⁷⁰ reported a DLS study of branched host-guest supramolecular dimmers/trimers based on β -CD and adamantane. The recorded hydrodynamic radii (≤ 10 nm) increased with increase in concentration/molecular weight of the polymer and the authors related this trend to the formation of elongated structures. In the case of polymer inclusion complexes (PICs), DLS has been shown to give columnar-type associates with large hydrodynamic radii of about 100–200 nm.^{71,72}

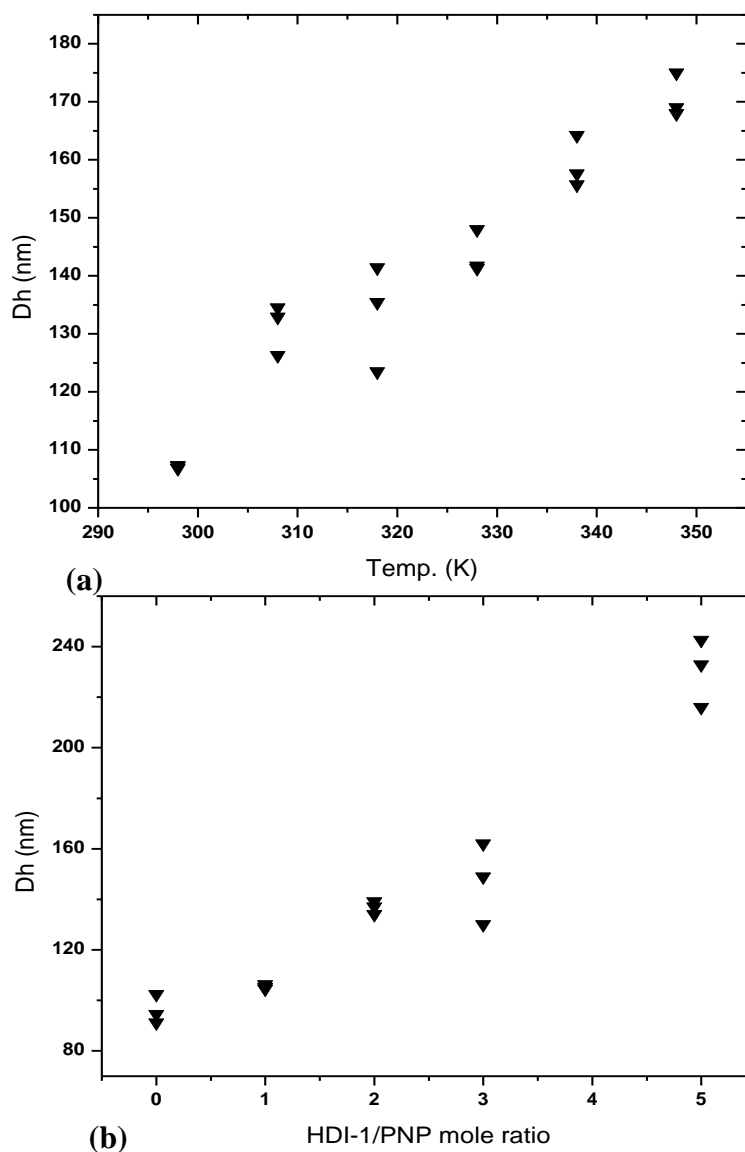


Figure 6.8 DLS results recorded as change in hydrodynamic diameter of HDI-1 copolymer with (a) temperature (298 to 348 K), and (b) relative PNP mole ratio (the x-axis in Figure 8b represents moles PNP per 1 mole HDI-1 monomer, where zero means absence of PNP).

The temperature dependence of hydrodynamic diameters in polymer materials is not straightforward to interpret since other phenomena (e.g., dehydration, micellization and aggregation) tend to dominate at certain polymer concentrations.⁷³⁻⁷⁵ However, a low concentration (<1 % w/w) of the polymer solution was used in this study. The increase in the hydrodynamic diameter of the HDI-1 copolymer in Figure 6.8 may be explained in terms of the

unwinding of the polymer chains due to temperature change and the inclusion of PNP guest⁷⁵ within the polymer chain. We hypothesize that PNP displaces the self-included linker chains from the β -CD cavity resulting in elongated structures as described in the VT study above. Other interesting observation from the DLS-VT study is the polydispersity index (PDI) which can be used to define the order-disorder phase transition in polymeric materials.⁷⁶ The lowest PDI value for the 1 % HDI-1 solution was obtained at 55 °C (0.34) and is consistent with the solution DSC which shows a transition around the same temperature range for the HDI-1 copolymer.

The formation of well-defined inclusion complexes is supported by the ¹H NMR (1-D and 2-D) and Raman spectroscopy, ICD, and DSC results, as described above. The reversible switching between *compact* and *extended* forms of the copolymer are supported according to the observed temperature effects and guest (i.e., PNP) concentration effects described by Schemes 6.2 and 6.5. In view of the substantial hydration and volumetric changes between the HDI-1 copolymer in its *compact* vs *extended* forms, the changes in hydration are consistent with a recent structural study of swelling phenomena of dextran-based hydrogels reported by Ferreira et al.⁷⁷ The textural and morphology properties of hydrogels in their hydrated and dry states are in good agreement with the well-established equilibrium swelling theory of Flory-Rehner,⁷⁸ and provide a theoretical framework for the further understanding of the “*Molecular Accordion*” behaviour observed for the HDI-1 urethane copolymer investigated in this study.

6.5 Conclusions

A urethane copolymer formed by the reaction of β -CD and hexamethylene diisocyanate at the 1:1 mole ratio (HDI-1) was investigated using ¹H NMR spectroscopy, Raman spectroscopy, ICD spectroscopy, and DSC in aqueous solution. Evidence of inclusion binding is supported by dipolar interactions between PNP and the β -CD inclusion sites of the HDI-1 copolymer according to ¹H ROESY NMR, Raman spectroscopy, ICD, and DSC.

Noncovalent interactions between HDI-1 and PNP occur primarily with the β -CD inclusion sites and secondarily with the hexamethylene linker domains at higher guest concentration and ambient temperature. The solution NMR structure of HDI-1 in the absence of guest was observed to adopt an *extended* or *compact* form at high vs low temperatures, respectively. The ambient temperature *compact* form of HDI-1 may be switched to the *extended*

conformation in the presence of PNP (*cf.* Scheme 6.5). The *compact* form of HDI-1 involves self-inclusion of the permethylene units in the annular hydroxyl region of β -CD (*cf.* Scheme 6.2).

The thermo- and chemo-reversible switching between the *compact* and *extended* forms of the hexamethylene unit of HDI-1 is herein referred to as a “*Molecular Accordion*”,⁷⁹ as illustrated by Schemes 6.2 and 6.5, respectively. The equilibrium switching of the HDI-1 “*Molecular Accordion*” is attributed to molecular recognition and hydrophobic hydration effects.^{30,34} Macrocyclic urethane copolymers of this type represent an emerging class of “*smart*” or “*functional*” supramolecular materials with improved solid phase extraction (SPE) and molecular recognition properties for numerous applications as sensors and in chemical separations.

6.6 Acknowledgements

The authors are grateful for the support provided by the Natural Sciences and Engineering Research Council (NSERC) and the University of Saskatchewan for support of this research. LDW wishes to acknowledge Natasha Dreaver for editorial assistance and M. H. Mohamed for provision of a research sample of HDI-1.

6.7 References

- (1) S. Polarz, S.; Antonietti, M. *Chem. Commun.* **2002**, 2593–2604.
- (2) Bender, M.L.; Komiyama, M. In *Cyclodextrin Chemistry*. Springer-Verlag.: Berlin, Heidelberg, New York, **1978**.
- (3) Steed, J.W.; Atwood, J.L. In *Supramolecular Chemistry*, 2nd ed.; John Wiley & Sons, Ltd.: West Sussex, UK, **2009**.
- (4) Asouhidou, D.D.; Triantafyllidis, K.S.; Lazaridis, N.K.; Matis, K.A. *Colloids Surf. A* **2009**, *346*, 83–90.
- (5) Chen, G.; Jiang, M. *Chem. Soc. Rev.* **2011**, *40*, 2254–2266.
- (6) (a) Soldatov, D.V. *J. Inclusion Phenom. Macrocyclic Chem.* **2004**, *48*, 3–9; (b) Rodríguez-Cabello, J. C.; Prieto, S.; Reguera, J.; Arias, F. J.; Ribiero, A. *J. Biomater. Sci. Polymer Edn.* **2007**, *18*(3), 269–286; (c) Aguilar, M. R.; Elvira, C.; Gallardo, A.; Vázquez, B.; Román, J. S. *Smart Polymers and Their Applications as Biomaterials, Topics in Tissue Engineering*, Vol. 3, **2007**, Eds. N Ashammakhi, R Reis & E Chiellini, Ch. 6, pp. 1–27.

- (7) Gao, J. H.; Gu, H. W.; Xu, B. *Acc. Chem. Res.* **2009**, *42*(8), 1097–1107.
- (8) Kopeček, J. *Biomaterials* **2007**, *28*, 5185–5192.
- (9) Crini, G. *Prog. Polym. Sci.* **2005**, *30*, 38–70.
- (10) Wenz, G. *Angew. Chem. Int. Ed. Engl.* **1994**, *33*, 803–822.
- (11) Yu, J. C.; Jiang, Z. -T.; Liu, H. -Y.; Yu, J.; Zhang, L. *Anal. Chim. Acta* **2003**, *477*(1), 93–101.
- (12) Mohamed, M. H.; Wilson, L.D.; Headley, J. V. *Carbohydr. Polym.* **2010**, *80*, 186–196.
- (13) Wilson, L.D.; Mohamed, M.H.; Headley, J.V. *Colloid Interface Sci. J.* **2011**, *357*, 215–222.
- (14) van de Manakker, F.; Vermonden, T.; van Nostrum, C.F.; Hennink, W.E. *BioMacromol.* **2009**, *10*, 3157–3175.
- (15) Ma, M.; Li, D. *Chem. Mater.* **1999**, *11*(4), 872–874.
- (16) Eftink, M. R.; Harrison, J. C. *Bioorg. Chem.* **1981**, *10*(4), 388–398.
- (17) Silva, O. F.; Fernández, M. A.; Pennie, S. L.; Gil, R. R.; de Rossi, R. H. *Langmuir* **2008**, *24*, 3718–3726.
- (18) Mohamed, M. H.; Wilson, L. D.; Headley, J. V.; Peru, K. M. *J. Colloid Interface Sci.* **2011**, *356*, 217–226.
- (19) García-Zubiri, I. X.; González-Gaitano, G.; Isasi, J. R. *J. Colloid Interface Sci.* **2009**, *337*(1), 11–18.
- (20) Pratt, D. Y.; Wilson, L. D.; Kozinski, J. A.; Morhart, A. M. *J. Appl. Polym. Sci.* **2010**, *116*, 2982–2989.
- (21) Mohamed, M. H.; Wilson, L. D.; Headley, J. V. *Carbohydr. Res.* **2011**, *364*, 219–229.
- (22) Rabolt, J. F.; Schlotter, N. E.; Swalen, J. D. *J. Phys. Chem.* **1981**, *85*, 4141–4141.
- (23) Berger, S.; Braun, S. In *200 and More NMR Experiments: A Practical Course*, Wiley-VCH: Weinheim, **2004**.
- (24) (a) Braunschweiler, L.; Ernst, R. R. *J. Mag. Res. Chem.* **1983**, *53*, 521–528; (b) Bax, A.; Davis, D. G. *J. Mag. Res. Chem.* **1985**, *65*, 355–360; (c) Bauer, C. J.; Freeman, R.; Frenkiel, T.; Keeler, J.; Shaka, A. J. *J. Mag. Res. Chem.* **1984**, *58*, 442–457; (d) Kessler, H.; Oschkihat, H.; Griesinger, C.; Bermel, W. *J. Mag. Res. Chem.* **1986**, *70*, 106–133.
- (25) Gerbaud, G.; Hediger, S.; Gadella, A.; Bardet, M. *Carbohydr. Polym.* **2008**, *73*, 64–73.
- (26) Yamaguchi, I.; Takenaka, Y.; Osakada, K.; Yamamoto, T. *Macromolecules* **1999**, *32*, 2051–2054.

- (27) Wilson, L. D.; Verrall, R. E. *Can. J. Chem.* **1998**, *76*, 25–34.
- (28) Memişgoğlu-Bilensoy, E.; Hincal, A. A.; Bochot, A.; Trichard, L.; Duchene, D. In *Microencapsulation - Methods and Industrial Applications*, 2nd ed.; Benita, S., Ed.; Taylor & Francis Group: Boca Raton, Florida, **2006**; Vol. 158, p 269–295.
- (29) Han, Y.; Cheng, K.; Simon, K.A.; Lan, Y.; Sejwal, P.; Luk, Y. *J. Am. Chem. Soc.* **2006**, *128*, 13913–13920.
- (30) Lombardo, D.; Longo, A.; Darcy, R.; Mazzaglia, A. *Langmuir* **2004**, *20*, 1057–1064.
- (31) Nozaki, T.; Maeda, Y.; Kitano, H. *J. Polym. Sci., Part A: Polym. Chem.* **1997**, *35*, 1535–1541.
- (32) Rekharsky, M. V.; Inoue, Y. *Chem. Rev.* **1998**, *98*, 1875–1918.
- (33) Yang, M.; Chu, L. -Y.; Xie, R.; Wang, C. *Macromol. Chem. Phys.* **2008**, *209*, 204–211.
- (34) Blokzijl, W.; Engberts, J. B. F. N. *Chem. Int. Ed. Engl.* **1993**, *32*, 1545–1579.
- (35) Wood, D. J.; Hruska, F. E.; Saenger, W. *J. Am. Chem. Soc.* **1977**, *99*, 1735–1740.
- (36) Schneider, H. -J.; Hacket, F.; Rüdiger, V. *Chem. Rev.* **1998**, *98*, 1755–1786.
- (37) (a) Yamamoto, Y.; Inoue, Y. *J. Carbohydr. Chem.* 1989, *8*, 29–46; (b) Inoue, Y.; Kanda, Y.; Yamamoto, Y.; Kobayashi, S. *Carbohydrate Res.* **1992**, *226* (2), 197–208.
- (38) Furrer, J. *J. Nat. Prod.* **2009**, *72*, 1437–1441.
- (39) Lamcharfi, E.; Kunesch, G.; Meyer, C.; Robert, B. *Spectrochim. Acta, Part A.* **1995**, *51*, 1861–1870.
- (40) Maeda, Y.; Kitano, H. *J. Phys. Chem.* **1995**, *99*, 487–488.
- (41) Ni, F.; Thomas, L.; Cotton, T.M. *Anal. Chem.* **1989**, *61*, 888–894.
- (42) Arrais, A.; Savarino, P. *J. Incl. Phenom. Macrocycl Chem.* **2009**, *64*, 73–81.
- (43) Witlicki, E.H.; Hansen, S.W.; Christensen, M.; Hansen, T.S.; Nygaard, S.D.; Jeppesen, J.O.; Wong, E.W.; Jensen, L.; Flood, A.H. *J. Phys. Chem. A.* **2009**, *113*, 9450–9457.
- (44) Iliescu, T.; Baia, M.; Miclăuș, V. *Eur. J. Pharm. Sci.* **2004**, *22*, 487–495.
- (45) Lamcharfia, E.; Kunescha, G.; Meyer, C.; Robert, B. *Spectrochimica Acta Part A* **1995**, *51*, 1861–1870.
- (46) Schmid, E. D.; Moschallski, M.; Peticolas, W. L. *J. Phys. Chem.* **1986**, *90*, 2340–2346.
- (47) Kumar, K.; Carey, P. R. *J. Chem. Phys.* **1975**, *63*, 3697–3707.
- (48) Kelley, A. M. *J. Phys. Chem.* **1999**, *103*, 6891–6903.
- (49) Šašić, S.; Kuzmanović, M. *J. Raman Spectrosc.* **1998**, *29*, 593–599.

- (50) Choi, S. -H.; Ryu, E-N.; Ryoo, J. J.; Lee, K-P. *J. Incl. Phenom. Macrocycl Chem.* **2001**, *40*, 271-274.
- (51) Lee, K. -P.; Choi, S-H.; Ryu, E. -N.; Ryoo, J. J.; Park, J. H.; Kim, Y.; Hyun, M. H. *Anal. Sci.* **2002**, *18(1)*, 31–34.
- (52) Vrielynck, L.; Lapouge, C.; Marquis, S.; Kister, J.; Dupuy, N. *Spectrochimica Acta Part A* **2004**, *60*, 2553–2559.
- (53) Rossi, B.; Verrocchio, P.; Viliani, G.; Scarduelli, G.; Mancini, I.; Guella, G.; Rossi, F. *Philos. Mag.* **2007**, *87*, 559-567.
- (54) Arrais, A.; Savarino, P. *J. Incl. Phenom. Macrocycl. Chem.* **2009**, *64*, 73–81.
- (56) Witlicki, E. H.; Hansen, S. W.; Christensen, M.; Hansen, T. S.; Nygaard, S. D.; Jeppesen, J. O.; Wong, E. W.; Jensen, L.; Flood, A. H. *J. Phys. Chem. A* **2009**, *113*, 9450–9457.
- (57) Li, W.; Lu, B.; Sheng, A.; Yang, F.; Wang, Z. *J. Mol. Struct.* **2010**, *981*, 194–203.
- (58) Sardo, M.; Amado, A.M.; Riberio-Claro, P.J.A. *J. Raman Spectrosc.* **2009**, *40*, 1624–1633.
- (59) Li, K.; Guo, L.; Liang, Z.; Thiyagarajan, P.; Wang, Q. *J. Polym. Sci., Part A: Polym. Chem.* **2005**, *43*, 6007–6019.
- (60) Yang, C.; Ni, X.; Li, J. *J. Mater. Chem.* **2009**, *19*, 3755–3763.
- (61) Krois, D.; Brinker, U. H. In *Cyclodextrins and Their Complexes*; Dodziuk, H., Ed.; Wiley-VCH GmbH & Co. KgaA: Weinheim, **2006**; Chapter 10.4.
- (62) Mendicuti, R. F.; González-Álvarez, M. J. *J. Chem. Educ.* **2010**, *87*, 965–968.
- (62) Berbenni, V.; Marini, A.; Bruni, G. *Thermochim.Acta* **1998**, *322*, 137–151.
- (63) Hu, J.; Liu, B.; Liu, W. *Text. Res. J.* **2011**, *76*, 853–860.
- (64) Akiyoshi, K.; Sasaki, Y.; Sunamoto, J. *Bioconj.Chem.* **1999**, *10(3)*, 321–324.
- (65) Xie, J.; Hsieh, Y. *J. Appl. Polym. Sci.* **2003**, *89*, 999–1006.
- (66) a) Yang, C.; Ni, X.; Li, J. *J. Mater. Chem.* **2009**, *19*, 3755–3763.
- (67) Alvarez-Rodríguez, R.; Arias, F. J.; Santos, M.; Testera, A. M.; Rodríguez –Cabello, J. C. *Macromol. Rapid Commun.* **2010**, *31*, 568–573
- (68) Aschi, A.; Mbarek, N.; Othman, M.; Gharbi, A. *Mat. Sci. Eng. C* **2008**, *28*, 594–600
- (69) Dev, S.; Surolia, A. *J. Biosci.* **2006**, *31(5)*, 551–556,
- (70) Galantini, L.; Jover, A.; Leggio, C.; Meijide, F.; Pavel, N. V.; Tellini, V. H. S.; Tato, J. V.; Tortolini, C. *J. Phys. Chem. B* **2008**, *112*, 8536–8541

- (71) Topchieva, I. N.; Panova, I. G.; Kurganov, B. I.; Spiridonov, V. V.; Matukhina, E. V.; Filippov, S. K.; Lezov, A. V. *Colloid J.* **2008**, *70*(3), 356–365.
- (72) Liu, J.; Sondjaja, H. R.; Tam, K. C. *Langmuir* **2007**, *23*, 5106–5109
- (73) Uguzdogan E.; Camli, T.; Kabasakal, O. S.; Patir, S.; Ozturk, E.; Denkbas, E. B.; Tuncel, A. *Eur. Polym. J.* **2005**, *41*, 2142–2149.
- (74) Isojima, T.; Lattuada, M.; Vander Sande, J. B.; Hatton, T. A. *ACS Nano*, **2008**, *2* (9), 1799–1806.
- (75) Liu, J.; Chen, G.; Guo, M.; Jiang, M. *Macromolecules* **2010**, *43*, 8086–8093.
- (76) Lynda, N. A.; Meulerb, A. J.; Hillmyer, M. A. *Prog. Polym. Sci.* **2008**, *33*, 875–893
- (77) Ferreira, L.; Figueiredo, M.M.; Gil, M.H.; Ramos, M.A. *J. Biomed. Mater. Res. Part B* **2006**, *77B*, 55–64.
- (78) Flory, P. J.; Rehner, J. *J. Chem. Phys.* **1943**, *11*, 521–527.
- (79) (a) Cates, M. *Nature* **1991**, *351*, 102–102; (b) Ringsdorf, H.; Venzmer, J.; Winnik, F. *Angew. Chem. Int. Ed. Engl.* **1991**, *30*, 315–318.

CHAPTER 7

Manuscript 6

Description

The study in this manuscript is an extension of the work of chapter 6 and the earlier chapters. The adsorption properties of Macromolecular (CD)-based Imprinted Materials (MIMs), were analyzed towards PFCs using various adsorption isotherm models (BET, Sips). The soluble HDI-1 copolymer described in Chapter 6, along with other insoluble copolymer adsorbents with higher linker loading ratios (i.e., HDI-3 and -6; where the ratios of HDI linker are 3 and 6, respectively, and that of β -CD comonomer is unity) were used. PFOA was used as the model PFC guest due to its abundance as an environmental marker. The adsorption properties of MIMs towards PFOA were assessed and compared to octanoic acid (OA; hydrocarbon analogue of PFOA) results. The respective adsorption behaviors of MIMs towards PFOA and OA were compared to similar studies using conventional granular activated carbon (GAC) adsorbents.

Author's Contribution

The idea of using adsorption isotherm models to analyze the interaction of CD-based copolymer adsorbents towards PFOA was proposed by myself. All of the copolymer materials synthesis, adsorption sample preparations, batch adsorption tests, and analyses of the data were done by myself. I prepared the first draft of the manuscript and subsequent editing was done by Dr. Wilson.

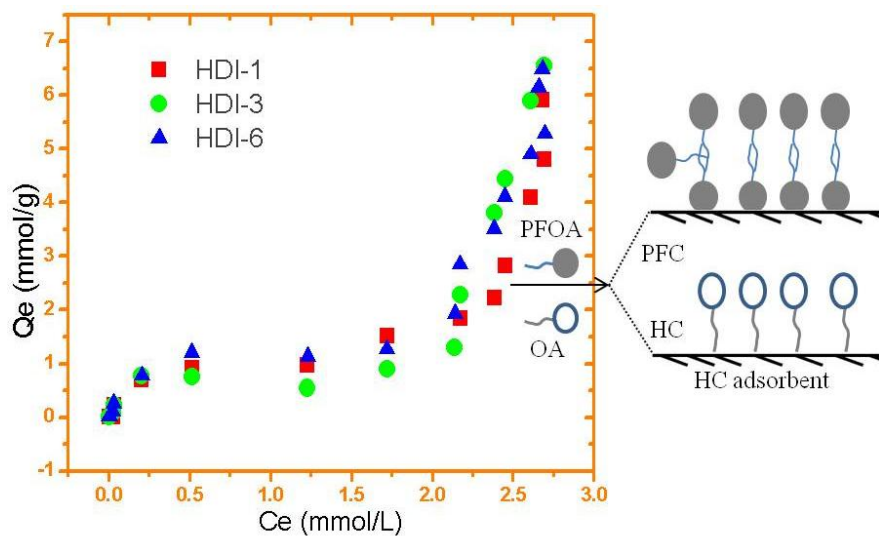
Relation of Manuscript 3 to Overall Objective of this Project

The work of this manuscript is important to the overall objective of this project because it provides an insight into the structure of host-guest systems containing a polymeric host. This study combines the findings of chapters 2–6 on the structure and dynamic properties of host-guest systems to assess how CD-based copolymer materials can be used to efficiently adsorb PFCs (e.g. PFOA).

Research Highlights

- The adsorption properties of MIMs are tunable according to the availability of apolar β -CD inclusion sites and polar functional groups (non-inclusion sites) at the surface of the copolymer (MIMs).
- The equilibrium binding constant of Poly-CD(MIMs)/PFOA is reduced by ~one to two orders of magnitude compared to similar value for native CD/PFOA because of reduced specific interactions in the former.
- MIMs generally displayed greater uptake for PFOA compared to GAC
- PFOA displayed multilayer adsorption with MIMs compared to monolayer adsorption for OA.

Graphical Abstract



7. Tunable Macromolecular-based Imprinted Materials for the Adsorption of Hydrocarbon and Perfluorocarbon Octanoate Anions

*Abdalla H. Karoyo and Lee D. Wilson**

Department of Chemistry, University of Saskatchewan, 110 Science Place (Room 156 Thorvaldson Building), Saskatoon, Saskatchewan, S7N 5C9

*Corresponding Author

7.1 Abstract

The sorption properties of tunable urethane-based copolymer materials containing β -cyclodextrin (β -CD) are evaluated with the carboxylate anions of perfluorooctanoic acid (PFOA) and octanoic acid (OA) in aqueous solutions, respectively. The copolymer materials are herein referred to as Macromolecular Imprinted Materials (MIMs) since the design strategy of such materials incorporates a porogenic macromolecule (β -CD) within a cross-linked framework with hexamethylene diisocyanate (HDI). We report the tunable uptake of OA and PFOA from aqueous solution with adsorption modes in accordance with the composition of the MIMs at variable mole ratios of β -CD and HDI. The sorption results were compared with results using granular activated carbon (GAC) at 295 K and pH values that exceed the pK_a of OA and PFOA, respectively. The BET and Sips models provided estimates of the monolayer sorption capacity (Q_m) and equilibrium sorption parameters. The upper Q_m value of GAC with PFOA was ~ 1.4 mmol/g; whereas, a greater Q_m value for the MIMs with PFOA (up to 2.6 mmol/g) was observed. GAC displays greater sorption of PFOA at relatively low C_e values with saturation of the monolayer at $C_e \sim 0.5$ mM. In contrast, the MIMs displays monolayer completion with PFOA at $C_e \sim 1$ mM with multilayer sorption at $C_e > 1$ mM. Equilibrium sorption of PFOA onto MIMs occurs at non-inclusion binding sites of the polymeric framework and the inclusion sites of β -CD. The former occurs through the interaction between the carboxylate head group of PFOA and dipolar domains of the MIMs framework. The inclusion sites of MIMs are favourable for PFOA and OA anions and display tunable and versatile sorption properties when compared with GAC.

7.2 Introduction

Perfluorinated compounds (PFCs) are an emerging class of persistent organic pollutants which represents significant concern to human health due to their recalcitrant nature in aquatic environments and ecosystems.¹ Perfluorooctane sulfonate (PFOS, C₈F₁₇SO₃H) and PFOA (C₈H₁₅O₂H) are among the most commonly studied types of PFCs. PFOA and PFOS have been detected in drinking water, ground water and surface water supplies,^{1,2} industrial waste water effluents,^{3,4} soil and sediments,⁵ and other aquatic environments.^{6,7} They have relatively high water solubility (PFOA ~9.5 g/L)⁸ and variable mobility in aqueous environments. In order to effectively remove PFCs and minimize their impact on the environment, efficient and proper treatment methods are required. PFOS and PFOA are generally not amenable to conventional chemical (e.g., oxidation and reduction) or biological treatment due to the great stability of C-F bonds.^{9,10} Alternatively, ultrasonic¹¹ and ultraviolet irradiation¹² techniques were reported as potential decomposition methods for PFOA and PFOS. However, these approaches are limited due to their demanding capital cost and time requirements. Adsorption methods using activated carbon offer an approach for the physical removal of PFCs¹³⁻¹⁷ due to its general utility as a sorbent, technical simplicity, and relatively low cost. A disadvantage of carbonaceous materials is their limited sorption capacity, regeneration costs, and longer equilibration times required for the sorption of PFCs. Carbon nanotubes (CNTs) were recently evaluated as potential adsorbent materials for the removal of PFOA and other PFCs from aquatic environments.^{18,19} For example, Xiaona et al.¹⁸ reported a study of electrochemical assisted sorption of PFOA onto multi-walled CNTs where a moderate sorption capacity ($Q_m = 0.98$ mmol/g) was reported. One disadvantage of carbonaceous materials is the limited uptake of PFCs due to their inert character and relative immiscibility with hydrocarbon materials.^{20,21} Thus, there is a defined need to develop improved sorbent materials with greater sorption capacity, reduced equilibration times, and improved recyclability with facile regeneration for sorptive applications of PFCs.

Macromolecular imprinted polymers have application as biosensors, sorptive removal of macromolecular toxins from the body, and as diagnostic materials due to their molecular recognition properties.²² We hypothesize that improved molecular recognition with target substrates is possible with synthetically engineered adsorbent materials through the incorporation of macromolecular template units within copolymer frameworks. The incorporation of macromolecular-based porogens with copolymer frameworks using a *bottom-up* approach offers

the advantage of tuning the physicochemical properties of the adsorbent by controlling the reagent ratios and reaction conditions. A paucity of such studies has been reported for the sorption of PFCs using copolymer sorbent materials and may be attributed to limitations regarding materials design strategy. For example, Deng et al.²³ reported the selective removal of PFOS from aqueous solution using molecularly imprinted polymers (MIPs) with PFOA as the molecular template. In contrast, a number of reports have documented the sorption of PFCs onto commercially available resins.^{16,24,25} It was reported that such resins had substantially higher levels of sorption for PFOS and perfluorooctanoate (~ 2.9 mmol/g)¹⁶ relative to activated carbon materials (~ 0.20 – 0.39 mmol/g).¹⁴⁻¹⁶ The incorporation of macromolecular units (e.g., β -CD) within urethane copolymer materials reported herein provides tunable sorption sites with variable accessibility and binding affinity for lipophilic adsorbates.²⁶ In contrast to carbonaceous sorbents such as GAC, urethane-based copolymer materials have promising potential as filtration and separation media with controllable morphology (e.g., films, fibers, and beads).²⁷

In this study we report a *bottom-up* design strategy that employs the incorporation of a macromolecule (β -CD) cross linked with hexamethylene diisocyanate (HDI) to form a copolymer framework, hereafter referred to as macromolecular imprinted materials (MIMs). As well, we report the sorption of the carboxylate anions of PFOA and octanoic acid (OA) in aqueous solution, respectively, with granular activated carbon (GAC) and various MIMs prepared from cross-linking between β -CD and HDI at variable mole ratios (i.e., HDI-1, HDI-3, and HDI-6). The results of this study are anticipated to contribute to improved sorbent design and a greater understanding of the sorption processes with hydrocarbon and perfluorocarbon carboxylate anion species, respectively.

7.3 Materials and Methods

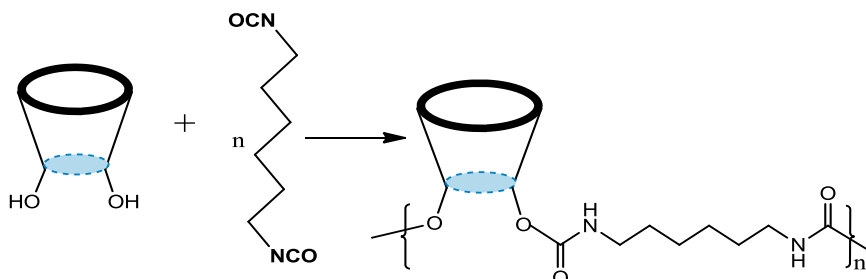
7.3.1 Chemicals

Perfluorooctanoic acid (PFOA; 96%) was purchased from SynQuest Laboratories USA (Alachua, FL). Octanoic acid (OA) and β -CD were purchased from VWR Canada Ltd. 1,6-hexamethylene diisocyanate (HDI), dimethyl acetamide (DMA), methanol (99.8% HPLC grade), sodium hydroxide (NaOH) and 4Å (8-12 mesh) molecular sieves were purchased from Sigma-Aldrich Canada Ltd. (Oakville, ON). All materials were used as received unless specified otherwise.

7.3.2 Adsorbents

The adsorbents used in this study include granular activated carbon (GAC) and polyurethane based MIMs containing variable amounts of β -CD and HDI. Norit Rox 0.8 GAC (VWR Canada Ltd.), was pretreated by refluxing in methanol for ~24 h followed by drying under vacuum ~70 °C to remove any impurities before further use.

The synthesis of polyurethane copolymers containing β -CD (HDI-1, -3 and -6) was adapted from a previous report,²⁸ as illustrated by Scheme 7.1. DMA was dried with 4Å (8–12 mesh) molecular sieves. MIMs containing β -CD and HDI at variable mole ratios (1:1, 1:3, and 1:6, respectively) denoted as HDI-1, -3, and -6 were prepared. 1 mmol of dried β -CD was dissolved in a round bottom flask with stirring in 10 mL of DMA followed by the addition of HDI (1, 3, or 6 mmol equivalents) in 30 mL of DMA to the reaction mixture. The solution was further stirred with heating at ~68 °C for 24 h under argon and subsequently cooled to room temperature. Excess DMA was removed under vacuum (pressure ~1 mbar), followed by the addition of cold methanol (~0 °C). The gelled product was filtered through Whatman no. 2 paper to obtain a crude product and subsequently washed with methanol in a Soxhlet extractor for 24 h.



Scheme 7.1 Reaction between β -CD and 1,6-hexamethylene diisocyanate (HDI) to form the HDI-X copolymers; where X = 1, 3 and 6.

The copolymer was dried in a pistol dryer for 24 h, ground into a powder, and passed through a 40-mesh sieve to ensure uniform particle size. A second cycle of washing for 24 h in the Soxhlet extractor with anhydrous diethyl ether was followed by drying, grinding, and sieving, as outlined above. The copolymer materials were characterized using FT-IR and NMR spectroscopy, thermoanalytical methods, and elemental analyses, as outlined previously.²⁸ Table 7.1 lists the sorbent materials and some of their selected physicochemical properties.^{26,29}

Table 7.1 Physicochemical Properties of the Adsorbent Materials and the Dye-based Equilibrium Binding Constants*

Adsorbent	SA (m ² /g)	K _{eq} (M ⁻¹) x10 ^{3c}	β-CD mol %	Accessible % β-CD ^d	% Linker content ^e
GAC	1100 ^a	~1.0	-	-	-
HDI-1	<1 ^b	~5.2	87.1	100	12.9
HDI-3	<1 ^b	~4.6	69.2	4.78	38.7
HDI-6	NR	~15	52.9	~0	77.4

^a Supplier's BET surface area, ^b BET surface area (Ref. 29), ^c Estimated from the Sips binding affinity (Table 3), ^d Estimated from % removal of *p*-nitrophenol from aqueous solution (Ref. 26), ^e Estimated from the initial monomer ratios for HDI-1.

7.3.3 Adsorbates

The pH conditions used for perfluorocarbon and hydrocarbon adsorbates used in this study vary for PFOA (pH ~3.8) and octanoic acid (OA) (pH ~8.5). The pH of the aqueous solution for each adsorbate was maintained above its respective pK_a value to ensure anion formation. The physicochemical characteristics of the adsorbates are listed in Table 7.2.^{30,31} The pK_a of PFOA is reported to range from -0.5–3.8;³² herein, a pK_a value of 2.5³³ was adopted.

Table 7.2 Physicochemical Properties of Adsorbate Materials*

Adsorbates	Molecular formula	Molecular weight	pKa	cmc (mM)	Water solubility(g/L)
PFOA	CF ₃ (CF ₂) ₆ CO ₂ H	414.06	2.5	8.7-10.5 ^b	3.4 (also 9.5)
Octanoic acid	CH ₃ (CH ₂) ₆ CO ₂ H	144.21	4.89 ^a	~400 ^b	0.68 ^c

^aRef. 30, ^bRef 35 (0.4 M refers to the cmc of the octanoate ion), ^cRef. 31.

7.4 Batch Sorption Studies

All sorption isotherms were conducted in duplicate and the term “sorption” will be adopted throughout this study to account for both adsorption and absorption processes.³⁴ The concentration of the adsorbates was maintained below their reported critical micelle concentration (cmc) values for all experiments (*cf.* Table 7.2).³⁵

7.4.1 Sorption of Perfluorooctanoate (PFOA)

Sorption studies were carried out using 4 dram glass vials that were loaded with ~2 mg MIMs (or ~20 mg in the case of GAC) in 10 mL of aqueous PFOA over a range of concentrations (~5 μ M–5 mM) in milli-Q water at pH ~3.85.

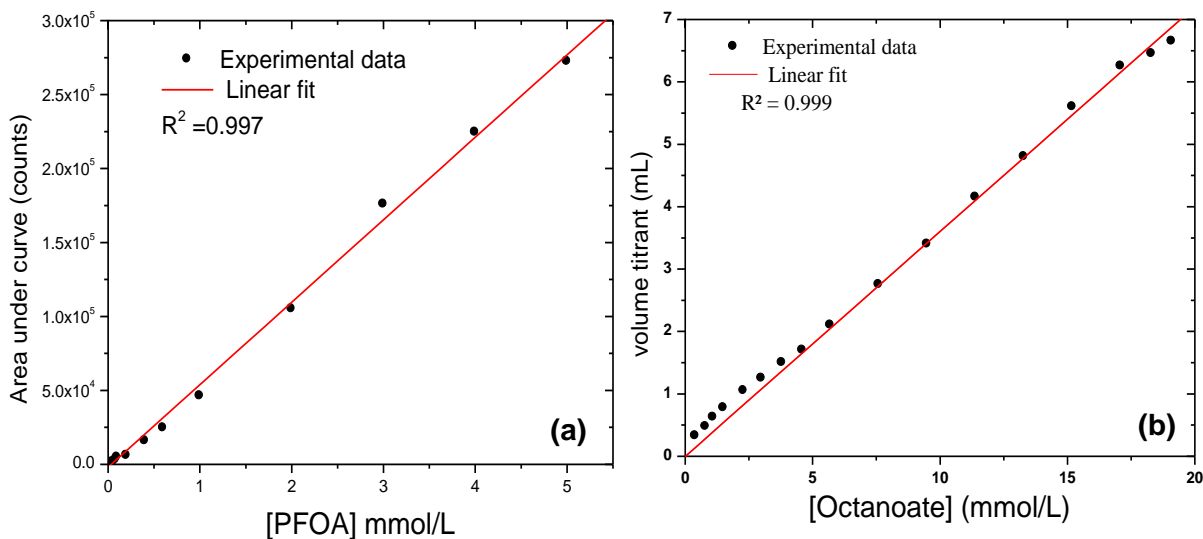


Figure 7.1 Calibration results and “best-fit” linear regression for the (a) ESI-MS results for PFOA and (b) titration of OA.

The vials were sealed with parafilm before incubating samples on a mechanical shaker at ~135 rpm and 295 K. The equilibration times were 24 h for the MIMs/adsorbate systems and 168 h for the GAC/adsorbate systems. After equilibration, the adsorbent systems were left to settle for ~24 h. Thereafter, 25 μ L aliquots of the supernatant was removed and diluted to 25 mL with HPLC grade methanol for mass spectrometry analysis. The use of methanol as a diluent matrix was previously described to ensure complete dissolution of the PFOA.¹⁵ The equilibrium residual PFOA in the supernatant aqueous phase was quantified using hybrid quadrupole-TOF (Qstar)

MS/MS mass spectrometer with electrospray ionization (ESI-MS) in negative ion mode. Calibration curves yielded linear calibrations ($R^2 > 0.99$) as shown in Figure 7.1a. Solutions of PFOA were eluted with acetonitrile/water (60:40 v/v %) and 10 μ L was injected into the HPLC system in a nitrogen stream at 295 K.

7.4.2 Sorption of Octanoate (OA)

Sorption studies were carried out using 4 dram glass vials containing ~10 mg of the adsorbent material and 10 mL octanoate solution (pH ~8.50) at variable concentration (i.e., 1–20 mM). The pH of the aqueous octanoate solution was adjusted with NaOH. The samples were incubated for 24 h, as described above. The residual amount of octanoate was analyzed by back titration with 0.01 M NaOH solution using methyl blue as the indicator to the reddish-green endpoint. The calibration curve for the titration results yielded a reproducible linear calibration ($R^2 > 0.99$), as shown in Figure 7.1b. The residual amounts of OA were not analyzed using ESI-MS since electrolytes such as NaOH affect the sensitivity of ESI-MS in the form of blockages and the suppression of ion formation.

7.4.3 Sorption Isotherms

The sorption isotherms were expressed as the plots of equilibrium uptake from aqueous solution of adsorbate species into the adsorbent phase (Q_e ; mmol/g or mg/g) against the equilibrium concentration of unbound (residual) adsorbate species (C_e ; mmol/L or mg/L) in aqueous solution as described by eqn 7.1. C_o refers to the initial adsorbate (i.e., PFOA or OA) concentration before sorption, m is the mass (g) of adsorbent, and V is the volume (L) of the solution, as previously described.^{36,37}

$$Q_e = \frac{(C_o - C_e) \times V}{m} \quad \text{Equation 7.1}$$

7.4.4 Models and Equations

The experimental sorption results were fitted using the Brunauer-Emmett-Teller (BET; eqn 2)³⁸ and the Sips (eqn 3)³⁹ models, where K_S and K_{BET} are the equilibrium sorption constants (K; L/g), Q_m is the monolayer sorption capacity of the adsorbent (mmol/g), C_S is the saturated

concentration of the adsorbate in aqueous solution (mmol/L), and n_s is an exponent parameter representing the degree of heterogeneity on the adsorbent surface.⁴⁰ All other parameters are defined as in eqn 7.1. In the case of the parameter C_s , an average value was estimated from eqn 7.2 by allowing C_s to vary as an adjustable parameter, until satisfactory “best fits” ($R^2 \geq 0.96$) were obtained. The “best fit” calculated value of C_s was ~ 4.0 mmol/L (*cf.* Table 7.3).

$$Q_e = \frac{Q_m K_{BET} C_e}{(C_s - C_e) \left[1 + (K_{BET} - 1) \left(\frac{C_e}{C_s} \right) \right]} \quad \text{Equation 7.2}$$

$$Q_e = \frac{Q_m (K_s C_e)^{n_s}}{1 + (K_s C_e)^{n_s}} \quad \text{Equation 7.3}$$

The BET model is widely used for multilayer sorption and is considered as an extension of the Langmuir model.⁴¹ The Sips isotherm shares common features to the Langmuir and Freundlich models, and it describes a range of sorption behaviour including surface heterogeneity.⁴⁰

Differential error analysis of eqn 7.1 was carried out to assign error contributions for Q_e (i.e., ΔQ_e) as described previously.⁴² Error contributions are assigned to uncertainties in the mass of the adsorbent (Δm), and the concentrations (ΔC_o and ΔC_e) of adsorbate. Thus, it is necessary to differentiate Q_e with respect to each quantity as described by eqns 7.4–7.6. The relative contributions by eqns 4–6 were used to compute the total error for Q_e .

$$\Delta Q_e = 2 \left| \frac{C_o - C_e \times V}{m^2} \times \Delta m \right| \quad \text{Equation 7.4}$$

$$\Delta Q_e = 2 \left| \frac{V}{m} \times \Delta C_o \right| \quad \text{Equation 7.5}$$

$$\Delta Q_e = 2 \left| \frac{V}{m} \times \Delta C_e \right| \quad \text{Equation 7.6}$$

7.5 Results and Discussion

7.5.1 PFOA sorption

In Figure 7.2, the sorption behavior of PFOA with GAC and MIMs are illustrated as plots of Q_e vs C_e . GAC displays a type I (Langmuir)⁴³ sorption isotherm with a monotonic increase of Q_e with C_e until it reaches a plateau ~ 0.5 mM. In contrast, the MIMs display type IV⁴³ behavior with saturation of the monolayer at greater C_e values (>1 mM). At greater C_e values (>2 mM), an asymptotic rise in Q_e is observed for the MIMs and is consistent with multilayer sorption processes.²³ In the case of MIMs, the experimental data are well-described using the multilayer BET isotherm. In contrast, the Sips model described monolayer sorption behaviour for GAC; where $R^2 \geq 0.96$ for each model, respectively. The best-fit sorption parameters derived from the BET and Sips models are listed in Table 7.3. The average sorption capacity (Q_m ; mmol/g) according to each respective model for the various adsorbents with PFOA are listed in descending order as follows; GAC (1.39) \sim HDI-1 (1.35) $>$ HDI-3 (0.97) $>$ HDI-6 (0.87). The monolayer sorption of PFOA onto MIMs was also fitted using the Sips model (See insets in Fig. 7.2) and the estimated Q_m values are as follows: 2.36 (HDI-1), 1.38 (HDI-3) and 1.28 (HDI-6) (*cf.* Table 7.3). The overestimation of the Q_m values using the Sips model in the case of MIMs is related to the errors unaccounted for in the Sips model due to the occurrence of multilayer sorption behaviour. Table 7.1 lists the physicochemical properties of the adsorbents where the MIMs vary due to the relative composition of β -CD and HDI which contribute to the surface chemistry, morphology, and the textural properties²⁹ (i.e., pore structure characteristics and surface area). It is worthwhile noting that the sorption capacity decreases for the MIMs as the HDI content increases (*cf.* Table 7.3 and Figure 7.2, insets).

The variable sorption behaviour of PFOA with MIMs, as compared with the GAC, indicates that the MIM sorbents have favourable sorption sites for PFOA due to the tunable surface chemistry sites (i.e., inclusion and non-inclusion). Previous sorption studies of HDI-based urethanes with mixtures of alkyl carboxylates reported by Mohamed et al.²⁹ indicate that the adsorbates were bound at dual sorption sites of the copolymer framework. Spectroscopic evidence for the presence of dual binding sites of HDI-1 copolymer was provided in chapter 6.

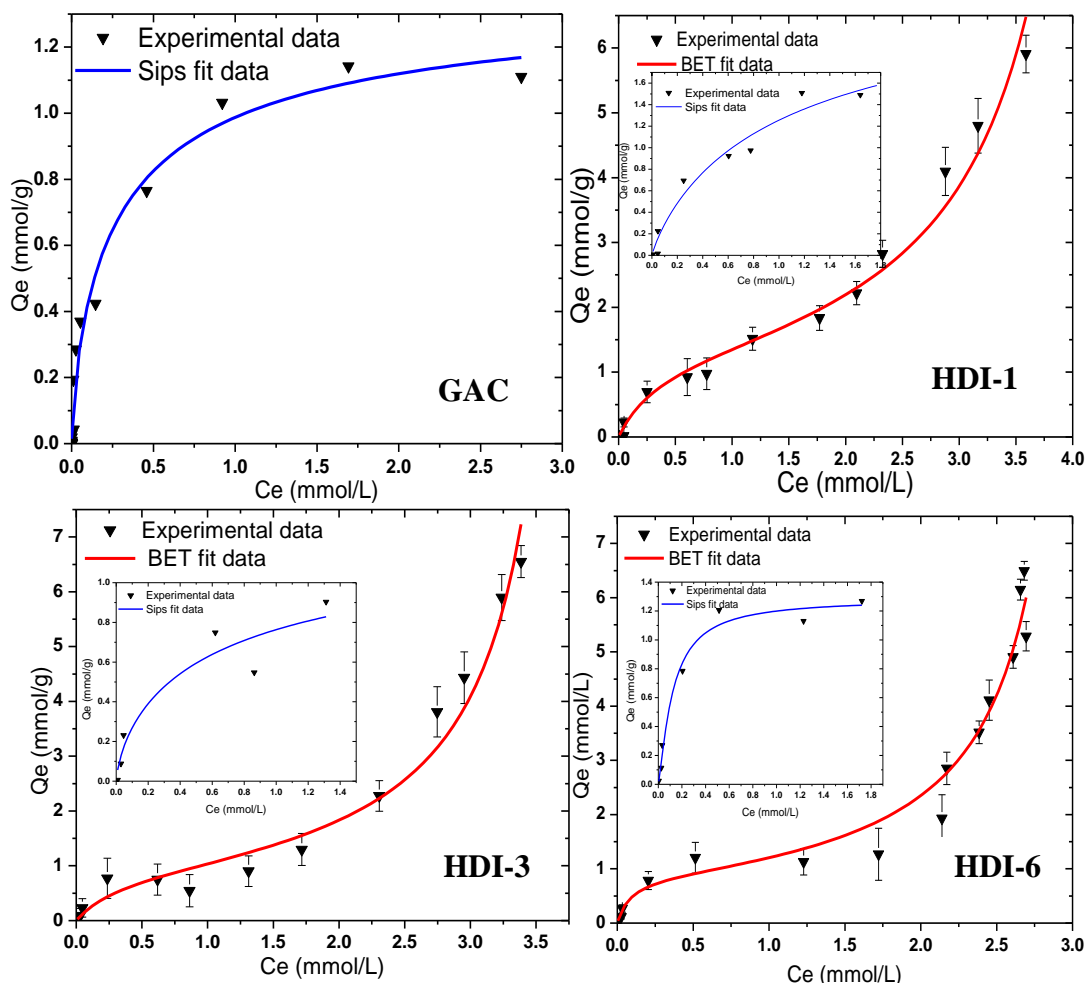


Figure 7.2 Sorption isotherms of PFOA onto GAC, HDI-1, HDI-3, and HDI-6 at pH 3.85 and 295 K. The “best-fit” lines correspond to the BET (copolymers) and Sips (GAC and copolymers; see insets) models.

The inclusion sites of copolymers due to β -CD exhibit greater binding affinity than the non-inclusion sites.^{26,44} Previous NMR studies in aqueous solution of complexes between β -CD and the anion of PFOA display favourable complex stability between the apolar PFC chain and the cavity interior of β -CD.⁴⁵ The inclusion domains within the MIMs copolymer framework offer potential binding sites favourable for PFOA, neglecting any steric effects. In cases where the cross-link density of the framework increases, steric effects are known to occur at the inclusion sites and sorption occurs alternatively at the non-inclusion sites (linker domains). The greater Q_m value observed for HDI-1 (1.35 mmol/g) relative to HDI-3 and -6 is related to the relative accessibility of the inclusion sites (*cf.* Table 7.1).

Table 7.3 Isotherm Sorption Parameters for PFOA onto GAC and the Urethane-copolymers (MIMs) Obtained from the BET and Sips Models at 295 K and pH ~ 3.85.

BET					Sips			
Sorbent	$Q_m(\text{mmol/g})$	$K(\text{L/g})$	$C_s(\text{mmol/L})$	R^2	$Q_m(\text{mmol/g})$	n_s	$K_s(\text{L/g})$	R^2
GAC	-	-	-	-	1.39±0.2	0.74±0.1	2.39±1.1	0.98
HDI-1	1.35±0.05	12.6±5.6	4.5	0.98	2.63±1.6	0.87±0.3	0.91±1.2	0.96
HDI-3	0.97±0.04	11.2±9.5	3.9	0.97	1.38±2.1	0.71±0.5	1.23±4.1	0.92
HDI-6	0.87±0.03	36.1±18.7	3.2	0.96	1.28±0.2	1.26±0.3	14.1±10.6	0.98

The Q_m value of HDI-1 derived using the Sips model reported in Table 7.3 for PFOA is comparable to that reported by Yu et al. (2.92 mmol/g)¹⁶ for an ion exchange resin. The Q_m values for GAC (1.39 mmol/g) and HDI-1 (1.35 mmol/g) are similar but greater than those for HDI-3 (0.97 mmol/g) and HDI-6 (0.87 mmol/g), according to their respective isotherm models. Relatively low Q_m values for GAC/PFOA systems were reported by Zhao et al. ($Q_m \sim 0.3$ mmol/g Calgon F600 GAC; $SA_{\text{BET}} 670 \text{ m}^2\text{g}^{-1}$)¹⁵ and Yu et al. (~ 0.4 mmol/g; $SA_{\text{BET}} 712 \text{ m}^2\text{g}^{-1}$).¹⁶ Variable Q_m values are attributed to the nature of the surface functional groups and the textural properties of the MIMs. The greater Q_m values reported in Table 7.3 for GAC are attributed to its greater surface area.

In general, the equilibrium constants according to the respective isotherm models are given as follows; HDI-6 ($1.5 \times 10^4 \text{ M}^{-1}$; BET) > HDI-1 ($5.2 \times 10^3 \text{ M}^{-1}$; BET) ~ HDI-3 ($4.6 \times 10^3 \text{ M}^{-1}$; BET) > GAC ($9.9 \times 10^2 \text{ M}^{-1}$; Sips). The equilibrium constants (K_{eq}) for the MIMs are greater than those for GAC indicating favourable binding occurs for PFOA onto MIMs. The relatively large K_{eq} value for HDI-6 indicates that more favourable interactions or multiple sorption sites are involved. It can be concluded from the magnitude of K_{eq} that the affinity for the inclusion and non-inclusion binding sites differ as the linker (HDI) content of the MIMs vary. In a previous dye sorption study with urethane copolymer adsorbents, the inclusion site accessibility was attenuated as the content of HDI (i.e., cross-linking) increased.²⁹ In the case of PFOA, non-inclusion binding onto the surface domains of the cross-linker sites of the copolymer framework

is anticipated.³⁶ The inclusion site accessibility of phenolphthalein with HDI-6 was approximately zero (*cf.* Table 7.1); therefore, PFOA may undergo preferential adsorption at the non-inclusion sites of MIMs with greater HDI content. Interactions between the carboxylate anion head group of PFOA and the non-inclusion sites of MIMs occur via dipolar interactions. The latter are anticipated to be more favourable ($\sim 10^2$ kJ/mol) than London-dispersion interactions (1–10 kJ/mol)⁴⁶ mediated via the interaction of the apolar perfluoroalkyl tail and the β -CD cavity sites of the copolymer. Thus, the greater equilibrium binding affinity of HDI-6 compared to HDI-1 and -3 (*cf.* Table 7.1) has direct correlation to increased linker content. Note that the K_{eq} (M^{-1}) values presented in Table 7.1 were estimated from the Sips model (*cf.* eqn 7.3) by multiplying the respective equilibrium constants (K_{Sips}/K_{BET} ; L/g) with the relative molar mass of the perfluorooctanoate anion (g/mol).

The 1:1 binding constant ($K_{1:1}$) for the HDI-1/PFOA system was independently determined according to results obtained from a ^{19}F NMR chemical shift titration in solution where the chemical shifts of the central methylene (CF_2) group of PFOA were monitored. The 1:1 binding model described by Connors⁴⁷ for a substrate (S) and a ligand (L) to form a complex (SL) was employed where a calculated value of $K_{L:1} \sim 1.02 \times 10^3 M^{-1}$ was obtained from a non-linear least squares (NLLS) fitting procedure (eqn 7.7), reported by Ramstad et al.⁴⁸ The parameters in eqn 7.7 are defined as follows; $\Delta\delta = \delta_{obs} - \delta_S$, $\Delta\delta_{max} = \delta_{SL} - \delta_S$, [S] is the concentration of the free substrate ($[PFOA]_f$). $[PFOA]_f$ was determined from the total substrate concentration ($[PFOA]_t$) as shown in eqn 7.8, where the value of $\Delta\delta_{max}$ is the hyperbolic asymptote which was determined using a non-linear regression analysis. The experimental and ‘best-fit’ results for the analysis of the binding affinity ($K_{L:1}$) is given in Figure 7.3. The value for $K_{1:1}$ for the HDI-1/PFOA system agrees well with independent estimates for the β -CD/sodium perfluorooctanoate system in aqueous solution.⁴⁹ The equilibrium constants derived from the BET and Sips models are composite values that reflect contributions due to inclusion and non-inclusion binding which may not be readily compared from ^{19}F NMR chemical shift results, especially if adsorption occurs via the apolar chain of PFOA and the carboxylate head group, respectively.

$$\Delta\delta = \frac{\Delta\delta_{\max} K_{1:1} [PFOA]_f}{1 + K_{1:1} [PFOA]_f} \quad \text{Equation 7.7}$$

$$[PFOA]_f = [PFOA]_i - [HDI1]_i \left(\frac{\Delta\delta}{\Delta\delta_{\max}} \right) \quad \text{Equation 7.8}$$

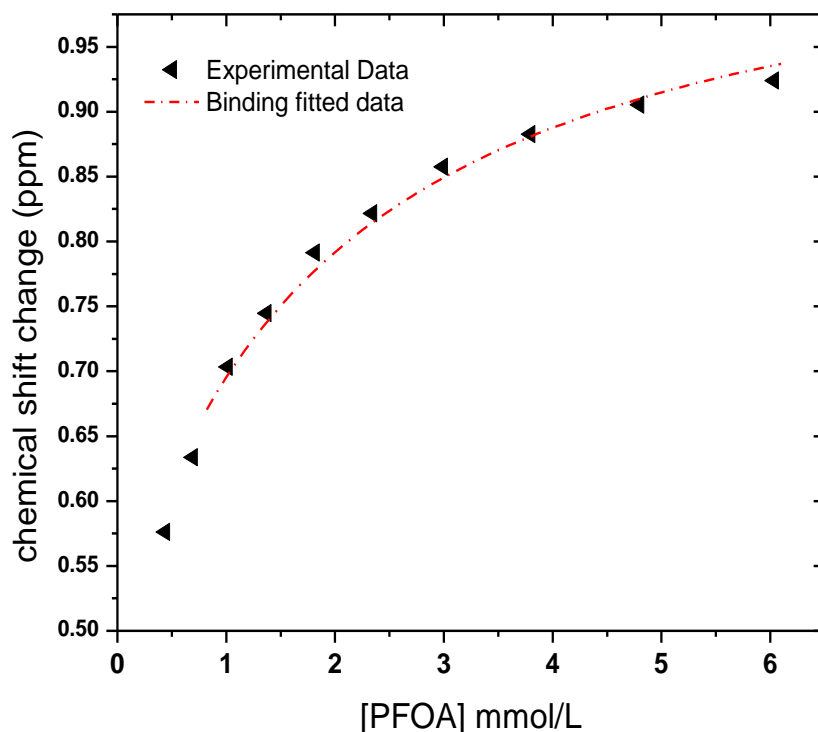


Figure 7.3 ^{19}F NMR chemical shifts (CF_2) and “best-fit” 1:1 equilibrium binding model for the titration of PFOA in the presence of HDI-1 (1 g/L) in aqueous solution at 298 K and pH ~ 5.

7.5.2 OA sorption

By comparison, the sorption isotherms for OA in its anion form with GAC and the MIMs are shown in Figure 7.4. In all cases, Q_e increases monotonically as C_e increases for each adsorbent system. The concentration dependence for each isotherm is well described using the Sips isotherm ($R^2 \geq 0.99$) and the best-fit parameters are listed in Table 7.4.

The Sips-derived monolayer sorption capacity (Q_m ; mmol/g) values for OA are listed in descending order as follows; GAC (117.5) > HDI-6 (27.8) > HDI-3 (19.8). In contrast to the Q_m

values for PFOA, the sorption capacity of OA is substantially greater for both GAC and MIMs. The results for the HDI-1/OA system are not reported due to the partial solubility of HDI-1 at these experimental conditions. The residual levels of unbound octanoate (i.e., C_e) in solutions containing HDI-1 cannot be readily deconvoluted by this titration method.

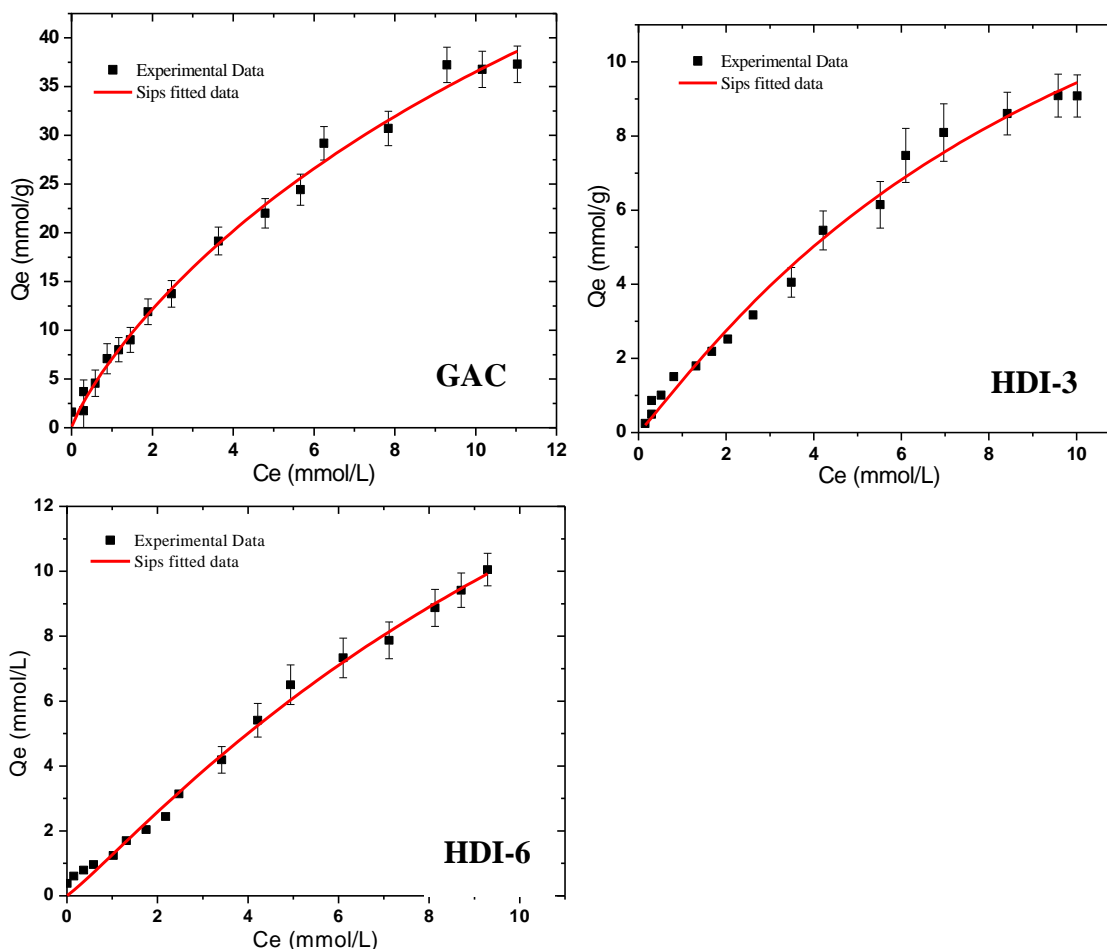
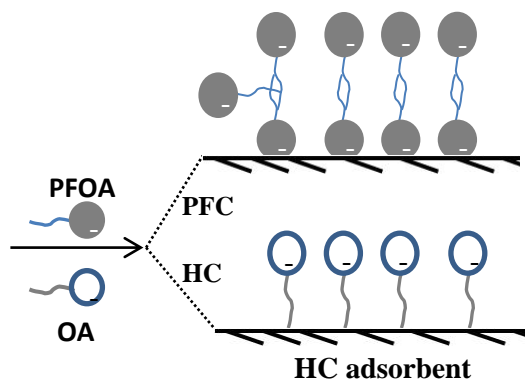


Figure 7.4 Sorption isotherms of octanoate onto GAC, HDI-3, and HDI-6 at pH 8.50 and 298 K. The “best-fit” lines correspond to the Sips model.

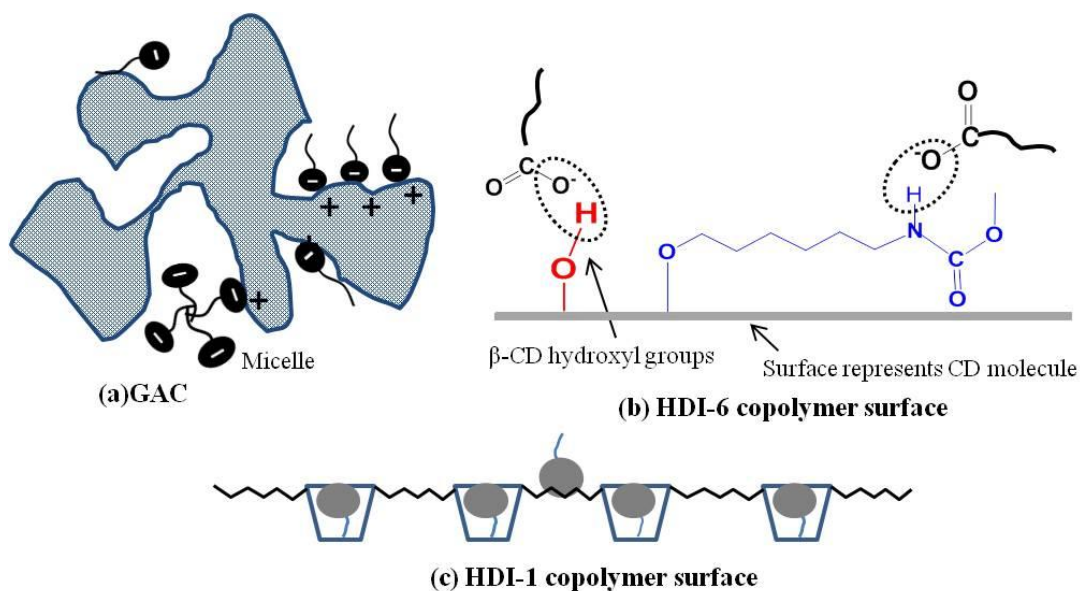
The greater sorption of octanoate by GAC compared with the copolymers is attributed to the greater surface area of GAC ($\sim 10^3$ m²/g; Table 7.1) relative to the lower surface area of the MIMs (< 1 m²/g; Table 7.1). On the other hand, greater Q_m values observed for OA relative to PFOA are related to the mutual compatibility of the hydrocarbon framework of MIMs and the apolar alkyl chain of OA. The phase separation of hydrocarbons (HCs) and perfluorocarbons

(PFCs) was previously reported²⁰ and attributed, in part, to dipole-dipole repulsions and other factors. Moreover, the relative incompatibility of the molecular polarizability values of the GAC/PFOA system is a principal factor contributing to the low levels of sorption in the case of PFOA. In contrast, the surface chemistry of the MIMs is variable due to the presence of heteroatoms (i.e., N and O) at the linker and inclusion site domains on the copolymer surface in accordance with the HDI content of the materials. The presence of polar and apolar domains present various binding sites for PFOA via the carboxylate head group or via the apolar perfluoroalkyl tail. Interactions between the carboxylate head group of PFOA and the adsorbent surface agree with the observation of well-defined monolayers and multilayers. Scheme 7.2 depicts a combination of multi-layer and monolayer sorption for PFOA and OA, respectively, onto the surface of a heterogeneous HC adsorbent.



Scheme 7.2 Sorption of PFOA and OA onto the hydrocarbon (HC) sorbents; Top: Binding of PFOA via the carboxylate head group and formation of tail-to-tail bilayer structures (with possible hemi-micelle and micelle formation), and Bottom: Monolayer binding of OA via the apolar alkyl chain.

Comparison with the known cmc value of PFOA (8.7–10.5 mM) in bulk solution³⁵ suggests the potential formation of molecular aggregates at the MIMs interface. Previous reports of hemi-micelle/micelle formation due to adsorption at the adsorbent surface is reported to occur at PFOA concentrations below its cmc value in bulk solution.^{19,50} Based on the foregoing discussion, a possible sorption mechanism of PFOA/OA binding onto the surfaces of HDI-1, HDI-6, and GAC vary according to the type of intermolecular interactions depicted in Scheme 7.3.



Scheme 7.3 Sorption modes of the PFOA/OA anion onto (a) activated carbon via electrostatic and hydrophobic interactions, (b) HDI-6 adsorption occurs via non-inclusion sites through ion-dipole interactions with hydroxyl groups and/or amide-NH groups as donor molecules and -COO^- as the acceptor (the wavy line displays the perfluoroalkyl tail of PFOA), and (c) HDI-1 adsorption occur via inclusion and non-inclusion sites of the copolymer framework where the toroids represent β -CD, spheres with tails represents PFOA, and the zig-zag lines represent HDI linker sites. Note that the head group of PFOA and perfluoroalkyl chain is not drawn to scale.

Apart from the favourable hydrophobic interactions affecting the adsorption of PFCs,⁵¹ electrostatic, ion-dipole and van der Waals interactions between the carboxylate head group and polar functional groups (i.e., -NH and -OH) at the sorbent surface may also occur. HDI-1 is a unique type of MIM because the β -CD inclusion sites are relatively accessible in comparison with HDI-3/-6 due to the greater cross linking and steric effects for increased HDI content. The textural and sorption properties of the MIMs are tunable by varying the relative composition of β -CD and HDI, as observed by the controlled uptake of PFOA and OA reported herein. The enhanced sorption observed for HDI-6 relative to HDI-3 with OA is related to the variable HDI content (*cf.* Table 7.1). Additional cross linking may attenuate or completely block the inclusion site accessibility which results in the availability of non-inclusion binding sites. In Table 7.4, the K_{Sips} for copolymer adsorbent/OA systems are an order of magnitude lower than the

corresponding values for PFOA in Table 7.3. The results agree with the nature of the noncovalent adsorbent/adsorbate interactions. Hydrophobic effects are concluded as the driving force for the sorptive association between the *n*-octyl group of OA and the adsorbent surface. As well, hydrophobic effects⁵² drive the inclusion of PFOA with the β -CD inclusion sites; whereas, dipolar interactions between the carboxylate head group of PFOA and the polar non-inclusion sites of the adsorbent surface are anticipated. The relative immiscibility of HC/PFC materials plays a key role in the known phase separation phenomena and this contributes to the observation of bilayers or aggregation via apolar association of the perfluoroalkyl chain of PFOA. This effect is illustrated in Scheme 7.3 for adsorption processes onto substrates with multiple binding sites.

Table 7.4 Isotherm Sorption Parameters for Octanoate onto GAC and the Urethane-copolymers (MIMs) Obtained from the Sips Model at 295 K and pH ~ 8.50.

	Q_m (mmol.g ⁻¹)	n_s	K_s (L g ⁻¹)	R^2
GAC	117.5 ±53.9	0.85 ±0.09	0.064 ±0.03	0.99
HDI-3	19.8 ±6.0	1.07 ±0.1	0.077 ±0.02	0.99
HDI-6	27.8 ±9.8	1.10 ±0.1	0.048 ±0.02	0.99

7.6 Conclusions

A systematic and comparative study of the equilibrium sorption properties of PFOA and OA with various adsorbents (i.e., GAC and MIMs) was investigated. Variable adsorption properties were observed depending on the nature of the adsorbent/adsorbate system. In the case of PFOA, the greatest sorption was observed for HDI-1. The sorption of PFOA at non-inclusion sites occur in two stages: (i) monolayer sorption via the head group with sorbent surface, and (ii) self-association of the apolar chains of PFOA to form multi-layers and/or aggregates. The adsorption properties of urethane copolymers are tunable according to the availability of apolar β -CD inclusion sites and polar functional groups (i.e., -NH and -OH) at the surface of MIMs. The GAC/OA system displayed the greatest overall sorption capacity in accordance with its greater

surface area. In all cases, OA is adsorbed as monolayers via the apolar *n*-octyl chain in accordance with hydrophobic effects.⁵¹ In all cases, MIMs possess inclusion and non-inclusion sites that offer favourable binding sites according to the nature of the adsorbate system. The differences in the physicochemical properties of perfluorocarbons and hydrocarbons are aptly demonstrated by their contrasting sorption properties with GAC and urethane copolymers containing β -CD. A key to the understanding of PFOA sorption is related to the relative compatibility of hydrocarbon-hydrocarbon vs. hydrocarbon-fluorocarbon materials.^{44,48} The greater lipophilicity of PFCs relative to HCs provides a basis for understanding the tendency of such materials to undergo phase separation and/or to form monolayer vs. multilayer structures in aqueous solution. MIMs are unique adsorbents due to the presence of inclusion sites and non-inclusion binding sites. The relative accessibility and affinity of these sites are tunable by varying the composition of the cross-linker and the macromolecule. This study is anticipated to contribute favourably to the future development of synthetically engineered MIMs for the controlled uptake of diverse organic contaminants in aquatic environments.

7.7 Acknowledgements

The authors are grateful for the support provided by the University of Saskatchewan and the Natural Sciences and Engineering Research Council of Canada (NSERC) for this research. AHK wishes to acknowledge Kenneth Thoms (Saskatchewan Structural Sciences Centre) for his expertise and technical assistance in obtaining the ESI-MS results. LDW acknowledges Computers for Schools (Saskatoon, SK.) for the donation of a desktop computer.

7.8 References

- (1) Fujii, S.; Polprasert, C.; Tanaka, S.; Lien, N. P. H.; Qiu, Y. J. *Water Supply: Res. Technol. AQUA* **2007**, *56.5*, 313–326.
- (2) Post, G. B.; Cohn P. D.; Cooper, K. R. *Environ. Res.* **2012**, *116*, 93–117.
- (3) Liou, J.S.-C.; Szostek, B.; DeRito, C. M.; Madsen, E. L. *Chemosphere* **2010**, *80*, 176–183.
- (4) Becker, A. M.; Suchan, M.; Gerstmann, S.; Frank, H. *Environ. Sci. Pollut. Res.* **2010**, *17*, 1502–1507.
- (5) Orata, F.; Maes, A.; Werres, F.; Wilken, R. D. *Soil Sediment Contam.* **2011**, *20*, 129–141.

- (6) Fernández-Sanjuan, M.; Meyer, J.; Damásio, J.; Faria, M.; Barata, C.; Lacorte, S. *Anal Bioanal. Chem.* **2010**, *398*, 1447–1456.
- (7) Zainuddin, K.; Zakaria, M. P.; Al-Odaini, N. A.; Bakhtiari, A. R.; Abdul Latif, P. *Environ. Forensics* **2012**, *13*, 82–92.
- (8) Li, M-H. *Environ. Toxicol.* **2009**, *24*, 95–101.
- (9) Prevedouros, K.; Cousins, I. T.; Buck, R.C.; Korzeniowski, S. H. *Environ. Sci. Technol.* **2006**, *40*, 32–44.
- (10) Schröder, H. F. *J. Chromatogr. A* **2003**, *1020*, 131–151.
- (11) Moriwaki, H.; Takagi, Y.; Tanaka, M.; Tsuruho, K.; Okitsu, K.; Maeda, Y. *Environ. Sci. Technol.* **2005**, *39*, 3388–3392.
- (12) Yamamoto, T.; Noma, Y.; Sakai, S. I.; Shibata, Y. *Environ. Sci. Technol.* **2007**, *41*, 5660–5665.
- (13) Hansen, M. C.; Børresen, M. H.; Schlabach, M.; Cornelissen, G. J. *Soils Sediments* **2010**, *10*, 179–185.
- (14) Ochoa-Herrera, V.; Sierra-Alvarez, R. *Chemosphere* **2008**, *72*, 1588–1593.
- (15) Zhao, D.; Cheng, J.; Vecitis, C. D.; Hoffmann, M. R. *J. Phys. Chem. A* **2011**, *115*, 2250–2257.
- (16) Yu, Q.; Zhanga, R.; Deng, S.; Huang, J.; Yu, G. *Water Res.* **2009**, *43*, 1150–1158.
- (17) Qu, Y.; Zhanga, C.; Li, F.; Bob, X.; Liu, G.; Zhou, Q. *J. Hazard. Mater.* **2009**, *169*, 146–152.
- (18) Li, X.; Chen, S.; Quan, X.; Zhang, Y. *Environ. Sci. Technol.* **2011**, *45*, 8498–8505.
- (19) Deng, S.; Zhang, Q.; Nie, Y.; Wang, H. W. B.; Huang, J.; Yu, G. *Environ. Pollut.* **2012**, *168*, 138–144.
- (20) Qaqish, S. E.; Urquhart, S. G.; Lanke, U.; Brunet, S. M. K.; Paige, M. F. *Langmuir* **2009**, *25*, 7401–7409.
- (21) Asakawa, T.; Amada, K.; Miyagishi, S. *Langmuir* **1997**, *13*, 4569–4573.
- (22) Kryscio, P. D. R.; Peppas, N. A. *Acta Biomater.* **2012**, *8*, 461–473.
- (23) Deng, S.; Shuai, D.; Yu, Q.; Huang, Y.; Yu, G. *Front. Environ. Sci. Engin. China* **2009**, *3*, 171–177.
- (24) Senevirathna, S. T. M. L. D.; Tanaka, S.; Fujii, S.; Kunacheva, C.; Harada, H.; Shivakoti, B. R.; Okamoto, R. *Chemosphere* **2010**, *80*, 647–651.

- (25) Xiao, F.; Davidsavor, K. J.; Park, S.; Nakayama, M.; Phillips, B. R. *J. Colloid Interface Sci.* **2012**, *36*, 505–511.
- (26) Mohamed, M. H.; Wilson, L. D.; Headley, J. V. *Carbohydr. Polym.* 2010, *80*, 186–196.
- (27) Elyashevich, G. K.; Olifirenko, A. S.; Pimenov, A. V. *Desalin.* 2005, *184*, 273–279.
- (28) Mohamed, M. H.; Wilson, L. D.; Headley, J. V. *Carbohydr. Res.* **2011**, *364*, 219–229.
- (29) Wilson, L. D.; Mohamed, M. H.; Headley, J. V.; *J. Colloid Interface Sci.* **2011**, *357*, 215–222.
- (30) Lide, D. R. CRC Handbook of Chemistry and Physics, 70th ed., **1990**, Boca Raton (FL): CRC Press.
- (31) Budavari, S. The Merck Index: An Encyclopedia of Chemicals, Drugs, and Biologicals, 12th ed., **1996**.
- (32) Burns, D.C., Ellis, D.A., Li, H.X., McMurdo, C.J.; Webster, E. *Environ. Sci. Technol.* **2008**, *42*, 9283–9288.
- (33) USEPA, 2002. Revised Draft Hazard Assessment of Perfluorooctanoic Acid and its Salts (http://www.ewg.org/files/EPA_PFOA_110402.pdf).
- (34) Accardi-Dey, A.; Gschwend, P. M. *Environ. Sci. Technol.* **2008**, *37*, 99–106.
- (35) (a) Hoffmann, H.; Wurtz, J. *J. Mol. Liq.* 1997, *72*, 191–; (b) Zemb, T.; Drifford, M.; Hayoun, M.; Jehanno, A. *J. Phys. Chem. J. Phys. Chem.* 1983, *87*, 4524–; (c) Kissa, E. *Fluorinated Surfactants and Repellents*, 2nd ed., Marcel Dekker, New York. **2001**.
- (36) Wilson, L. D.; Mohamed, M. H.; Berhaut, C. L. *Materials* **2011**, *4*, 1528–1542.
- (37) Pratt, D. Y.; Wilson, L. D.; Kozinski, J. A.; Morhart, A. *J. App. Polym. Sci.* **2010**, *16*, 2982–2989.
- (38) Brunauer, S.; Emmett, P. H.; Teller, E. *J. Am. Chem. Soc.* **1938**, *60*, 309–316.
- (39) Sips, R. *J. Chem. Phys.* **1948**, *16*, 490–495.
- (40) Foo, K. Y.; Hameed, B. H. *Chem. Eng. J.* **2012**, *156*, 2–10.
- (41) Langmuir, I. *J. Am. Chem. Soc.* 1916, *38*, 2221–2295.
- (42) Kwon, J. H.; Wilson, L. D. *J. Env. Sci. Health Part A* **2010**, *45*, 1793–1803.
- (43) Brunauer, S.; Deming, L.S.; Deming, W.E.; Teller, E. *J. Am. Chem. Soc.* 1940, *62*, 1723–1732.
- (44) Wilson, L. D.; Guo, R. *J. Colloid Interf. Sci.* **2012**, *387*, 250–261.

- (45) Wilson, L. D.; Sidall, S. R.; Verrall, R. E. *Can. J. Chem.* 1997, 75, 927–933; and references cited therein.
- (46) Eissa, A. S.; Khan, S. A. *Food Hydrocolloids* **2006**, 20, 543–547.
- (47) Connors K. A. *Binding Constants: The Measurement of Molecular Complex Stability*, John Wiley & Sons, **1987**.
- (48) Ramstad, T.; Hadden, C. E.; Martin, G. E.; Speaker, S. M.; Teagarden, D. L.; Thamann, T. *J. Int. J. Pharm.* **2005**, 296, 55–63.
- (49) Wilson, L. D.; Verrall, R. E. *Langmuir* **1998**, 14, 4710–4717; and references cited therein.
- (50) Sharma R. *Small-Molecule Surfactant Adsorption, Polymer Surfactant Adsorption, and surface Solubilization: An Overview*, Materials Science and Engineering Division, Eastman Kodak Company Rochester, NY 14650-2158
- (51) Johnson, R. L., Anschutz, A. J., Smolen, J. M., Simcik, M. F., Penn, R. L. *J. Chem. Eng. Data* **2007**, 52, 1165–1170.
- (52) Wilson, L. D.; Verrall, R. E. *J. Phys. Chem. B* **1997**, 101, 9270–9279; references cited therein.

CHAPTER 8

Manuscript 7

Description

The study in this manuscript describes the interaction of MIMs (*cf.* Chapter 7) with PFOA/OA at the solution-solid interface using spectroscopic (FT-IR), thermanalytical (DSC), and calorimetric (ITC) methods, and measurements of contact angles. The equilibrium adsorption properties of perfluorooctane sulfonate (PFOS) were used to provide further independent support for the sorptive process and interaction between PFOA and the copolymer (MIMs) adsorbent surface.

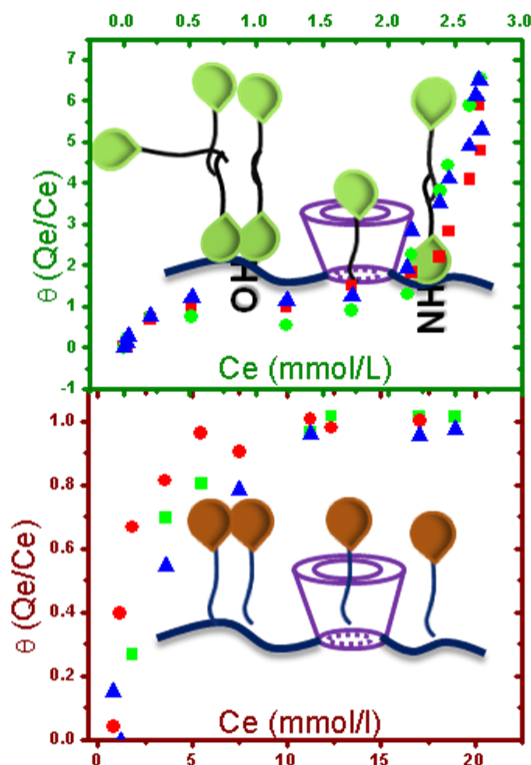
Author's Contribution

The idea of spectroscopically probing the interaction between PFOA and the adsorbent surface was proposed by Dr. Wilson. The use of some of the techniques (DSC, FT-IR and DLS) was proposed by myself, others (ITC and contact angle) were proposed by Dr. Wilson. All of the structural characterization, batch adsorption tests, and analyses of the data were done by myself. The first draft of the manuscript was prepared by myself and subsequently edited Dr. Wilson.

Relation of Manuscript 3 to Overall Objective of this Project

Since this study describes the interaction between PFOA and a CD-based copolymer adsorbent material, it provides an insight into the structure of host-guest systems at the solution-solid interface. The work in this manuscript is relevant to the study of the structure of supramolecular host-guest systems with emphasize on the use of polymeric host materials.

Graphical Abstract



Research Highlights

- The interaction of a fluorocarbon (FC; PFOA) guest onto the surface of hydrocarbon-based copolymers (MIMs) differs significantly from that of a hydrocarbon (HC) analogue (OA) due to differences in hydrophobicity of PFOA vs OA.
- In a non-ideal FC-HC interaction, the PFOA is adsorbed onto the MIMs' surface via head group interactions to form monolayers, with subsequent interaction of the methyl (CF_3) groups to form bilayers and multilayers.
- In an ideal HC-HC interaction, the OA is adsorbed onto the MIMs' surface via the tail group to form monolayer structure.
- The unique role of the head group interactions was concluded from comparison of the respective adsorption isotherms of MIMs with PFOA (carboxylate) and PFOS (sulfonate), respectively.

8. Investigation of the Adsorption Processes of Alkyl and Perfluoroalkyl Carboxylates onto Macromolecular Imprinted Materials

*Abdalla H. Karoyo and Lee D. Wilson**

University of Saskatchewan, Department of Chemistry, Saskatoon, SK, S7N 5C9, Canada

*Corresponding Author

8.1 Abstract:

The isotherm adsorption properties of synthetically engineered copolymer materials containing β -cyclodextrin (β -CD), hereafter referred to as macromolecular imprinted materials (MIMs), are reported with perfluorooctane sulfonate (PFOS), perfluorooctanoic acid (PFOA), and octanoic acid (OA) anions. The equilibrium sorption parameters derived from the Sips and BET models reveal variable surface interactions between the MIMs with the perfluorinated and hydrocarbon anions. Monolayer adsorption of OA onto the MIMs surface occurs via the hydrocarbon alkyl tail; whereas the interaction of PFOA is mediated via the carboxylate head group, followed by multilayer adsorption via the perfluoroalkyl tail. Supporting evidence for the nature of these unique interactions is evidenced by contact angle, vibrational frequency shifts and intensity changes, differential scanning calorimetry (DSC), and isothermal titration calorimetry (ITC). The formation of mono- and multilayer structures can be understood in terms of the hydrophobic effect and the unique thermodynamic properties of perfluorocarbon and hydrocarbon anions at copolymer interfaces.

8.2 Introduction

The adsorption of alkyl carboxylates and sulfonates from aqueous solution onto solid copolymer surfaces has been previously studied using solid-solution isotherms.¹⁻³ The adsorption of such alkyl anions onto copolymer surfaces was reported to form well defined structures such as aggregates, monolayers, bilayers, and multilayers.^{4,5} The occurrence of diverse interactions at the solid-liquid interface depends on the chemical compatibility of the adsorbent surface and the adsorbate because the hydration characteristics of the overall system can give rise to monolayer vs. multilayer adsorption.⁶ The preparation of multilayered structures through adsorption of a surfactant on a surface has been previously reported with industrial applications that range from paint technology and dispersion-flocculation to oil recovery processes.⁷ More importantly,

multilayer structures at interfaces are increasingly being recognized as exceptional structural features for biological applications (e.g., cell patterning, drug delivery, and anti-bacterial coating).⁸ The adsorption of surfactant anions onto copolymer surfaces containing β -CD to form monolayer and multilayer structures were recently reported.⁹ In the case of multilayer adsorption, the adsorbent surface is initially covered by a monolayer of the adsorbate anions (e.g. PFOA) whose polar head groups are adsorbed onto the polar domains (e.g., -NH and -OH) of the copolymer surface. As well, complex formation between the apolar tails of PFOA and the inclusion sites of β -cyclodextrin (β -CD; *cf.* Scheme 8.1) may occur. Additional adsorption of PFOA onto the preformed monolayer can yield bilayer and multilayer at elevated concentration of PFOA. The characterization of such types of surface interactions on solid surfaces requires various techniques such as spectroscopic (e.g., NMR, FT-IR, UV, and Raman), DSC, and contact angle.¹⁰⁻¹²

In a previous study,¹³ the adsorption between alkyl carboxylate anions and copolymers containing β -CD was inferred from isotherm adsorption parameters. To gain a better understanding of the molecular level details of the unique surface interactions for these adsorbent/adsorbate systems, we report a detailed study of the equilibrium adsorption between the anions of perfluorooctanoic acid (PFOA), octanoic acid (OA), and perfluorooctane sulfonate (PFOS) in aqueous solution. Herein, we report spectroscopic (FT-IR), thermal analyses (DSC), contact angle and calorimetric (ITC) results to study the adsorption processes for the alkyl carboxylate anions with MIMs. The adsorption results of PFOS were compared to provide further independent support for the mechanism of interaction between PFOA and the copolymer adsorbent surface.

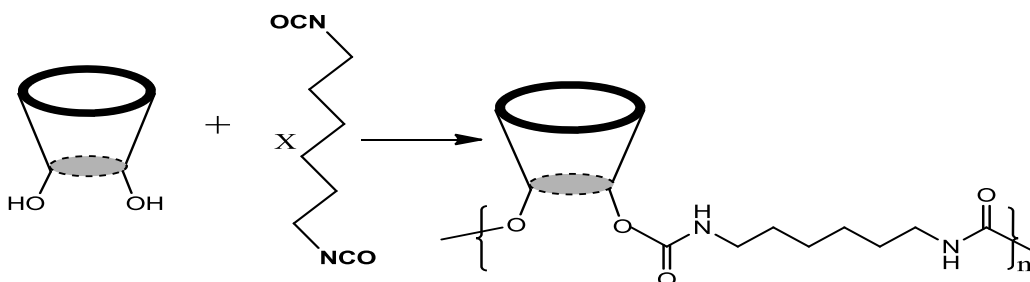
8.3 Chemicals

Perfluorooctanoic acid (PFOA; 96%) and perfluorooctane sulfonic acid (PFOS; 98%) were purchased from SynQuest Laboratories USA (Alachua, FL.). Octanoic acid (OA) and β -CD were purchased from VWR Canada Ltd. Sodium hydroxide (NaOH) and Potassium hydrogen phosphate (KH_2PO_4) were purchased from Sigma-Aldrich Canada Ltd. (Oakville, ON). All materials were used as received unless specified otherwise.

8.4 Methods

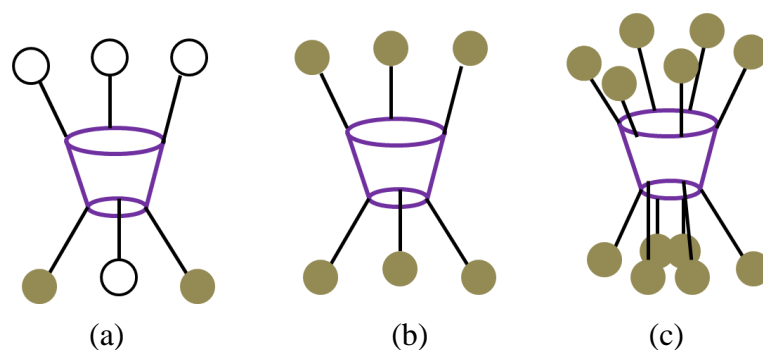
8.4.1 Synthesis of macromolecular (β -CD)-based copolymers (MIMs)

The synthesis of copolymers containing β -CD (MIMs; e.g., HDI-1 and -6), hereafter referred to as macromolecular imprinted materials (MIMs), was reported previously^{13,14} (*cf.* Scheme 8.1). Two types of MIMs (HDI-1; water soluble and HDI-6; water insoluble) were used in this study. The numeric values ($x = 1$ or 6) represent the relative mole quantity of diisocyanate linker units in relation to the moles of β -CD which is unity.



Scheme 8.1 Reaction between β -CD (toroid) and 1,6-hexamethylene diisocyanate (HDI) to form the HDI-X copolymers; where $X = 1$ or 6 . Note that for the 1:1 mole ratio, the cross linker is hypothesized to attach at the primary annular hydroxyl sites ($-\text{C}_6\text{H}_2\text{-OH}$) of β -CD.

According to Scheme 8.1 above, the number of linker substituents in the annular regions of β -CD is estimated at two linker moieties per annular face. In particular, the primary hydroxyl groups of β -CD are more reactive than the secondary hydroxyl groups; therefore, substitution of the diisocyanate linker occurs preferentially at the primary hydroxyl sites. This is applicable for the 1:1 β -CD/HDI copolymer (HDI-1). As the linker ratio increases (i.e., $X > 1$), the number of linker substituents increase up to three units per annular face.¹⁵ It should be noted here that the steric effects of the MIMs directly correlates with the linker content, as will be shown in the forthcoming results and discussion. Scheme 8.2a–c illustrates the proposed substitution of the diisocyanate linker units on the primary and secondary hydroxyl groups at the annular of β -CD for the low (1:1; HDI-1) to high (1:6; HDI-6) β -CD:HDI cross-linking.



Scheme 8.2 Schematic presentation of the sites of substitution of HDI cross linker to the primary (narrow rim) and secondary (wide rim) hydroxyl groups in the annular region of β -CD copolymer. The filled spheres represent covalently attached sites and illustrate (a) low (e.g. 1:1), (b) medium (e.g. 1:3), and (c) high (e.g. 1:6) cross-linking; whereas, the open spheres represent unreacted sites. Adapted from ref. 15.

8.4.2 Preparation of MIMs/carboxylate anion mixtures

Samples of the insoluble MIM (HDI-6) were equilibrated with PFOA (pH \sim 4) and OA (pH \sim 8.5) at several different concentrations to obtain mixtures that correspond to monolayer and multilayer surface coverage (*cf.* Figures 7.2 and 7.4, and Table 7.1, chapter 7). In the case of PFOA, 100 mg of HDI-6 was weighed in three separate 250 ml beakers containing 100 mL of 7 mM (multilayer), 4 mM (mono-/multi-layer), and 1 mM (monolayer) PFOA in MilliQ water at ambient pH conditions (pH \sim 4), respectively. As for OA, the following monolayer concentrations were used: 18 mM, 4 mM and 1 mM at pH 8.5 (i.e., pH $>$ pK_a OA) adjusted using small amounts ($<$ 1%) of NaOH solution. The solution mixtures were stirred for 24 h and filtered through Whatman no. 2 filter paper followed by washing with MilliQ water to remove excess PFOA or OA. The resulting equilibrated solid copolymer samples were analyzed using DSC and FT-IR spectroscopy. For the sake of discussion, the MIMs with PFOA and OA samples are denoted as HDI-6/PFOA-7, HDI-6/PFOA-4, HDI-6/PFOA-1, HDI-6/OA-18, HDI-6/OA-4, and HDI-6/OA-1, respectively. The foregoing numeric designation refers to the relative concentrations of the carboxylate anion (mM).

8.4.3 FT-IR Spectroscopy

Fourier Transform-IR spectra were obtained on the hydrated samples using a Bio-Rad FTS-40 spectrometer with a resolution of 4 cm⁻¹. All spectra were obtained with spectroscopic grade KBr

which constituted ~80% (w/w) of the total sample. The FT-IR of octanoic acid (OA) was obtained by adding a drop of the neat liquid sample on KBr.

8.4.4 Differential Scanning Calorimetry (DSC)

Differential scanning calorimetry (DSC) of the samples was acquired using a TA Q20 thermal analyzer over a temperature range of 30 °C to 150 °C. The scan rate was set at 10 °C/min and dry nitrogen gas was used to regulate the sample temperature and sample compartment gas purging. Samples were analyzed as aqueous pastes in hermetically sealed aluminum pans with a small exhaust hole punched in the lid of the pan to allow release of gas. Sample weights ranged between 10–12 mg.

8.4.5 Contact Angle

Contact angle measurements were acquired using CT Scan vintage 50 contact angle goniometer at ambient temperature (22±1 °C). Liquid drops containing variable levels of PFOA (7 mM, 4 mM and 1 mM) and OA (18 mM and 1 mM) in MilliQ water were placed on the surface of an air-dried copolymer film of HDI-6. The films (~20 µm thick) were prepared by drop-casting 1 mL of DMSO solution containing ~0.5 mg HDI-6 onto a 0.5”x1.5” silicon wafer to afford relatively smooth and even films.¹⁷ The use of silicon wafers as a substrate for contact angle measurements was previously reported.¹² The average contact angles were obtained from measurements on 4 drops of each liquid, where 10 µL drops were placed on the films using a 250 µL syringe and contact angle measurements were made on both sides of the drops. The reported contact angle corresponds to the static contact angle values at equilibrium measured within 1 minute of droplet addition to the surface. The contact angles of water, PFOA, and OA on untreated silicon wafer surface were also measured as controls where the contact angles were constant to within ± 1°.

8.4.6 Isothermal Titration Calorimetry (ITC)

ITC measurements were carried out at 25 °C on a Calorimetry Sciences Corp. (CSC) calorimeter using native β-CD and the soluble copolymer (HDI-1) as the host substrates. All samples employing OA titrations were prepared in phosphate buffer at pH ~8.5, while samples for PFOA titrations were prepared at ambient pH conditions (pH ~4) in Milli-Q water. The ITC

experiments were conducted by injecting the carboxylate anion solutions (OA, or PFOA; ~6 mM) as the titrants, at 200 s intervals between injections and 200 s standard equilibration time, using a 250 μ l injection syringe into a stainless steel sample cell (1.430 mL) containing the host substrates (β -CD; ~0.3 mM, or HDI-1; ~0.4 mg/mL). The ITC thermodynamic parameters for β -CD were measured against HDI-1 for comparison. The aqueous solutions containing β -CD or HDI-1 in the cell were stirred at 300–400 rpm. The integrated heat effects of each injection were corrected by subtraction of the corresponding heats of dilution; i.e., heat effects due to dilution of PFOA and OA solutions in Milli-Q water and phosphate buffer, respectively. In the case of the OA titrations, the heats of dilution for the phosphate buffer into the host substrates were also subtracted.

The experimental data obtained from the calorimetric titration were analyzed using CSC built-in BindWorks 3.1 software. A single binding model with an independent set of multiple binding sites was used for the non-linear regression. The enthalpy of binding (ΔH), the binding constant (K_i), and the number of binding sites (n) were estimated from the BindWorks 3.1 software using the independent and the multiple (β -CD/PFOA) models of the software, respectively. The change in standard Gibbs free energy (ΔG°) and the corresponding change in standard entropy (ΔS°) were obtained using equation (8.1). It should be noted here that β -CD forms 1:1 ($n = 1$) and 2:1 ($n = 2$) inclusion compounds with PFOA.¹⁸ Therefore, two distinct binding sites are available for PFOA to bind to β -CD. In the case of HDI-1, a 1:1 (β -CD/PFOA) complex is anticipated as the predominant stoichiometry. Hydrocarbon analogues, e.g. OA are generally known to form 1:1 CD/OA complexes,¹⁹ but higher stoichiometries (e.g., 2:1) have been reported in a previous ITC study.²⁰

$$\Delta G^\circ = -RT \ln K = \Delta H^\circ - T\Delta S^\circ \quad \text{Equation 8.1}$$

8.5 Adsorption Isotherms

Adsorption isotherms for PFOA and OA were expressed as plots of adsorbent surface coverage (Θ) against the equilibrium concentration of unbound (residual) adsorbate species (C_e ; mM) in aqueous solution. The surface coverage (Θ ; Q_e/Q_m) for both the adsorption isotherms

(i.e., PFOA and OA with MIMs) were determined as the ratio of the amount of adsorbed species (Q_e ; mmol/g) relative to the monolayer sorption capacity (Q_m ; mmol/g).

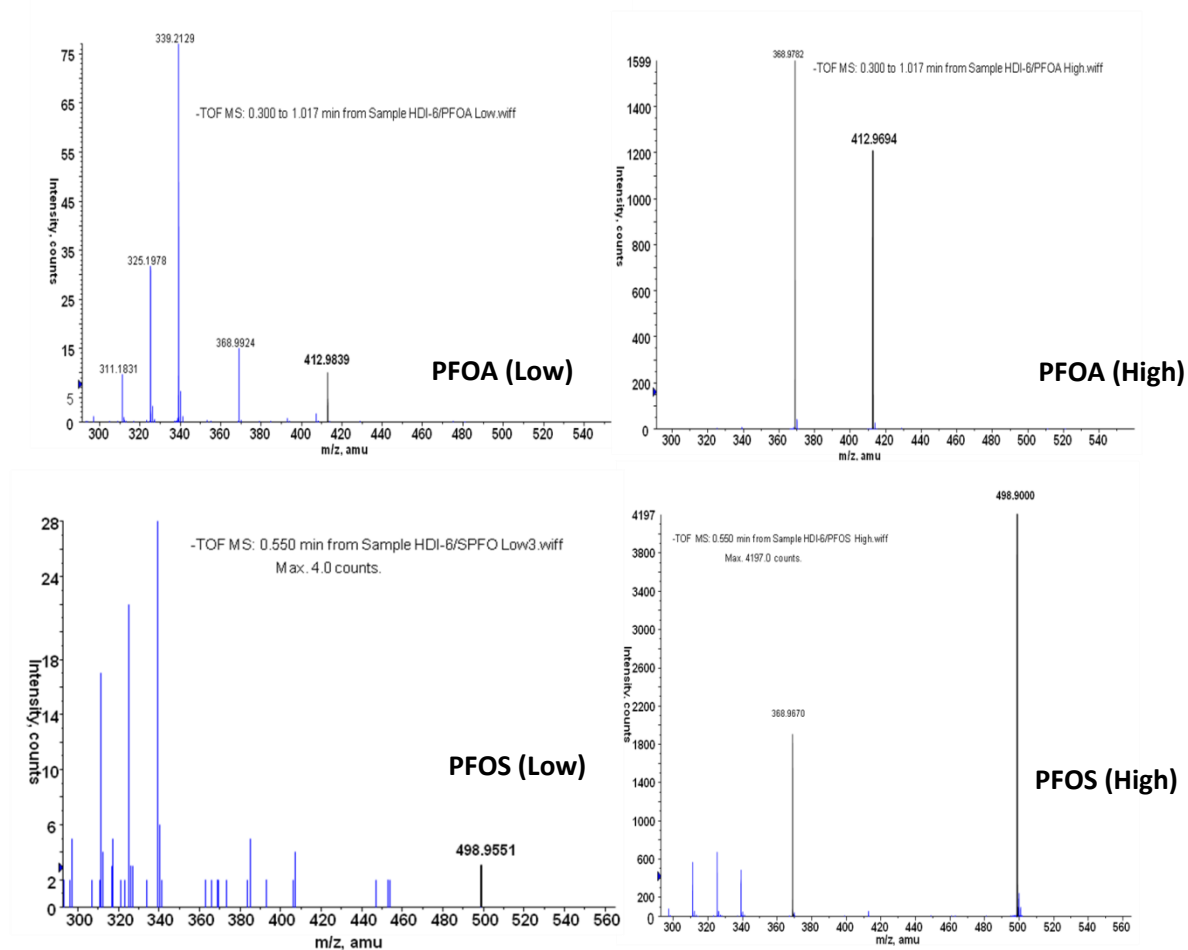


Figure 8.1 Typical ESI-MS spectra of the solutions of PFOA (pH 3.8) and PFOS (pH ~3) at low and high loading concentrations in the presence of HDI-6 copolymer.

Adsorption isotherms for PFOS were expressed as plots of Q_e (mmol/g) vs C_e (mmol/l), where the experimental sorption data was evaluated using the Brunauer-Emmett-Teller (BET) model.¹⁶ All equations and other parameters were defined in a previous report.¹³ Hybrid quadrupole-TOF (Q-star) MS/MS mass spectrometer with electrospray ionization (ESI-MS) in negative ion mode was used to evaluate the C_e values for the PFCs (i.e., PFOA and PFOS). The ESI-MS was not used to evaluate the equilibrium concentrations for OA since samples containing electrolytes (e.g., sodium) and fatty acids pose problems that limit the sensitivity of ESI-MS in the form of ion suppression and blockage effects. The residual amounts of OA were analyzed by back

titration using 0.02 M HCl solution and bromophenol blue as the indicator. Typical ESI-MS spectra for the equilibrium concentrations of PFOA (amu \sim 412.9) and PFOA (amu \sim 498.9) are shown in Figure 8.1a,b for low and high PFC loadings, after adsorption with HDI-6.

The use of Θ vs. C_e plots for PFOA and OA sorption with MIMs, respectively, allows for direct comparison of the type of interaction (monolayer; $\Theta \sim 1$ vs. Multilayer $\Theta > 1$) between the bound adsorbate and adsorbent surface. In the case of PFOS, the sorption equilibrium parameters obtained from the Q_e/C_e isotherms provide some insight concerning the adsorptive process of PFOS onto MIMs relative to that of PFOA.

8.6 Results and Discussion

8.6.1 Sorption Studies for PFOA, OA, and PFOS

8.6.1.1 Surface Coverage of PFOA and OA (Monolayer vs. Multilayer)

Figure 8.2 shows the binding sorption isotherms expressed as surface coverage (Θ) against the equilibrium residual concentrations (C_e ; mmol/L) of PFOA and OA in aqueous solution, respectively. The binding of the PFOA anion onto the various MIMs (Figure 8.2) leads to surface coverage greater than unity and this is consistent with the formation of a multilayer isotherm. In contrast to PFOA, the adsorption of OA onto the MIMs surface represents a typical monolayer isotherm described by the Langmuir equation.²¹

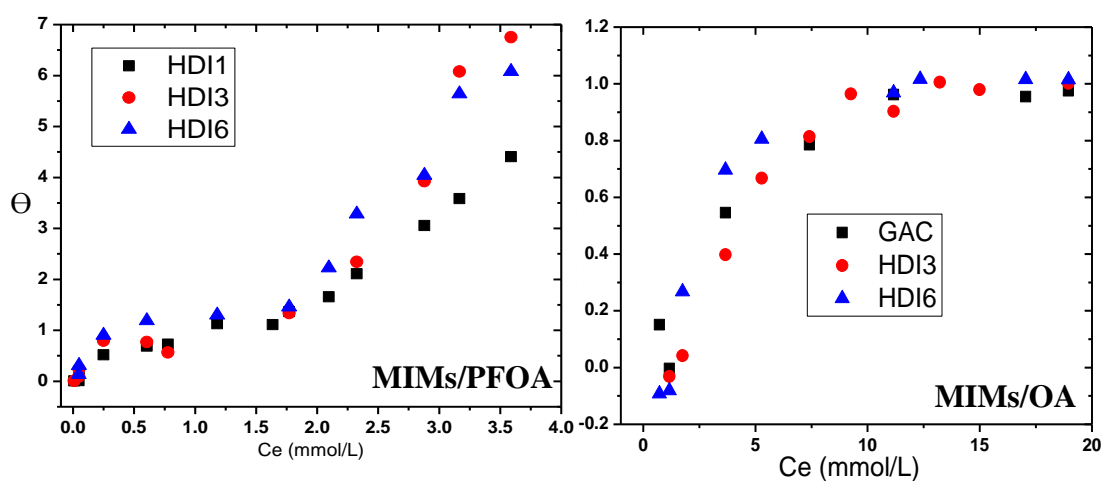


Figure 8.2 Sorption isotherms for MIMs/PFOA (Left) and MIMs/OA (Right) systems expressed as surface coverage (Θ) against equilibrium concentration (C_e).

Table 8.1 Physicochemical Properties of the Adsorbent and Adsorbate

Adsorbent	SA (m ² /g)	β -CD (mol %)	Accessibility of β -CD sites (%)	HDI content (mol %)
GAC	1100 ^a	-	-	-
HDI-1	3 ^{15,b}	87.1	100	12.9
HDI-3	5 ^{15,b}	69.2	4.78	38.7
HDI-6	NR	52.9	~0	77.4
Adsorbates	Molecular formula	pK _a	cmc (mM)	Water solubility (g/L at 25°C)
PFOA	CF ₃ (CF ₂) ₆ COOH	2.5 ²⁵	8.7-10.5 ²⁶	3.4 ²⁷
OA	CH ₃ (CH ₂) ₆ COOH	4.9 ²⁸	350 ²⁹	0.68 ³⁰

^aSupplier's BET surface area, ^bBET surface area.

A surface coverage of unity implies that a single layer of OA is adsorbed onto the MIMs surface at higher concentrations ($C_e \geq 10$ mM; *cf.* Fig. 8.2 for MIMs/OA).²² We concluded in a previous study¹³ that the binding of the OA anion onto the MIMs surface occurs via the apolar alkyl tail to minimize the surface free energy because the polar carboxylate head group is appreciably hydrated. In the case of the PFOA anion, binding onto the MIMs surface likely occurs between the carboxylate anion of PFOA and the dipolar domains (i.e., -NH and -OH) of the copolymer surface (*cf.* Scheme 8.1). This mode of binding is consistent with the reduced hydration of PFOA head group due to inductive effects of the neighbouring CF₂ groups. Inductive effects will reduce the overall negative charge on the carboxylate head group, in agreement with the low pK_a value of PFOA relative to OA.²³ Furthermore, interactions between the carboxylate head group of PFOA and the polar surface domains of the adsorbent lead to the formation of well-defined multilayers due to the occurrence of cooperative aggregation at higher PFOA concentration ($C_e > 1.5$ mM; Figure 2a).²⁴ In cases where the inclusion sites of β -CD are accessible, typical host-guest inclusion complexes are anticipated for OA and PFOA,

respectively. Table 8.1 lists the physicochemical properties of the various adsorbent materials (i.e. sorbent surface area, % accessibility of β -CD sites, and linker content) and the adsorbate (i.e. cmc, solubility, and pK_a).

8.6.1.2 Sorption and Equilibrium Binding Parameters for PFOA and OA

The equilibrium sorption binding parameters for PFOA and OA are listed in Table 8.2. Based on the Q_m values, it is worthwhile to note that the sorption of PFOA by the MIMs was shown to be comparable to GAC. The relatively high Q_m values for the MIMs/PFOA (2.63 mmol/g; Sips) systems exceed GAC (1.35 mmol/g; Sips) and is attributed to the formation of multilayers in the former. The formation of multilayers is significant in spite of the lower surface area of the copolymers relative to GAC (*cf.* Table 8.1).

The minimum equilibrium saturation concentrations ($C_{e,sat}$; mmol/l) of adsorbate for monolayer/multilayer profiles were estimated from the respective isotherm models (Sips/BET) in Table 8.2. The Q_m values enclosed in brackets in Table 8.2 represent values obtained from the Sips model. In general, complete coverage of the PFOA monolayer occurs at $C_e \sim 1.0$ mM and multilayer formation occurs at $C_e > 1.5$ mM with saturation at $C_e \geq 3.5$ mM. In the case of OA, monolayer saturation occurs at $C_e \sim 10$ mM. The equilibrium binding constants (K_{eq} ; M^{-1}) in Table 8.2 were estimated from the “best-fit” parameters obtained from the Sips isotherm model. The K_{eq} values for PFOA are greater than the corresponding values for the OA/MIMs systems. Adsorption processes of surface active species are strongly governed by hydrophobic effects and the variable hydrophobicity of PFOA and OA are consistent with their relative cmc values (*cf.* Table 8.1). The interaction of both alkyl carboxylates (i.e., PFOA and OA) with MIMs will likely involve London-dispersion forces; however, PFOA has some localized dipoles such as the α - and β -CF₂ groups, along with the terminal CF₃ group, in agreement with the chemical shift data of these nuclei.¹⁸ By contrast, the OA alkyl chain is an apolar hydrocarbon, and its greater cmc (*cf.* Table 8.1) suggests that it is less hydrophobic than PFOA.

The greater pK_a of OA relative to PFOA illustrates differences in the charge density and hydration of the carboxylate head group of each anion, as indicated above. Therefore, the greater K_{eq} for PFOA from Table 8.2 suggests that dipolar interactions occur with the polar surface groups at the MIMs interface. This is in addition to secondary binding at the inclusion sites of β -CD which occurs via the perfluoroalkyl group. In the case of OA, secondary London/dispersion

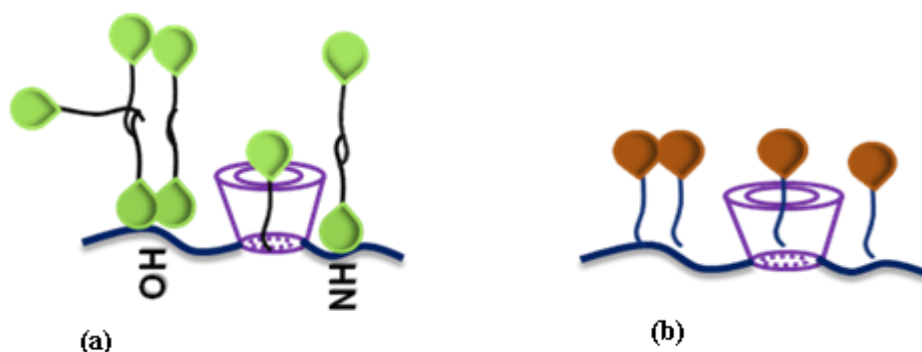
Table 8.2 BET and Sips Isotherm Sorption Parameters for PFOA and OA with GAC and MIMs at 295 K and pH 4 and 8.5, respectively.*

	GAC	HDI-1	HDI-3	HDI-6
PFOA				
	Sips	BET (Sips)		
Q_m (mmol/g)	1.39	1.35 (2.63)	0.97 (1.38)	0.87 (1.28)
K_{Sips} (L/g)	2.39	0.91	1.23	14.1
K_{eq} ($10^3 M^{-1}$)	~1	0.4	0.5	5.8
n_s	0.74	0.87	0.71	1.26
$C_{e, sat.}$ (mmol/L)	~0.5	~1/>3.5	~1/>3.5	~0.5/>3
OA				
Q_m (mmol/g)	1.98	NR	0.84	1.02
K_{Sips} (L/g)	0.07	-	0.01	0.04
K_{eq} (M^{-1})	10	-	1.4	5.8
n_s	2.1	-	3.1	3.2
$C_{e, sat.}$ (mmol/L)	~10	-	~10	~8

*The Q_m values enclosed in brackets in Table 2 represent values estimated from the Sips model; NR = not recorded.

intermolecular forces are anticipated with the apolar linker domain of the copolymer material, relative to the favourable inclusion of the β -CD sites.¹⁹ Dipolar interactions (e.g., H-bonding) are $\sim 10^1$ kJ/mol compared with weak dispersion forces ($< 10^1$ kJ/mol).³¹ Furthermore, the heterogeneity constant (n_s) derived from the Sips model indicates the presence of variable surface interactions between PFOA and OA with the MIMs, respectively. The large deviation of the n_s values ($n_s = 2-3$) from unity for the OA/MIMs system suggests the presence of

heterogeneous (i.e. two or more) surface sites on the material. The heterogeneity factor is lowered for PFOA sorption and supports that unique adsorbate/adsorbent interactions occur that agree with multilayer formation. Various types of subtle interactions are proposed for PFOA and OA anions at the MIMs surface that lead to multilayer and monolayer formation, as illustrated in Scheme 8.3a,b.



Scheme 8.3 Proposed adsorption modes of the carboxylate anions within the inclusion sites of β -CD via tail groups and onto the linker domains of the copolymer for (a) PFOA via ion-dipole interactions of the head group and subsequent formation of multilayers, and (b) OA adsorption occurs via the alkyl tails to form a monolayer.

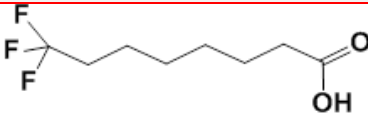
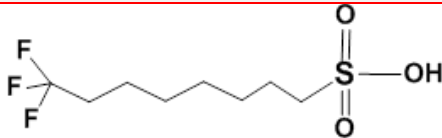
8.6.2 Sorption and Equilibrium Binding Parameters for PFOS

The sorption and equilibrium binding parameters of MIMs/PFOA systems were compared with the corresponding values for PFOS to further understand the mode of sorption by variation of the head group anion. Several structural and physicochemical properties of PFOA and PFOS are summarized in Table 8.3.

The most notable structural difference between PFOA and PFOS is the nature of the head group. The relative head group size, cmc, and pK_a values for PFOA and PFOS are expected to result in unique modes of adsorption with the MIMs surface, according to Scheme 8.3. The isotherms for PFOS with HDI-1 and -6 were obtained using the protocol described in a previous study.¹³ The concentration of PFOS was varied over a wide range of 0.01–5 mmol/l, while the weight of the adsorbent was fixed (~2 mg). The sorption behavior of PFOS at pH ~3 with MIMs was expressed graphically as plots of Q_e (mmol/g) vs C_e (mmol/l). Ambient pH values that exceed the respective pK_a values were used for the adsorption studies of both PFOA (~3.8) and PFOS (~3.0). The use of salts and buffers was avoided because they limit the sensitivity of ESI-

MS in the form of ion suppression and blockage effects, as described previously.¹³ At the given pH conditions, the anion species account for ~95 % and >99% for PFOA and PFOS, respectively. Therefore, the PFOA and PFOS species exist predominantly in their anion forms at the specified conditions.

Table 8.3 Molecular Structures and Physicochemical Properties of PFOA and PFOS*

	PFOA	PFOS
Molecular Structure		
Molecular weight (g/mol)	500	414
Solubility (g/L) at 25 °C	3.40	0.570 ³²
Melting point (°C)	45-55	>400
Vapor pressure (mmHg) at 20 °C	0.017 ²⁵	2.48x10 ^{-6 25,c}
pKa	2.5	<1 ³²
cmc (mmol/L)	8.7-10.5	2.0 ³²

*^cVapor pressure value for PFOS corresponds to the potassium salt.

The most notable structural difference between PFOA and PFOS is the nature of the head group. The relative head group size, cmc, and pK_a values for PFOA and PFOS are expected to result in unique modes of adsorption with the MIMs surface, according to Scheme 8.3. The isotherms for PFOS with HDI-1 and -6 were obtained using the protocol described in a previous

study.¹³ The concentration of PFOS was varied over a wide range of 0.01–5 mmol/l, while the weight of the adsorbent was fixed (~2 mg). The sorption behavior of PFOS at pH ~3 with MIMs was expressed graphically as plots of Q_e (mmol/g) vs C_e (mmol/l). Ambient pH values that exceed the respective pK_a values were used for the adsorption studies of both PFOA (~3.8) and PFOS (~3.0). The use of salts and buffers was avoided because they limit the sensitivity of ESI-MS in the form of ion suppression and blockage effects, as described previously.¹³ At the given pH conditions, the anion species account for ~95 % and >99% for PFOA and PFOS, respectively. Therefore, the PFOA and PFOS species exist predominantly in their anion forms at the specified conditions.

The sorption isotherms for PFOS in the presence of HDI-1 and -6 are shown in Figure 8.3. The equilibrium sorption parameters (e.g. sorption capacity and equilibrium constant) are listed in Table 8.4. The experimental data were well described by the BET model with $R^2 > 0.99$. In Figure 8.3, MIMs display a type III sorption isotherm with PFOS according to BET classification;³³ where an asymptotic rise for Q_e is observed at $C_e \sim 3.0$ mmol/l and 3.5 mmol/l for HDI-1 (a) and -6 (b), respectively (*cf.* Figure 8.3 and Table 8.4). This is contrary to the MIMs/PFOA system which displayed type IV isotherms. Type III sorption isotherms describe weak adsorbate-adsorbent interactions, therefore adsorbate-adsorbate interactions may play a more important role in the sorption of PFOS onto MIMs.³⁴ In contrast, PFOA sorption is characterized by moderately strong interactions at low C_e (*cf.* Figure 8.3 insets and Figure 7.2 in chapter 7), as evidenced by the higher magnitude of Q_e in the region where monolayer adsorption occurs. Relatively weak interactions are evidenced for the MIMs/PFOS isotherm, according to the negligible sorption onto the adsorbent surface for $C_e < 3$ mM (*cf.* Figure 8.3). These findings are consistent with the more pronounced ion/dipolar interactions of the carboxylate anion relative to the weaker ion/dipolar interactions of the sulfonate anion with the MIMs surface.

The dipolar domains on the MIMs surface consist of –NH and –OH functional groups (*cf.* Scheme 8.1), where these domains can serve as H-bond donor or acceptor sites. Ion-dipole interactions are possible between the carboxylate anions of either PFOA and PFOS, which depend on the hydration and charge distribution characteristics of the anions and the surface. The occurrence of inductive effects from the methylene groups in PFOA and PFOS affects the charge distribution of the carboxylate and sulfonate head groups to a differing extent. The ionic charge

of the carboxylate group is distributed over three atoms vs four atoms in the case of the sulfonate group. Therefore, the greater charge density of the carboxylate anion may result in more pronounced ion-dipole interactions with the MIMs surface. This is supported by the offset in binding affinity between PFOA vs PFOS, according to the differing K_{eq} value of each anion species (*cf.* Tables 8.2 and 8.4).

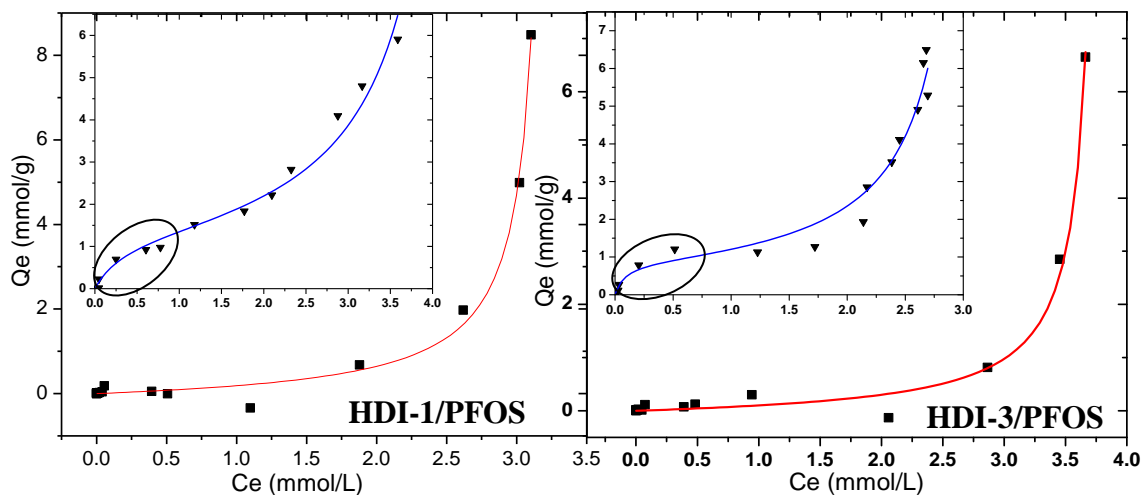


Figure 8.3 Sorption isotherms of PFOS onto HDI-1, and (b) HDI-6 MIMs at pH ~3 and 295 K. The “best-fit lines” correspond to the BET model. **Insets:** The corresponding sorption isotherms of PFOA onto HDI-1, and HDI-3 MIMs surfaces are compared where the circled regions at low C_e show favourable adsorbate-adsorbent interactions.

The values for the monolayer sorption capacity (Q_m ; mmol/g) of the MIMs with PFOS are listed in Table 8.4 as follows: 0.38 (HDI-1) and 0.69 (HDI-6). The Q_m results for PFOS (Table 8.4) are lower than the corresponding values for PFOA according to the BET model (*cf.* Table 8.2). The values in Table 8.4 for PFOS are in good agreement with those reported by Yu and coworkers.³⁵ For example, the maximum sorption capacity values for PFOS at pH 5 reported by Yu et al.³⁵ were 1.04 mmol/g on powdered activated carbon, 0.37 mmol/g on granular activated carbon, and 0.42 mmol/g for an ionic resin AI400. Hence, the MIMs uptake values reported herein have Q_m values for PFOS that are comparable or greater than other types of organic adsorbents. It is worthwhile to note that Q_m values of such PFCs is dependent on the solution pH and concentration, as anticipated according to Scheme 8.3.

The lower Q_m values for PFOS relative to PFOA can be related to different modes of sorption due to several adsorbate properties: (1) cmc values, (2) hydrophobicity, (3) molecular size, and 4) nature of the head group, as described above. For example, PFOA displayed higher Q_m values with HDI-1 (1.35 mmol/g) compared to HDI-6 (0.87 mmol/g) according to the BET model. However, the opposite trend was observed for PFOS where the Q_m value for HDI-6 (0.69 mmol/g) was greater than that for HDI-1 (0.38 mmol/g). Furthermore, the Q_m value of HDI-1/PFOS system was greatly attenuated relative to HDI-1/PFOA. The greater charge density of the carboxylate anion of PFOA imparts greater hydrophilic character, as compared to the sulfonate anion. As such, PFOS is less hydrated with a reduced charge density relative to the PFOA anion. The difference in size and charge dispersion of carboxylate and sulfonate head groups account for the observed differences with the MIMs.

MIMs adsorbents possess two types of binding sites; *i*) β -CD inclusion sites, and *ii*) interstitial domains due to the cross-linker framework. The inclusion sites of HDI-1 were reported by Mohamed et al.¹⁵ to be approximately 100% accessible (i.e., negligible steric effects) according to a dye-based method, as listed in Table 8.1. Steric effects at the inclusion sites of such copolymers typically increase as the level of crosslinking increases (i.e., HDI-6 > HDI-1). As well, HDI-1 forms a linear copolymer with high inclusion site accessibility, whereas; HDI-6 forms a more highly branched copolymer with low inclusion site accessibility (*cf.* Scheme 8.2). Given the lower cmc value and the greater molecular size^{35,36} of PFOS relative to PFOA (*cf.* Table 8.3), hemi-micelles and micelles are more likely to form for PFOS. The formation of surface-bound complexes will lower the overall concentration of unbound adsorbate which lowers the available adsorbate for inclusion binding processes. Yu et al.³⁵ reported the formation of micelles and hemi-micelles to explain the reduced adsorption of PFOS onto AI400 resin relative to that of PFOA. A similar effect may occur for the adsorption of PFOS onto HDI-1, as evidenced by its reduced binding affinity with the MIMs.

It is noteworthy that the equilibrium constant for HDI-1/PFOS ($0.57 \times 10^3 \text{ M}^{-1}$) in Table 8.4 is ~10 times lower than the value for HDI-1/ PFOA ($5.2 \times 10^3 \text{ M}^{-1}$) according to BET model, in accordance with the lower cmc of PFOS. In the case of HDI-6, greater adsorption of PFOS occurs relative to HDI-1 and may correlate with greater number of linker domains for the HDI-6 copolymer. The effect agrees with the onset of isotherm saturation for HDI-6 at a higher level of adsorbate ($C_{e, \text{sat}} \geq 3.5 \text{ mmol/L}$), relative to HDI-1 ($C_{e, \text{sat}} \geq 3.0 \text{ mmol/L}$). The inclusion site

accessibility for HDI-6 is approximately zero¹⁵ (Table 8.1); therefore binding at the cross-linker domains of the copolymer network is preferred over the inaccessible inclusion sites of β -CD. The lower K_{eq} for HDI-6 reveals that reduced uptake occurs for PFOS relative to PFOA, in agreement with the decreased charge density of PFOS described above.

It is concluded from the foregoing discussion that hydrophobic interactions are mainly responsible for the sorption of PFOS onto the MIMs surface, and hemi-micelles and micelles are formed near the cmc of the adsorbate.²⁴ Micelle formation and multilayer structures are favoured for PFOS over that of PFOA due to the greater surface activity of PFOS. As C_e approaches the cmc, multilayers and aggregates play a key role for the cooperative adsorption of PFOS at these copolymer surfaces. By comparison, the sorption of PFOA onto the MIMs surface is dominated by relatively strong dipolar interactions due to surface binding between the anion head group with the copolymer $-NH$ and/or $-OH$ groups. The adsorption of PFOA and PFOS onto the MIMs surface is summarized by Scheme 8.4. Additional evidence of these adsorptive processes between PFOA and OA with the MIMs surface is provided in a forthcoming section (§8.6.2).

Table 8.4 BET Isotherm Sorption Parameters* for PFOS with HDI-1 and -6 MIMs at 295 K and pH ~ 3.

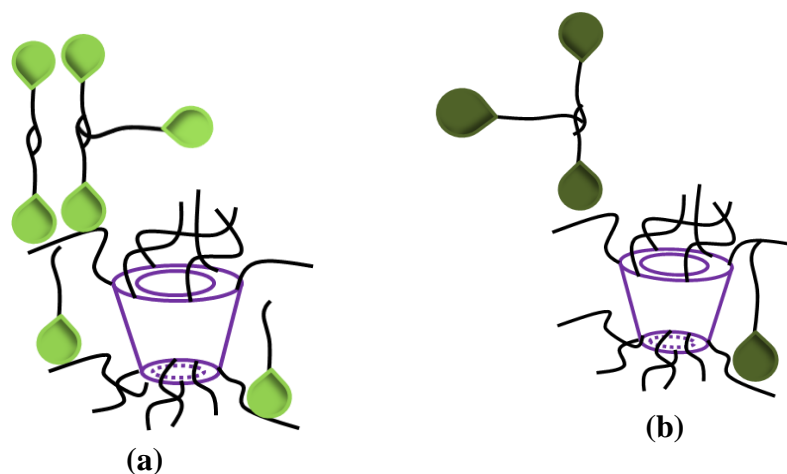
	Q_m (mmol/g)	K_{BET} (L/g)	K_{eq} ($10^3 M^{-1}$)	R^2	ϵ_R (%/g)	$C_{e, sat}$ (mmol/L)
HDI-1	0.38±0.07	1.15±1.09	0.57	0.994	37	≥3.0
HDI-6	0.69±0.07	0.14±0.04	0.07	0.995	34	≥3.5

* ϵ_R denotes the level of uptake of PFOS defined as $(C_o - C_e) \times 100\% / C_o$, where C_o and C_e are the initial and residual adsorbate concentrations, respectively. All other parameters are defined in Table 2.

8.6.3 The interaction of PFOA/OA with MIMs

8.6.3.1 DSC

DSC is a highly sensitive tool used for the study of the thermal and hydration properties of food, polymeric materials, and gels.³⁷⁻³⁹ Figures 8.4 and 8.5 show the DSC results of HDI-6/PFOA and HDI-6/OA mixtures as hydrated solid pastes, respectively.



Scheme 8.4 Proposed adsorption modes for (a) HDI-6/PFOA, and (b) HDI-6/PFOS systems. PFOA confers stronger ion-dipole interactions with the dipolar regions of the MIMs surface than PFOS. Adsorption via head group interactions prevail due to the low β -CD inclusion site accessibility and the greater number of urethane linkages of HDI-6 on the MIMs framework. Note: Inclusion sites accessibility for HDI-6 ~ 0 due to steric effects.

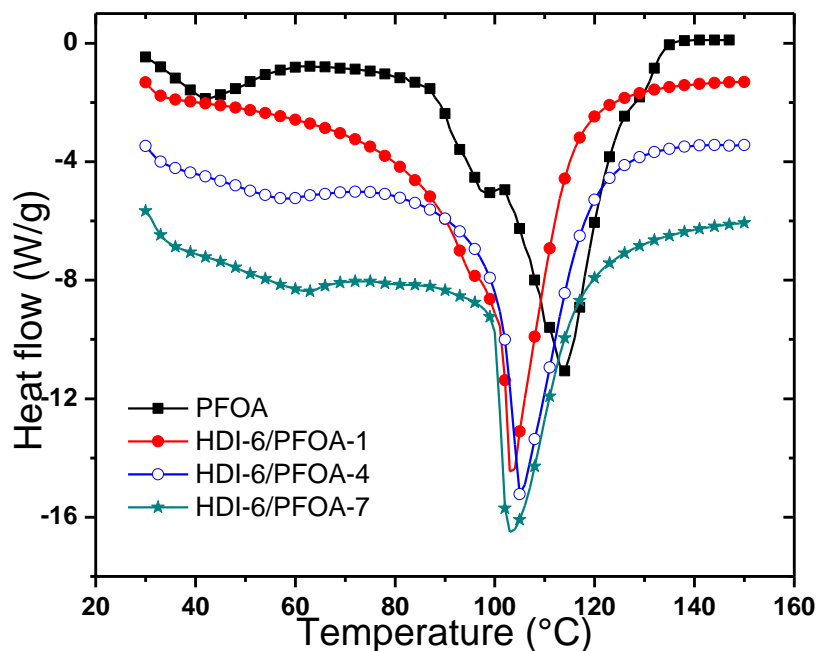


Figure 8.4 DSC thermograms of the hydrated samples of PFOA and mixtures containing HDI-6 at different PFOA loadings.

In Figure 8.4, the DSC traces for unbound PFOA and the HDI-6/PFOA system are shown. The DSC of free PFOA consists of an endotherm at lower temperature (~45 °C) which is attributed to a melting transition. The melting endotherm of PFOA appears to increase in temperature as the loading of PFOA increases, especially at 4mM and 7mM. The dehydration transition of the free PFOA is composed of two main contributions ~97 °C and 113 °C, in addition to a small broad peak ~130 °C. The endotherms at 97 and 113 °C are attributed to dehydration processes adjacent to the perfluoroalkyl chain and the head group, respectively.

Knowlton and White⁴⁰ used DSC endotherms to describe three types of water bound to zeolite; external (bulk), loosely bound, and tightly bound waters. By analogy, different regions of hydration are anticipated for the adsorbate anions and the MIMs surface due to the variation in hydrophile-lipophile domains,⁴¹ according to the isotherm results herein. Thus, such strongly bound water to the carboxylate head group are expected to desorb at much higher temperatures compared to bulk or loosely bound waters.⁴² The DSC region between 30–70 °C in Figure 8.4 is more revealing due to the “*semi-solid*” phase transitions attributed to monolayer and multilayer adsorption. For instance, the DSC of the HDI-6/PFOA-1 (monolayer) reveals an endotherm similar to that for free PFOA with the two dehydration processes at 95 and 105 °C. The lowering of these two endotherms is related to reduced hydration of PFOA due to competitive adsorption/dehydration of PFOA at the HDI-6 surface.

A comparison of the loading of PFOA from low to high values for HDI-6/PFOA-1 illustrates the emergence of a melting endotherm of PFOA ~60 °C, which increases at medium loading (HDI-6/PFOA-4; mono-/multilayer) to higher loading (HDI-6/PFOA-7; multilayer). The emergence of the PFOA endotherm ~60°C coincides with the disappearance of the dehydration endotherms at lower temperatures. The broader dehydration endotherm for HDI-6/PFOA-7 agrees with multilayer adsorption processes. Several studies of polyelectrolyte multilayers reveal that significant levels of water can enter such multilayer structures^{43,44} and contribute to broad dehydration endotherms. In general, shifting of the dehydration endotherms to lower temperatures in the HDI-6/PFOA mixtures relative to the free PFOA suggests a different environment for PFOA in the bound state. Therefore, the PFOA anion is bound via dipolar interactions onto the surface of HDI-6 through the polar domains (–NH/–OH) of the copolymer framework. The importance of such H-bonding interactions for stabilizing multilayer structures is relatively well established.¹⁰ The onset of the melting endotherm for adsorbed PFOA to higher

temperature (~ 62 °C) and the offset of the dehydration endotherm to lower temperature (103 °C) for the HDI-6/PFOA-7 system, relative to free PFOA, provides support of well-defined multilayers. The DSC results indicate that the monolayer and multilayer structures of the MIMs/PFOA system are stabilized by H-bonding and ion-dipole interactions, in agreement with the above isotherm results.

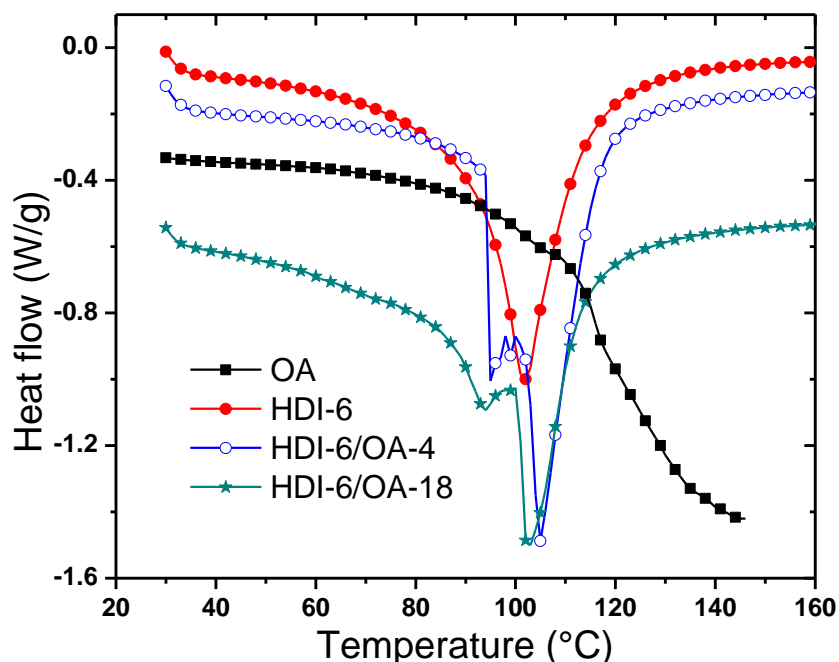


Figure 8.5 DSC thermograms of the hydrated samples of OA and its mixtures with HDI-6 at different loading levels of OA.

In contrast to PFOA, the DSC thermograms of the HDI-6/OA systems in Figure 8.5 are characterized by two well defined endotherms ~ 90 and 100 °C, attributed to dehydration processes. The DSC of unbound OA consists of a very broad dehydration transition at higher temperature (~ 140 °C) that is characteristic of fatty acids, in agreement with the strong ion-dipole interactions in water.⁴⁵ On the other hand, DSC thermograms for the HDI-6/OA mixtures are characterized by at least two dehydration events ~ 94 °C and 105 °C due to bulk and bound waters, respectively. Higher temperature transitions are characterized by sharp signals due to monolayer formation. The lower enthalpy of dehydration for HDI-6/OA mixtures relative to HDI-6/PFOA mixtures is hypothesized due to the formation of monolayers containing reduced

hydration. In contrast, multilayer structures can ingress greater amounts of water which result in broader transitions and increased dehydration enthalpy,⁴⁴ as for the HDI-6/PFOA system.

8.6.3.2 FT-IR Spectroscopy

FT-IR spectroscopy is a useful method for characterizing H-bond formation in polyurethanes and related compounds.^{32,46} FT-IR has also been used to probe spectral differences between self-assembled structures such as mono- and multi-layers,¹⁰ since these systems are often stabilized by dipolar interactions. The FT-IR spectra of HDI-6/PFOA and HDI-6/OA systems were studied to evaluate H-bonding and dipolar interactions. The results are shown in Figures 8.6 and 8.7, where the vibrational bands in Tables 8.5 and 8.6 are in agreement with previous reports.³²

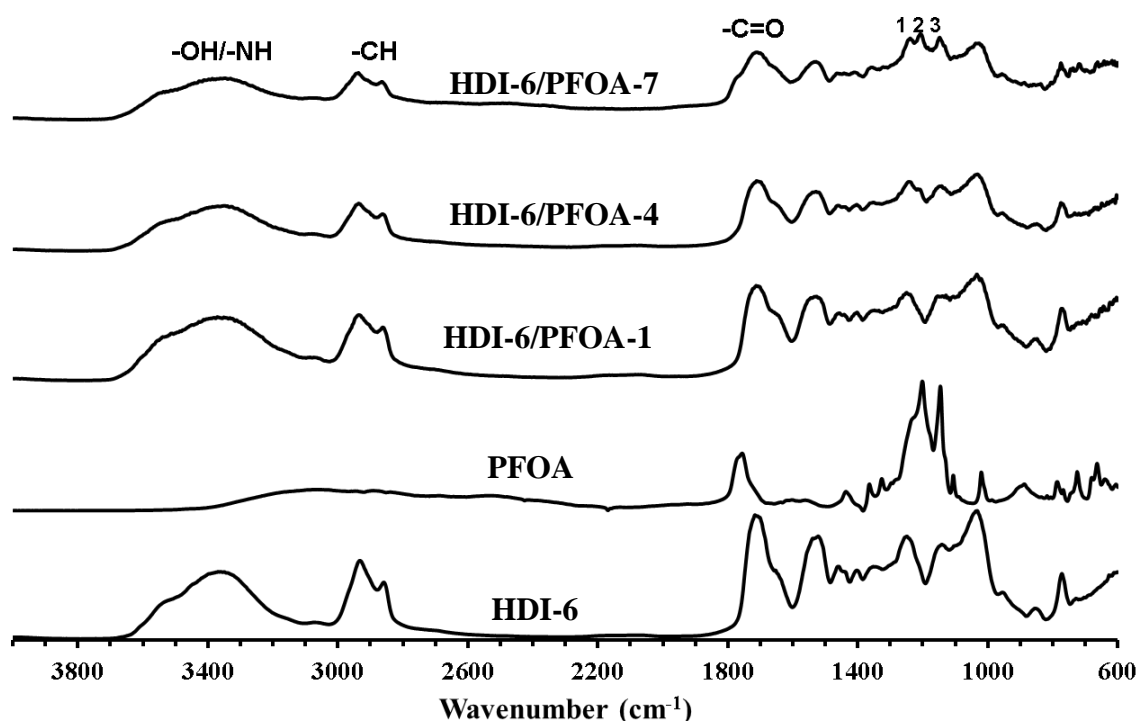


Figure 8.6 FT-IR spectra of hydrated solids HDI-6, PFOA, and HDI-6/PFOA-1, HDI-6/PFOA-4, and HDI-6/PFOA-7 systems at 295 K. The numbered bands (1–3) show the CF_2/CF_3 stretching bands of PFOA.

The FT-IR spectra for the HDI-6/PFOA system (Figure 8.6) are dominated by absorption bands due to the copolymer. The spectrum of unbound PFOA is characterized by a broad -OH

stretching band extending $\sim 3300\text{--}2600\text{ cm}^{-1}$ which is typical of carboxylic acids, due to the formation of H-bonded dimers.⁴⁷ The most important vibrational bands for the HDI-6/PFOA systems are summarized in Table 8.5. In general, broad --OH ($\sim 3400\text{ cm}^{-1}$) and --C=O ($\sim 1700\text{ cm}^{-1}$) bands are observed for the mixtures with respect to the HDI-6 and unbound PFOA, providing indirect evidence of the dipolar interactions between HDI-6 and PFOA.⁴⁸ Furthermore, the --C=O bands of the mixed systems are shifted by as much as 60 cm^{-1} (blue shift) and 13 cm^{-1} (red shift) relative to the free PFOA and HDI-6 copolymer, respectively.

The amide I region for HDI-6 and the mixtures in Figure 8.6 consistently show a band $\sim 1710\text{ cm}^{-1}$ (urethane --C=O vibrational band) and a shoulder at lower frequency ($\sim 1650\text{ cm}^{-1}$), assigned to a H-bonded urethane carbonyl band.⁴⁷ An additional band $\sim 1787\text{ cm}^{-1}$ was recorded for the HDI-6/PFOA-7 system with a blue shift of approximately 10 and 67 cm^{-1} , relative to the free acid and copolymer, respectively.

The band $\sim 1787\text{ cm}^{-1}$ is assigned to multilayers of PFOA that are unique to the HDI-6/PFOA-7 system. In its adsorbed state, PFOA at the MIMs interface exists in its acidic form due to H-bonding with --OH/--NH groups, unlike the carboxylate moieties at the subsequent layers. The IR frequencies of the acidic forms of benzoic and salicylic acids in solution were shown to increase by ~ 80 wavenumbers from ~ 1620 to 1700 cm^{-1} relative to the position of the respective unbound carboxylate anions.⁴⁹ As well, the formation of weak H-bonds may result in shortened X-H bonds with subsequent attenuation of the FT-IR bands and resulting blue frequency shifts.⁵⁰ The observed frequency shifts and variation in the relative intensities of the COO^-/COOH bands for the HDI-6/PFOA system, relative to free PFOA and HDI-6, provide support of such dipolar interactions between PFOA and the MIMs surface.⁵¹

In addition to the carbonyl bands, evidence of frequency shifts and change in band intensities of the amide II ($\sim 1500\text{ cm}^{-1}$) and the guest CF_2/CF_3 ($\sim 1200\text{ cm}^{-1}$) stretching bands (bands **1–3** in Figure 8.6) are noted. The amide II band ($\sim 1500\text{ cm}^{-1}$) results from the N-H bending and C-N stretching and displays a decreased frequency of up to 20 cm^{-1} , as compared to HDI-6 (*cf.* Table 8.5). These frequency shifts are accompanied by a reduced intensity of the --NH band $\sim 1500\text{ cm}^{-1}$ for the mixtures (i.e. HDI-1 > HDI-1/PFOA-1 > HD-1/PFOA-4 > HDI-1/PFOA-7). An increase in H-bonding of amides was reported to attenuate the wavenumber position of the amide II band.⁵²

Table 8.5 FT-IR Absorption Bands of HDI-6, PFOA and their Adsorbed Complexes.

Assigned Bands	Wavenumber (cm ⁻¹)				
	HDI-6	PFOA	HDI-6/PFOA-1	HDI-6/PFOA-4	HDI-6/PFOA-7
$\nu(\text{OH})$	3538	Broad	3534	3533	3530
$\nu(\text{N-H})$	3367	-	3363	3351	3344
$\nu_{\text{as}}(\text{CH})+\nu_{\text{s}}(\text{CH})$	2934, 2859	-	2934, 2862	2935, 2863	2947, 2868
$\nu(\text{C=O})$	1720, 1653	1777	1717, 1645	1719, 1645	1787, 1707, 1647
$\delta(\text{NH}) + \nu(\text{C-N})$	1545	-	1533	1529	1527
$\nu(\text{C-N})$	1250	-	1252	1246, 1180	1250, 1190
$\nu_{\text{as}}(\text{CF}_2)+\nu_{\text{as}}(\text{CF}_3)$	-	1205	-	1228	1228
$\nu_{\text{as}}(\text{CF}_2), \nu_{\text{s}}(\text{CF}_2)$	-	1242, 1149	1269, 1167	1263, 1167	1257, 1173

In Figure 8.6 and Table 8.5, the FT-IR shift and intensity changes of the guest ~ 1200 cm⁻¹ (band **2**; $\nu_{\text{asym}}\text{CF}_2 + \nu_{\text{asym}}\text{CF}_3$) and ~ 1250 cm⁻¹ (**3**; $\nu_{\text{sym}}\text{CF}_2$) and 1150 cm⁻¹ (**1**; $\nu_{\text{sym}}\text{CF}_2$) were observed. The intensity of the CF₃ band **2** increases at the expense of the CF₂ band **3**. Viana et al.¹⁰ reported integrated areas of the FT-IR bands to characterize multilayer structures. In Figure 8.6, an increase of the relative intensity of the CF₃ bands (**2**) ~ 1205 cm⁻¹ for the HDI-6/PFOA-7 system provides further support of multilayer adsorption processes.

The FT-IR results for the HDI-6/OA mixtures are shown in Figure 8.7 and Table 8.6. The spectra of the OA mixtures are similar with minor shifts (2–4 cm⁻¹) for the amide I and II bands. The -OH band ~ 3400 – 2400 cm⁻¹ for OA overlaps with the C-H bands (~ 2900 cm⁻¹), and is typical for fatty acids.⁵³ The shifts of the -C=O and -NH range from 13 to 20 cm⁻¹ up to 60 cm⁻¹ for the PFOA/copolymer systems, however; there are minimal wavenumber shifts for the OA/copolymer systems, in agreement with the monolayer isotherm results in Figure 8.2 and Scheme 8.3 for MIMs/OA system. Furthermore, the relative intensity of the -NH band ~ 1550 cm⁻¹ is not significantly affected by incremental amounts of OA in solution. The results suggest

that H-bonding interactions are not evident for the HDI-6/OA system, in agreement with the monolayer isotherm and hydration of the head groups, as described above. It is noteworthy that the principal mode of adsorption is via the alkyl chain with the MIMs surface where hydration of the head group is well defined.

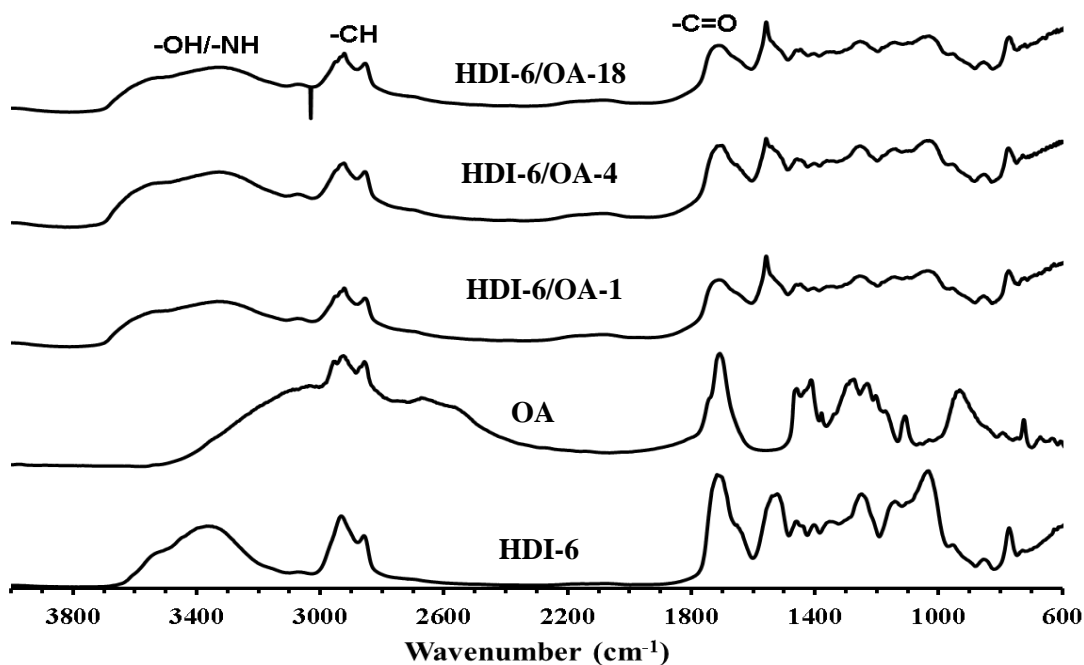


Figure 8.7 FT-IR spectra of hydrated solids HDI-6, OA, and HDI-6/OA-1, HDI-6/PFOA-4, and HDI-6/PFOA-18 systems at 295 K.

Table 8.6. FT-IR absorption bands for HDI-6, OA, and HDI-6/OA systems

Assigned Bands	HDI-6	OA	HDI-6/OA-1	HDI-6/OA-4	HDI-1/OA-18
$\nu(\text{OH})$	3538	Broad	3576	3582	3582
$\nu(\text{NH})$	3386	Broad	3337	3347	3347
$\nu_{\text{as}}(\text{CH}) + \nu_{\text{s}}(\text{CH})$	2934, 2859	2942, 2876	2949, 2873	2942, 2873	2946, 2876
$\nu(\text{C}=\text{O})$	1720, 1653	1748, 1715	1724, 1661	1722, 1659	1722, 1655
$\delta(\text{NH}) + \nu(\text{C-N})$	1545	-	1562	1564	1562

8.6.3.3 Contact Angle

Contact angles were measured to ascertain the nature of the surface interactions between HDI-6 with PFOA and OA, respectively. Contact angle measurements have been successfully used to characterize the surface properties of films and coatings.⁵⁴ Moreover, important information regarding the interactions at solid interfaces can be obtained from the wetting behaviour of films revealed by contact angle, especially when the chemical nature and surface roughness are controlled.^{55,56}

Table 8.7 Static Contact Angles (θ) of PFOA and OA on an HDI-6 Copolymer Film at Variable Loading Levels at 295 K.

Contact angle of PFOA/OA on HDI-6 surface at ambient temperature (22±1°C)						
Sample	OA-1	OA-18	PFOA-1	PFOA-4	PFOA-7	
Contact angle (°)	87	83	82	79	75	

Static contact angles of droplets containing aqueous solutions of PFOA and OA were measured at ambient conditions. HDI-6 films were drop-casted onto silicon wafer substrates, and the θ values are listed in Table 8.7. The static θ value for water on the untreated silicon wafer substrate was close to 90°, while the value on the HDI-6 film was 82±1°. The results suggest that the surface of the silicon wafer is more hydrophobic relative to the HDI-6 film.⁵³ The θ values for water measured by Arkales⁵⁴ on silicon ranged between $\theta = 86$ –88°. In Table 8.7, the greater θ values for OA (1 and 18 mM) and PFOA (1 mM) may result from repulsive interactions with the HDI-6 surface film. Tavana et al.⁵⁵ studied the relationship of dipole moments for a series of naphthalene compounds interacting with a fluorinated acrylate polymer film using θ values. A decrease in θ was observed for naphthalene derivatives containing highly electronegative compounds (e.g., fluorine), further confirming that specific adhesive interactions occur at the solid-liquid interface. The low θ values for HDI-6/PFOA-7 suggest that favourable adhesive interactions occur between the MIMs surface and PFOA. Comparable θ values for OA and PFOA may preclude a detailed quantitative analysis of the results. Furthermore, the HDI-6 films were drop-casted from a solution of DMSO which may influence surface roughness of the copolymer and the presence of trace solvent residues may affect the θ values. However, the

contact angle results reported here are in good agreement with previous reports,¹² and further support the conclusion from the isotherms, FT-IR spectra, and DSC results.

8.6.3.4 ITC

ITC has been reported for the characterization of CD-based complexes.^{56,57} The binding constants and the thermodynamic parameters of such host-guest complexes provide a basis for a detailed understanding of non-covalent binding processes.⁵⁶ The main interactions that occur for the binding of PFOA and OA with the MIMs are noncovalent in nature (i.e., H-bonding, van der Waals and electrostatic interactions) which are amenable to ITC studies. In the case of PFOA, dipolar interactions between the carboxylate head group and the polar domains of the MIMs surface are hypothesized, in addition to secondary interactions between the perfluoroalkyl groups to form bilayers and multilayers. In contrast to PFOA, the apolar alkyl group of OA adsorbs at the MIMs surface resulting in well-defined monolayers.

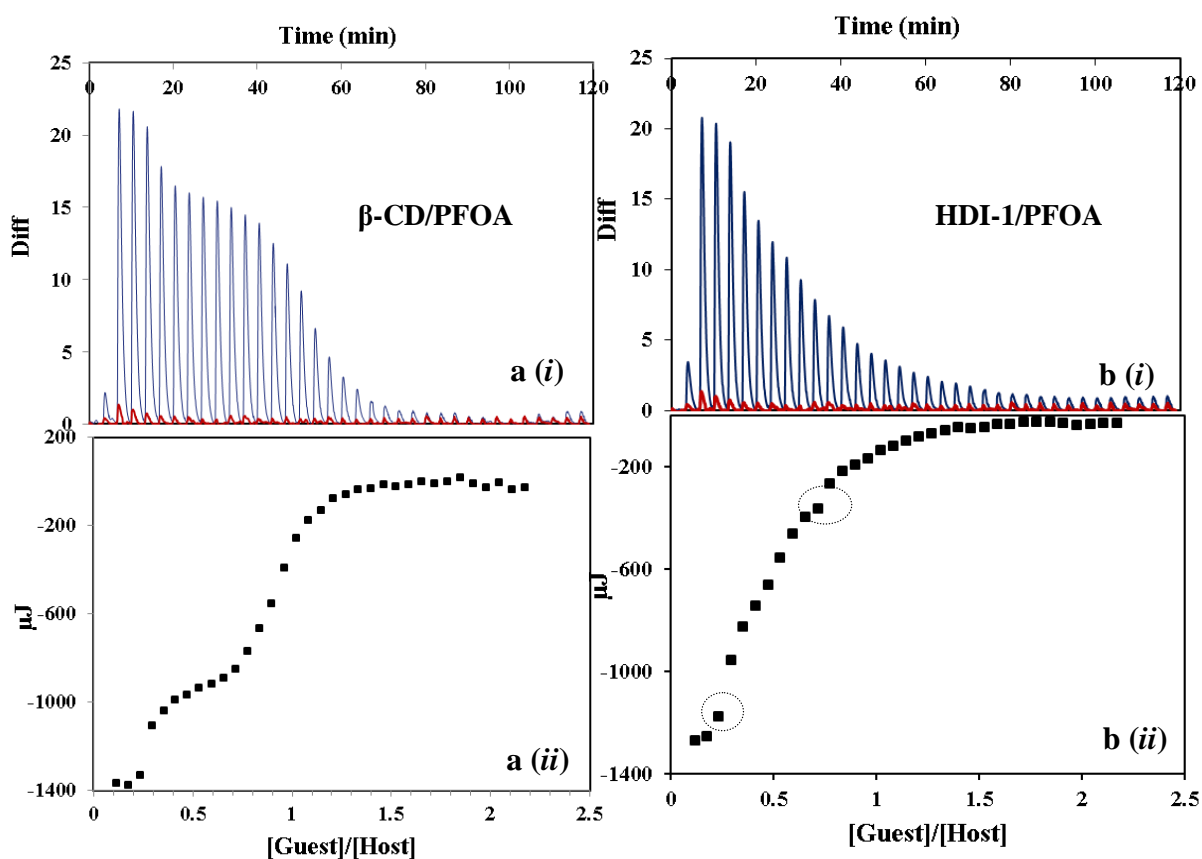


Figure 8.8 Calorimetric titration of (a) β -CD/PFOA, and (b) HDI-1/PFOA at pH \sim 4 and 298 K, respectively. The ITC isotherms reveal 1:1 and 2:1 β -CD/PFOA (a-ii), and 1:1 HDI-1/PFOA (b-ii).

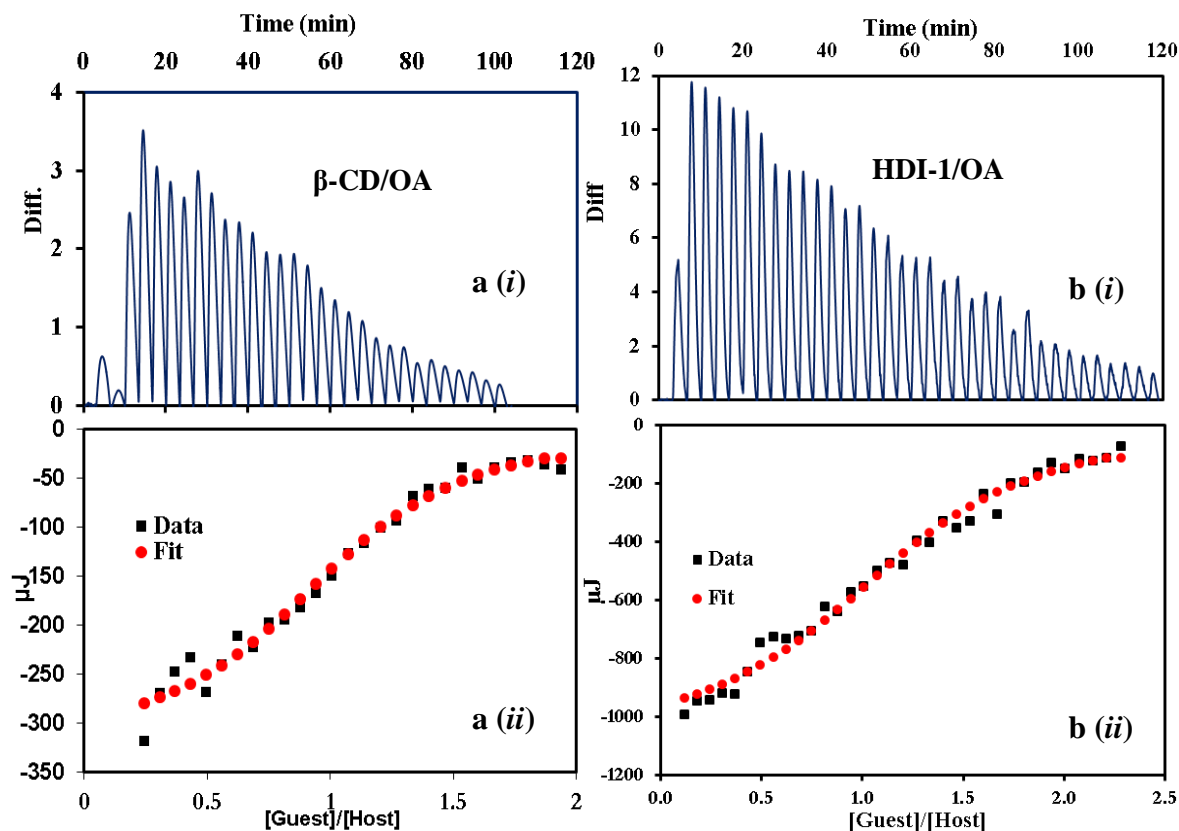


Figure 8.9 Calorimetric titration of (a) β -CD/OA, and (b) HDI-1/OA systems at pH \sim 8 and 298 K.

The ITC results for β -CD/PFOA and HDI-1/PFOA were compared at ambient temperature, as shown in Figures 8.8. Similar results for β -CD/OA and HDI-1/OA systems are shown in Figure 8.9 and the corresponding thermodynamic parameters are listed in Table 8.8. The ITC-based thermodynamic parameters for β -CD/PFOA^{18,58,59} and β -CD/OA²⁰ complexes (Figures 8.8a and 8.9a, and Table 8.8) indicate two types of binding equilibria in accordance with the formation of 1:1 β -CD/OA and 1:1 plus 2:1 (β -CD/PFOA) complexes.

In Figure 8.8a-ii, the molar enthalpy for the 1:1 complex (800 μ J) is greater than for the 2:1 complex (400 μ J), consistent with the relative binding affinity (i.e., $K_{1:1} > K_{2:1}$; cf. Table 8.8) and the partial inclusion geometry of the 2:1 complexes, described previously.⁵⁹ The structure of the HDI-1 copolymer does not favour the formation of 2:1 complexes with PFOA due to the linear topology of the copolymer. Furthermore, the polymeric framework of HDI-1 does not favour such 2:1 channel-type structures with PFOA due to the random orientation and spatial distribution of β -CD along the polymer backbone. Therefore, 1:1 complexes are anticipated for

HDI-1/PFOA system. However, the inflection point beyond the 1:1 complex in Figure 8.8b-ii (marked with a circle ~0.5 guest/host mole ratio) may be attributed to secondary binding of PFOA in the interstitial regions of the HDI-1 copolymer. The formation of inclusion complexes for the HDI-1/PFOA is consistent with the inclusion site accessibility and the favourable binding affinity at the copolymer inclusion sites.

Table 8.8 Binding constants (K_i ; $i = 1:1$ or $2:1$) and Standard Enthalpy (ΔH) and Entropy Changes ($T\Delta S$) for Inclusion Complexes of PFOA and OA with HDI-1 at pH ~4 (PFOA) and pH ~8.5 (OA, in phosphate buffer) at 298 K*

H/G System	Model	n	ΔG (kJ/mol)	$K_{1:1}$	$K_{2:1}$	ΔH (kJ/mol)	$T\Delta S$ (kJ/mol)
β-CD/PFOA	1:1	1.0(\pm 0.1)	-28.8	$1.1(\pm 0.7) \times 10^5$		-39.7 \pm 4.9	-10.9
	2:1	1.8(\pm 0.2)	-22.7	-	$9.7(\pm 11.) \times 10^3$	-69.1 \pm 16.	-46.4
HDI-1/PFOA	1:1	1.0(\pm 0.1)	-25.2	$2.6(\pm 1.0) \times 10^4$		-51.1 \pm 8.1	-25.9
β-CD/OA	1:1	1.0(\pm 0.3)	-19.3	$2.4(\pm 1.8) \times 10^3$		-11.1 \pm 6.2	+8.20
HDI-1/OA	1:1	1.2(\pm 0.1)	-25.8	$3.4(\pm 3.0) \times 10^4$		-28.2 \pm 5.2	-2.40

* $K_{1:1}$ (Lmol⁻¹), $K_{2:1}$ (Lmol⁻¹)², R = 8.3145 J/mol.K

The values of binding constants for β -CD/PFOA ($K_{1:1} \sim 1.1 \times 10^5$, $K_{2:1} \sim 9.7 \times 10^3$)^{59,60} and β -CD/OA (2.4×10^3)²⁰ complexes are listed in Table 8.8, in good agreement with previously reported values.⁵⁹ In Table 8.8, the Gibbs energy change (ΔG) of complex formation for PFOA are largely enthalpy (ΔH) driven; whereas the enthalpy of complex formation for OA was less negative and entropy driven in most cases. The binding of OA to CD/HDI-1 is generally characterized by increased entropies and $|\Delta H| < |T\Delta S|$ for these systems. The higher entropies are attributed to favourable desolvation contributions of the complex. The fact that the binding process in this system is entropy-driven reveals that factors such as the configurational entropy of the host, guest, and solvent must be considered, in addition to the favourable enthalpy to complex stability.^{61,62} Furthermore, the decreased entropy in the PFOA binding suggests the presence of complementary *size-fit* for this host-guest system and the important role of the hydrophobic effect in governing complex stability.⁶³

8.7 Conclusions

A systematic study was carried out to investigate the interaction of PFOA and OA anions with macromolecular-based copolymers (MIMs) in aqueous solution. The MIMs adsorbents contain β -CD within a urethane framework which afford two types of binding sites; β -CD inclusion sites and hexamethylene cross-linker sites with polar (-OH/-NH) domains. The adsorptive properties of the inclusion and cross-linker sites were studied using FT-IR spectroscopy, DSC, contact angle, and ITC. The unique role of the head group interactions was concluded by comparison of the isotherms of perfluorocarbon anions with sulfonate and carboxylate head groups (i.e. PFOS and PFOA) with copolymer adsorbents. The unique adsorption of perfluorocarbon anions onto the MIMs surface differs significantly relative to a hydrocarbon anion (*n*-octyl carboxylate). Perfluorocarbon anions are firstly adsorbed onto the MIMs surface via head group interactions with the polar (-OH, -NH) domains of the MIMs surface to form monolayers. Thereafter, bilayers and multilayer structures (e.g., micelles and hemi-micelles) form at higher concentration (*cf.* Scheme 8.3). Hydrocarbon adsorbates form a conventional monolayer mediated by apolar interactions between the *n*-octyl chain and the MIMs surface (Scheme 8.3). At low cross-link density (i.e. HDI-1), inclusion binding of adsorbates is the dominant process, whereas; inclusion binding is secondary for copolymers such as HDI-6 with reduced accessibility of β -CD. The various modes of adsorption for PFOA (monolayer/multilayers) and OA (monolayer) are supported by FT-IR, contact angle, ITC, and DSC results.

8.8 Acknowledgments

The authors are grateful for the support provided by the University of Saskatchewan and the Natural Sciences and Engineering Research Council of Canada (NSERC) for this research. A.H.K. wishes to acknowledge Jason Maley and Kenneth Thoms (Saskatchewan Structural Sciences Centre) for their expertise and technical assistance in obtaining the ITC and ESI-MS results, respectively. L.D.W. acknowledges Computers for Schools (Saskatoon, SK) for the donation of a desktop computer.

8.9 References

- (1) Yu, Q.; Deng, S.; Yu, G. *Water Res.* **2008**, *42*, 3089–3097.
- (2) Maddikeri, G. L.; Pandit, A. B.; Gogate, P. R. *Ind. Eng. Chem. Res.* **2012**, *51*, 6869–6876.
- (3) Senevirathna, S.T.; Tanaka, S.; Fujii, S.; Kunacheva, C.; Harada, H.; Shivakoti, B. R.; Dinh, H.; Ariyadasa, T. *Water Sci Technol.* **2011**, *63*, 2106–2113.
- (4) Lee, C. C.; Pedram, E. O.; Hlnes, A. L. *J. Chem. Eng. Data* **1986**, *31*, 133–136.
- (5) Somasundaran, P.; Krishnakumar, S. *Colloids Surf. A* **1997**, *123-124*, 491–513.
- (6) Krister Holmberg, Bo Jonsson, Bengt Kronberg, and Bjorn Lindman. *Surfactants and Polymers in Aqueous Solution*. John Wiley & Sons, Ltd. Chichester, West Sussex, England, **2003**.
- (7) (a) Ulman, A. *Chem. Rev.* **1996**, *96*, 1533–1554; (b) Harwell, J. H.; Hoskins, J. C.; Schechter, R. S.; Wade, W. H. *Langmuir* **1985**, *1*, 251–262.
- (8) Berg, M. C.; Zhai, L.; Cohen, R. E.; Rubner, M. F. *Biomacromolecules* **2006**, *7*, 357–364.
- (9) Bonenfant, D.; Mimeault, M.; Niquette, P.; Hausler, R. *Water Techno.* **2012**, *66(1)*, 224–230.
- (10) Viana, A. S.; Abrantes, L. M.; Jin, G.; Floate, S.; Nichols, R. J.; Kalaji, M. *Phys. Chem. Chem. Phys.* **2001**, *3*, 3411–3419.
- (11) Schonherr, H.; Ringsdorf, H. *Langmuir* **1996**, *12*, 3891–3897.
- (12) Ito, Y.; Virkar, A. A.; Mannsfeld, S.; Oh, J. H.; Toney, M.; Locklin, J.; Bao, Z. *J. Am. Chem. Soc.* **2009**, *131*, 9396–9404.
- (13) Karoyo, A. H.; Wilson, L. D. *J. Colloid. Interface Sci.* **2013**, *405*, 196–203.
- (14) Mohamed, M. H.; Wilson, L. D.; Headley, J. V. *Carbohydr. Res.* **2011**, *364*, 219–229.
- (15) Mohamed, M. H.; Wilson, L. D.; Headley, J. V. *Carbohydr. Polym.* **2010**, *80*, 186–196, and references cited therein.
- (16) Brunauer, S.; Emmett, P. H.; Teller, E. *J. Am. Chem. Soc.* **1938**, *60*, 309–319.
- (17) Gupta, A.; Mandal, S.; Katiyar, M.; Mohapatra, Y. N. *Thin Solid Films* **2012**, *520*, 5664–5670.
- (18) Karoyo, A. H.; Sidhu, P.; Wilson, L. D. *J. Phys. Chem. B* **2013**, *117*, 8269–8282.
- (19) Palepu, R.; Richardson, J. E.; Reinsborough, V. C. *Langmuir* **1989**, *5*, 218–221.
- (20) Parker, K. M.; Stalcup, A. M. *J. Chromatogr. A* **2008**, *1204*, 171–182.
- (21) Langmuir, I. *J. Am. Chem. Soc.* **1916**, *38(11)*, 2221–2295.

- (22) Gauglitz, G.; Vo-Dinh, T. *Handbook of Spectroscopy*. Wiley-VCH Verlag GmbH & Co. KGaA, Weinheim, **2013**.
- (23) Jing, P.; Rodgers, P. J.; Amemiya, S. *J. Am. Chem. Soc.* **2009**, *131*, 2290–2296.
- (24) Levitz, P. *Langmuir* **1991**, *7*, 1595–1608.
- (25) Emerging Contaminants–Perfluorooctane sulfonate (PFOS) and Perfluorooctanoic acid (PFOA). EPA, **2012**.
- (26) Hoffmann, H. J. Wurtz, J. *Mol. Liq.* *72* (1997) 191; E. Kissa, *Fluorinated Surfactants and Repellents*, second ed., Marcel Dekker, New York, **2001**.
- (27) Li, M.-H. *Environ. Toxicol.* **2009**, *24*, 95–101.
- (28) Lide, D. R. *CRC Handbook of Chemistry and Physics*, 70th ed., CRC Press, Boca Raton, FL, **1990**.
- (29) Wilson, L. D.; Sidall, S. R.; Verrall, R. E. *Can. J. Chem.* **1997**, *75*, 927–933, and references cited therein.
- (30) Budavari, S. *The Merck Index: An Encyclopedia of Chemicals, Drugs, and Biologicals*, 12th ed. Whitehorse Station, NJ; Merck, **1996**.
- (31) Eissa, A. S.; Khan, S. A. *Food Hydrocolloids* **2006**, *20*, 543–547.
- (32) Gao, X.; Chorover, J. *Environ. Chem.* **2012**, *9*, 148–157.
- (33) Tu, A.; Kwag, H. R.; Barnette, A. L.; Kim, S. H. *Langmuir* **2012**, *28*, 15263–15269.
- (34) Sing, K. S. W.; Everett, D. H.; Haul, R. A. W.; Moscou, L.; Pierotti, R. A.; Rouquerol, J.; Siemieniowska, T. *Pure Appl. Chem.* **1986**, *57*, 603–619.
- (35) Yu, Q.; Zhang, R.; Deng, S.; Huang, J.; Yu, G. *Water Res.* **2009**, *43*, 1150–1158.
- (36) Zhang, Q.; Deng, S.; Yu, G.; Huang, J. *Bioresource Technol.* **2011**, *102*, 2265–2271.
- (37) Mathlouthi, M. Water Content, Water Activity, Water Structure and the Stability of Foodstuffs. *Food Control* **2001**, *12*, 409–417.
- (38) Ito, K.; Yoshida, K.; Ujimoto, K.; Yamaguchi, T. *Anal. Sci.* **2013**, *29*, 353–359.
- (39) Ping, Z. H.; Nguyen, Q. T.; Chen, S. M.; Zhou, J. Q.; Ding, Y. D. *Polymer* **2001**, *42*, 8461–8467.
- (40) Knowlton, D. G.; White, T. R.; McCague, H. L. *Clays and Clay Minerals* **1981**, *29*(5), 403–411.

- (41) Volkov, V. V.; Nuti, F.; Takaoka, Y.; Chelli, R.; Papini, A. M.; Righini, R. *J. Am. Chem. Soc.* **2006**, *128*, 9466-9471; DeRuiter, J. *Carboxylic Acid Structure and Chemistry: Part 1 Tutorials*, **2005**.
- (42) Wang, R.; Wang, Q.; Li, L. *Polym. Int.* **2003**, *52*, 1820-1826.
- (43) Kohler, K.; Mohwald, H.; Sukhorukov, G. B. *J. Phys. Chem. B* **2006**, *110*, 24002-24010.
- (44) Schonhoff, M.; Ball, V.; Bausch, A. R.; Dejugnat, C.; Delorme, N.; Glinel, K.; Klitzing, R.; Steitz, R. *Colloid Surface A* **2007**, *303*, 14-29.
- (45) Meier, M. M.; Luiz, M. T. B.; Szpoganicz, B.; Soldi, V. *Thermochim Acta* **2001**, *375*, 153-160.
- (46) Yilgo, E.; Yilgo, I.; Yurtsever, E. *Polymer* **2002**, *43*, 6551-6559.
- (47) Meaurio, E.; Cesteros, L. C.; Katime, I. *Macromolecules* **1997**, *30*, 4567-4573.
- (48) Shinde, S. S.; Patil, S. S.; Mevekari, F. I.; Satpute, A. S. *Int. J. Adv. Pharm. Sci.* **2010**, *1*, 299-308.
- (49) Guan, X.; Chen, G.; Shang, C. *J. Environ. Sci.* **2007**, *19*, 438-443.
- (50) Jorly, J.; Eluvathingal, D. J. *J. Am. Chem. Soc.* **2007**, *129*, 4620-4632.
- (51) Sari, A.; Akcay, M.; Soylak, M.; Onal, A. *J. Sci. Ind. Res.* **2005**, *64*, 991-996.
- (52) Shakirova, L.; Grubea, M.; Goodacre, R.; Gavarea, M.; Auzinaa, L.; Zikmanisa, P. *Vib. Spectrosc.* **2013**, *64*, 51-57.
- (53) Max, J-J.; Chapados, C. *J. Phys. Chem. A* **2004**, *108*, 3324-3337.
- (54) Arkles, B. Hydrophobicity, Hydrophilicity, and Silane. Gelest Inc., Morrisville, PA. **2009**.
- (55) Tavana, H.; Hair, M. L.; Neumann, W. *J. Phys. Chem. B* **2006**, *110*, 1294-1300.
- (56) Bouchemal, K.; Mazzaferro, S. *Drug Discov. Today* **2012**, *17*, 623-629.
- (57) Wszelaka-Rylik, M.; Gierycz, P. *J. Therm. Anal. Calorim.* **2013**, *111*, 2029-2035.
- (58) Guo, W.; Fung, B. M.; Christian, S. D. *Langmuir* **1992**, *8*, 446-451.
- (59) Wilson, L. D.; Verrall, R. E. *Langmuir* **1998**, *14*, 4710-4717.
- (60) Xing, H.; Lin, S.; Yan, P.; Xiao, J.; Chen, Y. *J. Phys. Chem. B* **2007**, *111*, 8089-8095.
- (61) Cooper, A.; Johnson, C. M.; Lakey, J. H.; Nollmann, M. *Biophys. Chem.* **2001**, *93*, 215-230.
- (62) Dunitz, J. D. *Chem Biol.* **1995**, *2*, 709-712.
- (63) Blokzijl, W.; Engberts, J. F. B. N. *Angew Chem Int Ed Engl.* **1993**, *32*(11), 1545-1579.

CHAPTER 9

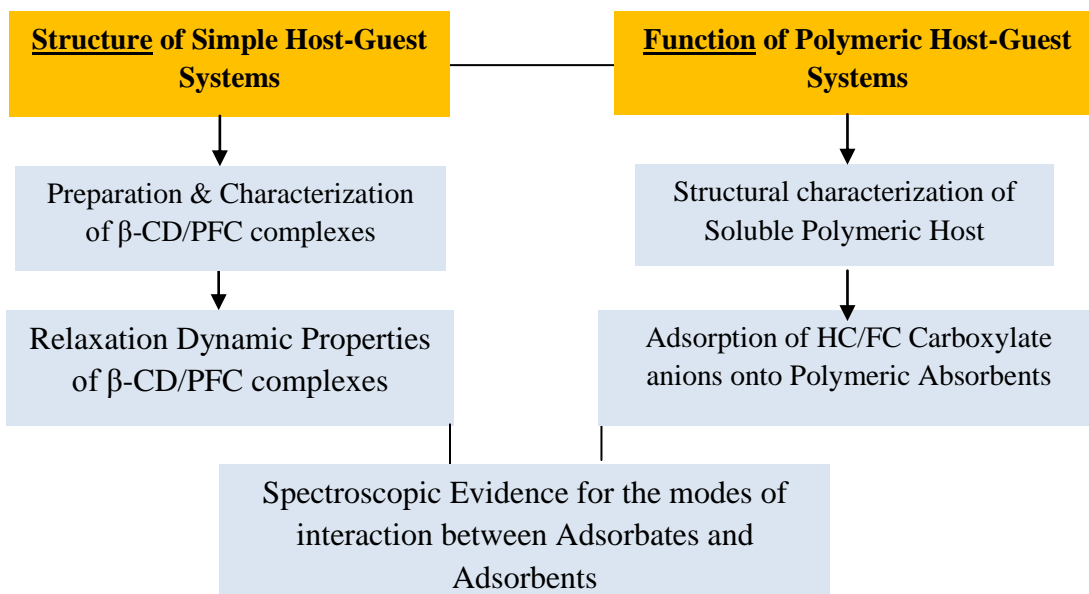
9. Summary, Conclusions and Future Work

9.1 Summary

This PhD thesis research describes the structure and function of various supramolecular host-guest systems. In chapter 1, the different types of supramolecular host-guest systems were discussed with an emphasis on β -CD and its copolymers as host materials. Cyclodextrins are known to form stable host-guest inclusion complexes in solution and the solid state with a wide range of organic molecules due to their unique nature imparted by their structure (*cf.* §1.2.1). CDs can be cross-linked with bi-functional reagents such as epichlorohydrin, diacid chlorides, and diisocyanates to form polymers that have properties suitable for adsorption-based applications in the areas of biomedicine, controlled-release of pharmaceuticals, environmental remediation, and advanced materials (e.g. molecular switches and sensors). A range of methods (e.g. NMR, DSC, PXRD, FT-IR, ICD, etc.) have been used to characterize the structure and function of CD-based materials. Of particular interest is the use of NMR techniques in aqueous solution and the solid state (*cf.* §1.5) because such methods are versatile (suitable for a range of nuclei e.g. ^1H , ^{19}F , ^{13}C , etc.) and provide valuable structural information related to host-guest supramolecular systems, which comprises one of the main objectives of this study (chapters 2 – 5). Understanding the structure and dynamic properties of host-guest systems is essential in the design of functional supramolecular materials with improved physicochemical properties.

The two types of host/guest systems that were studied in this thesis are: Type 1) simple macrocyclic CD host/aliphatic (HCs and PFCs) guests, and Type 2) CD-based urethane copolymer hosts/aliphatic guest systems. In the case of Type 1 host-guest systems (chapters 2 – 5), β -CD was used as the host to prepare a series of host-guest inclusion compounds (ICs) with a variety of perfluorinated compounds (PFCs) in aqueous solution and in the solid state. The PFCs studied represent medium chain perfluorooctanoic acid/PFOA-C8 (chapters 2 and 3), short chain perfluorobutyric acid/PFBA-C4 (chapter 4), and the sodium salt of PFOA i.e., sodium perfluorooctanoate/SPFO-C8 (chapter 5). β -CD/PFC complexes in the solid state were prepared at the 1:1 and 2:1 host-guest mole ratios using dissolution methods. The structure (guest binding geometry and conformation, host packing arrangement, etc.) and dynamic properties of the guest in the complexes were further characterized by using $^1\text{H}/^{19}\text{F}/^{13}\text{C}$ solid/solution NMR and FT-IR spectroscopic methods, thermal analyses (DSC, TGA), and powder X-ray diffraction.

In the case of Type 2 (CD-based cross-linked urethane polymer hosts/aliphatic guests) host-guest systems (chapters 6 – 8), CD-based copolymers were synthesized at various cross-linking ratios. β -CD was cross-linked with hexamethylene diisocyanate (HDI) at stoichiometric mole ratios (i.e. 1, 3, and 6) to form HDI-1, -3, and -6, respectively, where the β -CD mole content was set at unity. The structural characterization of the soluble HDI-1 copolymer in aqueous solution was evaluated to characterize the behavior of these materials as a function of guest concentration and temperature (chapter 6). The adsorption properties of the polymeric hosts (i.e. HDI-1, 3, and -6; herein referred to as Macromolecular-based Imprinted Materials or MIMs) with PFOA, PFOS (perfluorooctane sulfonate), and OA (octanoic acid) were evaluated using the Sips and BET isotherm models to assess their potential for chemical separation phenomena (chapter 7). Spectroscopic (FT-IR, DSC, contact angle, etc.) evidence for the modes of interaction between the MIMs and the various fluorocarbon (FC) and hydrocarbon (HC) adsorbate materials was provided in chapter 8. The overall research is outlined in Scheme 9.1.



Scheme 9.1 Organization of the PhD Thesis; The Boxes in Bold Represent the Two Main Themes of the Study, the Boxes under the Arrows Represent the Sub-topics, and the Box between the lines Represent the Intersection of the Structure and Function Themes.

9.2. Concluding Remarks

In conclusion, a detailed study of the preparation, characterization, and a comparison of the structure and dynamic properties of the complexes formed between β -CD and a variety of perfluorinated guest compounds (i.e., PFOA, PFBA, and SPFO) in aqueous solution and the solid state was presented. As well, the structural properties of a soluble CD copolymer (HDI-1) as a function of temperature and guest concentration in aqueous solution was studied. The sorption properties of a series of CD-based copolymers (HDI-1, -3, and -6) towards fluorocarbons (PFOA and PFOS) and hydrocarbon (OA) guests were evaluated and compared to a conventional activated carbon adsorbent material.

In the case of macrocyclic CD host/aliphatic guest systems (Type 1), various structural parameters were studied using several techniques. These include the local molecular environments and possible geometry of the guests ($^1\text{H}/^{19}\text{F}/^{13}\text{C}$ CIS values, $T_1/T_2/T_{1\rho}$ relaxation data), guest conformation ($^1\text{H}/^{19}\text{F}/^{13}\text{C}$ NMR and CIS values, FT-IR), host packing arrangements (PXRD), hydration properties (DSC, PXRD), and motional dynamics of the guests ($T_1/T_2/T_{1\rho}$ NMR relaxation parameters). The structural and dynamic properties of the different guest molecules (i.e., PFOA, PFBA, and SPFO) are distinct and depend on differences in the guest chain length (*size-fit* considerations), hydrophobicity, nature of counterion (H^+ vs Na^+) species, and solvation properties. PFC chains with carbon number ≥ 8 (e.g. PFOA and SPFO) have been reported to adopt the helical (*gauche*) conformation in their native form; whereas, shorter chains (carbon number ≤ 8) PFCs (e.g. PFBA) exist in the zigzag (*trans*) form.¹

The IR and solution NMR results revealed that PFOA and SPFO form 1:1 and 2:1 host-guest complexes with β -CD, where the PFC guests adopt the *gauche* and *trans* conformations, respectively. In contrast, PFBA mainly forms a 1:1 host-guest complex with β -CD where the *gauche* conformation of the guest is favoured. Secondary contributions such as 1:2 and 2:1 host-guest associations for PFBA were concluded from deconvolution of various contributions from the DSC/TGA and ^{19}F NMR results.

NMR CIS values of $^1\text{H}/^{19}\text{F}/^{13}\text{C}$ nuclei in solution and the solid state were used to provide insights on the geometry of the various guests in their complexed form with β -CD. The binding mode of SPFO was concluded to involve a deeper inclusion of the guest within the host cavity. Stronger binding affinity for the CD/SPFO complex (chapter 5) was related to the presence of the sodium counterion because it stabilizes the complex due to electrostatic effects.

The dynamic properties of PFOA, PFBA and SPFO varied in accordance with the structure of the pure guests and their geometry in the bound states with β -CD. Two types of motional dynamics were concluded for the PFC guests; 120° rotations of the fluoromethyl (CF_3) group, and C-F bonds rotations (axial or librational motions) of the fluoromethylene (CF_2) groups. The magnitudes and distribution of such motions depend on the host-guest stoichiometry and the geometry of the guests in the complexes. Simulation of the ^{19}F spectra of unbound PFBA and its complexes with β -CD in solution reveal that the fluoromethyl group experiences extensive rotation about its 3-fold axis, whereas, a significant level of C-F bond rotation occurs in the main chain. The dynamics of PFBA is generally greater compared to PFOA and SPFO guests (chapter 4). The dynamics of PFOA and SPFO are modulated by the presence of hydronium and sodium counterions, respectively, among other factors. The 2:1 β -CD/SPFO complex resembles a pseudo-rotaxane where the fluoromethyl and carboxylate ends are capped, whereas the central body experiences axial motions of the C-F bonds. In the case of the 1:1 β -CD/SPFO complex, the axial motions are affected by the extensive rotation of the CF_3 group and the presence of the sodium counterion which can act as an anchor. The dynamics of the guest in the β -CD/PFOA complexes undergo appreciable CF_3 rotations and C-F bond rotations. Some of the structural properties of the complexes formed by PFOA, PFBA, and SPFO with β -CD, respectively, are summarized in Table 5.6 (chapter 5).

Chapter 6 describes the study of CD-based cross-linked urethane polymer hosts/aliphatic guest systems (Type 2), wherein the structure of HDI-1 copolymer and PNP as a model guest showed that there are two binding sites; *inclusion* (cavity) and *non-inclusion* (interstitial) sites within the copolymer materials where a guest can potentially bind. The equilibrium binding constant (K) of HDI-1/PFOA ($K \sim 1.0 \times 10^3 \text{ M}^{-1}$)² system was evaluated (chapter 6) and was found to be comparable (about one to two orders of magnitude smaller) to values reported for native β -CD/PFC systems in solution ($K \sim 4 \times 10^4 \text{ M}^{-1} - 9.0 \times 10^4 \text{ M}^{-1}$).^{3,4} These findings address important knowledge gaps identified from a controversial report by Ma and Li.⁵ The anomalously large K values for CD-based urethane polymer/PNP complex reported in ref. 5 was five to six orders of magnitude greater when compared to the K values for the 1:1 β -CD/PNP complex. The determination of K by Ma and Li used UV-vis spectroscopy and the assumption that the guest was bound solely at the *inclusion* (cavity) site of the polymer framework. Based on the binding studies in this thesis and the attenuated K values by comparison of native CD to

polymeric CD, it was concluded that the *non-inclusion* sites were inadequately accounted for in the thermodynamic equilibrium model reported by Ma and Li. A detailed account of the anomalous binding behaviour described in Ref. 5 was described in chapters 6 and 7, and further outlined by Wilson and Mohamed in a recent mini-review.⁶

The copolymer materials (i.e. HDI-1, -3, and -6) reported herein were shown to adsorb PFCs (PFOA and PFOS) from aqueous solution with tunable sorption capacity (Q_m) that exceed those for other related synthetic polymeric adsorbent materials described elsewhere.^{7,8} The adsorptive uptake properties for the copolymer materials reported herein meet or exceed those reported for conventional activated carbon adsorbents.²

The results presented in this thesis are anticipated to contribute to a better understanding of host-guest complexes and their molecular structure (i.e. guest conformation and binding geometry, host packing arrangements, equilibrium binding constants, modes of interaction, etc.) and dynamics of perfluorocarbon compounds in their bound and unbound states. An improved knowledge of the structure and dynamics is crucial in understanding the properties of such host-guest systems in aqueous solution and the solid state. Moreover, the study provides useful insight relevant to the rational design of such supramolecular materials for targeted application in chemical separations, drug delivery, and environmental remediation.

The design of polymeric adsorbent materials with optimal function requires a better understanding of the host-guest structural properties such as geometry and dynamics. The dynamics of the guest in host-guest systems are expected to differ in solution and the solid state since exchange dynamics and overall tumbling rates prevail in solution. However, there are some similarities in certain aspects of the dynamic motions such as the rotation of methyl groups, as observed elsewhere in proteins in solution and solid phases, respectively.⁹ In this thesis, the dynamics of the short PFBA chain in the solid state involve extensive rotations of the CF_3 group and significant axial motions of the main perfluorocarbon chain. Such dynamics may contribute to increased dissociation rates and reduced overall binding constants for its complexes. Similarly, the geometry for medium (C8) chain PFCs (PFOA and SPFO) were reported to involve intra- and extra-cavity binding sites for the CF_3 group where its motional dynamics vary with the host-guest geometry; thereby, influencing complex stability (*cf.* Scheme 5.3c). In contrast, the channel-type structure of the 2:1 β -CD/SPFO complex and the geometry and affinity of SPFO guest for CD are expected to result in reduced motional dynamics (*cf.* Scheme 5.3b). For longer

guest chains, the dissociation rates of complexes containing two CDs are generally lower compared to similar complexes at the 1:1 stoichiometry.¹⁰

Rational design strategies for polymeric adsorbent materials may involve a number of strategies, such as the use of modified CDs to enhance the hydrophobicity of the CD interior and increase the cavity size, thus enhancing the complex stability between the host and guest.^{11,12} Okano et al.¹² have shown that subtle effects on the binding efficacy and dynamics are possible by affording small modifications to the CD structure. Such properties can be explored when designing functional supramolecular systems containing CDs. For example, substitution of a hydroxyl group in the annular region of a CD macrocycle with a functional group (e.g. a methyl or a moderate length ester pendant) affords ‘effective lengthening’ of the cavity dimensions of the host. The result leads to the ability of such modified CDs to accommodate medium as well as long chain guest molecules with alteration of the dynamics and their dissociation rates. The presence of additional inclusion or association sites for the guest to bind alters the complex stability. For example, the value of K for the binding of xanthone improved by 3-fold for methylated β -CD as compared to native β -CD.¹²

Chapter 8 describes a study where the nature of the surface interactions occurring between the MIMs with alkyl (OA) and perfluoroalkyl (PFOA and PFOS) adsorbates, respectively, are spectroscopically probed. The use of PFOS, whose head group bears a sulfonate ion compared to a carboxylate ion for PFOA, provided a comparison of head group effects on complex stability and hydration phenomena. The adsorption of PFOA by MIMs was concluded to proceed via the interaction of the carboxylate head ($R-COO^-$; where R = perfluoroalkyl moiety) group with the surface of the MIMs ($-NH$, $-OH$); whereas, the interaction of OA occurred via the alkyl tail with the MIMs surface. Such modes of interaction resulted in the respective formation of multilayer and monolayer structures for the PFOA and OA, where the adsorption processes varied according to the nature of the surface interactions. Adsorption of the guest with the *inclusion* (cavity) site is possible as long as there are no steric effects.

This thesis reports novel findings on the structure and dynamic properties of the guest for Type 1 host-guest systems. The findings are supported by additional results for the physicochemical properties of a soluble polymeric host material (HDI-1) in aqueous solution, with a comparison of the adsorption properties of a series of polymeric hosts (type 2) with various guest systems. Spectroscopic studies provide further evidence of the nature of binding

sites (structure) and the modes of interaction (function) between the hosts and guests. Knowledge of the structure-dynamics relationship of simple host/guest systems, equilibrium structural parameters, and modes of interaction of polymeric host/guest systems provide useful insights for the uptake properties of polymer adsorbent materials. The systematic studies described in this thesis will contribute to the rational design of polymeric adsorbent materials with improved physicochemical properties for applications in chemical separation phenomena, environmental remediation, drug delivery and biosensors.

9.3 On the Application of MIMs in Environmental Remediation

The study presented in this thesis offers important findings that are crucial to the rational design of polymeric adsorbent materials with improved physicochemical properties (e.g. binding properties, pore structure, surface chemistry, etc) for optimum function. The urethane-based macromolecular imprinted materials (MIMs) reported herein are unique in several ways; 1) they contain an intrinsic imprint (the *inclusion* site) where the guest can preferentially bind, 2) they have additional binding sites within the interstitial (*non-inclusion*) domains, and 3) the physicochemical properties (e.g. binding sites, pore structure and surface chemistry) can be tuned for tailored applications.

The versatility and potential of the MIMs adsorbents for removal of perfluorinated and other structurally related organic contaminants surpass that of the synthetic molecularly imprinted materials (MIPs) reported in the literature. The superiority of MIMs relative to traditional MIPs is related to the presence of an intrinsic and functional *inclusion* site imprint due to the macrocyclic host system. In the case of MIPs, the synthetic process of creating molecular imprints using templates has raised serious questions on several fronts; 1) was the imprint actually created, 2) do the physicochemical properties (e.g. size-fit and binding properties, functionality, etc.) of the imprint resemble those of the template upon its removal, and 3) is templating feasible at a more complex polymeric level. The main unique feature of MIMs is that the structure/functionality of the imprint is preserved even for complex polymeric units.

The potential of MIMs in environmental remediation, particularly in the removal of PFCs, is very promising. This is because the design strategy of MIMs adsorbents is able to address the challenges associated with the FC-HC demixing that are known to limit the performance of hydrocarbon-based polymeric materials. The uptake levels of MIMs for PFCs have been shown

in this thesis report to exceed similar values using activated carbon and MIPs (chapter 7). The use of commercially available ion-exchange resins and carbon nanotubes (CNTs) has been reported to improve the uptake of PFCs; however, such approaches are limited due to high regeneration costs, longer equilibration times, and demanding capital cost. MIMs have been shown to have superior sorption capacity, easy regeneration (by heating or chemical washing), and easy tunability. Furthermore, the surface area and function of the solid MIMs adsorbent such materials can be enhanced by immobilizing the material on a solid surface, and the use of materials in the form of beads or membranes. The cost effectiveness of MIMs adsorbents for industrial application relative to carbonaceous materials (e.g. GAC) is based on a number of factors; 1) their overall uptake performance, 2) the ability to regenerate the MIMs with relative ease, and 3) the multiple number of cycles the MIMs can be re-used to remove contaminants.

9.4 Proposed Future Work

Further studies are required to supplement the results reported in this thesis, and may include the following;

- 1) To understand the three-dimensional structure of guest molecules, especially PFOA/SPFO, and its complexes with β -CD in terms of its conformation (torsional angles), dynamics, precise bond angles and geometry in the bound state.
- 2) To supplement the relaxation dynamic studies in order to provide better understanding and comparison of the dynamics of the different guests (PFOA, SPFO, and PFBA) in their unbound and bound states with β -CD,
- 3) To further probe the dipolar interactions involved in the complexes formed between PFOA and MIMs in the solid state with methods such as NMR in order to provide better understanding of the structure and function of these materials as potential adsorbents.

In item 1, a single crystal structure of PFOA or SPFO will provide valuable structural information that is not readily available using other solid state techniques (e.g. NMR). Crystallographic studies of compounds containing perfluorinated chains is generally very difficult owing to the challenges associated with obtaining good quality crystals. PFCs are well-known to have a high tendency to undergo phase separation in solution,¹³ and although not always a bad thing, it can cause problems in growing and mounting single crystals.

Understanding the unit cell dimensions and the precise symmetry of PFOA will help enhance the understanding of how it binds to β -CD and related host materials in the solid state. Moreover, a single crystal structure of CD/PFC complex will reveal the exact geometry of the guest and role of the aqueous solvent in the complex.

Further information on the dynamics of the guest molecule and its complexes with β -CD can be obtained using other specialized 2-D NMR techniques to supplement the information obtained from dynamic relaxation data. J-resolved spectroscopy is an important NMR technique that can be used to study the conformations of host/guest systems that occur in solution which may not be amenable to X-ray crystallography techniques.¹⁴ J-resolved 2-D spectroscopy is a two-dimensional NMR technique that can separate chemical shifts from overlapping resonance lines, thereby improving the resolution and conveniently separating the individual signals in a spectrum. Ellis et al.¹⁵ applied J-resolved pulse sequence (*cf.* Figure 9.1)¹⁶ for PFBA where the individual signals were well resolved and separated. Interpretation of the splitting patterns based on individual coupling constants revealed that the fluorine atoms within each of the CF_2 moieties were non-equivalent; whereas, all the three atoms on the CF_3 group were equivalent, resulting in a $A_3\text{MNXY}$ spin system. For that to be the case, Ellis et al.¹⁵ concluded that the fluorocarbon chain must be held relatively rigid while there is a free rotation of the CF_3 group on a three-fold axis. In our study (*cf.* chapter 5), a slightly different picture of the dynamics of PFBA emerged. Simulation of the resonance lines of PFBA revealed that in addition to the free rotation of the CF_3 group, the C-F bonds experience appreciable axial motion. This is understood in terms of the fact that a rigid perfluorocarbon chain would yield separate sub-spectra of the individual rotamers (i.e., *gauche+*, *gauche-*, and *trans*) (*cf.* Fig. 4.7). J-resolved experiments can be applied to the complexes of PFBA and PFOA with β -CD in solution, where the dynamics of the free guests can be compared with that of the complexes. In the case of the host/guest complexes, the dynamics of the guest are expected to vary because it is coupled to the host.

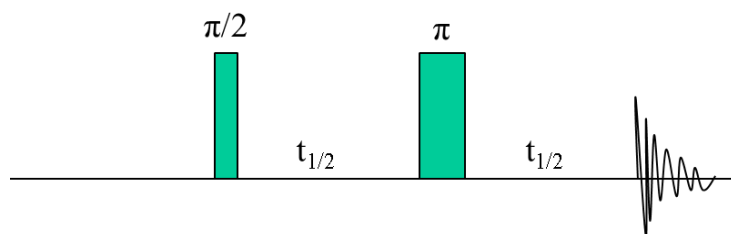


Figure 9.1 Pulse Sequence for 2D J-Resolved NMR Technique.

The interfacial structure of MIMs/PFOA mixture can be further probed using solid-state NMR, Raman spectroscopy and atomic fluorescence microscopy (AFM). The procedure for solid-state NMR involves doping the copolymers with variable concentrations of the guest and running the solid spectra of the complexes to probe changes in line shapes/widths for diagnostic resonance lines (e.g. the carbonyl) as well as appearance of new lines, particularly for the guest compound.

The Raman and AFM measurements can be acquired on film-based preparations of the polymers using drop- or spin-casting methods. Polymeric thin films (~10 μm) can be achieved using established spin coating or drop casting methods using appropriate non-aqueous solvents or water. The Raman/AFM analyses of such films doped with different concentrations of PFOA can provide useful information regarding the structure of MIMs/PFOA mixtures. Raman spectroscopy has been used to investigate the intermolecular interactions at polymer/dye and glass/dye interfaces.¹⁷ Frequency shift and intensity changes of the vibrational bands assigned to the guest (e.g., PFOA) and host (e.g. a copolymer) have been used to gain an insight into the relative strength of adhesive forces (e.g. H-bonding, ion-dipole, van der Waals, etc.) at the surface. On the other hand, AFM methods can be used to provide additional evidence for the formation of monolayer and multilayer PFOA structures on the surface of a copolymer film. Sample preparation for AFM involves formation of a monolayer by spreading PFOA solution at low concentration (~1 mM) onto the copolymer surface.¹⁸ Multilayer structures can be achieved either by repeatedly spreading PFOA solution at low/medium (~2 mM) concentration onto the film or by using a highly concentrated (~5 mM) PFOA solution.¹⁹ The thickness profiles of the monolayer and multilayers structures can be determined using contact mode AFM where the results can be compared to those of un-doped film. In a previous report,²⁰ contact mode AFM was used to intentionally and carefully scratch a monolayer deposited onto a film, whereas a line profile determined across the scratch allowed for the determination of the monolayer thickness from the depth of the scratch. Combined AFM and spectroscopic ellipsometry techniques have been used to analyze the morphology and thickness of surfactant films.²¹

9.4. References

1. Moynihan, R. E. *J. Am. Chem. Soc.* **1959**, *81*, 1045–1050.
2. Karoyo, A. H.; Wilson, L. D. *J. Colloid. Interf. Sci.* **2013**, *402*, 196–203

3. Wilson, L. D.; Verrall, R. E. *Langmuir* **1998**, *14*, 4710–4717
4. Xing, H.; Lin, S.; Yan, P.; Xiao, J.; Chen, Y. J. *Phys. Chem. B* **2007**, *111*, 8089–8095.
5. Ma, M.; Li, D. *Chem. Mater.* **1999**, *11*, 872–874
6. Wilson, L. D.; Mohamad, M. H. "A Novel Dye-Based Method for the Characterization of Polymers and Materials Containing β -Cyclodextrin", *Beilstein J. Org. Chem.* **2014**, Manuscript Submitted (ID 5623068).
7. Deng, S.; Shuai, D.; Yu, Q.; Huang, Y.; Yu, G. *Front. Environ. Sci. Eng. China* **2009**, *3*, 171-177.
8. Yu, Q.; Deng, S.; Yu, G. *Water Res.* **2008**, *42*, 3089-3097.
9. Reif, B.; Xue, Y.; Agarwal, V.; Pavlova, M. S.; Hologne, M.; Diehl, A.; Ryabov, Y. E.; Skrynnikov, N. R. *J. Am. Chem. Soc.* **2006**, *128*, 12354-12355.
10. Barros, T. C.; Stefaniak, K.; Holzwarth, J. F.; Bohne, C. *J. Phys. Chem. A* **1998**, *102*, 5639.
11. Christoff, M.; Okano, L. T.; Bohne, C. *J. Photochem. Photobio. A. Chemistry* **2000**, *134*, 169-176.
12. Okano, L. T.; Barros, T. C.; Chou, D. T. H.; Bennet, A. J.; Bohne, C. *J. Phys. Chem.* **2001**, *105*, 2122-2128.
13. Liu, Y.; Pellerin, C. *Polymer* **2009**, *50*, 2601–2607.
14. Morris, G. A. Two-Dimensional J-Resolved Spectroscopy. John Wiley & Sons Ltd. Manchester, UK, 2007, pp1–6.
15. Ellis, D. A.; Denkenberger, K. A.; Burrow, T. E.; Mabury, S. A. *J. Phys. Chem. A* **2004**, *108* (46), 10099–10106.
16. Lehmler, H. -J.; Rama Rao, V.V.V.N.S.; Nauduri, D.; Vargo, J. D.; Parkin, S. *J. Fluorine Chem.* **2007**, *128*, 595–607
17. Rabolt, J. F.; Schlotter, N. E. *J. Polym. Sci.: Polym. Phys.* **1983**, *21*, 1–9.
18. Zhavnerko, G. K.; Zhavnerko, K. A.; Agabekov, V. E.; Gallyamov, M. O.; Yaminsky, I. V.; Rogach, A. L. *Colloids Surf., A* **2002**, *198*, 231–238.
19. Deger, G.; Hong, J. D.; Schmitt, I. *Thin Films* **1992**, *210/211*, 831–835.
20. Anariba, F.; DuVall, S. H.; McCreery, R. L. *Anal. Chem.* **2003**, *75*, 3837–3844.
21. Finot, E.; Markeya, L.; Haneb, F.; Amreinc, M.; Leonenkob, Z. *Colloids Surf., B* **2013**, *104*, 289–293

Appendices (Supplementary Data)

1. Appendix A (Chapter 2)

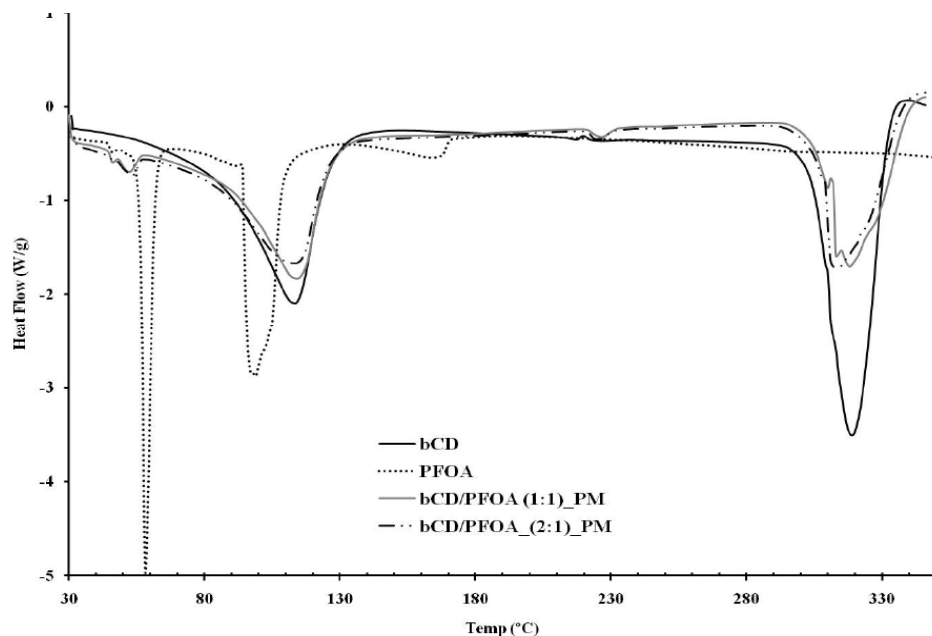


Figure A2.1 DSC thermograms for β -CD, PFOA, and the 1:1 and 2:1 Physical Mixtures of β -CD and PFOA.

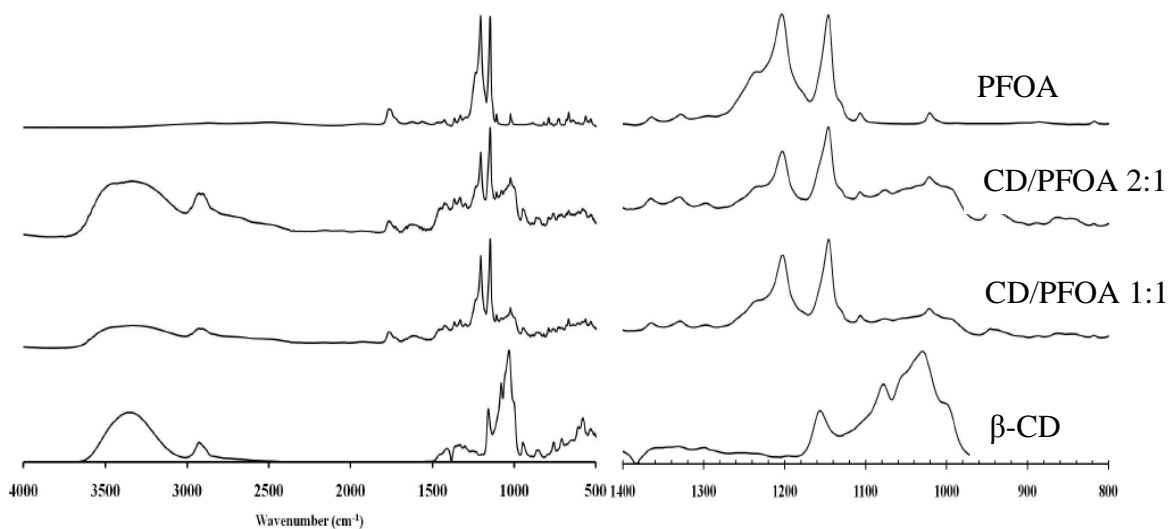


Figure A2.2 FT-IR spectra of β -CD, PFOA, and the 1:1 and 2:1 Physical Mixtures of β -CD and PFOA.

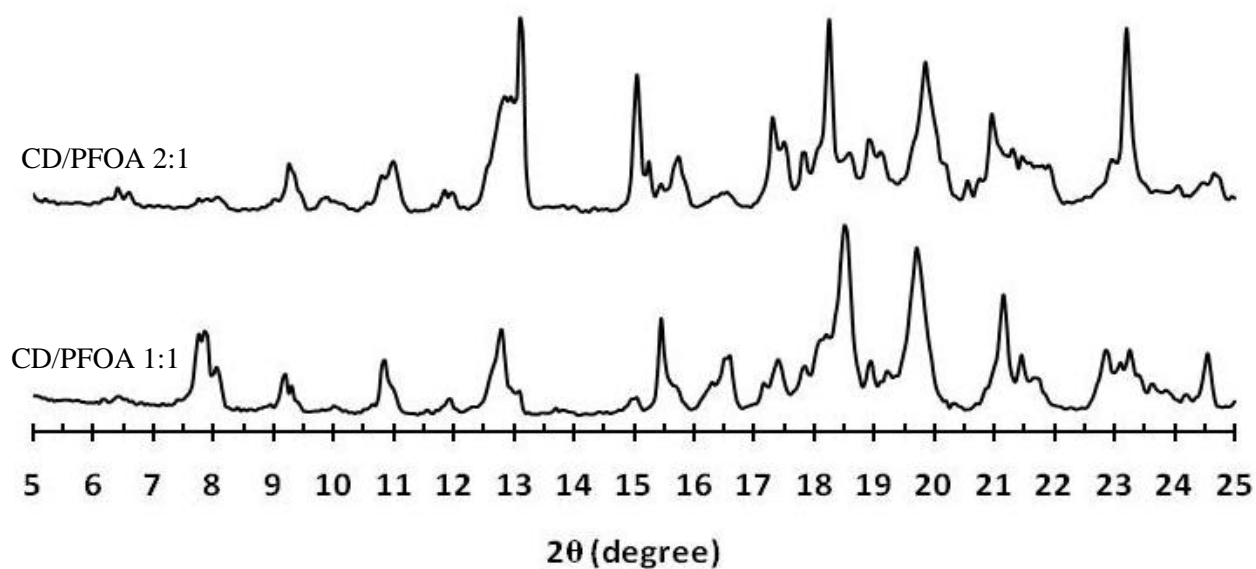


Figure A2.3 XRD Patterns for the 1:1 and 2:1 Physical Mixtures of β -CD and PFOA

2. Appendix B (Chapter 3)

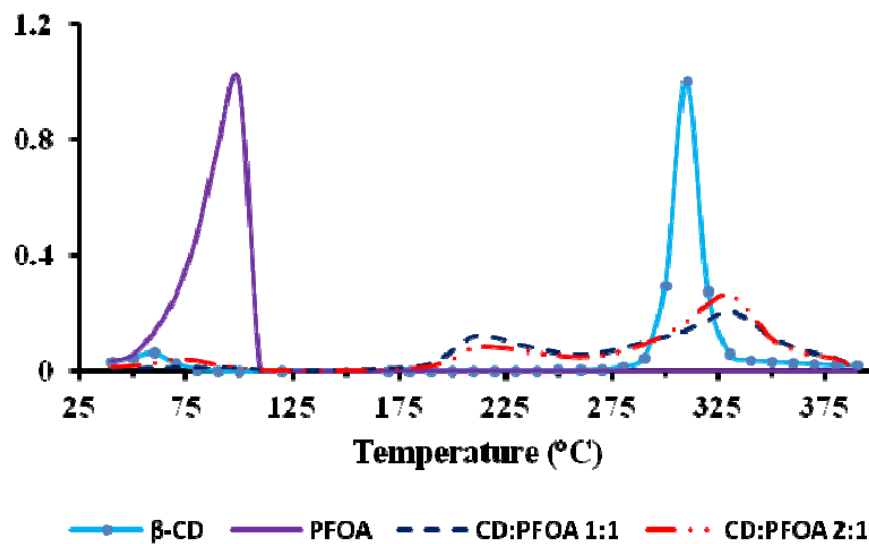


Figure B3.1 TGA thermograms for β -CD, PFOA, and the 1:1 and 2:1 β -CD/PFOA cocomplexes prepared by the modified dissolution method.

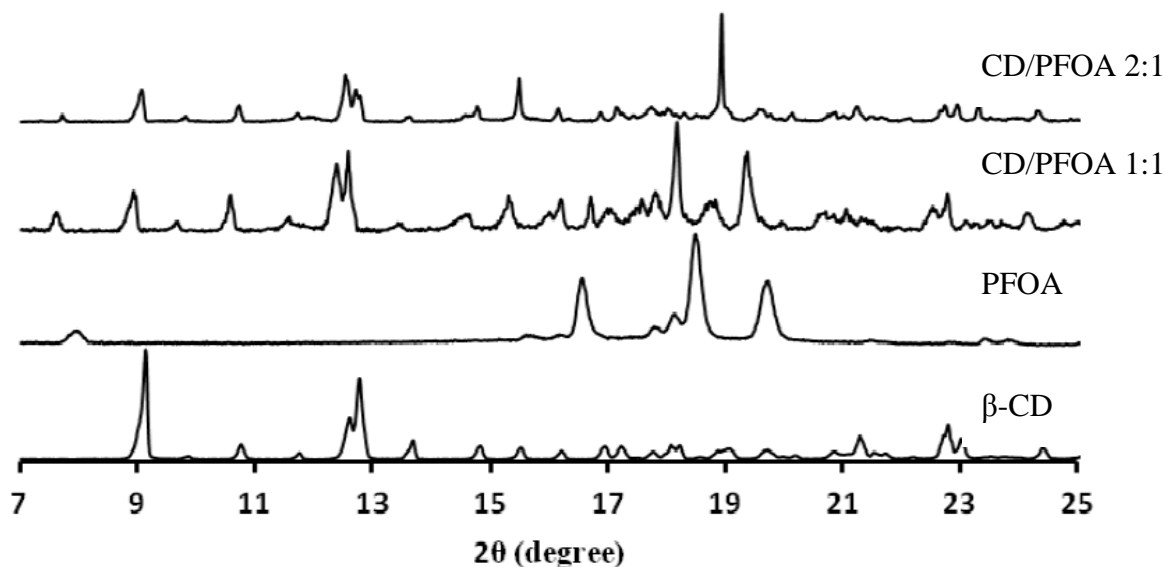


Figure B3.2 PXRD diffractograms for β -CD, PFOA, and the 1:1 and 2:1 physical mixtures of β -CD and PFOA.

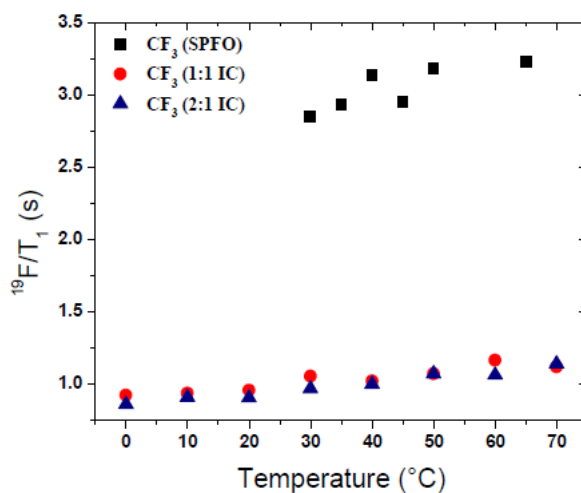


Figure B3.3 ^{19}F T_1 relaxation times for the CF_3 group of SPFO, the the 1:1 and 2:1 β -CD/PFOA inclusion complexes as a function of temperature.

Table B3.1. ^{19}F NMR spectral parameters Generated by Fitting the CF_3 Signal of the 1:1 β -CD/PFOA Complex to Two Lorentzian Peaks (CF_3 -in Cavity, CF_3 -out of Cavity (ref. Figure 3.6)

Temperature	chemical shift (ppm)	Height (a.u.)	Linewidth (Hz)	Area (a.u.)	Lorentz/Gauss (Ratio)
25°C (CF_3 in)	-81.178	3.40	731	512.0	1.00
30°C (CF_3 in)	-81.092	3.30	731	496.2	1.00
40°C (CF_3 in)	-81.014	3.18	720	471.0	1.00
50°C (CF_3 in)	-80.900	2.92	708	425.1	1.00
60°C (CF_3 in)	-80.785	2.82	724	420.0	1.00
70°C (CF_3 in)	-80.666	2.61	758	408.0	1.00
25°C(CF_3 out)	-80.117	0.74	1001	152.5	1.00
30°C(CF_3 out)	-79.966	0.72	997	148.1	1.00
40°C(CF_3 out)	-79.876	0.76	951	148.3	1.00
50°C(CF_3 out)	-79.695	0.80	939	155.5	1.00
60°C(CF_3 out)	-79.617	0.76	924	144.0	1.00
70°C(CF_3 out)	-79.360	0.70	912	132.3	1.00

Table B3.2. ^{19}F NMR spectral parameters Generated by Fitting the CF_3 Signal of the 2:1 β -CD/PFOA Complex to One Lorentzian Peak (CF_3 -in Cavity; ref. Figure 3.6).

Temperature	chemical shift (ppm)	Height (a.u.)	Linewidth (Hz)	Area (a.u.)	Lorentz/Gauss (Ratio)
25°C (CF_3 in)	-81.552	7.56	793	1235.0	1.00
30°C (CF_3 in)	-81.489	7.54	783	1215.5	1.00
40°C (CF_3 in)	-81.733	7.21	779	1155.3	1.00
50°C (CF_3 in)	-81.632	7.04	767	1118.7	1.00
60°C (CF_3 in)	-81.526	6.85	775	1093.7	1.00
70°C (CF_3 in)	-81.756	6.19	860	1099.4	1.00

3. Appendix C (Chapter 4)

Table C4.1a Deconvolution Parameters for the CF₃ and the CF₂ high and low field resonance lines of ¹⁹F spectrum of the 1:1 β-CD/PFBA Complex acquired at MAS 20 kHz and 295 K.

Resonance	Assigned configuration	Shift (ppm)	Height	Width (Hz)	L/G	Area
CF ₃	3 (2:1)	-82.36	91.87	259	0.50	2224.832
	2 (1:1)	-81.79	45.43	604	0.50	2568.604
	1 (1:2)	-80.77	17.98	262	0.50	440.426
CF ₂ (hf)	2 (1:1)	-118.96	26.63	634	0.75	1659.241
	3 (2:1)	-119.98	10.89	620	0.75	662.730
CF ₂ (lf)	2 (2:1)	-127.24	41.69	403	0.75	1652.790
	1 (1:2)	-126.77	6.63	574	0.75	374.460
	3 (1:1)	-128.19	14.34	468	0.75	659.958

Table C4.1b Deconvolution Parameters for the CF₃ and the CF₂ high and low field resonance lines of the ¹⁹F spectrum of the 2:1 β-CD/PFBA Complex acquired at MAS 20 kHz and 295 K.

Resonance	Assigned Configuration	Shift (ppm)	Height	Width (Hz)	L/G	Area
CF ₃	3 (2:1)	-82.42	91.89	246	0.50	2116.215
	2 (1:1)	-81.86	22.06	366	0.50	755.868
	1 (1:2)	-80.97	8.06	485	0.50	366.058
	-	-83.13	5.34	200	0.50	100.093
CF ₂ (hf)	3 (2:1)	-119.08	23.22	555	0.75	1264.956
	2 (1:1)	-120.16	3.99	932	0.75	365.698
CF ₂ (lf)	3 (2:1)	-127.30	39.09	384	0.75	1475.419
	2 (1:1)	-128.36	5.28	429	0.75	222.373

4. Appendix D (Chapter 5)

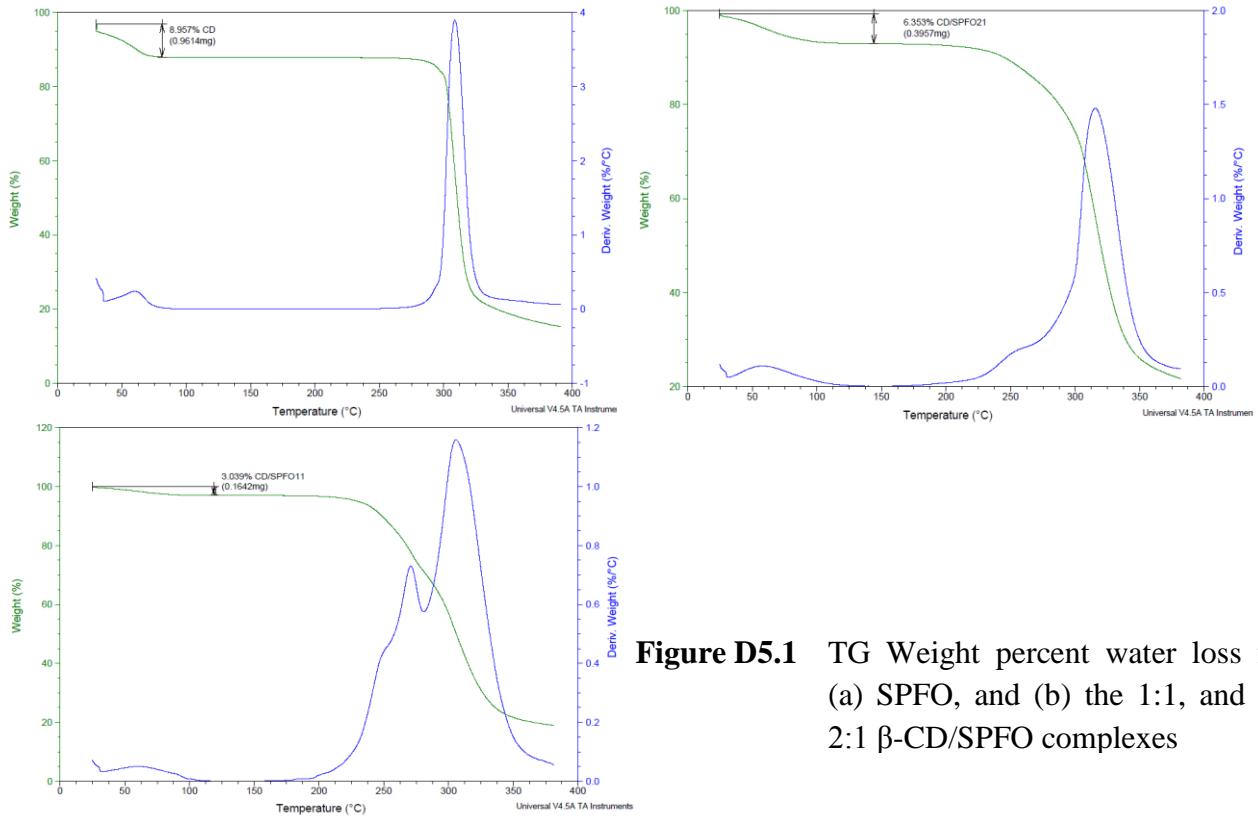


Figure D5.1 TG Weight percent water loss for (a) SPFO, and (b) the 1:1, and (c) 2:1 β -CD/SPFO complexes

Table D5.1 Deconvolution Parameters for the CF₃ Line Shape of pure SPFO, the 1:1, and 2:1 β-CD/SPFO Complexes.

Complex	Chemical shift	Height	width	Area
SPFO	-83.922	557.73	550	51620.443
	-83.866	428.18	220	15851.757
	-83.693	122.21	99	2039.734
1:1 IC	-80.921	35.29	435	2583.214
	-82.481	18.57	435	1359.291
	-83.980	38.13	435	2791.178
	-80.909	52.59	210	1858.327
	-81.253	69.96	220	2589.948
	-81.599	118.63	210	4192.147
	-82.001	76.07	220	2816.411
	-82.394	73.73	210	2605.556
2:1 IC	-82.930	50.27	210	1776.306
	-80.921	38.02	435	2783.077
	-81.660	73.62	435	5388.986
	-82.481	245.80	435	18003.010
	-82.771	29.67	142	709.540
	-83.756	15.02	435	1100.382

5. Appendix E (Chapter 6)

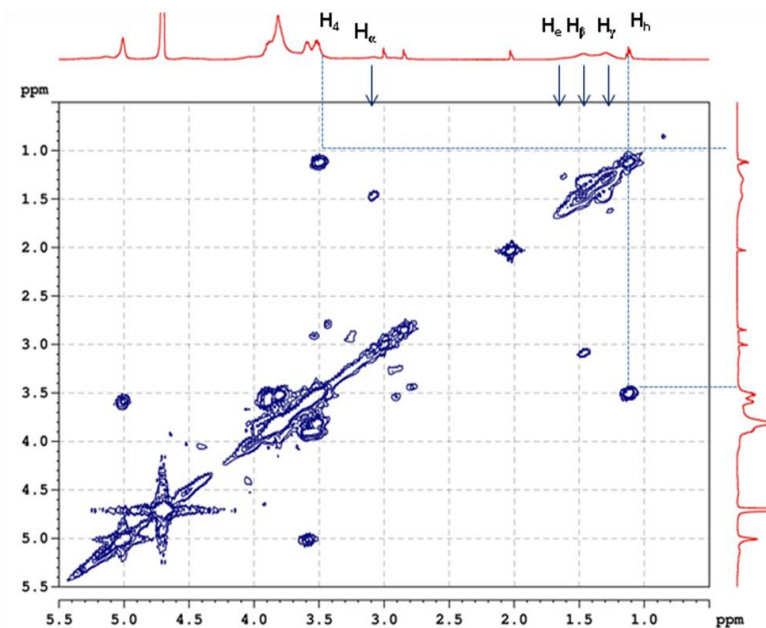


Figure E6.1 2-D ¹H COSY NMR Results of HDI-1 copolymer showing connectivity of the protons of the HDI cross-linker.

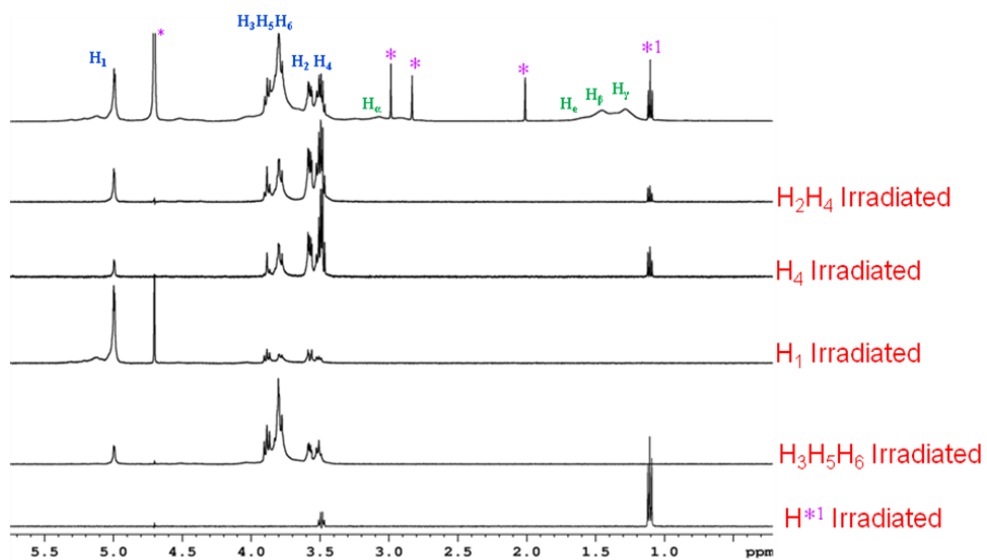


Figure E6.2 1-D TOCSY NMR spectra for HDI-1 copolymer. The ¹H nuclei of β-CD (H₁-H₄) were irradiated.

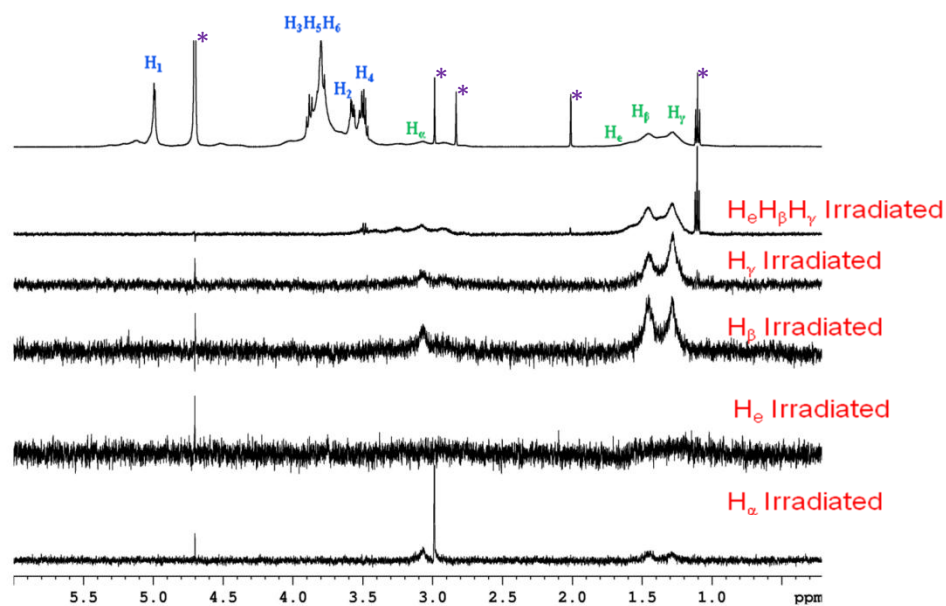


Figure E6.3 1-D TOCSY NMR spectra for HDI-1 copolymer. The ¹H nuclei of HDI cross-linker were irradiated.

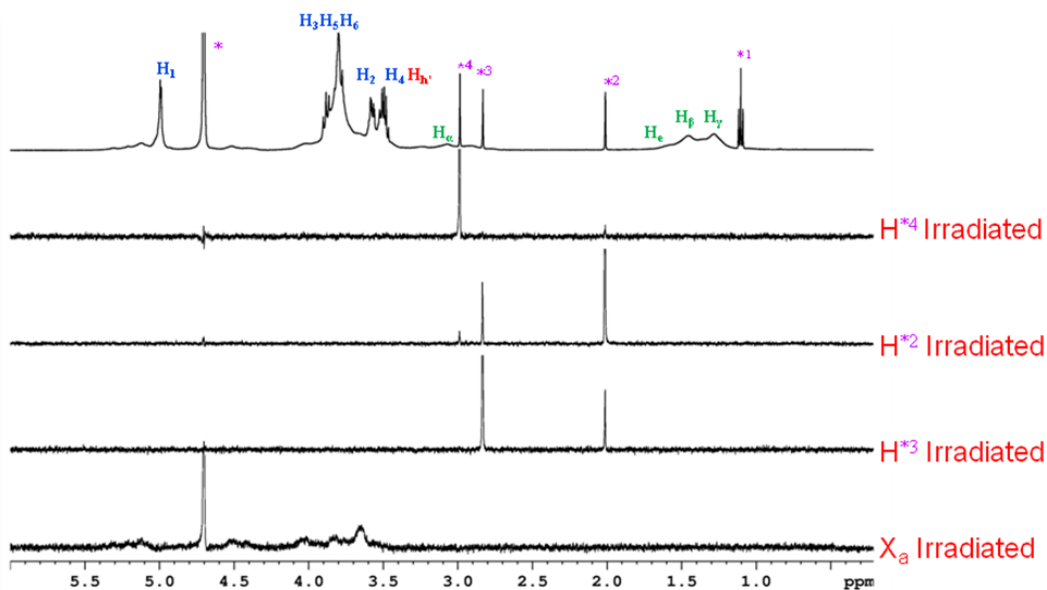


Figure E6.4 1-D TOCSY NMR spectra for HDI-1 copolymer. The ^1H nuclei of the solvents (diethyl ether, Dimethyl Acetamide) were irradiated.

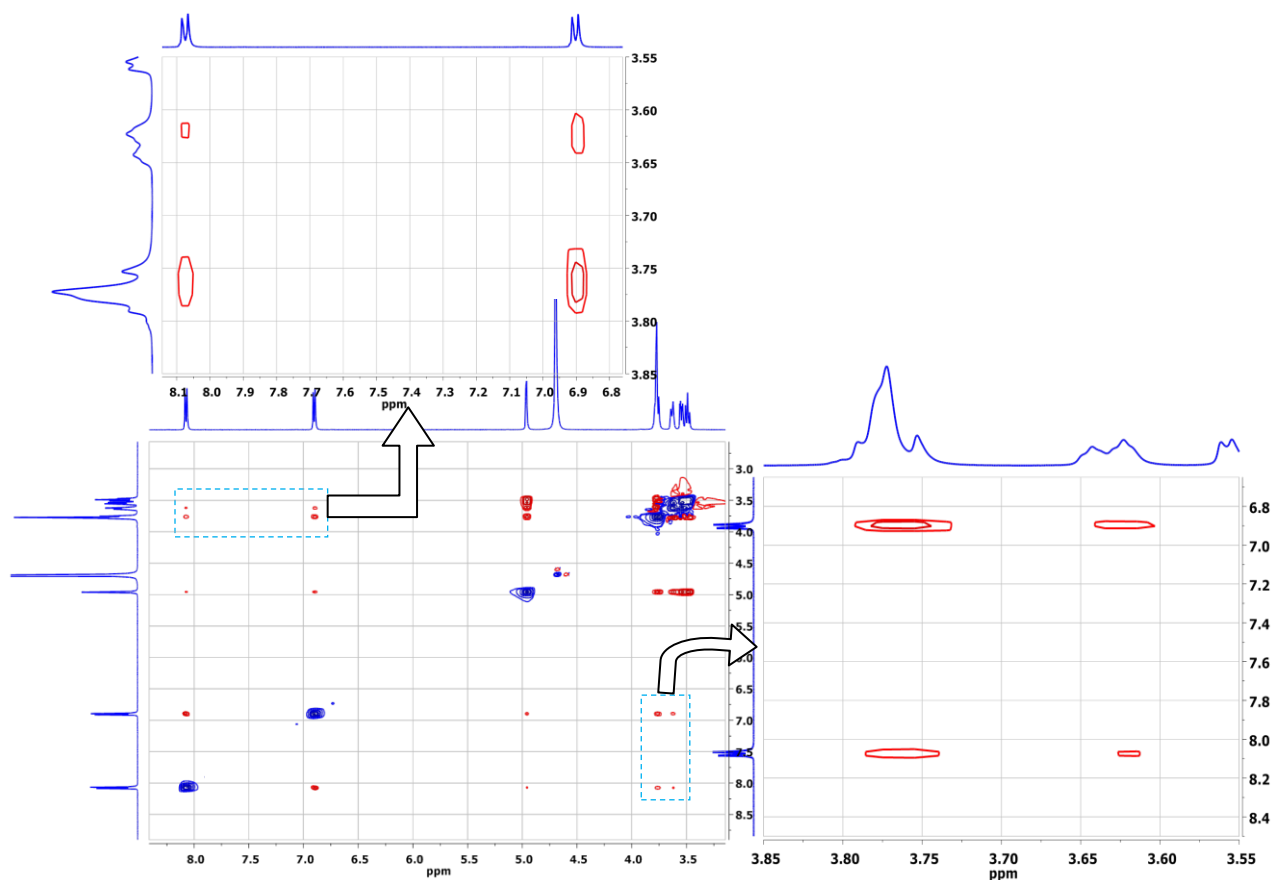


Figure E6.5 2-D ROESY NMR results for HDI-1/PNP complex. Cross peaks show directed inclusion of PNP within the Cavity of β -CD (see expanded regions).